

Engineering Principles of Agricultural Machines

2nd Edition

Ajit K. Srivastava

Michigan State University

Carroll E. Goering

University of Illinois

Roger P. Rohrbach

North Carolina State University

Dennis R. Buckmaster

The Pennsylvania State University

**Copyright © 2006 by the
American Society of Agricultural and Biological Engineers**
All rights reserved.

ASABE is an educational and scientific organization
dedicated to the advancement of engineering
applicable to agricultural, food, and biological systems.

**Editing by Peg McCann
Cover design by Melissa Miller
Production assistance by
Patricia Howard and Marcia Stults McCavit**

**Cover photo of a Massey Ferguson combine
courtesy of AGCO Corporation.**

This book may not be reproduced
in whole or in part by any means
without the permission of the publisher.

For information, contact the
American Society of Agricultural and Biological Engineers
2950 Niles Road, St. Joseph, MI 49085-9659 USA
Phone: 269-429-0300 Fax: 269-429-3852 E-mail: hq@asae.org

Library of Congress Card Number (LCCN) 2005937948
International Standard Book Number (ISBN) 1-892769-50-6
ASAE Publication 801M0206

The American Society of Agricultural and Biological Engineers is
not responsible for the statements and opinions advanced
in its meetings or printed in its publications.
They represent the views of the individuals to whom
they are credited and are not binding on the Society as a whole.

PREFACE

We are pleased to offer the second edition of the textbook *Engineering Principles of Agricultural Machines*. To arrive at the revisions in the second edition, we called some instructors of the first edition and conducted lengthy phone interviews to seek their thoughts and suggestions for revisions. We interviewed Dr. Dennis Buckmaster of Penn State University, Dr. Dan Humburg of South Dakota State University, Dr. Lei Tian of the University of Illinois, and Dr. Ranal Taylor of Kansas State University. Based on their input we prepared a survey form listing the many changes suggested. The survey forms were sent to all instructors, in the U.S. and abroad, who were using the textbook. We compiled the responses and rated each suggestion. We also held a user forum during the 2005 ASABE conference in Tampa, Florida to share the results of our survey and to seek additional input. Items receiving a 3 or higher score on a 5-point scale were marked for inclusion in the revised edition.

The changes can be divided in four categories. These are: reorganization of chapters into shorter modules to allow instructors greater flexibility in selecting topics to match their needs; the addition of a new chapter on agricultural information systems in response to the growth in precision agriculture technology since the first edition; addition of simulation problems; and adding a supplemental CD that includes a spreadsheet and many simulations. We feel the CD will add a new dimension to student learning and give them the opportunity to develop a deeper understanding of the process under study as affected by the various system parameters.

We are very pleased that Dr. Dennis Buckmaster has joined the list of authors. Dennis has been an avid user of the textbook and has developed much supplemental simulation material during the course of teaching principles of agricultural machines at Penn State University. We have included much of his material in the accompanying CD. Dennis also revised the chapter on hay and forage harvesting.

Finally, we would like to thank the many people who have been helpful in the process of preparing this edition. We thank Monte Dickson for providing a thorough review of the new chapter on agricultural information systems (Chapter 6). We would also like to acknowledge Frank Zoz for letting us include his traction prediction model in the CD, and Al Hanson for letting us use his engine simulator in the CD.

As always, we welcome your feedback and suggestions for improvement. Please feel free to contact any of us. Additions and changes will be posted to the ASABE Technical Library at <http://asae.frymulti.com/toc.asp> (scroll down to the listing of textbooks). For specific questions we ask that you direct your inquiries to Ajit Srivastava for Chapters 1, 4, 8, 10, 12, and 14; to Carroll Goering for Chapters 2, 3, 5, 6, 7, 9, and 15; to Roger Rohrbach for Chapter 13; and to Dennis Buckmaster for Chapter 11 and the accompanying CD.

Ajit Srivastava (srivasta@msu.edu)

Carroll Goering (cgoering@uiuc.edu)

Roger Rohrbach (rohrbach@eos.ncsu.edu)

Dennis Buckmaster (drb3@psu.edu)

The authors wish to dedicate this edition to their wives
Barbara Srivastava,
Carol Goering,
Jeanette Rohrbach,
and
Corinne Buckmaster
for their unwavering support and encouragement throughout our lives.

CONTENTS

Chapter 1

Agricultural Mechanization and Some Methods of Study 1

Introduction	1
1.1 History of Mechanized Agriculture.....	1
1.2 Farming Operations and Related Machines	3
1.3 Functional Analysis of Agricultural Machines.....	4
1.3.1 Basic processes of agricultural machines.....	5
1.3.2 Process diagrams.....	6
1.4 Dimensional Analysis	7
1.4.1 Scope.....	7
1.4.2 Physical dimensions.....	7
1.4.3 Units of measurement	8
1.4.4 Developing a prediction equation	9
1.4.5 Buckingham's Theorem.....	10
1.4.6 Systematic calculation of the dimensionless products	12
1.4.7 Transformation of dimensionless products	13
Problems.....	14

Chapter 2

Engine Power for Agricultural Machines 15

Introduction	15
2.1 The power in fuel.....	15
2.2 Combustion	16
2.2.1 Combustion chemistry	16
2.2.2 Energy release in combustion	19
2.3 Thermodynamic limits to Engine Performance.....	21
2.4 Heat Losses and Power at the Pistons	25
2.5 Mechanical Losses and Power at the Flywheel.....	26
2.6 Engine Torque and Efficient Engine Loading.....	28
2.7 Control of Engine Speed	29
2.8 Engine performance simulator	33
2.9 Turbocharging and Intercooling Engines.....	35
2.9.1 Operation of turbochargers	36
2.9.2 Intercoolers	39

2.9.3 Turbocharging and intercooling for versatility	39
Problems	41
Simulation Problems.....	43

Chapter 3

Electrical Power for Agricultural Machines 45

Introduction	45
3.1 Motor Components.....	45
3.2 Motor Classifications	46
3.3 Principles of Operation Of Induction Motors.....	47
3.4 Types of Single-Phase Induction Motors	49
3.4.1 Split-phase induction motors.....	49
3.4.2 Capacitor-start, induction-run motors	50
3.4.3 Two-value-capacitor, induction-run motors.....	52
3.4.4 Repulsion-start, induction-run motors.....	52
3.5 Three-Phase Induction Motors	53
3.6 Dual-Voltage Motors	54
3.7 Torque-Speed Characteristics of Induction Motors.....	56
3.8 Motor Nameplate Information	57
3.9 Motor Starters	59
3.10 Motor Enclosures	59
3.11 Variable- Speed Electric Motors	59
3.12 Motor Efficiency	60
Problems	61
Simulation Problems.....	63

Chapter 4

Mechanical Power Transmission 65

Introduction	65
4.1 V-Belt Drives	65
4.1.1 V-belt types and standardization.....	66
4.1.2 V-belt drive geometry	67
4.1.3 Kinematics of V-belt drives	68
4.1.4 Mechanics of V-belt drives	69
4.1.5 Stresses and service life	72
4.1.6 Variable-speed V-belt drives.....	74
4.1.7 V-belt drive design.....	76
4.2 Chain Drives	76
4.2.1 Types of chains and standardization	76
4.2.2 Geometry of chain drives	79
4.2.3 Kinematics of chain drives.....	79
4.2.4 Design of chain drives.....	82

4.3	Power-Take-Off Drives.....	83
4.4	Overload Safety Devices.....	87
4.4.1	Shear devices.....	87
4.4.2	Jump clutch devices.....	88
4.4.3	Friction devices.....	89
	Problems.....	90

Chapter 5

Fluid power, mechatronics, and control

91

	Introduction.....	91
5.1	Basic Principles and Elements Of Fluid Power.....	91
5.2	Pumps.....	92
5.3	Valves.....	96
5.3.1	Pressure control valves.....	96
5.3.2	Volume control valves.....	98
5.3.3	Directional control valves.....	99
5.4	Actuators.....	102
5.4.1	Hydraulic motors.....	102
5.4.2	Hydraulic cylinders.....	102
5.5	Reservoirs, Fluids, Filters, and Lines.....	104
5.6	Types of Fluid Power Systems.....	107
5.6.1	Open-center systems.....	107
5.6.2	Pressure-compensated systems.....	109
5.6.3	Load-sensing systems.....	109
5.7	Pressure Transients.....	111
5.8	Hydrostatic Transmissions.....	112
5.9	Mechatronics and System Control.....	114
5.9.1	An introduction to mechatronics.....	114
5.9.2	System control.....	115
	Problems.....	117
	Simulation Problems.....	121

Chapter 6

Precision agriculture

123

	Introduction.....	123
6.1	Sensors.....	124
6.1.1	Sensor types.....	124
6.1.2	Sensor applications.....	124
6.1.3	Advanced sensors.....	124
6.2	Global Positioning System.....	125
6.2.1	GPS for civilian use.....	125
6.2.2	Military GPS.....	125

6.2.3	Differential GPS.....	125
6.2.4	Carrier-phase GPS	126
6.2.5	Real-time kinematic GPS.....	126
6.2.6	Accuracy measures	126
6.2.7	Coordinate transformation	127
6.3	Geographic Information System	130
6.3.1	Data input to a FIS	130
6.3.2	Map coordination	131
6.3.3	Data analysis in the FIS	133
6.3.4	Data persistence	133
6.4	Variable Rate Applications	133
6.4.1	Approaches	133
6.4.2	Applications	134
6.4.3	Application resolution.....	134
6.4.4	Control systems.....	134
6.4.5	Automatic guidance	135
6.5	Controller Area Networks	135
	Problems	137

Chapter 7

Tractor Hitching, Traction, and Testing 139

	Introduction	139
7.1	Hitching Systems	139
7.1.1	Principles of hitching	139
7.1.2	Types of hitches	139
7.1.3	Hitching and weight transfer.....	142
7.1.4	Control of hitches.....	144
7.2	Tires and Traction	144
7.2.1	Basic tire design.....	146
7.2.2	Traction models	149
7.2.3	Traction predictor spreadsheet	153
7.3	Soil Compaction.....	154
7.4	Traction Aids.....	155
7.5	Tractor Testing.....	156
7.5.1	Basic principles of tractor testing.....	156
7.5.2	Official tractor tests.....	158
	Problems	165
	Simulation Problems.....	166

Chapter 8

Soil Tillage 169

	Introduction	169
--	--------------------	-----

8.1	Tillage Methods and Equipment	169
8.1.1	Primary tillage in conventional tillage systems.....	170
8.1.2	Secondary tillage in conventional tillage systems.....	179
8.1.3	Tillage in conservation tillage systems	184
8.2	Mechanics of Tillage Tools.....	185
8.2.1	Soil texture	185
8.2.2	Physical properties of soils	187
8.2.3	Mechanical properties of soils	189
8.2.4	Mechanics of a simple tillage tool	200
8.3	Performance of Tillage Implements	207
8.3.1	Moldboard plows	207
8.3.2	Disk implements	209
8.3.3	Cultivators.....	211
8.3.4	Rotary tillers.....	214
8.4	Hitching of Tillage Implements	215
8.4.1	Forces on tillage tools	215
8.4.2	Pull-type implements.....	221
8.4.3	Mounted implements.....	226
	Problems	229

Chapter 9

Crop Planting

231

	Introduction	231
9.1	Methods and Equipment	231
9.1.1	Broadcast seeding	231
9.1.2	Drilling.....	232
9.1.3	Precision planting.....	233
9.1.4	Transplanting	234
9.2	Functional Processes	235
9.2.1	Seed metering.....	235
9.2.2	Seed transport.....	245
9.2.3	Furrow opening and covering	255
9.2.4	Transplanting	258
9.3	Evaluating Planter and Transplanter Performance	262
9.3.1	Broadcast seeders.....	262
9.3.2	Drills	264
9.3.3	Precision planters	264
9.3.4	Transplanters.....	265
	Problems	265

Chapter 10
Chemical Application **269**

Introduction	269
10.1 Application of Granular Chemicals.....	269
10.1.1 Methods for application of granular chemicals.....	270
10.1.2 Equipment for application of granular chemicals	270
10.1.3 Functional processes of granular chemical applications	273
10.2 Application of Liquid Chemicals	280
10.2.1 Methods for application of liquid chemicals.....	280
10.2.2 Equipment for application of liquid chemicals	280
10.2.3 Functional processes of applying liquid chemicals.....	286
10.3 Performance Evaluation	310
10.3.1 Uniformity of coverage of granular chemical application	310
10.3.2 Calibration of fertilizer spreaders.....	312
10.3.3 Liquid chemical application.....	315
10.3.4 Sprayer calibration	321
Problems	322

Chapter 11
Hay and Forage Harvesting **325**

Introduction	325
11.1 Methods and Equipment	325
11.2 Functional Processes	331
11.2.1 Cutting mechanics and plant structure	331
11.2.2 Cutting and chopping.....	343
11.2.3 Curing and preservation of forage	370
11.2.4 Windrowing	374
11.2.5 Baling.....	380
11.3 Performance Evaluation	392
Problems	395

Chapter 12
Grain Harvesting **403**

Introduction	403
12.1 Methods and Equipment	403
12.1.1 Direct harvesting.....	403
12.1.2 Cutting and windrowing.....	408
12.2 Functional Processes	409
12.2.1 Gathering, cutting, pickup, and feeding	410
12.2.2 Threshing	415
12.2.3 Separation	420
12.2.4 Cleaning	427

12.2.5 Power requirements.....	433
12.3 Combine Testing.....	433
Problems.....	435

Chapter 13

Fruit, Nut, and Vegetable Harvesting

437

Introduction	437
Natural constraints.....	438
Economic constraints.....	438
13.1 The Functional Processes.....	439
13.1.1 Removal.....	439
13.1.2 Control.....	440
13.1.3 Selection.....	440
13.1.4 Transportation.....	441
13.2 Methods and Equipment	441
13.2.1 Root crops.....	442
13.2.2 Surface crops.....	447
13.2.3 Bush and trellis crops.....	452
13.2.4 Tree crops.....	459
13.3 Theoretical Considerations.....	464
13.3.1 Aerodynamic concepts.....	464
13.3.2 Fundamentals of bush and tree shakers.....	468
13.3.3 Vibrational detachment during harvest.....	475
13.3.4 Impact models and mechanical damage.....	476
13.4 Performance Factors.....	483
13.4.1 Damage.....	484
13.4.2 Efficiency.....	484
13.4.3 Reliability.....	484
Problems.....	486

Chapter 14

Conveying of Agricultural Materials

491

Introduction	491
14.1 Screw Conveyors	491
14.1.1 Screw conveyor methods and equipment.....	491
14.1.2 Theory of screw conveyors.....	492
14.1.3 Screw conveyor performance.....	494
14.2 Pneumatic Conveyors.....	499
14.2.1 Pneumatic conveyor methods and equipment.....	499
14.2.2 Theory of pneumatic conveyors.....	502
14.2.3 Pneumatic conveyor performance.....	510
14.3 Bucket Elevators	511

14.3.1	Theory of bucket elevators.....	512
14.3.2	Bucket elevator capacity	514
14.3.2	Bucket elevator power	514
14.4	Forage Blowers	515
14.4.1	Theory of forage blowers.....	516
14.4.2	Energy requirements of forage blowers	519
14.4.3	Forage blower performance	521
14.5	Miscellaneous Conveyors	521
14.5.1	Belt conveyors	521
14.5.2	Bulk or mass conveyors	523
	Problems.....	524

Chapter 15

Machinery Selection and Management

525

	Introduction	525
15.1	Field Capacity and Efficiency	525
15.1.1	Field capacity	525
15.1.2	Field efficiency	526
15.2	Draft and Power Requirements	529
15.3	Machinery Costs.....	535
15.3.1	Ownership costs.....	535
15.3.2	Operating costs.....	538
15.3.3	Timeliness costs	540
15.4	Machinery Selection and Replacement.....	545
15.4.1	Machinery selection.....	545
15.4.2	Machinery replacement.....	548
	Problems	549
	Simulation Problems.....	551

Selected Bibliography..... 553

Appendix A..... 566

Appendix B 568

Subject Index 571

AGRICULTURAL MECHANIZATION AND SOME METHODS OF STUDY

1

INTRODUCTION

Many factors have contributed to agricultural mechanization. Reducing human drudgery, increasing productivity, improving timeliness of agricultural operations such as planting and harvesting, and reducing peak labor demands are among the most compelling. Farm work is physically demanding and the working conditions are often harsh. It is less strenuous to drive a tractor than to till the soil with a spade all day long. A tractor pulling a plow can cultivate a larger area than a human with a spade in the same amount of time, thereby increasing productivity and timeliness. Timeliness is an important factor in agricultural production. Completing certain farming operations such as planting and harvesting in a timely manner increases yields and improves profitability. Farming operations are seasonal with fluctuating labor demand. More labor is needed during planting and harvesting than during other periods of plant growth. This fluctuation in labor demand creates labor management problems. With mechanization it is possible to reduce peak labor demand and maintain a more stable labor force on the farm.

1.1 HISTORY OF MECHANIZED AGRICULTURE

Even though great changes have taken place in the field of agriculture, soil still has to be tilled; seeds still have to be planted in the soil; the growing crop still has to be tended and cared for; and the crops still have to be harvested and threshed. However, the manner in which these operations are performed have changed drastically.

One of the earliest plows used to till soil was a wooden plow pulled either by humans or draft animals. As we learned to work with steel, moldboard plows were developed. The moldboard plow was a major development, since it turned the soil for better weed control and soil aeration. The seeds were planted by broadcasting them by hand. A major development in planting occurred when we learned to plant seeds in rows using dibble sticks in the early stages and later on with planters. Planting in rows had the advantage of controlling the plant population and facilitated better weed control during the plant growth period.

Crop harvesting was done by hand using sickles or scythes. The cut crop was bundled and carried to a central location where it was threshed either by beating it with a stick or by having hooped animals walk on it. The threshed crop was separated from chaff and straw by winnowing in natural wind. The threshed crop mixture would be slowly dropped from a height and the wind would blow the chaff and small pieces of straw away leaving the clean grains to fall in a pile. The process was repeated until the grain was totally free of chaff and other debris. Later, the grain was cut by mowers that used a reciprocating sicklebar. The crop was still bundled by hand. Reapers combined the cutting and binding process in one machine. The development of steam engines made it possible to develop stationary threshers. Stationary threshers were used to thresh a bundled crop at a central location. The cleaning operation was still done by winnowing but it was done by a fan instead of the natural wind. The development of the internal combustion engine made it possible to combine the cutting, threshing, and cleaning functions. The name “combine” became popular because the machine combined the three operations.

The power for early farming operations was primarily human labor. Later, draft animals were used as the source of power. Horses, water buffalo, oxen, camels, and even elephants were used as power sources. Mechanical power became the primary source with the development of steam engines in 1858. In 1889 the first tractor with an internal combustion engine was built. Tractors powered by internal combustion engines were lighter and more powerful than steam-powered tractors. In the 1930s the high compression diesel engine was adopted for tractors and became very popular. Today’s modern tractor is a very sophisticated machine with hydrostatic drive, electrohydraulic servos to control draft force and the operating depth, and an ergonomically designed, climate-controlled operator’s station. Developments in technologies such as global positioning systems (GPS) and geospatial information systems (GIS) have led to the development of what is commonly known as *precision agriculture* in which soil variability and fertility data are stored in an on-board computer that controls the application rate of chemicals such as fertilizers, pesticides, and herbicides.

It needs, however, to be pointed out that in many parts of the world, especially the Third World countries, animal and human labor continue to be the major source of power for farming operations. Even in the most advanced countries, manual labor is still used for fresh-market fruit and vegetable harvesting operations because of the delicate nature of the products. The level of mechanization depends upon the availability of human labor and the level of industrialization within each country.

Mechanization of agriculture was an important factor in reducing labor demands for farming and making it available to develop other industries. In 1900 nearly two-thirds of the U.S. population was engaged in farming. While only 3% of the American population is engaged in production agriculture now, an American farmer produces enough food to feed 60 people and one farm family can manage up to 1200 ha of farmland. Agricultural mechanization has transformed American agriculture from subsistence farming to a major industry. Today, in monetary value, exports from the agriculture sector are second only to the sale of weapons to foreign countries.

Mechanized agriculture is, however, energy and capital intensive. Energy costs and the availability of capital to buy machines determine the level of mechanization in a

society. Thus, production agriculture is facing many challenges. Rising energy costs, greater competition in the global marketplace, and the growing concerns for the environment pose new challenges that agricultural engineers must face to keep agriculture productive and affordable. The area of agricultural machines is dynamic and will continue to evolve to meet the changing needs of production agriculture.

1.2 FARMING OPERATIONS AND RELATED MACHINES

Plants are the primary production units of agriculture. They receive carbon dioxide from the air through their leaves, and receive water and nutrients from the soil through their roots. Using carbon dioxide, water, nutrients, and solar energy, plants produce seeds, fruits, roots, fibers, and oils that people can use.

The growth of plants happens in nature without any human intervention. However, agriculture arises when people exert control over plant growth. Machines are used as an extension of people's ability to produce and care for plants. This book focuses on many of the machines used by farmers to produce crops in plant agriculture.

A *crop* is a group of similar plants which are growing within the same land area. For example, if a farm produces rice and wheat, that farm is said to produce two crops. A farmer must complete certain operations in order to successfully produce a crop. The first operation is a mechanical stirring of the soil, called *tillage*, to prepare the seed bed. The second operation is called *planting* and it places the seeds in the tilled soil at the correct depth with the appropriate spacing between seeds. When the required soil temperature and soil water content are present, the seeds will germinate and then grow leaves and roots. For some crops the seeds are planted in a small area called a nursery and then the small plants are transplanted to the fields where they will grow to maturity.

As the plants grow the farmer must protect them from pests such as weeds (unwanted plants), insects, other animals, and diseases. Mechanical cultivation (tillage between the plants) is used to control weeds in some cases. Chemicals are frequently used to control weeds, insects, and diseases. Fences and/or noise-making devices may be used for protection from larger animals.

The final crop production operation is the *harvesting* of the plant parts which have economic value for the farmer. In some cases, more than one part of the plant may have economic value. For example, a farmer may use rice straw (stems and leaves) as an energy resource after the rice seeds have been removed from the plants. In other cases, the crop residue (unused plant parts) is stirred into the soil during tillage for the next crop.

The period of time on the calendar which passes from the beginning of the planting operation until the end of the harvest operation is called the *growing season*. The weather in some tropical farming areas is such that the growing season is continuous. In these areas, a crop can be planted any time during the year, and it can be harvested whenever it is mature. In many farming areas, however, the growing season is restricted because of weather conditions. For example, the planting operation may begin during spring when the soil temperature is increasing, and the harvest operation is

Table 1.1. Example of a crop rotation with four crops.

Year	Area 1	Area 2	Area 3	Area 4
1	Crop A	Crop B	Crop C	Crop D
2	Crop B	Crop C	Crop D	Crop A
3	Crop C	Crop D	Crop A	Crop B
4	Crop D	Crop A	Crop B	Crop C

completed during fall before cold weather begins. In other climates, the growing season depends on rainfall patterns with the planting operation done at the beginning of the rainy season so that the plants have adequate water for growth. Some farming areas have weather conditions which cause a short growing season that allows only one crop per calendar year, while other areas have a longer growing season which allows two or more crops each year from a given field. When the growing season is weather dependent, the planting and harvesting operations are very labor intensive in order to complete these operations in a timely way. If planting and harvesting are not completed in a timely way, the crop yield will be lowered.

Agricultural crops such as rice and wheat are *annual plants* which have one harvest after each planting. The annual plants die after they reach maturity and a new crop must be planted before another harvest can be achieved. Crops like hay (used for live-stock feed) are *perennial plants* which live for several years and can be harvested several times after a single planting operation.

Field crops include grains, hay, and sugar beets, while *horticultural crops* include fruit and vegetables. The crops which farmers choose for their own farm depends on soil type, climate, labor availability, machine availability, profit potential, social customs, government programs, and the farmer's skills.

Many farmers produce more than one type of crop during each calendar year. For example, a farm may be divided into four land areas with a different crop grown on each of the four areas. Alternating these crops in a fixed sequence is called a *crop rotation* and an example is illustrated in Table 1.1. Using a crop rotation spreads the farmer's work load over a longer period of time and reduces the economic risk in case one crop fails. A good crop rotation can also improve crop yield and the soil. Crop rotation affects the set of machines that must be available on the farm. For example, if wheat, corn, and soybeans are all grown, then the farmer needs a grain drill and a row-planter to plant crops, and a grain head and a row crop head as attachments to the combine to harvest crops. A broad selection of machines adds to capital cost and must be taken into account when selecting a crop rotation system.

1.3 FUNCTIONAL ANALYSIS OF AGRICULTURAL MACHINES

An agricultural machine has components that work together as a system in order for the machine to perform its intended function. Any machine, however simple, may be divided into many subcomponents. To understand how a machine works, consider the machine as a collection (or system) of several subsystems made up of components and subcomponents. In this section, we will learn how to identify the various systems found in a modern agricultural machine and the functions performed by the subsystems.

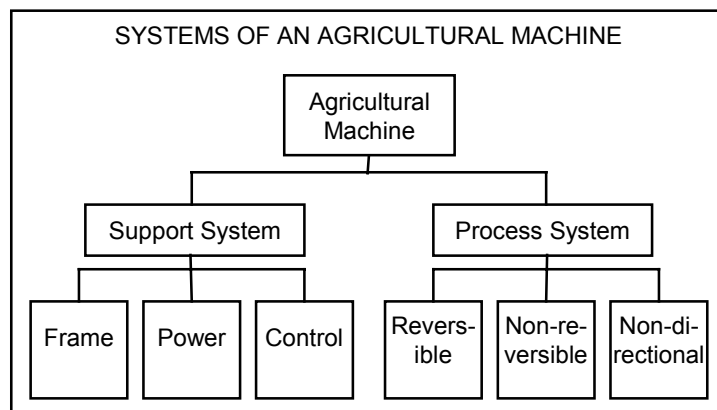


Figure 1.1 – Systems of agricultural machines.

It is often useful to look at a complex machine, such as an agricultural machine, as including two kinds of systems: process systems and support systems. The *process systems* are those components of the machine that actually perform the function(s) that the machine is designed to perform, i.e., cut, separate, mix, etc. The *support systems* are the parts that support or aid the process systems in performing their functions.

Process systems may be divided into three types: reversible, non-reversible, and non-directional. Reversible processes include processes such as separation and compaction. Non-reversible processes include cutting and grinding. Examples of non-directional processes are conveying, metering, and storing materials.

Support systems may be divided into three subsystems: the framing, control, and power subsystems. The framing system consists of all structural parts of the machine that hold pieces together so they function properly. The control system provides control over the process system. Controls may be automatic or manual. Power systems supply the power to the process systems. Self-propelled machines contain both the power source (the engine) and the power transmission devices (the drivetrain). Machines that depend on the tractor as a power source contain power transmission devices such as chains, belts, gears, PTO shafts, etc. Together these devices form the power system, which drives the process system.

A breakdown of the types of systems found in an agricultural machine is given in Figure 1.1. This illustration should aid in developing the concept of the agricultural machine as a system.

1.3.1 Basic processes of agricultural machines

In this book we will concentrate on process systems of agricultural machines. The process systems of a machine include all parts that perform reversible, non-reversible, or non-directional processes, whereas these processes are the functions the machine was designed to perform. For example, the hay baler was designed to package hay material in the form of a bale so it can be transported and stored for later feeding to animals. In order to perform this task, several processes must be performed on the hay

Table 1.2. Basic processes of agricultural machines.

Reversible Processes		Non-Reversible Processes	Non-Directional Processes
Mix	Separate	Dissociate	Convey
Fluff	Pack	Cut	Meter
Pickup	Deposit	Crush	Store
Scatter	Position	Grind	

material. They include non-reversible processes such as cutting, reversible processes such as pickup and compaction, and non-directional processes such as conveying and metering of hay. Table 1.2 lists the processes commonly found in various agricultural machines. The reversible processes are listed in opposing pairs under the appropriate category in the table. The list is not comprehensive, but it includes most commonly found processes in modern agricultural machines.

1.3.2 Process diagrams

An exercise that can be helpful in understanding the operation of an agricultural machine is to draw a diagram of the processes that occur in the machine. The diagram is formed by following the flow of material through the machine and listing the processes in order. The processes can be connected with lines to indicate the flow of the material through the machine.

Any of the processes can occur either totally within the machine or with machine mobility as part of the process. For example, the forward motion of a baler is essential to pick up hay. However, after hay is picked up, it will be baled regardless of the forward motion of the machine. When machine mobility is a part of the process, the process is, in this book, enclosed in a box. A process occurring totally within the machine is enclosed in a circle or an oval.

A few examples should be helpful in understanding the concept of process diagramming. A good first example is the moldboard plow. The first step is to determine what processes occur as the plow moves through the soil. As the plow moves forward, the soil is cut, picked up, positioned, and deposited. The second step is to determine whether the processes are dependent upon forward motion. In the case of a moldboard plow, all functions would cease as soon as the plow is stopped. The process diagram for the moldboard plow is given in Figure 1.2. The processes of picking up and positioning occur simultaneously and, therefore, are diagrammed as a pair.

A more complex machine to diagram is the conventional hay baler. The processes that occur in the machine are pickup, convey, meter, cut, pack, bind, convey, and deposit. The process which is dependent upon forward motion of the baler is pickup. The process diagram is given in Figure 1.3.

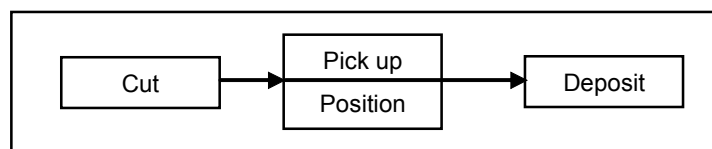


Figure 1.2 – Process diagram for a moldboard plow.

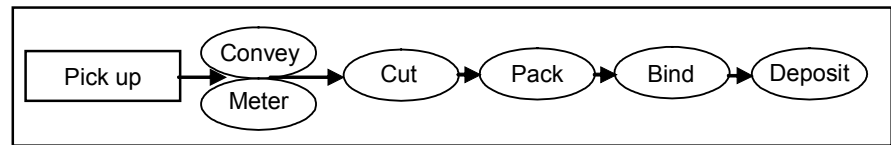


Figure 1.3 – Process diagram of for a hay baler.

The concepts of machine systems and process diagramming are introduced here as tools to aid students in learning more about the makeup and operation of agricultural machines. It is hoped that these concepts will provide a new and more interesting way to study agricultural machines, or any machine for that matter.

1.4 DIMENSIONAL ANALYSIS

Engineers like to develop predictive models to study a process or a phenomenon. Ideally we would like to develop a model that is based on the natural laws that govern the process. For example, to predict the droplet size and its distribution in a sprayer nozzle we need to understand basic fluid mechanics and the physics of a jet breakup in another fluid such as air. However, this can be a very complex process and does not lend itself to easy modeling. In cases like these another technique which is often useful is *dimensional analysis*. In dimensional analysis we need only to identify all pertinent physical quantities that influence the process. We then combine these quantities in groups so that each group is dimensionless. Experiments are then carried out to develop a power law model to relate the dependent dimensionless group to the independent ones. Dimensional analysis can be applied to highly complex processes to develop a prediction equation; however, the basic underlying natural laws are not necessarily revealed. It is, however, better than regression models in that the number of variables that must be studied are reduced substantially. Below is an abbreviated discussion of dimensional analysis.

1.4.1 Scope

Dimensional analysis is a method by which we deduce information about a phenomenon from the single premise that the phenomenon can be described by a dimensionally correct equation among pertinent variables.

The result of a dimensional analysis of a problem is a reduction in the number of variables in the problem. This results in a considerable savings in both cost and labor during the experimental determination of the function.

1.4.2 Physical dimensions

Scientific reasoning is based on such abstract entities such as force, mass, length, time, accelerations, velocity, temperature, specific heat, and electric charge. Each of these entities is assigned a unit of measurement. Of these entities, mass, length, time, temperature, and electric charge are in a sense independent and their units of measurement are specified by international standards. Furthermore, specified units of these entities determine the units of all other entities. There is, however, nothing fundamental in the set of entities, mass, length, time, temperature, and electric charge. A great many possibilities exist for choosing five mutually independent entities. Frequently, unit of force is prescribed, rather than the unit of mass. The unit of mass is determined

by Newton's law, $F = ma$. In this case the system of measurement is called a *force system*. Dimensions are a code for telling us how the numerical value of a quantity changes when the basic units of measurement are subjected to prescribed changes. The symbols [F], [M], [L], [T], and [θ] have been employed to denote dimensions of force, mass, length, time, and temperature, respectively, and any entity that has no units is denoted by [1] (Table 1.3).

Table 1.3. Dimensions of entities.

	Mass System	Force System
Length	L	L
Time	T	T
Temperature	θ	θ
Force	MLT^{-2}	F
Mass	M	$FL^{-1}T^{-2}$
Mass density	ML	$LF^{-4}T^2$
Pressure and stress	$ML^{-1}T^{-2}$	LF^{-2}
Energy, work	ML^2T^{-2}	FL
Viscosity	$ML^{-1}T^{-1}$	$FL^{-2}T$
Mass movement of inertia	ML^2	FLT
Surface tension	MT^{-2}	FL^{-1}
Strain	1	1
Poisson's ratio ^[a]	1	1

^[a] Any ratio of like-dimensioned quantities (i.e., unitless) has the dimension of one.

1.4.3 Units of measurement

CGS (Centimeter Gram Second) System

Force, measured in dynes, is defined as the force required to accelerate a 1 gram mass with 1 cm/s^2 acceleration. Thus, the weight of a gram mass is:

$$\begin{aligned} W &= mg \\ &= (1 \text{ g}) (981 \text{ cm/s}^2) \\ &= 981 \text{ (g} \cdot \text{cm/s}^2) \\ &= 981 \text{ dynes} \end{aligned}$$

U.S. Customary System

Force = pound (lb)

Length = foot (ft)

Time = second (s)

Mass, measured in slugs, is defined as that mass which will require a 1 lb force in order to accelerate with 1 ft/s^2 acceleration. Thus, the weight of 1 slug is:

$$\begin{aligned} W &= mg \\ &= (1 \text{ slug}) (32.2 \text{ ft/s}^2) \\ &= 32.2 \text{ (slug} \cdot \text{ft/s}^2) = 32.2 \text{ lb} \end{aligned}$$

SI (International) System

Force, measured in Newtons, is defined as the force required to accelerate a 1 kg mass with 1 m/s^2 acceleration. Thus, the weight of a kilogram mass is:

$$\begin{aligned} W &= mg \\ &= (1 \text{ kg}) (9.81 \text{ m/s}^2) \\ &= 9.81 \text{ kg} \cdot \text{m/s}^2 \\ &= 9.81 \text{ Newtons} \end{aligned}$$

Conversion Factors

1 m = 3.281 ft

1 ft = 0.3048 m

1 kg = 0.06852 slug

1 slug = 14.594 kg

1 Newton = 0.2248 lb

1 lb = 4.448 Newtons

1° C = 1.9° F

1.4.4 Developing a prediction equation

A critical step in dimensional analysis is to decide what physical quantities enter the problem. It is important that there be no redundancy and that no pertinent quantities are left out. To list pertinent variables, it is useful to develop an understanding of the basic phenomena or laws that affect the system. For example, let us consider that we want to develop an equation to predict the period of oscillation of a simple pendulum, that is, a mass is attached to one end of a string while the other end is attached to a support in a way such that the mass is allowed to swing with no friction. We will also neglect the aerodynamic effects. An equation of the following form may be written:

$$T = C_{\alpha} l^a m^b g^c \quad (1.1)$$

where T = period, a time entity denoted by dimension $[T]$

C_{α} = a dimensional coefficient denoted by dimension $[1]$

l = string length, a length entity denoted by dimension $[L]$

m = mass, an entity denoted by dimension $[M]$

g = acceleration due to gravity, denoted by dimension $[LT^{-2}]$

a , b , and c = dimensionless exponents

Substituting the dimension of each physical quantity in Equation 1.1 we get:

$$[T] = [1] [L]^a [M]^b [LT^{-2}]^c \quad (1.2)$$

It may clarify the next step to place the $[L]$ and $[M]$ dimensions on both sides of the equation, each with a zero exponent:

$$[M]^0 [L]^0 [T] = [1] [L]^a [M]^b [LT^{-2}]^c$$

Then, collecting and equating the exponents of the above equation we get:

for $[M]$: $0 = b$, because the $[M]$ exponent on the left is 0 and the $[M]$ exponent on the right is b ;

for $[L]$: $0 = a + c$, thus $a = -c$, because the $[L]$ exponent on the left is 0 and on the right the collected $[L]$ exponents are $a + c$; and similarly,

for $[T]$: $1 = -2c$
 $c = -1/2$
 $a = 1/2$

Substituting the values of a , b , and c in Equation 1.1 we get

$$T = C_{\alpha} l^{1/2} m^0 g^{-1/2}$$

or

$$T = C_{\alpha} \sqrt{l/g}$$

or

$$\frac{T}{\sqrt{l/g}} = C_{\alpha} \quad (1.3)$$

Note that the quantity on the left hand side of Equation 1.3 is a dimensionless group. Also note that mass, m , dropped off. This is true since we know that the period of oscillation does not depend on mass as heavier objects do not fall faster. The coefficient C_{α} needs to be determined experimentally. We know from mechanics that the

value of the constant is 2π . Also note that we began with four physical quantities and we reduced the equation by three (a number equal to the number of basic dimensions in the problem) to one dimensionless term in Equation 1.3.

1.4.5 Buckingham's Theorem

Buckingham's Theorem states that "If an equation is dimensionally homogeneous, it can be reduced to a relationship among a complete set of dimensionless products."

Suppose that we are interested in the drag force, F , acting on a sphere of diameter, D , submerged in a fluid with an average velocity, V , and having density, ρ , and viscosity, μ . Consider tentatively the relationship:

$$F = C_\alpha V^a D^b \rho^c \mu^d \quad (1.4)$$

where C_α = dimensionless coefficient; and a, b, c, d = dimensionless exponents.

In order for the equation to be *dimensionally homogeneous* both sides of the equation should have the same dimensions. This is similar to checking your units in a complicated equation; they must be the same on each side. This is accomplished by replacing the variables by their dimensions (Table 1.3) in the above equations. (Note that we use the force system since our objective is to develop a prediction equation for drag force. This can be done in the mass system, but the result will not be intuitive since force will need to be expressed as mass times the acceleration.) Replacing the variables by their dimensions results in:

$$[F] = [1] [LT^{-1}]^a [L]^b [FL^{-4}T^2]^c [FL^{-2}T]^d \quad (1.5)$$

$$\begin{aligned} \text{for } [F]: & 1 = c + d \\ \text{for } [L]: & 0 = a + b - 4c - 2d \\ \text{for } [T]: & 0 = -a + 2c + d \\ & a = 2 - d \\ & b = 2 - d \\ & c = 1 - d \end{aligned}$$

Substituting the values in Equation 1.4 we get:

$$F = C_\alpha V^2 D^2 \left(\frac{\mu}{V D \rho} \right)^d \quad (1.6)$$

$$\text{rearranging,} \quad \left(\frac{F}{\rho V^2 D^2} \right) = C_\alpha \left(\frac{\rho V D}{\mu} \right)^n \quad (1.7)$$

Note that the pressure coefficient, $\bar{P} = \left(\frac{F}{\rho V^2 D^2} \right)$, and the Reynolds number,

$N_{Re} = \left(\frac{\rho V D}{\mu} \right)$, can be substituted into the rearranged equation, which then simplifies to:

$$\bar{P} = f(N_{Re}) \quad (1.8)$$

where f is any general function.

Both \bar{P} , the pressure coefficient, and N_{Re} , Reynolds number, are dimensionless quantities. In general, a dimensional equation can be reduced to dimensionless quantities (call the *pi-terms*) related by a general function f . Notice that there are only two terms in the dimensionless form of the equation (Equation 1.8) whereas there are five variables in the dimensional form (Equation 1.7).

Stated generally, Buckingham's Theorem allows us to conclude that if n variables are connected by an unknown dimensionally homogeneous equation, it can be expressed in the form of $n - r$ dimensionless products, where r is the number of basic dimensions.

We follow up with Equation 1.7 while noting that the projected area of a sphere is $A = (1/4) \pi D^2$. Substituting, we obtain:

$$\left(\frac{F}{PV^2A} \right) = \frac{1}{2} \frac{8}{\pi} f(N_{Re}) \quad (1.9)$$

The term $\frac{8}{\pi} f(N_{Re})$ is called the drag coefficient, C_D . Thus, the equation for drag on a sphere can be written as:

$$F = \frac{1}{2} C_D PV^2A \quad (1.10)$$

where C_D is a function of N_{Re} . It is plotted in Figure 1.4. The figure is an experimental graph for smooth spherical bodies. It gives complete information concerning the drag forces on smooth spherical bodies of all sizes in an incompressible fluid with any speed of flow. To provide the same information without using dimensional analysis would require about 25 graphs that would show separately the effects of each of the variables V , D , ρ , and μ .

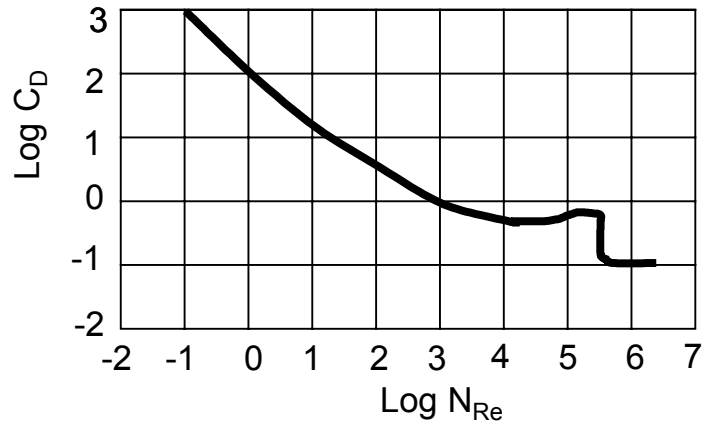


Figure 1.4 – Drag coefficient as a function of Reynolds number for smooth spherical bodies.

1.4.6 Systematic calculation of the dimensionless products

Consider the problem of computing dimensionless products of variables P, Q, R, S, T, U, V, whose dimensional matrix is given below:

	k_1	k_2	k_3	k_4	k_5	k_6	k_7
	P	Q	R	S	T	U	V
M	2	-1	3	0	0	-2	1
L	1	0	-1	0	2	1	2
T	0	1	0	3	1	-1	2

The first step is to calculate the r , rank of the matrix. The determinant to the right hand side of the matrix is:

$$\begin{vmatrix} 0 & -2 & 1 \\ 2 & 1 & 2 \\ 1 & -1 & 2 \end{vmatrix} = 1 \quad (1.11)$$

Since the determinant is not zero, $r = 3$. The number of dimensionless groups is the number of variables minus the rank of the dimensional matrix, i.e., the number of dimensionless groups, or $7 - 3 = 4$. The corresponding algebraic equations are:

$$2k_1 - k_2 + 3k_3 - 2k_6 + k_7 = 0$$

$$k_1 - k_3 + 2k_5 + k_6 + 2k_7 = 0$$

$$k_2 + 3k_4 + k_5 - k_6 + 2k_7 = 0$$

There are seven variables in the above three equations. This implies that four variables may be assigned any arbitrary values and the other three may be solved using the above equation. Since the value of the determinant as computed above corresponds to k_5 , k_6 , and k_7 , is non-zero, we will use these as dependent variables. In other words, k_1 , k_2 , k_3 , and k_4 may be assigned arbitrary values and k_5 , k_6 , and k_7 may be solved explicitly. While any value may be assigned to k_1 through k_4 , it is prudent to select a set of values that results in simplicity in calculations.

Let $k_1 = 1$ and $k_2 = k_3 = k_4 = 0$ and find $k_5 = -11$, $k_6 = 5$, and $k_7 = 8$. Similarly, let $k_2 = 1$ and $k_1 = k_3 = k_4 = 0$ and find $k_5 = 9$, $k_6 = -4$, and $k_7 = -7$.

The above procedure can be repeated and the solutions arranged as follows:

	Solution Matrix						
	k_1	k_2	k_3	k_4	k_5	k_6	k_7
	P	Q	R	S	T	U	V
π_1	1	0	0	0	-11	5	8
π_2	0	1	0	0	9	-4	-7
π_3	0	0	1	0	-9	5	7
π_4	0	0	0	1	15	-6	-12

From the above matrix the dimensionless products can be written as follows:

$$\pi_1 = \frac{PU^5V^8}{T^{11}} \quad \pi_2 = \frac{QT^9}{U^4V^7}$$

$$\pi_3 = \frac{RU^5V^7}{T^9} \quad \pi_4 = \frac{ST^{15}}{U^6V^{12}}$$

These products are linearly independent of each other. Using these dimensionless terms the following prediction equation can be written:

$$\pi_1 = C_\alpha \pi_2^a \pi_3^b \pi_4^c \quad (1.12)$$

1.4.7 Transformation of dimensionless products

New dimensionless products can be determined by forming the products of powers of the old terms. For example, the following set of dimensionless products may be transformed if necessary:

$$\pi_1 = \frac{PF}{\mu^2} \quad \pi_2 = V^3 \sqrt{\frac{P}{\mu g}} \quad \pi_3 = L^3 \sqrt{\frac{P^2 g}{\mu^2}}$$

Suppose we have determined that μ is not important. Even so, we cannot drop all terms containing μ . Instead, we transform the existing set in such a way that μ appears only in one group, which can then be discarded if necessary. This is done as follows:

$$\pi_1^* = \frac{\pi_1}{\pi_2^2 \pi_3} = \frac{F}{PV^2L^2}$$

$$\pi_2^* = \pi_2 \pi_3 = \frac{VLP}{\mu}$$

$$\pi_3^* = \frac{\pi_2^2}{\pi_3} = \frac{V^2}{\mu}$$

where π^* denotes the transformed dimensionless products. Now μ appears only in one term, which we may decide to disregard in order to simplify the investigation.

PROBLEMS

- 1.1 Show by dimensional analysis that the centrifugal force of a particle is proportional to its mass, proportional to the square of its velocity, and inversely proportional to radius of curvature of its path.

14 CHAPTER 1 AGRICULTURAL MECHANIZATION AND SOME METHODS OF STUDY

- 1.2 Complete a dimensional analysis to predict the traction force of a wheel on soil. With the help of your instructor identify soil properties that should be included in dimensional analysis. Express the prediction equation as a function of dimensionless groups.
- 1.3 Suppose it is desired to obtain an expression of the draft force of a tillage tool operating in soil. List all variables that affect the draft force and complete a dimensional analysis of the problem suitable for plotting data from experimental tests.
- 1.4 An agricultural spray nozzle is used to atomize fluid in air. Complete a dimensional analysis to predict the droplet mean diameter of the spray.

ENGINE POWER FOR AGRICULTURAL MACHINES

2

INTRODUCTION

The earliest farm equipment made use of human power and, for a period in the 19th and 20th centuries, animals supplied the power needs of farm equipment. Modern agricultural equipment, however, is powered by *internal combustion (IC) engines* and, since the 1970s, nearly all new agricultural engines have been *compression ignition (CI) engines* that burn diesel fuel. The engine can be a part of the machine itself, as on a self-propelled combine, or can provide the power for an agricultural tractor.

Engines consume fuel to produce power. The power is delivered to some load through the crankshaft and flywheel of the engine. Much of the energy in the fuel is lost before it is converted to useful power. The purpose of this chapter is to clarify the processes by which an IC engine produces power and to provide insights into how engines may be made to operate efficiently. By reading this chapter, you will also learn the important terminology of diesel engines.

2.1 THE POWER IN FUEL

Liquid fuels are a highly concentrated form of chemical energy storage. Burning the fuel at even a modest rate releases a large amount of energy that can be calculated using Equation 2.1:

$$P_{fe} = \frac{H_g \dot{m}_f}{3600} \quad (2.1)$$

where P_{fe} = fuel equivalent power, kW

H_g = gross heating value of the fuel, kJ/kg

\dot{m}_f = fuel consumption rate, kg/h

The heating values are measured by burning a sample of fuel in a calorimeter. The heating values are defined as gross (H_g) or net (H_n) depending on whether the water created in combustion is recovered as liquid or vapor, respectively. The terms higher

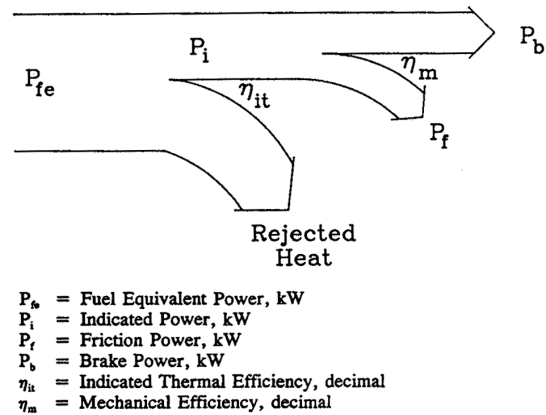


Figure 2.1 – Energy flows through an engine.

and lower are sometimes used instead of gross and net, respectively. Heating values tabulated in books (see Table 2.1) are gross values unless otherwise indicated. Less than half of the fuel equivalent power is available for useful work at the flywheel of an engine (see Figure 2.1). In the remainder of this chapter, the various power losses are identified.

2.2 COMBUSTION

Combustion is a very complex process, particularly in a CI engine. The fuel must vaporize and mix with air to form a combustible mixture. Burning of the fuel-air mixture generates exhaust emissions, but also generates increased pressure to drive the pistons. The rate of pressure rise affects engine performance and durability.

2.2.1 Combustion chemistry

Insights that are very useful in understanding engines can be obtained by making two simplifying assumptions regarding *combustion chemistry*. The first is that all of the hydrogen in the fuel links with oxygen to form water. The second is that all of the carbon in the fuel is converted to carbon dioxide (CO_2) and carbon monoxide (CO), so that no free carbon appears in the combustion products. Most conventional, petroleum-based engine fuels are mixtures of a variety of hydrocarbon molecules, but representative molecules are given in Table 2.1 for each of the common petroleum-based fuels. Alcohols, which may become engine fuels of the future, are also listed. Atomic weights of 12 for carbon, 1 for hydrogen, 16 for oxygen and 14 for nitrogen may be used in the combustion calculations. Although various gases are in the earth's atmosphere, it is common practice in combustion calculations to neglect all gases except oxygen and nitrogen. The composition of earth's atmosphere is such that 3.76 molecules of nitrogen (N_2) accompany every molecule of oxygen (O_2). Combustion chemistry then becomes a simple matter of counting atoms, as indicated in Example Problem 2.1.

Table 2.1. Comparison of properties of several fuels.

Fuel	API Gravity, degrees	Density, kg/m ³	Higher Heating Value, kJ/kg	Research Octane Number	Boiling Range, °C	Formula	Stoichiometric Air-Fuel Ratio
Butane	112	580	49,500	98	0	C ₄ H ₁₀	15.5
Propane	146	509	50,300	111	- 42	C ₃ H ₈	15.7
Reg. gasoline	61	735	47,600	93	30 - 230	C ₆ H ₁₈	15.2
No. 1 diesel	40	823	45,700	40 ^[a]	160 - 260	C ₁₂ H ₂₆	15.0
No. 2 diesel	38	834	45,500	40 ^[a]	200 - 370	C ₁₆ H ₃₄	15.0
Methanol	---	792	22,700	110	65	CH ₄ O	6.49
Ethanol	---	785	29,700	110	78	C ₂ H ₆ O	9.03
Methyl soyate	---	885	38,379	51 ^[b]		C ₁₉ H ₃₆ O ₂	12.5

^[a] Minimum cetane rating for diesel fuel

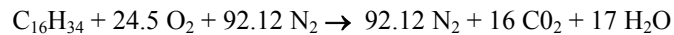
^[b] Cetane rating

Example Problem 2.1

Calculate the *stoichiometric* (chemically correct) air/fuel ratio when diesel fuel is burned with air. Also analyze the products of combustion when No. 2 diesel is burned.

Solution

From Table 2.1, the cetane molecule (C₁₆H₃₄) is used to represent diesel fuel. Under the standard simplifying assumptions, the complete combustion reaction becomes:



The reaction is balanced on the basis of one molecule of fuel. The hydrogen balance determines the amount of water in the combustion products, while the carbon balance determines the amount of CO₂. Then enough O₂ must be supplied to form the CO₂ and H₂O; each mole of O₂ is accompanied by 3.76 moles of N₂. The nitrogen is nearly inert and simply appears in the combustion products. The *stoichiometric air/fuel ratio* is:

$$A/F = (24.5 \times 32 + 92.12 \times 28) / 226 = 14.9$$

Note that 17 moles of water appear in the exhaust for each mole of fuel burned or, on a mass basis, 1.35 kg of water appear per kilogram of fuel burned. The difference between the gross and net heating values of the fuel is exactly equal to the latent energy of the water produced by combustion, i.e., the energy needed to convert that liquid water to vapor. A major reason why quick warm up of engines is important is to cause the combustion water to exit the engine as vapor rather than liquid. If the fuel contains sulphur impurities, the sulphur compounds created in combustion can react with liquid water to form sulfuric acid and corrode the engine.

Engine exhaust gases are normally analyzed on a dry, volume basis. Since the exhaust gases are intermingled at the same temperature and pressure, each molecule occupies the same volume according to Avogadro's Law. Thus, the analysis of the dry exhaust gases in Example Problem 2.1 is:

$$92.12 / (92.12 + 16) = 0.852 \text{ volume fraction (85.2\%)} \text{ is occupied by } N_2,$$

and $16 / (92.12 + 16) = 0.148 \text{ volume fraction (14.8\%)} \text{ is occupied by } CO_2.$

The equivalence ratio, ϕ , is a measure of mixture richness. It is defined as follows:

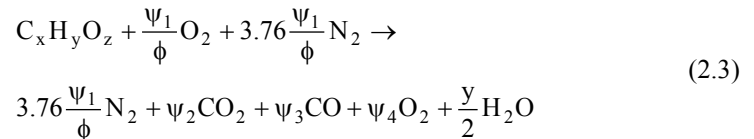
$$\phi = \frac{(F/A)_{\text{actual}}}{(F/A)_{\text{stoichiometric}}} \quad (2.2a)$$

or

$$\phi = \frac{(A/F)_{\text{stoichiometric}}}{(A/F)_{\text{actual}}} \quad (2.2b)$$

Note that the F/A ratio is just the inverse of the A/F ratio. Thus, in Example Problem 2.1, the stoichiometric ratios were $A/F = 14.9$ or $F/A = 0.0671$. An air-fuel mixture is rich if $\phi > 1$, stoichiometric if $\phi = 1$, or lean if $\phi < 1$. A rich mixture contains more fuel than the available oxygen can combust, while a lean mixture contains more oxygen than is theoretically needed to combust all the fuel. When $\phi > 1$, not enough oxygen is available to convert all the carbon in the fuel to CO_2 ; consequently, CO appears in the exhaust. When $\phi < 1$, not all of the oxygen is needed in combustion and free oxygen appears in the exhaust products. For a spark ignition engine, ϕ must be reasonably close to unity to sustain combustion. For a compression ignition engine, ϕ should not exceed 0.7 to prevent engine damage.

The following *generalized combustion reaction* is valid for any air-fuel mixture under the two simplifying assumptions given earlier:



where x = number of carbon atoms in fuel molecule

y = number of hydrogen atoms in fuel molecule

z = number of oxygen atoms in fuel

$$\Psi_1 = x + y/4 - z/2$$

$$\Psi_2 = x \quad \text{for } \phi \leq 1$$

$$x - 2\Psi_1 (1 - 1/\phi) \quad \text{for } \phi > 1$$

$$\Psi_3 = 0 \quad \text{for } \phi \leq 1$$

$$2\Psi_1 (1 - 1/\phi) \quad \text{for } \phi > 1$$

$$\Psi_4 = \Psi_1 (1/\phi - 1) \quad \text{for } \phi < 1$$

$$0 \quad \text{for } \phi \geq 1$$

Note that the Combustion Reaction 2.3 accommodates *oxygenated fuels*, such as the alcohols in Table 2.1. The number of carbon, hydrogen, and oxygen atoms need not be integer numbers. The stoichiometric air/fuel ratio for the combustion is:

$$A / F = \frac{137.3\Psi_1}{\phi(12x + y + 16z)} \quad (2.4)$$

The theoretical concentrations of the *dry* exhaust products on a volume basis are:

$$\text{Conc. N}_2 = 3.76 \Psi_1 / (\phi T) \quad (2.5a)$$

$$\text{Conc. CO}_2 = \Psi_2 / T \quad (2.5b)$$

$$\text{Conc. CO} = \Psi_3 / T \quad (2.5c)$$

$$\text{Conc. O}_2 = \Psi_4 / T \quad (2.5d)$$

where $T = \Psi_2 + \Psi_3 + \Psi_4 + 3.76\Psi_1/\phi$.

Equations 2.5a through 2.5d give good approximations to actual exhaust emissions, except that minute amounts of other gases also appear. A small amount of oxygen and nitrogen react with each other to form oxides of nitrogen, i.e., NO and NO₂. The combined NO and NO₂ gases are commonly referred to as NO_x. Also, ϕ is typically not uniform throughout all of the combustion chambers of an actual engine. Thus, small amounts of CO and O₂ may appear in the exhaust whether the overall ϕ is less than or greater than one. Some free carbon may also appear, as well as trace amounts unburned hydrocarbons (HC), hydrogen, and other gases.

2.2.2 Energy release in combustion

The purpose of the combustion reaction is to release energy to drive the pistons. A cross section of a typical diesel engine is shown in Figure 2.2. The combustion process can be carried out in either two or four strokes of the piston, but the four-stroke cycle is most common. Unless otherwise indicated, all engines discussed in this book will be assumed to use the four-stroke cycle.

Through a combined experimental and analytical technique, it is possible to infer the *rate of energy release* throughout the combustion process. The technique relies on measurement of combustion chamber pressures in a running engine while simultaneously measuring the crankshaft rotation, and computing the volume within the combustion chamber. The spatially averaged temperature in the combustion chamber can be calculated from the pressure and volume. Then, from changes in pressure, volume, and temperature, the heat loss through the chamber walls, work done on the piston, and changes in internal energy of the mixture in the combustion chamber can be calculated. The energy released from the fuel is equal to the sum of the heat loss, work, and increases in internal energy. Figure 2.3 shows a typical energy release diagram for a diesel engine; the rate of energy release is plotted versus crankshaft position.

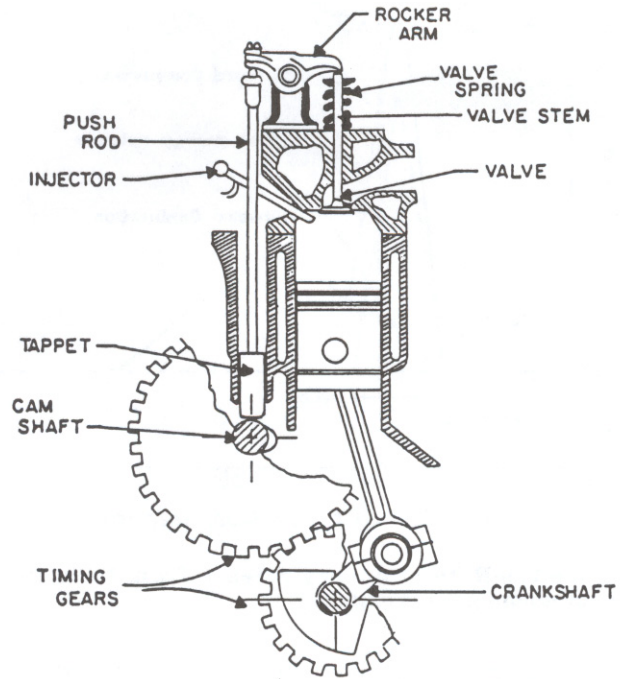


Figure 2.2 – Cross section of a typical diesel engine.

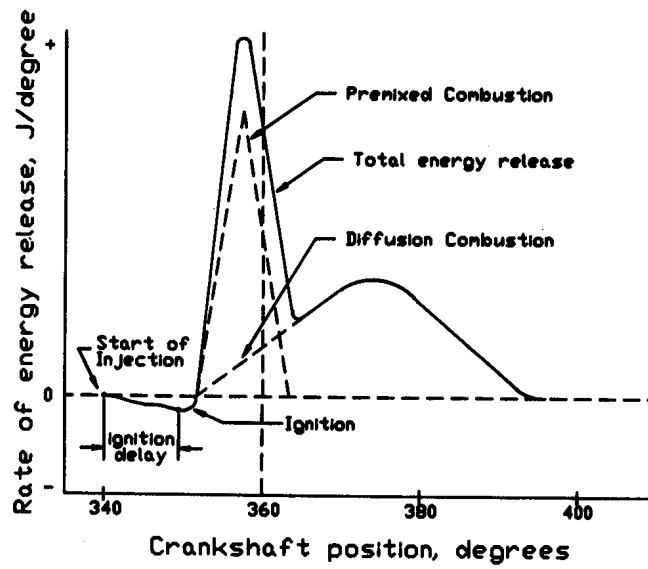


Figure 2.3 – Rate of energy release from fuels in a compression ignition engine.

In a diesel engine, air without fuel is taken in during the intake stroke and compressed. Late in the compression stroke, at approximately 20° before HDC (Head Dead Center), injection of fuel into the combustion chamber begins. An apparent negative energy release rate appears initially as energy is withdrawn from the chamber to evaporate the injected fuel. The evaporated fuel mixes with air and undergoes certain pre-reactions during an ignition delay period. Then ignition occurs and all of the air-fuel mixture prepared during the ignition delay burns suddenly to produce a sharp, triangular-shaped energy release pattern identified as *premixed combustion*. For combustion to continue, fuel vapor and air must diffuse toward each other across the regions burned out in the premixed combustion. The rate of diffusion limits the latter combustion, which is identified as *diffusion combustion*. The total energy release is the sum of the premixed and diffusion combustion. Premixed combustion is efficient and, except for the production of NO_x , is also clean combustion. However, the rapid release of energy produces the greatest stress on the engine and also most of the combustion noise. The slower diffusion burning is quieter and less stressful on the engine, but produces exhaust smoke and most of the CO emissions and is less efficient. Using fuels of higher cetane rating and less-advanced injection timing shifts more of the combustion from the premixed to the diffusion mode; the converse is also true.

In a diesel engine, the air supply is never throttled to control the engine speed. Rather, control is achieved by controlling only the fuel delivery rate. Consequently, ϕ is close to zero when the engine is idling without load and increases as more fuel is injected with increasing load. To limit smoke emissions and avoid excessive engine temperatures, it is necessary to operate a diesel engine with ϕ below approximately 0.7. As Reaction 2.3 and Equation 2.5d would show, considerable free oxygen appears in the exhaust when $\phi = 0.7$ or less. Engine users sometimes increase the fueling rate to diesel engines to take advantage of the extra oxygen and boost the power output of the engine, but at the cost of reduced engine life. For their own protection, engine manufacturers put a seal on the injector pumps of their engines; if the seal is broken to increase the fueling rate, the engine warranty is automatically voided.

2.3 THERMODYNAMIC LIMITS TO ENGINE PERFORMANCE

The effective pressure that can be obtained from fuel to drive the pistons and also the combustion efficiency have thermodynamic limits which are defined in this section. The engine is designed to carry out the combustion cycle in four strokes of the piston. As is required in an engine with a *four-stroke cycle*, the timing gears in Figure 2.2 are arranged such that the crankshaft makes two revolutions for each revolution of the camshaft. Valve timing in a four-stroke cycle is shown on a valve-timing spiral, as illustrated in Figure 2.4. Valve timing is designed to maximize airflow through the engine and may differ somewhat from that shown in Figure 2.4. The cycle begins just before *HDC (Head Dead Center)* with the opening of the intake valve, and the air intake process ends well after *CDC (Crank Dead Center)* with the closing of the intake valve. As the piston approaches HDC on the compression stroke, fuel is injected and, after a short delay, ignites and forces the piston down on the power stroke. The

exhaust process begins with the opening of the intake valve late in the power stroke and ends with the closing of the exhaust valve soon after HDC. Thus, the four strokes of the cycle are intake, compression, power, and exhaust. Note that there is valve overlap, i.e., both valves are open simultaneously during a brief part of the cycle. Alternate terms used in the literature are TDC (Top Dead Center) instead of HDC and BDC (Bottom Dead Center) instead of CDC.

The *dual cycle* of Figure 2.5 is the best thermodynamic model of the modern diesel engine. It illustrates the theoretical variations in combustion gas pressure and cylinder volume during an engine cycle. The dual cycle is a combination of the Otto cycle, which represents spark ignition engines, and the original Diesel cycle that Dr. Rudolph Diesel proposed to represent his engine. Parameter γ defines the relative proportion of energy input to the dual cycle at constant pressure, i.e.:

$$\gamma = \frac{q_p}{q_p + q_v} \quad (2.6)$$

where q_p = energy input at constant pressure
 q_v = energy input at constant volume

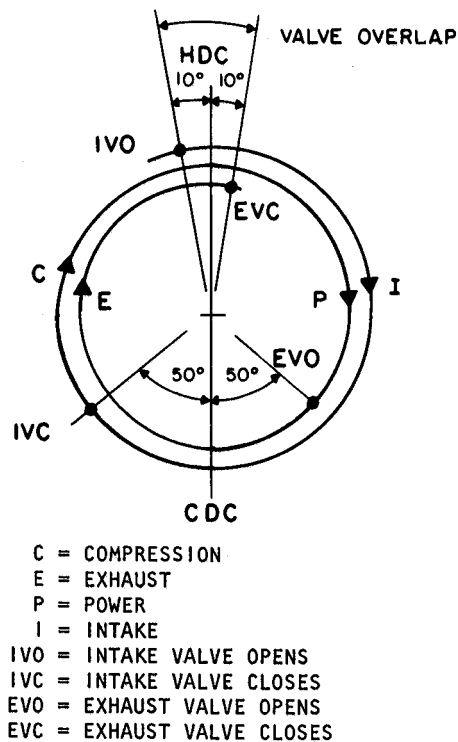


Figure 2.4 – Valve timing spiral showing typical valve timing.

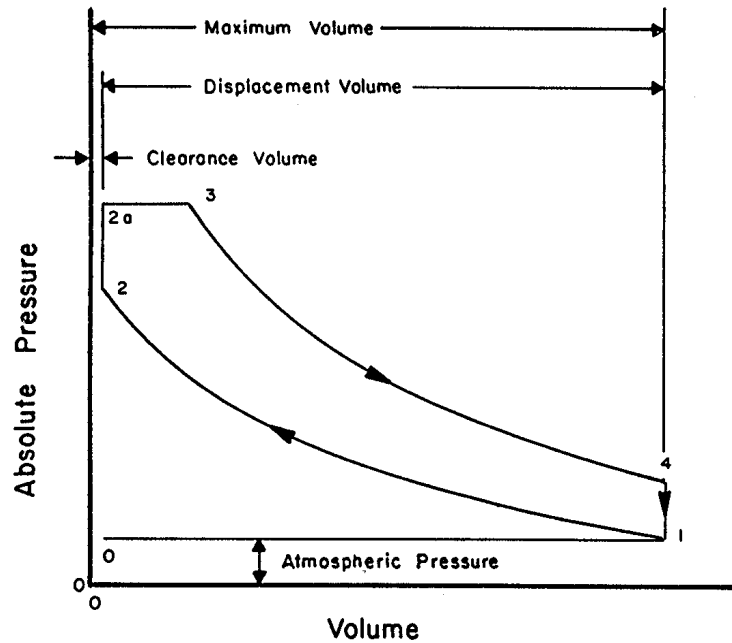


Figure 2.5 – The theoretical dual cycle.

When $\gamma = 0$, the dual cycle becomes the Otto cycle with points 2a and 3 becoming coincident (Figure 2.5). When $\gamma = 1$, the dual cycle becomes the original Diesel cycle with points 2 and 2a becoming coincident.

In the dual cycle, 0-1 is the intake process, followed by compression, 1-2. Process 2-2a is energy input to the cycle at constant volume and 2a-3 is constant-pressure energy input. Work is extracted from the cycle between points 2a and 3, followed by heat rejection, 4-1. Process 1-0 is exhaust, at which point the cycle starts over. The cylinder volume at CDC, V_1 , is the *maximum gas volume*. The cylinder volume at HDC, V_2 , is called the *clearance volume*. The *displacement* of a single cylinder is:

$$V_c = V_1 - V_2 \quad (2.7)$$

The displacement, V_c , of a multi-cylinder engine is simply V_c times the number of cylinders. The compression ratio of the engine is:

$$r = \frac{V_1}{V_2} \quad (2.8)$$

The *cycle mean effective pressure* is the net area within the p-v diagram of Figure 2.5 divided by V_c . Multiplying the cycle mean effective pressure by the piston area and stroke length gives the actual work performed by each power stroke. The cycle mean effective pressure can be calculated from:

$$\frac{p_{cme}}{p_1} = \frac{r - r^k + \Theta_r (r - r^{2-k} r_{co}^{k-1} + r r_{co}^{-1} (k-1)(r_{co} - 1))}{(k-1)(r-1)} \quad (2.9)$$

where p_{cme} = cycle mean effective pressure, kPa

p_1 = absolute pressure at beginning of compression, kPa

$\Theta_r = \Theta_3/\Theta_1$

$\lambda = k(\gamma^{-1} - 1)$

$r_{co} = (\lambda + 1)/(\lambda + (\Theta_3/\Theta_1)r^{k-1})$ = fuel cutoff ratio

$k = 1.4$ for air standard cycle

The pressure, p_1 , is very nearly equal to the atmospheric pressure unless the engine is turbocharged. The fuel cutoff ratio is defined as the proportion of the power stroke during which energy is being released into the cycle from the burning fuel. The *cycle efficiency* is defined as:

$$\eta_{cy} = \frac{q_v + q_p - q_{out}}{q_v + q_p}$$

where each heat transfer quantity is calculated from the mass (M) in the combustion chamber, multiplied by the appropriate specific heat and temperature difference, i.e.:

$$q_v = Mc_v (T_{2a} - T_2)$$

$$q_p = Mc_p (T_{2a} - T_3)$$

$$q_{out} = Mc_v (T_4 - T_1)$$

where c_v = specific heat at constant volume, J/kg °K

c_p = specific heat at constant pressure, J/kg °K

$k = c_p/c_v$

The temperatures are those at the corresponding points in the cycle of Figure 2.5. Note that the mass (M) cancels out in the efficiency equation. Through use of the definition of k , the specific heats also cancel out of the efficiency equation. Then, in a lengthy derivation making use of the ideal gas law, the temperatures can be reduced to volume ratios (r or r_{co}) and the inlet pressure, p_1 . The result is the following equation for cycle efficiency:

$$\eta_{cy} = 1 - \frac{\gamma(r_{co}^k - 1) + k(r_{co} - 1)(1 - \gamma)r^{1-k}}{k(r_{co} - 1)} \quad (2.10)$$

The theoretical values, p_{cme} and η_{cy} , cannot be achieved in practice, but are thermodynamic upper limits and targets against which practical designs can be compared.

Example Problem 2.2

Assume that the compression ratio of a NA (naturally aspirated, i.e., not turbocharged) diesel engine is $r = 14.5$. For typical conditions, estimate the cycle mean effective pressure and the cycle efficiency if $\gamma = 0.2$.

Solution

An estimate is needed for the ratio, Θ_3/Θ_1 . If the ambient temperature is 27°C , then $\Theta_1 = 300^\circ\text{K}$. It is common practice to estimate Θ_3 as being equal to the equilibrium flame temperature for hydrocarbon fuels, i.e., $\Theta_3 = 2700^\circ\text{K}$. Thus, for a NA diesel engine, a good estimate is $\Theta_3/\Theta_1 = 9$. Then, using Equations 2.9, 2.10, and the supplementary equations that support them:

$$\Theta_r = 8.078$$

$$r_{co} = 1.114$$

$$p_{cme}/p_1 = 11.36$$

$$\eta_{cy} = 0.655$$

Theoretically, the specified cycle can convert 65.5% of the input energy to useful work. For a NA diesel engine, p_1 is approximately equal to barometric pressure or, approximately, $p_1 = 100 \text{ kPa}$. Then $p_{cme} = 1136 \text{ kPa}$. Because of friction and other losses, the theoretical efficiency and mean effective pressure cannot be achieved in practice, but it is possible to achieve at least 75% of the theoretical values.

2.4 HEAT LOSSES AND POWER AT THE PISTONS

Energy is liberated from the fuel when Combustion Reaction 2.3 occurs. The released energy causes a sharp rise in cylinder pressure but the pressure diminishes as the piston moves toward CDC. Through proper instrumentation, it is possible to obtain a plot similar to Figure 2.5, except that actual (not theoretical) cylinder pressure is plotted versus volume. Historically, cylinder pressures were plotted on indicator diagrams and thus the net area within the actual p-v diagram, divided by V_c , is called the indicated mean effective pressure, p_{ime} . Multiplying p_{ime} by the top area of the piston gives the average force exerted on the piston during the power stroke. Multiplying force by the stroke length gives the work per stroke and multiplying by the number of strokes per unit time gives the indicated power for a single-cylinder engine. Finally, multiplying by the number of cylinders gives the indicated power for the entire engine. Note, however, that the product of piston area times stroke times number of cylinders gives the engine displacement, V_e . Thus, the *indicated power* (power generated at the head of the pistons) for an engine can be calculated from:

$$P_i = \frac{p_{ime} V_e n_e}{2(60,000)} \quad (2.11)$$

where P_i = indicated power, kW

p_{ime} = indicated mean effective pressure, kPa

V_e = engine displacement, L

n_e = engine speed, rev/min

The factor 2 is in the denominator of Equation 2.11 because 2 revolutions of the crankshaft are required for each power stroke in a four-stroke cycle engine. The factor 60,000 is simply a units constant. Equation 2.11 brings out the important point that only three ways are available to increase engine power. They are (1) increase the size (V_e) of the engine, (2) increase its speed (n_e), or (3) increase the pressure levels (p_{ime}) in the engine.

The indicated power is always less than the fuel equivalent power. The *indicated thermal efficiency* of an engine is defined as:

$$\eta_{it} = \frac{P_i}{P_{fe}} \quad (2.12)$$

The fraction $(1 - \eta_{it})$ of P_{fe} is not converted into work but is rejected as heat (Figure 2.1). Some of the rejected heat can be recovered using heat exchangers if there is a need for heat in the vicinity of the engine; otherwise the heat is lost. The cycle efficiency, η_{cy} , is an upper limit for η_{it} and a target against which achieved values of η_{it} can be compared.

2.5 MECHANICAL LOSSES AND POWER AT THE FLYWHEEL

After combustion and mechanical losses are subtracted, the remaining power reaching the flywheel is called *flywheel power*. The earliest devices used to measure engine power were called prony brakes, and thus flywheel power is more commonly called *brake power*. With modern technology, a device called a dynamometer is used to measure the torque and speed of the power shaft connected to the engine flywheel. If T_b is the torque in a shaft, the work accomplished per revolution of the shaft is equal to $2\pi T_b$. Then, since the engine speed gives the revolutions per unit of time, the brake power can be calculated from the following equation:

$$P_b = \frac{2\pi T_b n_e}{60,000} \quad (2.13)$$

where P_b = brake power, kW

T_b = engine brake torque, N·m

The factor 60,000 is a units conversion factor.

The *mechanical efficiency*, η_m , is the fraction of P_i that is converted to brake power (Figure 2.1), i.e.:

$$\eta_m = \frac{P_b}{P_i} \quad (2.14)$$

By definition, all of the indicated power not converted to brake power is called *friction power*, i.e.:

$$P_f = P_i - P_b \quad (2.15)$$

What is included in friction power? All the friction of moving parts in the engine is included, as the name implies, but power to operate the fan, oil pump, alternator, and other engine accessories is also included.

Engine users are interested in the overall efficiency of the engine in converting fuel equivalent power to brake power. The overall efficiency is called the *brake thermal efficiency*, i.e.:

$$\eta_{bt} = \frac{P_b}{P_{fe}} \quad (2.16a)$$

It is easy to show that the following equation is true:

$$\eta_{bt} = \eta_{it} \eta_m \quad (2.16b)$$

Thus, for good overall efficiency, engine designers must design an efficient combustion process (high η_{it}) and a high percentage of the resulting power must be transmitted to the flywheel (high η_m).

Equation 2.11 shows that, for a given engine running at a given speed, P_i is proportional to p_{ime} . Engine designers have broadened that concept in defining *brake mean effective pressure*, p_{bme} , as:

$$p_{bme} = \frac{2(60,000)P_b}{V_e n_e} \quad (2.17)$$

and in defining friction mean effective pressure, p_{fme} , as:

$$p_{fme} = \frac{2(60,000)P_f}{V_e n_e} \quad (2.18)$$

In a diesel engine, p_{fme} is almost entirely a function of speed, i.e.:

$$p_{fme} = C_0 + C_1 n_e + C_2 n_e^2 \quad (2.19)$$

where C_0 , C_1 and C_2 are constants that vary from engine to engine. The following approximate values were presented by SAE for the purpose of estimating the mechanical efficiency of a diesel engine:

$$C_0 = 139.3 \text{ kPa}$$

$$C_1 = -0.0259 \text{ kPa} \cdot \text{min/rev}$$

$$C_2 = 22.97 \times 10^{-6} \text{ kPa}/(\text{rev/min})^2$$

More accurate values can be obtained for a specific engine by fitting a curve to friction mean effective pressure values at various engine speeds. An important practical

consequence of Equation 2.19 is that engine friction power can be reduced and engine efficiency can be increased by running engines at reduced speeds.

The reader is encouraged to derive a relationship between the several mean effective pressures and to express η_m in terms of mean effective pressures.

2.6 ENGINE TORQUE AND EFFICIENT ENGINE LOADING

Combining Equations 2.12, 2.13, 2.15, and 2.19 provides an equation which gives insights into how an engine produces torque, i.e.:

$$T_b = \frac{H_g \eta_{it}}{4\pi} \left[\frac{C_f \dot{m}_f}{n_e} \right] - \frac{V_e}{4\pi} p_{fme} \quad (2.20)$$

where $C_f = 2(1000/60) =$ units conversion factor

$(C_f \dot{m}_f / n_e) =$ grams of fuel injected per engine cycle

In Equation 2.20, the term between the equal sign and the minus sign is called indicated torque, while the last term in the equation is *friction torque*. Thus, the net or brake torque is the indicated torque minus the friction torque. Since H_g (the heating value of the fuel) is constant and η_{it} varies only a little with changes in torque and speed, the indicated torque varies nearly proportionally with the quantity of fuel injected into each engine cycle. As explained in Section 2.2.7, the quantity of fuel injected into each cycle is controlled by an *engine governor*.

Combining Equations 2.14, 2.15 and 2.16a gives the following alternate equation for brake thermal efficiency:

$$\eta_{bt} = \eta_{it} P_b / (P_b + P_f) \quad (2.16c)$$

Figure 2.6 is a plot of Equation 2.16c and illustrates the relationship of engine efficiency to load. All engines are most efficient at full load and are especially inefficient as the engine load approaches zero.

Engine designers have developed the term *SFC (Specific Fuel Consumption)* to indicate how much fuel is burned by an engine to accomplish a given amount of work. It is defined as:

$$SFC = \frac{\dot{m}_f}{\text{power}} \quad (2.21)$$

Because of losses in the transmission of power, it is important to use an adjective with SFC to indicate the point of power measurement. The two most common SFC terms in the literature are BSFC (for Brake SFC, i.e., when the denominator of Equation 2.21 is brake power) and ISFC (for Indicated SFC). Like η_{bt} , BSFC is an indicator of overall engine efficiency, except that BSFC is lowest when the engine is most efficient.

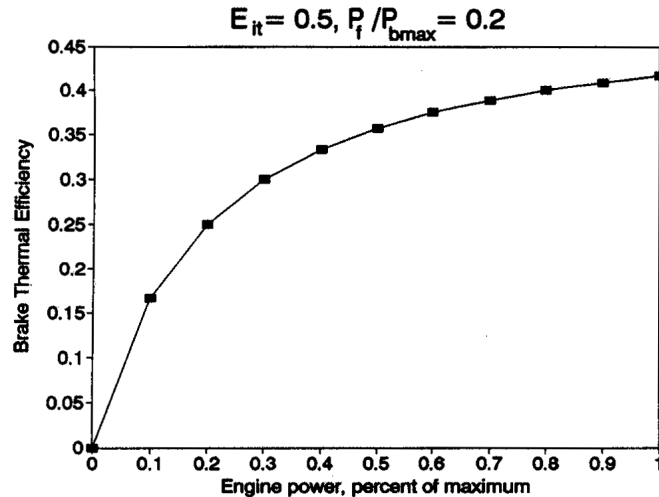


Figure 2.6 – Variation of brake thermal efficiency with engine load.

2.7 CONTROL OF ENGINE SPEED

It is desirable to perform many agricultural operations at nearly constant speed. Governors control speed by reducing fuel delivery to the engine when the speed is too high and increasing fuel delivery when the speed is too low. A *flyweight governor* is illustrated in Figure 2.7. The flyweights are hinge-connected to the governor shaft, which typically rotates at one-half of crankshaft speed. In the unit shown in Figure 2.7a, centrifugal force from increasing engine speed causes the weights to swing outward and the flyweight linkage forces the thrust bearing downward. The governor linkage rotates counterclockwise, stretching the spring and reducing fuel delivery. Conversely, reductions in engine speed allow the spring to contract, forcing the flyweights inward and increasing fuel delivery.

The force induced on the thrust bearing by centrifugal force on the flyweights varies proportionally with the radius of the path of the flyweights and with the square of the engine speed. Figure 2.7b shows curves for the limiting cases when the path radius is smallest (weights in) and largest (weights out). The governor can only operate between these two limiting curves.

If an ungoverned engine was receiving fuel at even a moderate rate and was running without load, the speed would quickly become excessive and destroy the engine. In a governed engine, however, the flyweights would swing out to their limit and fuel delivery would fall to a level sufficient to provide only the friction power of the engine. The engine would operate at point A on Figures 2.7b and 2.7c, which is called the *High Idle point* because the speed is high and the engine is idling (not doing any work). As an increasing torque load is applied to the engine, the flyweights move

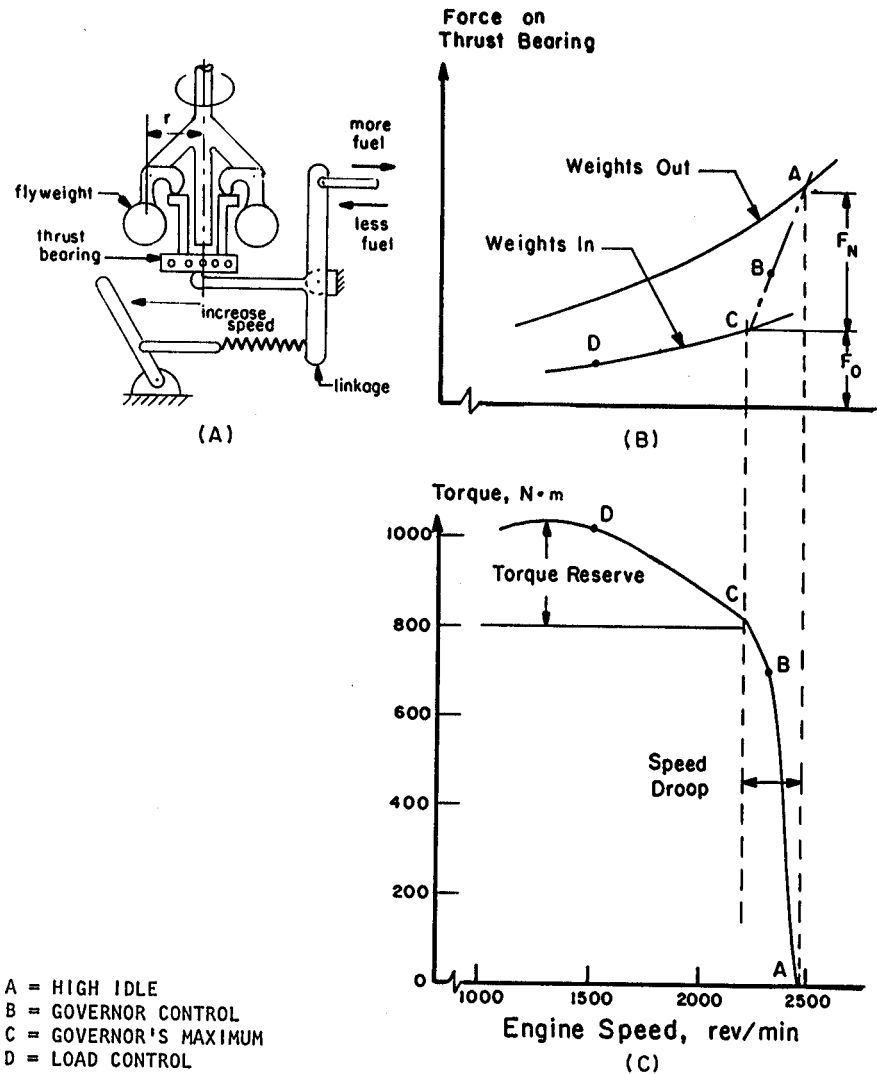


Figure 2.7 – Action of an engine governor.

inward to increase the stroke of the fuel injector pump and supply the fuel needed to provide that torque (see Equation 2.20). At point C in Figure 2.7, the flyweights are at their innermost position and cannot move the governor linkage or increase the injector pump stroke any further; thus Point C is called *Governor's Maximum*. With further increases in torque, the speed begins to fall rapidly because the governor cannot increase the fuel delivery per cycle. At points to the left of point C in Figure 2.7c, speed is controlled only by the torque load on the engine. Thus, the engine is under

governor control at points between A and C and under load control at points to the left of point C. Torque increases are possible in the *load-controlled range* because friction torque declines with speed (see Equation 2.20) and because injector pumps gain somewhat in pumping efficiency as speed decreases.

Governors cannot maintain perfectly uniform speed, even in the governor-controlled range. The *governor regulation*, as calculated in Equation 2.22, is a measure of how closely the governor controls the engine speed.

$$\text{Reg}_g = \frac{200(n_{\text{HI}} - n_{\text{GM}})}{(n_{\text{HI}} + n_{\text{GM}})} \quad (2.22)$$

where Reg_g = governor regulation, %

n_{HI} = engine speed at high idle, rev/min

n_{GM} = engine speed at governor's maximum, rev/min.

The curves in Figures 2.7b and 2.7c show the governor controlling the engine at one speed setting. By moving the hand lever to the right, the operator can decrease the initial tension in the governor spring and thereby decrease the speed required to move the flyweights outward. The effect is to move curve ABC to the left, where it meets the load-control curve at some higher value of torque (see Figure 2.8a). Conversely, if the linkage stop will permit it, the operator can increase the speed setting of the engine by moving the speed control lever to the left. Manufacturers typically rate their engines at the governor's maximum speed that corresponds to the fastest setting of the governor. In Figure 2.8, for example, the highest governor's maximum speed is at 2200 rev/min and that would be the rated speed of the engine.

As shown in Figure 2.7c, *torque reserve* is defined as the difference between the peak torque of the engine and the torque at *rated speed*. Large torque reserve is desirable to prevent the engine from stalling during momentary overloads. Torque reserve is expressed as a percentage of rated torque. In Figure 2.7c, for example, the peak torque is 1020 N·m and the rated torque is 820 N·m, so the torque reserve would be 24.4%. It is also desirable for the torque peak to be well to the left of governor's maximum. In Figure 2.7c, the torque peak is at 1300 rev/min while rated speed is 2200 rev/min. Therefore, the torque peak appears at 59% of rated speed.

Figure 2.8b shows a power versus speed curve that results from the torque versus speed curve of Figure 2.8a. From Equation 2.13, the power rises nearly linearly with torque in the governor-controlled range because the speed varies little. Torque varies only modestly in the load-controlled range, so power falls in nearly direct proportion to the fall in speed. Some engine manufacturers market "constant power" engines; these are engines with sufficient torque rise to offset the falling speed in the load-controlled range, so that the power doesn't begin to fall until operation has moved some distance into the load-controlled range.

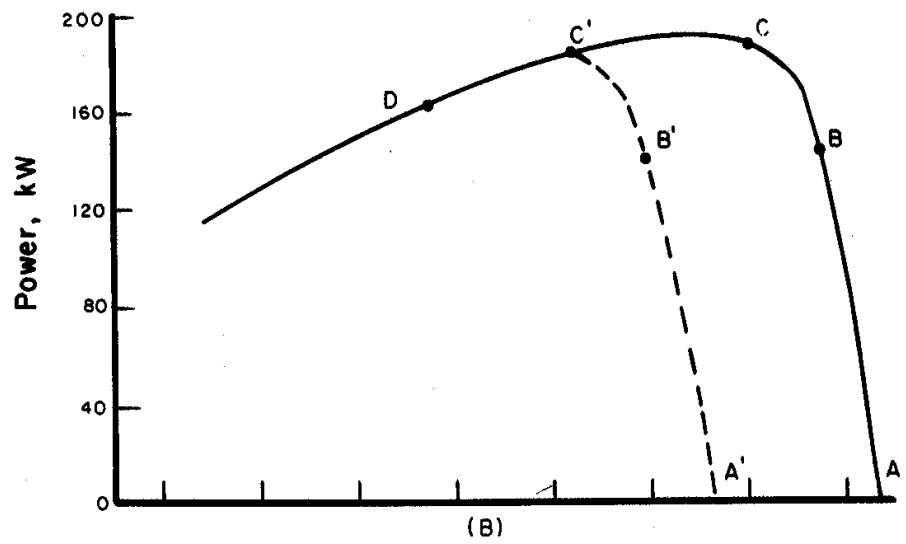
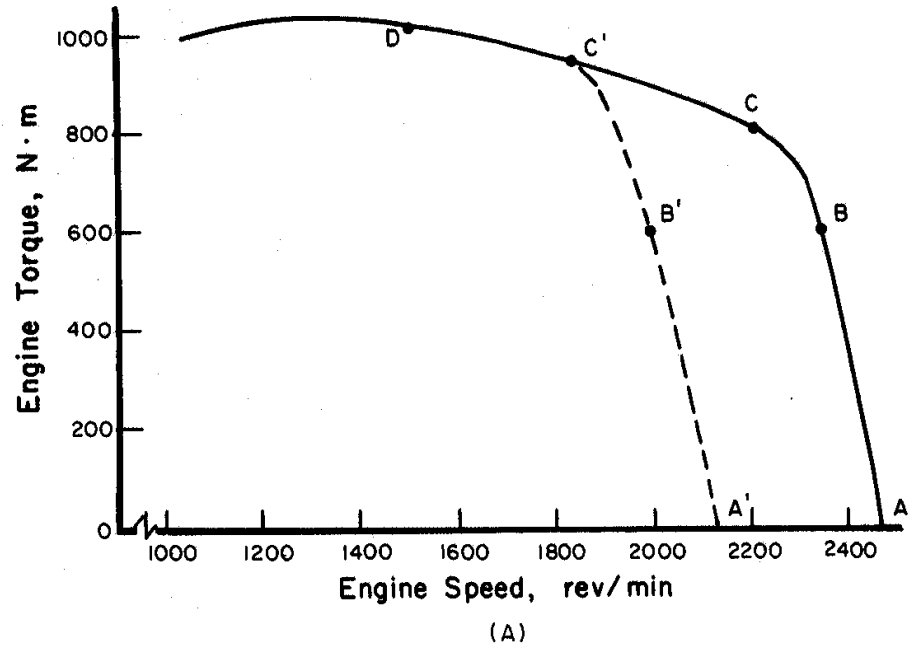


Figure 2.8 – Torque-speed and power-speed curves for a governed engine.

2.8 ENGINE PERFORMANCE SIMULATOR

A computer-based engine simulator (in the CD included with this book) was developed by the authors to allow the user to explore the operation of a compression-ignition engine. The simulator incorporates the same controls that would be found when performing a dynamometer test on an engine. The simulator user input data to specify the engine operating limits. Given these limits, the simulator computes operating variables under user-specified speed and load settings using equations from this chapter.

The simulator includes two screens. The first, Figure 2.9, is used to define the operating properties of an engine and the fuel. The second, Figure 2.10, is the engine control/display console. The model assumes that governor control is along a straight line between the high idle and governor's maximum points, while load control is on another straight line between the governor's maximum and peak torque points. The first five inputs in the specifications page fix the high idle, governor's maximum, and peak torque points on the engine map. The simulated torque is set by the position of the engine load slider on the console (Figure 2.10), and engine speed is calculated to maintain operation on the torque-speed lines described above. The remaining engine

Engine Specifications

Engine High Idle (r/min): 2500.....

Governor Regulation(%): 8.3.....

Torque at Rated Speed(Nm): 630.....

Engine Speed at Peak Torque (r/min): 1200.....

Torque Rise(% of Rated Speed): 20.....

Engine Displacement (L): 7.6.....

Volumetric Efficiency-NA(%): 90.....

Turbocharged (Y/N): Y.....

Fuel Specifications

Gross Heating Value of Fuel (kJ/kg): 45000.....

Carbon: 16.....

Hydrogen: 34.....

Oxygen: 0.....

[Go to Engine Panel](#)

Figure 2.9 – Engine and fuel specifications panel.

specifications are the engine displacement, volumetric efficiency under naturally aspirated (NA) conditions, and whether the engine is fitted with a turbocharger or not. The volumetric efficiency is used with the engine displacement and speed to calculate the air consumption at each simulated point selected by the user. Also at each point, the program calculates the brake power and estimates the brake thermal efficiency, then uses these data and the heating value of the fuel to calculate the fuel consumption needed to produce the brake power. Values of engine speed, torque, power and fuel consumption are displayed on the lower left quadrant of the control panel (Figure 2.10).

The volumetric efficiency of a naturally-aspirated engine is held at 85%. For a turbocharged engine, the volumetric efficiency is assumed to be 85% until load is applied to the engine. At each simulated engine load, the program estimates the turbocharger boost, then uses pressure and temperature ratios to estimate the volumetric efficiency. The program uses the calculated airflow and fuel consumption to calculate the fuel-air ratio of the combustion and the equivalence ratio.

The engine control and display console (Figure 2.10) allows the user to interact directly with the engine to observe its responses on an instantaneous basis. The display console has four quadrants. The top quadrants have user controls. Sliders allow adjustment of the governor setting and the engine load. Engine operating states are reported. Lights indicate when the engine is operating under governor control or load

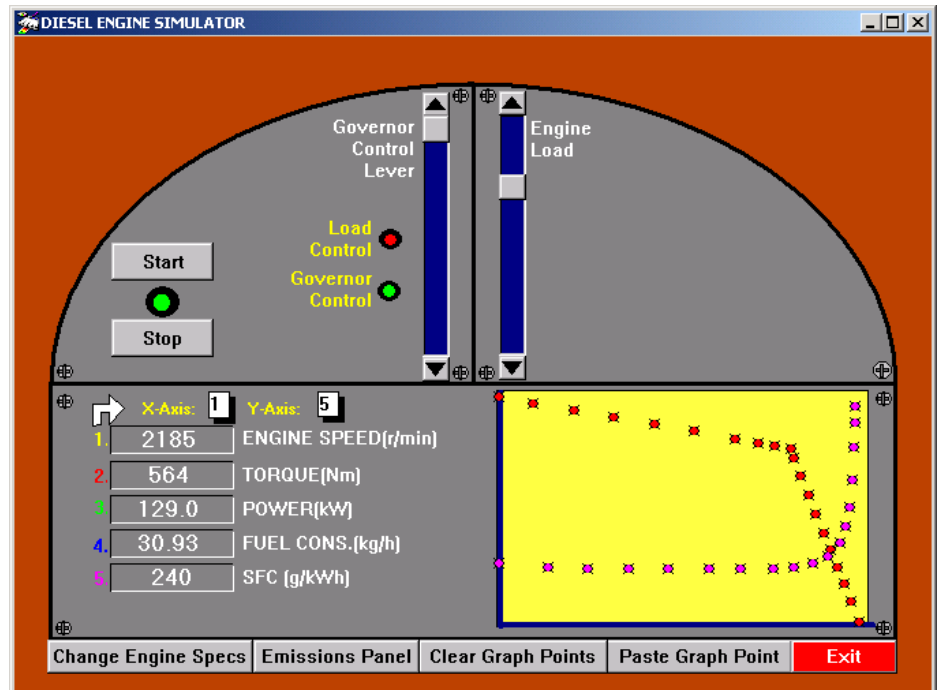


Figure 2.10 – Engine control and display console.

control and whether the engine is turbocharged. Clicking on the start button “starts” the engine and the red light below this button changes to green. Then the user adjusts the two sliders to control the governor setting and load. If the engine reaches stall, for instance when the engine is overloaded, a stall message appears and it is necessary to restart the engine. An emissions panel is displayed in the top right quadrant when activated by a button at the bottom of the console.

The bottom left quadrant of the simulator reports the current speed, torque, power, fuel consumption, and specific fuel consumption (SFC). The operator can also select these variables as axes for the graphical portion of the simulator in the lower right quadrant. The graphical window allows the user to visualize the operating characteristics of the simulator as load or the governor control sliders are adjusted. The current state of the engine is represented as a red dot. Buttons at the bottom of the console are used to paste points onto the graph and also to clear them. The different variables are color-coded so that they can be identified on the graph. As the governor setting or engine load are changed, the point on the graph moves.

As with any simulation, the user to must provide realistic inputs. For example, specifying a rated torque that is too high for the specified engine displacement and high idle speed will result in a too-rich fuel-air mixture (as indicated by the equivalence ratio) when the engine is fully loaded. As discussed earlier, the equivalence ratio of a compression-ignition engine should not go much above 0.7 to avoid engine overheating and damage.

2.9 TURBOCHARGING AND INTERCOOLING ENGINES

Power generation in an engine increases in proportion to the fueling rate, as indicated by Equation 2.1. To keep the equivalence ratio below 0.7, the air delivery rate must be much larger than the fuel delivery rate; thus it is air handling capacity that truly limits the power producing capacity of an engine. The *air handling capacity* can be calculated using the following equation:

$$\dot{m}_a = C_a V_e n_e \rho_a \eta_v \quad (2.23)$$

where \dot{m}_a = air handling capacity, kg/hr

$C_a = 0.03$ = constant to convert units

V_e = engine displacement, L

n_e = engine speed, rev/min

ρ_a = density of the air entering the engine, kg/m³

η_v = *air delivery ratio* of the engine, a decimal

The air delivery ratio, or *volumetric efficiency* as it is sometimes called, is a measure of the air-pumping efficiency of an engine. It is equal to the ratio of the actual air handling capacity divided by the theoretical capacity that could be obtained at the same engine speed if each cylinder filled entirely with atmospheric air during each intake stroke. If the engine has no turbocharger, pressure drops in the intake system cause the air delivery ratio to be less than one. Conversely, a turbocharger delivers

pressurized air for intake and the air delivery ratio can be greater than one. The following equation, which was derived from the *ideal gas law*, can be used to calculate ρ_a if the barometric pressure and the ambient temperature are known:

$$\rho_a = \frac{29p_a}{8.314\Theta_a} \quad (2.24)$$

where p_a = air pressure, i.e., barometric pressure, kPa

Θ_a = ambient air temperature, °K

Under most atmospheric conditions, ρ_a will be between 1.1 and 1.2 kg/m³.

The air delivery ratio of a typical *naturally-aspirated (NA)* diesel engine is approximately 0.85; the air-handling capacity of a NA diesel engine can only be increased by increasing the displacement or the engine speed. However, the air delivery ratio and air handling capacity can be greatly increased by adding a turbocharger to the engine.

2.9.1 Operation of turbochargers

A *turbocharger* consists of a *compressor* directly coupled to an exhaust-driven *turbine* as illustrated conceptually in Figure 2.11. Ambient air enters the compressor at point 1 and is compressed before entering the intake manifold at point 2. Hot exhaust gases in the exhaust manifold at point 3 drive the turbine before exiting at point 4. Thus, the turbocharger uses energy extracted from the engine exhaust to pressurize the air entering the combustion chamber. The *boost* is the increase in pressure provided by the compressor, i.e.:

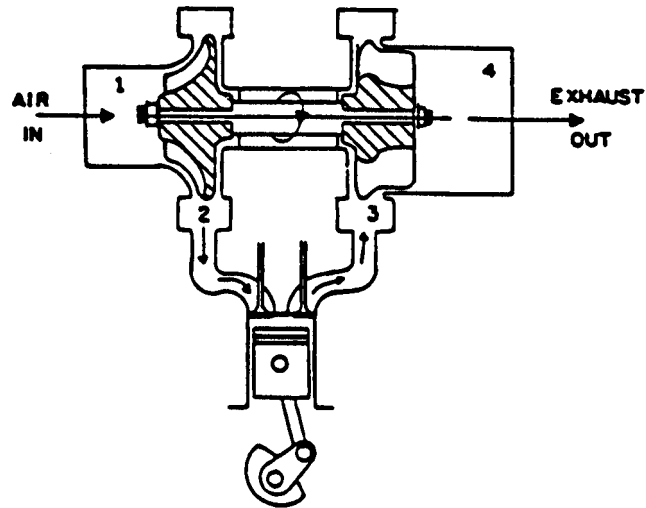


Figure 2.11 – The concept of a turbocharger.

$$\text{boost} = p_2 - p_1 \quad (2.25)$$

where p_1 and p_2 are the absolute pressures at points 1 and 2, respectively. The pressure ratio across the compressor, p_{rc} , is also important and is defined as:

$$p_{rc} = \frac{p_2}{p_1} \quad (2.26)$$

The temperature ratio across the compressor, Θ_{rc} , can be calculated from the following equation:

$$\Theta_{rc} = 1 + \frac{p_{rc}^{0.286} - 1}{\eta_c} \quad (2.27)$$

where η_c = compressor efficiency.

A turbocharger is ineffective when the engine is idling. The turbocharger becomes increasingly effective as load is put on the engine, because the fraction $(1-\eta_{it})$ of the increased fuel supplied is available to drive the turbine; the turbocharger reaches maximum effectiveness near governor's maximum. When the engine is well loaded, the air delivery ratio of the engine can be estimated with acceptable accuracy using the following equation:

$$\eta_v = p_{rc} / \Theta_{rc} \quad (2.28a)$$

Equation 2.28a fails when the engine is idling, but then η_v is close to 0.85. Example Problem 2.3 illustrates the use of Equations 2.23 through 2.28a.

Example Problem 2.3

A turbocharger is to be fitted to a 6.5 liter engine. A boost pressure of 110 kPa is desired when the engine is running under full load at 2200 rev/min. The map of the turbocharger compressor is shown in Figure 2.12. Ambient conditions are 27°C and 100 kPa. Determine the compressor (a) airflow, (b) efficiency, and (c) speed.

Solution

From Equation 2.24, the ambient air density is:

$$\rho_a = 29 \times 100 / (8.314 \times 273 + 27) = 1.16 \text{ kg/m}^3$$

From Equations 2.25 and 2.26, the desired pressure ratio across the compressor is:

$$p_{rc} = (p_1 + \text{boost}) / p_1 = (100 + 110) / 100 = 2.1$$

The remainder of the problem must be solved by iteration, because the compressor efficiency, engine volumetric efficiency, and engine airflow are all unknown and

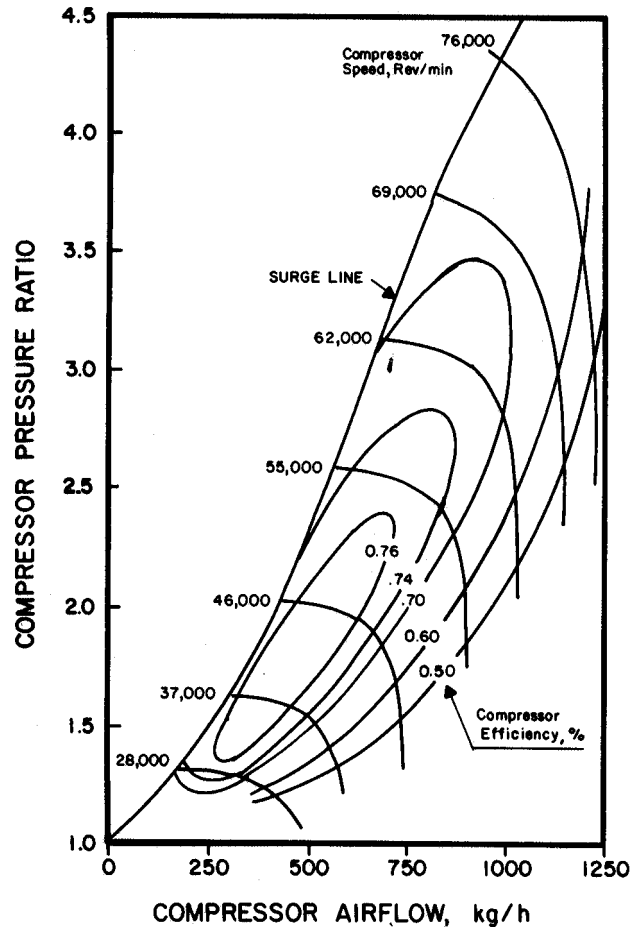


Figure 2.12 – A turbocharger compressor map.

interdependent. Begin by assuming a compressor efficiency of 70%. Then, from Equation 2.27, the initial estimate of the temperature ratio is:

$$\Theta_{rc} = 1 + (2.1^{0.286} - 1)/0.7 = 1.338$$

The estimated volumetric efficiency is, from Equation 2.28a:

$$\eta_v = 2.1/1.338 = 1.57$$

Finally, from Equation 2.23, the initial estimate of airflow into the engine is:

$$\dot{m}_a = 0.03 \times 6.5 \times 2200 \times 1.16 \times 1.57 = 781 \text{ kg/h}$$

Now we can check on the accuracy of the initial choice of compressor efficiency. From Figure 2.12, when the pressure ratio is 2.1 and the airflow is 781 kg/h, the

corresponding compressor efficiency is 72%. Using the new value for compressor efficiency, the new estimate of temperature ratio is 1.328, the new volumetric efficiency is 1.58, and the new airflow is 787 kg/h. From Figure 2.12, the compressor efficiency corresponding to pressure ratio of 2.1 and airflow of 787 kg/h is very close to 72%, so no further iteration is needed. Thus (a) the airflow into the turbocharged engine would be 787 kg/h, (b) the compressor efficiency would be 72%, and (c), interpolating between the adjacent speed curves on Figure 2.12, the compressor speed would be approximately 51,000 rev/min. It should be noted that pressure ratio-airflow combinations to the left of the surge curve in Figure 2.12 produce unstable, surging airflow and are therefore unacceptable. The solution to Example Problem 2.3 is to the right of the surge curve and is therefore acceptable.

Selection of the compressor operating point does not complete the problem of fitting a turbocharger to an engine; it is also necessary to select a compatible operating point for the turbine. The turbine must rotate at the same speed as the compressor while supplying the power necessary to drive the compressor. In addition, the flow rate through the compressor is $\dot{m}_a(1+FA)$, where FA is the fuel-air ratio of the turbocharged engine, that is, the mass airflow rate divided by the mass fuel flow rate. A turbine map (not shown in this book) is used to insure that the values selected for turbine flow rate, pressure ratio, speed, and efficiency are mutually compatible.

2.9.2 Intercoolers

Equation 2.27 can be used to show that the temperature of the air leaving the compressor can be very hot, i.e., well above the boiling point of water. An *intercooler* (sometimes called an *aftercooler*) may be used to reduce the temperature of the compressed air. An intercooler is a heat exchanger through which the compressed air is passed in giving up heat energy to a secondary fluid. The engine coolant is the most common secondary fluid used, but ambient air is used in some intercoolers. Intercooling is a constant-pressure process. When an intercooler is used, the volumetric efficiency of the turbocharged, intercooled engine can be estimated using the following equation:

$$\eta_v = \frac{p_{rc}}{\Theta_{rc}} \frac{\Theta_2}{\Theta_{2i}} \quad (2.28b)$$

where Θ_2 = temperature of air leaving compressor, °K

Θ_{2i} = temperature of air leaving intercooler, °K

2.9.3 Turbocharging and intercooling for versatility

In recent years, engine manufacturers have used turbocharging and intercooling to reduce the costs of manufacturing a *family of engines* and of maintaining an inventory of replacement parts for the engines. The procedure is illustrated in Example Problem 2.4.

Example Problem 2.4

An engine manufacturer wants to provide four engine models from one basic design of a 6-cylinder, 7.636 L, diesel engine that is to run at a rated speed of 2200 rev/min. The desired power levels of the four engines are to increase in approximately 15 kW increments from a base level of 75 kW for the NA version of the engine. How might turbocharging and intercooling be used to accomplish the objective? The intercooler is to use the engine coolant as the secondary fluid, and the thermostat provides a coolant temperature of 90°C. Tests have shown that the NA engine can achieve BSFC of 0.3 kg/kWh.

Solution

The assumed atmospheric conditions will be 300°K and 100 kPa. Thus, from Equation 2.24, the ambient air density is:

$$\rho_a = (29 / 8.314) (100 / 300) = 1.16 \text{ kg/m}^3$$

Assuming $\eta_v = 0.85$ for the base, NA engine, Equation 2.23 gives the air consumption as:

$$\dot{m}_a = 0.03 \times 7.636 \times 2200 \times 1.16 \times 0.85 = 497 \text{ kg/h}$$

The fuel consumption of the 75 kW, NA engine would be:

$$\dot{m}_f = P_b \times \text{BSFC} = 75 \times 0.3 = 22.5 \text{ kg/h}$$

The stoichiometric air-fuel ratio for diesel fuel is 14.9 (see Example Problem 2.1) and the actual air-fuel ratio is $497/22.5 = 22.1$. Thus, from Equation 2.2b, ϕ for the NA engine is:

$$\phi = 14.9 / 22.1 = 0.674$$

This ϕ is well below the recommended maximum of 0.7 discussed in Section 2.2.2. For the 120 kW engine, assume that a turbocharger is added to provide a boost of 90 kPa. Then, from Equations 2.25 and 2.26, $p_{rc} = 1.9$. A reasonable value for compressor efficiency is $\eta_c = 0.7$ and, from Equation 2.27:

$$\Theta_{rc} = \Theta_2 / \Theta_1 = 1 + (1.9^{0.286} - 1) / 0.7 = 1.288$$

Since $\Theta_1 = 300^\circ\text{K}$ (27°C), note that the temperature of the air leaving the compressor would be $1.288 \times 300 = 386^\circ\text{K}$ (113°C), which is very hot. Thus an intercooler will be added; it can reduce the air temperature to within approximately 10°C of the coolant temperature, i.e., to 100°C (373°K). From Equation 2.28b, the estimated volumetric efficiency of the 120 kW, turbocharged, intercooled (TC, IC) engine would be:

$$\eta_v = (1.9 / 1.288) (386 / 373) = 1.53$$

Then, using the new value for η_v in Equation 2.23, the air consumption of the TC, IC engine would be 895 kg/h. Assuming the BSFC remained at 0.3 kg/kW h, the approximate fuel delivery rate would be:

$$\dot{m}_f = P_b \times \text{BSFC} = 120 \times 0.3 = 36 \text{ kg/h}$$

After the engine was constructed, the actual fueling rate could be adjusted to produce exactly the 120 kW of brake power desired. The ϕ corresponding to the 36 kg/h fueling rate would be:

$$\phi = 14.9 / (895 / 36) = 0.60$$

The proposed increase in fueling rate, from 22.5 kg/h for the 75 kW, NA version to 36 kg/hr for the 120 kW, TC, IC engine, would be acceptable since ϕ would remain below 0.7.

The intermediate sized engines (90 and 105 kW) could be achieved by using appropriate fueling rates; the rates would be approximately $90 \times 0.3 = 27$ kg/h and $105 \times 0.3 = 31.5$ kg/h for the 90 and 105 kW engines, respectively. These fueling rates, being less than the 36 kg/h used for the 120 kW engine, would reduce the turbocharger boost below 90 kPa and the temperature of the air leaving the compressor (Θ_2) would fall below the 113°C calculated for the TC, IC engine. If Θ_2 fell close to 100°C or below, not enough temperature differential above the coolant temperature would exist to permit cooling of the air. Thus, intercooling would probably be impractical except for the 120 kW engine.

In summary, a family of four engines ranging from 75 to 120 kW in power could be obtained from one basic engine. The family would include a 75 kW NA engine, 90 and 105 kW TC engines, and a 120 kW TC, IC engine. The advantage would be that all four engines would share a common inventory of parts except that a larger injector pump and fuel injectors might have to be used on the largest engines. The three smaller engines would be over-designed, since they would have to have the same strength as the 120 kW engine. That disadvantage would be more than offset by the greatly reduced parts inventory that was achieved, and thus engine manufacturers have adopted the strategy of Example Problem 2.4.

PROBLEMS

- 2.1 A 5-liter engine with a 15:1 compression ratio consumed 11.5 liters of fuel in 30 minutes. The heating value of the fuel was 45,400 kJ/kg and the fuel density was 0.835 kg/liter. The engine is operating with a brake thermal efficiency of 18% and is running at 2400 rpm. Calculate (a) the fuel equivalent power, (b) the brake power, and (c) the brake torque.
- 2.2 An engine was tested on a dynamometer and produced 450 N·m of torque at a speed of 2400 rpm. (a) Calculate the power output. (b) If the engine reaches a peak of 22% torque rise at 1900 rpm, what is the maximum torque the engine

will produce? (c) Sketch curves for torque and power versus speed, to scale, and label all known points. Low and high idle for the engine are 800 and 2700 rpm, respectively.

- 2.3 (a) Determine the concentrations of N_2 , CO , CO_2 , and O_2 in the exhaust on a dry, volume basis when butane is combusted in air. Let ϕ vary from 0 to 1.5 in increments of 0.1 and plot the concentrations of the exhaust constituents versus ϕ . Note that use of a computer spreadsheet will greatly simplify the calculations. Repeat part (a) except with (b) propane, (c) regular gasoline, (d) methanol (methyl alcohol), (e) ethanol (ethyl alcohol), and (f) butanol (butyl alcohol) as fuel. (g) Repeat part (a) except use No. 1 diesel as the fuel, and mark the typical range of ϕ values for diesel engines on the graph. (h) Repeat part (g) except use No. 2 diesel as the fuel.
- 2.4 Let the maximum instantaneous pressure in the dual cycle be p_{peak} . It can be shown that:

$$p_{peak}/p_1 = (r/r_{co}) (\Theta_3/\Theta_1)$$

Given a dual cycle with $\Theta_3/\Theta_1 = 9$, and compression ratios ranging from 14 to 30, plot p_{cme}/p_1 and p_{peak}/p_1 , both versus compression ratio. Show curves for γ values of 0.1 and 0.2. Considering that engine stress increases with p_{peak} while cycle work increases with p_{cme} , what conclusions can you draw from your plots concerning desirable values for r and γ ?

- 2.5 Given a dual cycle with $\Theta_3/\Theta_1 = 9$, and compression ratios ranging from 14 to 30, plot η_{cy} versus compression ratio. Include curves for $\gamma = 0.1$ and 0.2. Which is more influential on increasing η_{cy} , increasing r or reducing γ ?
- 2.6 A 6-cylinder, turbocharged diesel engine has a displacement of 8.268 liters and a compression ratio of 17.3:1. While running at 2200 rev/min engine speed, it produces 634 N · m of torque while consuming No. 2 diesel fuel at the rate of 30.6 kg/h. Through a study of the friction characteristics of the engine, it is determined that the constants in Equation 2.19 for this engine are:

$$C_o = 77.0 \text{ kPa}$$

$$C_1 = -0.0143 \text{ kPa/(rev/min)}$$

$$C_2 = 1.271E-5 \text{ kPa/(rev/min)}^2$$

Making use of data given in this problem and in Table 2.1, calculate the (a) brake, (b) friction, and (c) indicated mean effective pressures. Also calculate the (d) fuel equivalent, (e) indicated, (f) brake, and (g) friction power. Finally, calculate the (h) indicated thermal, (i) mechanical, and (j) brake thermal efficiencies, and (k) the BSFC (brake specific fuel consumption).

- 2.7 Continue Problem 2.4 by assuming that the torque is increased sufficiently to maintain constant brake power while the engine speed is reduced to 1800 rev/min. You may also assume that the indicated thermal efficiency remains constant during the change in speed (this is a reasonably accurate assumption). For the engine running at 1800 rev/min as described, calculate the (a) brake,

- (b) friction, and (c) indicated mean effective pressures; the (d) indicated and (e) fuel equivalent power; (f) the brake thermal efficiency, (g) the new rate of fuel consumption, and (h) the new BSFC. (i) comparing results from Problems 2.4 and 2.5, does the engine run more efficiently at the lower or higher speed? Why?
- 2.8 (a) Using equations in Sections 2.2.4 through 2.2.6, derive the following equation:

$$\text{BSFC} = \frac{3600}{\eta_{it} H_g} \left(1 + \frac{P_f}{P_b} \right)$$

(b) Assume that the indicated thermal efficiency is 0.45 and take the heating value of No. 2 diesel fuel from Table 2.1. Engine load is to be varied from zero to a maximum while speed remains constant. Thus, friction power will also remain constant. You can estimate the friction power, P_f , from the following equation:

$$P_f = P_b \left(\frac{1 - \eta_m}{\eta_m} \right)$$

Let the maximum brake power, P_b , be 100 kW and, at maximum brake power, assuming that the mechanical efficiency is 0.8, calculate the friction power. Then make a plot of BSFC versus percent of maximum brake power. Note that BSFC becomes infinite at zero brake power, so let the percent brake power vary from 10% to 100%. Your graph will show the characteristic shape when BSFC is plotted versus brake power.

- 2.9 Rework Example Problem 2.3, except assume the engine displacement is 7.0 liters and the engine speed is 2000 rev/min.

SIMULATION PROBLEMS

- S2.1 Use the engine simulator to study the performance of the engine of Figure 7.10. Using data from Figure 7.10, verify the following input data for the simulator:

High idle speed = 2237 rpm
 Governor regulation = 11.2%
 Torque at rated speed = 1000 N·m (assumes 14% power loss in PTO drive)
 Speed for peak torque = 1402 rpm
 Torque rise = 48.8%
 Engine displacement = 8.268 L
 Volumetric efficiency = 0.85% (assumed value with engine at idle)
 Turbocharged (Y/N) = Y
 Fuel: Heating value = 45,500 kJ/kg (from Table 2.1)
 Chemical formula $C_{16}H_{34}$

- (a) Start the engine and move the governor control slider to maximum high idle speed and turn on the emissions panel. (b) While loading the engine with the load slider, use the plotting feature to plot a torque-speed curve. Use close spacing of the points near governor's maximum to clearly define governor's maxi-

mum. Observe changes in the equivalence ratio and in SFC during the loading test. (c) Next, reset the y-axis selection to 3 and repeat step b but plot a power-speed curve. (d) Next, reduce the load to 60% of the rated torque to simulate a part load; record the brake power, the fuel consumption, and the SFC. (e) Next, with the load reduced to zero, reduce the high idle speed by 20% (i.e., to 1790 rpm), then increase the load until the power level reaches that in step d; note the fuel consumption and the SFC. (f) Step (e) was a demonstration of possible fuel savings resulting from a “shift up and throttle back” technique to save fuel at part load. Calculate the percent fuel savings from using the technique.

S2.2 Rework Problem S2.1, but use methyl soyate as the fuel; its properties are given in Table 2.1.

S2.3 Rework Problem S2.1, except use an engine assigned by your instructor.

S2.4 Rework Problem S2.3, but use methyl soyate as the fuel; its properties are given in Table 2.1.

Relevant websites

(Warning: The following websites were relevant at time of publication of the book, but webmasters are free to change or eliminate websites at any time).

<http://auto.howstuffworks.com/diesel1.htm>

<http://science.howstuffworks.com/two-stroke2.htm>

ELECTRICAL POWER FOR AGRICULTURAL MACHINES

3

INTRODUCTION

Electric motors are devices that convert electric power into mechanical power. They are often chosen over engines for applications in which an electrical power supply is available. Compared to engines, electric motors are quieter, more readily adaptable to automatic or remote control, and do not produce exhaust emissions. Unlike engines, which will stall and stop consuming fuel when overloaded, an electric motor will continue to absorb electricity when overloaded. To prevent self-destruction, therefore, means must be provided to prevent an electric motor from overheating and breaking down the insulation on the windings. Typically, a thermal protector is provided to disconnect the electrical power when the windings reach a limiting temperature. Various types of electric motors are discussed in this chapter.

3.1 MOTOR COMPONENTS

A wide variety of electric motors are in commercial use, but all motors have certain features in common. A frame holds all parts in their proper orientation. Bearings (sleeve, roller, or ball) hold the rotating shaft in the frame. The stator includes electrical windings on a laminated magnetic core. The windings are arranged to provide at least two electrical poles, that is, a north and a south pole. Electric current flowing through the windings produces a magnetic field across a rotor, which rotates with the motor shaft. A fan within motors helps to provide cooling. The housings of some electric motors have external fins to aid in cooling. A terminal housing with a removable cover is attached to motors to allow access to the certain wires within the motor. On most motors, a means of terminating an equipment grounding wire is provided in the terminal housing. Finally, information relating to the internal wiring and the motor application is given on a nameplate attached to the motor.

3.2 MOTOR CLASSIFICATIONS

There are four classification systems that help to describe the differences between motors. First, motors can be classified as to the type of electrical power required, that is, *alternating current* (AC) or *direct current* (DC). Secondly, the electrical power can be *single-phase* (1- ϕ) or *three-phase* (3- ϕ). The rotor can be designed as a *squirrel-cage* or a *wound rotor*. The squirrel-cage design is less expensive because it has no windings; rather, induced currents flow in the bars and end plates (Figure 3.1). A wound rotor has many loops of wire wrapped on the rotor; the wound rotor in Figure 3.2 is for a DC motor used as an electric starter, but AC motors with wound rotors are

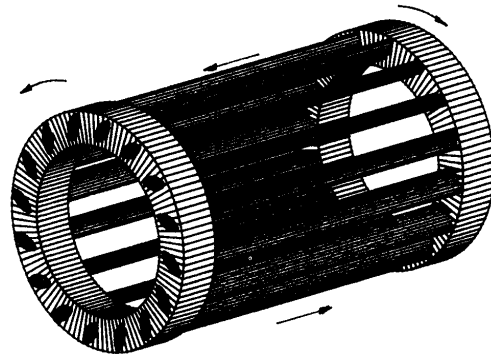


Figure 3.1 – A squirrel-cage rotor of an electric motor.

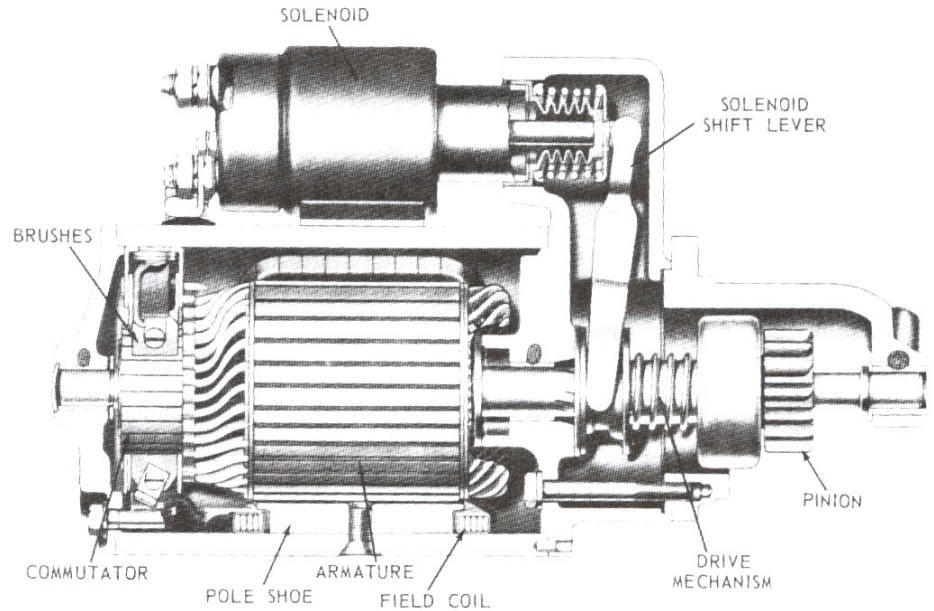


Figure 3.2 – An electric motor with a wound rotor.

also available. The loops terminate at *commutator* segments on which stationary brushes can ride to make electrical contact with the loop connected to a particular set of commutators. Rotors containing such windings and commutators are called armatures. Finally, motors can be classified as induction or *synchronous motors*. Synchronous motors turn at a speed that is governed by the frequency of the electrical voltage and the number of poles but is independent of motor load. Conversely, loading of *induction motors* causes slippage, which in turn causes the rotor to turn slower than the synchronous speed. Most of the rest of this chapter is concerned with AC, induction-type motors with a squirrel-cage rotor, since these motors are in the most widespread use. Smaller motors of this design run on single-phase power, while three-phase power is used for larger motors. DC motors will also be discussed. Other types of electrical motors will be described only briefly.

3.3 PRINCIPLES OF OPERATION OF INDUCTION MOTORS

The motor of Figure 3.3 is not a practical motor, but it illustrates the principles of operation of induction motors. A squirrel-cage rotor similar to the one in Figure 3.1 is surrounded by a permanent magnet with two poles (one a north pole and the other a south pole). The rotor in this case is made from aluminum, a material that conducts electrical current but is not attracted to magnets. Imagine that the rotor is initially stationary, but the permanent magnet is made to rotate clockwise, as indicated by the arrows. The rotor is thus positioned in a rotating magnetic field. Due to the relative motion between the rotor and rotating field, the aluminum bars in the rotor cut across the magnetic lines of force flowing from the north pole to the south pole and electrical currents are induced in the bars. The currents flow toward the reader in the conductors nearest the north pole (as indicated by the dots) and away from the reader in the conductors nearest the south pole (as indicated by the plus signs). These induced currents in turn generate magnetic fields around each conductor; these circular fields are counterclockwise about the conductors nearest the north pole. The counterclockwise fields add to the rotating flux field on the left side of each conductor and subtract on the right side. Consequently, the bars tend to move to the right into the weaker flux field. Near the south pole, similar logic shows that the bars tend to move to the left into a weaker flux field. The net result is that the rotor rotates clockwise, that is, in the same direction that the magnetic flux field is rotating. However, the rotor cannot attain the same rotational speed as the rotating magnetic field or there would be no relative motion to induce currents in the bars of the squirrel cage.

The motor in Figure 3.4 is similar to the one in Figure 3.2, except that the outer frame is now held stationary (it becomes a stator) and the permanent magnets are replaced with electromagnets wired in series. The electromagnets are connected to a source of alternating current. Thus, as the AC current goes through a full sine wave, the top electromagnet starts at zero magnetism, builds to a strong north pole, diminishes to zero, builds to a strong south pole, diminishes to zero again, and the cycle repeats. Because of the arrangement of the windings, the bottom magnet is going through a similar pattern, except that its magnetic polarity is opposite that of the top

magnet. Note that, along a vertical line through the center of the squirrel-cage rotor, the variation of the magnetic field is the same as if the permanent magnet of Figure 3.3 was rotating, that is, the magnetic flux builds to a maximum in the downward direction, diminishes to zero, builds to a maximum in the upward direction, diminishes to zero, etc. Thus, the motor of Figure 3.4 can be viewed as having a rotating field. The *synchronous speed*, that is, the speed at which the field appears to rotate, can be calculated by using the following equation:

$$n_s = \frac{120f}{\lambda_p} \quad (3.1)$$

where n_s = synchronous speed, rev/min
 f = line frequency, Hz
 λ_p = number of poles

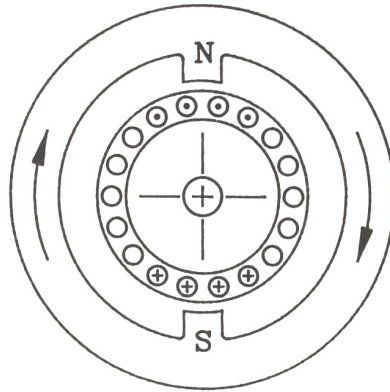


Figure 3.3 – Illustration of the principle of operation of an induction motor.

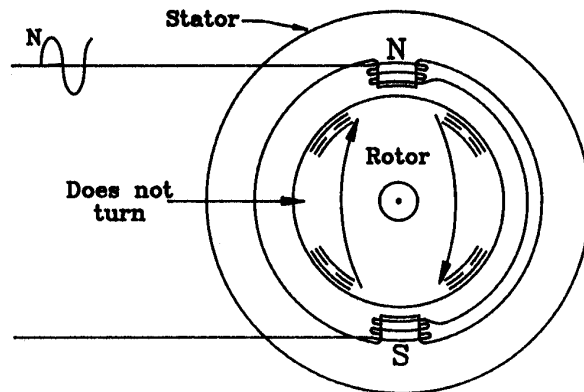


Figure 3.4 – Illustration of an induction motor without starting means (adapted from Surbrook and Mullin, 1985).

In the United States, the standard *line frequency* is 60 Hz. Then, for the motor of Figure 3.3 with two poles, the synchronous speed would be 3600 rev/min. The rotor cannot turn as fast as the synchronous speed in an induction motor, that is, there is some slip, defined as:

$$s = \frac{n_s - n_r}{n_s} \quad (3.2)$$

where s = slip, decimal

n_r = rotor speed (and shaft speed), rev/min

Combining Equations 3.1 and 3.2 gives the following equation for rotor speed:

$$n_r = \frac{120f(1-s)}{\lambda_p} \quad (3.3)$$

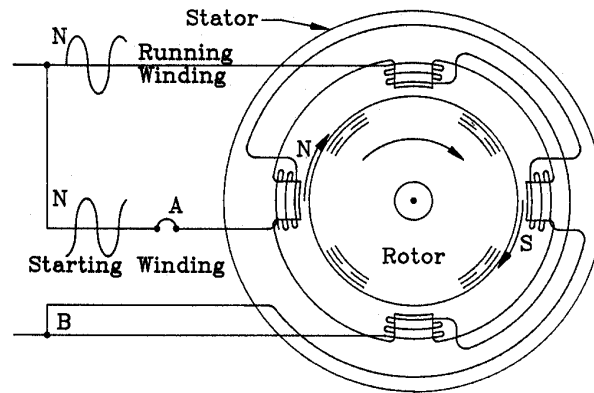
The *slip* $s = 1.0$ at startup and declines to some small value when the motor reaches full speed. For example, if the two-pole motor of Figure 3.4 was driven with 60 Hz AC current and the slip was 4.17%, the rotor speed would be 3450 rev/min. Note that, if the bottom pole in Figure 3.4 was positioned 90° from the top pole instead of 180° , the magnetic field would rotate only half a revolution in each voltage cycle. Another set of poles could be added to allow the magnetic field to complete the full revolution in two voltage cycles. Doubling the number of stator poles to four would reduce the synchronous speed to 1800 rev/min and, if the slip was 4.17%, the rotor speed would be 1725 rev/min.

The motor of Figure 3.4 has no provision for starting the rotor into motion. Once started, the rotor would continue to run in the initial direction because of the alternating magnetic field. As explained in the next section, there are various types of single-phase induction motors, each differing in the means used to start the rotor into motion.

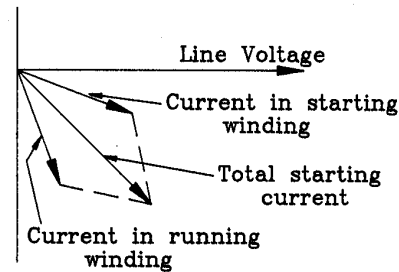
3.4 TYPES OF SINGLE-PHASE INDUCTION MOTORS

3.4.1 Split-phase induction motors

The motor of Figure 3.5a is called a *split-phase induction motor*. A set of starting windings has been added on poles that are rotated 90° from the running windings. Compared to the running windings, the starting windings have fewer turns of higher-resistance wire. Because of the lower resistance and higher inductance of the starting windings, the current in the starting windings is displaced in phase from the running windings (see Figure 3.5b). Consequently, a clockwise-rotating magnetic field is established that starts the rotor into clockwise motion. A centrifugal switch in series with the starting windings opens when the motor has attained sufficient speed and the motor then continues to run as an ordinary induction motor. If the leads are brought out to the terminal housing, the direction of rotation can be reversed by reversing the leads, A and B, of the starter-windings circuit. The split-phase motor is generally available in sizes from 0.04 to 0.25 kW ($1/20$ to $1/3$ hp). Compared to other single-phase induction motors, it has higher starting current and lower starting torque. It is best suited to fans and other machines that do not start under heavy load.



(a)

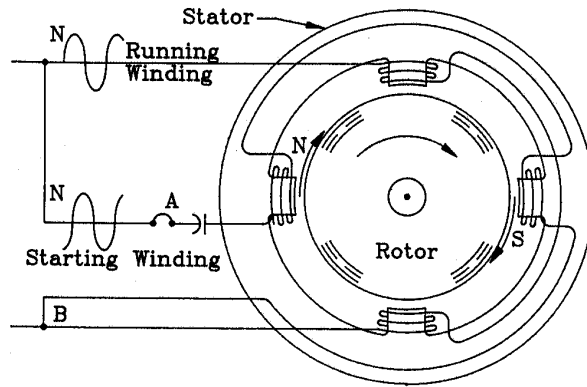


(b)

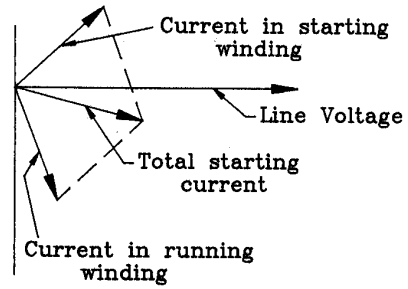
Figure 3.5 – Illustration of a split-phase induction motor (adapted from Surbrook and Mullin, 1985).

3.4.2 Capacitor-start, induction-run motors

A *capacitor-start, induction-run motor* is illustrated in Figure 3.6a. An electrolytic capacitor has been inserted in series with the starting windings to shift the phase of the starting current as shown in Figure 3.6b. The electrolytic capacitor is not designed for continuous duty and thus, when the motor reaches 75% to 80% of synchronous speed, a centrifugal switch opens and disconnects the starter-winding circuit. Comparing Figures 3.5b and 3.6b shows that the capacitor-start motor has much lower starting current than the split-phase motor; typically, the starting current of the capacitor-start motor is three to four times that required for running. The starting torque capability of the capacitor-start motor is typically is about twice that of a split-phase motor. The capacitor-start, induction-run motor is available in sizes from 0.13 to 2.3 kW ($\frac{1}{6}$ to 3 hp) and is the most widely used motor for farm equipment. As with the split-phase motor, the direction of rotation can be reversed by reversing the leads, A and B, to the starter-winding circuit.



(a)



(b)

Figure 3.6 – Illustration of a capacitor-start induction-run motor (adapted from Surbrook and Mullin, 1985).

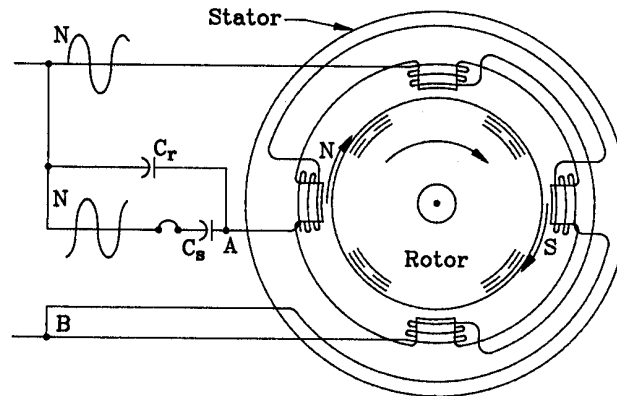


Figure 3.7 – Illustration of a two-value-capacitor, induction-run motor (adapted from Surbrook and Mullin, 1985).

3.4.3 Two-value-capacitor, induction-run motors

A schematic diagram of a *two-value-capacitor, induction-run* motor (also called a *capacitor-start, capacitor-run motor*) is shown in Figure 3.7. The auxiliary winding used for starting is also used for running. An oil-filled capacitor (C_r) capable of continuous operation is placed in series with the auxiliary winding. An electrolytic capacitor (C_s) is connected in parallel with the oil-filled capacitor while starting but is disconnected by a centrifugal switch when the motor comes up to speed. The two-value-capacitor induction-run motor is commonly available in sizes up to 7.5 kW (10 hp) and develops high starting torque. Again, the direction of rotation can be reversed by reversing the leads, A and B, to the auxiliary-coil circuit.

3.4.4 Repulsion-start, induction-run motors

A *repulsion-start, induction-run motor* is illustrated schematically in Figure 3.8. Unlike the previous induction motors, the repulsion-start motor does not use auxiliary starting windings on the stator. Instead, a wound rotor is used. Unlike the squirrel-cage rotor in which all of the conductor bars are shorted together by washer-shaped end plates, the conductors of the wound rotor are brought out to commutator segments, that is, the rotor is an armature. The two brushes which ride on opposite sides of the commutator are shorted together, as shown in Figure 3.8. Thus, at any instant, one set of windings on the armature are connected into a coil whose axis is tilted relative to the axis of the stator winding. The stator magnetic field induces a current in the coil on the armature which, in turn, generates a magnetic flux from the armature coil. The repulsion of the stator and armature electromagnets forces the armature to turn. After the motor comes up to speed, a centrifugal device shorts all of the commutator segments together and the motor runs similar to a squirrel-cage induction motor. The direction of rotation can be changed by shifting the angle of the brushes relative to the axis of the stator coil. The repulsion-start, induction-run motor develops very high starting torque with relatively low starting current and is available in sizes from 0.37

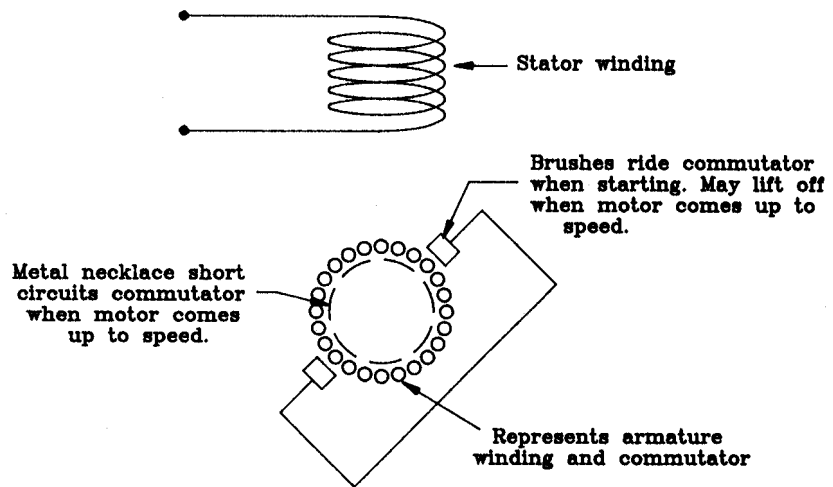


Figure 3.8 – Illustration of a repulsion-start, induction-run motor.

to 7.5 kW ($\frac{1}{2}$ to 10 hp). However, because of the high cost of manufacturing the armature, the repulsion-start, induction-run motor is less widely used than the capacitor-start and two-value-capacitor motors.

3.5 THREE-PHASE INDUCTION MOTORS

Single-phase motors become impractical in sizes much above 7.5 kW (10 hp) and, for larger power requirements, three-phase motors become the practical choice. *Three-phase, induction-type motors* are available in sizes up to 150 kW (200 hp). A three-phase induction motor is illustrated in Figure 3.9a. The rotor has the squirrel-cage

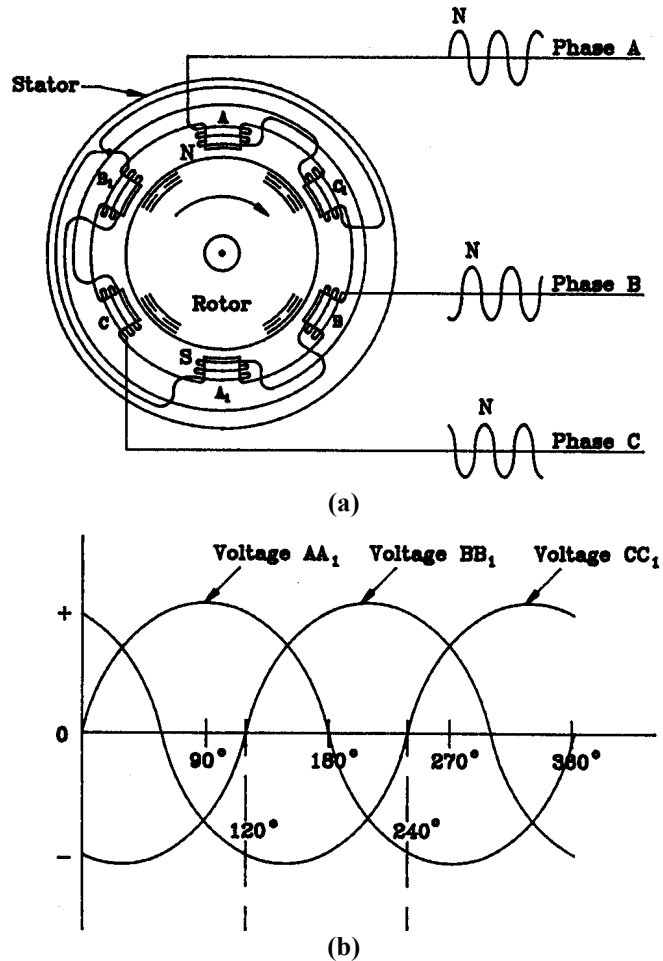


Figure 3.9 – Illustration of a three-phase induction motor (adapted from Surbrook and Mullin, 1985).

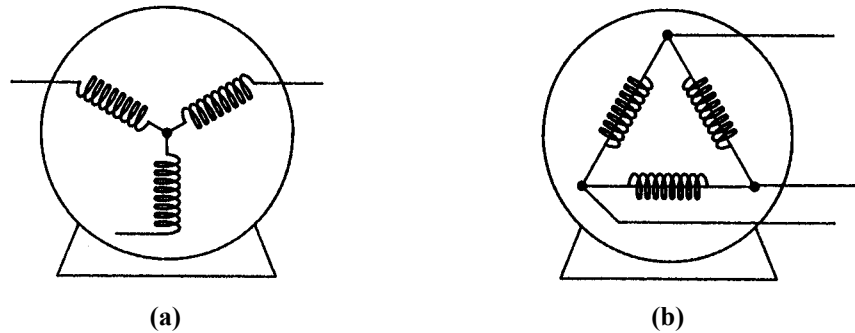


Figure 3.10 – Three-phase induction motor with (a) wye and (b) delta connections (adapted from Surbrook and Mullin, 1985).

design of Figure 3.1. The voltage to the motor (Figure 3.9b) is supplied through the three electrical conductors of a three-phase line. The voltage waveform BB_1 lags AA_1 by one third of the wavelength or 120° or, for 60 Hz voltage, by 0.0056 seconds; Voltage CC_1 lags AA_1 by 240° or 0.0111 seconds. As waveform AA_1 goes through its sinusoidal variation, electromagnet A in Figure 3.9a builds from zero to a strong north pole, diminishes to zero, builds to a strong south pole, diminishes to zero, and so forth. Electromagnets B and C follow a similar pattern except for their respective phase delays. Thus, the north pole of the magnetic field across the rotor appears to rotate from electromagnet A to B to C to A and so forth, that is, the field appears to rotate clockwise. Thus, as was discussed in Section 3.3, the rotor also rotates clockwise. The synchronous speed, slip, and rotor speed can be calculated by using Equations 3.1, 3.2, and 3.3, respectively. Thus, for 60 Hz current, the synchronous speed would be 3600 rev/min for the two-pole motor shown in Figure 3.9a. If the slip at full load was 4.17%, the rotor would turn at 3450 rev/min at full load. A four-pole motor uses twice as many windings to create two sets of north and south poles simultaneously. As was described in Section 3.3, the magnetic field then rotates halfway around the stator in each cycle of voltage and the synchronous speed becomes 1800 rev/min.

The direction of rotation of the three-phase induction motor can be reversed by reversing any two of the three leads to the motor. Some contemplation will show that reversing any two leads reverses the direction of rotation of the magnetic field and thus reverses the direction of rotation of the rotor.

Three-phase electricity from the electric power grid is provided for either wye or delta connections and motors are available for either type of power. Figure 3.10a shows a wye-type motor while a delta-type motor is shown in Figure 3.10b.

3.6 DUAL-VOLTAGE MOTORS

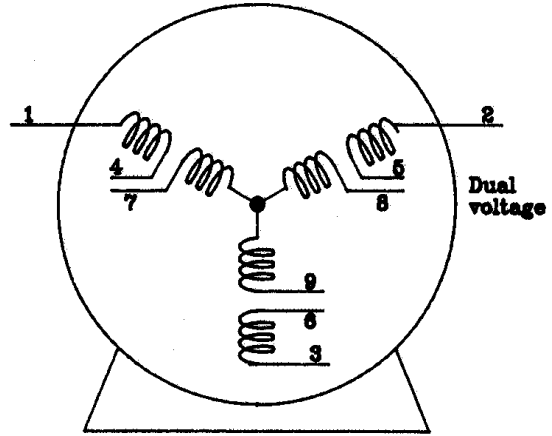
Many motors are designed to be operated at either of two different voltages. For example, the three-phase motors of Figure 3.11 can be connected to operate on 230-volt or 460-volt electrical power. Note that two separate coils are wrapped on each electromagnet and all leads are brought out to the terminal housing on the motor. The numbering diagrams beside each motor show how to connect the coils. The lower

voltage can be used when the two coils on each electromagnet are connected in parallel, and the coils are connected in series to permit use of the higher voltage. Many single-phase motors are similarly designed for dual-voltage operation. For a given power output, the current draw of the motor will be only half as large when the higher voltage is used; thus, whenever the higher voltage is available, it should be used.

230-V connection

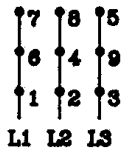


480-V connection

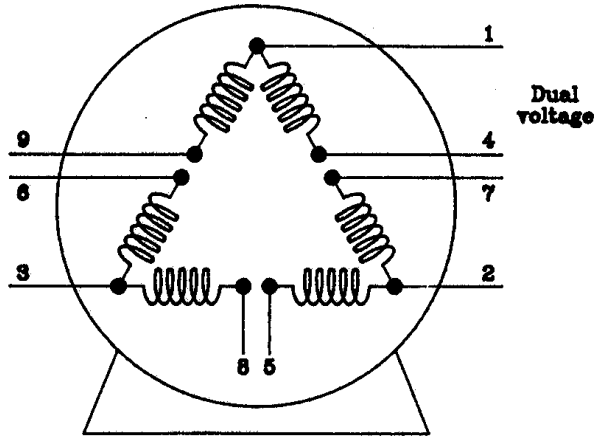
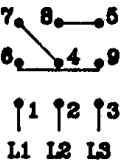


(a)

230-V connection



480-V connection



(b)

Figure 3.11 – Three-phase motors with dual voltage connections (after Surbrook and Mullins, 1985).

3.7 TORQUE-SPEED CHARACTERISTICS OF INDUCTION MOTORS

The torque produced by a motor must be sufficient to start the connected machine and keep it operating under normal loading. Figure 3.12 shows variations in torque as three-phase and single-phase motors accelerate from rest. The locked-rotor torque (Figure 3.12a), defined as the torque at zero speed, must be large enough to start the machine in motion. Once started, the motor will stall if the load exceeds the breakdown torque. Motor manufacturers do not indicate the breakdown torque on the nameplate, but do use it in rating the power capacity of the motor. Note that the rotor cannot achieve synchronous speed while producing torque, that is, there must be some slip. Thus, full-load torque is produced at a rated speed slightly below the synchronous speed. The motor speed will fall below rated speed when the load is increased above the full-load torque, but will regain the speed when the load is reduced. Due to the steepness of the curve near the rating point, moderate increases in torque load produce only small decreases in speed, thus the power output increases with increased load until the speed begins to drop more rapidly near the point of breakdown torque. To prevent overheating and damage to a motor, it should never be loaded so heavily that the point of operation approaches the breakdown point.

The torque characteristic of single-phase motors combines two separate curves (Figure 3.12b). Starting from rest, the torque output of the motor is produced by the combined effects of the starting and running windings. After the centrifugal switch opens and the starting winding is disconnected, only the running winding remains to produce torque. Otherwise, the terminology and description of the torque characteristics of the single-phase and three-phase motors are similar.

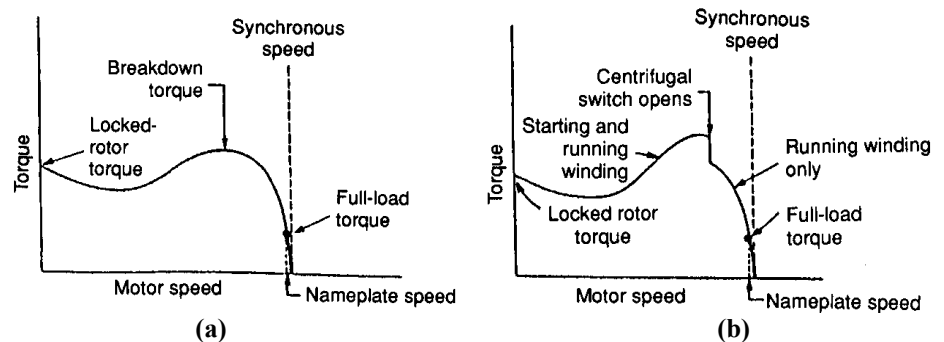


Figure 3.12 – Torque-speed characteristics of induction motors (after Surbrook and Mullin, 1985).

3.8 MOTOR NAMEPLATE INFORMATION

Design and rating standards developed by the *National Electrical Manufacturer's Association* (NEMA) permit the comparison of motors from different manufacturers. Information on the nameplate may include any or all of the following:

- *VOLTS*, the proper operating voltage, may be either a single value or, for dual-voltage motors, a dual value.
- *AMPS* is the full-load current draw in amperes with the proper voltage supply. When a dual number is listed, the motor will draw the smaller amperage when connected to the higher voltage source.
- *RPM* is the rotor speed when the motor runs at the full-load point on the torque-speed curve (Figure 3.12).
- *HZ* is the design operating frequency of the electrical supply. In the United States, it is 60 cycles per second. A standard frequency of 50 cycles per second is used in some countries.
- *FR* is one of the standard frame numbers used by manufacturers to insure interchangeability. For motors with power ratings below 0.75 kW (1.0 hp), common frame numbers are 42, 48, and 56. The frame number divided by 6.3 (16) gives the height in cm (inches) from the bottom of the mounting to the shaft centerline. Letters may be added to specify the type of mounting, for example, T-frame or the heavier U-frame. A replacement motor with the same frame number as the original motor will fit on the same mounting.
- *DUTY* indicates whether the motor is rated for continuous or intermittent; *HOURS* may be used to indicate the length of time the motor can be safely operated during intermittent duty.
- *TEMPERATURE RISE* (°C) may be stated as the allowable temperature rise above a 40°C (104°F) ambient temperature while the motor is operating at full load. Often, a motor can be operated at 10% to 15% overload without damage, but the motor temperature should never exceed 55°C (131°F). If, while operating, a motor is not too hot to touch, it is not overheated.
- As an alternative to temperature rise, the allowable *AMBIENT TEMPERATURE* may be listed. Then the motor can be operated at full load in environments with temperatures below the stated ambient temperature.
- *SF*, the service factor, is multiplied by the rated power to obtain the permissible loading. For example, a service factor of 1.10 means the motor could be operated at 10% overload without overheating. Service factors for farm-duty motors can be 1.35 or more.
- *INSULATION CLASS* is a temperature-resistance rating of the insulation on the wires in the motor. Typical classes are A, B, F, or H, where class A is the lowest temperature rating. Class A or B insulation is used in most farm-duty motors.
- The *CODE LETTER* is used to determine the maximum rating of the motor branch-circuit protection and is based on the locked-rotor current drawn by the

motor. The following equation may be used to calculate the locked-rotor starting current from the code letter:

$$\text{amps} = \frac{1000(\text{kVA}) \text{ hp}}{\text{volts } C_{\text{ph}}} \quad (3.4)$$

where amps = starting current in amperes

kVA = rating from the National Electric Code (NEC)

hp = rated power from nameplate, in hp

volts = supply voltage in volts

C_{ph} = constant = 1.0 for single-phase motor or 1.73 for three-phase motor

- A *DESIGN* letter may be given on the nameplate as an indication of their starting-to-rated currents and starting-to-rated torques. The five classes for squirrel-cage motors are A, B, C, D, and F, with A and B being the most common. Design A has starting current 6 to 7 times rated current and starting torque 150% of rated. Design B has starting current 5.5 to 6 times rated current and starting torque 150% of rated.
- A *THERMAL PROTECTION* indication on the nameplate indicates the motor is equipped with such protection to prevent overheating the windings. Protection may be provided by sensing motor current or temperature in the windings and shutting off the motor when either becomes excessive. After shutdown, the motor must be reset manually unless it is equipped with an automatic reset.

Example Problem 3.1

For a 50 hp, three-phase, 230/460-volt motor with a code letter G on the nameplate, determine the starting currents when the motor is used at 230 volts and at 460 volts.

Solution

Table 430-7(b) of the NEC (provided at the beginning of the homework problems) lists the kilovolt-amperes per hp (kVA/hp) for code letter G as 5.6 to 6.29. Thus, from Equation 3.4, the minimum locked-rotor starting current while operating at 230 volts would be:

$$\text{amps} = \frac{1000 (5.6) 50}{230 (1.73)} = 704\text{A}$$

Using the same equation at the higher end of the range, the maximum locked-rotor starting current would be 790 amperes. These are very high starting currents. The starting currents could be reduced to the range of 352 to 395 amperes by using the motor on a 460-volt supply.

3.9 MOTOR STARTERS

The starting current of squirrel-cage motors can be up to 7 times higher than the running current and, as Example Problem 3.1 indicates, the starting current for large electric motors can be very high. The high starting current can cause an excessive voltage drop on the electric supplier's power lines, thus interfering with neighboring customers. Means are available to reduce the excessive starting current. Sometimes it is possible to start the motor under zero load and then apply the torque load after the motor is running. Also, *autotransformers* can be used to temporarily reduce the supply voltage at starting and thus reduce the starting current. Other types of starters are also available for reducing the starting current. When starting current is not excessive, a simple *across-the-line* starter can be used. Typically, across-the-line starters are used for motors up to 22 kW (30 hp) in size.

3.10 MOTOR ENCLOSURES

Motors used in agricultural applications are often exposed to harsh environments, including dust, high humidity, combustible vapors, rodents, and insect pests. Thus, the design of the motor enclosure is important. Available enclosures include open, drip-proof, splash-proof, totally-enclosed and explosion-proof. Open enclosures are least expensive but offer the least protection. The openings for ventilation air for drip-proof motors are designed to prevent entry of rain, but not of dust. Air openings in splash-proof motors are even more secluded to reduce the possibility of liquids splashing into the motor. Totally enclosed motors prevent the entry of dust; cooling air is circulated within the motor but heat can only be dissipated by conduction through the enclosure. A fan may be located externally on the motor shaft to blow air over the exterior of the enclosure for cooling. Explosion-proof motors are totally enclosed and are designed to prevent the entry of combustible vapors into the interior of the motor; they are used on fuel-dispensing pumps and for other applications where combustible vapors may be present.

3.11 VARIABLE- SPEED ELECTRIC MOTORS

Although AC induction motors are designed to run at constant speed, permanent split-capacitor motors are capable of some speed variation, as shown in Figure 3.13. The torque-speed curve for the load is shown superimposed on the torque-speed curves for the motor at two different supply voltages. By reducing the supply voltage from V_A to V_B , the operating speed is reduced from n_a to n_b . Notice that the motor has less torque available as the speed is reduced, and therefore, as shown by Equation 2.13 in the previous chapter, the power output falls rapidly as the supply voltage is reduced. Thus, the technique will work only if the power demand of the driven machine falls rapidly at decreased speed. A fan represents such a load and thus the technique of Figure 3.13 is sometimes used to provide variable speeds to a fan.

As Equation 3.3 indicates, the speed of an induction motor is proportional to the frequency of the supplied electrical power. Based on Equation 3.3, a special controller

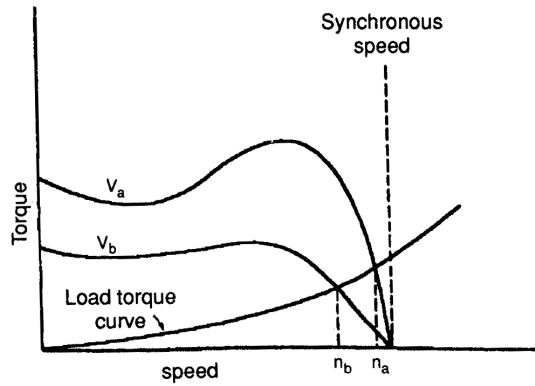


Figure 3.13 – Illustration of means of changing speed of induction motors (after Surbrook and Mullin, 1985).

may be used to control the speed of three-phase induction motors. The controller rectifies the AC voltage to direct current and then inverts it back to AC current at a controllable frequency. When frequency is reduced, the voltage is also reduced to prevent overheating of the motor. The controller generally maintains constant output torque from the motor. Thus, as shown by Equation 2.13, the power output varies proportionally with the motor speed. Using the controller, the motor speed typically can be controlled from 20% to 110% of the motor nameplate speed, and wider variation is also possible.

A multiple-speed induction motor can be achieved by electrical switching to change the number of stator poles. If the shaft of the two-pole motor turned at 3450 rev/min, for example, Equation 3.3 indicates that switching it to a four-pole motor would reduce the speed to 1725 rev/min. Other speed ratios are also possible; for example, it is possible to switch between four and six poles or between two and six poles. Note that switching the number of poles provides only two discrete speeds, whereas the previously mentioned techniques permit infinitely variable speed changes.

A motor in which a wound rotor is connected in series with the stator coils is called a universal motor because it will operate on either AC or DC electrical power. The speed of a universal motor can be reduced by reducing the electric current supplied to the motor, for example, by lowering the supply voltage. An electric drill motor is an example of a universal motor. Speed control of the drill motor is achieved by use of an SCR (Silicon-Controlled Rectifier) to control the AC input current. Variable speed could also be obtained by operating a universal motor on a variable voltage DC supply, but AC current is more widely available than DC current.

3.12 MOTOR EFFICIENCY

Not all of the electrical power delivered to a motor is converted to mechanical power. The most important losses are in the windings, in the magnetic core, and in mechanical friction. The power efficiency of a motor can be calculated by using the following equation:

$$\eta_m = \frac{2\pi T_m n_m}{60 C_{ph} V I \cos(\phi)} \quad (3.5)$$

where η_m = power efficiency of the motor, decimal

T_m = motor output torque in N·m

n_m = motor shaft speed in rev/min

C_{ph} = constant = 1.0 for single-phase motor or 1.73 for three-phase motor

V = voltage supplied to the motor in Volts

I = current draw by the motor in amperes

ϕ = phase angle between the voltage and current

A motor running without load must absorb electrical power to overcome mechanical friction and thus its no-load power efficiency is zero. Most motors are designed to achieve peak efficiency at 80% to 120% of rated load. The following example problem illustrates the calculation of power efficiency.

Example Problem 3.2

A single-phase, 115 V electric motor absorbs 7.8 amperes while running at 1725 rev/min and developing 3.1 N·m of torque. The phase angle between the voltage and current is 38°. Calculate the power efficiency of the motor.

Solution

All of the data required in Equation 3.5 are given in the problem statement. The solution is:

$$\eta_m = \frac{2\pi(3.1)1725}{60(115)7.9\cos(38)} = 0.79$$

Thus, the power efficiency of the motor is 79%.

PROBLEMS

Table 430-7(b) in the National Electrical Code is useful for calculating the locked-rotor starting current of electric motors. The table below shows the data for the most common code letters.

Code Letter	kVA/hp
G	5.6 - 6.29
H	6.3 - 7.09
J	7.1 - 7.99
K	8.0 - 8.99
L	9.0 - 9.99

- 3.1 What is the shaft speed of a four-pole synchronous motor operating from a 60 Hz supply?
- 3.2 A four-pole, single-phase induction motor runs at 1750 rev/min while being supplied with 60 Hz electrical power. Calculate (a) the synchronous speed and (b) the slip.
- 3.3 Rework Problem 3.2, except assume the motor runs at 1730 rev/min.
- 3.4 A capacitor-start, induction-run, single-phase electric motor has a starting torque 300% of rated torque and runs at 1750 rpm. Sketch the torque versus speed performance curve to scale and label synchronous speed, rated speed, full load torque, and locked rotor torque.
- 3.5 A 37.3 kW (50 hp) electric motor runs on 230/460 VAC, 60 Hz, 3-phase power. It draws 119.6/59.8 amperes at full load while running at 1775 rev/min. Its code letter is G and its service factor is 1.15. Assuming the motor is connected for 460-volt operation, calculate (a) the full-load torque, (b) the locked-rotor starting current, (c) the ratio of starting current to full-load current, (d) the maximum allowable power output, and (e) the power efficiency at full load if the phase angle between the current and voltage is 35° . (f) Is this motor suitable for an across-the-line starter, or should a reduced-current starter be used? (g) How many poles does this motor have?
- 3.6 Rework Problem 3.5, except use a 0.75 kW (1.0 hp) motor that runs on 115/230 VAC, 60 Hz, single-phase power, draws 12.8/6.4 amperes at full load while running at 1725 rev/min, has code letter K and service factor 1.25. Assume the motor is connected for 115 VAC operation.
- 3.7 Rework Problem 3.5, except use a 0.25 kW ($\frac{1}{3}$ hp) motor that runs on 115/230 VAC, 60 Hz, single-phase power, draws 6.0/3.0 amperes at full load while running at 3450 rev/min, has code letter L and service factor 1.75. Assume the motor is connected for 115 VAC operation.
- 3.8 A dual voltage, 3-phase, 3.7 kW (5 hp) electric draws 18 amperes at full load if connected to a 230V supply. If the motor is properly connected to a 460V supply, (a) what is its current draw, and (b) what will be its power output at full load?
- 3.9 Why is it important to give specifications for both single and 3-phase motors for some applications?
- 3.10 An electric motor has a number 56 frame. What is the height of the shaft above the mounting surface?
- 3.11 A potato slurry conveyor is to be powered by an electric motor. A 3.7 kW (5 hp) motor has been determined to be sufficient. Specify a motor type and other factors such as enclosure type, phase, type of running and starting, and bearing type. Give brief reasons for each choice.

SIMULATION PROBLEMS

The simulation problems for Chapter 3 use the AC motor simulator on the CD-ROM. The data in Table S3.1 are for use in the simulation problems.

Table S3.1 Properties of several AC electric motors.

Factor	Motor 1	Motor 2	Motor 3	Motor 4	Motor 5	Motor 6	Motor 7	Motor 8
Phase	1	1	3	1	1	3	3	3
Poles	4	4	6	4	4	4	4	4
Volts	115	115	230	115	115	220	220	220
Amps	6.1	6.9	2.8	13.8	25.6	13.2	26.0	51.6
Hertz	60	60	60	60	60	60	60	60
Rated rpm	1725	1750	1140	1725	1715	1760	1760	1760
Rated hp	0.333	0.5	0.75	1	2	5	10	20
Phase, deg.	63	52	48	51	50	30	30	30

S3.1 An electric motor is to be direct-coupled to a machine input shaft that requires up to $5.5 \text{ N}\cdot\text{m}$ of torque. The shaft speed must not fall below 1700 rpm. (a) Using the simulator, selected the smallest motor from Table S3.1 that will meet these requirements. (b) How much heat, in kJ/min, must the cooling system dissipate to keep the motor temperature from rising? (Hint: Find the row that has the shaft torque closest to $5.5 \text{ N}\cdot\text{m}$, then adjust the percentage in Column A iteratively until the shaft torque is exactly $5.5 \text{ N}\cdot\text{m}$; finally, check to see if the corresponding speed is at or above 1700 rpm for the selected motor).

S3.2 Rework Problem S3.1, except the shaft requires up to $1.0 \text{ N}\cdot\text{m}$ of torque and the speed must not fall below 1745 rpm.

S3.3 Rework Problem S3.1, except that the shaft requires up to $50 \text{ N}\cdot\text{m}$ of torque and the speed must not fall below 1745 rpm.

Relevant websites

(Warning: The following websites were relevant at time of publication of the book, but webmasters are free to change or eliminate websites at any time).

<http://electronics.howstuffworks.com/motor6.htm>

<http://www.baldor.com/>

<http://hyperphysics.phy-astr.gsu.edu/hbase/magnetic/elemot.html>

MECHANICAL POWER TRANSMISSION

4

INTRODUCTION

In Chapter 1 we introduced the concept of support and process systems of an agricultural machine. In Chapters 2 and 3 we presented the main sources of power for agricultural machines, i.e., the diesel engine for self-propelled machines and the electrical motor for many stationary machines used on the farmstead. Pull-type machines must receive propulsion and rotary power from the tractor. Power is transmitted from the tractor to the machine by means of traction, power-take-off drives (PTO), and/or by fluid power. Rotary power is also transmitted by means of belts and chains. Topics related to rotary power transmission are presented here. Fluid power transmission is presented in Chapter 5

4.1 V-BELT DRIVES

V-belts are employed extensively in agricultural machinery applications in which it is not necessary to maintain exact speed ratios. V-belts tend to cushion shock loads, do not require lubrication, and are less likely to become misaligned than are other types of drives. They can be operated at speeds as high as 33 m/s, although speeds in agricultural machinery applications seldom exceed 15 m/s. V-belts are not suitable for high torque at low speeds.

V-belts may be used singly or in matched sets, although single belts are the most common on agricultural machines. Banded, multiple V-belts are sometimes employed on drives having high power requirements, pulsating loads, and inherent instability problems. A banded belt consists of a matched set of two or more conventional V-belts with a thin tie band connecting their tops. Tying the strands together minimizes lateral belt whip and improves the load distribution among the belts.

Because a V-belt wedges into the sheave grooves, it can transmit a given amount of power with less overall shaft pull than a flat-belt drive. V-belts can be operated with relatively small arcs of contact, as in close-center shaft arrangements with large shaft-speed ratios. A single belt on an implement often drives several components in an arrangement known as a serpentine drive. V-belts permit considerable latitude in possible orientation and arrangement of the shafts involved in a drive.

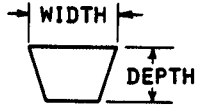
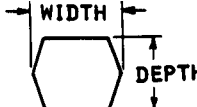
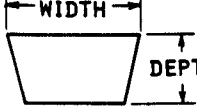
V-belts are adaptable to clutching arrangements. A close-fitting guard may be needed to maintain proper belt orientation and move the belt away from the driver when the tension is released. Under certain conditions it is convenient or economically desirable to drive a relatively large flat pulley with V-belts from a smaller, grooved sheave. This is known as a V-flat drive.

4.1.1 V-belt types and standardization

Three types of V-belts specially designed for agricultural machines are known as agricultural V-belts, agricultural double V-belts, and adjustable-speed belts. These are illustrated in Table 4.1. Banded belts made from agricultural V-belts are also available. Agricultural V-belts and double V-belts are distinguished from the corresponding cross-sectional sizes of industrial V-belts by the prefix H.

The cross-sectional dimensions of agricultural V-belts are identical with those of industrial belts but the construction is different because of the different type of use. Agricultural V-belts are more likely to be subjected to excessive shock loads, heavy pulsating loads, and other adverse conditions. Whereas V-belts in industrial drives are expected to last for several years of continuous operation, a life expectancy of 1000 to 2000 h is adequate for most farm machinery applications. Hence, agricultural V-belt loadings can be higher than in industrial applications.

Table 4.1. Agricultural V-belt cross-sectional dimensions, sheave groove angles, and differences between sheave effective outside diameters and pitch diameters.*

Type	Belt Cross Section	Nominal Belt Width		Nominal Belt Depth		Sheave Groove Angle (deg.)†	Effective OD Minus PD for Std-Groove Sheave	
		(mm)	(in.)	(mm)	(in.)		(mm)	(in.)
Conventional V-belts								
	HA	12.7	0.50	7.9	0.31	30-38	6.35	0.250
	HB	16.7	0.66	10.3	0.41	30-38	8.89	0.350
	HC	22.2	0.88	13.5	0.53	30-38	10.16	0.400
	HD	31.8	1.25	19.0	0.75	30-38	15.24	0.600
	HE	38.1	1.50	23.0	0.91	32-38	20.32	0.800
Double V-belts								
	HAA	12.7	0.50	10.3	0.41	30-38	6.35	0.250
	HBB	16.7	0.66	13.5	0.53	30-38	8.89	0.350
	HCC	22.2	0.88	17.5	0.69	30-38	10.16	0.400
	HDD	31.8	1.25	25.4	1.00	30-38	15.24	0.600
Adjustable-speed V-belts								
	HI	25.4	1.00	12.7	0.50	26	7.6	0.30
	HJ	31.8	1.25	15.0	0.59	26	9.4	0.37
	HK	38.1	1.50	17.5	0.69	26	11.4	0.45
	HL	44.4	1.75	19.8	0.78	26	13.2	0.52
	HM	50.8	2.00	22.2	0.88	26	15.2	0.60

* ASAE Standard S211.3.

† For V-belts and double V-belts, sheave groove angle increases as diameter is increased.

Table 4.2 Diameters of ASAE standard adjustable-speed sheaves.^[a]

Belt Cross Section	Recommended Minimum OD, mm (in)	Maximum PD with Minimum OD, mm (in)	Maximum Belt Diameter Change, mm (in)
HI	177.8 (7.00)	170.2 (6.70)	72.1 (2.84)
HJ	222.2 (8.75)	2112.8 (8.38)	94.7 (3.73)
HK	266.7 (10.5)	255.3 (10.05)	117.3 (4.62)
HL	311.2 (12.25)	298.0 (11.73)	140.2 (5.52)
HM	355.6 (14.0)	340.4 (13.40)	162.8 (6.41)

^[a] ASAE Standard S211.3.

Double V-belts are employed in *serpentine drives* where the direction of rotation of one or more shafts is reversed, thus requiring that power be transmitted to grooved sheaves from both the inside and outside of the belt. Adjustable-speed belts are discussed later in the chapter.

The American Society of Agricultural Engineers (ASAE; now called ASABE, the American Society of Agricultural and Biological Engineers) has established a standard for agricultural V-belts. This standard covers cross-sectional dimensions (Table 4.1), belt lengths generally available, groove specifications, minimum diameters for idlers, procedures and examples for calculating required belt lengths, installation and take-up allowances, twisted-belt drives, and belt-measuring specifications. Table 4.2 includes diameters of ASAE standard adjustable-speed sheaves.

The ASAE standard is similar in many respects to the standard established by the Rubber Manufacturers Association (RMA) for industrial V-belts. There are minor differences in groove dimensions and in available belt lengths. The RMA standard specifies pitch lengths for belts, whereas the ASAE standard specifies effective outside lengths. The RMA standard is intended primarily for two-sheave drives and includes formulas and charts for power ratings. The ASAE standard covers a broad range of drive configurations and does not include power ratings. In designing an agricultural drive, the allowable load is related to the expected number of hours of actual operation for a specific drive.

4.1.2 V-belt drive geometry

Belts are generally used to connect parallel shafts so that the sheaves rotate in the same direction or in the opposite direction as shown in Figure 4.1. The angle of wrap is defined as the angle of belt contact around the sheave. For the open belt drive, the angles of wrap (rad) are

$$\theta_2 = \pi - 2 \sin^{-1} \frac{D_3 - D_2}{2C} \quad (4.1)$$

and

$$\theta_3 = \pi + 2 \sin^{-1} \frac{D_3 - D_2}{2C} \quad (4.2)$$

where D_2 and D_3 are the outside sheave diameters.

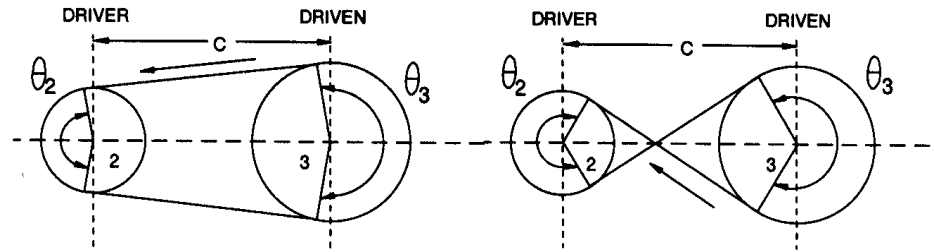


Figure 4.1 – Geometry of V-belt drives.

The angles of wrap for the crossed-belt drive are equal and are given by:

$$\theta_2 = \theta_3 = \pi + 2 \sin^{-1} \frac{D_3 - D_2}{2C} \quad (4.3)$$

The belt length for an open drive is approximated by:

$$L = 2C + \frac{\pi}{2}(D_3 + D_2) + \frac{(D_3 - D_2)^2}{4C} \quad (4.4)$$

and for the crossed belt drive the length is:

$$L = 2C + \frac{\pi}{2}(D_3 + D_2) + \frac{(D_3 + D_2)^2}{4C} \quad (4.5)$$

4.1.3 Kinematics of V-belt drives

As a belt bends to conform to the sheave curvature, the outer section stretches and the inner section is compressed. The location of the neutral axis, which establishes the pitch diameter of the sheave, is determined by the position of the load-carrying cords within the belt cross-section. Differences between sheave effective outside diameters and pitch diameters are included in Table 4.1. Pitch diameters, rather than outside diameters, should always be used in calculating speed ratios and belt speeds.

The belt speed (m/s) is calculated as:

$$v = \pi n_2 D_{p2} = \pi n_3 D_{p3} \quad (4.6)$$

where n_2, n_3 = angular speeds of rotation of sheaves 2 and 3, respectively, in rev/s

D_{p2}, D_{p3} = pitch diameters of sheaves 2 and 3, respectively, m

From the above equation we get the following relationship:

$$\frac{n_2}{n_3} = \frac{D_{p3}}{D_{p2}} \quad (4.7)$$

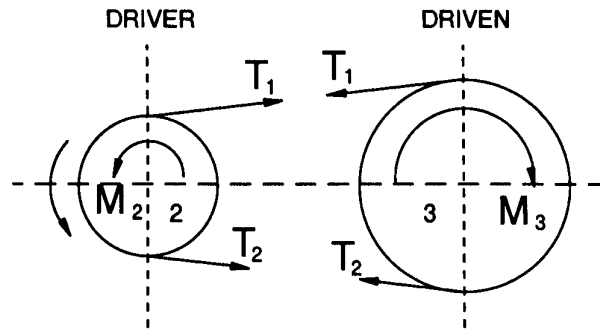


Figure 4.2 – Belt tensions and moments on the sheaves.

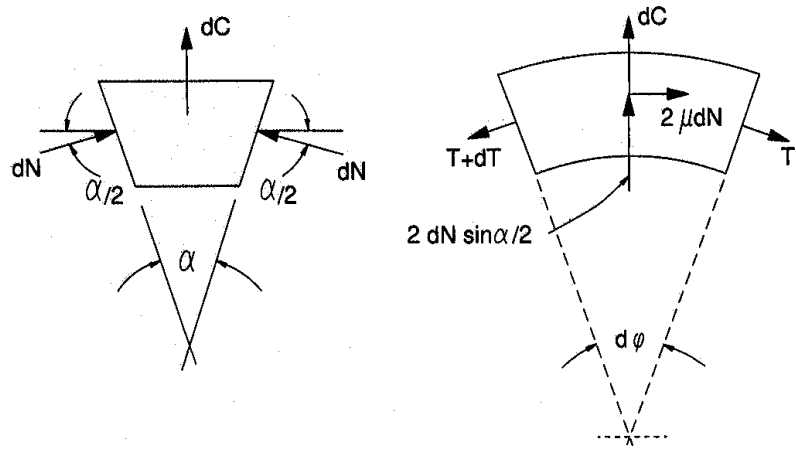


Figure 4.3 – Forces acting on an element of V-belt.

4.1.4 Mechanics of V-belt drives

A V-belt transmits power by virtue of the difference in belt tensions between the point at which it enters a sheave and the point at which it leaves (Figure. 4.2). This difference in tension is developed through friction between the belt sidewalls and the sides of the sheave groove. The wedging effect as the belt is pulled into the groove because of belt tension greatly increases the potential driving force.

Figure 4.3 shows the forces acting on a segment of the belt as it wraps around the sheave. In a belt drive there is a tight side and a slack side of the belt. In the free body diagram as shown in Figure 4.3, $T + dT$ represents the tight side tension, T represents the slack side tension, dC is the centrifugal force, dN is the normal sheave reaction force, and μdN is the frictional force.

The centrifugal force (dC) is given by:

$$dC = \frac{dm v^2}{R} \quad (4.8)$$

where dm = mass of the belt element, kg
 R = pitch radius, m
 v = belt speed, m/s

Elemental belt mass (dm) can be obtained by multiplying the density of the belt material by its volume as follows:

$$dm = \rho_b a R d\phi \quad (4.9)$$

where ρ_b = density of the belt material, kg/m^3
 a = belt cross-section area, m^2
 $d\phi$ = elemental wrap angle, rad

Substituting Equation 4.9 into Equation 4.8 we obtain:

$$dC = \rho_b a v^2 d\phi \quad (4.10)$$

Summing forces in the radial direction we get:

$$dC + 2dN \sin(\alpha/2) - T \sin(d\phi/2) - (T + dT) \sin(d\phi/2) = 0 \quad (4.11)$$

Let $dN = p_N R d\phi$, where p_N is the normal reaction force per unit belt length. Substituting the expressions for dC and dN in Equation 4.11 and taking the limit we get:

$$\rho_b a v^2 + 2p_N R \sin(\alpha/2) - T = 0 \quad (4.12)$$

If the belt is not transmitting any power, the tension in the belt would only be due to the centrifugal force, i.e., $T_c = \rho_b a v^2$. Substituting T_c in Equation 4.12 and solving for p_N we get:

$$p_N = \frac{T - T_c}{2R \sin(\alpha/2)} \quad (4.13)$$

Summing forces in the tangential direction we get:

$$(T + dT) \cos(d\phi/2) - T \cos(d\phi/2) - 2\mu p_N R d\phi = 0 \quad (4.14)$$

which in the limit becomes:

$$dT - 2\mu p_N R d\phi = 0 \quad (4.15)$$

Substituting for p_N , letting $k = \mu / \sin(\alpha/2)$, and rearranging we get:

$$\frac{dT}{T - T_c} = \frac{\mu}{\sin(\alpha/2)} d\phi \quad (4.16)$$

Integrating we get:

$$\int_{T_2}^{T_1} \frac{dT}{T - T_c} = k \int_0^{\theta} d\phi \quad (4.17)$$

Carrying out the integration, applying the limits, and rearranging we get:

$$\frac{T_1 - T_c}{T_2 - T_c} = e^{k\theta} \quad (4.18)$$

If the belt speed is low, T_c may be eliminated in the above equation. The k is sometimes referred to as the effective coefficient of friction.

Power transmitted by a V-belt drive is determined by the effective pull and the belt speed as given by the following equation:

$$P = \frac{(T_1 - T_2)v}{1000} \quad (4.19)$$

where T_1 = tight-side tension, N
 T_2 = slack-side tension, N
 P = power transmitted, kW
 v = belt speed, m/s
 $T_1 - T_2$ = effective pull, N

It is customary to calculate tensions on the basis of a design power load that is somewhat greater than the average load to be transmitted, thus allowing for the effects of overloads or fluctuating loads. The design power for each driven wheel in a drive system is determined by multiplying the actual power by an appropriate service factor. Recommended values for service factors in agricultural machinery applications are included in Table 4.3 and range mostly from 1.2 to 1.5.

Table 4.3. Service factor and service life for some agricultural machines (Gates rubber company).

Machine or Operating Unit	Service Factor	Service Life, h
Combine cylinder	1.5	1000-2000
Sickle bar	1.5	1000-2000
Straw walker	1.0	1000-2000
Cleaning shoe	1.0	1000-2000
Stalk shredder	1.5	400-1000
Hay rake	1.2	600-1200
Ensilage cutter	1.5	500-1000
Ensilage blower	1.5	500-1000
Hay conditioner	1.5	800-2000
Delivery auger	1.3	400-1000
Tree shaker harvester	1.5	400-1000
Peanut digger	1.3	800-1600
Orchard sprayer	1.3	800-2000

If the ratio between the tight-side and slack-side tensions is too great, belt slippage will be excessive. Slippage in a properly designed drive should not exceed 1% to 2%. If the ratio is smaller than it needs to be, unnecessarily high tensions will be needed for a given effective pull, thereby reducing belt life. The maximum allowable tension ratio is:

$$R_{a\theta} = \frac{T_1}{T_2} = e^{k\theta} \quad (4.20)$$

In designing a drive with a V-belt in a V-sheave, a tension ratio of $R_{aB} = 5$ (allowable tension ratio for 180° arc of contact) is commonly assumed. This gives a value of $k = 0.512$. A somewhat higher tension ratio is permissible if automatic tensioning is provided. For a V-belt running on a flat pulley, a value of $R_{aB} = 2.5$ is satisfactory ($k = 0.292$).

When the arc of contact is less than 180° , the allowable tension ratio is less, as indicated by Equation 4.20, thus requiring higher values of T_1 and T_2 for a given effective pull and power. For example, if an effective pull of 360 N is required for the design power, values of T_1 and T_2 would be 450 N and 90 N, respectively, if the arc of contact on a grooved sheave is 180° ($R_{aB} = 5$). But if the arc of contact is only 120° , the maximum allowable tension ratio is 2.9, requiring tensions of 549 and 189 N. Flat, backside idlers are often employed to effect tensioning and, at the same time, increase the arcs of contact on the loaded sheaves.

In a two-sheave drive without an idler, the smaller sheave is the critical one in regard to tension ratio (slippage) because it has the smaller arc of contact. In a V-flat, two-wheel drive without an idler, the sheave and the flat pulley have equal maximum allowable tension ratios when the arc of contact is about 130° on the sheave and 230° on the flat pulley. When a drive has more than one driven sheave or pulley, tensions must be determined in a cumulative manner. All tensions in the system must be adjusted so that no wheel has a tension ratio greater than its allowable value. In a multi-wheel drive, the driver is usually the one most likely to slip.

4.1.5 Stresses and service life

Stresses in a V-belt drive arise from the effective pull needed for the power load, slack-side tension needed to prevent slippage, bending around each wheel, and centrifugal forces acting on the belt. The bending tension, T_b , in the outer fibers of a belt with a given cross section is inversely proportional to the wheel diameter. The tension due to centrifugal force may be expressed as:

$$T_c = wv^2 \quad (4.21)$$

where T_c = centrifugal tension, N

w = belt mass, kg/meter of belt length

The tensions in a three-sheave drive are illustrated in Figure 4.4. The slack-side tension is T_3 and the differences, $T_2 - T_3$, $T_1 - T_2$, and $T_1 - T_3$, represent the effective pulls needed to transmit the power. Note that there is one peak tension at each wheel. It has been determined experimentally that a V-belt usually fails from fatigue caused by repetition of peak tensions and that the average fatigue life of a belt is predictable if loads are accurately known or can be estimated.

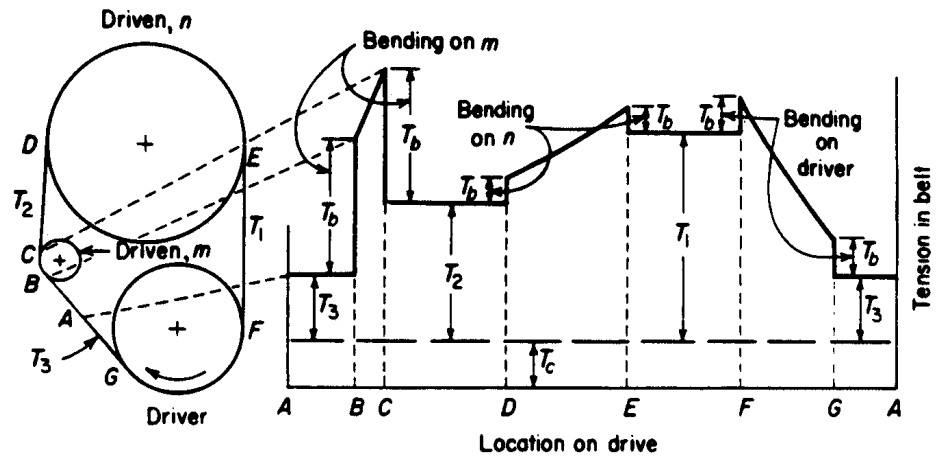


Figure 4.4 – Belt tensions in relation to position on a three-sheave drive (Gates Rubber Co.; reprinted from Kepner et al., 1978).

The Gates Rubber Co. has developed a design method for predicting the service life of a V-belt that includes the effects of the following factors:

- The number of wheels on the drive.
- The design power for each wheel (including an appropriate service factor for each driven wheel).
- The belt speed.
- The arc of contact for each wheel.
- The sequence of loaded wheels and idlers on the drive.
- The pitch diameter of each wheel.
- The stress-fatigue characteristics and cross-sectional dimensions of the particular type and cross-section of belt being considered.
- The belt length.

The Gates system is based on the determination (from an empirical equation or nomographs) of a “fatigue rate” corresponding to the peak tension for each wheel at a given belt speed. The units of the fatigue rate are millimeters of belt length per 100 h of life. The fatigue rates for the individual wheels are added together to obtain the total fatigue rate for the particular size and type of belt being considered for the drive. The calculated average service life of the belt at a given speed is:

$$\text{Belt Service Life (h)} = \frac{\text{Belt length(mm)} \times 100}{\text{Total Fatigue Rate}} \quad (4.22)$$

For a given tight-side tension and wheel pitch diameter, increasing the belt speed increases the fatigue rate, primarily because of the greater frequency of stress cycles but also because of increased centrifugal tension at high speeds. (The transmitted power would be increased also.)

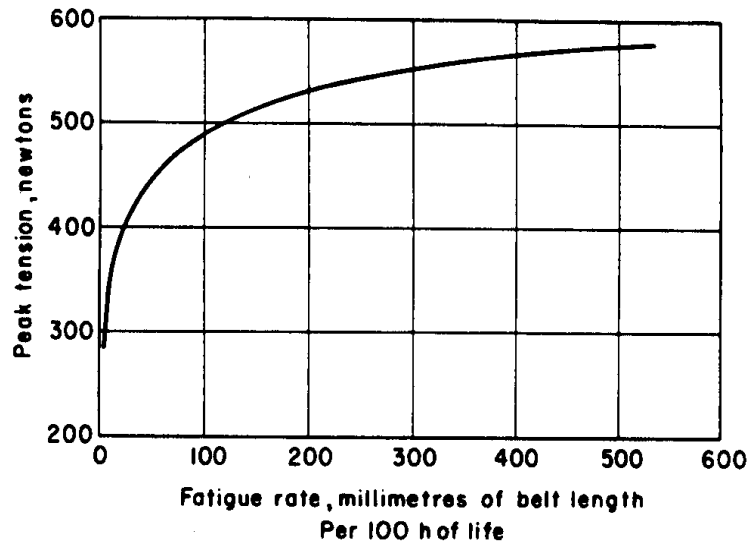


Figure 4.5 – Typical relation between tension and fatigue rate for one V-belt cross section and one speed (Gates Rubber Co.; reprinted from Kepner et al., 1978).

The relation of fatigue rate to tension and speed for each type or quality of belt and each cross section is determined experimentally by means of durability tests in the laboratory, from which constants in a generalized equation are evaluated. A typical curve for one speed is shown in Figure 4.5. Essentially, a tension-fatigue-rate curve is the inverse of the usual S-N curve (stress vs. fatigue cycles).

In designing a drive, the sequence of the driven sheaves or pulleys affects the magnitudes of the peak tensions and hence the service life. If a multiple sheave drive can be arranged so the belt leaving the driver comes to the driven sheaves in order of increasing power requirements, the magnitudes of tension peaks for the low-power sheaves will be minimized. Exceptionally small-diameter sheaves should be in belt spans of lesser tension to avoid the combination of a high tight-side tension and a high bending tension. An idler, if used, should be in the span with the least tension.

Increasing the sheave diameters on a particular drive, if feasible, reduces both the bending stresses and the required effective pull and may even permit the use of a smaller belt cross section. Centrifugal tension is seldom a limiting factor at speeds encountered in agricultural machinery drives.

4.1.6 Variable-speed V-belt drives

An adjustable-pitch V-belt sheave has provision for moving one face axially with respect to the other, thus changing the radius at which the belt operates. Some adjustable-pitch sheaves can be changed only when stopped, but others can be changed while in motion (Figure. 4.6). In this textbook, the term “variable-speed drive” implies the ability to change the speed ratio over the entire range of control while the drive is in operation and under load.

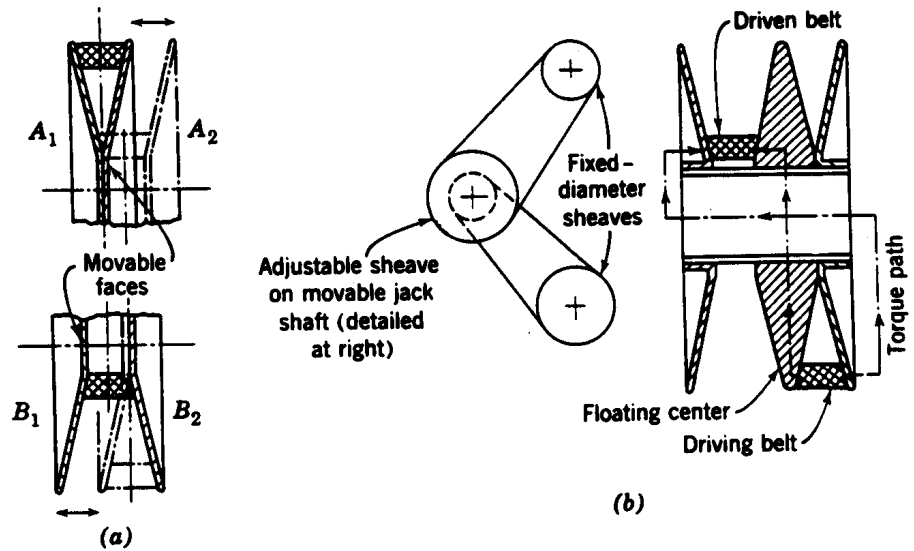


Figure 4.6 – (a) Arrangement with two adjustable-pitch sheaves on fixed centers. (b) Double adjustable-pitch sheave with floating center (reprinted from Kepner et al., 1978).

Belts designed specifically for variable-speed drives are wider than conventional V-belts in relation to their thickness. The extra width is necessary to obtain reasonable ranges of speed ratio as well as increased load capacities. Relatively thin belts are needed because minimum operating diameters are generally small in this type of drive.

With adjustable-speed sheaves and V-belts as shown in Tables 4.1 and 4.2, maximum speed-range ratios ranging from 1.75 for HI belts to 1.9 for HM belts are obtainable when one adjustable pitch sheave of the minimum allowable diameter is used in conjunction with a fixed-diameter sheave. The range for a given belt size varies inversely with the sheave diameter, since the maximum change in pitch diameter is fixed by the 26° groove angle and the belt top width (Figure 4.6a).

The speed range for a combination of two adjustable-pitch sheaves is the product of the two individual ranges. When both sheaves have the minimum recommended diameter, the maximum speed ratio varies from 3.0 for HI belts to 3.7 for HM belts. The most common arrangement is with the two sheaves on fixed centers, as shown in Figure 4.6a. If the faces A₁ and B₂ are fixed axially while A₂ and B₁ are moved simultaneously, proper belt alignment is maintained at all speed ratios because the entire belt moves axially.

A third arrangement has two adjustable-speed belts in tandem and a double adjustable-pitch sheave with floating center section, as shown in Figure 4.6b. The speed ratio is changed by moving the adjustable-pitch sheave along a path that keeps the sum of the required belt lengths constant as the floating center changes its lateral position. This system is subject to belt misalignment as discussed above for arrangements employing a single adjustable pitch sheave.

4.1.7 V-belt drive design

The Gates design procedure is summarized below:

1. Determine the design power of the drive by multiplying the actual power demand by the service factors. Table 4.3 shows examples of service factors as recommended by the Gates Rubber Co.
2. Determine the belt type and cross section based on the design power. The selection of belt type and cross-section is based on the pitch diameter of the driver and the drive sheaves and their speeds. Graphs used to select appropriate belt sections based on the speed of faster shaft and the design power are given by Gates Rubber Co. (1976). As the design power increases for a constant shaft speed larger belt sections are required. Also, if the shaft speed decreases, bigger belts would be necessary to transmit the same power.
3. Layout the drive and determine pitch diameters of the driver and all driven sheaves, and calculate approximate belt length. Also, find arc of contact for each sheave.
4. The next step is to determine belt tension ratios, effective pull, and span tensions. These are computed using the equations given above.
5. Determine total fatigue rate and service life by peak tension at a given belt speed. The nomograms to determine the fatigue rate are given in the Gates manual.
6. The estimated belt life should be compared with the recommended values as given in Table 4.3. If the calculated belt life is not acceptable then make one or more of the following changes:
 - Increase the number of belts.
 - Increase the smallest diameter.
 - Change the belt cross section.
 - Increase the belt length or reduce speed.
 - Reduce the torque.

4.2 CHAIN DRIVES

Perhaps the first use of a chain drive was made in a reaper by Cyrus McCormick in 1837. Today chain drives play an important part in many agricultural machines such as hay balers, corn pickers, combines, cotton pickers, and beet harvesters. As opposed to V-belt drives, chain drives are used where it is important to maintain an exact speed ratio. Another benefit is that chain drives are capable of transmitting a large amount of power at slower speeds. However, chain drives require better shaft alignment and more maintenance than V-belt drives.

4.2.1 Types of chains and standardization

Roller chains are of two types, either standard-pitch or double-pitch. Other types of chains include detachable-link chains, cast roller chains, and pintle chains.

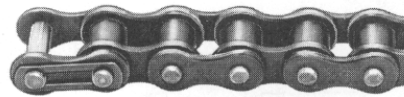
Standard-pitch roller chain, double-pitch roller chain (the pitch of a chain is the effective length of one link), and detachable-link chain (Figure. 4.7) are commonly used in agricultural machines. All roller chains are so constructed that the rollers rotate when contacting the teeth of the sprocket. Roller chains may be used in a single or

multiple strand arrangement. Standardized dimensions for each of these types have been adopted by the American Standards Association (ASA). The standard dimensions of roller chains are given in Table 4.4.

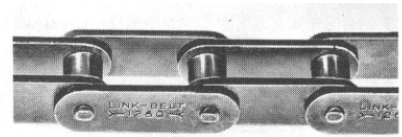
Standard-pitch roller chain drives are satisfactory at linear speeds from less than 0.5 m/s up to 20 m/s and are well suited for heavy loads requiring a compact drive. The maximum permissible speed decreases as the pitch is increased. Multiple-width chains of short pitch can be used for extremely compact drives at high speeds. Roller chains are precision-built and under favorable conditions may have efficiencies as high as 98% to 99%.

Sprockets may be driven from either the inside or the outside of a roller chain. Although oil-bath lubrication is recommended for high-speed drives, this system often is not practical on agricultural machines. Standard-pitch roller chain is several times as expensive as steel detachable-link chain.

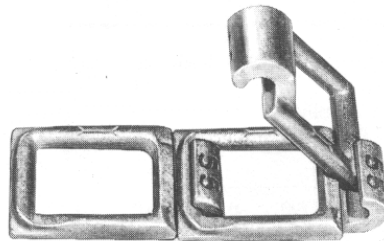
Double-pitch roller chain employs the same pins, bushings, and rollers as standard-pitch roller chain, but the side plates have twice the pitch. Thus, double-pitch chains have the same strength and precision as corresponding standard-pitch chains but less mass. They are less expensive than standard-pitch roller chains, but considerably more expensive than steel detachable-link chain. Double-pitch chains are suitable for slow and moderate-speed drives. Because the roller diameter is only $\frac{5}{16}$ of the pitch, there is ample space for sprocket teeth, and precision, cast-tooth sprockets are satisfactory (and more economical than machine-cut teeth).



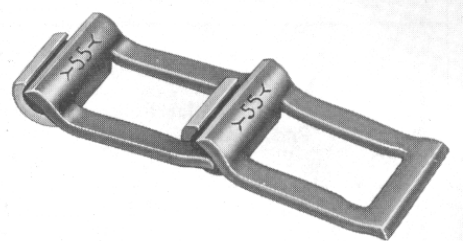
Standard-pitch roller chain



Double-pitch roller chain



**Malleable-cast-iron,
detachable-link chain**



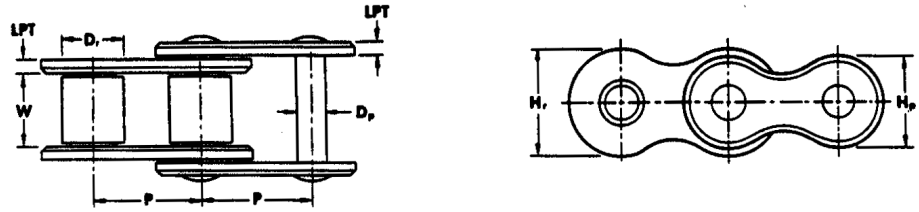
**Pressed-steel,
detachable-link chain**

**Figure 4.7 – Four types of drive chain common on farm machines
(reprinted from Kepner et al., 1978).**

During the 1950s several companies developed chains that are physically interchangeable with standard-pitch and double-pitch roller chains but which are self-lubricating. Self-lubricating chain has oil-impregnated, sintered-steel bushings at the joints, replacing the bushings and rollers of conventional roller chain. It was designed for applications where external lubrication is impossible or impractical. Many farm machinery applications fall into this category. However, because this chain does not have rollers, it is not recommended for high speeds or extremely heavy loads.

The cost of standard-pitch or double-pitch self-lubricating chain is the same as that of the corresponding size of conventional roller chain. Ultimate strengths are perhaps 5% to 20% lower. Laboratory tests and field experience have indicated that, for a given load and a given allowable percentage elongation due to wear, the service life of a self-lubricating chain is several times as great as that of non-lubricated conventional roller chain. But, where a conventional chain can be adequately lubricated, it will outperform the self-lubricating chain.

Table 4.4. General chain dimensions, in mm (inches). (Reproduced from *Identification, installation, lubrication and maintenance of power transmission roller chains in ANSI B29.1 and ANSI B29.3*, by permission of the American Chain Association, Rockville, MD.)



Standard Chain No.	Pitch P	Max. Roller Diam. D_r	Nominal Width W	Nominal Pin Diam. D_p	Link Plate Thickness LPT	
					Standard Series	Heavy Series
25	6.35 (0.250)	3.30 (0.130)*	3.18 (0.125)	2.30 (0.090)	0.76 (0.030)	—
35	9.52 (0.375)	5.08 (0.200)*	4.78 (0.188)	3.58 (0.141)	1.27 (0.050)	—
41	12.70 (0.500)	7.77 (0.306)	6.35 (0.250)	3.58 (0.141)	1.27 (0.050)	—
40	12.70 (0.500)	7.92 (0.312)	7.92 (0.312)	3.96 (0.156)	1.52 (0.060)	—
50	15.88 (0.625)	10.16 (0.400)	9.52 (0.375)	5.08 (0.200)	2.03 (0.080)	—
60	19.05 (0.750)	11.91 (0.469)	12.70 (0.500)	5.94 (0.234)	2.39 (0.094)	3.18 (0.125)
80	25.40 (1.000)	15.87 (0.625)	15.87 (0.625)	7.92 (0.312)	3.18 (0.125)	3.96 (0.156)
100	31.75 (1.250)	19.05 (0.750)	19.05 (0.750)	9.52 (0.375)	3.96 (0.156)	4.75 (0.187)
120	38.10 (1.500)	22.22 (0.875)	25.40 (1.000)	11.10 (0.437)	4.75 (0.187)	5.56 (0.219)
140	44.45 (1.750)	25.40 (1.000)	25.40 (1.000)	12.70 (0.500)	5.56 (0.219)	6.35 (0.250)
160	50.80 (2.000)	28.57 (1.125)	31.75 (1.250)	14.27 (0.562)	6.35 (0.250)	7.14 (0.281)
180	57.15 (2.250)	35.71 (1.406)	35.71 (1.406)	17.45 (0.687)	7.14 (0.281)	7.92 (0.312)
200	63.50 (2.500)	39.67 (1.562)	38.10 (1.500)	19.84 (0.781)	7.92 (0.312)	9.52 (0.375)
240	76.20 (3.000)	47.62 (1.875)	47.62 (1.875)	23.80 (0.937)	9.52 (0.375)	12.70 (0.500)

*Bushing diameter, these chains have no rollers.

An agricultural double-pitch roller chain has been developed that is dimensionally the same as the regular double-pitch chain but has a lower cost because of different materials and because the joints have more clearance, thus permitting greater manufacturing tolerances. Performance is said to be somewhat inferior to that of regular double-pitch chain.

Steel detachable-link chains are used extensively on agricultural implements, both for transmitting power and in conveyors and elevators. This is the least expensive type of chain and it is well suited for moderate loads at speeds not exceeding 2 to 2.5 m/s. Under dirty conditions, detachable-link chains are subject to greater wear than roller chains because of the loose-fitting, open hooks. Detachable-link chains usually are not lubricated, because the lubricant would tend to retain grit particles in the joint.

An improved type of “high-fatigue” steel detachable-link chain, developed in the early 1950s, is said to have one-third more tensile strength than conventional steel detachable-link chain, and more than twice the fatigue strength. The hook is rolled up from material in front of the link rather than from the material punched out from the center. It is more expensive than the conventional type.

Pintle chain is composed of identical links with hollow cored cylinders cast or forged integrally with two offset side bars. The links are jointed by pins inserted in holes in the ends of the side bars in through the cored cylinders.

4.2.2 Geometry of chain drives

The pitch diameter is a function of the chain pitch and the number of teeth in the sprocket. Referring to Figure 4.8, the pitch diameter is given by:

$$PD = \frac{P}{\sin(180/N)} \quad (4.23)$$

where P = the chain pitch

N = the number of teeth in the sprocket

The length (L) is determined in pitches and is approximated by the following formula:

$$\frac{L}{P} = \frac{2C}{P} + \frac{N_1 + N_2}{2P} + \frac{(N_2 - N_1)^2}{4\pi^2(C/P)} \quad (4.24)$$

where C is the center distance between the sprockets and N_1 and N_2 are the number of teeth on the two sprockets.

4.2.3 Kinematics of chain drives

Since a sprocket is essentially a polygon with as many sides as there are teeth or pitches, either the chain speed or the angular velocity of the sprocket must vary as the chain engages or leaves the sprocket due to the chordal action as shown in Figure 4.9.

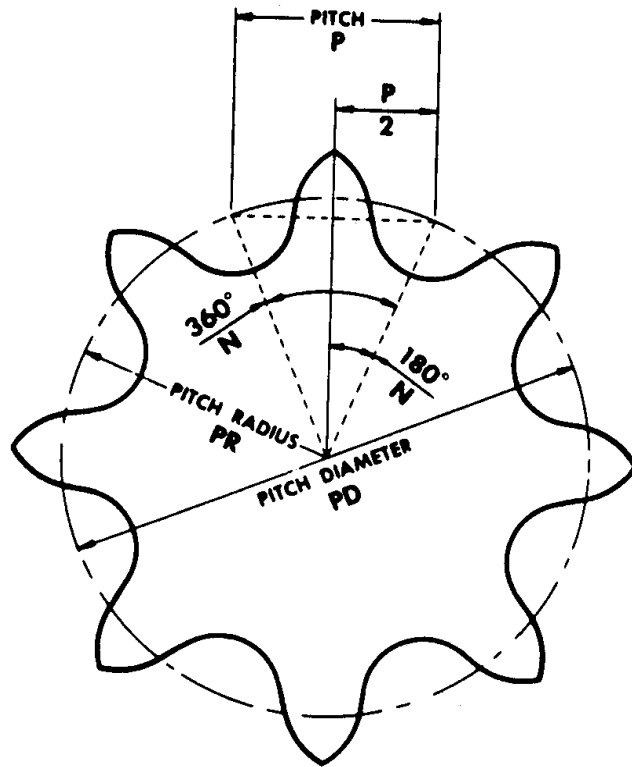


Figure 4.8 – Computation of sprocket pitch diameter
 (reproduced from *Chains for Power Transmission and Material Handling*,
 by permission of the American Chain Association, Rockville, MD).

The fewer teeth there are on the sprocket, the greater is the speed variation. Theoretically, a 10-tooth sprocket would give a variation of about 5%. Practically, however, small speed variations as well as sudden load shocks tend to be absorbed or cushioned by the natural elasticity of the chain and the catenary effect of the driving side. Although sprockets with as few as six teeth are available, sizes with less than 17 or 18 teeth are not recommended for high-speed drives. The chordal speed variation is given by:

$$\frac{\Delta v}{v} = \frac{\pi}{N} \left(\frac{1}{\sin(180/N)} - \frac{1}{\tan(180/N)} \right) \quad (4.25)$$

where the chain velocity is $v = NPn$ and $n =$ angular speed in rev/s.

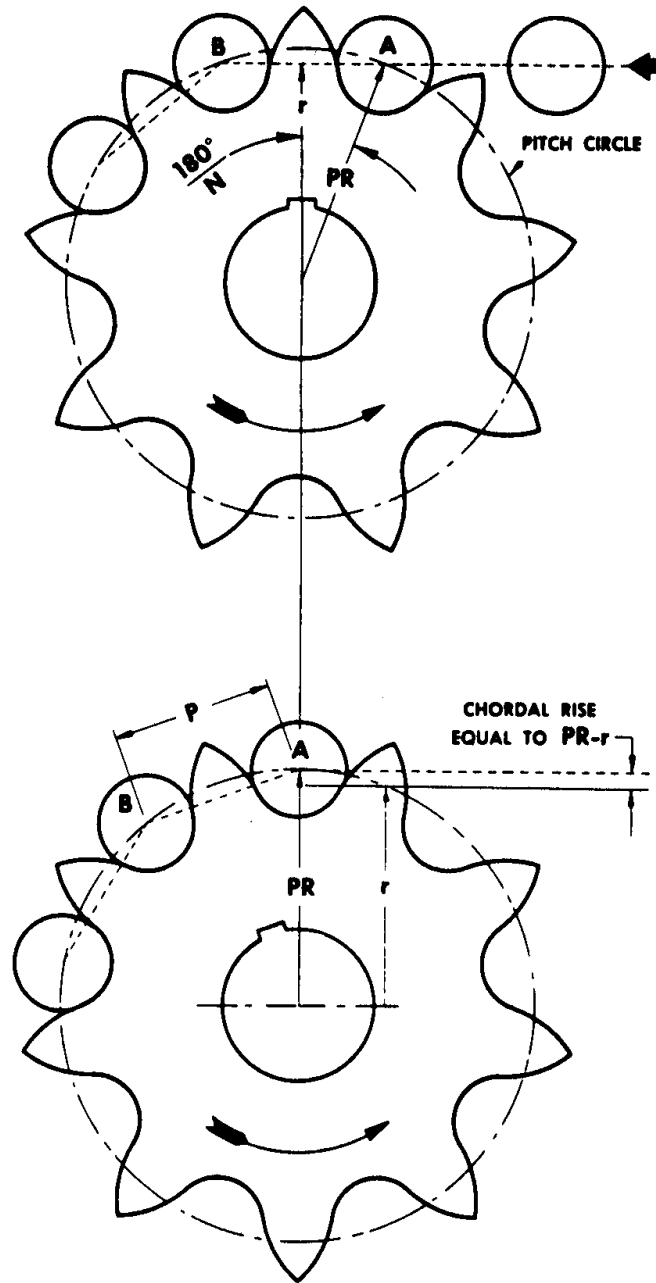


Figure 4.9 – Chordal action of chain
 (reproduced from *Chains for Power Transmission and Material Handling*,
 by permission of the American Chain Association, Rockville, MD).

4.2.4 Design of chain drives

In general, the load capacity of a chain is based upon the rate of wear rather than on the ultimate strength. Because wear is mainly due to the hinge action as the chain engages or leaves a sprocket, the rate of wear is greater with small sprockets than with large ones. The rate of wear is also directly related to chain speed and inversely related to chain length. As a chain wears, the pitch length increases and the chain rides farther out on the sprocket teeth. The more teeth a sprocket has, the sooner the chain will ride out too far and have to be replaced. For this reason, speed ratios should not exceed 10:1 for standard-pitch roller chain or 6:1 for other chains.

Power ratings published in chain catalogs are for the relatively long life expected in industrial applications. As in designing V-belt drives, actual power requirements are multiplied by appropriate service factors to obtain design power. Because of the shorter life requirements on agricultural machines in comparison with industrial applications, somewhat greater loadings are often acceptable. However, unfavorable environmental conditions may tend to shorten the life.

Chain selection for extremely slow drives is sometimes based on ultimate strength rather than wear rate. With roller chains, the recommended maximum ratios of working load to ultimate strength range from 0.2 at 0.13 m/s to 0.1 at 1.3 m/s. Conventional steel detachable-link chain has inherent stress concentration points that promote early fatigue failures if the chain is loaded to more than 10% of its ultimate strength. The pull required for a given power and speed can be determined from Equation 4.19. T_2 is assumed to be zero, since a chain should run with essentially no slack-side tension. Chain speed in meter per second = (chain pitch, mm/1000) \times (number of teeth on sprocket) \times (sprocket $r/\text{min} \div 60$).

The chain drive design procedure, in general, includes the following steps:

1. *Design power.* A service factor based on the type of power source and the nature of load is selected to determine the design power. Table 4.5 gives the recommended values for service factors. Design power is determined by multiplying transmitted power by the service factor.
2. *Tentative chain selection.* Once the design power is determined chain pitch is selected based on Figure 4.10.
3. *Selection of small sprocket.* The sprocket selected must be large enough to accommodate the shaft. For a given chain speed and power the effect of increasing the number of teeth on the sprocket is to increase the linear speed of chain and to decrease the pull and to decrease the chordal action. This results in a quieter drive with less impact.
4. *Selection of large sprocket.* After selecting the small sprocket the desired speed ratio is used to determine the number of teeth on the large sprocket. It is recommended that the speed ratios greater than 10:1 should not be attempted in a single drive.
5. *Determine chain length and center distance.* The chain length is a function of number of teeth on both sprockets and the center distance. It is preferred that the chain consist of an even number of pitches in order to avoid an offset link. The center distance is based on the physical requirements of the application. The chain length is calculated by using Equation 4.24.

Table 4.5. Service factors of roller chains (reproduced from *Chains for Power Transmission and Material Handling*, by permission of the American Chain Association, Rockville, MD).

Type of Driven Load	Type of Input Power		
	Internal Combustion Engine with Hydraulic Drive	Electric Motor or Turbine	Internal Combustion Engine with Mechanical Drive
Smooth	1.0	1.0	1.2
Moderate shock	1.2	1.3	1.4
Heavy shock	1.4	1.5	1.7

6.

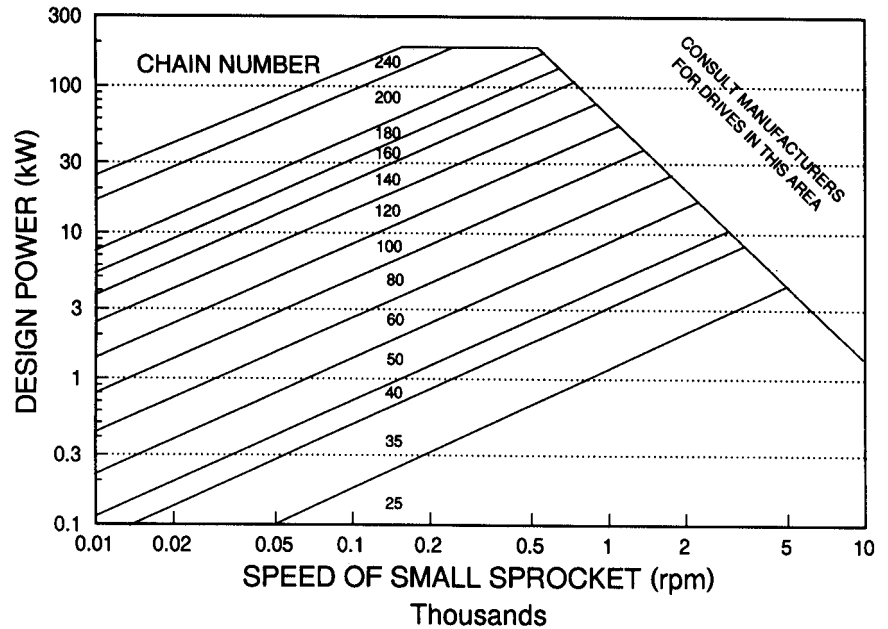


Figure 4.10 – Roller chain pitch selection chart (redrawn from *Chains for Power Transmission and Material Handling*, by permission of the American Chain Association, Rockville, MD).

4.3 POWER-TAKE-OFF DRIVES

A power-take-off (PTO) drive provides a means for transmitting rotary power to machines that are coupled to a tractor. The most common location for the PTO shaft is at the rear of the tractor (see Figure. 4.11), but some tractors have auxiliary PTO shafts at other locations. The direction of rotation, rotational speed, approximate location, and exact dimensions of the PTO shaft were standardized by the ASAE in 1926 so that equipment of different manufacturers could be interchanged. With growth in tractor

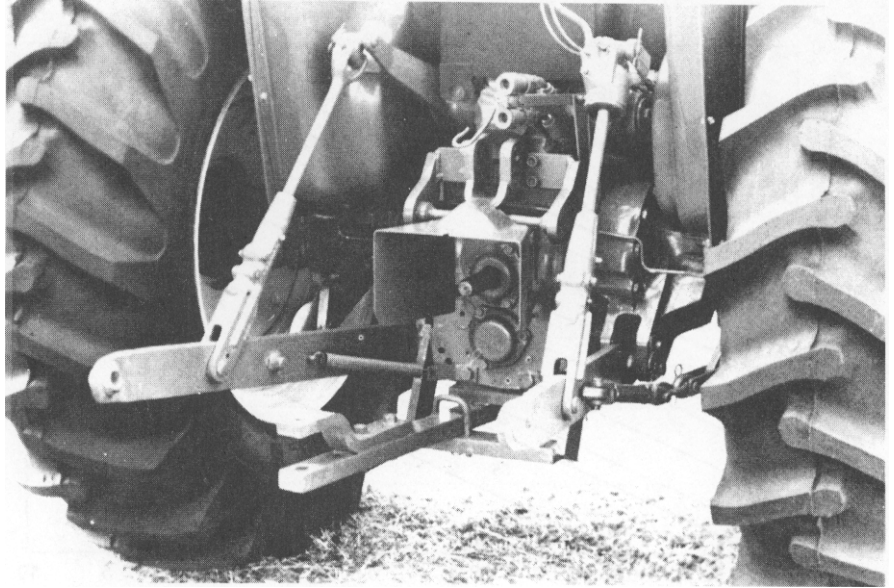


Figure 4.11 – A tractor PTO drive.

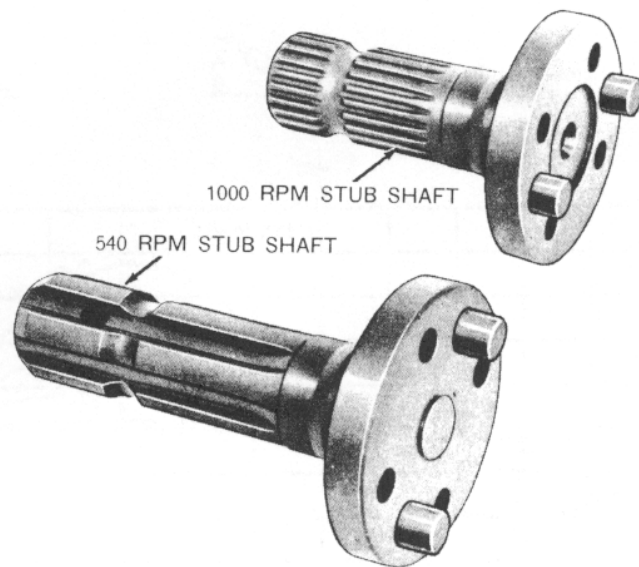


Figure 4.12 – Splines for 540 and 1000 rev/min PTO shafts (courtesy of Deere and Co.).

size, it became necessary to develop faster and larger PTO shafts to transmit the increased available power. There are now three standard PTO shafts. Illustrated in Figure 4.12 are the 35 mm (diameter) shafts with standard rotation speeds of 540 rev/min and 1000 rev/min. The shaft with a standard speed of 540 rev/min is used on tractors with up to 65 kW PTO power. The 35 mm shaft with a standard speed of 1000 rev/min is used on tractors with 45 to 120 kW of PTO power. Note the power overlap, i.e., tractors in the 45 to 65 kW power range could be equipped with either of the shafts in Figure 4.12. The 45 mm shaft with a standard speed of 1000 rev/min is not shown in Figure 4.12; it is similar in appearance to the other 1000 rev/min shaft, except that it is larger in diameter and has 20 splines instead of 21. It is used on tractors of 110 to 190 kW of PTO power. Some large, four-wheel-drive tractors, used primarily for traction, do not have PTO drives.

Early PTO drives were driven from the tractor transmission and stopped rotating whenever the traction clutch was disengaged. Present standard practice is to provide an independent PTO which is controlled by its own separate clutch. Figure 4.13 illustrates the most common type of universal joint drive that is used for transmitting power from the PTO shaft to an implement. Two Cardan universal joints are included and the connecting shaft is telescoping to accommodate changes in angularity and distance between the implement and tractor. An integral shield surrounds the shaft and partially surrounds each joint. The shield normally rotates with the shaft but can stop if it contacts a person or other object. A single Cardan joint creates fluctuations in drive line rotation when operating at an angle, as shown in Figure 4.14. The curves in Figure 4.14 are based on the following equation:

$$\tan(\phi_{jo}) = \cos(\alpha) \tan(\phi_{ji}) \quad (4.26)$$

where ϕ_{jo} = angular displacement of joint output shaft, radians

α = joint angle (see Figure. 4.14)

ϕ_{ji} = angular displacement of joint input shaft, radians

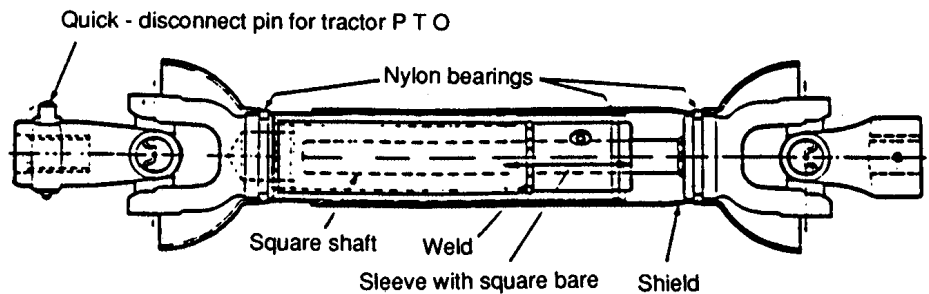


Figure 4.13 – A telescoping PTO shaft with integral safety shield (courtesy of Neapco Products, Inc.).

The relationship between shaft velocities is:

$$\frac{n_{jo}}{n_{ji}} = \frac{\cos(\alpha)}{1 - \sin^2(\alpha)\sin^2(\phi_{ji})} \quad (4.27)$$

where n_{ji} , n_{jo} = speeds of joint input and output shafts, respectively, in rev/min. When two Cardan joints are connected in series, as in Figure 4.13, the velocity fluctuations will cancel if the two joint angles are equal and the joints are 90° out of phase. Proper phasing is accomplished when the yokes connected to the two ends of the intermediate shaft are in line with each other. Then the velocity fluctuations are canceled in the output shaft but not in the intermediate shaft. Constant speed universal joints, such as the Bendix-Weiss joint, can transmit power through an angle without introducing the speed fluctuations of the Cardan joint. Although the Bendix-Weiss joints transmit torque more smoothly, they are not well suited for the high torque levels often encountered in agricultural equipment.

Experimental tests have shown that peak torques in a PTO driveline far exceed average torques. Thus, drive lines are designed on the basis of fatigue stresses imposed by repeated peak torques. One technique for reducing fatigue stresses is to limit the joint angles encountered during normal operations when the tractor and implement are not in a turn.

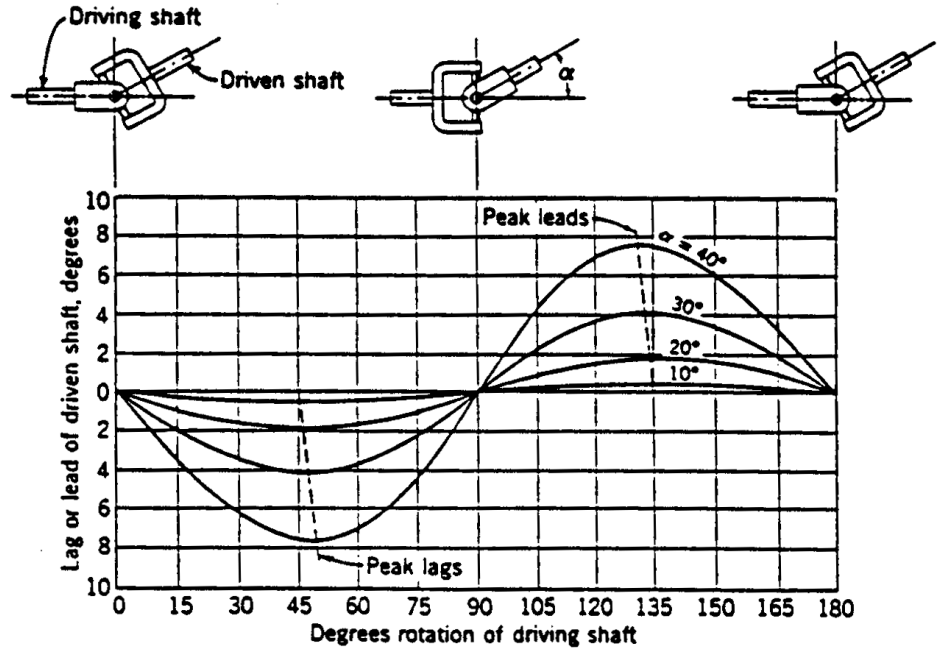


Figure 4.14 – Lead or lag of shaft driven by a Cardan-type universal joint, in relation to rotational position of the driving shaft (reprinted from Kepner et al., 1978).

4.4 OVERLOAD SAFETY DEVICES

In many types of farm machinery, a single power source drives various components that have widely differing power requirements and are subject to varying degrees of possible overload. In such a system some overload protection is almost mandatory, especially for the lower-powered components. Three general types of safety devices commonly used in rotary drives are:

- Those that depend upon shearing of a replaceable connecting member in the drive.
- Units in which spring force holds two corrugated members together, utilizing the principle of the inclined plane. These devices are also called jump clutches.
- Devices depending entirely upon friction.

4.4.1 Shear devices

Shear devices are simple and relatively inexpensive, but the sheared element must be replaced after each overload. Thus, they are most suitable where overloads are rather infrequent. Shear devices can be designed for almost any desired load rating, although pin or key sizes become rather small for low torque ratings unless a material with low shear strength is selected. Typical arrangements for shear devices are:

- Shear key between the shaft and hub (usually a brass key, with a tapered shaft and bore).
- Diametral shear pin through the hub and shaft (gives double shear).
- Flange-mounted shear pin parallel to the shaft, as illustrated in Figure 4.15.

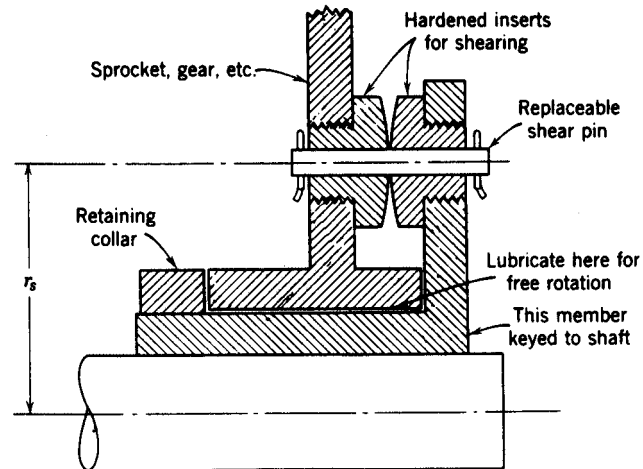


Figure 4.15 – An arrangement with a flange-mounted shear pin. The hardened shearing inserts could be omitted, particularly if overloads are expected only infrequently or if necked-down shear pins are used (reprinted from Kepner et al., 1978).

Regardless of the arrangement, the driving and driven members must rotate freely with respect to each other after the shear element has failed. With either of the first two types, the shaft or bore is likely to be scored by the sheared element. Removal of the hub from the shaft may be necessary in the first type to replace a sheared key.

The flange-mounted shear pin is the most easily replaced, but the unit is more costly than a diametral pin and not as well adapted to low torques because of the greater radius to the shear section. For experimental testing, interchangeable pins necked down to different diameters can be used to vary the load at which failure occurs. In production units, a full-sized pin of an ordinary material (such as hot-rolled steel) is desirable for convenience of replacement by the operator.

The torque at which a flange-mounted shear pin will fail, and the power, are given by the following equations:

$$T = r_s \left(\frac{\pi}{4} d_1^2 S_s \right) 10^{-3} \quad (4.28)$$

and
$$kW = \frac{2\pi NT}{60,000} = 8.225 N r_s d_1^2 S_s 10^{-8} \quad (4.29)$$

where N = shaft speed, rev/min

T = torque, N · m

r_s = distance between shaft center and shear pin center (Figure. 4.15), mm

d_1 = diameter of shear pin at shear section, mm

S_s = ultimate shear strength of shear pin, MPa

Similarly, a diametral shear pin (double shear) will fail when:

$$kW = 8.225 N D d_1^2 S_s 10^{-8} \quad (4.30)$$

where D = shaft diameter (diameter at which shear occurs), mm.

4.4.2 Jump clutch devices

A jump clutch has rounded, mating jaws or corrugations that are held together by an adjustable spring. In Figure 4.16, part A is keyed to the shaft and part B, the driving member, is free to rotate on the shaft when an overload occurs. The overload torque required to rotate B with respect to A and cause jumping is a function of the slope of the inclined corrugation faces, the coefficient of friction between the faces, the effective radius from the shaft centerline to the contact area, and the force required to compress the spring and permit axial movement of B with respect to A.

The spring must have sufficient deflection available so it is not compressed solid before the relative displacement of the two corrugated faces is sufficient to permit jumping. Although friction between the corrugated faces influences the magnitude of the torque required for jumping, the unit would function (at a lower torque) even if the coefficient of friction were zero.

Because of its automatic resetting feature, the jump clutch is more suitable than shear devices where overloads may occur rather frequently. There is no slippage until

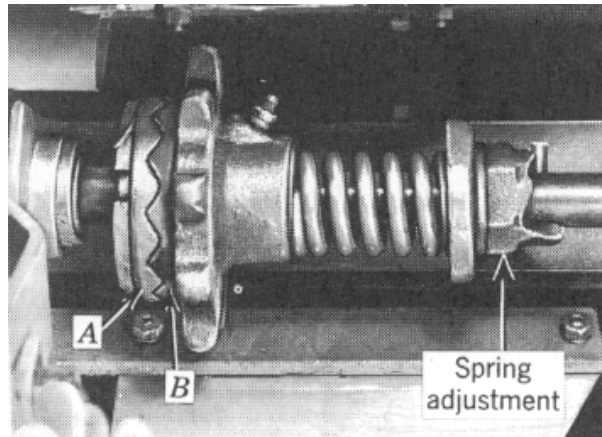


Figure 4.16 – Typical arrangement of a jump clutch (reprinted from Kepner et al., 1978).

the load exceeds the setting of the unit, and then the operator is warned audibly that an overload has occurred. Jump clutches are more expensive than shear devices and are not well suited to large loads because of the excessive physical size required. When they are jumping, they impose high shock loads upon the drive system.

The magnitude and variability of the friction force required to slide the movable member axially can have an important effect upon the torque required to cause jumping. To minimize the axial friction force, the torque should be transmitted to or from the movable member at a relatively large radius, as with a sprocket or sheave, rather than through splines or a key in the shaft.

4.4.3 Friction devices

A properly designed belt drive can serve as a friction safety device, although its performance is affected by variations in belt tension and by the increase in coefficient of friction as the percentage of belt slip increases. The performance is more consistent with a spring-loaded idler than with a fixed adjustment.

Single-plate clutches with two friction surfaces, similar to tractor or automotive clutches, are often used for overload protection. The spring pressure is adjusted to drive normal loads but slip under abnormal loads. In comparison with jump clutches, friction safety clutches have the advantages of more consistent breakaway torque and no damaging peaks during slippage. However, tests have shown that the momentary dynamic torque capacity under sudden load application may be two to three times the static value.

Friction clutches are very effective in protecting a drive from frequent peak torques. But under some conditions it is possible to have a friction clutch slipping sufficiently to become overheated without the operator being aware of the overload.

PROBLEMS

- 4.1 An HB-section V-belt is to transmit 5 kW at a belt speed of 17 m/s. The included angle between the sides of the belt cross section is 38° and the belt density is 1.25 g/cm^3 . The arc of contact of the smaller sheave is 150° . Tensioning is accomplished by changing the position of an adjustable idler (not automatic). Calculate T_1 and T_2 .
- 4.2 A V-belt drive has two sheaves with effective outside diameters of 125 mm and 348 mm. One shaft is to be movable for take-up and the desired center distance is about 460 mm. (a) Using the ASAE Standard S211 and the example therein, select the best normally available effective belt length for an HA belt and determine the maximum and minimum center distances needed for installation and take-up. (b) Calculate the speed of the larger sheave if the smaller sheave runs at 1250 rev/min.
- 4.3 (a) Compute the theoretical percentage variation in speed of a chain as it leaves an 8-tooth sprocket rotating at a uniform speed. (b) Repeat for an 18-tooth sprocket.
- 4.4 A 9-tooth sprocket operating at 200 rev/min drives a 23-tooth sprocket through No. 45 steel detachable-link chain. The pitch of this chain is 41.4 mm and the ultimate strength is 9.34 kN. Calculate the (a) average linear speed of chain in m/s, (b) recommended maximum power in kW, and (c) average torque applied to the drive shaft at recommended power.
- 4.5 The two universal joints of a pair are operating at joint angles of 30° and 22° . The input shaft, intermediate shaft, and output shaft are all in the same plane and the yokes on the two ends of the intermediate shaft are in line. (a) Calculate the lead or lag in each joint for each 15° increment of the input shaft from 0° to 90° . (b) Plot lead or lag versus degree rotation of the input shaft, showing a curve for each joint and one for the system. On each joint indicate where the peak occurs. (c) What changes might be made in this drive system to provide uniform rotation of the output shaft?
- 4.6 Two shafts are connected by a universal joint operating at a joint angle of 30° . The speed of the input shaft is 1000 rev/min. (a) Calculate and plot the speed of the output shaft through one full revolution of the input shaft. (b) Determine the angle of the input shaft at which acceleration of the output shaft is at a maximum.

FLUID POWER, MECHATRONICS, AND CONTROL

5

INTRODUCTION

When fluid power systems gained widespread use on agricultural equipment in the 1940s, physical strength was no longer a necessary qualification for equipment operators. Fluid power permits the raising and lowering of heavy implements with a minimum of physical effort. Also, fluid power can be transmitted to remote locations much more conveniently than mechanical power. In this chapter, you will learn the basic principles and be introduced to the elements of fluid power systems.

5.1 BASIC PRINCIPLES AND ELEMENTS OF FLUID POWER

There are five principles that are important to an understanding of fluid power circuits. They are: (a) liquids have no shape of their own but will flow to acquire the shape of their container, (b) liquids can be considered incompressible at the pressures used in fluid power systems, (c) liquids transmit pressure equally in all directions, (d) the rate of flow from a positive displacement pump varies proportionally with pump speed but is virtually independent of system pressure, and (e) any flow of liquid through a pipe or orifice is accompanied by a reduction in liquid pressure.

Fluid power systems include, at a minimum, a reservoir, one or more pumps to convert mechanical power into fluid power, one or more control valves, one or more actuators to convert the fluid power back into mechanical power, lines to join the various components, and filters to remove contaminants from the hydraulic fluid. Each of these components will be discussed, as well as the types of circuits in which the components can be used.

Making physical drawings of the many components in fluid power systems would be very time consuming and such drawings would not necessarily convey the system logic. Thus, a joint industry conference of the fluid power industry was convened to devise symbols for fluid power components. The resulting symbols were initially called JIC symbols. Later, they were standardized by the International Standards Organization and by the National Fluid Power Association and are now called NFPA symbols. The NFPA symbols are summarized in Appendix B. The NFPA symbols are

analogous to electrical symbols and they simplify the drawing of fluid power circuits in the same way that electrical symbols simplify the drawing of electrical circuits. The shape of every NFPA symbol was chosen to be as self explanatory as possible and you should be able to recognize and use the symbols very quickly. Physical drawings may be used to explain some fluid power components in this chapter, but the corresponding NFPA symbols will also be shown.

5.2 PUMPS

A pump is the heart of any fluid power system; it converts mechanical power into fluid power. Only positive displacement pumps are used in fluid power systems, thus the pump delivery is nearly independent of the pressure at the outlet port of the pump. The three basic types of pumps used in fluid power systems include *gear pumps*, *vane pumps*, and *piston pumps*.

Diagrams of gear and vane pumps are shown in Figure 5.1. The displacement of these pumps is the theoretical amount of liquid that would be moved from the inlet port to the outlet port in one revolution of the pump shaft. Liquid is carried in the tooth spaces of the gear pump but meshing of the gears prevents oil from making a full circle; thus the oil is forced out of the outlet port. Likewise, oil is carried in the spaces between the sliding vanes in the vane pump. Both the gear pump and the vane pump have fixed displacement, i.e., the displacement cannot be changed after the pump is manufactured.

Both axial-piston pumps (Figure 5.2) and radial-piston pumps (Figure 5.3) are available. The former have pistons parallel to the pump shaft, while the latter have pistons arranged radially to the shaft. The piston pumps in Figures 5.2 and 5.3 both have variable displacement, but piston pumps can also be designed with fixed displacement.

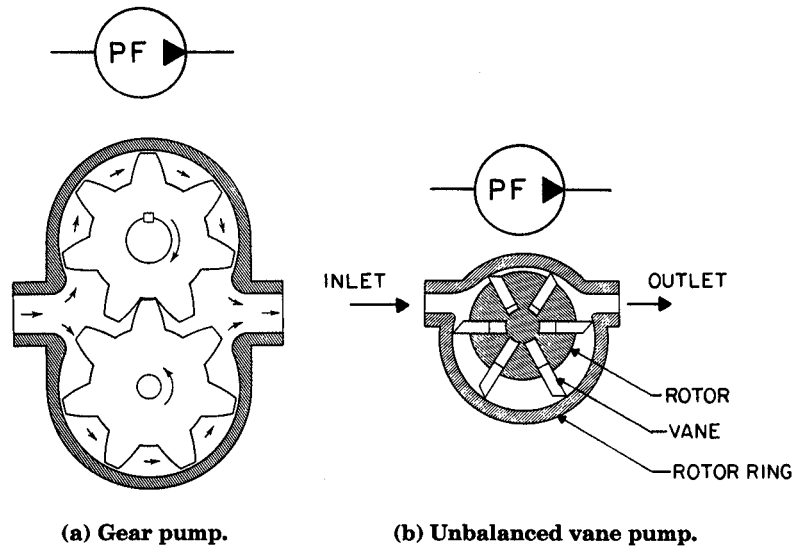


Figure 5.1 – Fixed-displacement pumps.

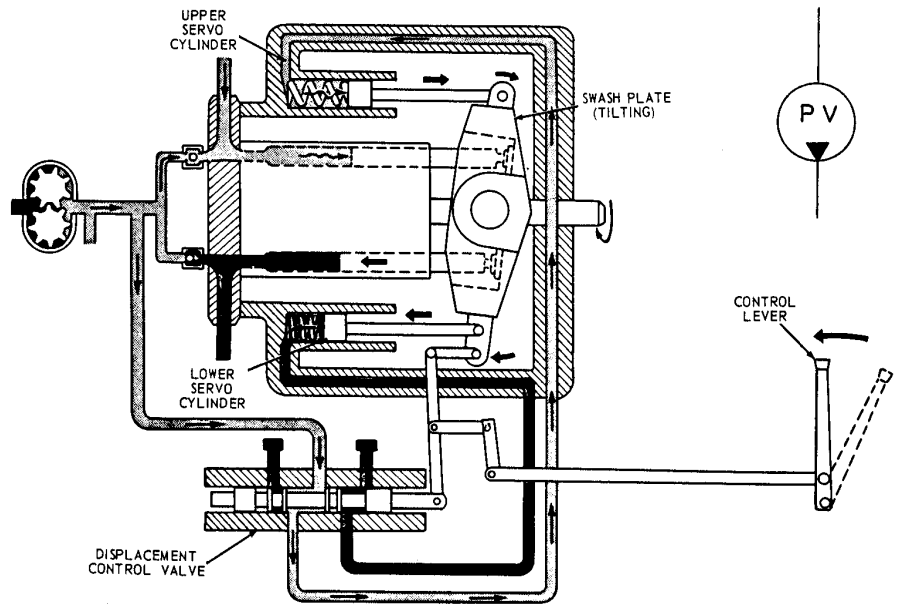


Figure 5.2 – Variable-displacement, axial piston pump (courtesy of Deere and Co.).

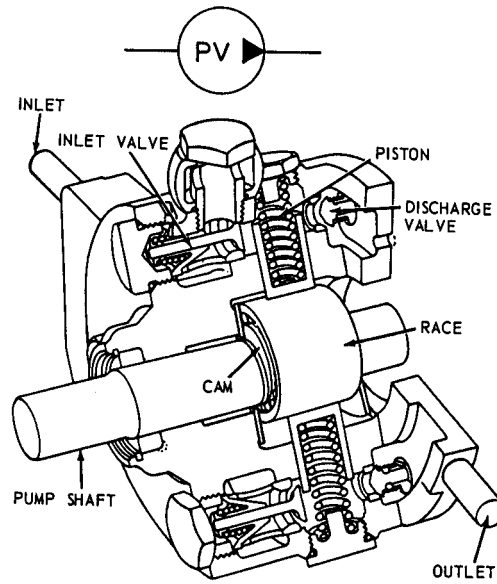


Figure 5.3 – Radial-piston pump (courtesy of Deere and Co.).

The delivery of oil from a pump can be calculated using Equation 5.1:

$$Q_p = \frac{V_p n_p \eta_{vp}}{1000} \quad (5.1)$$

where Q_p = pump delivery, L/min

V_p = pump displacement, cm^3/rev

n_p = pump speed, rev/min

η_{vp} = volumetric efficiency of the pump, decimal

Because of internal leakage within a pump, the volumetric efficiency is always less than one, i.e., the pump always delivers less than its theoretical delivery. Generally, internal leakage in a hydraulic component is directly proportional to the area of the leakage path and the pressure drop across the leakage path and inversely proportional to viscosity. The leakage flow is given by the following equation:

$$Q_L = \frac{(6 \times 10^7) C_L A \Delta p}{\mu} \quad (5.2)$$

where Q_L = leakage flow, L/min

C_L = leakage length constant, cm

A = cross-sectional area of the leakage path, cm^2

μ = dynamic viscosity of the fluid, $\text{mPa} \cdot \text{s}$

Δp = pressure drop, MPa

Therefore, the volumetric efficiency can be calculated as:

$$\eta_{vp} = \frac{Q_{tp} - Q_L}{Q_{tp}} = 1 - \frac{Q_L}{Q_{tp}} \quad (5.3)$$

where Q_{tp} is the theoretical pump delivery and can be calculated from Equation 5.1 by equating $\eta_{vp} = 1$.

The torque requirement of a pump can be calculated from Equation 5.4:

$$T_p = \frac{\Delta p V_p}{2\pi \eta_{tp}} \quad (5.4)$$

where T_p = torque required to drive the pump, $\text{N} \cdot \text{m}$

Δp = pressure rise across the pump, MPa

η_{tp} = torque efficiency of the pump, decimal

Because of friction within the pump, the torque efficiency is always less than one and more than the theoretical amount of torque required to drive the pump. The frictional torque (T_{fp}) is the amount of torque required to overcome friction within the pump. The frictional torque is given by:

$$T_{fp} = \frac{2\pi C_f \mu n_p}{6 \times 10^{10}} \quad (5.5)$$

where $C_f = \text{constant (cm}^3\text{)}$. The friction torque is called the damping torque since it is proportional to the shaft speed. There is an additional frictional torque due to shaft seals. The torque efficiency can be calculated as:

$$\eta_{tp} = \frac{T_{tp}}{T_{tp} + T_{fp}} = \left(1 + \frac{T_{fp}}{T_{tp}}\right)^{-1} \tag{5.6}$$

where T_{tp} is the theoretical torque and it can be calculated from Equation 5.4 by letting $\eta_{tp} = 1$.

The fluid power produced by a pump can be calculated using Equation 5.7:

$$P_{fl} = \frac{Q_p \Delta p}{60} \tag{5.7}$$

where P_{fl} = fluid power, kW. The shaft power required to drive a pump can be calculated from Equation 5.8:

$$P_{sp} = \frac{P_{fl}}{\eta_{pp}} \tag{5.8}$$

where P_{sp} = shaft power required to drive the pump, kW

$$\eta_{pp} = \eta_{vp} \times \eta_{tp} = \text{power efficiency of the pump}$$

Since both η_{vp} and η_{tp} are less than one, η_{pp} is also less than one and more than the theoretical amount of power is required to drive the pump.

The efficiencies of a pump vary with operating conditions, as illustrated in Figure 5.4. The internal leakage in a pump increases with Δp ; as pump speed approaches zero, the entire theoretical delivery can leak back to the inlet and η_{vp} goes to zero. As pump speed increases, however, the internal leakage becomes small relative to the

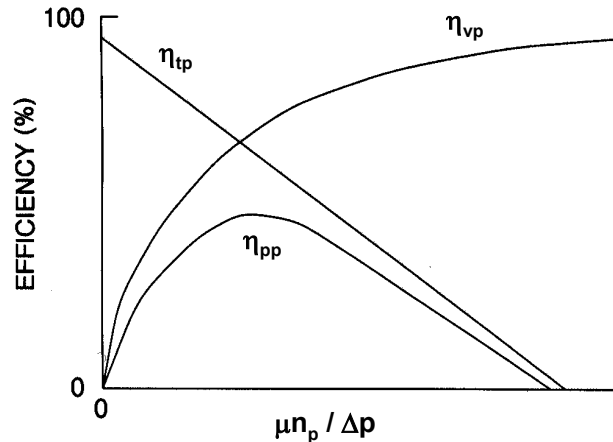


Figure 5.4 – Torque, volumetric, and power efficiencies.

theoretical delivery and η_{vp} approaches its maximum. Some shaft torque is used to overcome the friction which is always present in a pump; at high Δp , that friction torque is relatively small compared to the theoretical torque required and η_{tp} is at a maximum. Conversely, at low Δp , the friction torque is dominant and η_{tp} reaches zero. Since η_{pp} is the product of η_{vp} and η_{tp} , the shape of its curve on Figure 5.4 is defined by the shape of the torque and volumetric efficiency curves. Figure 5.4 implies that a pump must be operated within proper limits of speed and pressure or its power efficiency will drop to unacceptable levels.

5.3 VALVES

Valves are used in fluid power systems to control pressure, volume, and direction of flow. Valves are classified, accordingly, as *pressure control valves* (PCV), *volume control valves* (VCV), and *directional control valves* (DCV).

5.3.1 Pressure control valves

Liquid passes through orifices in control valves, resulting in pressure drops. Equation 5.9 relates the pressure drop across an orifice to the flow through it:

$$Q = 60C_oA_o\sqrt{\frac{2\Delta p}{\rho_f}} \quad (5.9)$$

where Q = flow through orifice, L/min

C_o = orifice coefficient, dimensionless

A_o = orifice area, mm²

Δp = pressure drop across the orifice, MPa

ρ_f = mass density of the fluid, kg/m³

In the usual case where A_o is much smaller than the upstream channel and flow is turbulent, $C_o = 0.60$ for a sharp-edged orifice, but can rise to more than 0.80 if the orifice edges are rounded. The orifice shape has little effect, i.e., C_o will be nearly the same for a long narrow orifice as for a circular one. For typical, petroleum-based fluids used in fluid power systems, $\rho_f = 850$ to 950 kg/m³.

The most common PCV is the relief valve. Relief valves are closed during normal operation, but open at a set pressure to discharge liquid to the reservoir. Thus, relief valves are intended to limit the pressure in a circuit to a safe level. Because direct-acting relief valves (Figure 5.5) have a large pressure override (Figure 5.6), pilot-operated relief valves are sometimes used (Figure 5.7). Pilot-operated relief valves have a light spring which allows a pilot relief valve (see numbers 3 and 4 in Figure 5.7) to open at the desired cracking pressure. The resulting flow passing through an orifice in the valve piston causes a pressure drop (see Equation 5.9) which raises the piston, thus opening the main relief valve. The pressure override, which is the full-flow pressure minus the cracking pressure, is thus much smaller in a pilot-operated relief valve than in a direct-acting relief valve. Note that the direct-acting relief valve is classified as a two-way valve, meaning that it has two ports for connection to the fluid power circuits. The pilot-operated relief valve would be classified as a three-way valve unless the drain was internally connected to the discharge port.

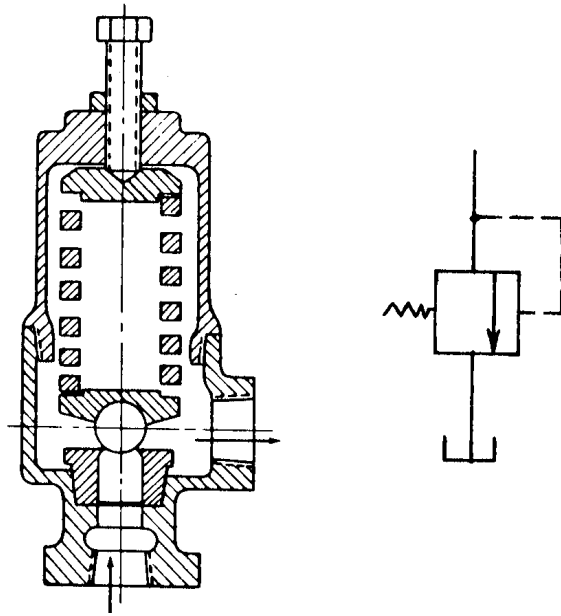


Figure 5.5 – A direct-acting relief valve.

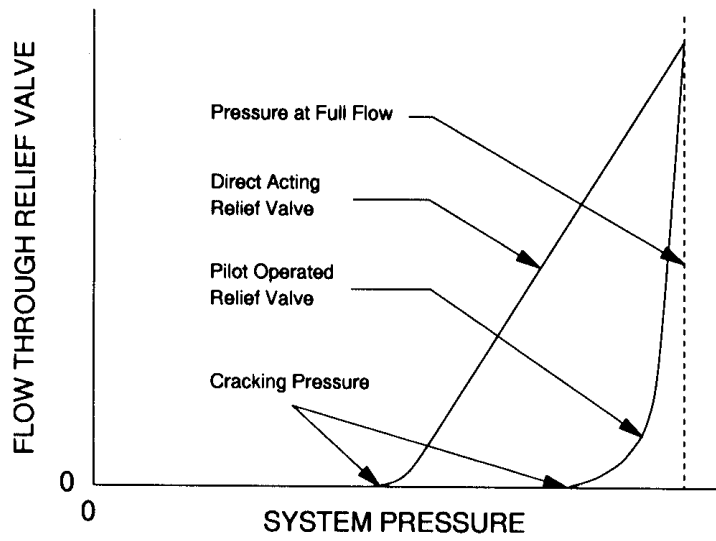


Figure 5.6 – Pressure override in a relief valve.

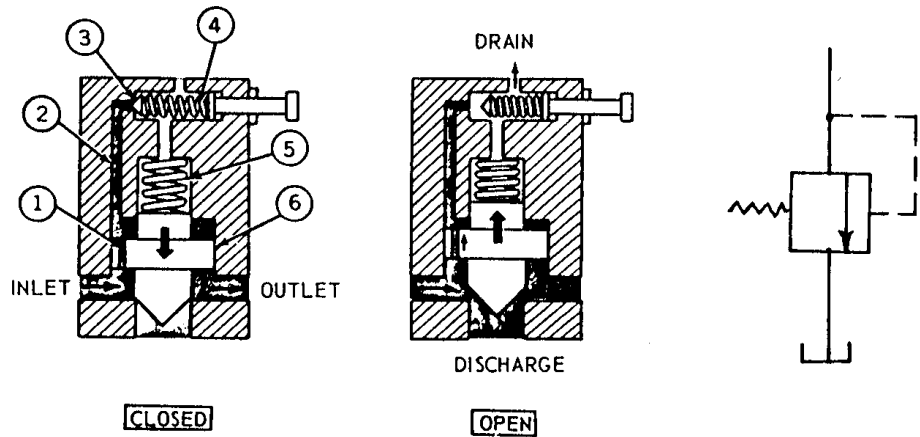


Figure 5.7 – A pilot-operated relief valve.

5.3.2 Volume control valves

The two most common VCVs are the throttling valve (Figure 5.8) and the flow-divider valve (Figure 5.9). The purpose of both valves is to regulate the flow to the outlet port regardless of downstream pressure. Both valves have a spring-loaded spool valve whose purpose is to maintain a constant pressure across an orifice and thus, in accordance with Equation 5.9, maintain constant flow to the outlet port. If the flow through the orifice increases, the pressure drop across the orifice will also increase in accordance with Equation 5.9 and the pressure within the spool will fall. The resulting pressure imbalance across the head of the spool will move the spool to the right to partially block the outlet port, thus reducing the flow to the outlet port. Conversely, if the flow through the orifice declines, the spool will move to the left to create a larger opening to the outlet port. Both the throttling valve and the flow-divider valve are pressure compensated, because they automatically compensate for changes in down-

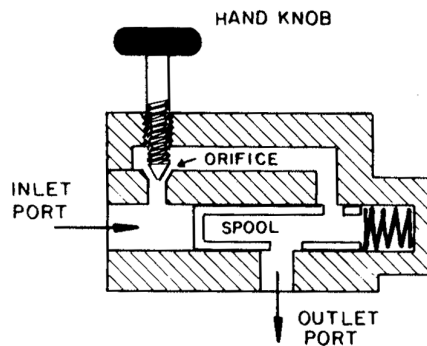


Figure 5.8 – A pressure-compensated throttling valve.

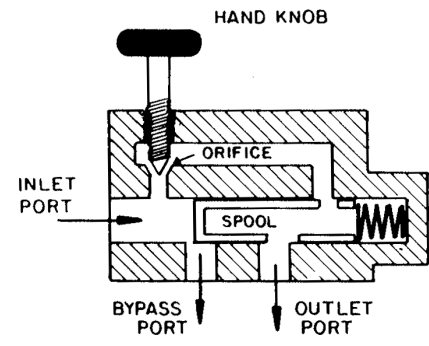


Figure 5.9 – A bypass-type flow-divider valve.

stream pressure. Both of the valves that are illustrated have adjustable flow rates, i.e., the operator can use the hand knob to set the desired flow level. Nonadjustable valves are also available.

The primary difference between the throttling valve and the flow-divider valve is that the latter has a third port for bypass flow. The throttling valve can only be used in systems in which the pump flow reduces automatically when the flow is throttled. In systems with fixed-displacement pumps, any surplus flow must be bypassed and thus only the flow-divider valve is suitable. The flow-divider valve can also be used as a priority valve, i.e., circuits with top priority (for example, steering circuits) are connected to the outlet port. Any excess flow passes to through the bypass port to circuits with lower priority.

5.3.3 Directional control valves

A directional control valve (DCV) is illustrated in Figure 5.10. It has four ports and is thus classified as a four-way valve. It is also classified as a three-position valve because the valve spool has three possible positions: right, centered, or left. In Figure 5.10a, the spool is to the right to connect port P (for pump) to B and port T (for tank, or reservoir) to A. These connections are reversed when the spool is to the left as in Figure 5.10c. An actuator can be connected to ports A and B and, by moving the DCV spool left or right, the direction of movement of the actuator can be reversed. With the spool centered, as in Figure 5.10b, all ports are blocked and thus the valve is also classified as a closed-center valve, in circuits in which pump flow changes automatically to meet demand. In drawings of fluid power circuits, DCVs are always shown with the spool centered for simplicity and it is left to the reader to imagine the other spool positions.

The valve illustrated in Figure 5.11 is a four-way, three-position, open-centered DCV. It could be used with a fixed-displacement pump because, with the spool centered, pump flow can pass through the DCV to the reservoir. Note, however, that any actuator connected to the DCV would be free to move when the spool was centered. If the actuator was a hydraulic cylinder used to raise an implement, for example, the implement would lower as soon as the spool was centered. For that reason, open-centered DCVs are seldom used on agricultural equipment. Instead, if the fluid power system

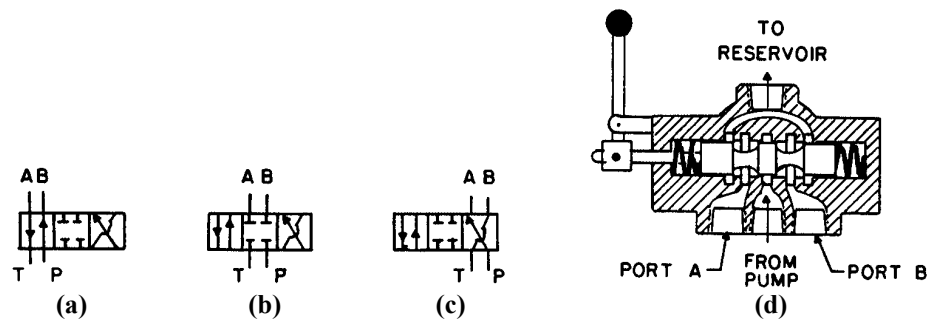


Figure 5.10 – A closed-center directional control valve.

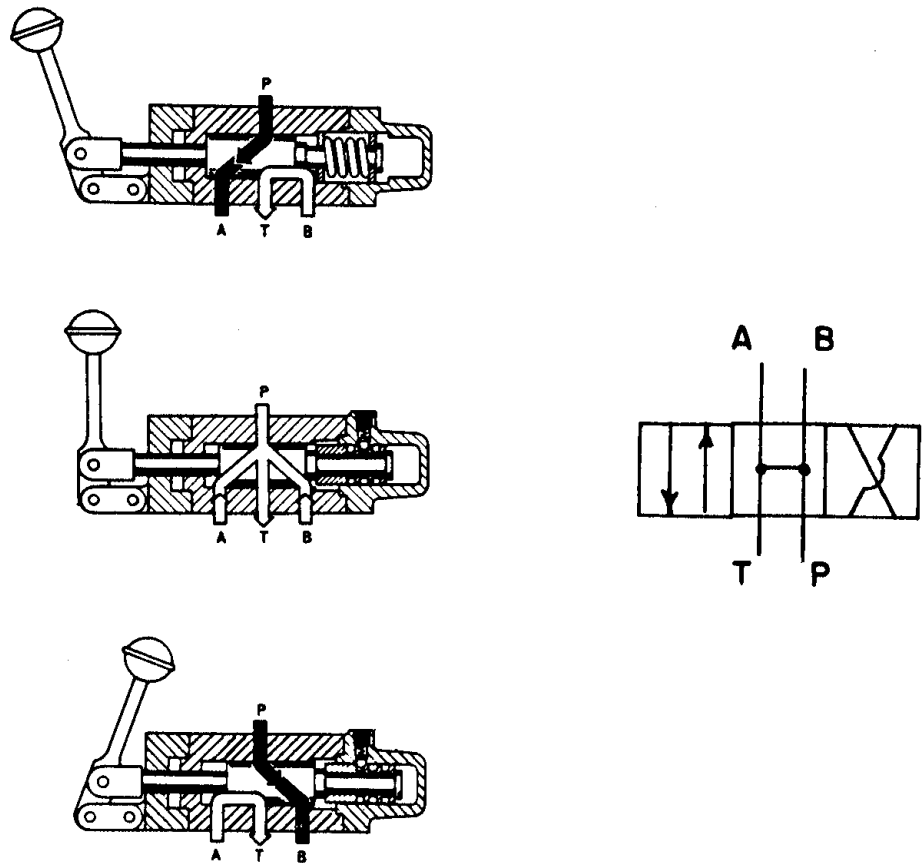


Figure 5.11 – An open-center directional control valve.

has a fixed-displacement pump, a tandem-centered DCV is used. A dual tandem-centered DCV is illustrated in Figure 5.12. With both spools centered, all actuator ports are blocked but the pump port is connected to the reservoir port. Moving either spool left or right blocks the pump connection to the reservoir and oil is forced to flow to an actuator.

Although the NFPA symbols do not reveal it, all DCVs also provide some degree of flow control. By partial movement of the spool to either the left or right, the orifice within the valve can be partially opened and, in accordance with Equation 5.9, can provide partial flow delivery to the actuator.

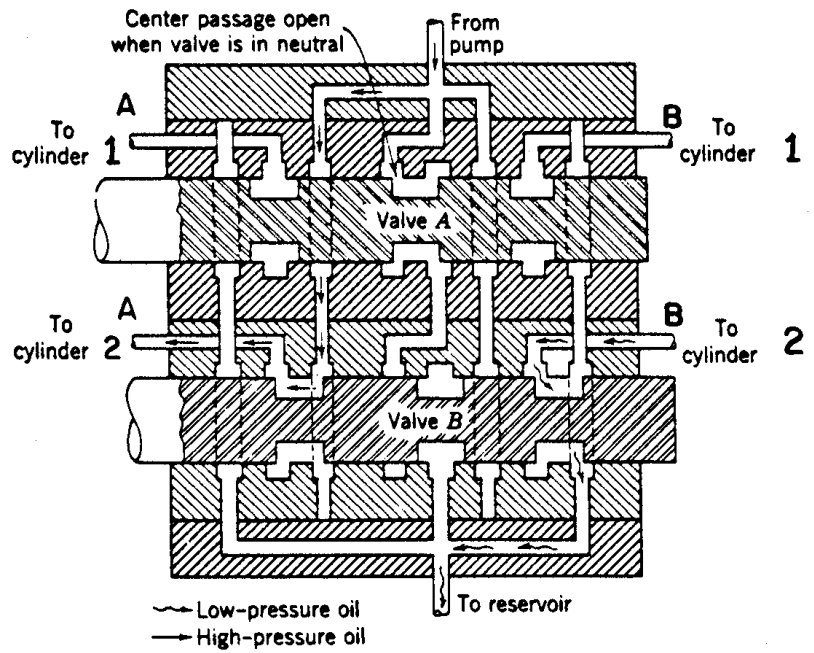
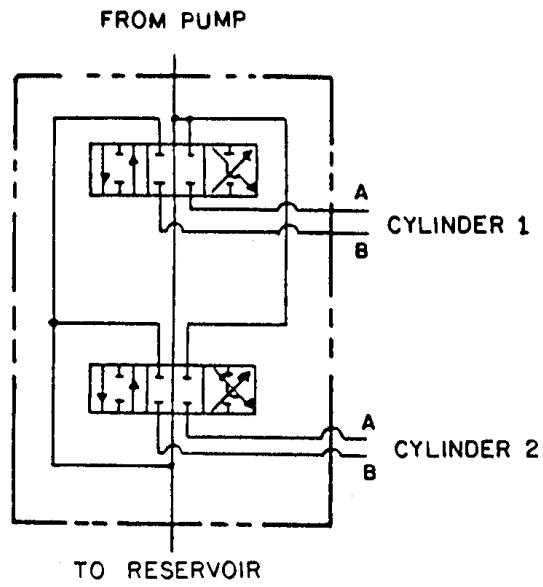


Figure 5.12 – A dual tandem-center directional control valve (reprinted from Kepner et al., 1978).

5.4 ACTUATORS

Actuators include hydraulic motors to provide rotary mechanical power and hydraulic cylinders to provide linear mechanical power.

5.4.1 Hydraulic motors

Motors are similar to pumps and, with suitable precautions, the pumps shown in Figure 5.1 could also be used as motors. To prevent seal damage, the shaft seals of most pumps and motors are internally vented to the low pressure port. Low pressure exits at the inlet of a pump but at the outlet of a motor and thus, to use a gear or vane pump as a motor, the direction of rotation must be reversed. Axial-piston motors of either fixed or variable displacement are also available.

Equations 5.10 to 5.12 are for the speed, torque, and power output, respectively, of a hydraulic motor:

$$n_m = \frac{1000Q\eta_{vm}}{V_m} \quad (5.10)$$

and

$$T_m = \frac{\Delta p V_m \eta_{tm}}{2\pi} \quad (5.11)$$

and

$$P_{sm} = \frac{Q\Delta p\eta_{pm}}{60} \quad (5.12)$$

where n_m = motor speed, rev/min

η_{vm} = volumetric efficiency of motor

V_m = motor displacement, cm^3/rev

T_m = motor torque, $\text{N}\cdot\text{m}$

η_{tm} = torque efficiency of motor

P_{sm} = motor shaft power, kW

$\eta_{pm} = \eta_{vm} \times \eta_{tm}$ = power efficiency of motor

Q = fluid flow through motor, L/min

Δp = pressure drop across motor, MPa

The volumetric, torque, and power efficiencies for a motor are analogous to those for a pump and vary as illustrated in Figure 5.4.

5.4.2 Hydraulic cylinders

Both single-acting and double-acting hydraulic cylinders are available. A cutaway of a double-acting cylinder is shown in Figure 5.13. Oil is forced into the port on the left to extend the cylinder and the piston movement forces oil out of the port on the right. Conversely, by reversing the port connections, the cylinder can be made to retract. The double-acting cylinder of Figure 5.13 could be converted into a single-acting cylinder by emptying the oil to the right of the piston and installing an air breather in the port to the right. A single-acting cylinder is used in those situations where an external load is available to make the cylinder retract. Dimensions for hydraulic cylinders to control implements have been specified in ASAE Standard S201.4.

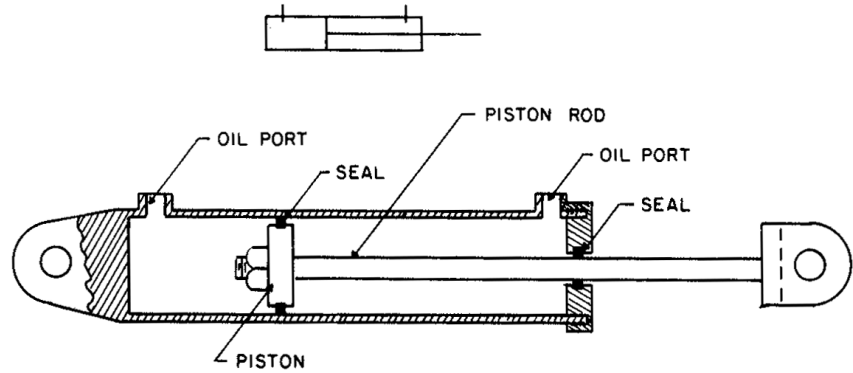


Figure 5.13 – A double-acting hydraulic cylinder.

The load capacity of a cylinder can be calculated using Equation 5.13:

$$F = \frac{p_1 A_1 - p_2 A_2}{10} \quad (5.13)$$

where F = force capacity of the cylinder, kN

A_1 = area of piston, cm^2

A_2 = area of piston minus area of piston rod, cm^2

p_1 = pressure (gage) acting on area A_1 , MPa

p_2 = pressure (gage) acting on area A_2 , MPa

The factor of 10 is simply a units conversion factor. A negative answer indicates the cylinder is retracting. In many situations, one of the ports will be connected to the reservoir and the corresponding pressure will be zero gage pressure.

The speed at which a cylinder extends or retracts can be calculated using Equation 5.14:

$$v = \frac{Q}{6A_i} \quad (5.14)$$

where v = speed of movement of rod, m/s

Q = flow into cylinder, L/min

A_i = A_1 if cylinder is extending or A_2 if retracting

Note that, for a given Q , the cylinder extends slower than it retracts, since $A_1 > A_2$. The return flow from a double-acting cylinder is calculated from the following equation:

$$Q_{cr} = 6A_j v \quad (5.15)$$

where Q_{cr} = cylinder return flow, L/min

A_j = A_2 if cylinder is extending or A_1 if retracting

Equations 5.14 and 5.15 will show that a cylinder returns less oil than it receives while extending and more oil than it receives while retracting. The reservoir must supply the flow deficit or absorb the excess flow.

5.5 RESERVOIRS, FLUIDS, FILTERS, AND LINES

A reservoir supplies oil to the pump and provides a place for oil to return from the circuit. The reservoir must be large enough to allow the oil to cool, i.e., a larger reservoir allows more resident time for the oil to cool in the reservoir. If the reservoir cannot provide sufficient cooling, an oil cooler can be used to provide supplementary cooling. A properly designed reservoir has internal baffles to reduce oil splashing and has its inlet and outlet ports arranged to prevent oil returning from the hydraulic circuit from immediately re-entering the pump. The return port should be below the oil surface to reduce air entrainment and foaming as the oil returns to the reservoir. Finally, the reservoir must be vented to the atmosphere to accommodate changing oil levels and the vent should have a filter to prevent dust entry. As the oil passes through lines, valves, and other devices that do no mechanical work, any pressure drops result in conversion of fluid power to heat. The power loss and heat generation rate can be calculated from Equation 5.16:

$$P_L = \frac{\Delta p Q}{60} \quad (5.16)$$

where P_L = power loss in a nonworking device, kW

Δp = pressure drop across the device, MPa

Q = flow through the device, L/min

The number 60 is a units constant

Viscosity is the most important property of a hydraulic fluid. Manufacturers generally recommend fluid viscosities between 12 and 49 mPa·s at the operating temperature of the pump. Fluid viscosities fall markedly with increased temperatures, but the viscosity dependence on temperature is less if the fluid has a high viscosity index. A high viscosity index is thus highly desirable for hydraulic fluids, since the fluid is subject to wide variations in temperature and pumps and motors become very inefficient when the viscosity is either too low or too high (see Figure 5.4). Petroleum-based hydraulic fluids are subject to oxidation. The oxidation rate doubles for every 10°C increase in temperature but is very low when the temperature is below 60°C. Additives are used in the fluid to reduce oxidation, foaming, and wear. A rust inhibitor is also generally used. The transmission case on tractors and self-propelled machinery is often used as the reservoir for the hydraulic system. Then the same fluid that serves as the hydraulic fluid must also lubricate the gears in the transmission.

Metal particles and other solid contaminants can be very damaging to hydraulic components. Clearances between mating parts are 10 μm or less in some hydraulic components and, if particles of that size pass between the mating parts, rapid failure can result. Thus filters are used to remove contaminants in fluid power systems. Three possible alternatives for locating a filter in a fluid power circuit include (a) between the reservoir and the pump inlet port, (b) immediately after the pump outlet port, and (c) just before the return inlet to the reservoir. Location (a) is seldom used because the pressure drop across the filter can cause subatmospheric pressures to be generated

within the pump, leading to cavitation and pump damage. Location (b) is seldom used because the filter would have to withstand very high pressures in that location. Thus, location (c) is usually chosen for filters that can remove particles as small as 10 μm. In addition, a strainer or porous filter may be used in location (a) to prevent the largest particles (typically larger than 150 μm) from reaching the pump.

Lines consist of hydraulic tubing and/or hydraulic hoses to convey fluid between the various devices in a fluid power circuit. Both the tubing and the hoses are treated as smooth conduits for which the correct diameter must be selected to avoid excessive pressure drops in the lines. The Reynolds number is used to determine whether flow in the lines is laminar or turbulent. Reynolds number is defined as:

$$N_{Re} = \frac{4C\rho_f Q}{\pi\mu d} \tag{5.17}$$

where N_{Re} = Reynolds number, dimensionless

$C = 16.67$ = units constant

ρ_f = fluid density, kg/m^3

Q = flow through conduit, L/min

μ = dynamic viscosity of oil, $mPa \cdot s$

d = inside diameter of conduit, mm

Flow is laminar for Reynolds numbers less than 2000 and fully turbulent for Reynolds numbers above 4000. Between these limits, flow is in a transition region. The Hagen-

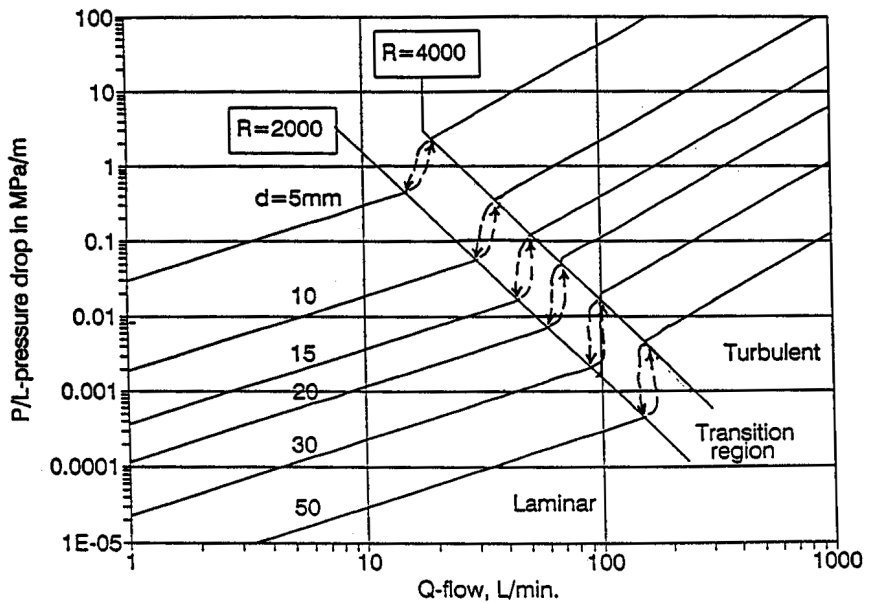


Figure 5.14 – Pressure drop in hydraulic conduits for $\rho_f = 850 \text{ kg/m}^3$ and $\mu = 27.6 \text{ mPa} \cdot \text{s}$.

Poiseuille law is used to compute pressure losses for laminar flow in conduits, i.e.:

$$\frac{\Delta p}{L} = \frac{2.13\mu Q}{\pi d^4} \quad (5.18)$$

where Δp = pressure drop, MPa.

L = length of conduit over which pressure drop occurs (m)

For fully turbulent flow, the pressure drop can be calculated from the following equation:

$$\frac{\Delta p}{L} = \frac{0.0333\mu^{0.25}\rho^{0.75}Q^{1.75}}{d^{4.25}} \quad (5.19)$$

where terms are defined as in Equation 5.18. For convenience, Equations 5.18 and 5.19 have been plotted in Figure 5.14.

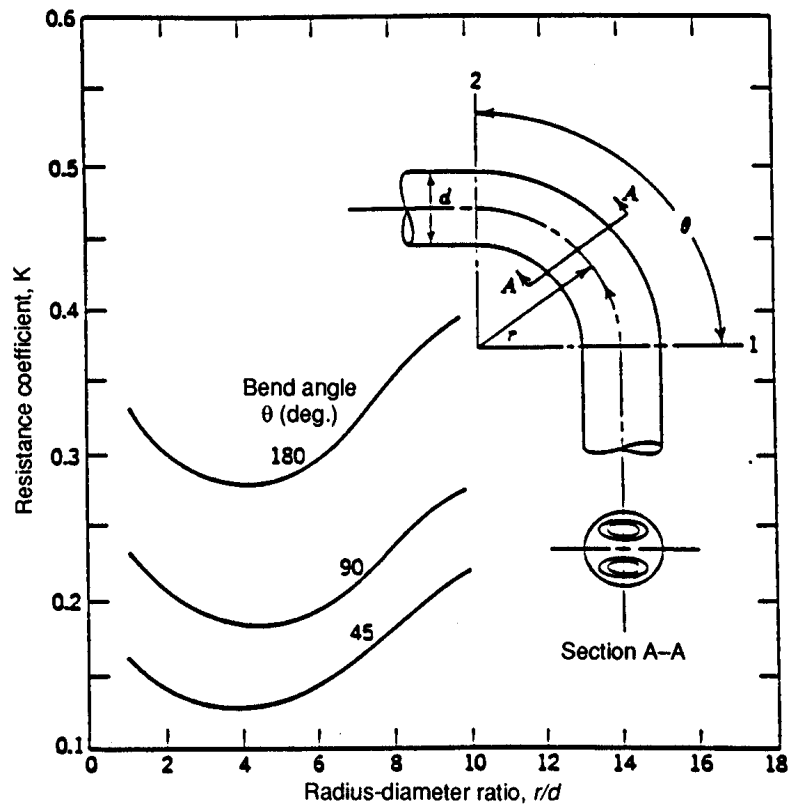


Figure 5.15 – Resistance coefficients of pipe bends (reprinted from J. J. Taborek, “Fundamentals of Line Flow,” *Machine Design Magazine*, 16 April 1959).

The term *minor losses* refers to pressure drops that result from fittings, bends, and sudden changes in cross section. The pressure drop associated with bends can be calculated from the following equation:

$$\Delta p = (1.39 \times 10^{-4}) K \rho_f \frac{Q^2}{A^2} \quad (5.20)$$

where Δp = pressure drop, MPa

K = dimensionless factor taken from Figure 5.15

ρ_f = fluid density, kg/m³

Q = flow in conduit, L/min

A = cross-sectional area of the conduit, mm²

The numerical constants in Equations 5.18 through 5.20 are unit conversion factors. The pressure drop calculated from Equation 5.20 is added to the pressure drop that would be calculated for a straight conduit of equal length. Pressure drops occur in the various elbows, valves, and other fittings that are used in connecting fluid power circuits. Data on these pressure drops can be obtained from component manufacturers or by measurement.

5.6 TYPES OF FLUID POWER SYSTEMS

On most modern agricultural equipment, the hydraulic pump is driven directly by the engine so that fluid power will be available whenever the engine is running. The fluid power system is said to be in standby when the pump is running but no fluid power is needed. Any power delivered to the pump during standby is converted into heat, so it is necessary to minimize shaft power to the pump during standby. As Equations 5.7 and 5.8 show, there are three ways to minimize standby power. They are to minimize (a) pump pressure, (b) pump delivery, or (c) pump delivery and pressure. These approaches have led, respectively, to the *open-center* (OC), *pressure-compensated* (PC), and *load-sensing* (LS) fluid power systems that are now available for use on agricultural equipment.

5.6.1 Open-center systems

An open-center fluid power system (Figure 5.16) was the first system used on agricultural equipment and is still used on some smaller tractors. It includes a fixed-displacement gear pump, a relief valve, a tandem-center DCV with one or more spools, and one or more actuators. A pressure-flow diagram for an OC system is shown in Figure 5.17. During standby, the system operates at full flow but very low pressure because the pump can discharge freely to the reservoir through the tandem-center DCV. When a DCV spool is displaced to send oil to an actuator, pressure rises only enough to move the load; flow declines slightly as η_{vp} falls with increasing pressure (see Figure 5.4). If the actuator load is too large, the relief valve cracks open and flow to the actuator declines as oil is diverted to the reservoir through the relief valve.

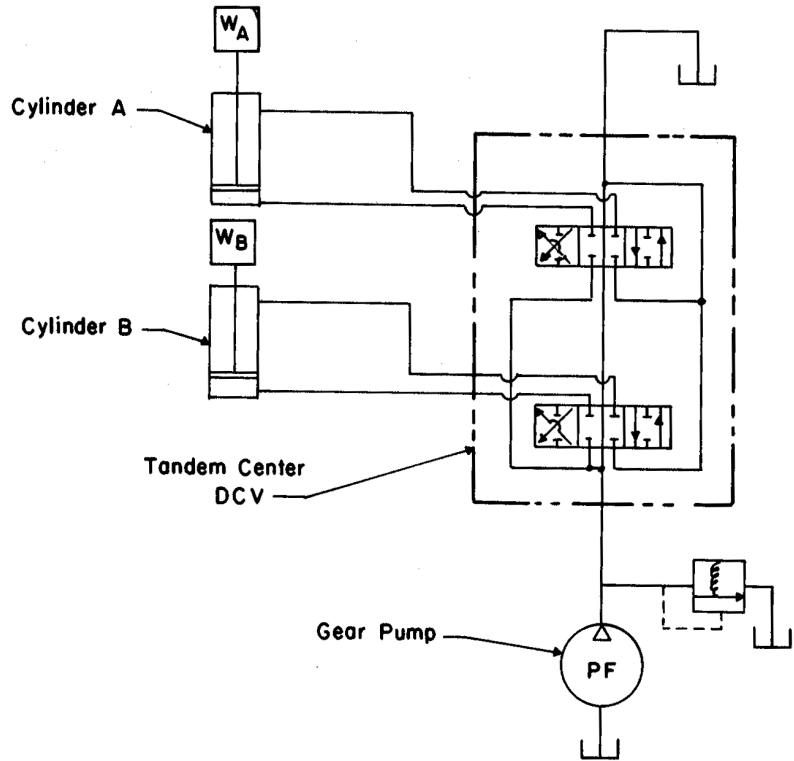


Figure 5.16 – An open-center hydraulic system.

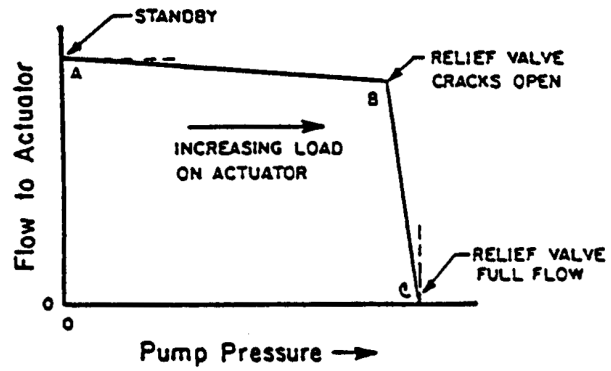


Figure 5.17 – A pressure-flow diagram of an open-center hydraulic system.

Maximum fluid power is produced just to the left of point B in Figure 5.17, i.e., just before the relief valve opens. When two or more spools in the DCV are displaced at the same time, oil flows to the actuator that requires the least pressure; the remaining actuators are stalled until the pressure can rise. If cylinder load WA in Figure 5.16 was larger than cylinder load WB, for example, cylinder B would move first and cylinder A would be stalled until cylinder B reached the end of its stroke. Such action is called sequencing and is a major disadvantage of OC systems.

5.6.2 Pressure-compensated systems

The pressure-compensated system (Figure 5.18) was developed to overcome some of the limitations of the OC system. The heart of the system is a pressure-compensated pump (see Figure 5.3) that automatically adjusts its delivery to meet demand. When no flow is needed, the stroke control valve opens to admit oil to the pump crankcase, holds the radial pistons away from the cam, and causes delivery to cease. If pressure falls, for example, when a DCV spool is displaced, the pressure in the crankcase drops and the pump again begins delivering oil. The stroke-control valve eliminates the need for a relief valve. Notice that the PC system includes a closed-center DCV, thus the pump flow is zero at standby, as shown in Figure 5.19. Any number of actuators can be connected simultaneously; since the pump automatically adjusts its stroke to maintain full pressure, no sequencing will occur unless the pump reaches full stroke. If oil demand is more than the pump can supply at full stroke, the system moves to the left of point B in Figure 5.19 and behaves like the OC system of Figure 5.17. Thus, sequencing can occur in the PC system if one of the connected actuators has a high flow demand and a low pressure demand.

5.6.3 Load-sensing systems

The most recent innovation in fluid power systems is the load-sensing (LS) system illustrated in Figure 5.20, alternatively called a pressure-flow-compensated system. It includes a closed-center DCV, so that flow is near zero at standby. Unlike the PC system, however, pressure is also low at standby and rises only high enough to meet the highest pressure demand in the system. Thus, sequencing is eliminated. The heart of the LS system is a pressure-compensated, axial-piston pump whose stroke is controlled by a differential-pressure compensating valve (DPCV). With port B of the DPCV blocked, the system would behave like a PC system with very low standby pressure, since a weak spring is used in the DPCV. Thus, standby pressure is low, typically about 1.4 MPa. When a DCV spool is displaced, the pressure demand of the load is transmitted to port B of the DPCV via a sensing line, thus assisting the spring and allowing the pump outlet pressure to rise to 1.4 MPa above the actuator demand. The same differential pressure of 1.4 MPa appears across the throttling valve (see Figure 5.8) which regulates flow to the actuator. When two or more actuators with differing pressure demands are engaged simultaneously, the highest pressure is transmitted to port B of the DPCV. A pressure drop larger than 1.4 MPa appears across those throttling valves controlling the actuators with smaller pressure demands. Each throttling valve has a manual adjustment to allow the operator to control the speed of the associated actuator. The pressure-flow diagram for the LS system is similar to that

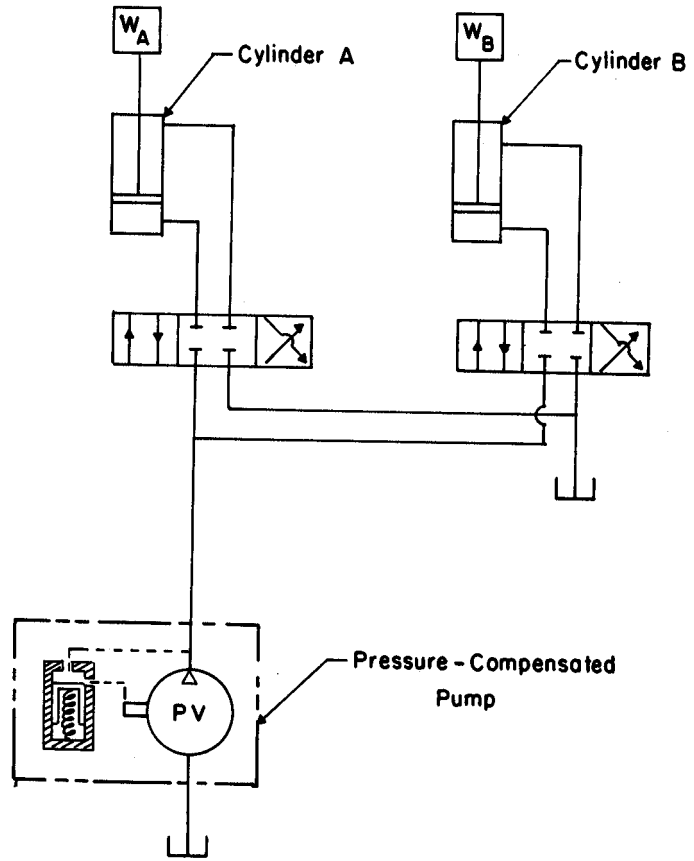


Figure 5.18 – A pressure-compensated hydraulic system.

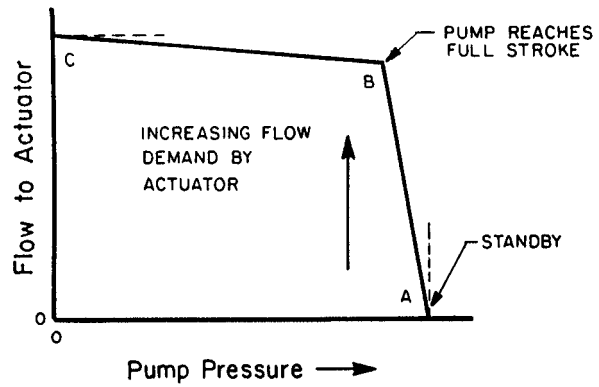


Figure 5.19 – A pressure-flow diagram of a pressure-compensated hydraulic system.

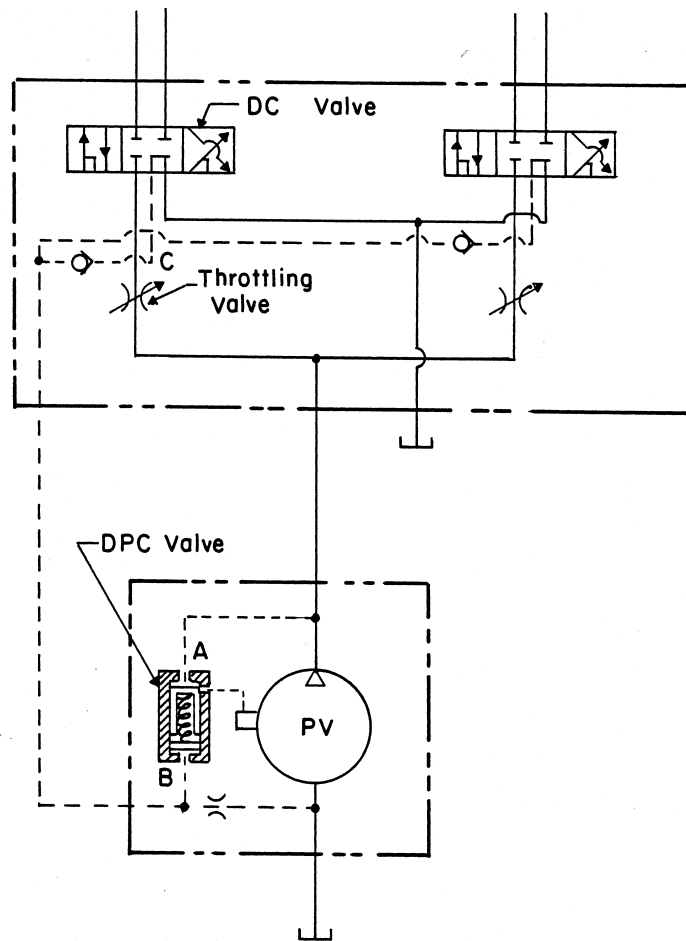


Figure 5.20 – A load-sensing hydraulic system.

of Figure 5.19, except that the system can operate at any point under the curves. Pressure is controlled by actuator demand and flow is controlled by the throttling valves. Standby for the LS system is near the origin in Figure 5.19, not at point A.

5.7 PRESSURE TRANSIENTS

The equations that have been presented up to this point are for the steady-state behavior of fluid power systems. They are generally sufficient for analyzing and designing manually controlled fluid power systems. Pressure transients must be considered in automatically controlled systems that incorporate feedback, or the systems may exhibit unstable behavior. The equations that describe transient behavior are beyond the scope of this textbook. However, software packages are available that enable the use of computers to simulate transient behavior of fluid power systems.

5.8 HYDROSTATIC TRANSMISSIONS

A hydrostatic transmission consists of a pump connected to a hydraulic motor, as illustrated in Figures 5.21 and 5.22. The output speed of the transmission can be calculated from:

$$n_m = \eta_{vp} \eta \frac{V_p}{V_m} n_p \quad (5.21)$$

Two equations are available for calculating output torque:

$$T_m = \eta_{tp} \eta_{tm} \frac{V_m}{V_p} T_p \quad (5.22)$$

or

$$T_m = \frac{V_m \eta_{tm}}{2\pi} \Delta p \quad (5.23)$$

Variables in Equation 5.21 through 5.23 are as defined previously.

Equation 5.22 calculates the output torque, subject to the maximum pressure limit expressed by Equation 5.23. To provide a variable speed ratio, the pump or the motor or both must have variable displacement. Equations 5.21 and 5.23 show that a transmission with a variable V_p and fixed V_m is a constant-torque transmission; decreasing V_p reduces the output speed but the output torque is limited by the pressure rating of the transmission and cannot be increased. Thus, power capability declines with decreasing output speed. Constant-torque hydrostatic transmissions are used in some lighter-duty vehicles which require only limited output torque.

A transmission with constant V_p and variable V_m is a constant-power transmission because, as V_m is increased to reduce the output speed, the output torque is automatically increased with no increase in system pressure. All gear-type transmissions have the constant-power feature, which is desirable in a transmission. However, the constant-power hydrostatic transmission is seldom used because of its limited range; V_m cannot reach the infinite value that would be needed to bring the output speed to zero. Also, V_m cannot reach zero without blocking the pump flow, so the tilt of the motor swash plate (see Figure 5.22) cannot be reversed and the transmission cannot reverse the direction of travel of the vehicle.

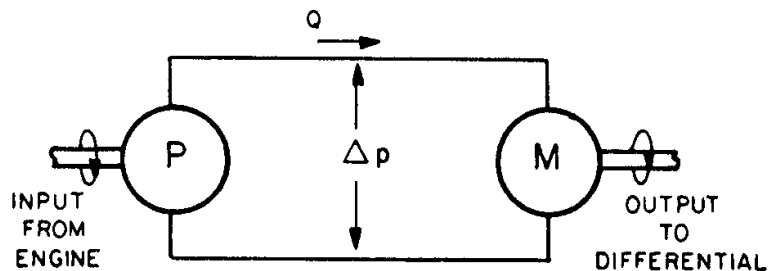


Figure 5.21 – A hydrostatic drive.

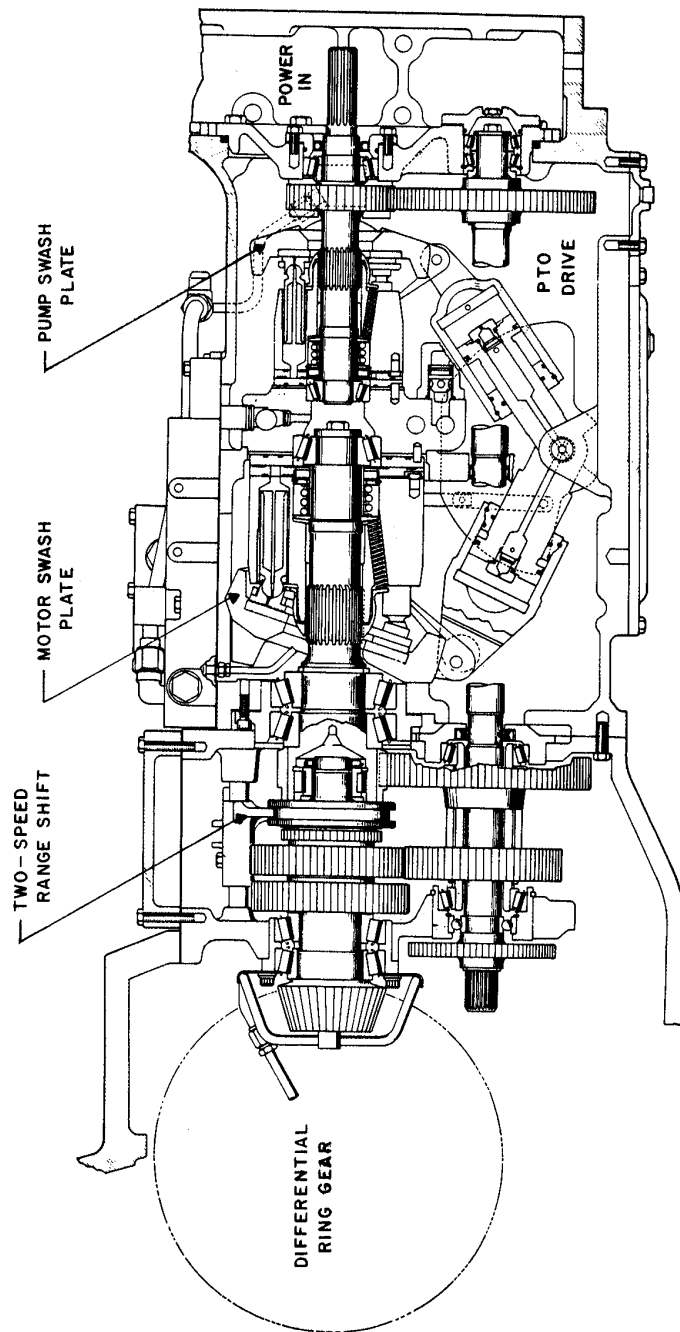


Figure 5.22 – A heavy-duty hydrostatic transmission in series with a manual shift transmission (courtesy of CNH).

As Figure 5.22 illustrates, hydrostatic transmissions for heavy-duty tractors include a variable-displacement pump and a variable-displacement motor. The variable V_p allows linear control of output speed and full reversing capability. The variable V_m allows some increase in output torque as the output speed declines. Theoretically the hydrostatic transmission can provide full-range speed control but, as Figure 5.4 illustrates, the transmission efficiency would be very low at either low or high speed ratios. To improve efficiency, a mechanical transmission is often used in series with the hydrostatic transmission, as shown in Figure 5.22. The mechanical transmission allows the hydrostatic transmission to work over a much narrower speed range and thus better maintain its efficiency.

5.9 MECHATRONICS AND SYSTEM CONTROL

Many functions accomplished by hydraulics were previously accomplished by mechanical devices in earlier machines. However, the great flexibility of hydraulic systems has allowed them to replace mechanical systems in many cases. Hydraulic systems and especially mechatronic systems allow much more precise and flexible control than mechanical systems.

5.9.1 An introduction to mechatronics

Electrohydraulic valves have been used in hydraulic circuits for many years to allow control of the valves at locations remote from the valves. Microprocessors are becoming ever more widely used in the control of off-road vehicles. Microprocessor control of electrohydraulic valves is one example of the emerging field of *mechatronics*. The microprocessors in mechatronic devices allow such devices to have unique capabilities and great flexibility. Figure 5.23 is an example of a prototype mechatronic valve.

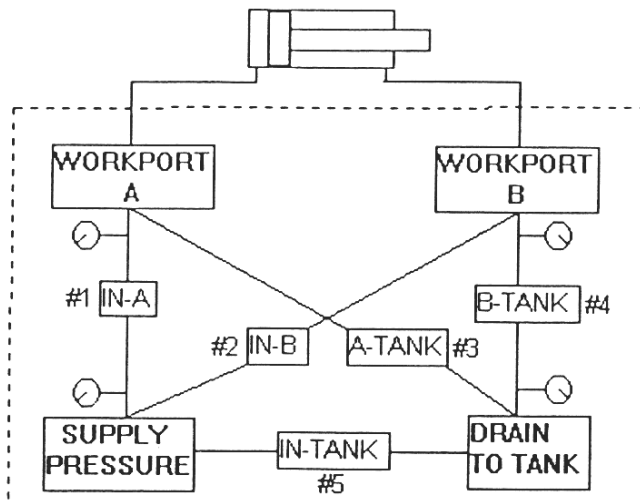


Figure 5.23 – A mechatronic directional control valve (from Book and Goering, 1999).

Through microprocessor control, the valve in Figure 5.23 can perform many functions in a hydraulic circuit. The valve has four ports, as in an ordinary, single-spool DCV. Five proportional cartridge valves can block or open any of the possible passages between the four ports. A pressure transducer in each port allows the microprocessor to determine the pressure in each port. Cartridge valve 5 is normally open but can be closed on signal from the microprocessor. The other four cartridge valves are normally closed but can be opened on signal from the microprocessor. Although the mechatronics valve of Figure 5.23 can perform many functions, only a few will be discussed.

The mechatronics valve removes the distinction between open-center and closed-center DCVs. The computer keeps cartridge valve 5 closed to simulate a closed-center valve. For the mechatronics valve to function in an open-center circuit, the computer keeps cartridge valve 5 open until actuator action is needed; to extend a hydraulic cylinder, for example, the computer might open cartridge valves 1 and 4, then smoothly close cartridge valve 5 to cause a smooth start to cylinder extension. When the pressure in work port A indicated the cylinder had reached the end of its stroke, the computer would close cartridge valves 1 and 4 while opening cartridge valve 5. The reader can deduce which cartridge valves the computer would need to control to cause the cylinder to retract.

The mechatronic valve of Figure 5.23 has built-in pressure relief. If the pressure in the supply pressure port became too high, for example, the computer could cause cartridge valve 5 to open to provide a flow path to the tank. Compared to ordinary relief valves, the mechatronics relief valve could have near zero pressure override (see Figure 5.6).

In addition to providing relief against excessively high pressures, the mechatronics valve can provide protection against sub-atmospheric pressures and cavitation. Consider the situation if a hydraulic motor was powering a high-inertia load at high speed when the controlling DCV was closed to stop the motor. Momentarily, the external load would drive the motor, causing it to function as a pump to remove fluid from the motor supply line and pump fluid into the motor discharge line. With the DCV closed, there would be no inflow to the supply line or outflow from the discharge line. The pressure in the supply line would fall below atmospheric pressure and could possibly cause collapse of the line. If the mechatronic valve was used in place of the DCV, the computer could sense the approach of sub-atmospheric pressure and open cartridge valve 3 to allow oil from the reservoir to relieve the vacuum. Note also that the mechatronics valve could also close cartridge valve 4 in a controlled way to stop the hydraulic motor without causing excessively high pressures in the motor discharge line.

5.9.2 System control

Many machine functions are powered and controlled by hydraulics and space does not permit a discussion of all of them. Instead, we will discuss only one control function, i.e., the control of the hitch used to link implements to tractors. Hitches are discussed more fully in Chapter 7. Many types of hitches have been used in the past, but the *three-point hitch* illustrated in Figure 7.2 has become the standard hitch. Figure 7.6 is an example of a mechanical system for controlling a three-point hitch. A single-

acting hydraulic cylinder rotates lift arms for raising the two lower links. The weight of the attached implement provides the force for lowering the hitch.

The earliest use of three-point hitches was for mounting a plow to a tractor. Undulating soil surfaces caused difficulties during plowing with a fully mounted plow. When the tractor front wheels encountered an incline or the tractor rear wheels encountered a swale, the plow depth could increase until the tractor engine approached stall. Operators found they could avoid shifting to a lower gear by raising the hitch to reduce the plowing depth somewhat, thus reducing the load on the tractor. The operator would lower the hitch when the soil surface became level again. Tractor designers automated this practice by adding a load control lever and linkage. In Figure 7.6, the lower link points are attached to arms on a torsionally rigid torque tube. One end of a torsion bar is attached to the torque tube, while the other end of the torsion bar is anchored to the vehicle frame. With increasing pull on the lower links, the torsion bar allows increasing rotation of the torque tube. An arm near the center of the torque tube moves to control the DCV actuating linkage as the torque tube rotates. An increasing load signals the DCV to raise the hitch while a decreasing load signals the DCV to lower the hitch. The operator uses the load control handle to set the desired load on the hitch. Note that the system of Figure 7.6 has two control levers, one for load control and one for position control. The two controls together control the hitch. Pulling the load control lever to the rear increases the hitch sensitivity to implement draft, which can result in erratic plowing depth in variable soils. Conversely, moving the draft control lever forward decreases hitch sensitivity to draft and provides for more constant plowing depth on level ground. The three-point hitch enhances weight transfer from the front to the rear wheels of the tractor, thus improving traction and reducing the need for tractor ballast.

While mechanical linkages were able to control three-point hitches successfully, the complex linkages were expensive to manufacture and were subject to wear. Thus, such linkages are being replaced by mechatronic devices. In the mechatronic equivalent of the hitch shown in Figure 7.6, each control handle is replaced by a very small handle that sets the position of a potentiometer. Another potentiometer senses the rotation of the shaft that rotates the lower-link lift arms. The lower hitch links are linked to the tractor by special pins that produce an electric signal proportional to the shear in the pins. The mechanically controlled DCV is replaced by an electrically controlled DCV. For position control, the microprocessor senses the setting of the position-control handle, compares it with the current hitch position, and signals the DCV to raise or lower the hitch as needed. For load control, the microprocessor senses the setting of the load-control lever, compares it with the load as measured by the lower link pins, and raises or lowers the hitch as needed. In addition to having fewer moving parts subject to wear, the mechatronic system offers enhanced control of the hitch. For example, while controlling load, the microprocessor might restrict the raising and lowering of the hitch to programmed limits to avoid excessive variation in tillage depth.

PROBLEMS

- 5.1 A hydrostatic drive includes a pump with $C_f = 9.9 \times 10^8 \text{ cm}^3$ and $A C_L = 4.53 \times 10^{-8} \text{ cm}^3$; equations for pump efficiencies are given in Problem 5.5. The pump is hydraulically coupled to a motor whose efficiency equations are given in Problem 5.8 and with $C_f = 2.5 \times 10^8 \text{ cm}^3$ and $A C_L = 4.0 \times 10^{-8} \text{ cm}^3$. The viscosity of the oil in the hydrostatic drive is $27 \text{ mPa} \cdot \text{s}$. Assume the pump speed is held constant at 2200 rev/min . The pump displacement (V_p) can be changed from $120 \text{ cm}^3/\text{rev}$ for forward travel to $120 \text{ cm}^3/\text{rev}$ for reverse travel. Motor displacement (V_m) is $120 \text{ cm}^3/\text{rev}$ when $V_p = 0$ and changes linearly with V_p to a minimum of $60 \text{ cm}^3/\text{rev}$ when $V_p = 120 \text{ cm}^3/\text{rev}$. Assuming the torque load on the transmission is such that $\Delta p = 39 \text{ MPa}$, calculate the following variables at 10 increments of V_p from 0 to $120 \text{ cm}^3/\text{rev}$: (a) η_{vp} , (b) η_{tp} , (c) η_{pp} , (d) torque, and (e) power required to drive the pump, (f) oil flow rate in the pump-motor circuit (g) η_{vm} (h) η_{tm} , and (i) η_{pm} , (j) motor output speed, (k) torque, and (l) power and (m) overall power efficiency of the hydrostatic drive. Note that this is a good spreadsheet problem. Also, with pump delivery known, n_m depends on and 0_{vm} vice versa so iteration is required.
- 5.2 Same as Problem 5.1, except $\Delta p = 32 \text{ MPa}$ because of reduced torque load on the hydrostatic drive.
- 5.3 A hydraulic piston pump with a displacement of $10.54 \text{ cm}^3/\text{rev}$ has a rated speed of 1800 rev/min and rated pressure of 10.3 MPa . The leakage flow is given by:

$$Q_{Lp} = 0.00368 \Delta p$$

Using the equation in this problem and in the text, (a) calculate the speed (in terms of Δp) at which $\eta_{vp} = 0$. (b) Starting at this minimum speed and ending at rated speed, plot η_{vp} versus pump speed for Δp values of 5 and 10 MPa, i.e., plot two curves on the graph. (c) Specify the speed and pressure ranges in which this pump can be operated if η_{vp} is to be 0.95 or greater.

- 5.4 For the pump of Problem 5.3, the friction torque can be calculated using the following equation:

$$T_{fp} = 0.0014 n_p$$

where T_{fp} = friction torque in $\text{N} \cdot \text{m}$ and n_p = pump speed in rev/min . Calculate the (a) friction torque when the pump is running at rated speed, (b) theoretical, and (c) actual shaft torque, and (d) torque efficiency when the pump is working at rated pressure. (e) Also plot η_{tp} versus pump pressure for pressures ranging from 0.1 MPa to rated pressure and for pump speeds of 900 and 1800 rev/min , i.e., plot two curves on the graph. (f) Specify the speed and pressure ranges in which this pump can be operated if η_{tp} is to be 0.85 or greater.

- 5.5 (a) Using equations from the text and from Problem 5.3, derive the following equation for the volumetric efficiency of a pump:

$$\eta_{vp} = 1 - \left(\frac{2\pi A C_L}{V_p} \right) \left(\frac{\mu n_p}{C_u \Delta p} \right)^{-1}$$

where μ = viscosity (mPa·s)

n_p = pump speed (rev/min)

Δp = pressure rise (MPa)

$C_u = (3 \times 10^{10})/\pi$ = constant inserted to make a dimensionless variable

Note that, for normal values of μ , n_p , and Δp , the magnitude of the dimensionless variable is very small. The quantity $(2\pi A C_L/V_p)$ is also dimensionless when V_p = pump displacement in cm^3/rev , A = leakage area in cm^2 , and C_L = leakage constant in cm. (b) Using equations from the text and from Problem 5.4, derive the following equation for the torque efficiency of a pump:

$$\eta_{tp} = \left[1 + \left(\frac{2\pi C_f}{V_p} \right) \left(\frac{\mu n_p}{C_u \Delta p} \right) \right]^{-1}$$

The quantity, $(2\pi C_f/V_p)$ will be dimensionless when C_f = friction constant in cm^3 . (c) Assume that $\mu = 25$ mPa·s, $\Delta p = 30$ MPa, $V_p = 120$ cm^3/rev , $A C_L = 4.53 \times 10^{-8}$ cm^3 and $C_f = 9.91 \times 10^8$ cm^3 . Letting n_p range from 200 to 2500 rev/min, plot η_{vp} , η_{tp} , and η_{pp} all versus the dimensionless variable $(\mu n_p/C_u \Delta p)$. Compare your results with the curves plotted in Figure 5.4.

- 5.6 A pump with characteristics as given in Problems 5.3 and 5.4 is operated at rated speed and pressure. Calculate the (a) pump delivery in L/min, (b) required torque to drive the pump, and (c) the shaft power.
- 5.7 In a throttling valve as illustrated in Figure 5.8, let the pressure be p_i at the inlet port, p_o at the outlet port and p_x in the passage between the hand-controlled orifice and the spool-controlled orifice. Let the flow area of the hand-controlled orifice be A_m (for manually controlled) and the area through the spool be A_a (for automatically controlled). (a) Starting with Equation 5.9, derive an equation for p_x in terms of p_i , p_o , A_m , and A_a . (b) Calculate the value of p_x when $p_i = 14$ MPa, $p_o = 6$ MPa, and $A_m = A_a$. (c) Also calculate the value of A_m and A_a required to deliver 70 L/min of flow through the valve. (d) Assuming the pressure at outlet port rises to 8 MPa with no change in A_m , to what value must A_a automatically change to maintain 70 L/min of flow through the valve? (e) Repeat part (d) except let the pressure at the outlet port fall to 4 MPa.
- 5.8 The leakage and friction equations for a motor are the same as those for a pump as given in Problems 5.3 and 5.5, respectively. (a) Derive the following equation for volumetric efficiency of a motor:

$$\eta_{vm} = \left[1 + \left(\frac{2\pi C_L A}{V_m} \right) \left(\frac{\mu n_m}{C_u \Delta p} \right)^{-1} \right]^{-1}$$

(b) Derive the following equation for torque efficiency of a motor:

$$\eta_{tm} = 1 - \left(\frac{2\pi C_f}{V_m} \right) \left(\frac{\mu n_m}{C_u \Delta p} \right)$$

where in both of the above equations, symbols are as defined in Problem 5.5 except that subscript m denotes a hydraulic motor. (c) Assume that $\mu = 25 \text{ mPa} \cdot \text{s}$, $\Delta p = 25 \text{ MPa}$, $V_m = 60 \text{ cm}^3/\text{rev}$, $C_L = 0.4 \times 10^{-7} \text{ cm}^3$, and $C_f = 1.9 \times 10^7 \text{ cm}^3$. Letting n_m vary from 200 to 2000 rev/min, plot η_{vm} , η_{tm} , and η_{pm} all versus the dimensionless variable and compare your results with Figure 5.4.

- 5.9 On the double-acting cylinder of Figure 5.13, let port 2 be the port on the right (the rod-end of the cylinder) and port 1 be the port on the left. The piston and rod have diameters of 75 mm and 25 mm, respectively, and the maximum stroke length of the cylinder is 200 mm. One port of the cylinder is to be connected to a hydraulic system which has a rated pressure of 10 MPa and produces a maximum flow of 50 L/min; the other cylinder port is to be connected to the reservoir, which is at zero gage pressure. When the cylinder is extending with port 2 connected to the reservoir, calculate (a) the maximum force that can be exerted, (b) the rod speed, and (c) the length of time required to fully extend the cylinder. (d) Also calculate the flow rate of oil delivered from port 2 to the reservoir. Next, with port 1 connected to the reservoir while retracting the cylinder, calculate (e) the maximum force, (f) rod speed, and (g) length of time to fully retract the cylinder. (h) Also calculate the flow rate of oil from port 1 to the reservoir.
- 5.10 Rework Problem 5.9, but use dimensions of a cylinder assigned by the instructor.
- 5.11 The flow through the throttling valve of Figure 5.8 is 50 L/min while the pressure drop across the valve is 10 MPa. (a) Compute the rate of heat generation (in kW) due to the power loss in the valve. (b) If the throttling valve discharges into a reservoir whose capacity is 20 L, how much time would be required to completely displace all of the oil in the reservoir? (c) During the time calculated in part b, how much heat energy would be delivered from the valve to the reservoir? (d) If no energy was dissipated from the reservoir during that time, how much would the oil temperature increase in the reservoir? Assume the oil density is 900 kg/m^3 and the specific heat of the oil is $2.3 \text{ kJ/kg}^\circ\text{C}$. (Note that the true temperature rise would be less than that of part d because heat is dissipated from the reservoir).
- 5.12 A hydraulic fluid with dynamic viscosity of $27.6 \text{ mPa} \cdot \text{s}$ and density of 850 kg/m^3 is to be conveyed through hydraulic tubing at the rate of 75 L/min. Calculate (a) the smallest diameter tubing which would permit laminar flow, (b) the pressure drop per meter of tubing, and (c) the power loss per meter of tubing. (d) Use Figure 5.14 to do an approximate check on the calculated pressure drop.
- 5.13 Same as Problem 5.12, except use the smallest diameter tubing which would give fully turbulent flow.

- 5.14 A 90° bend of radius 40 mm is to be formed in the hydraulic tubing of Problem 5.12. Calculate the additional pressure drop that would occur in the tubing due to the bend.
- 5.15 Same as Problem 5.14, except use the hydraulic tubing of Problem 5.13.
- 5.16 Assume both hydraulic cylinders of Figure 5.16 have a bore of 60 mm, a rod diameter of 25 mm, and a maximum stroke of 200 mm. The relief valve cracks open at a pressure of 15 MPa. A load of 30 kN rests on cylinder A while a load of 40 kN rests on cylinder B. The pump delivers a flow rate of 60 L/min at rated speed. Note that the pump pressure is zero when both DCVs are in the neutral position. If the operator moves the handles on both DCVs simultaneously to try to raise both loads and continues to hold the handles in the raise position, the pump pressure will increase from zero to one level, later to a second level, and still later to a third level, i.e., there will be three phases of operation. Neglecting line losses, (a) calculate the pressure level during the first phase, (b) calculate the duration of the phase, and (c) describe the oil flow, i.e., where would the system be operating on Figure 5.17 and to where would the pump be delivering the oil? For answers (d), (e), and (f), repeat steps (a), (b), and (c) for phase 2. For answers (g), (h), and (i), repeat steps (a), (b), and (c) for phase 3.
- 5.17 Repeat Problem 5.16, except the relief valve cracks open at 10 MPa. Also, the number of phases may not be equal to three, as in Problem 5.16; you are to determine how many phases will occur.
- 5.18 In the PC system of Figure 5.18, the cylinders have the same dimensions as in Problem 5.16. On Figure 5.19, the pressures are 15.5 MPa at point A and 15 MPa at point B; the pump deliveries are 60 L/min at point B and 63 L/min at point C. The loads on the cylinders are the same as those in Problem 5.16. Neglecting line losses, predict the behavior of the system if the operator holds both DCV handles to try to extend both cylinder loads simultaneously, i.e., calculate system pressures, flows, and durations of those conditions as in Problem 5.16.
- 5.19 Assume that cylinder A of Figure 5.20 is connected to the left DCV of Figure 5.20 and the flow is controlled by throttling valve A. Cylinder B is connected to the right DCV and the flow is controlled by throttling valve B. The cylinders have the same dimensions as given in Problem 5.16. A weight of 30 kN rests on cylinder A while 40 kN of weight is on cylinder B. The pressure drop across the DPCV is 1.4 MPa. The pump is capable of delivering 60 L/min and both throttling valves are set to transmit 25 L/min. Now assume that the operator holds both DCV handles to attempt to raise both cylinder loads simultaneously. Neglecting line losses, calculate (a) the pump outlet pressure, the pressure on the piston of (b) cylinder A, and (c) cylinder B, the pressure drop across (d) throttling valve A, and (e) throttling valve B, and the power loss in (f) throttling valve A, and (g) throttling valve B.
- 5.20 Repeat Problem 5.19 except that the weight is 40 kN on each cylinder.

SIMULATION PROBLEMS

Two spreadsheets, Hydraulic Pump Simulator and Hydraulic Motor Simulator, are on the CD-ROM for your use in working the simulation problems below. The simulators are based on theory presented in Chapter 5. Each simulator is calibrated using data from one operating point of the pump or motor. The simulation accuracy degrades as predictions are made further from the calibration point. However, both simulators accurately depict performance trends.

S5.1 Enter the following data into the pump efficiency spreadsheet to calibrate the equations for a certain pump:

Pump displacement = 67 cm ³ /rev	Pump outflow = 91.6 L/min
Pump speed = 1500 rpm	Pump shaft power = 25.4 kW
Pump pressure = 13.8 Mpa	Oil temperature = 70.8°C

(a) Use the spreadsheet to prepare a graph showing the variation of the volumetric, torque, and power efficiencies as the pump speed is varied from 500 to 10,000 rpm at a pump pressure of 14 Mpa when the oil temperature is 70°C. (b) Prepare a graph showing the variation of these same efficiencies as the pump pressure is changed from 2 to 20 MPa while the speed is held at 2500 rpm and the oil temperature remains at 70°C. (c) Next, prepare a graph showing the variation of these same efficiencies as the oil temperature is changed from 0 to 100°C while the pressure is held at 14 MPa and the pump speed is held at 2500 rpm. (d) Inspect the graphs and consider whether the variations in efficiency seem logical.

S5.2 Enter the following data into the motor efficiency spreadsheet to calibrate the equations for a certain motor:

Motor displacement = 8.2 cm ³ /rev	Motor inflow = 15.0 L/min
Motor speed = 1720 rpm	Motor shaft power = 2.2 kW
Inlet pressure = 10.3 Mpa	Oil temperature = 74°C

Use the spreadsheet to prepare a graph showing the variation of the volumetric, torque, and power efficiencies as the inflow is varied from 2 to 50 L/min at outlet pressure of 10.3 Mpa when the oil temperature is 74°C. (b) Prepare a graph showing the variation of these same efficiencies as the outlet pressure is changed from 2 to 20 MPa while the inflow is held at 20 L/min and the oil temperature remains at 74°C. (c) Next, prepare a graph showing the variation of these same efficiencies as the oil temperature is changed from 0 to 100°C while the outlet pressure is held at 10.3 MPa and the inflow is held at 20 L/min. (d) Inspect the graphs and consider whether the variations in efficiency seem logical.

Relevant websites

(Warning: The following websites were relevant at time of publication of the book, but webmasters are free to change or eliminate websites at any time).

<http://www.hydraulic-supply.com/html/productline/mfgprod/vickers-hydraulics.htm>

<http://science.howstuffworks.com/hydraulic2.htm>

PRECISION AGRICULTURE

6

INTRODUCTION

The conversion from human powered to animal powered operations in the early 1800s transformed agriculture. Invention of the reaper and other animal powered machines greatly reduced the drudgery and increased the productivity of farming. A second transformation occurred in the early 1900s, when tractor powered machines replaced the animal powered machines and productivity increased even further. A third transformation is now underway, the transition to information-based agriculture. Electronics, including microprocessors, have become an integral part of modern farm equipment. The mechatronic systems discussed in Chapter 5 are only one example of such usage. Another is *site-specific crop management* (SSCM), also called *precision agriculture*.

In conventional farming, fields are treated uniformly. For example, the rate of fertilizer application remains constant over an entire field even though the field itself is not uniform. On hilly land, for example, the soil near the top of a hill sheds rainfall while soil near the foot of the hill can capture extra water. The aim of SSCM is to take advantage of such spatial differences within a field, for example, by applying less fertilizer to areas that receive less rainfall (and therefore have lower yield potential) and more to areas that receive more rainfall (and therefore have higher yield potential). The concept is not new. In 1929, C.M. Linsley and F.C. Bauer published Circular No. 346 from the University of Illinois. It described a procedure for sampling soil and preparing maps to guide the application of lime on a spatially variable basis, i.e., less lime was applied to less acid areas of a field and more to the more acid areas. The concept applies to many agricultural operations, e.g., variable application rates for seed, fertilizer, or pesticides.

SSCM was impractical in 1929, but more recent innovations have allowed the concept to be revived. These include sensors for sensing soil and crop conditions, the *global positioning system* (GPS) for determining the position of a machine within a field at all times, *geographic information systems* (GIS) for handling the large quantities of data involved in SSCM, and electronic control systems to automatically change application rates as a machine traverses a field. One or more microprocessors are included in modern tractors to handle the automatic control and the data input to guide the control. When more than one microprocessor is included on a tractor, there are advantages in having these microprocessors communicate with each other. This has led to the replacement of conventional wiring harnesses by a *controller area network* (CAN) that features a standardized CAN bus.

6.1 SENSORS

A sensor is a device used to measure some quantity of interest and produce a signal (usually electrical) representing that measurement.

6.1.1 Sensor types

A variety of sensor types have been developed to measure many different phenomena of interest to agriculture. Strain gage sensors measure micro deflections of surfaces to which they are glued. Because deflections are caused by forces, strain gages can be used to measure forces and pressures as well as deflections. Piezoelectric sensors are crystals that produce an electrical signal when subjected to stress. Ion-selective field effect transistors (ISFETs) are sensors that can measure concentrations of chemical substances. They utilize special membranes that generate a differential charge while selectively passing ions; the membrane is coated on a field effect transistor to generate a useable signal. For example, an ISFET that selectively passed nitrate ions could measure nitrate concentrations in a soil-water slurry. Vision sensors use a digital camera to continuously capture images and then use image analysis software to continuously capture useable information from the images.

6.1.2 Sensor applications

Detailed analysis of the various sensors is beyond the scope of this book. Sensor development has become a critical need for the continued advance of SSCM. The ASABE technical library includes more than 1,000 web-accessible documents that relate to sensor development. Sensors in existence or under development are aimed at the following measurements supporting SSCM:

- soil moisture
- soil air permeability
- soil strength
- concentrations of soil nutrients (nitrates, potassium, etc.)
- soil surface profile
- crop nitrogen stress
- crop leaf area
- plant population
- crop moisture content (grain, forage, etc.)
- crop flow rate into harvester (grain, forage, cotton, etc.)
- quality of crop/grain into harvester (protein, oil, etc.)
- weed sensor
- flow rates of fertilizer, pesticides, etc. in an applicator

6.1.3 Advanced sensors

Miniaturization has allowed development of smart sensors, wireless sensors, and sensor fusion. A smart sensor is made by integrating a microprocessor with a sensor to produce a more useful signal. When using a differential pressure transducer to measure the pressure drop across an orifice, for example, the signal would vary linearly with the pressure differential but with the square root of the flow rate through the orifice (see Equation 5.9). Integrating a microprocessor into the transducer could produce a signal that varied linearly with the flow rate. Sensor fusion combines more than one sensor and a microprocessor into a single unit. Combining a grain moisture sensor with a flow rate sensor, for example, could produce a sensor that measured the grain flow rate on a dry weight basis. Finally, a wireless sensor incorporates a radio trans-

mitter to allow the sensor data to be transmitted without a wire. Such a sensor could be very useful if installed on a rotating shaft or in other applications where use of wire connections would be very inconvenient.

6.2 GLOBAL POSITIONING SYSTEM

Development of the *global positioning system*, or GPS, began in 1973 under the leadership of Colonel Bradford Parkinson of the US Air Force; the system is still operated and maintained by the US military for military use, but is also available for civilian use. The system includes 24 satellites that orbit the earth at altitudes more than 11,000 miles up, in six orbital planes spaced 60° apart. This constellation allows a GPS receiver to access five to eight satellites from any point on earth at any time.

6.2.1 GPS for civilian use

For civilian use, the satellites broadcast a coded signal on a 1575.42 MHz (L1) carrier frequency. When a GPS receiver receives the coarse acquisition (C/A) coded signal, it compares it to an internal signal in the receiver and uses the phase shift between the two signals to compute the time required for the signal to travel from the satellite to the receiver. Because signals travel at the speed of light (which is known), the receiver can calculate the distance from the satellite to the receiver. The signal from one satellite thus determines that the receiver must be on the surface of a sphere whose radius is equal to the distance to the satellite. Because the intersection of two spheres is a circle, receiving the signal from a second satellite places the receiver on a circle in space. Receiving the signal from a third satellite pinpoints the receiver location to one of two points in space. Normally, the receiver tracks four or more satellites to calculate its position. Typically, a C/A based GPS can determine horizontal position within 100 meters and vertical position within 160 meters. These accuracies and those in the following sections are based on the 2SD accuracy system (see Section 6.2.6).

6.2.2 Military GPS

GPS positioning accuracy can be degraded by a number of causes. For example, the earth's atmosphere delays transmission of the signals from satellites to the receiver differently depending upon the orientation of the satellites relative to the earth. To provide increased accuracy, each satellite also broadcasts a second (L2) carrier frequency, at 1227.60 MHz, to measure the atmospheric delay. The latter signal can only be received by military receivers authorized to use this precise positioning service (PPS). The PPS receivers can determine horizontal position within 22 meters and vertical position within 28 meters. When the GPS system was first developed, the US military was concerned that adversaries would use the C/A based receivers in attacks on the US. To forestall such attacks, the military instituted selective availability (SA) that intentionally degraded the accuracy of C/A based positioning. Since May, 2000, the US military no longer degrades the GPS signal with SA.

6.2.3 Differential GPS

Differential GPS involves the use of two receivers. One is at a fixed location whose coordinates are accurately known, while the other is a roving receiver. By comparing the GPS reading of the fixed receiver with the known coordinates, the fixed receiver

can calculate correction factors that can be applied to the roving receiver. The corrections can be applied in real time using a radio link between the receivers, or in a post-processing mode. Differential C/A based GPS can determine horizontal positions within a few meters. A number of organizations now provide GPS correction signals for a fee. The FAA provides Wide Area Augmentation System (WAAS) correction signals without a fee. Generally, the roving receivers must be within 160 km (100 miles) or less of the base station receiver for accurate corrections. GPS receivers now available include antennas for both the GPS signals and the correction signals and software that will cause the GPS receiver to automatically display the corrected coordinates.

6.2.4 Carrier-phase GPS

Carrier-phase tracking provides the most highly accurate positioning. These receivers use both the L1 and L2 carrier signals. The receivers are able to distinguish individual cycles in the L1 carrier wave, which has a wavelength of 19 cm. By using two carrier-phase receivers in a differential mode and keeping the receivers no more than 30 km (20 miles) apart, positions can be determined within 5 cm, i.e., with sufficient accuracy for surveying. The technique requires keeping the roving receiver in each position to be determined for at least 15 minutes; the multiple readings taken during that time are averaged by the receiver software to improve accuracy. The corrections from the fixed receiver are applied to the roving receiver in a post-processing mode.

6.2.5 Real-time kinematic GPS

Real-time kinematic (RTK) surveying is similar to the carrier-phase tracking described above, except that a radio link between the two receivers allows the corrections to be applied to the roving receiver in real time.

6.2.6 Accuracy measures

GPS positioning errors tend to be normally distributed (Figure 6.1). The equation for the normal distribution is:

$$p(x) = \frac{1}{\sigma\sqrt{2\pi}} e^{-\left[\frac{(x-\mu)^2}{2\sigma^2}\right]} \quad (6.1)$$

where $x = \text{err} = \text{GPS positioning error}$

$p(x) = \text{probability of that error}$

$\mu = \text{mean value of the distribution}$

$\sigma = \text{standard deviation of the distribution}$

Areas under the normal curve represent cumulative probabilities. For example, 68% of the area is within \pm one standard deviation of the center of the distribution. Thus, 68% of a set of GPS measuring errors would be expected to be within one standard deviation of the mean error. Several measures are used to show the accuracy of GPS positions. The two-standard-deviations (2SD) error is calculated from repeated position measurements at a given location; 95% of the measurements will then be within two standard deviations of the mean error. The root-mean-square (RMS) error corres-

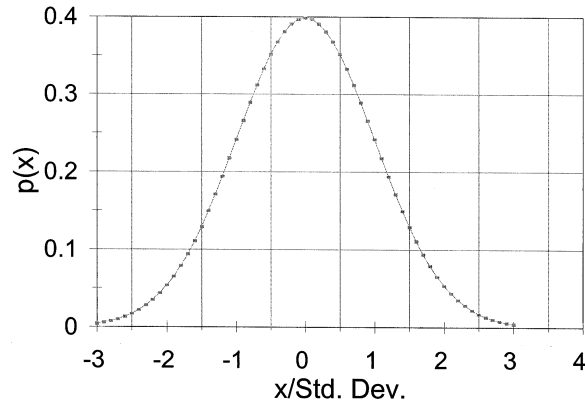


Figure 6.1 – The standard normal distribution.

ponds to one standard deviation, i.e., 68% of the measurements at a given location will be within one standard deviation of the mean error. The circular-error-probable (CEP) is the radius of a circle within which 50% of the measurements are expected to fall. This radius corresponds to 0.68 standard deviations on the normal curve.

6.2.7 Coordinate transformation

GPS readings are given as latitude-longitude pairs, but are transformed into x,y coordinates for use in a field coordinate system. The transformation assumes the earth is an ellipsoid with properties as given by J.P. Snyder (1987) and makes use of the following differential equations:

$$dx = \frac{a \cos(\text{Lat})d\text{Lon}}{[1 - e^2 \sin^2(\text{Lat})]^{0.5}} \quad (6.2)$$

and

$$dy = \frac{a(1 - e^2)d\text{Lat}}{[1 - e^2 \sin^2(\text{Lat})]^{1.5}} \quad (6.3)$$

and

$$e = \sqrt{1 - \frac{b^2}{a^2}} \quad (6.4)$$

where Lat = latitude, expressed in radians

Lon = longitude, expressed in radians

dLat = differential of latitude

dLon = differential of longitude

dx = differential of x-dimension (east-west)

dy = differential of y-dimension (north-south)

a = equatorial radius = 6,378,135 m

b = polar radius = 6,356,750 m

Equations 6.2 and 6.3 must be integrated to obtain the plane coordinates. If two points in a field are sufficiently close (usually within 1 minute change in longitude or latitude), the integrations result in the following closed form approximations:

$$x - x_o = K_x (\text{Lon} - \text{Lon}_o) \quad (6.5)$$

and
$$y - y_o = K_y (\text{Lat} - \text{Lat}_o) \quad (6.6)$$

where $x - x_o$ = displacement in east-west direction, m
 $y - y_o$ = displacement in north-south direction, m

$$K_x = \frac{a \cos(\text{Lon}_o)}{[1 - e^2 \sin^2(\text{Lon}_o)]^{0.5}}$$

$$K_y = \frac{a(1 - e^2)}{[1 - e^2 \sin^2(\text{Lon}_o)]^{1.5}}$$

Variables with subscript $_o$ refer to a reference position, for example, one corner of a field.

Example Problem 6.1

A GPS reading (in degrees, minutes, seconds format) in the northeast corner of a rectangular field gave the coordinates $88^\circ, 12', 34.50''$ west longitude, $40^\circ, 4', 21.20''$ north latitude. The GPS reading in the southwest corner of the same field gave coordinates $88^\circ, 12', 60.4''$ west longitude, $40^\circ, 4', 8.1''$ north latitude. Calculate (a) the field dimensions in m and (b) the field area in ha.

Solution

The first step is to convert all of the longitude and latitude readings to radians, as follows:

$$\text{Lon, NE corner} = (88 + 12/60 + 34.50/3600)(\pi/180) = 1.53955 \text{ radians}$$

$$\text{Lat, NE corner} = (40 + 4/60 + 21.20/3600)(\pi/180) = 0.69940 \text{ radians}$$

$$\text{Lon, SW corner} = (88 + 12/60 + 60.4/3600)(\pi/180) = 1.53967 \text{ radians}$$

$$\text{Lat, SW corner} = (40 + 4/60 + 8.1/3600)(\pi/180) = 0.69933 \text{ radians}$$

Next,

$$K_x = \frac{6,348,135 \cos(0.69940)}{[1 - (0.081819)^2 \sin^2(0.69940)]^{0.5}} = 6,378,135 \text{ m/radian}$$

and
$$K_y = \frac{6,348,135 [1 - (0.081819)^2]}{[1 - (0.081819)^2 \sin^2(0.69940)]^{1.5}} = 6,335,438 \text{ m/radian}$$

Then,

$$x - x_o = 6,378,135 (1.53967 - 1.53955) = 800.9 \text{ m}$$

$$y - y_o = 6,335,438 (0.69933 - 0.69940) = -402.4 \text{ m}$$

The minus sign merely indicates the SW corner is further south than the reference corner. The dimensions of the field are thus 800.9 m in the east-west direction and 402.4 m in the north-south direction. A hectare contains 10,000 m² and thus the area of the field is:

$$\text{Area} = (800.9)(402.4)/10,000 = 32.2 \text{ ha}$$

Example Problem 6.2

In Example Problem 6.1, the coordinates for the northeast corner of the field were precisely determined by survey and the point was marked as a permanent benchmark. A GPS user has purchased a C/A code-based, differential GPS unit and wishes to determine its accuracy. The user places the GPS antenna on the benchmark and records a reading at five different times throughout a day. The results are:

	Longitude	Latitude
Benchmark	88° 12' 34.50"	40° 4' 21.20"
Reading 1	88° 12' 34.55"	40° 4' 21.22"
Reading 2	88° 12' 34.43"	40° 4' 21.25"
Reading 3	88° 12' 34.49"	40° 4' 21.11"
Reading 4	88° 12' 34.52"	40° 4' 21.24"
Reading 5	88° 12' 34.54"	40° 4' 21.23"

Analyze these readings and express the GPS errors in (a) 2SD, (b) RMS, and (c) CEP terms.

Solution

The K_x and K_y are the same as for Example Problem 6.1 because the same reference point was used for both. The first step is to convert each GPS reading from degrees-minutes-seconds to radians. Then, for each reading, Equations 6.5 and 6.6 are used to calculate the distances from the true benchmark position. For Reading 1, for example:

$$\text{Lon, Reading 1} = (88 + 12/60 + 34.55/3600)(\pi/180) = 1.53955 \text{ radians}$$

$$\text{Lat, Reading 1} = (40 + 4/60 + 21.22/3600)(\pi/180) = 0.69940 \text{ radians}$$

and

$$x - x_o = 6,378,135 (1.53955 - 1.53955) = 1.55 \text{ m}$$

$$y - y_o = 6,335,438 (0.69941 - 0.69940) = 0.61 \text{ m}$$

Then the radial distance error is:

$$\text{err} = \sqrt{\Delta x^2 + \Delta y^2} = \sqrt{(1.55)^2 + (0.61)^2} = 1.66 \text{ m}$$

Carrying through a similar analysis for the remaining points gives the following results:

Reading	Δx , m	Δy , m	err, m
1	1.55	0.61	1.66
2	-2.16	1.54	2.65
3	-0.31	-2.76	2.78
4	0.62	1.23	1.38
5	1.24	0.92	1.54

The mean of these five errors is 2.00 m and the standard deviation is 0.592 m. Thus, from this set of trial readings,

(a) the 2SD error = $2.00 + 2(0.592) = 3.18$ m,

(b) the RMS error = $2.00 + 0.592 = 2.59$ m, and

(c) the CEP = $2.00 + 0.68(0.592) = 2.40$ m.

Recall that 50% of all errors are expected to be no larger than the CEP error, 68% no larger than the RMS error and 95% no larger than the 2SD error. In this small sample, none of the individual errors were larger than the 2SD error, but two were larger than the RMS and the CEP errors.

6.3 GEOSPACIAL INFORMATION SYSTEM

As used in SSCM, a geospatial information system, or GIS, is a computer-based system for storing, analyzing, and displaying spatially-referenced data. The coverage of a GIS is selected to encompass the entity of interest and can be as large as a country, state, or county. For SSCM, GIS is used as a tool to aid crop management decisions. The coverage of each GIS is that of a single farm field and such a GIS could be considered a *Field Information System* (FIS).

6.3.1 Data input to a FIS

Input to a FIS can include any available data relevant to crop management decisions. The data can come from a variety of sources. Data on soil nutrients, moisture, texture, etc., can come from soil samples manually extracted from the soil at regular intervals in the field and processed in a soils laboratory. Alternatively, when appropriate sensors are available, the sensors can be positioned on an implement-mounted blade that is pulled through the soil. Machine vision sensors to capture crop-relevant data can be carried on low-flying aircraft or on satellites in space. Crop yield data can be captured by harvesters equipped with yield monitors, as discussed in later chapters in this book.

Typically, because the data vary spatially across a field, maps are used to represent the data in the FIS. For example, the map in Figure 6.2 shows spatially variable nitrogen application rates for a particular field. Other maps could show soil concentrations of potassium, phosphorous, or other factors relevant to crop production.

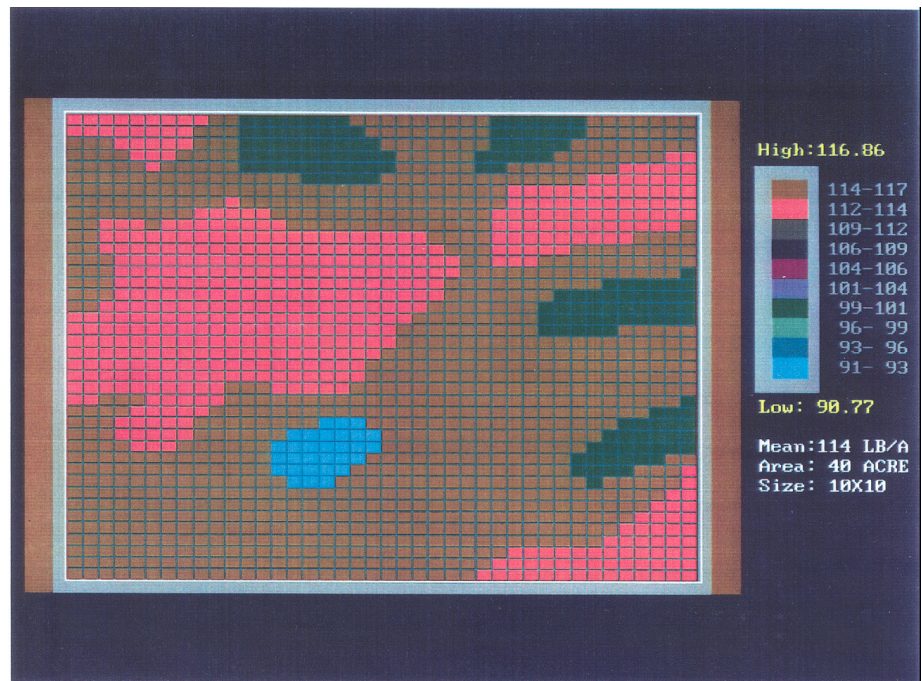


Figure 6.2 – A nitrogen application rate map.

6.3.2 Map coordination

The data inputs to a FIS can be in a variety of formats. Manual soil samples are taken at grid intersections in the field. Some implement-mounted sensors can produce continuous signals, but only along the paths of the sensors across the field. Data from satellites are often presented in the form of geo-referenced images. The images can be converted into geo-spatial maps.

In making decisions regarding management of any given point in a field, it is desirable to consider all of the data relevant to that point. These data are present in the form of overlying maps (see Figure 6.3) in the FIS, but the maps must be coordinated. Each map must have the same perimeter boundary, the same horizontal scale and each point within the boundary must be represented by data. A data interpolation scheme is used to estimate the given crop production factor at unmeasured points. *Kriging* is an interpolation technique that makes use of a semivariogram, i.e., a measure of the spatial dependence between samples of a given production factor. A semivariogram (see Figure 6.4) shows the increase in variance of some factor (e.g., soil potassium) between samples as one moves away from a given point in the field. Beyond a certain point (about 50 m in Figure 6.4), the variance no longer increases with distance and the area within this distance of the point is called the neighborhood of the point. Interpolation by kriging puts increasing weight on samples that are increasingly close to the point

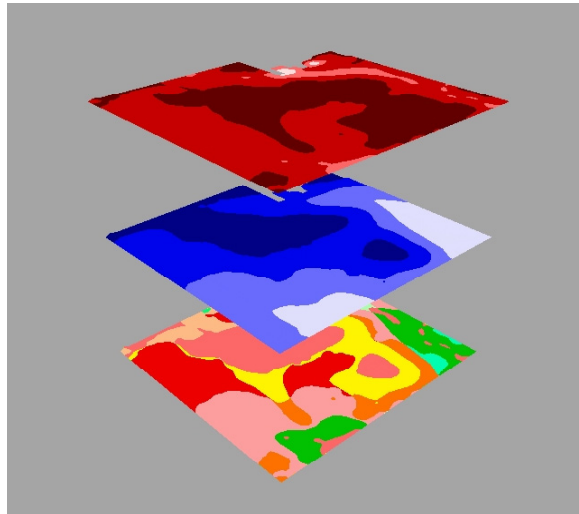


Figure 6.3 – Overlying maps in a GIS.

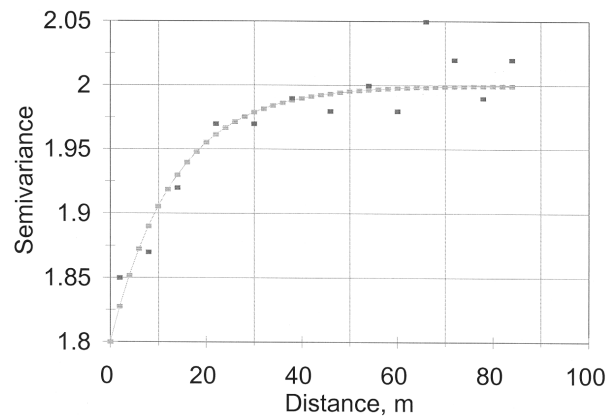


Figure 6.4 – A semivariogram.

whose data value is to be estimated. Because the calculations become onerous if too many sample points are included in the interpolation, only those data within the neighborhood of the point are used. The mathematics of kriging is beyond the scope of this book.

It is impractical to map the precise level of a crop production factor at every point in a field. Instead, the field is subdivided into smaller areas in which a crop production factor varies within defined limits and is considered uniform. Maps can be in either raster format or vector format. In raster format, the field is subdivided into small square grid cells, within each of which a crop production factor is considered to be

uniform. In vector format, straight-line (vectors) are linked, end-to-end, to enclose polygons within which a crop production factor is uniform. Each vector is represented by the coordinates of its two end points. The map in Figure 6.2 is in raster format. Note that multiple adjacent cells can make up larger areas of a uniform crop production factor and these larger areas approximate the polygons of the vector-based maps. The smaller the square cells, the more nearly the raster maps resemble the vector-based maps. The overlying maps of Figure 6.3 are vector-based maps. Software is available to convert maps from raster format to vector format or vice versa.

6.3.3 Data analysis in the FIS

An important use of a FIS is to generate application maps. For example, a potassium application map would show the desired application rate at every subarea in a field. Algorithms in the FIS are used to generate application maps based on an analysis of all of the relevant crop production factors mapped in the FIS. Generating target yield maps is an intermediate step, because nutrient needs increase with target yield.

There are three different approaches to generating target yield maps. One approach is to develop a mathematical model to predict yield based on the soil factors mapped in the FIS and on the probable weather, especially rainfall, in the coming season. Because of the complexity of crop growth and the unpredictability of weather, this approach has met with only limited success. A second approach is to map the actual yields of a crop, e.g., corn (see Chapter 12), for a number of years when the entire field is being farmed conventionally, i.e., uniformly. The idea is to identify subareas that yield consistently low or high as an indication of the yield potential of these subareas. This approach has also given only limited success because of poor repeatability. For example, a poorly drained low spot in a field might have very low yields in a wet year, but have the highest yields in a dry year. The third approach is to use a vision sensor or other radiometric device to sense the condition of the crop during the growing season and to apply fertilizer at rates appropriate to the condition of the crop in each part of the field. More research is needed on the generation of target yield maps and application rate maps.

6.3.4 Data persistence

Some crop production factors persist longer than others. At one extreme, the soil texture in a field is essentially constant over many years. At the other extreme, soil nitrates can vary widely over a short time as drainage removes the water-soluble nitrates and microorganisms form new nitrates. There is little benefit in mapping soil nitrate levels, because the levels will likely have changed before the map can be used. Only those crop production factors whose levels persist over time are usually mapped.

6.4 VARIABLE RATE APPLICATIONS

6.4.1 Approaches

There are three different approaches to variable rate applications. In the map driven approach (MDA), a digitally represented map is consulted by the controller of the variable rate applicator to determine the desired application rate as the applicator moves across the field. In the sensor driven approach (SDA), a sensor mounted on the

applicator senses some factor, e.g., soil nitrate, and the variable rate applicator uses the sensor signal to determine the appropriate application rate as the applicator moves across the field. The third approach is the map and sensor driven approach (MSDA) that uses a combination of the two approaches. In MSDA applications of nitrogen fertilizer, for example, an application map could indicate the amount of nitrogen needed to meet the target yield in each subarea of the field, while a nitrate sensor indicated the amount of nitrogen already present; the applicator could then apply only the additional nitrogen needed to meet the target yield.

6.4.2 Applications

A variety of agricultural operations can benefit from variable rate technology. For example, sensors have been developed to sense the density of weed populations across a field. Variable rate sprayers have been developed to spray only those areas of a field that contain significant weed populations. Some research has been done on sensing the spatial variation of soil compaction, so that deep chiseling can be done on only those areas needing this high-energy tillage operation. These are only two examples and additional uses for variable-rate technology continue to be developed.

6.4.3 Application resolution

Resolution refers to the smallest area that is treated by variable-rate technology. Crop scientists who have studied the spatial variability of various crop production factors have found significant variability over distances as small as one meter. However, practical considerations prevent applications from being responsive to such small-scale variation. For example, some fertilizer applicators apply a uniform rate of fertilizer over the entire width of the applicator and the applicator width can be ten meters or more. Such an applicator could change the application rate continuously along its path of travel, but not over the width of the applicator. In general, SDA-type applicators can achieve high resolution in the direction of travel but resolution across the width of an applicator depends on the design of the applicator.

There are other factors that provide practical limits to resolution. For MDA applications, it is pointless to try to achieve resolution smaller than the uncertainty error of the GPS unit that determines the applicator location in the field. GPS uncertainty can be several meters depending upon the GPS unit being used. Also, if applications are tied to soil samples that are taken and analyzed manually, economic considerations greatly limit the number of such samples in a field. If the soil sampling points are separated by tens of meters, the data interpolation technique will be incapable of providing accurate interpolations of the data to the one-meter level. Thus, resolution choices require a compromise involving the length scale of crop production factors and practical considerations that often limit the resolution to larger length scales.

6.4.4 Control systems

Automatic control systems can be either open loop or closed loop. Consider, for example, a sprayer whose application rate is being controlled by varying the speed of the pump that delivers herbicide to spray nozzles. If the pump has fixed displacement, as discussed in Chapter 5, the flow rate will vary proportionally with pump speed. In an open loop system, the pump speed would be controlled accordingly to produce a

flow rate consistent with the travel speed of the sprayer and the desired herbicide application rate. The actual flow rate to the nozzles would not be measured. If internal wear in the pump reduced the flow rate, the open-loop controller would not be able to detect the error in application rate.

By adding a flow meter to measure the actual flow rate to the nozzles, the above controller could be converted to a closed-loop controller. The controller would compare the actual flow rate to the flow rate needed to produce the desired application rate at the current applicator speed and adjust the pump speed accordingly. In this case, the accuracy of the closed loop controller depends only on the accuracy of the flow meter and that of the travel speed sensor. Closed-loop controllers are generally more accurate than open-loop controllers but introduce new problems. One of these is that the controller may become unstable, i.e., its control signal may oscillate. There are design techniques to deal with controller stability, but they are beyond the scope of this book.

6.4.5 Automatic guidance

Automatic guidance is a newly emerging part of precision agriculture. GPS has improved to the point that it can provide a dependable guidance reference of acceptable accuracy. Although a tractor or machine with automatic guidance might not need a human operator for steering, an operator of such a tractor or machine might still be needed for detecting contingencies and making decisions. For example, a combine operator might see a rock about to enter the header and stop the combine before damage occurs. To provide sensors and control systems to guard against every such possible contingency would be very expensive. Automatic guidance can be economically justified even if it doesn't replace the operator. For example, the added cost of automatic guidance is near the cost of a set of mechanical markers on a modern corn planter and can eliminate the need for the markers. Also, automatic guidance can prevent excessive overlaps or skips in spraying operations. Farm equipment manufacturers have begun offering automatic guidance systems as options on farm equipment.

GPS can pinpoint the geographic location of a tractor or machine within a field with sufficient accuracy. Before a steering error can be calculated, the desired location of the tractor or machine must be known at each instant in time. Desired travel paths within a field can be included as one map layer in a GIS. The guidance system can continually interrogate the GIS and the GPS to determine needed steering corrections. Although much theoretical analysis has been done on automatic guidance for agricultural machines, the theory is beyond the scope of this book.

6.5 CONTROLLER AREA NETWORKS

Modern tractors and implements contain multiple microprocessors, or *electronic control units* (ECUs), to provide sophisticated control of various functions. A radar unit can deliver pulses to an ECU that uses the pulse frequency to compute and display travel speed. An ECU might also accept a signal from a flow rate sensor and the two signals might be used to control a spray application rate. The ECUs, together with sensors and actuators, are the fundamental components of modern control systems. Each ECU can be programmed to perform its function or functions. The programs can

be stored in an EPROM (erasable programmable read-only memory) or an EEPROM (electrically erasable programmable read-only memory).

Advantages can be gained by allowing the various ECUs to intercommunicate. For example, the ECU on a tractor might contain digitized application maps, while a different ECU on a variable rate sprayer might control the actual spray applications. The *controlled area network* (CAN) was developed to allow intercommunication between ECUs. To allow ECUs from different manufacturers to communicate, the CAN has been standardized in ISO Standard 11783 (covering agricultural tractors and implements) and in SAE Standard 1936 (covering construction equipment), i.e., ISO 11782 provides for an open architecture system. The communication occurs via a CAN bus consisting of two wires in a twisted quad to communicate data. The other two wires in the twisted quad are used to deliver electrical power to the ends of the bus. Each bus must have a terminator at both ends. A special automatic terminating bus breakaway connection at the hitch point automatically provides termination when an implement is unplugged.

The maximum length of a bus is 40 m. ECUs can be connected at any point on the bus, but must be at least 0.1 m apart. A bridge must be used to interconnect bus segments, e.g., a tractor bus with an implement bus. In ISO Standard 11783, an ECU on the tractor may serve as the bridge. The bridge ECU may do filtering to reduce traffic on certain bridge segments. For example, the high traffic associated with timing of individual fuel injections to an engine would be filtered to prevent it from reaching the implement bus because the implement-controlling ECU does not need data on individual fuel injections.

Messages between ECUs consist of groups of digital bits that are sent serially. The first bits in each group are message identifiers, while the remaining bits carry data. Identifier bits include the source address of the sending ECU and the destination address of the receiving ECU. Each ECU attempts to claim an address upon power-up and an arbitration protocol handles conflicts. The ISO 11783 standard provides for a bus able to handle up to 250,000 bits/s of information. The protocol imbedded in each ECU requires the ECU to check the bus before sending a message to be sure no other ECU is currently using the bus and a prioritization scheme to allow the bus to prioritize messages.

The ISO 11783 standard provides for an operator interface called a *virtual terminal* (VT). The VT provides information to the operator and allows the operator to input information to the system. The VT may be switched between ECUs to allow monitoring and control of any part of the system. For example, the VT might be used to monitor engine performance at certain times and to monitor and control implement functions at other times. The VT can be used to download masks and soft-key menus. The masks define the panels displayed on the screen, while the soft-key menus allow operator input to the system.

ISO Standard 11783 includes a message classification scheme. Classification I is for basic information and lighting control. Example messages include engine speed, PTO speed, hitch position, and control of turn signals, stop lights, and illumination lights. Classification II adds ground-based distance and direction data, implement

draft, etc. Classification III adds control information, e.g., set points for hitch position and PTO speed.

Work on CAN buses during the 1990s led to the development of ISO Standard 11783. Earlier, electronic devices had to be developed to accommodate the often-unfavorable environment (temperature, humidity, shock, and so forth) encountered on farm tractors. Manufacturers began to market agricultural tractors equipped with CAN buses soon after the development of ISO Standard 11783 and rapid widespread adoption of such systems is expected.

PROBLEMS

Note: For your convenience in working the problems below, EXCEL spreadsheet “GPS Calculations” has been provided on the CD-ROM.

- 6.1 A GPS unit was used to determine the coordinates of the following two corners in a rectangular field:
- Point 1: $88^{\circ} 12' 86.30''$ W Longitude, $40^{\circ} 4' 8.15''$ N Latitude
Point 2: $88^{\circ} 12' 112.20''$ W Longitude, $40^{\circ} 3' 42.10''$ N Latitude
- (a) Find the N-S and E-W dimensions of the field in m, (b) find the area of the field in hectares, and (c) for each GPS reading, determine whether it is the NE, NW, SE, or SW corner of the field. (Hint: Longitude increases moving westward while, in the northern hemisphere, latitude increases moving northward).
- 6.2 A GPS unit was used to determine the coordinates of the following two corners in a rectangular field:
- Point 1: $88^{\circ} 12' 86.30''$ W Longitude, $40^{\circ} 4' 8.15''$ N Latitude
Point 2: $88^{\circ} 12' 112.20''$ W Longitude, $40^{\circ} 3' 55.10''$ N Latitude
- (a) Find the N-S and E-W dimensions of the field in m, (b) find the area of the field in hectares, and (c) for each GPS reading, determine whether it is the NE, NW, SE, or SW corner of the field. (Hint: Longitude increases moving westward while, in the northern hemisphere, latitude increases moving northward).
- 6.3 Rework Problem 6.1, but use data you acquired yourself or provided by your instructor.
- 6.4 For evaluating the accuracy of a GPS unit, the following readings were taken:
- Benchmark: $88^{\circ} 12' 34.50''$ W Longitude, $40^{\circ} 3' 21.20''$ N Latitude
Point 1: $88^{\circ} 12' 34.56''$ W Longitude, $40^{\circ} 3' 21.23''$ N Latitude
Point 2: $88^{\circ} 12' 34.44''$ W Longitude, $40^{\circ} 3' 21.24''$ N Latitude
Point 3: $88^{\circ} 12' 34.48''$ W Longitude, $40^{\circ} 3' 21.16''$ N Latitude
Point 4: $88^{\circ} 12' 34.53''$ W Longitude, $40^{\circ} 3' 21.18''$ N Latitude
Point 5: $88^{\circ} 12' 34.55''$ W Longitude, $40^{\circ} 3' 21.22''$ N Latitude
Point 6: $88^{\circ} 12' 34.47''$ W Longitude, $40^{\circ} 3' 21.17''$ N Latitude
- Calculate the (a) RMS, (b) 2SD, and (c) CEP errors in m.
- 6.5 For evaluating the accuracy of a GPS unit, the following readings were taken:

Benchmark: $88^{\circ} 12' 34.49''$ W Longitude, $40^{\circ} 3' 21.17''$ N Latitude

Point 1: $88^{\circ} 12' 34.56''$ W Longitude, $40^{\circ} 3' 21.23''$ N Latitude

Point 2: $88^{\circ} 12' 34.44''$ W Longitude, $40^{\circ} 3' 21.24''$ N Latitude

Point 3: $88^{\circ} 12' 34.48''$ W Longitude, $40^{\circ} 3' 21.16''$ N Latitude

Point 4: $88^{\circ} 12' 34.53''$ W Longitude, $40^{\circ} 3' 21.18''$ N Latitude

Point 5: $88^{\circ} 12' 34.55''$ W Longitude, $40^{\circ} 3' 21.22''$ N Latitude

Point 6: $88^{\circ} 12' 34.47''$ W Longitude, $40^{\circ} 3' 21.17''$ N Latitude

Calculate the (a) RMS, (b) 2SD, and (c) CEP errors in m.

- 6.6 Rework Problem 6.4, but use data you acquired yourself or provided by your instructor.

Relevant websites

(Warning: The following websites were relevant at time of publication of the book, but webmasters are free to change or eliminate websites at any time).

http://www.Colorado.edu/geography/gcraft/notes/gps/gps_stoc.html

<http://www.gis.com/whatisgis/>

<http://www.gisdevelopment.net/tutorials/tuman006.htm>

TRACTOR HITCHING, TRACTION, AND TESTING

7

INTRODUCTION

Tractors frequently serve as the power source for field machines. A hitch connects the implement to the tractor. The tractor provides the tractive force to move the implement through the field. Thus, this chapter deals with tractor hitching and traction. Standard testing procedures have been developed for tractors and tractor testing is also discussed in this chapter.

7.1 HITCHING SYSTEMS

7.1.1 Principles of hitching

Most agricultural operations involve hitching some type of implement to a tractor. The forces transmitted through a hitch can affect the performance of both the tractor and the implement. Modern hitches include feedback for automatic control of pull and/or depth of tillage implements. In addition to transmitting forces, the hitch may also be required to carry the implement for transport.

7.1.2 Types of hitches

Early tractors included only a *drawbar* hitch, which permitted pulling but not carrying an attached implement. The three-point hitch has now become standard equipment on most tractors. The tractor of Figure 7.1 is equipped with both a drawbar and a *three-point hitch*. Terminology of a three-point hitch is illustrated in Figures 7.2 and 7.3. The points of attachment of the hitch links to the tractor are called link points, while the links are attached to the implement at the hitch points. Quick-attaching couplers (Figure 7.4) have been developed to allow faster attachment of three-point hitches to implements. Dimensions of three-point hitches have been standardized by ASAE (now ASABE) since 1959. Table 7.1 shows four of the hitch categories that have been standardized for different sized tractors; in addition, there is a category 0 hitch standard for garden tractors. The hitch dimensions that are standardized include

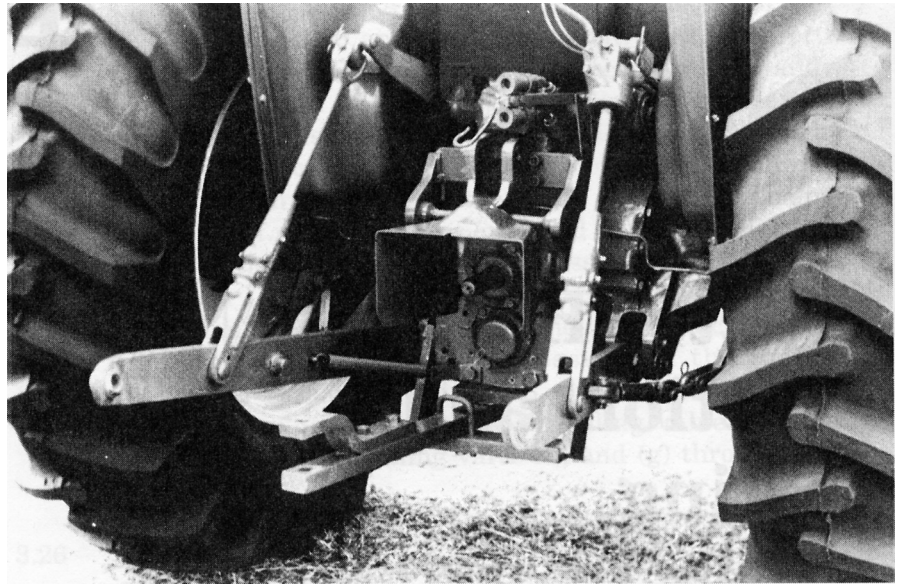


Figure 7.1 – A tractor with a drawbar and three-point hitch.

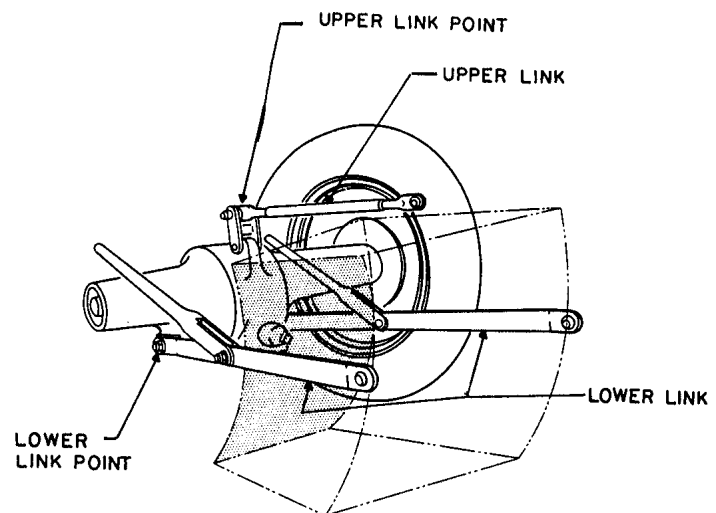


Figure 7.2 – A three-point hitch for a tractor (reprinted from ASAE Standard S217.10, Three-point, free-link attachment for hitching implements to agricultural wheeled tractors).

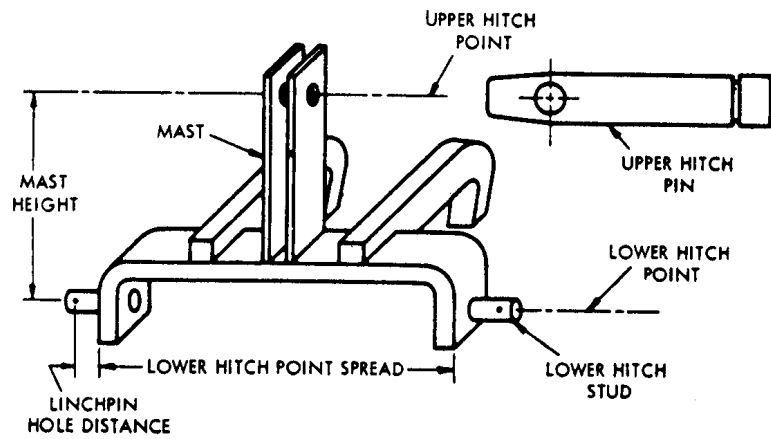


Figure 7.3 – Three-point hitch connections on an implement (reprinted from ASAE Standard S217.10, Three-point, free-link attachment for hitching implements to agricultural wheeled tractors).

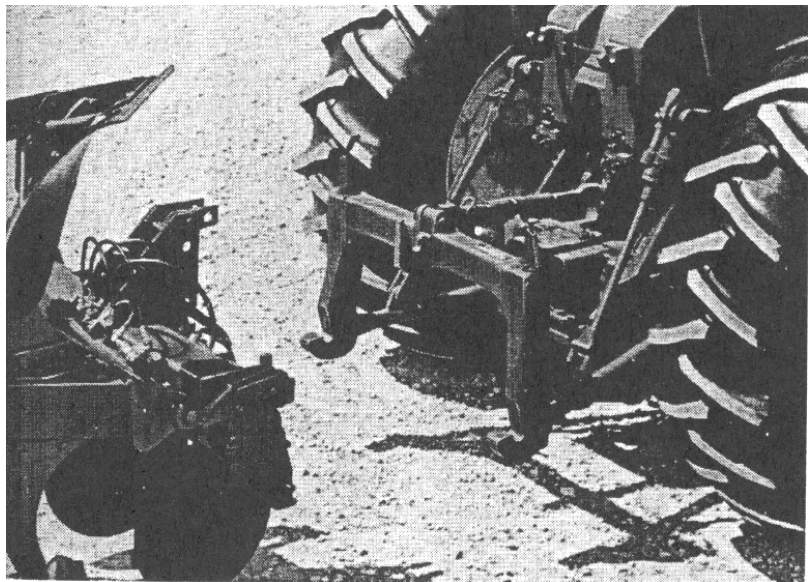


Figure 7.4 – Three-point hitch with quick-attaching coupler (courtesy of Deere and Co.).

Table 7.1. Three-point hitch categories (ASAE Standard S217.10).

Category	Maximum Drawbar Power, kW (hp)
I	15 - 35 (20 - 45)
II	30 - 75 (40 - 100)
III and III-N	60 - 168 (80 - 225)
IV and IV-N	135 - 300 (180 - 400)

hitch pin diameters, mast height, and lower hitch point spread. Exact dimensions can be found by referring to ASAE Standard S217. There are also ASAE standards relating to the drawbar; Standard S207 specifies minimum vertical loads that drawbars must withstand, while Standard S203 specifies the location of the drawbar hitch point relative to the *PTO shaft*.

An implement with a mast (Figure 7.3) can be carried entirely by the tractor and such implements are said to be *fully mounted*. *Semi-mounted* implements are attached to the tractor by only the two lower links and the ground must provide part of the implement support. Semi-mounted moldboard plows are the best known example of this type of hitch. Thus, the three types of hitching include *towed* (for implements hitched to the drawbar), semi-mounted, and fully mounted implements.

7.1.3 Hitching and weight transfer

Hitching affects both vertical and horizontal force relations between tractor and implement. Vertical effects on the tractor are of special interest because of their effect on the tractive performance of the tractor. The force imposed on the tractor by the implement (Figure 7.5) could be transmitted through a drawbar or through a semi-mounted or fully mounted hitch. The following equations can be obtained by taking moments about points C_2 and C_1 , respectively:

$$R_r = \frac{m_t g(x_1 - x_2)}{x_1} + \frac{F_{hx} z}{x_1} + F_{hz} \quad (7.1a)$$

and

$$R_f = \frac{m_t g x_2}{x_1} - \frac{F_{hx} z}{x_1} \quad (7.2a)$$

where R_r = total vertical soil reaction on rear wheels, kN

R_f = total vertical soil reaction on front wheels, kN

m_t = tractor mass, Mg

g = acceleration of gravity = 9.801 m/s²

F_{hz} = z-component of hitch force, kN

F_{hx} = x-component of hitch force, kN

x_1 = wheelbase of tractor, mm

x_2 = distance from rear axle center to tractor center of gravity, mm

z = distance from ground to intersection of R_r with line of pull, mm

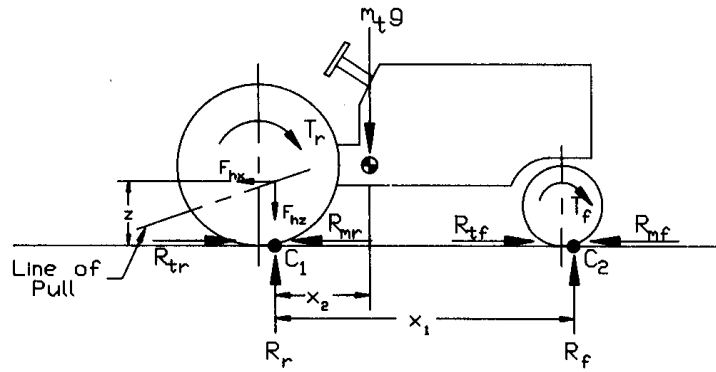


Figure 7.5 – Force and moment relations for a tractor when pulling an implement at a uniform velocity on level ground.

Points C_1 and C_2 are directly under the axle centers when a tractor is sitting on level ground with $F_{hx} = 0$, but move forward somewhat due to rolling resistance when the tractor is moving. The vertical wheel forces calculated from Equations 7.1a and 7.2a when $F_{hx} = F_{hz} = 0$ are called the static wheel reactions. The quantity, $(F_{hx} z/x_1)$, is called *weight transfer* because it is removed from the front wheel reaction and added to the rear wheel reaction due to the moment of the pull transmitted through the hitch. If the line of pull is inclined as shown in Figure 7.5, an additional term, F_{hz} , is also added to the rear wheel reaction. Some weight transfer is helpful on 2WD (two-wheel drive, typically rear-wheel drive) tractors because the tractive ability of the drive wheels is limited by the vertical soil reaction. However, too much weight transfer will bring R_f to zero, upon which the front wheels will raise off the ground. For 4WD (four-wheel drive) tractors, weight transfer is not helpful because tractive effort gained at the rear wheels is lost at the front wheels.

While Equations 7.1a and 7.2a give exact values for wheel reactions, they are difficult to use in practice. The distances x_2 and z are not easily measured and are constantly changing during agricultural operations. Thus, an approximate method has been developed for computing wheel reactions. The approximate equations are:

$$R_r = R_{r0} + C_{dw} F_{hx} \tag{7.1b}$$

$$R_f = R_{f0} - C_{dw} F_{hx} \tag{7.2b}$$

where $R_{r0} = m_t g(x_1 - x_2)/x_1$ = static rear wheel reaction, kN

$R_{f0} = m_t g x_2/x_1$ = static front wheel reaction, kN

C_{dw} = dynamic weight coefficient, dimensionless

Experimental studies have shown that the approximate values for C_{dw} are 0.20, 0.45, and 0.65 for towed, semimounted, and fully mounted hitching, respectively. The C_{dw} values were chosen to incorporate the effect of force F_{hz} on the rear wheels; thus Equation 7.2b somewhat overestimates the weight transfer from the front wheels.

7.1.4 Control of hitches

A single-acting hydraulic cylinder is usually provided to raise the lower links of a three-point hitch and lowering is accomplished by the weight of the attached implement. In the system illustrated in Figure 7.6, the cylinder rotates a rockshaft; arms attached to the ends of the rockshaft lift the lower links to raise the hitch. A feedback control system is provided as a standard feature of three-point hitches so that the hitch movement will mimic the movement of the hitch control lever. In the system shown in Figure 7.6, moving the position-control handle leftward pulls on the spool of the main control valve, initiating oil flow to the cylinder to raise the hitch. As the hitch raises, a cam on the rockshaft pushes on the spool of the main control valve so that hitch movement stops at a position corresponding to that of the position control handle. Conversely, when the position control handle is moved to the right, the hitch mimics that movement in lowering as the control valve releases oil from the cylinder.

With the first three-point hitches, when a tractor was pulling a heavy-duty tillage implement under varying field conditions, the operator would raise the hitch slightly when the pull became excessive in heavy soils and would again lower the hitch when the pull subsided in lighter soils. Engineers soon modified the three-point hitch controls to accomplish such raising and lowering automatically. In Figure 7.6, a torsion bar is used to sense force in the lower links; as the force increases, twisting of the torsion bar moves a linkage to pull out on the spool of the main control valve and causes the lower links to be lifted. Conversely, declining force in the lower links causes them to be lowered. Just as the position control handle is used to set the desired position of the lower links, the load (draft) control handle is used to set the desired amount of force in them. On some small tractors, *draft sensing* is accomplished by sensing compressive force in the top link. In recent larger tractors, the torsion bar and mechanical linkage are eliminated. Lower link sensing is accomplished by use of instrumented link pins that sense shear at the lower link points. Through circuitry that is provided, the voltage from the link pins is used to control an electrically actuated hydraulic valve which, in turn, controls raising and lowering of the hitch.

7.2 TIRES AND TRACTION

The power of a tractor engine may be transmitted through the PTO shaft, the hydraulic system, or through a hitch. The latter is the most common means of transmitting tractor power and the efficiency of transmission is limited by *tractive efficiency*. Thus, traction mechanics that support the design of efficient tractive devices is of great interest. Wheels are the tractive devices considered in this textbook. When a wheel works on soil, the soil must compress in order to acquire sufficient strength to provide a high tractive force to the wheel. The compression is provided by relative movement between the wheel and the soil. Consequently, some *wheel slip* must occur to provide traction, but excessive slip is inefficient. Traction mechanics provides a means for determining optimum wheel slip. The soil strength is an important factor in traction mechanics, and is represented by the *cone index*.

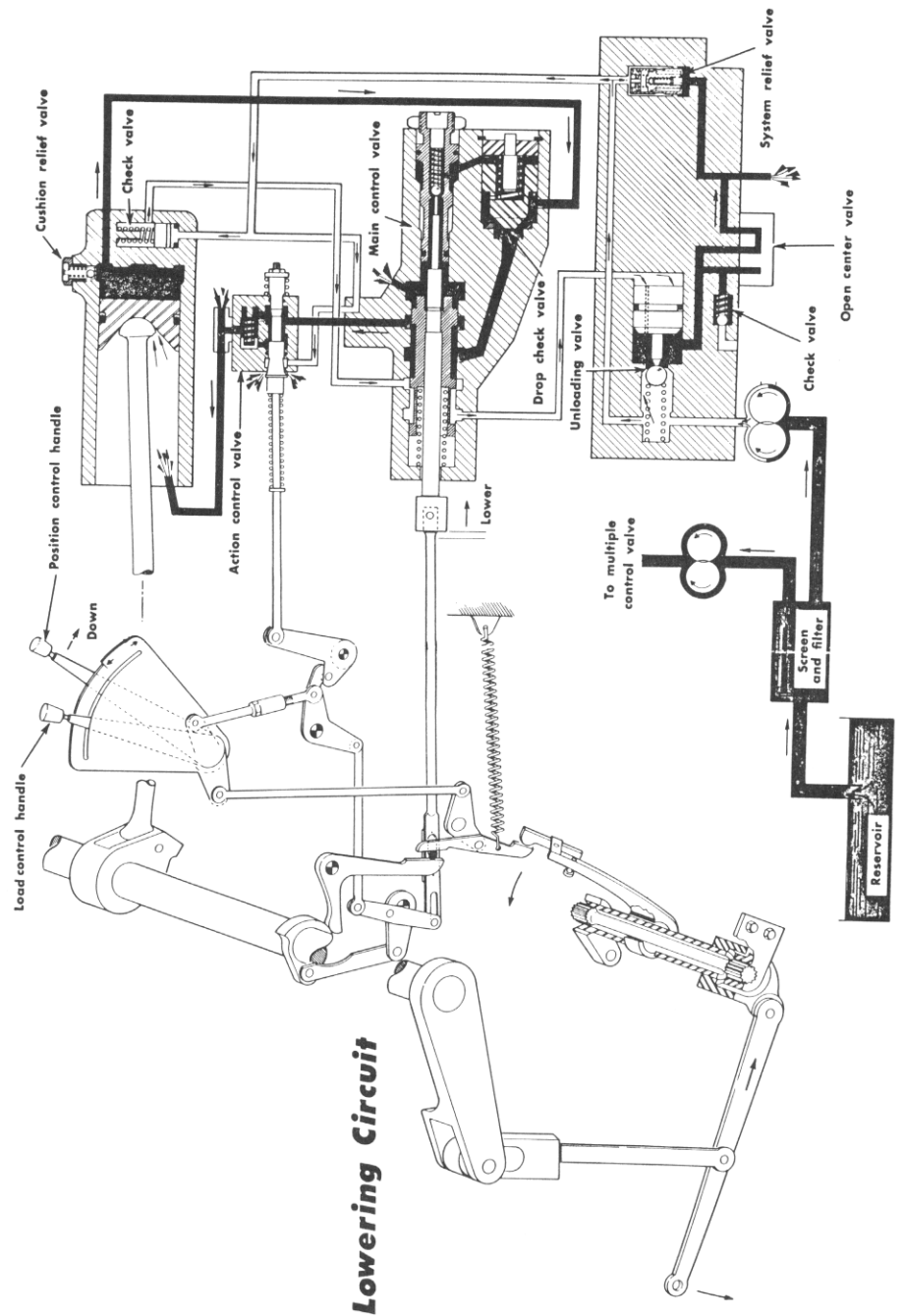


Figure 7.6 – A combination draft and position control system for a tractor hitch (courtesy of CNH).

7.2.1 Basic tire design

Dimensions associated with tires are illustrated in Figure 7.7. The *aspect ratio* of a tire is the *section height* divided by the *section width*. Typical aspect ratios range from 0.75 or less for low-profile tires to 1.0 or higher for high molded tires. Agricultural tires typically deflect about 19% of their section height at rated inflation pressure when the rated vertical load is applied, and thus the *loaded radius* (Figure 7.7) is less than half of the outside diameter of the tire. As the tire deforms under load, the section height decreases and the width increases. The dimensions for the loaded tire in Figure 7.7 are for a motionless tire. The stress distribution in a moving tire causes a slight lifting action and thus the rolling radius is slightly larger than the static loaded radius.

Agricultural tractors have not yet been converted to metric sizes. Thus, the tire size gives dimensions in inches. Consider the following tire, for example:

20.8-32, 8

The first number is the section width in inches, the second number is the rim diameter in inches, and the third number is the ply rating. The tire in the above example has a section width of 20.8 inches, a rim diameter of 32 inches, and it is an 8-ply tire.

Tire manufacturers specify the *load-carrying capacity* of their tires. The load-carrying capacity increases with tire size, *ply rating*, and inflation pressure. Travel speed affects the load rating and thus manufacturers of agricultural tires publish two

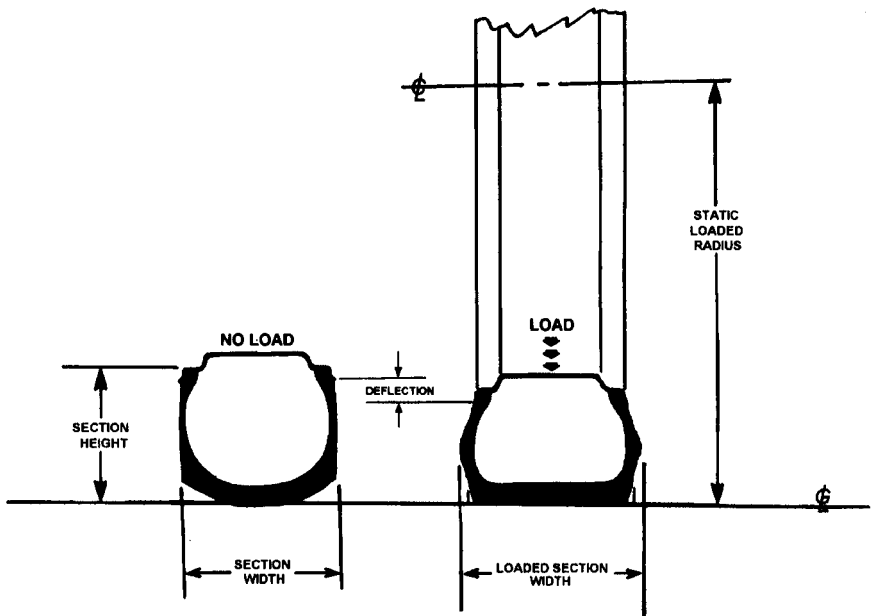


Figure 7.7 – Tire and rim dimensions.

sets of load rating tables. One table is for speeds up to 32 km/h and the other for speeds below 8 km/h. Considerably higher loading is permitted for the slower speeds. Lugged tires are used to convert axle torque to pull and, on such tires, the maximum tangential pull on the tire must be kept within allowable limits. Thus, the drawbar power must be limited to keep the tire bead from slipping on the rim and/or the tire sidewall from buckling. Figure 7.8 illustrates the use of dual tires to increase the tangential-pull-limited drawbar power. The figure is for bias-ply tires on a 2WD tractor. For example, if 20.8-34, 8 ply tires are on the rear axle, the maximum allowable drawbar power is 55 kW when the tractor is pulling at 4 km/h with a single tire on each rear axle. Pulling with duals (two 20.8-34, 8 ply tires on each rear axle) at 4 km/h would increase the allowable drawbar power to 96 kW. Notice that, at a given speed, the allowable power with duals is not double the power with singles; tire manufacturers derate the tangential pull on each tire by 12% when used in the dual configuration and by 18% when triples are used. Allowable drawbar power can also be increased by increasing the travel speed. When 20.8-34, 8-ply singles are used, for example, Figure 7.8 shows that the allowable drawbar power increases from 55 kW to 110 kW when the travel speed is increased from 4 to 8 km/h.

The previous discussion has been on agricultural tires with *bias-ply* construction, but *radial tires* are also available. Figure 7.9 illustrates differences between these two types of construction. With bias-ply construction, the reinforcing cords in the tire are

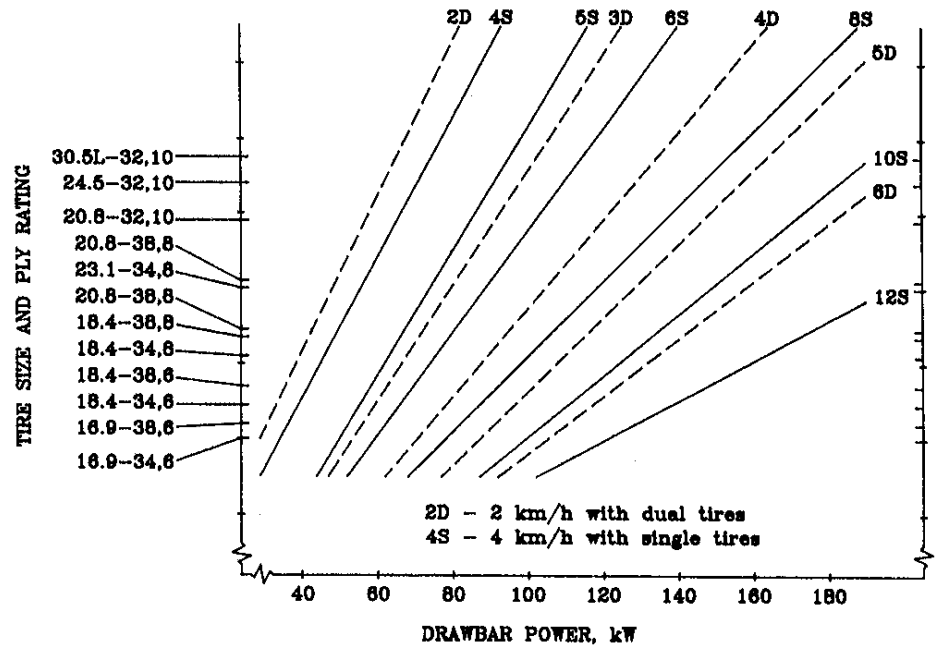


Figure 7.8 – Tangential-pull limited drawbar power.

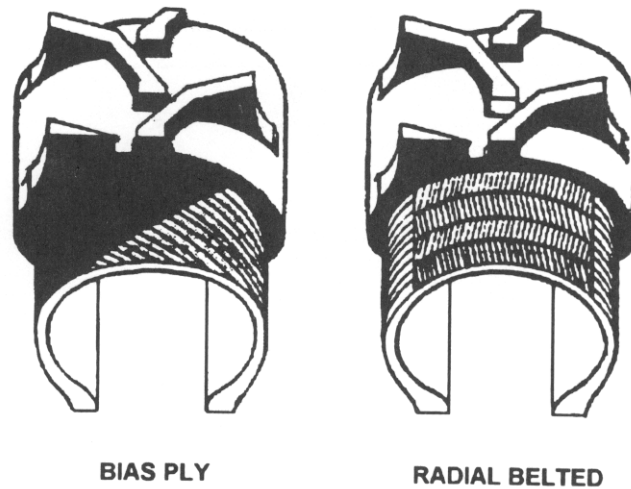


Figure 7.9 – Bias and radial-ply agricultural tires.

arranged diagonally across the tire from bead to bead. With radial construction, the cords are arranged perpendicular to the tire beads. An inextensible belt is positioned between the plies and the tread to restrict the flexing action of the radial tire. Radial construction permits increased radial deflection and increased bulging of the sidewall compared to bias-ply tires. Radial tires thus have a larger footprint, resulting in approximately 10% higher pull for a given slip or 15% to 25% reduced slip at a given pull compared to bias-ply tires.

The tires in Figure 7.9 have rubber lugs on the outer tread to provide better traction on soft soil. Agricultural tires without lugs are available for implements and for unpowered tractor wheels. The tire industry has established the codes listed in Table 7.2 to indicate the various types of tires. Only those with prefix R have lugs or knobs, to indicate that they are the *rear* tires on a 2WD tractor. R-type tires are also used on the front wheels of 4WD tractors. The terms *lugged* and *nonlugged* would be more descriptive of the tires, but the R-designation is still used by the tire industry to indicate lugged tires. R-2 tires have much taller lugs than R-1 tires to provide traction in the wet conditions encountered in rice production. The letter F in Table 7.2 is used to indicate *front* tires, that is, tires which are used on the front wheels of 2WD tractors. *Implement tires* have the prefix I and off-road *industrial tires* have the prefix E.

In selecting tires for a tractor or implement that is being designed, only a rough estimate of the tire loading may be available initially. It is good practice to base the tire selection on the lowest ply rating available when selecting a tire that can fit within available space and carry the estimated load. Also, the tires must provide a large enough contact area to carry the vertical load without excessive sinkage into soft soils. Tires on driving wheels must be able to transmit the required amount of power without exceeding the tangential pull limits. Thus many factors influence the initial tire selection. If refinement of the design shows increased tire loading, a larger ply rating can be selected to provide increased load-carrying capacity without increasing the tire size.

Table 7.2. Standard industry codes for tire types.^[a]

Type of Tire	Code
Front Tractor	
Rice tread	F-1
Single rib tread	F-2
Dual rib tread	F-2D
Triple rib tread	F-2T
Industrial tread	F-3
Drive Wheel Tractor (Rear)	
Rear wheel, regular tread	R-1
Cane and rice, deep tread	R-2 ^[b]
Shallow, non-directional tread	R-3
Industrial, intermediate tread	R-4
Implement	
Rib tread	I-1
Traction tread	I-3
Plow tail wheel	I-4
Smooth tread	I-6
Off-The-Road Tires (Industrial)	
Rib	E-1
Traction	E-2
Rock	E-3
Rock deep tread	E-4
Rock intermediate	E-5
Rock maximum	E-6
Flotation	E-7

^[a] Source: Reprinted with permission © 1970 Deere and Co., *Fundamentals of Service - Tires and Tracks*, 4.

^[b] Also includes similar treads for “G,” “L,” and “ML” series codes.

7.2.2 Traction models

The equations that govern traction were developed by grouping all of the relevant traction variables into dimensionless quantities (as discussed in Chapter 1). Then individual wheels were tested in a soil bin while forces, speed, and slip were measured. Using the dimensionless quantities, two basic equations were then developed to fit the soil bin data. One was for a *gross traction ratio* and another was for a *motion resistance ratio*. The equations are thus for single wheels, but the same equations can be assembled into a traction model for an entire vehicle. The gross traction ratio relates torques and forces on a wheel (see Figure 7.5) to wheel and soil parameters, i.e.:

$$\frac{T_i}{r_{Li}R_i} = C_{gi} = 0.88(1 - e^{-0.1B_{mi}})(1 - e^{-k_i s}) + k_2 \quad (7.3)$$

where T_i = traction-limited torque on wheel i , N·m
 i = f for a front wheel or r for a rear wheel

r_{Li} = static loaded radius of wheel i , mm

R_i = dynamic vertical load on wheel i , kN

C_{gi} = gross traction ratio for wheel i , dimensionless

B_{ni} = wheel numeric (See Equation 7.4)

k_1 = constant = 7.5 for bias-ply tires or 8.5 to 10.5 for radial tires

k_2 = constant = 0.04 for bias-ply tires or 0.03 to 0.035 for radial tires

S = wheel slip, decimal

The torque calculated using Equation 7.3 is the maximum torque that can be supported by traction. If the engine and power train attempts to deliver higher torque, wheel torque will increase somewhat until maximum wheel slip is reached but will not increase further. Note that, for a given C_{gi} , the maximum torque increases in direct proportion with the dynamic load on the wheel. Also, C_{gi} increases with wheel slip and with B_{ni} . The *wheel numeric*, B_{ni} , is defined as:

$$B_{ni} = \frac{CI_i b_i d_i}{1000R_i} \frac{1 + 5\delta_i / h_i}{1 + 3/r_A} \quad (7.4)$$

where B_{ni} = dimensionless wheel numeric for i th wheel

CI_i = effective cone index for i th wheel, N/mm²

b_i = section width of i th wheel, mm

d_i = outside diameter of i th wheel, mm

δ_i = deflection of i th tire due to vertical loading, mm

h_i = section height of i th wheel, mm

r_A = aspect ratio = section height over section width

The wheel numeric is the product of two dimensionless terms. The numerator of the first term is a measure of the load carrying capacity of the soil, while the denominator gives the actual loading. The second dimensionless term is a correction term to account for deformation of the tire under load. As Equation 7.4 indicates, B_{ni} increases with soil strength, wheel diameter, tire width, and tire deflection. The quantities, b_i , d_i , and r_{Li} , can be found in ASAE Standard S220 for specific tires. If the standard is not available or for tires not listed in the standard, d_i and r_{Li} can be calculated from the tire size specifications by using the following equations:

$$d_i = 25.4(d_{nri} + 2r_A b_{nri}) \quad (7.5)$$

and

$$r_{Li} = 25.4 \left(\frac{d_{nri}}{2} + 0.81r_A b_{nri} \right) \quad (7.6)$$

where d_{nri} = *nominal rim diameter* for the i th wheel, inches

b_{nri} = *nominal section width* for the i th wheel, inches

r_A = aspect ratio = section height over section width

Note the inclusion of a factor, 25.4, in the above equations to convert to mm from the tire size specifications in inches. Equation 7.6 is based on an assumed tire deflection of 19% of the section height. The following aspect ratios should be used in Equations 7.5 and 7.6:

- For low-profile, R-1 and R-2 type tires (indicated by an L in the tire size designation), use 0.70.
- For other R-1 and R-2 type tires, use an aspect ratio of 0.85.
- For low-profile F- or I-code tires (indicated by an L after the width in the size specification), use an aspect ratio of 0.78.
- For other F- or I-code tires, use an aspect ratio of 1.01.

These choices for aspect ratio and tire deflection generally allow calculation of d_i and r_{Li} with less than 10% error.

Two other tire parameters can be calculated using the following equations:

$$\delta_i = \frac{d_i}{2} - r_{Li} \quad (7.7)$$

and

$$h_i = \frac{d_i - 25.4d_{nri}}{2} \quad (7.8)$$

The motion resistance ratio, ρ_i , is defined as follows:

$$\frac{R_{mi}}{R_i} = \rho_i = k_2 + \frac{k_3}{B_{ni}} + 0.5SB_{ni}^{-0.5} \quad (7.9)$$

where R_{mi} = motion resistance force on i th wheel, kN (see Figure 7.5)

k_3 = constant = 1.0 for bias-ply tires or 0.9 for radial tires

ρ_i = motion resistance ratio for i th wheel, dimensionless

S = slip of powered wheels or zero for unpowered wheels

The motion resistance ratio is subtracted from the gross traction ratio to obtain the *net traction ratio* (C_{ni}) for the i th wheel, i.e.:

$$C_{ni} = C_{gi} - \rho_i \quad (7.10)$$

Wheel slip, S , is defined as:

$$S = 1 - \frac{V_a}{V_{ti}} \quad (7.11)$$

where V_a = actual travel speed of vehicle, m/s

V_{ti} = theoretical travel speed of i th wheel, m/s

The theoretical travel speed can be calculated from the engine speed, tire radius and drive train speed ratio, i.e.:

$$V_{ti} = \frac{\pi n_e r_{Li}}{30000 N_{pti}} \quad (7.12)$$

where n_e = engine speed, rev/min

N_{pti} = power train speed ratio for i th wheel

The tractive efficiency, η_{ti} , is the ratio of the tractive power out of the i th wheel divided by the rotational power in, i.e.:

$$\frac{(R_{ti} - R_{mi})V_i}{T_i\omega_i} = \eta_{ti} = \frac{(1 - S_i)C_{ni}}{C_{gi}} \quad (7.13)$$

where $R_{ti} - R_{mi}$ = net tractive force on i th wheel, kN (see Figure 7.5)

η_{ti} = tractive efficiency of i th wheel, dimensionless

ω_i = rotational speed of i th wheel, rad/s

The preceding equations can be used to calculate the tractive performance of an entire vehicle. By summing forces in the x-direction of Figure 7.5:

$$F_{hx} = C_{nr}R_r + C_{nf}R_f \quad (7.14)$$

In applying Equation 7.14, R_r is the combined dynamic load on all wheels on the rear axle, while R_f is the combined load on all front wheels. The value for b_i in Equation 7.4 must be the combined width of all tires on axle i . Equation 7.14 is valid for vehicles with two- or four-wheel drive. For two-wheel drive, $C_{gi} = 0$ for all nondriving wheels while V_{ti} is calculated only for the driving wheels.

Note that, for a specified s , F_{hx} must be calculated iteratively because B_{ni} for each axle depends on the dynamic weight on that axle, the dynamic weight depends on the weight transfer, and the weight transfer depends on F_{hx} . A suitable procedure is to assume zero weight transfer in the first iteration, which allows calculation of an initial value of F_{hx} . That value can be used in Equations 7.1b and 7.2b to find new dynamic weights, after which a new value of F_{hx} can be calculated. After a few iterations, the value of F_{hx} will converge to some constant. If the dynamic reaction on the front axle reaches zero during the iterations, the entire tractor weight is supported on the rear axle and no further iteration is necessary.

What value of slip should be used in the calculations? The form of Equation 7.3 is such that C_{gi} and, consequently, F_{hx} increase with slip. The draft of most soil-engaging implements increases with speed but, since slip reduces forward speed, greater slip reduces implement draft. Thus, when an equation for implement draft (see ASAE Data D497 for such equations) is added to the traction model presented above and the model is solved iteratively, the solution for the tractor-implement combination will converge to some equilibrium slip, S_e . The calculated S_e may not produce maximum tractive efficiency, so it may be desirable to change it until maximum η_t is achieved. The S_e can be increased by removing ballast to reduce the vertical loads on the powered wheels or by increasing implement draft, i.e., by use of a larger implement. The S_e can be reduced by the converse measures. The goal of traction is to transmit drawbar power, which can be calculated using Equation 7.15:

$$P_{db} = V_a F_{hx} \quad (7.15)$$

where P_{db} = drawbar power in kW. Increasing V_a reduces the F_{hx} and thus the ballast needed to transmit a given amount of drawbar power. To prevent overloading the tractor and excessively compacting the soil, it is recommended that V_a be at least 2 m/s or 7.2 km/hr.

The effective cone index is measured by pushing a cone penetrometer into the soil. Dimensions of the standard *penetrometer* and directions for using it are given in ASAE Standard S313. The cone index varies with depth but, by averaging the cone

index values over the first 150 mm of depth, an effective cone index is obtained for use in Equation 7.4 for wheels that run in undisturbed soil. Typically, effective cone indexes range from 0.33 N/mm² for soft soil to 1.75 N/mm² for firm soil. If the rear wheels run in the track of the front wheels, the effective cone index for the rear wheels is increased due to the compaction provided by the front wheels. The following equation can then be used to estimate the effective cone index for the rear wheels:

$$\frac{CI_a}{CI_b} = 1 + 1.8e^{-0.11B_{ni}} \quad (7.16)$$

where CI_a = effective cone index after wheel passage, N/mm²
 CI_b = effective cone index before wheel passage, N/mm²

7.2.3 Traction predictor spreadsheet

Frank Zoz developed a spreadsheet, “Predicting Tractor Field Performance,” that uses the above traction theory to predict the tractive performance of tractors. The spreadsheet, in EXCEL format, is in the CD-ROM that is included with this textbook. Instructions for using the spreadsheet are given in the spreadsheet itself. There are 11 pages in the spreadsheet. The calculations are done in customary units and displayed on page one. Page two shows the results of the page one calculations in SI units. Instead of entering tractor parameters directly, the user can select one of the tractors listed on page three of the spreadsheet and the parameters for that tractor are entered automatically. Page five has a list of “help” instructions. Page six is provided to enter parameters of the user’s “own” tractors. The remaining pages include an introductory page and various performance charts.

Soil strength is indicated in the spreadsheet by entering a soil cone index (CI) value. In practice, the soil cone index is measured by pushing a standardized soil penetrometer into the soil to measure the penetration resistance. ASAE Standard S313.2 gives dimensions of the standardized penetrometer. Soft soil CI values could range from 0 to 700 kN/m² (102 psi). Tilled soil values could range from 350 to 1200 kN/m² (51 to 174 psi). Firm soil would have a CI value of 1750 kN/m² (254 psi). For comparison with the theory above, 1 N/mm² = 1000 kN/m².

The parameters for the tractor selected for analysis are those that were present when the tractor received an official OECD/Nebraska tractor test. The spreadsheet user can change any of these parameters to study their effect. For example, a menu is provided to allow the user to change the size of tires used on the tractor and to specify whether singles, duals, or triples are used on each axle. The user can also change the type of hitch by which an implement is attached, i.e., the user can specify whether the implement is towed, semi-mounted, or integrally-mounted.

Two calculation modes are provided in the spreadsheet, i.e., a performance mode and a weight mode. In the performance mode, slip is increased until the calculated pull is sufficient to use all of the available engine torque. In the weight mode, the spreadsheet calculates the amount of tractor weight needed to achieve the calculated pull at a slip level selected by the user.

In the performance mode, after a tractor make and model are selected, the following parameter values appear automatically on the spreadsheet: static weight on front

axle, front power efficiency (if front wheels are driven), static weight on rear axle, rear power efficiency, wheel base, hitch point height, hitch point distance behind rear axle, pull angle below the horizontal, no-slip travel speed, maximum PTO power from the OECD/Nebraska test, and a load factor to de-rate the maximum power. Reducing the load factor reduces the pull proportionally. Outputs in performance mode include weight transfers to the rear axle from the front axle and from the implement, the resulting dynamic loads on the front and rear axles, drawbar pull, actual travel speed, slip, drawbar power, power delivery efficiency (drawbar power/PTO power), and pull-weight ratio (drawbar pull/tractor weight).

In weight mode, after a tractor make and model are selected, the parameters that automatically appear on the spreadsheet are the same as in performance mode with two exceptions. First, the static axle loads on the front and rear axles do not appear as parameters; instead, they are calculated as outputs. Also, in weight mode, the user must enter the percentage of the total dynamic weight that is to be carried on the front axle and the desired slip. Outputs are the same as in performance mode. Note that, by subtracting the front and rear static axle loads of the base tractor from the corresponding static axle loads calculated in the weight mode, the user can determine the amount of ballast needed on the front and rear axles.

Simulation problems at the end of this chapter provide an opportunity for the reader to experiment with the traction prediction spreadsheet.

7.3 SOIL COMPACTION

The passage of wheels over agricultural soils results in soil compaction, that is, an increase in soil cone index as indicated by Equation 7.16 and an accompanying increase in soil density. The cone index is a composite measure of soil strength that is a function of soil texture, density, and moisture. A proven relationship for field soils is not yet available, but Ayers and Perumpherl (1982) developed an equation to relate soil density to cone index and soil moisture for several artificial soils. The artificial soils consisted of mixtures of zircon sand, fire clay, and water. The following equation is equivalent to the one presented by Ayers and Perumpherl:

$$\frac{\rho_d}{\rho_{do}} = \left\{ \frac{CI}{CI_o} \left[1 + C_o \left(\frac{m_s}{m_{so}} - 1 \right)^2 \right] \right\}^n \quad (7.17)$$

where ρ_d = dry density of soil, Mg/m³

ρ_{do} = reference density of soil (a constant), Mg/m³

CI = soil cone index, kPa

CI_o = reference cone index (a constant), kPa

m_s = soil moisture content, percent, dry basis

m_{so} = reference moisture content (a constant), percent

C_o, n = dimensionless constants

The five constants in Equation 7.17 depend upon soil type. Although values are not yet available for field soils, one of the homework problems provides data for illustrating the use of the equation with artificial soils.

Compaction results in an increase in soil density, but the effect of soil density on crop growth and yield is complex. In a relatively dry growing season, increased soil density may help to keep plant roots in contact with moisture and provide increased crop yields. Conversely, in a wet season, internal drainage is retarded by dense soil and crop yields may be reduced. Even within a given growing season, there is an optimum soil density for maximum crop production. Vomicil (1955) proposed a relationship between crop yield and soil density which can be expressed as follows:

$$\frac{Y}{Y_i} = 1 - C_y \left(\frac{\rho_d}{\rho_{di}} - 1 \right)^2 \quad (7.18)$$

where Y = actual crop yield

Y_i = crop yield with ideal soil density

C_y = a soil-crop-climate constant

ρ_d = actual dry density of soil, Mg/m^3

ρ_{di} = ideal dry density of soil, Mg/m^3

Notice from Equation 7.18 that $Y = Y_i$ when $\rho_d = \rho_{di}$, and that the yield decreases with either smaller or larger values of ρ_d . Limited amounts of data are provided with one of the homework problems for illustrating the use of Equation 7.18.

7.4 TRACTION AIDS

A number of techniques are available for increasing the tractive performance of a tractor. One of the earliest techniques was to use dual or triple tires on each rear axle of a 2WD tractor. Careful studies have shown that such use of duals or triples provides little increase in C_{ni} or in η_t . However, the duals or triples increase the load-carrying capacity as discussed in Section 7.3.1, thus permitting much higher dynamic loads on the drive axles and, consequently, higher drawbar pull. In soft ground, duals or triples also reduce the *sinkage* of the tires into the soil. Whether single, dual, or triple tires are used, use of increased axle loads leads to increased soil compaction. Soil compaction can be avoided and axle stress can be reduced by use of travel speeds of 7.2 km/h or higher. As Equation 7.15 shows, use of higher travel speeds reduces the amount of pull needed to achieve a given drawbar power level.

Only the rear wheels of early 2WD tractors were powered; the front wheels produced motion resistance and thus only a negative contribution to tractor pull. Two methods have been used to power both front and rear wheels. Tractors designated as 4WD have all wheels powered. All of the wheels are of equal size and the rear wheels run in the tracks of the front wheels. Thus, in addition to the pulling contribution of the front wheels, the soil strengthening they provide (see Equation 7.14) increases the pulling capacity of the rear wheels. More recently, FWA (Front Wheel Assist, an alternate name is MFWD for Mechanical Front Wheel Drive) tractors have been designed as 2WD tractors with a front wheel assist option. The peripheral speeds of the front and rear wheels are closely matched with a slightly higher peripheral speed for the front wheels. The front wheels of FWA tractors are intermediate in size between conventional, unpowered front wheels and powered rear wheels; the front wheels on FWA tractors are also equipped with lugs to aid pulling. Since the rear tires of 2WD

and FWA tractors are always wider than the front tires, the rear tires must form part of their own rut and Equation 7.14 somewhat overestimates the effective cone index for the rear tires.

Optimum weight distribution varies according to type of tractor. For 2WD tractors, only enough dynamic weight is needed on the front axle to provide reliable steering. With typical weight transfer, reliable steering is achieved if approximately 25% to 30% of the static weight is carried on the front axle. For 4WD tractors, approximately 55% to 60% of the static weight is carried on the front axle; weight transfer then generates approximately equal dynamic loads on the front and rear axles. Ballasting of FWA tractors depends upon their use. When the optional FWA is disengaged, the tractor should be ballasted the same as a 2WD tractor. Conversely, when the FWA is engaged, ballasting should be that of a 4WD tractor.

To allow use of more ballast and to reduce sinkage in soft soils, some FWA tractors are equipped with dual or triple wheels on the rear axles, but steering considerations generally require use of a single tire on each front axle. Most 4WD tractors have articulated steering, i.e., the tractor has a vertical hinge between the front and rear axles that allows those axles to move out of their parallel orientation for a turn. Such tractors may be equipped with dual or triple tires on both the front and rear axles, i.e., there may be 8 or 12 tires on the tractor. As before, the benefit of the dual or triple tires is to reduce sinkage in soft soils and to allow the use of more ballast to increase traction.

The design of individual tires affects traction. Studies have been made of the effect of lug height, lug angle, and number of lugs on a tire, but few consistently clear trends have been observed from such studies. Bias-ply construction was used on all early tires, but tires with radial plies are now gaining wider use on farm equipment. Some studies have shown that radial tires provide a significant improvement in net coefficient of traction. Note that, in traction mechanics theory, traction parameters k_1 , k_2 , and k_3 for radial tires differ from those for bias ply tires. The reader can thus use the traction mechanics equations to assess performance differences between radial and bias ply tires under various conditions of tractor loading and soil strength.

Where rice is grown in flooded paddies, effective soil cone indexes will typically be less than 0.5 N/mm^2 . The performance of conventional tires becomes unacceptable in such conditions because of high wheel slippage and adhesion of sticky soil to the tires. One solution has been the use of tires with very high lugs. Another solution is to attach an auxiliary wheel with steel lugs to the side of each tire. The steel lugs improve the traction coefficient and, for road transport, may be folded to avoid contact with the road surface.

7.5 TRACTOR TESTING

7.5.1 Basic principles of tractor testing

Tractor testing provides data that may be used in comparing performance of various makes and models of tractors. When comparative tests are done by agencies independent of the tractor manufacturers, the resulting competition among the manufacturers also tends to promote improvements in tractor design. The original independent agency to do tractor testing was the University of Nebraska Tractor Testing Laboratory (NTTL). It was authorized by the 1919 session of the Nebraska legislature, which

passed a bill requiring testing and maintenance of service stations for all models of tractors sold within the state. The bill was prompted by the presence of inferior tractors on the market at that time. The provisions of the current law do not apply to tractors whose engines develop less than 30 kW (40 hp) nor to tractors manufactured or sold as nonagricultural tractors. Standard tests conducted at the NTTL were developed and are periodically updated by SAE (Society for Automotive Engineers) working in cooperation with ASAE (ASABE). The SAE/ASAE tractor tests are also in good agreement with International Standards Organization (ISO) test standards. Thus, these tests will be referred to as SAE/ASAE/ISO tests.

The NTTL served as a uniquely independent tractor testing agency for many years. As tractor manufacturing and marketing became global in the 1980s, the Organization for Economic Cooperation and Development (OECD) test codes became the commonly accepted official test procedure for world-wide marketing. These test codes were developed in Europe. The US was not a full participant during the development of the OECD test codes, but the Farm and Industrial Equipment Institute (FIEI) (re-named to EMI, the Equipment Manufacturer's Institute and more recently to AEM, the Association of Equipment Manufacturers) attended as a US observer; the OECD codes were in existence by about 1960. In 1986, the Nebraska legislature changed their tractor test law to accept OECD tests as well as those conducted by the NTTL as a prerequisite to selling tractors in the state. By 1988, the NTTL had been designated as an official OECD testing station for the United States. In addition, the NTTL has begun producing summaries of OECD tests conducted elsewhere if the tractor requires a Nebraska sales permit. The summaries are similar in format to the reports of the SAE/ASAE/ISO tests and are distributed to Nebraska farmers and other interested parties.

There are now three widely-recognized standard test procedures for testing tractors. They include the standard ASAE/SAE/ISO test, the OECD restricted test and the OECD long test. The OECD tests are described by code designations, as follows:

Code I: OECD Standard Code for the Official Testing of Agricultural Tractor Performance

Compulsory tests:

1. Main PTO
2. Hydraulic power and lifting force
3. Drawbar power, ballasted tractor
4. Turning area and turning circle
5. Position of center of gravity
6. Braking (wheeled tractors only)
7. External (bystander) noise (wheeled tractors only)

Tests performed and reported at manufacturer's option:

8. Engine
9. Performance at the belt or belt pulley shaft
10. Performance in a hot atmosphere
11. Low temperature starting
12. Drawbar power and fuel consumption for unballasted tractor

Code II: OECD Restricted Standard Code for the Official Testing of Agricultural Tractor Performance

Compulsory tests:

1. Main PTO
2. Hydraulic power and lifting force
3. Drawbar power and fuel consumption for unballasted tractor

In addition, tests 3 through 11 above from the Standard Code may be performed and reported at the manufacturer's option.

Code III: OECD Standard Code for the Official Testing of Protective Structures on Agricultural Tractors (Dynamic Test)**Code IV: OECD Standard Code for the Official Testing of Protective Structures on Agricultural Tractors (Static Test)****Code V: OECD Standard Code for the Official Measurement of Noise in Protective Structures on Agricultural Tractors**

The SAE/ASAE/ISO test and the OECD restricted test are similar; the ASAE/SAE/ISO procedure includes a 10-hour drawbar test at 75% load, whereas the OECD test requires only a 5-hour test. The OECD test report requires more detailed tractor specifications, including more design data on the engine, power train, brakes, etc. In some countries, either of the OECD tests can be conducted using the manufacturer's test facilities provided an OECD-authorized supervisor monitors the tests. Conversely, the SAE/ASAE/ISO tests are all performed at the NTTL by NTTL personnel. An OECD test can be carried out at more than one facility. For example, an SAE/ASAE/ISO test conducted at the NTTL can be supplemented by tests carried out in other countries to obtain an OECD test. NTTL is not equipped to conduct OECD Code III or Code IV tests, but NTTL personnel witness such tests conducted at the manufacturer's facility.

Manufacturing tolerances are an inherent part of mass production of tractors, but, because of such tolerances, there is variation between tractors produced on the same assembly line. Thus some procedure must be used to select the specific tractor used for testing. The procedure used for the SAE/ASAE/ISO test or either of the OECD tests is to permit the manufacturer to select a tractor from the assembly line and pre-test it before submitting it for an official test. In addition to pre-testing tractors prior to an official test, manufacturers routinely test tractors and their components for durability and to gain other useful information. For example, an engine may be tested to reveal which combinations of speed and torque produce the highest fuel economy.

7.5.2 Official tractor tests

Official OECD reports are too lengthy for distribution to the public. For every tractor model that is sold in the state of Nebraska and has an OECD test, however, the NTTL publishes a summary of the test in a format similar to that of the earlier Nebraska Tractor Test reports. An example of such a report is shown in Figure 7.10. The purpose of the summary reports is to allow prospective tractor buyers to compare tractors. Performance at the PTO is directly comparable by using either the OECD summaries or reports of SAE/ASAE/ISO tests. Care must be used in comparing drawbar performance because of differences in test procedures. For example, SAE/ASAE/ISO tests are run at rated engine speed, while OECD tests are run at the maximum power point.

**NEBRASKA OECD TRACTOR TEST 1828—SUMMARY 416
CASE IH MX 285 DIESEL
18 SPEED**

POWER TAKE-OFF PERFORMANCE

Power HP (kW)	Crank shaft speed rpm	Gal/hr (l/h)	lb/hp.hr (kg/kW.h)	Hp.hr/gal (kW.h/l)	Mean Atmospheric Conditions
MAXIMUM POWER AND FUEL CONSUMPTION					
Rated Engine Speed—(PTO speed—1003 rpm)					
242.24 (180.64)	2000	13.60 (51.50)	0.395 (0.240)	17.81 (3.51)	
Maximum Power (2 hours)					
276.12 (205.90)	1700	14.73 (55.75)	0.375 (0.228)	18.75 (3.69)	
VARYING POWER AND FUEL CONSUMPTION					
242.24 (180.64)	2000	13.60 (51.50)	0.395 (0.240)	17.81 (3.51)	Air temperature
214.39 (159.87)	2085	12.41 (46.99)	0.407 (0.248)	17.27 (3.40)	78°F (25°C)
163.89 (122.21)	2121	10.28 (38.91)	0.441 (0.268)	15.94 (3.14)	Relative humidity
111.45 (83.11)	2161	7.59 (28.74)	0.479 (0.291)	14.68 (2.89)	68%
56.70 (42.28)	2200	5.03 (19.05)	0.624 (0.380)	11.27 (2.22)	Barometer
1.07 (0.80)	2237	2.86 (10.82)	18.818 (11.446)	0.37 (0.07)	28.77" Hg (97.43 kPa)

Maximum Torque - 947 lb.-ft. (1283 Nm) at 1402 rpm
 Maximum Torque Rise - 48.8%
 Torque rise at 1600 engine rpm - 38%

**DRAWBAR PERFORMANCE
UNBALLASTED - FRONT DRIVE ENGAGED
FUEL CONSUMPTION CHARACTERISTICS**

Power Hp (kW)	Drawbar pull lbs (kN)	Speed mph (km/h)	Crank- shaft speed rpm	Slip %	Fuel Consumption lb/hp.hr (kg/kW.h)	Hp.hr/gal (kW.h/l)	Temp.°F (°C) cool- ing med	Air dry bulb	Barom. inch Hg (kPa)
Maximum Power—7th Gear									
203.74 (151.93)	18108 (80.55)	4.22 (6.79)	1990	6.17	0.470 (0.286)	14.95 (2.95)	188 (87)	60 (16)	28.88 (97.80)
75% of Pull at Maximum Power—7th Gear									
163.92 (122.23)	13579 (60.40)	4.53 (7.29)	2085	3.89	0.509 (0.310)	13.81 (2.72)	191 (88)	74 (23)	28.88 (97.80)
50% of Pull at Maximum Power—7th Gear									
113.45 (84.60)	9036 (40.20)	4.71 (7.58)	2129	2.11	0.565 (0.344)	12.44 (2.45)	187 (86)	81 (27)	28.83 (97.63)
75% of Pull at Reduced Engine Speed—9th Gear									
163.98 (122.28)	13575 (60.38)	4.53 (7.29)	1578	3.97	0.454 (0.276)	15.49 (3.05)	189 (87)	76 (24)	28.87 (97.77)
50% of Pull at Reduced Engine Speed—9th Gear									
113.82 (84.88)	9041 (40.21)	4.72 (7.60)	1615	2.20	0.487 (0.296)	14.45 (2.85)	185 (85)	83 (28)	28.82 (97.60)

DRAWBAR PERFORMANCE
BALLASTED - 1700 ENGINE RPM
MAXIMUM POWER IN SELECTED GEARS

Power Hp (kW)	Drawbar pull lbs (kN)	Speed mph (km/h)	Crank- shaft speed rpm	Slip %	Fuel Consumption lb/hp.hr (kg/kW.h)	Fuel Consumption Hp.hr/gal (kW.h/l)	Temp.°F (°C) cool- ing med	Air dry bulb	Barom. inch Hg (kPa)
3rd Gear									
184.07 (137.26)	30057 (133.70)	2.30 (3.70)	1994	9.91	0.512 (0.311)	13.74 (2.71)	185 (85)	62 (17)	28.78 (97.46)
4th Gear									
202.66 (151.12)	28487 (126.72)	2.67 (4.29)	1966	7.45	0.483 (0.293)	14.58 (2.87)	193 (90)	64 (18)	28.82 (97.60)
5th Gear									
212.51 (158.47)	27488 (122.27)	2.90 (4.67)	1857	7.19	0.487 (0.296)	14.44 (2.84)	197 (92)	65 (18)	28.82 (97.60)
6th Gear									
222.29 (165.76)	25986 (115.59)	3.21 (5.16)	1762	5.65	0.465 (0.283)	15.13 (2.98)	196 (91)	69 (21)	28.83 (97.63)
7th Gear									
235.01 (175.25)	24343 (108.28)	3.62 (5.83)	1692	4.92	0.444 (0.270)	15.86 (3.12)	198 (92)	70 (21)	28.83 (97.63)
8th Gear									
236.98 (176.72)	21200 (94.30)	4.19 (6.75)	1686	3.69	0.438 (0.267)	16.04 (3.16)	198 (92)	72 (22)	28.82 (97.60)
9th Gear									
235.71 (175.77)	18117 (80.59)	4.88 (7.85)	1686	2.79	0.442 (0.269)	15.92 (3.14)	199 (93)	76 (24)	28.82 (97.60)
10th Gear									
236.16 (176.11)	15772 (70.16)	5.62 (9.04)	1688	2.62	0.436 (0.265)	16.13 (3.18)	199 (93)	74 (23)	28.82 (97.60)
11th Gear									
233.41 (174.05)	13505 (60.07)	6.48 (10.43)	1690	2.10	0.443 (0.270)	15.87 (3.13)	200 (93)	75 (24)	28.82 (97.60)
12th Gear									
229.67 (171.27)	11563 (51.44)	7.45 (11.99)	1689	1.84	0.450 (0.274)	15.64 (3.08)	200 (93)	66 (19)	28.82 (97.60)
13th Gear									
226.20 (168.67)	9086 (40.42)	9.34 (15.02)	1690	1.35	0.460 (0.280)	15.30 (3.01)	200 (93)	68 (20)	28.82 (97.60)

THREE POINT HITCH PERFORMANCE(OECD Static Test)

CATEGORY: III

Quick Attach: Yes

Maximum force exerted through whole range: 16375 lb (72.8 kN)

i) Opening pressure of relief valve: NA

Sustained pressure at compensator cutoff: 3040 psi (209 bar)

ii) Pump delivery rate at minimum pressure and rated engine speed:

39.0 GPM (147.6 l/min)

iii) Pump delivery rate at maximum

hydraulic power: 38.5 GPM (145.7 l/min)

Delivery pressure: 2850 psi (196 bar)

Power: 63.9 HP (47.7 kW)

High Lift Option

17931 lb (79.8 kN)

NA

High Flow Option

3060 psi (211 bar)

52.4 GPM (198.3 l/min)

46.6 GPM (176.5 l/min)

2760 psi (190 bar)

75.1 Hp (56.0 kW)

**DRAWBAR PERFORMANCE
UNBALLASTED - FRONT DRIVE ENGAGED
MAXIMUM POWER IN SELECTED GEARS**

Power Hp (kW)	Drawbar pull lbs (kN)	Speed mph (km/h)	Crank- shaft speed rpm	Slip %	Fuel Consumption lb/hp.hr (kg/kWh)	Fuel Consumption Hp.hr/gal (kW.h/l)	Temp.°F (°C) cool- ing med	Air dry bulb	Barom. inch Hg (kPa)
5th Gear									
174.78 (130.34)	20820 (92.61)	3.15 (5.07)	2078	10.27	0.524 (0.319)	13.42 (2.64)	187 (86)	54 (12)	28.87 (97.77)
6th Gear									
190.03 (141.70)	19792 (88.04)	3.60 (5.79)	2023	8.11	0.493 (0.300)	14.26 (2.81)	187 (86)	58 (14)	28.88 (97.80)
7th Gear									
207.28 (154.57)	19081 (84.88)	4.07 (6.56)	1952	7.65	0.474 (0.289)	14.82 (2.92)	190 (88)	60 (16)	28.88 (97.80)
8th Gear									
220.22 (164.22)	18892 (84.04)	4.37 (7.03)	1826	7.61	0.467 (0.284)	15.07 (2.97)	194 (90)	61 (16)	28.88 (97.80)
9th Gear									
231.71 (172.79)	18511 (82.34)	4.69 (7.55)	1698	7.48	0.446 (0.271)	15.76 (3.11)	195 (91)	62 (17)	28.89 (97.83)
10th Gear									
234.72 (175.03)	15986 (71.11)	5.51 (8.86)	1696	5.28	0.440 (0.268)	15.99 (3.15)	196 (91)	63 (17)	28.89 (97.83)
11th Gear									
233.35 (174.01)	13705 (60.96)	6.38 (10.28)	1693	4.10	0.440 (0.267)	16.00 (3.15)	196 (91)	65 (18)	28.89 (97.83)
12th Gear									
231.67 (172.76)	11811 (52.54)	7.36 (11.84)	1681	2.98	0.440 (0.267)	16.00 (3.15)	197 (92)	67 (19)	28.89 (97.83)
13th Gear									
231.71 (172.78)	9332 (41.51)	9.31 (14.98)	1696	2.33	0.446 (0.271)	15.78 (3.11)	198 (92)	69 (21)	28.89 (97.83)

TRACTOR SOUND LEVEL WITH CAB

	dB(A)
At 75% load in 9th gear	72.0
Bystander in 18th gear	87.7

TIRES, BALLAST AND WEIGHT

	With Ballast	Without Ballast
Rear Tires -No., size, ply & psi (kPa)	Four 520/85R42;**,13(90)	Two 520/85R42;**,17(115)
Ballast - Duals (total)	1950 lb (885 kg)	None
- Cast Iron (total)	6145 lb (2787 kg)	None
Front Tires -No., size, ply & psi (kPa)	Two 420/90R30;**,23(160)	Two 420/90R30;**,17(115)
Ballast - Liquid (total)	None	None
- Cast Iron (total)	1600 lb (726 kg)	None
Height of Drawbar	17.5 in (445 mm)	17.0 in (430 mm)
Static Weight with operator - Rear	20265 lb (9192 kg)	12805 lb (5808 kg)
- Front	11235 lb (5096 kg)	9000 lb (4082 kg)
- Total	31500 lb (14288 kg)	21805 lb (9890 kg)

Location of Test: Nebraska Tractor Test Laboratory, University of Nebraska, Lincoln, Nebraska 68583-0832

Dates of Test: September 9 - October 24, 2003
Manufacturer: CNH America LLC, 700 State Street, Racine, WI. 53404 USA

FUEL, OIL and TIME: Fuel No. 2 Diesel Specific gravity converted to 60°/60°F (15°/15°C) 0.8447 Fuel weight 7.033 lbs/gal (0.843 kg/l) Oil SAE 15W40 API service classification SF/CD/CE Transmission and hydraulic lubricant Case IH Hy-Tran Ultra fluid Front axle lubricant SAE 85W-140 API GL-5 Total time engine was operated: 43.5 hours

ENGINE: Make Consolidated Diesel Corporation Diesel Type six cylinder vertical with turbocharger and air to air intercooler Serial No. *46273650* Crankshaft lengthwise Rated engine speed 2000 Bore and stroke 4.488" x 5.315" (114.0 mm x 135.0 mm) Compression ratio 17.0 to 1 Displacement 505 cu in (8268 ml) Starting system 12 volt Lubrication pressure Air cleaner two paper elements and aspirator Oil filter one full flow cartridge Oil cooler engine coolant heat exchanger for crankcase oil, radiator for hydraulic and transmission oil Fuel filter two paper elements and prefilter Fuel cooler radiator for pump return fuel Muffler vertical Cooling medium temperature control 2 thermostats and variable speed fan

ENGINE OPERATING PARAMETERS: Fuel rate: 92.8-102.0 lb/h (42.2 - 46.3 kg/h) High idle: 2180-2270 rpm Turbo boost: nominal 23.2-27.6 psi (160 - 190 kPa) as measured 24.6 psi (170 kPa)

CHASSIS: Type front wheel assist Serial No. *JAZ126247* Tread width rear 64.0" (1626 mm) to 129.0" (3277 mm) front 60.0" (1524 mm) to 88.0" (2235 mm) Wheelbase 118.3" (3005 mm) Hydraulic control system direct engine drive Transmission selective gear fixed ratio with full range operator controlled powershift Nominal travel speeds mph (km/h) first 1.96 (3.15) second 2.24 (3.61) third 2.58 (4.16) fourth 2.96 (4.77) fifth 3.41 (5.48) sixth 3.90 (6.28) seventh 4.55 (7.33) eighth 5.23 (8.41) ninth 6.02 (9.69) tenth 6.91 (11.12) eleventh 7.92 (12.75) twelfth 9.09 (14.63) thirteenth 11.33 (18.23) fourteenth 12.99 (20.91) fifteenth 14.98 (24.11) sixteenth 17.19 (27.66) seventeenth 19.72 (31.73) eighteenth 22.61 (36.39) reverse 2.81 (4.53), 3.23 (5.20), 6.56 (10.55), 7.52 (12.10) Clutch multiple wet disc electrohydraulically operated by foot pedal Brakes wet disc hydraulically operated by two foot pedals that can be locked together Steering hydrostatic Power take-off 1000 rpm at 1994 engine rpm Unladen tractor mass 21630 lb (9811 kg)

REPAIRS AND ADJUSTMENTS: The hydraulic supply hose to front suspension control valve was replaced. The viscous fan hub was replaced previous to the unballasted drawbar tests.

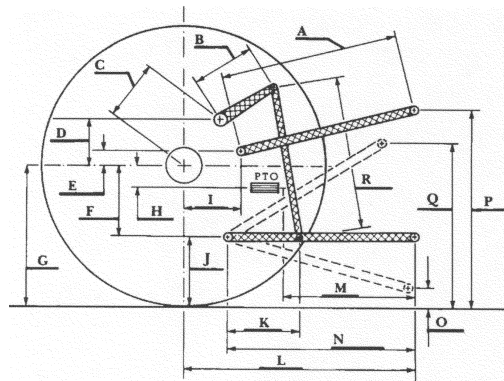
REMARKS: All test results were determined from observed data obtained in accordance with official OECD, SAE and Nebraska test procedures. For the maximum power tests the fuel temperature at the injection pump inlet was maintained at 115°F (46°C). This tractor did not meet the manufacturer's claim of 53.1 GPM (201 lpm) optional hydraulic flow. The pull in 3rd gear (ballasted tractor) was limited to avoid excessive tractor bouncing. The performance results on this summary were taken from OECD tests conducted under the Code II Test Code Procedure.

We, the undersigned, certify that this is a true and correct report of official Tractor Test No. 1828, Nebraska Summary 416, January 15, 2004.

Leonard L. Bashford
 Director

M.F. Kocher
 V.I. Adamchuk
 W.P. Campbell
 Board of Tractor Test Engineers

HITCH DIMENSIONS AS TESTED
 –NO LOAD



	inch	mm
A	28.2	718
B	20.5	520
C	22.9	581
D	20.7	525
E	10.5	266
F	15.7	400
G	36.4	925
H	3.5	90
I	20.9	530
J	20.7	525
K	30.2	768
L	46.1	1170
*L'	50.7	1287
M	20.1	511
N	38.2	970
O	9.0	230
P	47.6	1210
Q	40.7	1035
R	39.2	995

*L' to Quick Attach ends



CASE IH MX 285 DIESEL

Agricultural Research Division
 Institute of Agriculture and Natural Resources
 University of Nebraska–Lincoln
 Darrell Nelson, Dean and Director

Figure 7.10 – Nebraska OECD tractor test 1828 – Summary 416 (courtesy of the University of Nebraska Tractor Testing Laboratory).

If the tractor has a PTO shaft, a two-hour PTO test is run at the speed which produces maximum power. Short tests are also run at rated engine speed and at standard PTO speed of these speeds differ from the speed at maximum power. In the report of Figure 7.10, for example, rated engine speed was 2000 rev/min but maximum power

was at 1700 rev/min. A series of short, part-load PTO tests are run in the governor-controlled range. The engine is also loaded into the load-controlled range so that the torque reserve can be reported. In addition to power and speed, fuel consumption is measured during each PTO test. By neglecting power losses between the engine and PTO shaft, the approximate engine torque for each test can be calculated from power and speed by using Equation 2.13. As indicated by Equations 2.23 and 2.24, the ambient temperature and barometric pressure affect the mass air consumption of an engine and thus the atmospheric conditions prevailing during the PTO tests are reported. In SAE/ASAE/ISO testing, ambient conditions are recorded for every PTO test. As shown in Figure 7.10, however, the average ambient conditions during all PTO tests are recorded in OECD tests. Note that, in the Varying Power tests of Figure 7.10, the SFC (in kg/kW h) increases substantially as engine load decreases, as could be predicted from the discussion in Section 2.5.

In OECD tests, the tractor is tested in each gear provided that slip and speed limits are not exceeded. The first drawbar test reported in the NTTL summary (Figure 7.10) is for the best pulling gear, i.e., the gear that produces the most drawbar power. Next, the NTTL reports results of a 5-hour test at 75% of the pull that produces maximum power. Listed next in the report are results of a short test at 50% of the pull that produces maximum power. The next two tests listed are again at 75% and 50% of pull, but at reduced engine speed. In the latter two tests, the tractor is shifted to a higher gear (from 7th to 9th gears in this case) and the engine speed is reduced to give approximately the same travel speed as in the earlier tests.

The next two sections of the report are on series of drawbar tests in selected gears. The first series is drawbar performance of the unballasted tractor at maximum power. Note that, for the engine to produce maximum power, the drawbar load must be increased as the tractor is shifted to lower gears. Also note the increase in reported wheel slip as the drawbar pull was increased. First through fourth gears were not tested because the pull would have produced excessive wheel slip. The engine was running at 1700 rev/min to produce maximum power in the PTO test and, since that same engine speed prevailed, the engine was at maximum power during the tests in gears 9th through 13th. In 5th through 8th gears, however, the drawbar load was reduced to prevent excessive slip and the engine produced less than maximum power. Gears 14 through 18 were not tested to avoid use of excessive speeds.

The second series of maximum power tests of various gears was similar to the first series, except that the tractor was fully ballasted. The added ballast allowed testing of 3rd and 4th gears without exceeding the maximum allowable wheel slip. Atmospheric conditions, fuel consumption, and other performance parameters were reported for each of the drawbar tests mentioned above.

The test report contains details as to the fuel and lubricating oil used, engine specifications and operating parameters, and information about the chassis. The latter includes the gear selections available and advertised speeds in each gear. Data are given on the center of gravity location, axle loads, drawbar height, and tires used which would be useful in calculating tractive performance as described in Section 7.2.2. The lifting performance of the 3-point hitch is measured and reported. Finally, sound levels inside the cab and at a bystander location are measured and reported.

PROBLEMS

- 7.1 Use data from Nebraska test No. 1828 (Figure 7.10) to calculate (a) the governor regulation, and (b) the peak-torque speed as a percent of rated speed. (c) What is the engine torque reserve as reported on the Nebraska test? You can assume that governor's maximum speed is the same as rated speed in the Nebraska test.
- 7.2 Rework Problem 7.1, except use data from a Nebraska Test specified by the instructor.
- 7.3 Using data from the maximum power test in fifth gear of Nebraska Test No. 1828 (Figure 7.10), calculate (a) the ambient air density; (b) the theoretical air consumption rate of the turbocharged, intercooled engine; (c) the pressure and (d) the temperature of the air in the intake manifold; (e) the estimated volumetric efficiency of the engine; (f) air consumption by the engine; (g) air/fuel ratio; and (h) equivalence ratio of the engine. What would the (i) air consumption and (j) air/fuel ratio be if the intercooler was removed from the engine? In working part (c) of the engine, note that the measured boost at maximum power is given in the report. In working part (d), assume that the efficiency of the turbocharger compressor is 0.7.
- 7.4 Rework Problem 7.3, except use data from a Nebraska Test specified by the instructor.
- 7.5 Using data from Nebraska OECD Test 1828 (Figure 7.10), calculate (a) the distance x_2 , i.e., the horizontal distance from the rear axle center to the tractor center of gravity. (Note: the unballasted weight distribution in Figure 7.10 was obtained with the tractor unballasted except for full tanks and with 75 kg of mass on the tractor seat.) (b) Then, assuming that a level drawbar load is attached to the drawbar, calculate the dynamic weight coefficient, C_{dw} . (c) For each of the gears used in the drawbar tests of Maximum Power in Selected Gears, calculate R_r and R_f and plot these soil reactions versus drawbar pull.
- 7.6 Assume that the tractor of Problem 7.5 is operating on a soil with a soil cone index of 1.5 N/mm^2 (a very firm soil). (a) Making use of Equations 7.1b through 7.14 as needed, calculate the maximum drawbar pull that can be produced by the tractor at 10% wheel slip while pulling a semimounted plow. To simplify the problem, assume that the front wheel assist is disengaged. Note that ASAE Standard S220 can be used to obtain needed dimensions for the tires, or the dimensions can be calculated from the tire size as indicated in the text. Also note that an iterative solution is necessary, since the pull depends on the value of the wheel numerics, the wheel numerics depend on the tire loading and, because of weight transfer, the tire loading depends on pull. Thus you may save time by preparing a computer program to calculate the traction-limited pull. If, during the iterations, the pull becomes large enough to reduce the front wheel vertical reaction to zero, no further iteration is necessary since the entire tractor weight is then carried on the rear axle. (b) Repeat part (a) but use a wheel slip of 15%. (c) Repeat part (a) but use wheel slips of 10, 15, 20, 25, and 30%; then plot maximum pull versus wheel slip.

- 7.7 Same as Problem 7.6, except that the soil cone index is 0.5 N/mm^2 (a medium soil).
- 7.8 Same as Problem 7.7, except that the soil cone index is 0.25 N/mm^2 (a soft soil).
- 7.9 (a) Using data from Problem 7.6 and Equation 7.16, determine the cone index before and after passage of the rear wheels of the tractor (ignore any compaction due to passage of the front wheels). (b) Then use Equation 7.17 to estimate the dry density of the soil before and after wheel passage assuming $m_s = 17\%$. Use the following constants in Equation 7.17:
- $$\rho_{do} = 1.0 \text{ Mg/m}^3$$
- $$CI_o = 1000 \text{ kPa or } 1.0 \text{ N/mm}^2$$
- $$C_o = 5.1 \text{ (dimensionless)}$$
- $$m_{so} = 5\%$$
- $$n = 0.1333$$
- (c) Finally, use Equation 7.18 to assess the change in crop yield due to the passage of the rear wheels. Constants for use in Equation 7.18 are given in the table below. Assume conditions are similar to those for 1981 in the table. (Note: Equation 7.17 is very sensitive to m_s and Equation 7.18 is very sensitive to ρ_d . Thus the equations are useful for illustrating trends but not for reliable prediction of actual yields).
- 7.10 Same as Problem 7.9, except $m_s = 20\%$.

Data for Problems 7.9 and 7.10.

Year	Soil Type	Y_i Mg/ha	ρ_{di} Mg/m ³	C_y
1976	clay	16.0	0.99	5.74
1977, 1980	clay	12.3	1.13	17.96
1981	sandy loam	11.4	1.375	9.46

Crop: corn silage

Data source: Ayers and Perumpherl, 1982.

SIMULATION PROBLEMS

- S7.1 Use the Zoz spreadsheet to explore the effect of gear selection on PDE (Power Delivery Efficiency) of a John Deere 8410 tractor. The advertised (no-slip) speeds in km/hr (mph) for the tractor are: 1st, 2.18 (1.35); 2nd, 2.79 (1.73); 3rd, 3.55 (2.21); 4th, 4.53 (2.81); 5th, 5.49 (3.41); 6th, 6.19 (3.85); 7th, 7.01 (4.36); 8th, 7.91(4.92); 9th, 8.92 (5.54); 10th, 10.07 (6.26); 11th, 11.40 (7.08); 12th, 12.86 (7.99); 13th, 16.37 (10.17); 14th, 20.91 (12.99); 15th, 26.61 (16.53); 16th, 37.08 (23/04). (a) Find the gear that maximizes the PDE when the tractor is pulling an implement with the drawbar and has single tires on each of the front and rear axles. (b) Then, using that gear, explore whether singles, duals, or triples on the rear axles produce the highest PDE. Continue to use singles on the front. (c)

Then, using the solutions of parts (a) and (b), explore the effect of hitch type, i.e., whether the implement is attached via the drawbar, semi-integral or integral. (Note: You will need to work the problem on page 1 of the spreadsheet using customary units, but can see the results on page 2 in SI units if you wish).

- S7.2 For the tractor of Problem S7.1 equipped with singles on the front and rear axles, (a) find the ballasting that would produce 15% slip. (b) Repeat part (a), but use duals on the rear axles.
- S7.3 Repeat simulation Problem S7.1, except use a tractor selected by your instructor. Take the speeds in each gear from the advertised speeds in the Nebraska/OECD test report for the tractor.
- S7.4 Repeat simulation Problem S7.2, except use a tractor selected by your instructor.

Relevant websites

(Warning: The following websites were relevant at time of publication of the book, but webmasters are free to change or eliminate websites at any time).

<http://ianrpubs.unl.edu/farmpower/g1273.htm>

http://www.firestoneag.com/index.asp?_setLang=1

<http://www.goodyearag.com/indexflashnew.html>

SOIL TILLAGE



INTRODUCTION

Tillage may be defined as the mechanical manipulation of soil for any purpose, but usually for nurturing crops. In agriculture, the objectives of soil tillage are:

- To develop a desirable soil structure for a seedbed or a root bed. A granular structure is desirable to allow rapid infiltration and good retention of rainfall, to provide adequate air capacity and exchange within the soil, and to minimize resistance to root penetration. Compared to a root bed, a good seedbed has finer particles and greater firmness in the vicinity of the seeds, to enhance moisture absorption by the seeds needed for germination.
- To control weeds or remove unwanted crop plants (thinning).
- To manage plant residues. Thorough mixing of residue is desirable from the tilth and decomposition standpoints, whereas retention of residue on the soil surface or in the top layers reduces erosion. On the other hand, complete coverage is sometimes necessary to control over-wintering insects or to prevent interference with precision operations such as planting and cultivating certain crops.
- To minimize soil erosion by following such practices as contour tillage, listing, and proper placement of plant residue.
- To establish specific surface configurations for planting, irrigating, drainage, or harvesting operations.
- To incorporate and mix fertilizers, manure, pesticides, or soil amendments into the soil.
- To accomplish segregation. This may involve moving soil from one layer to another, removal of rocks and other foreign objects, or root harvesting.

8.1 TILLAGE METHODS AND EQUIPMENT

A *tillage tool* is defined in this textbook as an individual soil-engaging element, such as a plow bottom or a disk blade. A *tillage implement* consists of a single tool or a group of tools, together with the associated frame, wheels, hitch, control and protection devices, and any power transmission components. For tillage implements, the *process system* consists of the tillage tools, while the other components form the *support systems*.

Throughout the world farmers choose from a variety of implements for soil tillage. The set of implements that an individual farmer chooses depends on local customs, crop type, soil moisture level, soil type, and the amount of plant residue from the previous crop. Tillage implement selection is also affected by the availability of implements, power units, labor, and capital.

The three hitching configurations available for these implements are *integral* (mounted), *semi-integral* (semi-mounted), and *drawn* (pull-type). Integral and semi-integral implements are attached to the three-point hitch of a tractor, but a drawn implement is attached to the drawbar. An *integral* plow, in the transport position, is fully supported by the tractor. The rear furrow wheel of an integral implement provides vertical and lateral support along with the hitch when the implement is in its operating position. Plowing depth for an integral plow is usually controlled by changing the vertical position of the tractor's hitch. A semi-integral plow is supported at the front by the tractor's hitch and at the rear by the plow's furrow transport wheel in both the transport and operating positions. The front of the plow is raised and lowered by the tractor's hitch while the rear of the plow is raised and lowered by a remote hydraulic cylinder. A drawn plow/implement is fully supported by its own transport wheels and is raised and lowered by a remote hydraulic cylinder.

Tillage operations for seedbed preparation are often classified as *primary* or *secondary*, although the distinction is not always clear-cut. A primary tillage operation constitutes the initial, major soil-working operation after harvest of the previous crop; it is normally designed to reduce soil strength, cover plant materials, and rearrange aggregates. Secondary tillage operations are intended to create refined soil conditions following primary tillage. The final tillage operation prior to planting a crop is usually secondary tillage, but farmers may use more than one secondary tillage operation. In some situations, a tillage operation may fit the definition of both secondary and primary tillage. For example, a farmer may prepare a field for planting winter wheat with a single disking operation after harvesting soybeans. This single disking operation is both the initial tillage operation after harvest and the final tillage operation before planting.

Erosion of soil by wind or moving water is a problem that plagues agriculture in many parts of the world. The erosion process removes nutrients and other chemicals from land as well as soil. Some farmers in North America use conservation tillage, a practice which leaves plant residue on the soil surface to reduce erosion. Practicing *conservation tillage* can reduce the time and energy required for tillage, although this practice frequently requires better management than *conventional tillage*.

8.1.1 Primary tillage in conventional tillage systems

Most farmers use only one primary tillage operation after harvesting a crop. An exception is when a farmer uses a subsoiler in the fall shortly after harvest followed by another primary tillage in the spring. Implements used for primary tillage are moldboard plows, disk plows and tillers, chisel plows, subsoilers, stubble-mulch plows and tillers, rotary tillers, listers, and bedders.

8.1.1.1 Moldboard plows

All moldboard plows are equipped with one or more tillage tools called *plow bottoms* (Figure 8.1). Each plow bottom is a three-sided wedge with the landside and the horizontal plane of the share's cutting edge acting as flat sides and the top of the share and the moldboard together acting as a curved side. The primary functions of the plow bottom are to cut the furrow slice, shatter the soil, and invert the furrow slice to cover plant residue. Most moldboard plows are also equipped with tillage tools called *rolling coulters* (Figure 8.2) to help cut the furrow slice and to cut through plant residue which might otherwise collect on the shin or plow frame and cause clogging. The vertical edge of the furrow slice left uncut by the rolling coulters is cut by the *shin*. The bottoms along with the rolling coulters are responsible for the process function of the moldboard plow.

Moldboard plows are the most common implement used for primary tillage, but they are never used for secondary tillage. They are usually equipped with adjustments to ensure that the plow is level in the longitudinal and lateral directions and that the plow bottom is oriented with the landside parallel to the direction of travel. A five-bottom moldboard plow is shown in Figure 8.3.

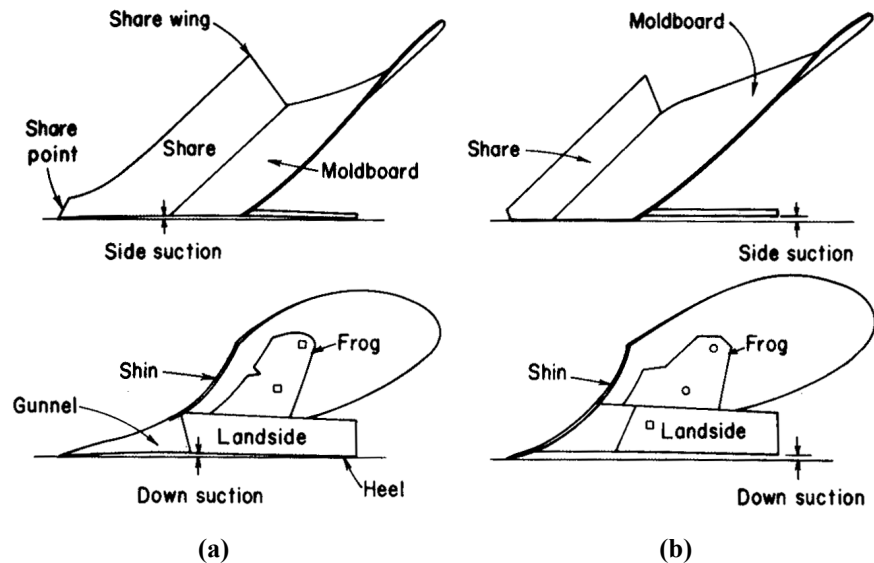


Figure 8.1 – Typical moldboard plow bottoms, (a) with gunnel-type share, showing method of measuring suction when no rear furrow wheel or depth control devices are used, (b) with throw-away share, indicating clearances when a rear furrow wheel is used (reprinted from Kepner et al., 1978).

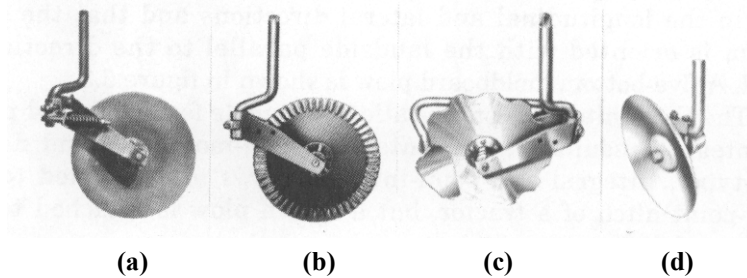


Figure 8.2 – (a) Plain coulters with spring, (b) ripple-edge coulters, (c) notched coulters with jointer attachment, (d) concave coulters or disk jointers (reprinted from Kepner et al., 1978).

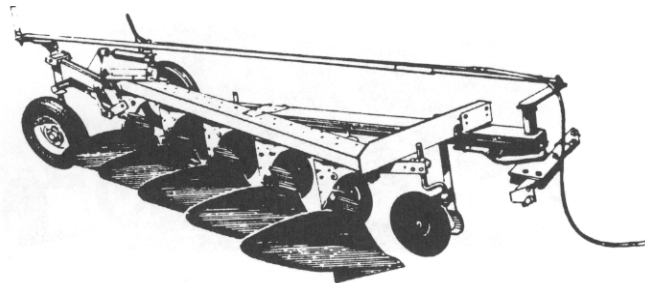


Figure 8.3 – A semi-integral five-bottom moldboard plow bottom.

Integral moldboard plows have the lowest purchase price and the best maneuverability for small and irregular fields. However, they are limited in size due to tractor stability and the lift capacity of the hitch. The furrow transport wheel of a semi-integral plow is automatically steered to provide more maneuverability than for a drawn plow. Both integral and semi-integral plows improve a tractor's traction by applying a downward force on the hitch. Drawn plows provide the most uniform plowing depth, but have the highest purchase price.

Moldboard plows are frequently equipped with automatic reset standards that allow a plow bottom to move rearward and upward to pass over an obstacle, such as a rock, without damage. A hydraulic cylinder or a spring mechanism automatically moves the bottom to its original position after it passes over the obstacle (Figure 8.4).

Most moldboard plows are designed to turn the furrow slices only to the right. Two-way plows, however, have two sets of opposed bottoms that can be used selectively. With this arrangement, all the furrows can be turned toward the same side of the field by using the right-hand bottoms for one direction of travel and the left-hand bottom on the return trip. The two sets of bottoms are mounted on a common frame that is rotated 180° about a longitudinal axis to change from one set to the other as shown in Figure 8.5. In most cases, rotation is accomplished with a hydraulic cylinder

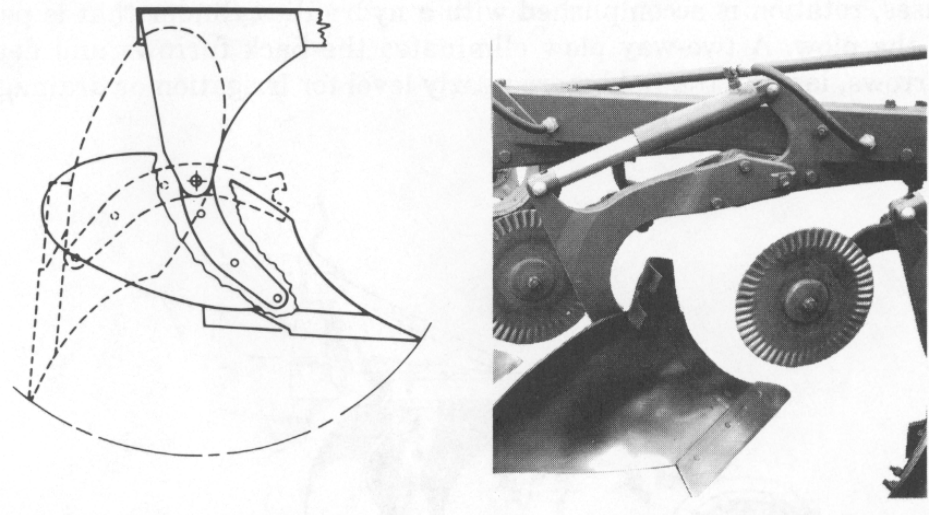


Figure 8.4 – Spring-trip (left) and hydraulic reset mechanisms (right) used as overload protection devices for moldboard plows (Left, reprinted from Kepner et al., 1978; right, courtesy of Deere and Co.).

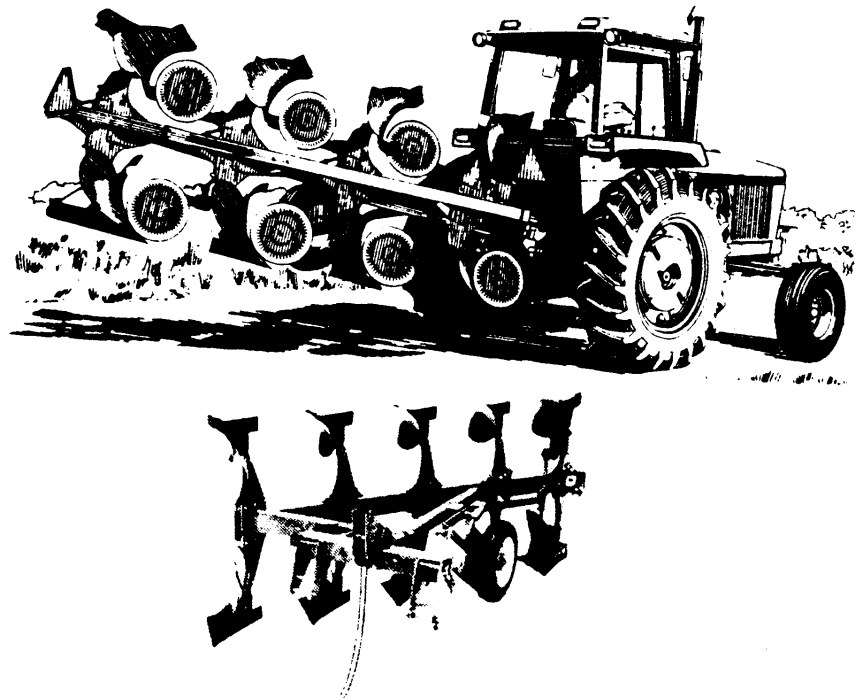


Figure 8.5 – A rear-mounted two-way plow.

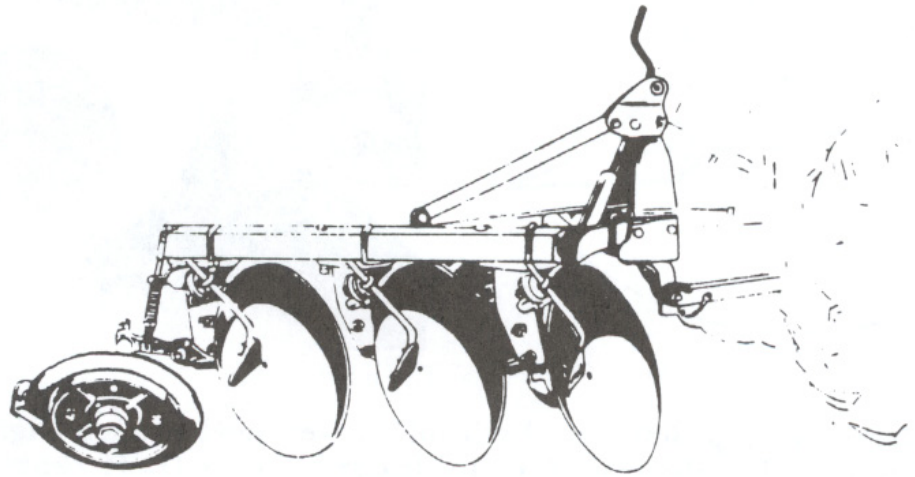


Figure 8.6 – A mounted three-bottom disk plow.

that is part of the plow. A two-way plow eliminates the back furrows and dead furrows, leaving the field more nearly level for irrigation or drainage. Two-way plows are also advantageous for terraced fields or contour plowing and for small fields of irregular shape.

8.1.1.2 Disk plows

The common *disk plow* consists of a series of disk blades mounted individually on a frame as shown in Figure 8.6. The disk blades are set at an angle, called the *disk angle*, from the forward line of travel, and also at a *tilt angle* from the vertical, as shown in Figure 8.7. Standard disk plows usually have three to six blades, spaced to cut 18 to 30 cm/disk. The disk angles vary from 42° to 45° and the tilt angles vary from 15° to 25° . The disk diameters are commonly between 60 and 70 cm.

The disks used in the disk implements are either conical or spherical (i.e., sections of hollow spheres). Both blades have a *spherical radius* associated with the *concavity* of the blades as shown in Figure 8.7. A conical blade has its outside surface flattened to a specific *cone angle*. The *blade angle* of a spherical blade is defined as the tangent at the edge surface area of the blade.

Disk plows are used for primary tillage and are available in integral, semi-integral, and drawn hitching configurations. They are most suitable for conditions under which moldboard plows do not work satisfactorily, such as in hard, dry soils, and in sticky soils where a moldboard plow will not scour. Scrapers, furnished as standard equipment on most disk plows, assist in covering plant residue and inverting the soil and prevent soil buildup in sticky soils. Reversible disk plows have an arrangement whereby the disk angle can be reversed at each end of the field to permit one-way plowing.

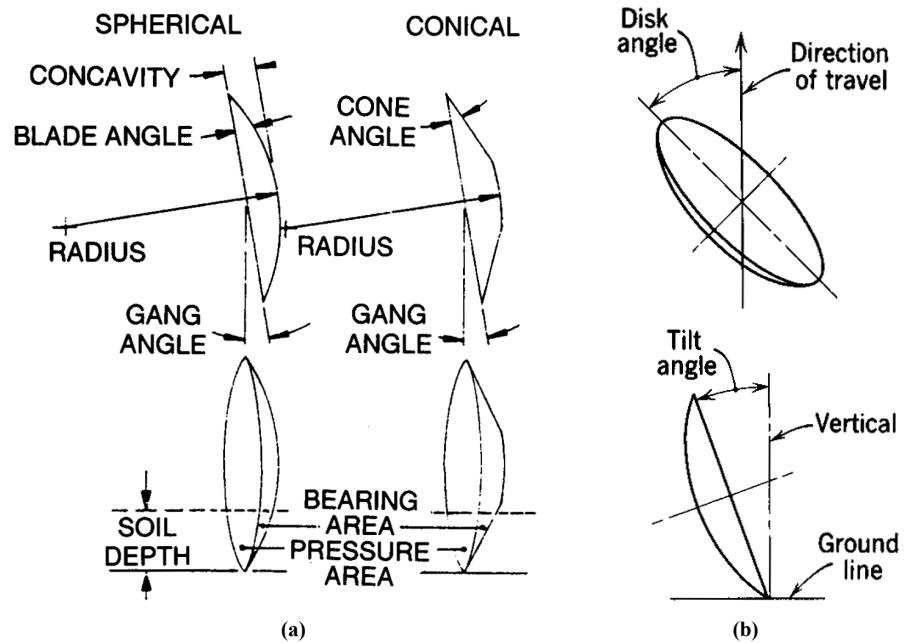


Figure 8.7 – (a) Disk blade geometry (Sommer et al., 1983), (b) disk and tilt angles (reprinted from Kepner et al., 1978).

Under most conditions, and particularly in hard, dry soils, any disk tool must be forced into the ground by its weight rather than depending upon suction as does a moldboard plow. Consequently, disk plows are built with heavy frames and wheels (total masses of 180 to 540 kg/disk blade), and even then additional mass must sometimes be added to obtain a desired depth. The soil penetration ability of a disk plow depends upon disk diameter, tilt angle, and disk angle. Whereas the moldboard plow absorbs side forces mainly through the landsides, a disk plow must depend upon its wheels for this purpose.

A standard disk plow does not have special attachments to protect its disk blades from damage due to impact with rocks buried in the soil. Usually, the disk plow is able to withstand impact forces because of its heavy frame and its lower operating speed.

8.1.1.3 Disk tillers

The disk tiller (Figure 8.8) is also known as one-way disk plow, vertical-disk plow, harrow plow, and wheatland plow. It is similar to a disk plow in regard to the frame, wheels, and depth control, but the disk tiller blades are uniformly spaced along one axle or gang bolt and clamped together through spacer spools so the entire gang rotates as a unit.

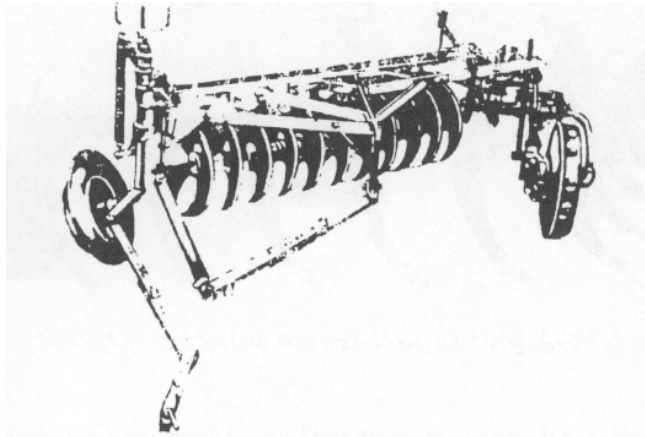


Figure 8.8 – A pull-type one-way disk tiller or wheatland plow.

This implement is used in dryland grain-growing regions for shallow tillage (often only 8 to 13 cm) and mixing plant residue with the soil. The soil surface is left rough with visible plant residue to reduce soil erosion. Disk tillers are used for primary tillage and are frequently used in subsequent operations for summer fallowing. Some disk tillers are equipped with seed and fertilizer attachments to accomplish seedbed preparation, seeding, and fertilizing in a single operation.

The blades of a disk tiller are somewhat smaller than those of a standard disk plow, the most common diameters being between 51 and 61 cm. They are generally spaced 20 to 25 cm apart along the gang bolt. The width of cut per blade depends upon the spacing and upon the gang angle (adjustable) between the gang axis and the direction of travel. Gang angles range from 35° to 55°, with 40° to 45° being most common. There is no tilt angle, and the disk angle is commonly between 35° and 55° (disk plow disk angles are 42° to 45°).

Since disk tillers are primarily for relatively shallow tillage, they are built much lighter than disk plows (usually 45 to 90 kg/blade). They are available with integral and drawn hitching configurations. Most disk tillers move the soil only to the right, but reversible models are available which can move the soil in either direction.

8.1.1.4 Chisel plows

A chisel plow (Figure 8.9) is an implement designed for primary tillage at depths from 15 to 46 cm. The soil engaging tools are shanks equipped with replaceable points or shovels. They shatter, mix, and aerate the soil with little soil inversion. They leave a rough soil surface with most of the plant residue remaining uncovered. This condition helps prevent wind and water erosion while improving water penetration into the soil, and the plant residue on the soil surface improves traction.

Chisel plows function most effectively when the soil is dry and firm because the tools can pass through wet soil with almost no shattering action.

A chisel plow requires approximately one-half of the draft of a moldboard plow with the same working width and operating at the same tillage depth. However, farmers usually operate a chisel plow at a greater depth than a moldboard plow to break up

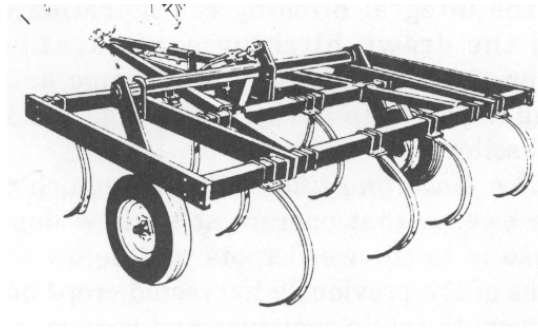


Figure 8.9 – A pull-type chisel plow with rigidly mounted shanks.

the plow sole for improved water and root penetration. Under those conditions the draft requirement of a chisel plow increases.

The plant residue left on the soil surface acts as an insulator and slows soil warm-up and soil drying in the spring compared with soil left bare from moldboard plowing. Some researchers have found a need for increased chemical application rates because chisel plowing does not bury weed seeds and because plant residue may absorb some of the chemicals.

Chisel plowing is usually completed in late summer or early fall and is followed by one or more secondary tillage operations during the following spring. Both the surface roughness and required draft increase with increased operating speed. Chisel plows are available with integral and drawn hitching configurations. The shanks are designed with spring-cushion, spring-reset, or spring-trip mountings to protect the tool and frame from impacts with buried rocks.

8.1.1.5 Subsoilers

Subsoilers (Figure 8.10) are used to break through and shatter compacted or otherwise impermeable soil layers and to improve rainfall penetration. They have heavy standards that can be operated at depths of 45 to 75 cm or more. Subsoilers do very little soil mixing and no soil inversion. They are most effective under dry and firm soil conditions. A subsoiling operation is usually followed by another primary tillage operation before secondary tillage is begun. Most subsoilers use the integral hitching configuration, but a few are available with the drawn hitching configuration. Subsoilers frequently rely on the heavy design of the frame and standards for protection during impact with buried rocks. Figure 8.10 shows a pull type V-frame subsoiler.

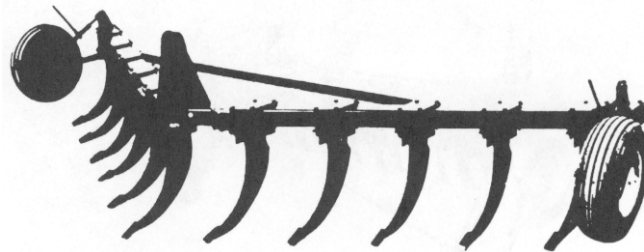


Figure 8.10 – A pull-type V-frame subsoiler.

8.1.1.6 Stubble-mulch plows and tillers

Stubble-mulch plows are made of wide V-shape sweeps that operate at shallow depth of 10 cm or less. The purpose is to cut weed roots just below the surface and leave the stubbles of the previously harvested crops on the surface to act as mulch (cover) to retain moisture and reduce soil erosion. The width of each sweep is in the range of 1.5 m. There may be several sweeps on a plow. Very wide plows have folding wings that fold during transport. These plows may be used as primary tillage tools right after the harvest or as secondary tillage tools before planting. When used for primary tillage it may be necessary to mix some surface residue into the soil using a disk tiller or a disk harrow (see below) before planting.

A stubble-mulch tiller is a combination of a chisel plow and a disk harrow. The disk section is in the front to cut stubbles, such as corn stalks, while the rear section is the chisel plow to accomplish deep tillage. Stubble-mulch tillers are used where it is essential to till deep to break old plow pan but it is not necessary to leave all crop residue for erosion control. Mixing some of the crop residue helps to improve organic matter in the soil.

8.1.1.7 Rotary tillers

Rotary tillers are also called power tillers because the power is transferred to the tiller from the tractor via the power-take-off drive. A shaft containing blades is located at 90° to the line of travel and rotates in the same direction as the forward travel of the tractor. Since the shaft turns at a rate that is considerably faster than the corresponding tractor speed, soil pulverization is accomplished. Also, the tiller pushes the tractor forward and generates a negative draft. Consequently, lighter tractors can be used for rotary tillage operations. Total power requirements for rotary tillers are generally higher than for conventional plows. However, one rotary tillage operation may be equivalent to several conventional tillage operations as far as the quality of the seed bed is concerned. Figure 8.11 shows a rotary tiller.

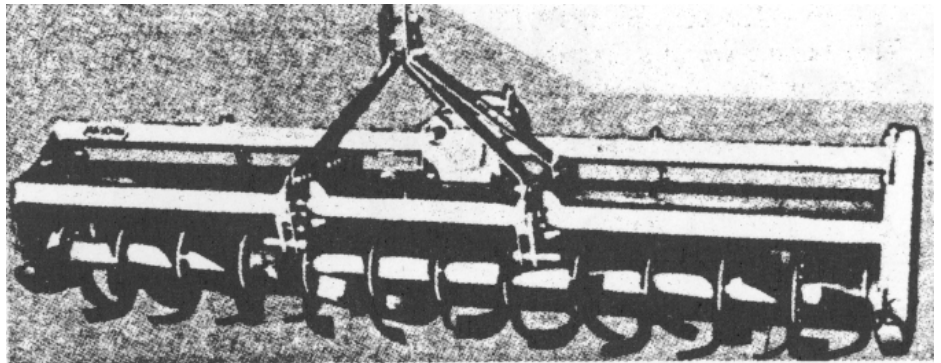


Figure 8.11 – A rear-mounted full width rotary tiller.

8.1.2 Secondary tillage in conventional tillage systems

Any tillage operations performed after the primary tillage are called secondary tillage. Generally, several secondary tillage operations are performed before the field is ready for planting. The main objective of secondary tillage is to break down large clods and to prepare an ideal seedbed for planting. An ideal seedbed is the one that allows for good seed-to-soil contact, conserves moisture needed for germination, and allows for vigorous and uninhibited root and shoot growth. The equipment used for secondary tillage are generally called *harrows*. The most common harrow is the disk harrow; spring tine harrows, spike tooth harrows, cultivators, and rotary hoes are other types. In dry climates, culti-packers are often used for the final tillage operation before planting. The purpose of a culti-packer is to increase the density of the top few centimeters of the soil depth. This tends to break the capillaries in this soil zone and prevent moisture from escaping.

8.1.2.1 Disk harrows

Disk harrows differ from disk plows in that there is no tilt angle and several blades are mounted on a common axis called the gang. They are lighter and have smaller wheels than disk tillers. In disk harrows, the gang may be arranged in different configurations as shown in Figure 8.12. The arrangements may be single-action, offset, or tandem. It should be noted that the gangs are always in pairs with opposite disk orientation to balance the side draft produced by each disk. Disk harrows may be either mounted or pull type. Smaller units tend to be mounted while larger units tend to be pull type with wheels for transportation. Remote hydraulic cylinders are used to raise or lower the implement from the driver's seat. Some very large units are designed to fold over for transportation. Pull type units with wheels allow for better depth control.

The size, weight, spacing, depth, and angles of the disks are selected based on the field conditions and the purpose of disking. Disk diameters range from 40 to 80 cm, and weights range from 20 to 200 kg/disk. Disking with larger disks should be followed by lighter disks for final seedbed preparation. Disk spacing increases with disk diameter. Narrow disk spacing of about 18 cm is used for final seedbed preparation when the ground is not hard with little surface residue. Disk spacing of about 23 cm is

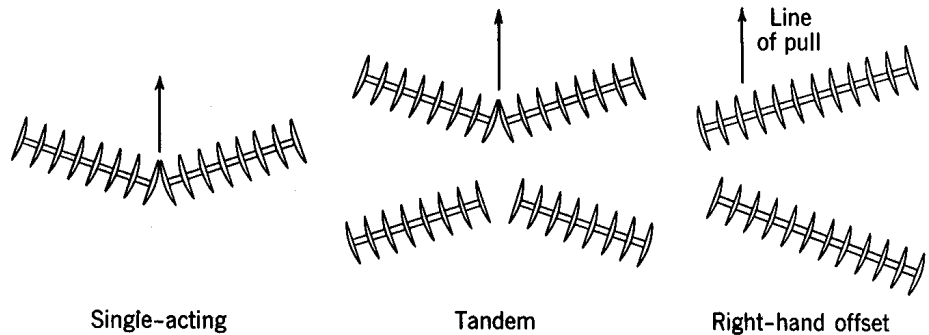


Figure 8.12 – Gang arrangements for three general types of disk harrows (reprinted from Kepner et al., 1978).

used for mixing of chemicals or cutting of surface trash. Spacing of about 28 cm and higher is needed for harder soils or when heavy surface residue is present. The operating depth is determined by the soil conditions and the weight per unit disk of the plow. The gang angle varies from 15° to 35° as measured from a line perpendicular to the line of travel. Gang angles may be changed to meet the field conditions. Increasing the gang angle makes the disks more aggressive, increasing their depth and power requirement.

8.1.2.2 Spike-tooth, tine-tooth, and spring-tooth harrows

These tillage tools are used in the final seedbed preparation. They are also used for post-planting operations to breakup soil crust and remove weeds. In a spike-tooth harrow, the spikes are rigidly mounted on a frame. However, the mounting bars may be spring-loaded (Figure 8.13). The angle of the spikes may be altered to change the aggressiveness, with vertical orientation being the most aggressive. Tine-tooth harrows, as shown in Figure 8.14, use spring tines that create additional action for soil breakup. The tines are closely spaced, about 3.8 to 5 cm apart, compared to spikes in spike-tooth harrows. Spring-tooth harrows (Figure 8.15) use round wire teeth made of spring steel. Due to the spring action, these harrows are more suited for stony ground. However, their lack of depth penetration limits their use to less than hard soils. All of these harrows may be used as attachments to other tillage tools such as moldboard plows and disk harrows because of their low draft requirements. Some units may be up to 16 m wide with fold-up frames for road transport.

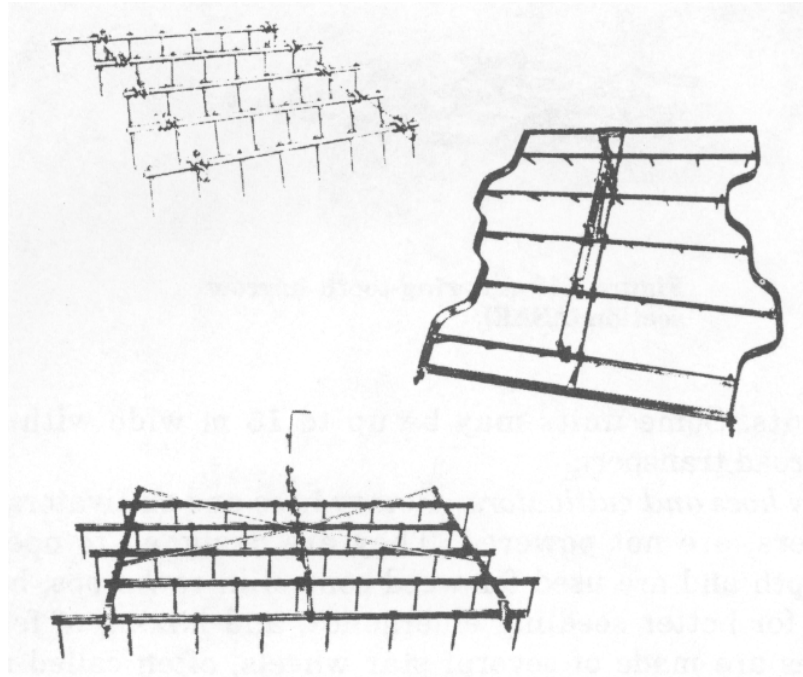


Figure 8.13 – Different sections used in spike-tooth harrows.

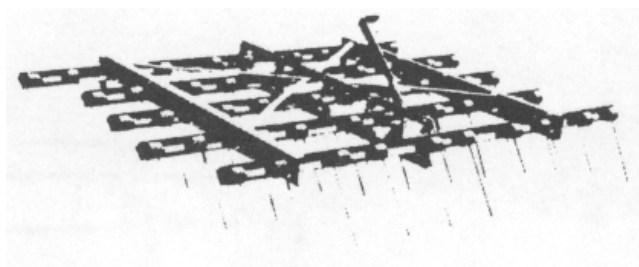


Figure 8.14 – A tine-tooth harrow.

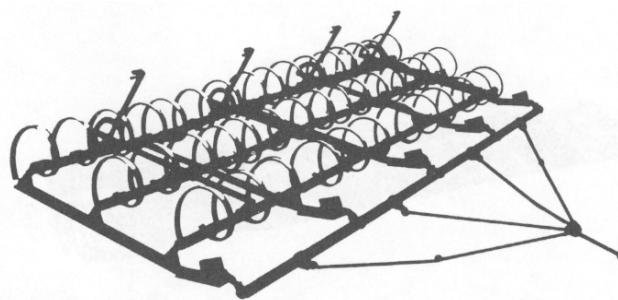


Figure 8.15 – A spring-tooth harrow section.

8.1.2.3 Cultivators

There are basically three types of cultivators: *field cultivators*, *row crop cultivators*, and *rotary cultivators*. Field cultivators are often used as secondary tillage tools for seedbed preparation. They are similar to chisel plows in appearance but they operate at much shallower depths. Figure 8.16 shows the different types of tools that can be attached to a cultivator shank for different applications. Field cultivators may be either mounted or pull type with wheels for depth control. Some very large units are designed to be folded while transporting. The lateral tine spacing may vary from 15 to 30 cm. Usually two or three rows of tines are used with fore and aft spacing ranging from 50 to 80 cm. Row crop cultivators have the tines spaced to go between the crop rows. They are used for cultivation and weed control operations during the active growth period of crops planted in rows.

8.1.2.4 Rotary hoes and rotary cultivators

Rotary hoes and cultivators, unlike rotary tillers, are not powered. They are both designed to operate at shallow depth and are used for weed control in row crops, breaking soil crests for better seedling emergence, and mixing of fertilizer.

Rotary hoes are made of several star wheels, often called spiders, mounted on a shaft at a spacing of about 15 cm to form a gang. Each spider has 10 to 16 teeth and the tip diameter ranges from 45 to 50 cm. Two staggered parallel gangs make a section and provide a working width of about 8 to 10 cm. Several sections are used in a given implement. The section width is such that they fit between the rows for row crop cultivation. The teeth in a rotary hoe have forward curvature for more aggressive cultivation. A rotary hoe is shown in Figure 8.17.

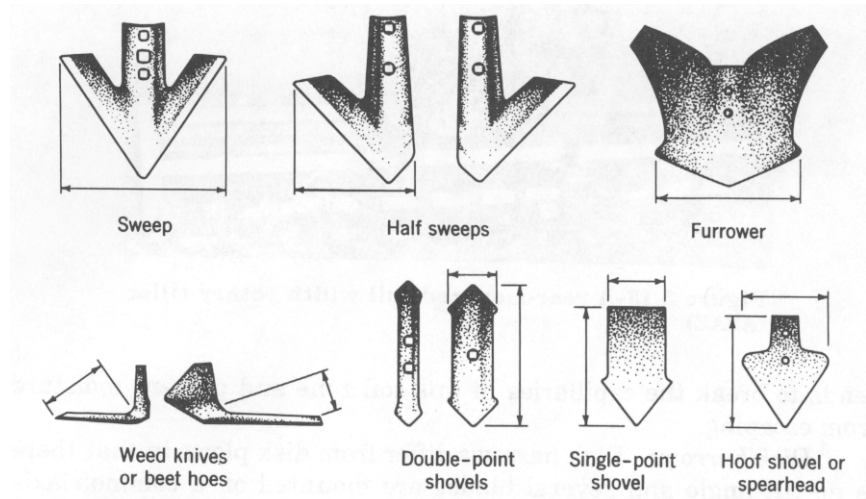


Figure 8.16 – Cultivator tools (reprinted from Kepner et al., 1978).

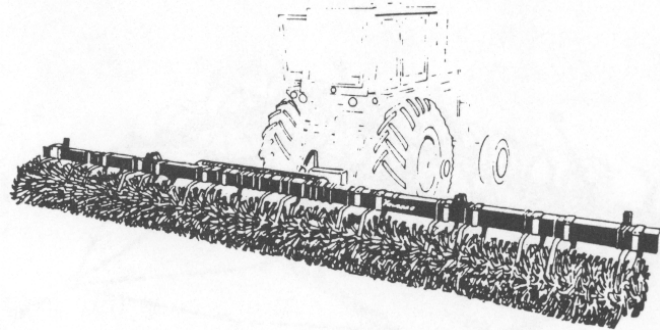


Figure 8.17 – A rear mounted rotary hoe with in-line sections on spring-loaded arms.

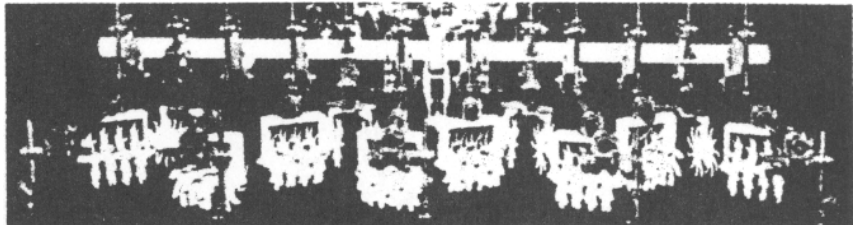


Figure 8.18 – A rear-mounted, row crop rotary cultivator with ground-driven finger wheels.

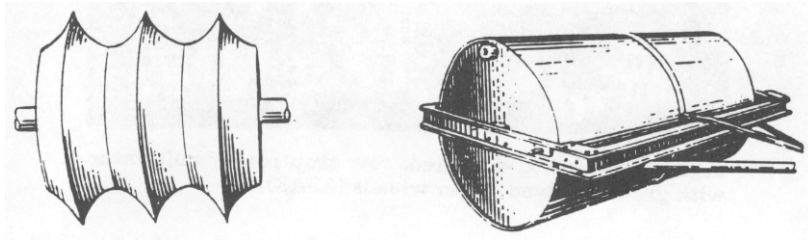


Figure 8.19 – Rollers and culti-packer.

Rotary cultivators have spiders similar to rotary hoes but the teeth are twisted and the ends are shaped like chisels. This creates a sideways movement of the soil. Only two spiders are mounted on a shaft, and each shaft is located at an angle from the forward line of travel. The spider wheels turn backward as the implement is pulled forward creating the necessary tilling action. The cultivator may be arranged to cultivate row crops or the entire field. A rotary cultivator is shown in Figure 8.18.

8.1.2.5 Culti-packers, rollers, and finishing boards

Often in dry conditions or when the soil has many clods, culti-packers, rollers (Figure 8.19), or finishing boards are used to break up soil clods and to conserve moisture for better seed germination. These tools are used almost always as attachment to harrows just before seeding.

8.1.2.6 Listers

Listers (Figure 8.20) look like double moldboard plows. They are used to create furrows for planting. Sometimes it is desirable to plant in furrows as opposed to on a flat surface to protect the plants from wind and to place seed down near the moisture. These ridges are flattened due to the cultivation performed during the growing season so by the time of harvest the field is level. Often planters are attached to listers to accomplish planting in the same operation.

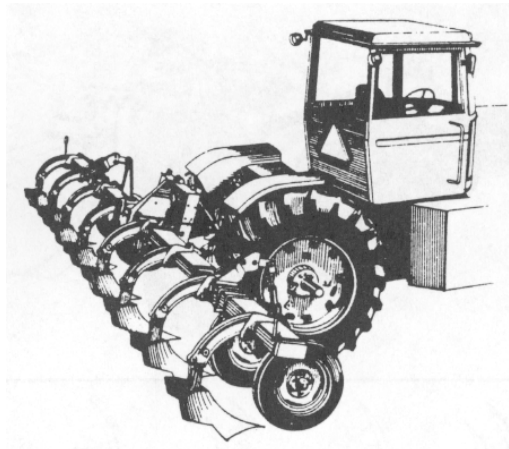
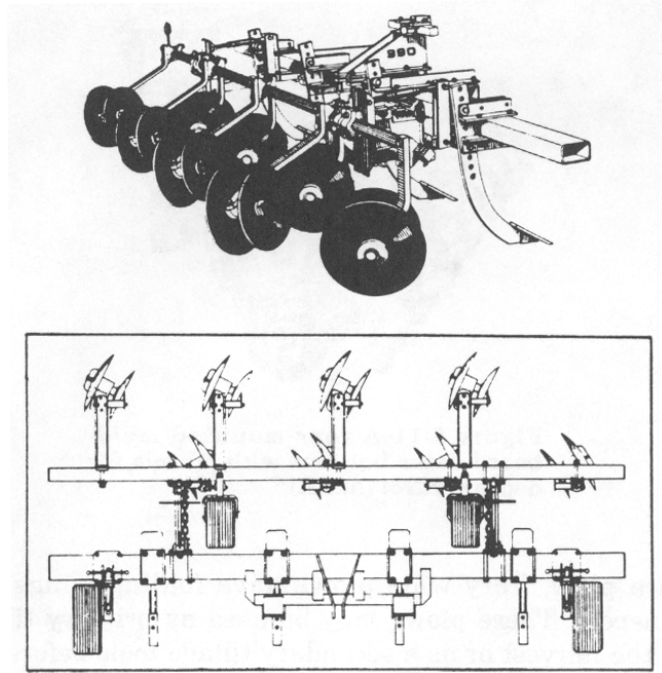


Figure 8.20 – A rear-mounted mold-board lister with wheels for depth control.



**Figure 8.21 – A rear-mounted bedder-ridger with disk-staggered gangs.
Shown with a subsoiler.**

8.1.2.7 Bedders

Bedders are used to make ridges or beds when it is desirable to plant on a higher soil level in areas of high rainfall. Bedders are made of disk implements that work in pairs to form the ridges as shown in Figure 8.21.

8.1.3 Tillage in conservation tillage systems

Conservation tillage systems are designed to conserve soil, water, and/or energy. In areas prone to wind soil erosion, it is advisable to leave surface cover on the soil to prevent or minimize soil erosion. Any primary tillage operation that turns the soil over and buries the surface residue under the soil is eliminated. In heavy soils subjected to compaction due to wheel traffic, it is recommended that primary tillage performed during the wet spring season be eliminated. In this situation weed control is accomplished by use of herbicides. Generally, conservation tillage systems require some other changes to be made in the methods and equipment. For example, planter changes are needed to cut through the surface residue in order to plant seeds. This is accomplished by adding a fluted coulter ahead of the furrow openers.

There are different levels of conservation tillage: minimum tillage, strip tillage, and zero tillage. Zero tillage system consists of no primary or secondary tillage operation. In a strip tillage system, a small band or strip of soil is tilled and the crop is planted in this strip. Elimination of any primary or secondary tillage operation results in the minimum tillage system.

8.2 MECHANICS OF TILLAGE TOOLS

8.2.1 Soil texture

One aspect of the physical properties of soil, its *texture*, is described by the percent of particles in various size classes (Table 8.1). Particle size is the defining difference between sand, silt, and clay, but of course the size of the particle has much to do with its other properties. Natural soils are nearly always mixtures of sand, silt, and clay particles, as well as organic matter and stones. One convenient method of naming soils is the soil texture triangle (Figure 8.22). The sides of the triangle are axes, each representing the percentages of sand, silt, and clay that constitute the soil. Special names are assigned to various combinations as designated by the areas within the triangle. Thus, if a soil is composed of 40% sand, 35% silt, and 25% clay, it is called a loam. This is noted by the * in the figure. Note that because of the importance of the surface area-to-volume ratio, soils with as little as 20% clay still are called clay soils.

There are various laboratory methods of measuring the relative amounts of sand, silt, and clay, but a field key such as Figure 8.23 gives useful results.

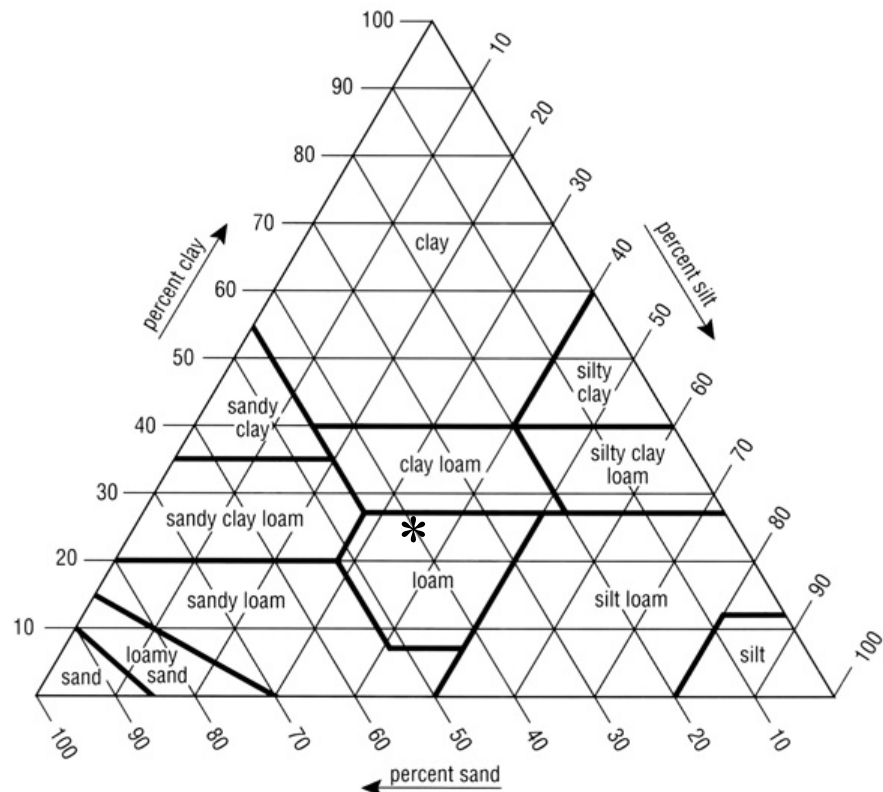


Figure 8.22 – USDA soil texture triangle showing the percentages of sand, silt, and clay in various soils. Note that these percentages are after sieving out particles > 2.0 mm (gravel and stones) and removing the organic matter.

Table 8.1. USDA soil particle size definitions.

Particle class	Size (diameter)
clay	less than .002 mm
silt	.002-.05 mm
sand	.05-2.0 mm
gravel, stone	larger

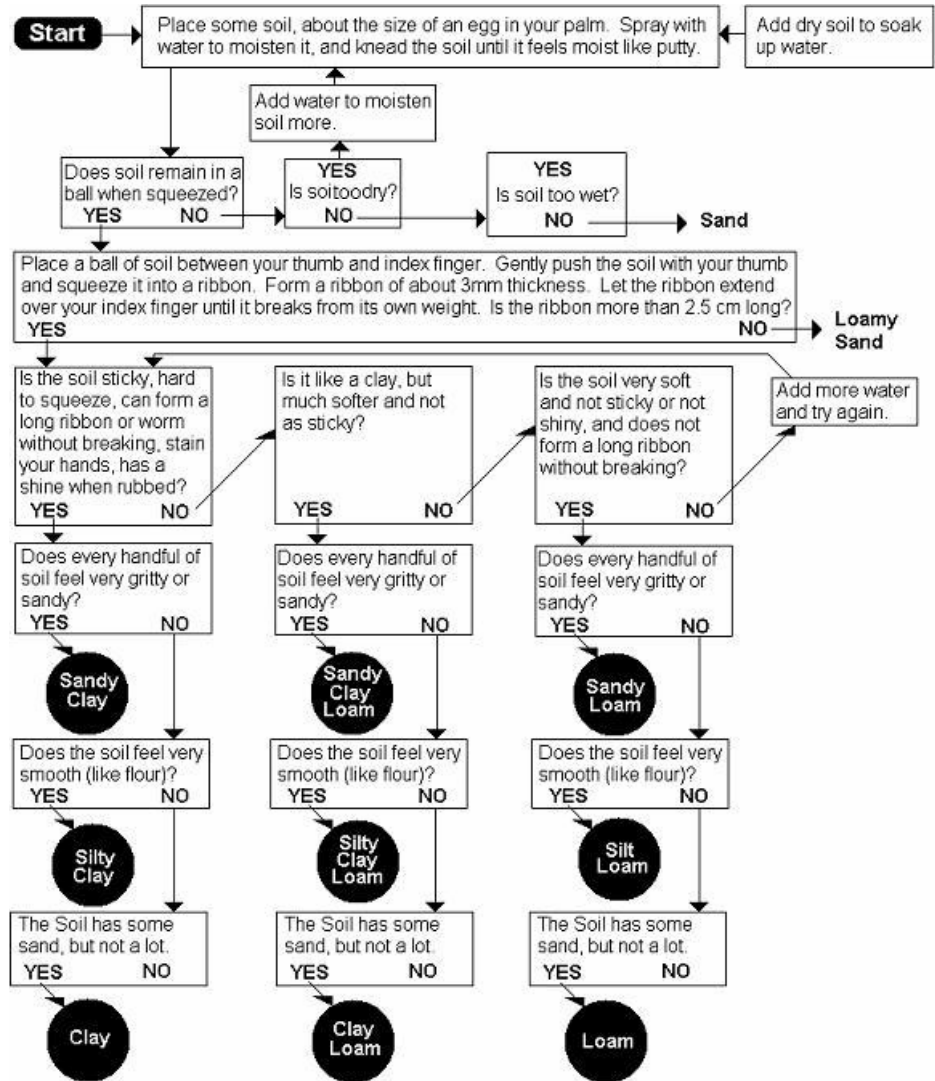


Figure 8.23 – Guide to soil texture by feel (from USDA-NRCS, http://soils.usda.gov/education/resources/k_12/lessons/texture/).

8.2.2 Physical properties of soils

Porosity, n , is a measure of the relative amount of voids in the soil. It is the ratio of the void volume, V_v , to the total volume, V , of the soil sample (Figure 8.24), or:

$$n = \frac{V_v}{V} \quad (8.1)$$

The *void ratio*, e , is the ratio of the void volume to the volume of the solids in a soil sample, or:

$$e = \frac{V_v}{V_s} \quad (8.2)$$

where V_s = volume of solids.

The *water content* of the soil, w , is the ratio of the weight of water, W_w , to that of the solids, W_s , expressed as a percentage, or:

$$w = \frac{100 W_w}{W_s} \quad (8.3)$$

The *degree of saturation*, S_r , is the percentage of void space that is occupied by water, or:

$$S_r = \frac{100 V_w}{V_v} \quad (8.4)$$

where V_w = volume of water.

The *unit weight* or *density*, γ , is defined as the weight divided by the volume. For soils:

$$\gamma = \frac{W}{V} = \frac{W_s + W_w}{V_s + V_w + V_a} \quad (8.5)$$

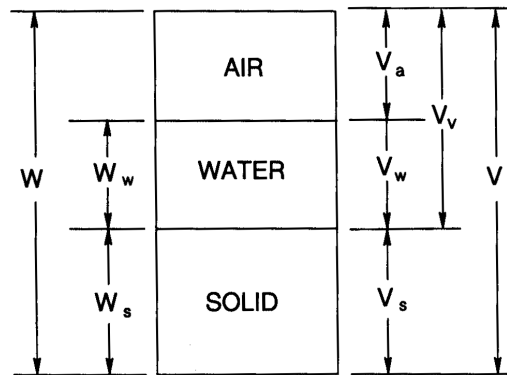


Figure 8.24 – Soil weight and volume fractions.

The *dry density*, γ_d , is the weight of solids divided by the total volume, or:

$$\gamma_d = \frac{W_s}{V} \quad (8.6)$$

Finally, the density of the solid particles in the soil, γ_s , is expressed as follows:

$$\gamma_s = \frac{W_s}{V_s} \quad (8.7)$$

The density of the solids in soils is found to be somewhat constant. It generally remains between 2.6 and 2.8 g/cm³. The average value is 2.65 g/cm³ for sand and silt and 2.75 g/cm³ for clay.

Example 8.1

A 100 cm³ soil sample weighs 165 g and its water content was found to be 49%. If the specific gravity of the solids is assumed to be 2.6, find the void ratio, porosity, degree of saturation, and dry density.

Solution

First, find the weights and volumes of all fractions of the soil specimen.

$$w = W_w/W_s = 0.49$$

$$W_w = 0.49 W_s$$

$$W_s + W_w = 165 \text{ g}$$

$$W_s + 0.49 W_s = 165 \text{ g}$$

$$W_s = 165/1.49 = 110.74 \text{ g}$$

$$W_w = 165 - 110.74 = 54.26 \text{ g}$$

$$V_s = W_s / \gamma_s = 110.7/2.6 = 42.59 \text{ cm}^3$$

$$V_w = W_w / \gamma_w = 54.26/1.0 = 54.26 \text{ cm}^3$$

$$V_a = V - V_s - V_w = 100 - 42.59 - 54.26 = 3.15 \text{ cm}^3$$

Now find the required ratios from the weight and volume values as computed above.

$$\begin{aligned} \text{Void ratio, } e &= V_v / V_s = (V_w + V_a) / V_s \\ &= (54.26 + 3.15) / 42.59 = 1.35 \end{aligned}$$

$$\text{Porosity, } \eta = V_v / V = (54.26 + 3.15) / 100 = 0.57$$

$$\begin{aligned} \text{Degree of saturation, } S_r &= 100 V_w / V_v \\ &= 100 (54.26) / 5741 = 0.95\% \end{aligned}$$

$$\text{Dry density, } \gamma_d = W_s / V = 110.74 / 100 = 1.107 \text{ g/cm}^3$$

8.2.3 Mechanical properties of soils

8.2.3.1 Shear strength

If a soil specimen is subjected to shear stress the shear stress-strain diagram may look like one of the curves in Figure 8.25, depending upon the soil conditions. A highly cemented soil will result in a well defined failure point as shown by curve A. Loose soil may not show any definite failure point and the stress may increase exponentially with strain reaching some maximum value as shown by curve B. Curve C is for a soil that is well compacted but not cemented.

The soil strength refers to the value of the shear stress on a plane within the soil sample where soil failure has taken place either by rupture or breakage. For curves A and C this point is clearly defined but for curve B soil failure is not distinct. In the case of curve C the failure is considered to have taken place by yielding or plastic flow and the asymptotic value of shear stress is taken as the shear strength for this case. The shear stress-strain curves shown in Figure 8.25 are for a given normal stress on the sample. If the normal stress is changed the shear stress-strain diagram will change and consequently the value of the maximum shear stress will also change. An increase in the normal stress would cause an increase in maximum shear. Therefore, the shear strength is a function of the normal stress on the failure plane.

Mohr-Coulomb failure theory states that failure in a material occurs if the shear stress on any plane equals the shear strength of the material. Furthermore, the shear strength (s) along any plane is a function of the normal stress (σ) on the plane, as shown below:

$$s = f(\sigma) \quad (8.8)$$

Coulomb, in 1776, conducted experiments to determine the maximum shear stress that could be applied on a plane within a sample of soil at varying levels of normal stress. He plotted the maximum shear stress values at failure against the corresponding normal stress on the failure plane and suggested the following linear relationship:

$$s = c + \sigma \tan(\phi) \quad (8.9)$$

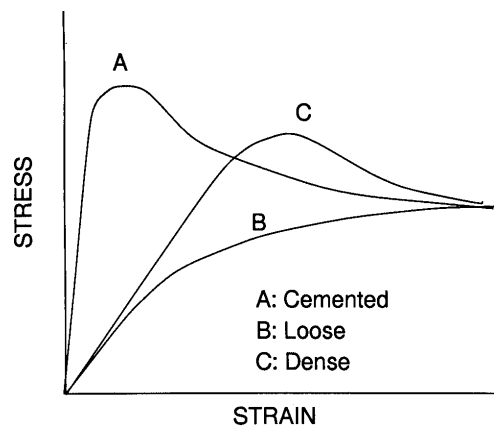


Figure 8.25 – Typical shear stress-strain diagrams for soils in three conditions.

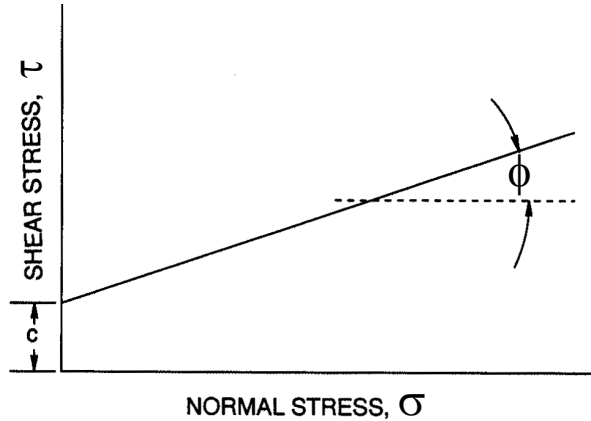


Figure 8.26 – Soil failure envelopes.

The Coulomb criterion is shown as a straight line in Figure 8.26, with an intercept on the shear stress (τ) axis equal to c and a slope equal to $\tan \phi$. The quantities c and ϕ are material properties frequently called cohesion and angle of internal friction, respectively. The shear strength as defined by Equation 8.9 represents the maximum shear stress that may be sustained on any plane in a given material. The strength function is called the failure envelope since it defines the limiting stress.

8.2.3.2 Determination of shear strength

Direct shear test and the *triaxial test* are the two most widely used methods for determining soil shear strength. The purpose of these tests is to determine the value of c and ϕ needed in Equation 8.9 to define the soil shear failure envelope.

The direct shear test. The direct shear test is performed using an apparatus as illustrated in Figure 8.27. The box consisting of an upper and a lower half contains the

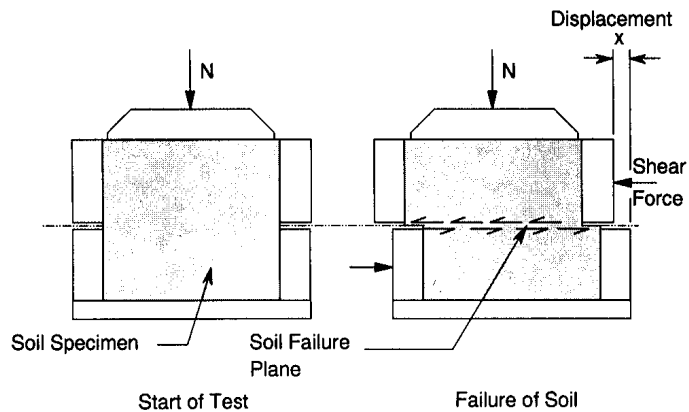


Figure 8.27 – Direct shear test apparatus.

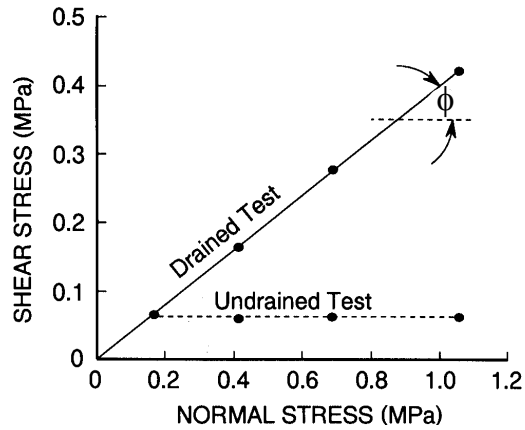


Figure 8.28 – Typical result of direct shear test.

soil sample to be tested. Drainage of water from the specimen is permitted using a porous stone at the bottom. The soil sample fails at the interface of the two halves. A normal stress is applied through a loading head, and the shear stress is increased until the specimen fails. A stress-strain curve is obtained by plotting the shear stress against the shear displacement.

To obtain the failure envelope, several tests utilizing different normal stresses are performed on specimens of the same soil. The specimens are then sheared at a slow rate to allow time for volume changes. If the shear strength is plotted against the normal stress, we obtain the solid line in Figure 8.28. The linear relationship between s and ϕ is the failure envelope.

The triaxial test. Consider a cylindrical soil sample subjected to a hydrostatic stress σ_3 as shown in Figure 8.29a and then an additional normal stress called the deviator stress (σ') as shown in Figure 8.29b. The deviator stress is increased until the soil fails. Figure 8.30a shows a two dimensional representation of stresses on the soil specimen. The soil failure plane orientation is shown by an angle (θ) from the horizontal. Figure 8.30b shows the shear and the normal stresses on the failure plane. Since the specimen failed the shear stress on this plane is equal to the shear strength. We now have to determine the values of the shear stress (τ) and the normal stress (σ) on this plane. These stresses can be determined by means of Mohr's circles as shown in Figure 8.31. Point A on the circle represents the failure plane. It should be noted that the angle or orientation of the failure plane is doubled in the Mohr's diagram. The coordinates of this point are the shear and the normal stresses on the failure plane. Using this diagram the following relationships can be written for these stresses:

$$\sigma = \frac{\sigma_1 + \sigma_3}{2} + \frac{\sigma_1 - \sigma_3}{2} \cos 2\theta \quad (8.10)$$

and

$$\tau = \frac{\sigma_1 - \sigma_3}{2} \sin 2\theta \quad (8.11)$$

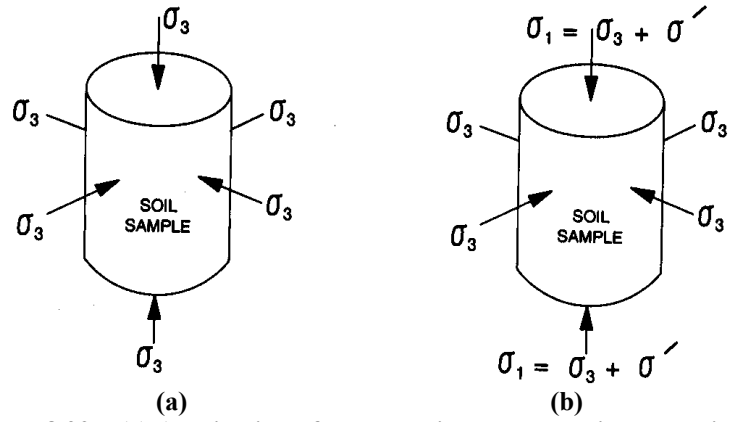


Figure 8.29 – (a) Application of hydrostatic stresses during consolidation, (b) application of the normal deviatoric stress to cause shear failure.

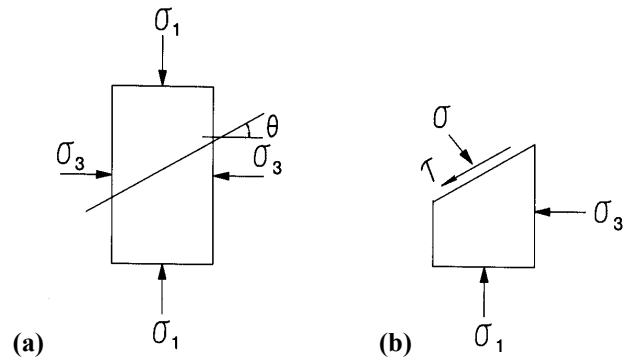


Figure 8.30 – (a) Two-dimensional representation of the stresses on a soil sample during the tri-axial shear test, showing (b) the shear and normal stress on the failure plane.

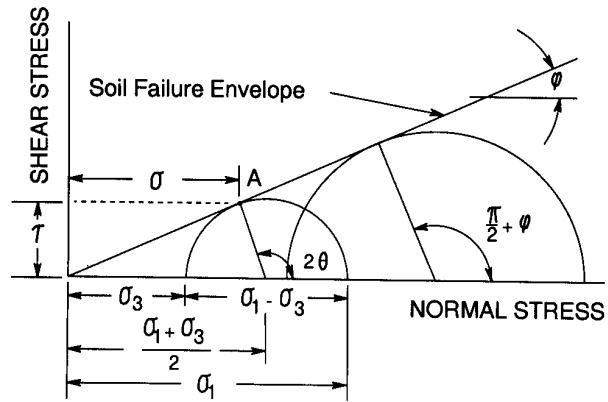


Figure 8.31 – Mohr's circle representation of principal stresses.

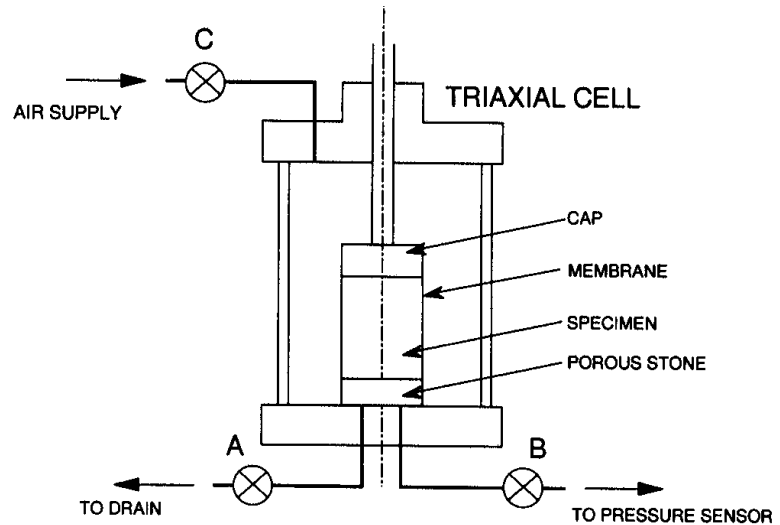


Figure 8.32 – A tri-axial shear test apparatus.

Figure 8.32 is a schematic diagram describing the triaxial apparatus and the application of stresses. The cylindrical soil specimen is enclosed within a thin rubber membrane and is placed inside a triaxial cell. The cell is then filled with a fluid. The specimen is subjected to a hydrostatic compressive stress (σ_3) by pressurizing the cell. This causes the soil sample to consolidate. An additional vertical stress (σ') is applied through the piston as shown in the figure. This deviator stress is steadily increased until failure of the specimen occurs. The specimen fails under a set of principal stresses $\sigma_3 + \sigma'$ and σ_3 .

Drainage of water from the specimen is measured by a burette, and valve A can be closed to prevent drainage from the specimen. Another line from the base leads to a pressure sensor to measure pore water pressure.

To obtain the failure envelope, several triaxial tests are performed on specimens of the same soil at different values of cell pressure (σ_3). A Mohr's circle is drawn for the principal stresses at failure for each specimen. These are shown in Figure 8.31 and the line tangent to these circles constitutes the failure envelope. The stress on the failure surface is represented by the point of tangency. From the geometry of Mohr's circle this plane makes an angle of $(\pi/2 + \phi)/2$ with the major principal stress plane.

The triaxial test may be performed as a drained (d), consolidated-undrained (c-u), or undrained test (u). In the drained test, water is allowed to seep out of the sample during the application of the hydrostatic and deviator stresses, and the pore water pressure is equal to zero. During the c-u test drainage is permitted during the application of the hydrostatic stress and the corresponding pore water pressure $u_a = 0$. When the deviator stress is applied, drainage is not permitted and the pore water pressure $u_b > 0$. In an undrained test, no drainage is permitted and the total pore water pressure is equal to u . The effective stress $\bar{\sigma}$ for the three drainage conditions may be calculated using the following equations:

Drained: $\bar{\sigma}_1 = \sigma_1$ $\bar{\sigma}_3 = \sigma_3$ (8.12)

Consolidated-Undrained $\bar{\sigma}_1 = \sigma_1 - u_b$ $\bar{\sigma}_3 = \sigma_3 - u_b$ (8.13)

Undrained $\bar{\sigma}_1 = \sigma_1 - u$ $\bar{\sigma}_3 = \sigma_3 - u$ (8.14)

Figure 8.33 illustrates typical Mohr's envelopes obtained from undrained, drained, and consolidated-undrained triaxial tests; the envelopes are constructed from the principal stresses at failure. The failure envelope corresponding to the drained test, called the effective failure envelope, may be determined from Equations 8.13 and 8.14 depending on the drainage condition of the test. Regardless of the type of the test performed, there exists an effective failure envelope unique to the soil being tested.

The effective-stress failure envelope is written as:

$$s = \bar{c} + \bar{\sigma} \tan \phi \tag{8.15}$$

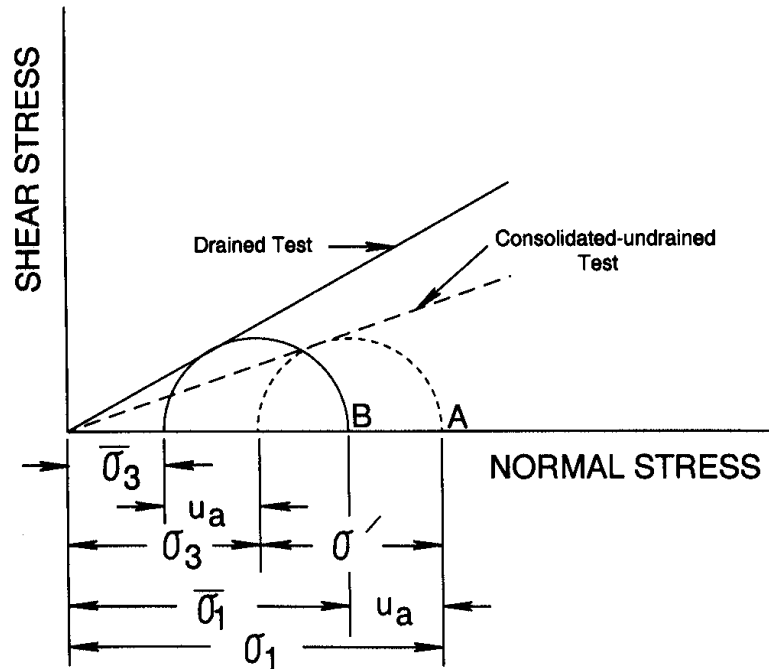


Figure 8.33 – Effective-stress and total-stress envelopes.

Example 8.2

A consolidated-undrained triaxial test was performed on a specimen of saturated clay. The value of the hydrostatic pressure (σ_3) was 200 kPa. The specimen failed when σ' was 280 kPa, $u = 180$ kPa. If the failure plane in this test makes an angle of 57° with the horizontal, calculate the normal and shear stresses on the failure surface.

Solution

The principal stresses at failure are calculated as:

$$\sigma_3 = 200 \text{ kPa} \quad \sigma_1 - \sigma_3 = 280 \text{ kPa} \quad \sigma_1 = 280 + 200 = 480 \text{ kPa}$$

On the 57° plane the normal and the shear stresses are calculated as follows:

$$\sigma = \frac{\sigma_1 + \sigma_3}{2} - \frac{\sigma_1 - \sigma_3}{2} \cos 2\theta = \frac{480 + 200}{2} - \frac{480 - 200}{2} \cos 114 = 283 \text{ kPa}$$

$$\tau = \frac{\sigma_1 - \sigma_3}{2} \sin 2\theta = \frac{480 - 200}{2} \sin 114 = 127 \text{ kPa}$$

The effective normal stress on the failure plane was:

$$\bar{\sigma} = \sigma - u = 283 - 180 = 103 \text{ kPa}$$

Example 8.3

If the value of cohesion for the sample in the above example was 80 kPa and the angle of internal friction was 24° , show why failure occurred on the plane $\theta = 57^\circ$ instead of the plane of maximum shear stress. What was the maximum shear stress within the sample?

Solution

The effective normal stress on the failure plane is 103 kPa. The corresponding shear strength on this plane is computed as:

$$s = c + \bar{\sigma} \tan \phi = 80 + 103 \tan 24 = 127 \text{ kPa}$$

The shear strength is equal to the shear stress on this plane and consequently failure occurs. The maximum shear stress occurs at a 45° plane and the normal effective stress on this plane is computed as:

$$\sigma = \frac{480 + 200}{2} + \frac{480 - 200}{2} \cos 2(45) = 340 \text{ kPa}$$

$$\bar{\sigma} = 340 - 180 = 160 \text{ kPa}$$

$$s = 80 + 160 \tan 24 = 151 \text{ kPa}$$

The maximum shear stress occurs on a plane oriented at 45° from the horizontal:

$$\tau_{\max} = \frac{\sigma_1 - \sigma_3}{2} = 140 \text{ kPa}$$

Failure does not occur at 45° plane because the strength is higher than the stress.

Shear strength of cohesionless soils. Sand and silt are cohesionless soils. Figure 8.34 shows a typical failure envelope of a cohesionless soil. The envelope passes through the origin. Thus, only one Mohr's circle is needed to establish the failure envelope. The following equations are used to determine the drained (effective) failure envelope for cohesionless soils.

$$s_{cu} = \sigma \tan \phi_{cu} \quad (8.16)$$

and

$$s = \bar{\sigma} \tan \bar{\phi} = (\sigma - u) \tan \bar{\phi} \quad (8.17)$$

The value of $\bar{\phi}$ for cohesionless soils ranges from about 28 to 42° . Generally, the value of $\bar{\phi}$ increases with increasing density. Extremely loose sands with an unstable structure may have a $\bar{\phi}$ as low as 10° .

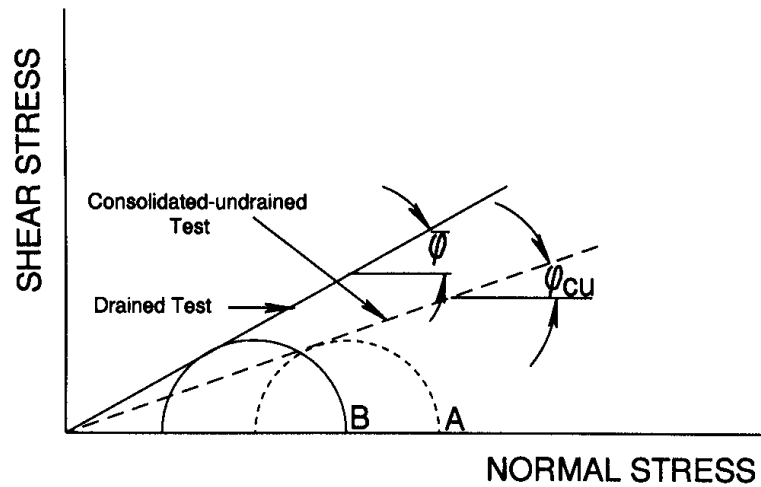


Figure 8.34 – Failure envelopes of cohesionless soils.

Field measurements of soil shear strength. The previously described direct shear and triaxial shear tests are laboratory procedures to measure the shear strength. Soil samples must be taken from the field to perform these tests. The samples may get disturbed and their shear strengths may be altered in the process. To avoid this, field methods to measure the shear strength have been developed. The first method is a round shear box which is rotated after it is inserted into the soil as shown in Figure 8.35. The box is driven into the soil until the top of the box is in contact with the soil surface. The soil is excavated carefully outside the box before applying the torque to shear the soil. The soil at the bottom of the box is sheared. The shear strength is calculated using the following equation:

$$s = \frac{3M}{2\pi r^3} \quad (8.18)$$

where s = soil shear strength
 M = moment at failure
 r = shear box radius

Markers are placed on the soil inside the box that are visible through small holes in the top of the box. The markers are used to ensure that the soil shears uniformly.

To overcome the problem that the soil located near the outer edge of the shear box must move considerably farther than that near the center, a narrow annulus has been designed as a shear box. Shear strength for the narrow annulus shaped box is calculated from the following equation:

$$s = \frac{3M}{2\pi (r_1^3 - r_2^3)} \quad (8.19)$$

where r_1 and r_2 are the inner and the outer radii of the annulus, respectively.

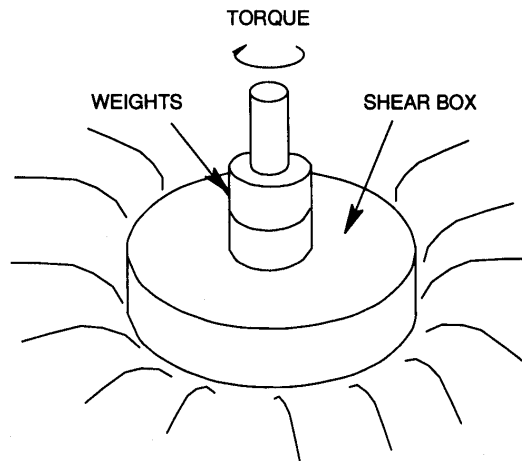


Figure 8.35 – A field soil shear apparatus.

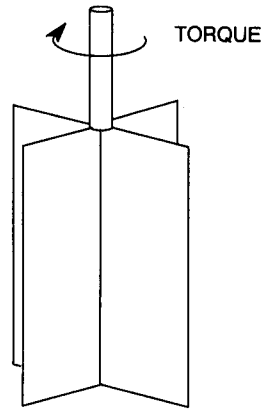


Figure 8.36 – A vane shear apparatus.

The field apparatus described above requires excavating the soil at the outside after inserting it into the ground. A vane type apparatus as shown in Figure 8.36 does not require excavation. Once driven into the soil the rotation causes shear of soil along the surface of the cylinder that is generated by the vanes. This device may be used at greater depths. Measurements can be made at increasing depths without extracting the shear device so that a rather complete strength profile of natural soil conditions can be obtained. The vanes have a height-to-radius ratio of 4:1. The vane shear apparatus provides no means of varying normal load. Shear strength is computed as:

$$s = \frac{3M}{28\pi r^3} \quad (8.20)$$

where r is the radius of the circle inscribed by vane tips.

8.2.3.3 Friction

There are three types of frictional parameters in problems involving soil dynamics. These are soil metal-friction (μ'), soil-soil friction (μ), and soil internal friction ($\tan \phi$). Soil internal friction has been discussed above in reference to soil shear strength. To determine soil-soil friction and soil-metal friction, we make use of Coulomb's concept of friction coefficient, or

$$\mu \text{ or } \mu' = \frac{F}{N} = \tan \psi \quad (8.21)$$

where F = frictional force tangent to the sliding surface

N = normal force to the sliding surface

ψ = friction angle

An apparatus to measure soil-metal friction is shown in Figure 8.37. Frictional force corresponding to different normal loads are measured and plotted against the normal loads. The slope of the line is the coefficient of friction. It must be pointed out that there is a difference between the soil-soil friction and the internal friction angle. In soil-soil friction phenomenon, the soil moves as a rigid body against another soil surface. The internal friction of soil comes into play when soil fails under shear load-

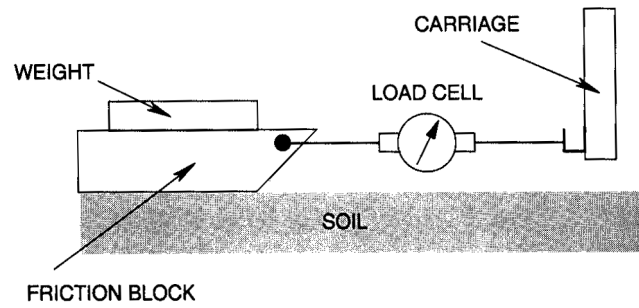


Figure 8.37 – Measuring soil-metal friction.

ing. Therefore, if we continue to apply shearing load in a shear test after failure then we will measure soil-soil frictional behavior.

8.2.3.4 Adhesion

Adhesion is defined as the force of attraction between two unlike bodies. In soil, adhesion is due to the film of moisture between soil particles and the surface contacting the soil. The force of adhesion is due to the surface tension of water and consequently it depends upon the value of surface tension and moisture content of the soil. However, it is virtually impossible to differentiate between friction and adhesion. Thus, an apparent coefficient of friction is often used to include effects of both friction and adhesion. Figure 8.38 shows the effect of moisture content on the apparent coefficient of friction. It can be seen that initially at low moisture content the friction is due to pure sliding action. As the moisture content increases, friction increases due to increased adhesion. As the moisture content is increased even further the friction reduces due to the lubricating effect created by the moisture film. The following model has been proposed to include adhesion:

$$F = a C_{\alpha} + N \tan \psi \quad (8.22)$$

where C_{α} = adhesion and a = surface area.

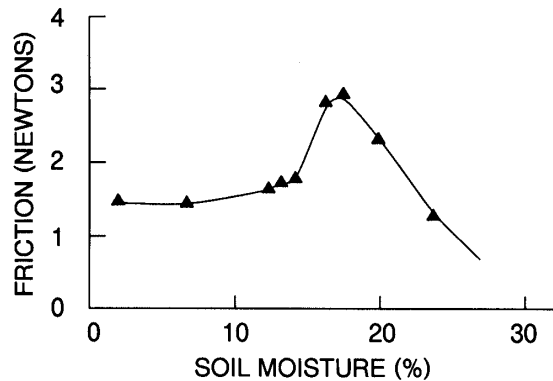


Figure 8.38 – Effect of soil moisture content on apparent coefficient of friction (Gill and Vandenberg, 1968).

8.2.4 Mechanics of a simple tillage tool

A discussion of soil-tool interaction as the tool travels through the soil is presented here. Consider a tillage tool in the shape of an inclined blade traveling through soil as shown in Figure 8.39. As the tool moves forward, the soil in front of the tool undergoes loading similar to that of an unconfined compression test. As the tool continues to move forward the loading increases until the soil fails in shear. Successive shear planes are formed and the soil mass between the shear planes travels along the surface of the tillage tool. W. Soehne (1956) analyzed the forces acting on the tillage tool and the soil to develop an expression for the total draft force needed to overcome the various soil reactions. Gill and Vandenberg (1968) have presented the work by Soehne.

Soehne (1956) concluded that soil-metal friction, shear failure, acceleration force for each block of soil, and cutting resistance act on the tillage tool as it moves through the soil. Figure 8.40a shows a free body diagram of a segment of soil as it reacts to the advancing tool. Forces CA_1 and μF_1 are due to soil shear and are those present at the instant incipient shear failure occurs. Forces due to soil-metal friction ($\mu'F_o$) and acceleration (B) are also present. The soil cutting resistance, defined as the cutting force per unit length of the cutting edge, is given by k . The forces acting on the tillage tool are shown in Figure 8.40b. These forces are soil cutting resistance (kb) obtained by multiplying the unit cutting resistance (k) by the cutting width (b); soil normal reaction (F_o); soil frictional reaction ($\mu'F_o$); and the tool support forces (V) and draft (D).

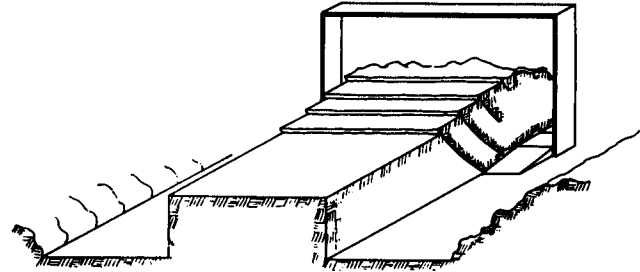


Figure 8.39 – An inclined plane tillage tool (Soehne, 1956, cited in Gill and Vandenberg, 1968).

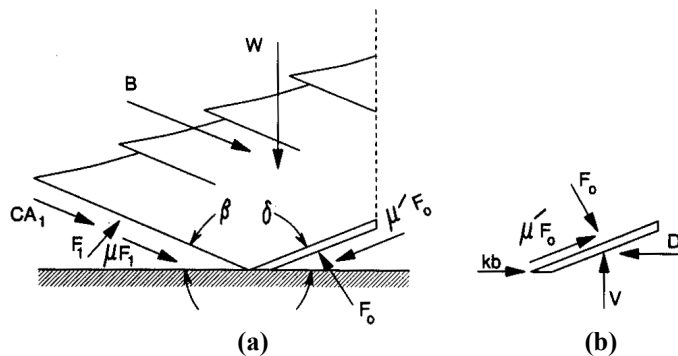


Figure 8.40 – Soil and tool reaction forces (Soehne, 1956, cited in Gill and Vandenberg, 1968).

Summing forces in the horizontal direction and equating them to zero the following equation is obtained:

$$D = F_o \sin \delta + \mu' F_o \cos \delta + kb \quad (8.23)$$

where D = horizontal draft force

F_o = normal load on the inclined plane

δ = tool lift angle

μ' = coefficient of soil-metal friction

k = soil cutting resistance

The specific draft force (D^*) is defined as:

$$D^* = D - kb$$

$$\text{or} \quad D^* = F_o \sin \delta + F_o \mu' \cos \delta \quad (8.24)$$

Summing all the vertical components of forces acting on the soil mass and equating them to zero for equilibrium results in the following equation:

$$\begin{aligned} W - F_o (\cos \delta - \mu' \sin \delta) - F_1 (\cos \beta - \mu \sin \beta) \\ + (CA_1 + B) \sin \cos \beta = 0 \end{aligned} \quad (8.25)$$

where W = soil weight, N

μ = coefficient of internal soil friction, no units

F_1 = normal force on the forward failure surface, N

β = angle of the forward failure surface, rad

C = soil cohesion, Pa

A_1 = area of forward shear failure surface, m^2

B = soil acceleration force, N

The horizontal forces on the soil segment can be summed and placed in equilibrium from the relations shown in Figure 8.40 to give:

$$F_o (\sin \delta + \mu' \cos \delta) - F_1 (\sin \beta + \mu \cos \beta) - (CA_1 + B) \cos \beta = 0 \quad (8.26)$$

Equation 8.25 can be used to solve for F_o . Substituting F_o in Equation 8.26 to solve for F_1 we get:

$$F_1 = \frac{D - (CA_1 + B) \cos \beta}{\sin \beta + \mu \cos \beta} \quad (8.27)$$

Substituting for F_o and F_1 in Equation 8.25 gives:

$$W - \left(D^* \frac{\cos \delta - \mu' \sin \delta}{\sin \delta + \mu' \cos \delta} \right) - \left[D^* - (CA_1 + B) \cos \beta \right] \left(\frac{\cos \beta - \mu \sin \beta}{\sin \beta + \mu \cos \beta} \right) + (CA_1 + B) \sin \beta = 0$$

Expanding and rearranging terms gives:

$$D^* \left(\frac{\cos \delta - \mu' \sin \delta}{\sin \delta + \mu' \cos \delta} + \frac{\cos \beta - \mu \sin \beta}{\sin \beta + \mu \cos \beta} \right) = W + \frac{CA_1 - B}{\sin \beta + \mu \cos \beta}$$

and by letting the geometric factor, z , be:

$$z = \left(\frac{\cos \delta - \mu' \sin \delta}{\sin \delta + \mu' \cos \delta} + \frac{\cos \beta - \mu \sin \beta}{\sin \beta + \mu \cos \beta} \right)$$

then
$$D^* = \frac{W}{z} + \frac{CA_1 + B}{z(\sin \beta + \mu \cos \beta)} \quad (8.28)$$

Equation 8.28 relates the forces acting in the soil-tool system. The weight of soil may be calculated from the volume of the soil supported by the inclined tool. Figure 8.41 shows a trapezoidal area that may be assumed to be supported by the tool. The area of the trapezoid multiplied by the depth of the area (width of tool) and the density of the soil gives the weight. By using the relationships in Figure 8.41, the weight of soil is:

$$W = \gamma b d^* \left(L_0 + \frac{L_1 + L_2}{2} \right) \quad (8.29)$$

where γ = wet bulk density of soil, kg/m^3

b = tool width, m

$d^* = d \{[\sin(\delta + \beta)] / \sin \beta\}$, m

d = tool depth, m

$L_1 = d \{[\cos(\delta + \beta)] / \sin \beta\}$, m

$L_2 = d^* \tan \delta$, m

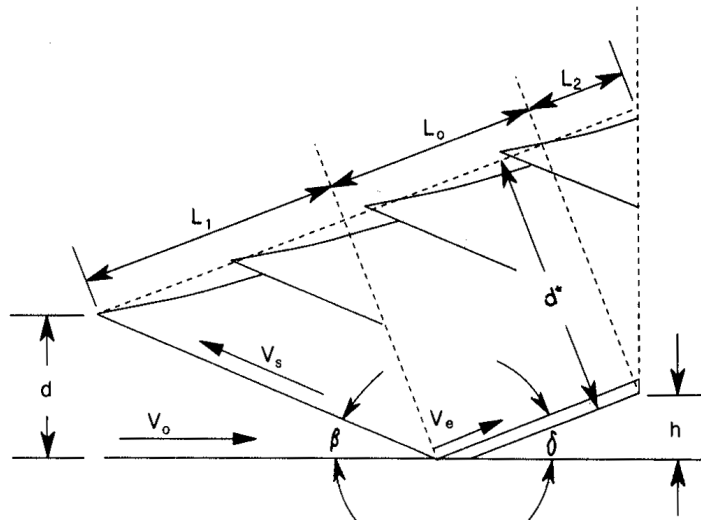


Figure 8.41 – Segment of soil on the inclined tillage plane tillage tool (Soehne, 1956, cited in Gill and Vandenberg, 1968).

The shear plane area, A_1 , can be determined easily from either Figure 8.40 or 8.41 and it is given by:

$$A_1 = \frac{bd}{\sin \beta} \quad (8.30)$$

The acceleration force, B , is the only item in Equation 8.27 that remains to be specified. Using Newton's Second Law of Motion:

$$B = m \frac{dv}{dt} \quad (8.31)$$

where m = accelerated soil mass, kg

v = soil velocity (uniform within the mass), m/s

t = time, s

The mass of the soil being accelerated or disturbed by the tool at time, t , is given by:

$$m = \frac{\gamma}{g} dbt_0 v_0 \quad (8.32)$$

where t_0 = average time a particle of soil is engaged by the tool, s

v_0 = tool velocity, m/s

g = acceleration due to gravity, m/s^2

After having developed an expression for the accelerated soil mass (m) in Equation 8.31, we must now develop an expression for the acceleration (dv/dt). Referring to Figure 8.41, v_s is the absolute velocity of the soil mass and v_e is the velocity of the soil mass relative to the tool. The direction of v_s is along the failure plane of the soil oriented at an angle β from the horizontal as shown in Figure 8.41. The relative velocity v_e is the sliding velocity along the surface of the tool oriented at an angle δ from the horizontal (Figure 8.41). The tool velocity (v_0) is directed horizontally as shown in the Figure. The three velocity vectors make a closed triangle as indicated by the following vector equation:

$$v_s = v_0 + v_e$$

Soehne assumed that:

$$\frac{dv}{dt} \approx \frac{\Delta v}{\Delta t} = \frac{v_s - 0}{t_0 - 0} = \frac{v_s}{t_0} \quad (8.33)$$

$v_0 = 0$ since the soil was initially at rest at time $t = 0$. In addition, since the velocity vectors (v_0 , v_s , and v_e) form a closed triangle, we can write the following relationship:

$$v_0 = v_s \cos \beta + v_e \cos \delta$$

and

$$v_s \sin \beta = v_e \sin \delta$$

so that v_e can be eliminated to give:

$$v_e = v_o \frac{\sin \delta}{\sin(\delta + \beta)} \quad (8.34)$$

Substituting Equations 8.32, 8.33, and 8.34 into 8.31 and simplifying gives:

$$B = \frac{\gamma}{g} b d v_o^2 \frac{\sin \delta}{\sin(\delta + \beta)} \quad (8.35)$$

Equations 8.28, 8.30, and 8.35 may be substituted into Equation 8.28 to provide a single equation in which parameters of the tool, soil, and mode of operation are related to the horizontal force to move the tool forward. Soil friction may be calculated from:

$$\mu = \tan \phi$$

where ϕ is the angle of internal friction. The angle β can be evaluated from the equation (see Figure 8.31):

$$\beta = (90^\circ - \phi)/2$$

Vertical forces on the tool can be placed in equilibrium to provide a relation similar to Equation 8.23. Equations 8.25 and 8.26 again can be used to calculate an equation similar to Equation 8.28. Equation 8.28 and its implied vertical counterpart thus constitute a simple mechanics for inclined tools. Soehne (1956) attempted to verify Equation 8.28 experimentally. He used an inclined tool supported in the center. Figure 8.42 compares the measured and the calculated values.

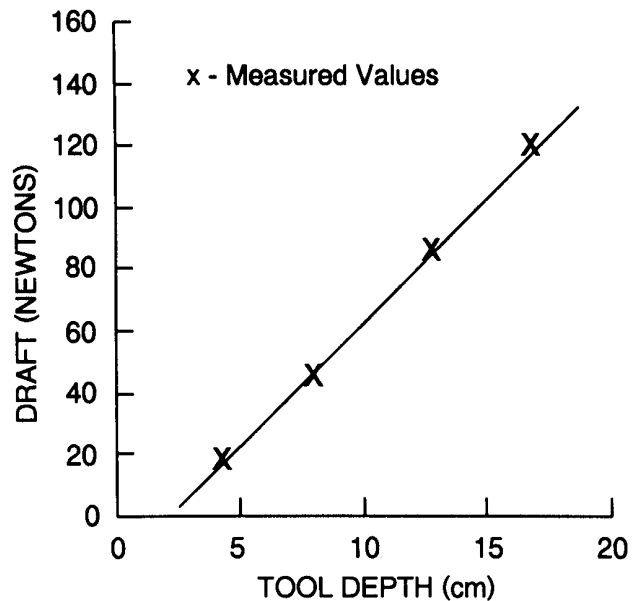


Figure 8.42 – Predicted and measured draft forces on a simple tillage tool in a sandy soil (Soehne, 1956, cited in Gill and Vandenberg, 1968).

There is a general agreement between the measured and predicted data indicating that the mechanics is sound. However, several factors may have contributed to the prediction error. Edge and supporting standard effects were present for the tool, but not for the mathematical model. Experimental determination of the dynamic soil parameters may have been in error. The shear failure may be a progressive failure rather than a simultaneous failing of the entire surface. Refinement in any one of these limiting factors will greatly improve prediction accuracy.

Example 8.4

An inclined blade tillage tool 25 cm wide and 10 cm long is operating at 25 cm depth in cohesionless soil with density equal to 1.2 g/cm^3 , and the angle of internal friction of 37° . The tool speed is 5 km/h and the soil metal friction is to be taken as 0.3. Assuming a negligible cutting resistance, determine the horizontal force acting on the tillage tool.

Solution

The following parameters are given by the problem statement:

$$\begin{array}{llll} \delta = 45^\circ & d = 25 \text{ cm} & \phi = 37^\circ & b = 25 \text{ cm} \\ L_o = 10 \text{ cm} & \mu' = 0.3 & \rho = 1200 \text{ kg/m}^3 & v_o = 1.389 \text{ m/s} \end{array}$$

Using Equation 8.34 the acceleration force can be computed. Note that $\rho = \gamma/g$ and $\beta = 1/2(90 - \phi) = 26.5^\circ$. Substituting these values in the equation we get:

$$B = 1200 \left(\frac{25}{100} \right) \left(\frac{25}{100} \right) (1.389)^2 \frac{\sin 45}{\sin(45 + 26.5)} = 108 \text{ N}$$

The area of shear plane, A_1 , ahead of the tool is calculated from Equation 8.30 as:

$$A_1 = \frac{(25)^2}{(100)^2 \sin 26.5} = 0.14 \text{ m}^2$$

The soil weight is calculated next from Equation 8.29 as follows:

$$d^* = \frac{25}{100} \frac{\sin(45 + 26.5)}{\sin(26.5)} = 0.53 \text{ m}$$

$$L_1 = \frac{25}{100} \frac{\cos(45 + 26.5)}{\sin(26.5)} = 0.178 \text{ m}$$

$$L_2 = 0.53 \tan(45) = 0.53 \text{ m}$$

$$W = 9.81(1200) \frac{25}{100} 0.53 \left(0.10 + \frac{0.178 + 0.53}{2} \right) = 710 \text{ N}$$

The geometric factor (z) is calculated as follows:

$$z = \left(\frac{\cos 45 - \mu' \sin 45}{\sin 45 + \mu' \cos 45} + \frac{\cos 26.5 - \mu \sin 26.5}{\sin 26.5 + \mu \cos 26.5} \right) = 1.037$$

Finally, the draft force (D^*) is calculated from Equation 8.28 as follows:

$$D^* = \frac{710}{1.037} + \frac{108}{10.62(\sin 26.5 + 0.75 \cos 26.5)} = 778\text{N}$$

Rowe and Barnes (1961) attempted to overcome some of the inherent limitations in the soil mechanics model. They used the physical arrangement shown in Figure 8.39 to eliminate the influence of extraneous forces along the sides of the soil block and the standard holding the tool. They also incorporated into the mechanics the influence of adhesion on the soil-metal sliding surface. The adhesion parameter (C_α) requires a change in the forces as shown in Figure 8.43. Incorporating the adhesion parameter changes Equation 8.28 to give:

$$D^* = \frac{W}{z} + \frac{CA_1 + B}{z(\sin \beta + \nu \cos \beta)} + \frac{C_\alpha + A_o}{z(\sin \delta + \mu' \cos \delta)} \quad (8.36)$$

where A_o = area of the inclined tool

C_α = soil-metal adhesion

Rowe and Barnes (1961) were primarily concerned with the influence of speed on the magnitude of the soil shear parameters, which would, in turn, influence the draft. Consequently, they measured the soil shear parameters at various speeds and assumed that the soil sheared at velocity (v_s) that can be calculated by Equation 8.34. The results of performing shear tests at different speeds are given in Table 8.2. The results of their measurements and calculations are shown in Figure 8.44. A reasonable agreement was obtained between calculated and measured values.

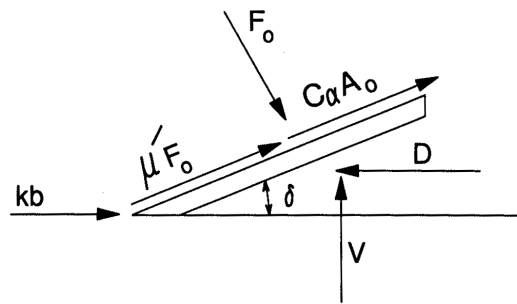


Figure 8.43 – A free body diagram of the tillage tool showing soil adhesion force (Rowe and Barnes, 1961, cited in Gill and Vandenberg, 1968).

Table 8.2. Soil shear strengths of various soils at different shear rates (Rowe and Barnes, 1961, cited in Gill and Vandenberg, 1966).

Rate of shear (in/sec)	Sand (psi)	Ida soil (psi)	Colo soil (psi)	Luton soil (psi)
0.76	1.15	1.67		3.14
8.27	1.27	1.96	2.72	3.69
15.76	1.45	2.31	3.28	4.39
22.95	1.46	2.24	3.28	
26.97			3.33	

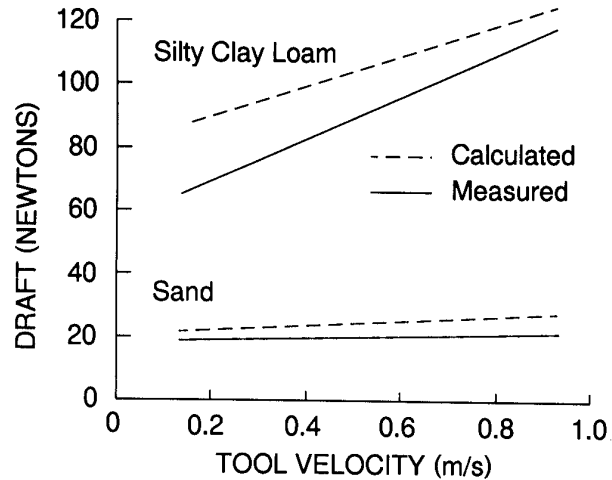


Figure 8.44 – Measured and calculated draft of an inclined tillage tool at various tool velocities (Rowe and Barnes, 1961, cited in Gill and Vandenberg, 1968).

8.3 PERFORMANCE OF TILLAGE IMPLEMENTS

The performance of tillage tools is determined by their draft and power requirements and the quality of work. The definition of quality of work depends upon the type of tillage tool. For a plow it is the degree of soil inversion and pulverization while for a harrow it is the level of clod break-up. However, no universally accepted method has been developed to quantify the quality of work. Therefore, in this section only the draft force acting on the tillage tools and their power requirements are presented. The effects of soil and tool parameters as well as the operating conditions on the draft force and power requirements are discussed.

8.3.1 Moldboard plows

The draft is defined as the component of tractor pull acting on the plow parallel to the line of travel. The specific draft is the draft divided by the cross-sectional area of

the furrow. Soil type and condition are by far the most important factors contributing to variations in specific draft. Values of specific draft range from 1.4 to 2 N/cm² (2 to 3 lb f/in.²) for sandy soils and up to 10 to 14 N/cm² (15 to 20 lb f/in.²) for heavy gumbo soils. Sandy or silt loams may have specific drafts from 2 to 5 N/cm² (3 to 7 lb f/in.²), whereas 4 to 8 N/cm² (6 to 12 lb f/in.²) would be typical for clay loams and heavy clay soils.

Soil moisture content is an important factor in regard to both draft and quality of work. A dry soil requires excessive power and also accelerates wear of the cutting edges. An increase of moisture content from 9.1% to 11.7% may reduce the specific draft in a fine sandy loam by 15% to 35%. Other pertinent soil factors include the degree of compaction and the type or absence of cover crop. The draft may increase 15% to 35% when the apparent specific gravity of a fine sandy loam changes from 1.68 to 1.83.

Most available evidence indicates that the specific draft of a plow generally decreases as the depth is increased to some optimum depth/width ratio and then increases as the depth is increased further. It has been reported that the minimum specific draft for a number of 36 cm (14 in.) bottoms was at depths of 13 to 18 cm (5 to 7 in.). It has been found that the specific draft was increased as the width of cut was reduced below 26 cm. Results from several sources indicate that the draft of a rolling coulter may be 10% to 17% of the total for the plow-coulter combination. Comparative tests in loam soils indicate about 5% to 7% reduction in draft by taking most of the side thrust on the rear furrow wheel rather than all on the landside.

McKibben and Reed (1952) consolidated the many speed-versus-draft test results. They plotted the percent increase in draft as a function of speed, taking the draft at 4.83 km/h (3 mph) as 100% in each case. This data includes several runs with mold-board plows, mostly at speeds from 1.6 to 13 km/h (1 to 8 mph). The data for mold-board plows can be represented reasonably well by the relation:

$$\frac{D_s}{D_r} = 0.83 + 0.00730S^2 \quad (8.37)$$

where D_r = draft at the reference speed, 4.83 km/h

D_s = draft at speed S , in same units as D_r

S = speed, km/h

Hendrick (CRC, 1988) gave the following equations for the specific draft (in N/cm²; S = speed in km/h) for different soil types:

Silty Clay (South Texas)	Specific draft = $7 + 0.049 S^2$
Decatur Clay Loam	Specific draft = $6 + 0.053 S^2$
Silt Clay (N. Illinois)	Specific draft = $4.8 + 0.024 S^2$
Davidson Loam	Specific draft = $3 + 0.020 S^2$
Sandy Silt	Specific draft = $3 + 0.032 S^2$
Sandy Loam	Specific draft = $2.8 + 0.013 S^2$
Sand	Specific draft = $2 + 0.013 S^2$

Once the specific draft is determined, the value of total draft can be calculated by multiplying the specific draft by the total cross-sectional area of the plow. The power requirement can then be determined by multiplying the total draft by implement speed.

8.3.2 Disk implements

The performance of disk implements is measured in terms of draft, specific draft, power requirements, and depth. Unlike moldboard plows, the depth of penetration of disk implements is determined by the implement weight and soil condition. Thus, the ability to maintain a uniform desired depth becomes an important performance criterion.

Disk plows. Hendrick (CRC, 1988) developed equations for the specific draft of a furrow slice for a 66 cm disk, 22° tilt and 45° disk angles. Specific draft (in N/cm^2 ; S = speed in km/h) is given by the following equations:

$$\text{Decatur Clay} \quad \text{Specific draft} = 5.2 + 0.039 S^2$$

$$\text{Davidson Loam} \quad \text{Specific draft} = 2.4 + 0.045 S^2$$

Disk harrows. For disk harrows the draft (in N) is a function of mass M (in kg) for any speed as follows:

$$\text{Clay} \quad \text{Draft} = 14.7 M$$

$$\text{Silt Loam} \quad \text{Draft} = 11.7 M$$

$$\text{Sandy Loam} \quad \text{Draft} = 7.8 M$$

The typical weight for disk harrows ranges from 160 to 210 kg/m of width for mounted tandem type with 41 to 51 cm diameter disks. The mass for wheel type is 240 to 510 kg/m with 41 to 66 cm diameter disks. For offset pull-type harrows with wheels the mass is 390 to 890 kg/m with 56 to 81 cm diameter disks. The numbers also apply for harrows with no wheels and 61 to 81 cm disks.

Disk tillers. Sommer et al. (1983) summarized results of a five-year study for a primary tillage disk with a 610 mm diameter blade and masses from 55 to 120 kg per blade. The tests focused on the effects of gang angle, mass per blade, blade type, blade spacing, and speed on the performance parameters such as concave specific draft, depth, and draft. Concave specific draft is calculated by dividing the total draft by the concave pressure area. The concave and the projected areas are given in Figure 8.45.

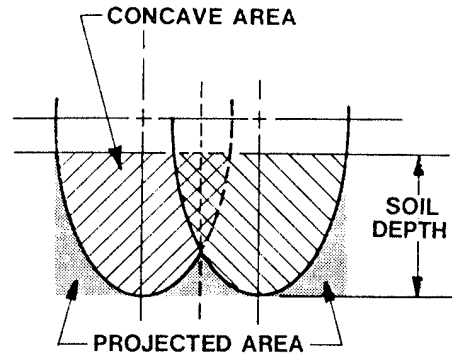


Figure 8.45 – Concave and projected pressure areas (Sommer et al., 1983).

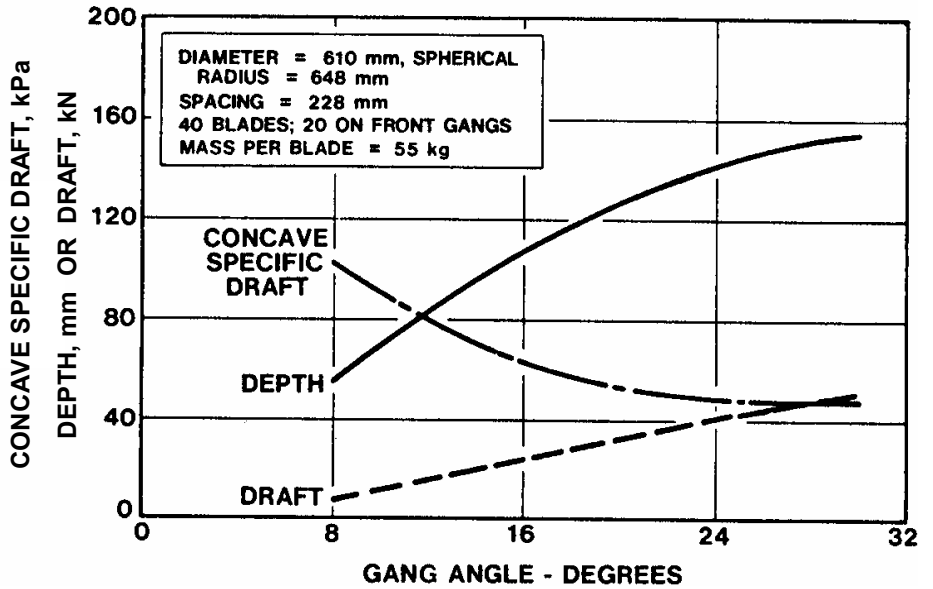


Figure 8.46 – Effect of gang angle on disk performance (Sommer et al., 1983).

They developed prediction equations using a base disk with 610 mm blade diameter and a 648 mm spherical radius. The disk spacing was 228 mm with 55 kg per disk. There were a total of 40 blades on the tandem double offset disk implement. Figure 8.46 shows the effect of gang angle. The draft and the depth increased with an increase in the gang angle but the concave specific draft reduced. The following prediction equations were developed:

$$\text{Depth (mm)} = -0.15 (\alpha^2 - 67.3\alpha + 104) \quad (8.38)$$

$$\text{Draft (kN)} = -0.013 (\alpha^2 - 181\alpha + 808) \quad (8.39)$$

where α = gang angle, degrees.

Figure 8.47 shows the effect of mass per blade for a gang angle of 18° . As the mass per blade increases, concave specific draft, depth, and draft increase. The increase in the concave specific draft indicates that the draft increases faster than the tilled area. The following equations were developed:

$$18^\circ \text{ gang angle: } \text{Depth (mm)} = K_d (-4.93\beta - 509) \quad (8.40)$$

$$\text{Draft (kN)} = K_f (-39.2\beta + 42) \quad (8.41)$$

$$22^\circ \text{ gang angle: } \text{Depth (mm)} = K_d (-2.9\beta - 733) \quad (8.42)$$

$$\text{Draft (kN)} = K_f (-36.2\beta + 700) \quad (8.43)$$

where β = mass per blade, kg. The values of K_d and K_f have been found to be -0.15 and -0.013 , respectively.

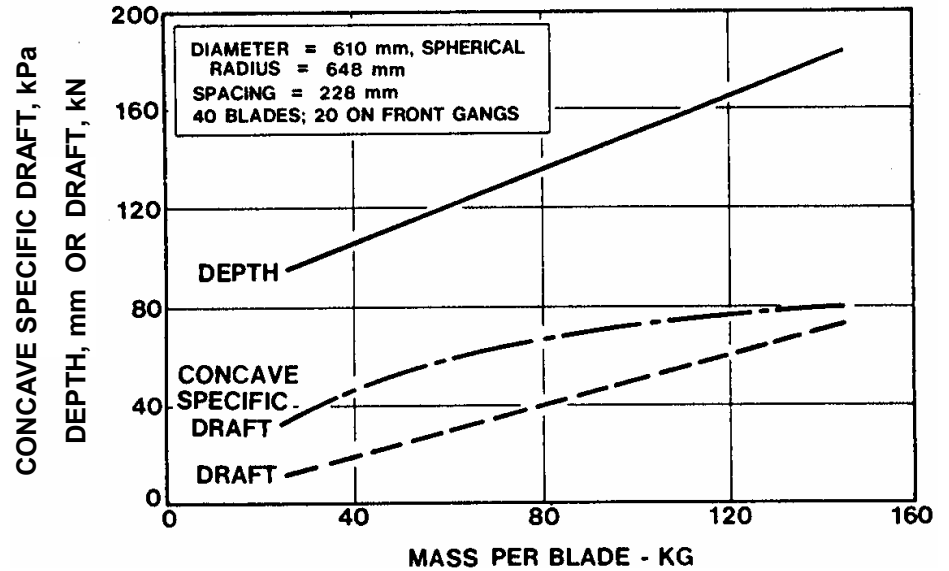


Figure 8.47 – Effect of mass per blade on disk performance (Sommer et al., 1983).

8.3.3 Cultivators

Gullacher and Coates (1980) studied the effect of cultivator sweep pitch on tillage forces. They measured both the draft and suction forces. Suction is defined as the vertical force that the soil exerts on the sweep. Figure 8.48 shows three typical shank assemblies used for mounting cultivator sweeps. The angle that the bottom of the sweep makes with the horizontal is known as the sweep pitch. A positive pitch angle is defined when the sweep tip is lower than its heel. During tillage, soil forces on the sweep causes the pitch to increase as shown in Figure 8.49. The increase in pitch at low to moderate forces is due to the flexing of the shank. But as the forces exceed spring preload, the shank begins to rotate upward and the pitch angle increases more rapidly.

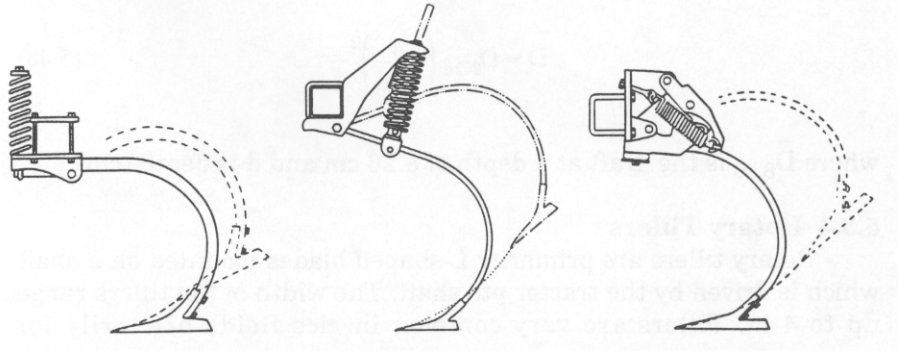


Figure 8.48 – Typical shank assemblies (Gullacher and Coates, 1980).

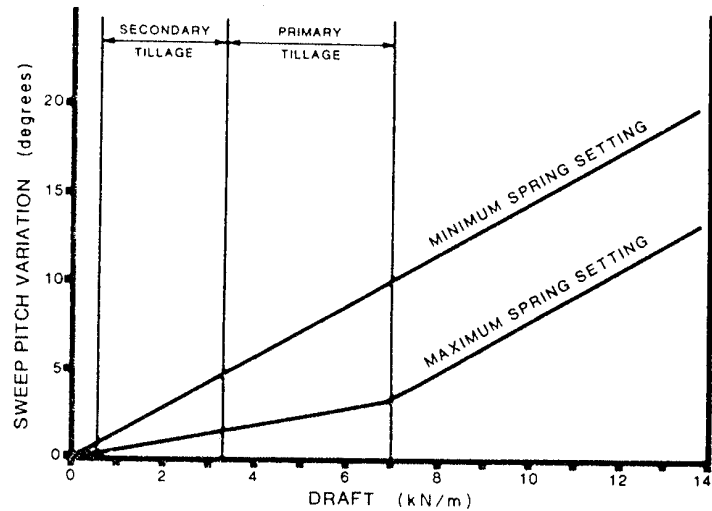


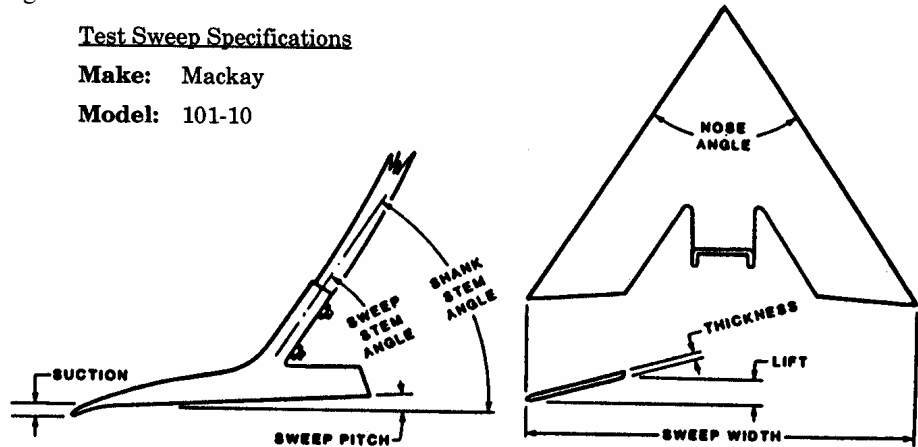
Figure 8.49 – Variation in sweep pitch over a range of normal tillage forces for one shank assembly (Gullacher and Coates, 1980).

Figure 8.50 shows the geometry and dimension of the sweep used in their study. They found that during the primary tillage operation, the draft per unit width increased 31% from 1.7 kN/m at 2.5° pitch to 2.3 kN/m at 18.5°. These results were obtained at a depth of 40 mm and at a speed of 8 km/h. This represents an increase of about 2% per degree change in the pitch angle. In secondary tillage operation in Oxbow loam under similar operating conditions the draft increased from 0.8 kN/m to 1.7 kN/m, an increase of 106%. At 60 mm depth the increase was 78%. These data are shown in Figures 8.51 and 8.52.

Test Sweep Specifications

Make: Mackay

Model: 101-10



Dimensions: sweep width, 258 mm lift, 20 mm thickness, 4.9 mm
nose suction, 6 mm nose angle, 60.5° sweep stem angle, 48°

Figure 8.50 – Specifications of the test sweep (Gullacher and Coates, 1980).

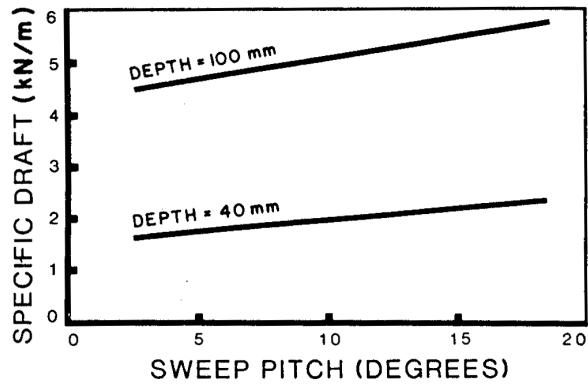


Figure 8.51 – Variation in specific draft with sweep pitch for primary tillage in Oxbow loam at 8 km/h (Gullacher and Coates, 1980).

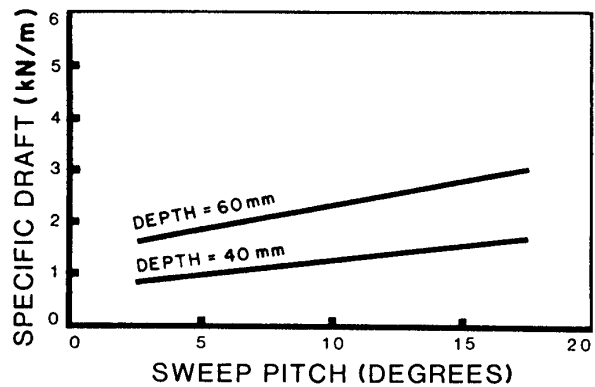


Figure 8.52 – Variation in specific draft with sweep pitch for secondary tillage in Oxbow loam at 8 km/h (Gullacher and Coates, 1980).

Hendrick (CRC, 1988) reported the draft for chisel plows and field cultivators in firm soil spaced at 30 cm apart and operating at a depth of 8.26 cm and traveling at 5.5 to 10.5 km/h as follows:

$$\begin{aligned}
 \text{Loam (Saskatchewan):} & \quad \text{Draft (N)} = 520 + 49.2 S \\
 \text{Clay Loam (Saskatchewan):} & \quad \text{Draft (N)} = 480 + 48.1 S \\
 \text{Clay (Saskatchewan):} & \quad \text{Draft (N)} = 527 + 36.1 S
 \end{aligned} \tag{8.44}$$

Draft at other depths is given by:

$$D_d = D_{8.26} \left(\frac{d}{8.26} \right)^2 \tag{8.45}$$

where $D_{8.26}$ is the draft at a depth of 8.26 cm and d is depth in cm.

8.3.4 Rotary tillers

Rotary tillers are primarily L-shaped blades mounted on a shaft which is driven by the tractor PTO shaft. The width of the tillers range up to 4 m. Tillers are very common in rice fields, primarily for puddling operation. Rotary tillers produce a high degree of soil pulverization but have high power requirements.

Figure 8.53 shows an L-shape blade for a conventional rotary tiller and the cutting path as followed by the blade. The rotor rotates in the same direction as the forward travel. The tillers make two to three cuts per revolution of the blade. The bite length is defined as the amount of forward travel per cut. The bite length is affected by the speed of rotation and the forward travel speed.

The rotor develops a forward and an upward soil reaction. The forward reaction generates a negative pull on the tractor while the upward pull reduces the implement weight. Under hard soil conditions the tiller may “walk” out of the ground due to excessive upward soil reaction. Both force reactions increase with operating depth. The forward reaction represents negative power requirements that is generally less than 7% of the PTO shaft power but can be as high as 20% depending on the bite length.

Increasing bite length reduces specific energy requirements. Specific energy is defined as the total energy required divided by the volume of soil disturbed by the tiller. Energy requirements are influenced by the ratio of the depth to the rotor diameter. As shown in Figure 8.54, even the lowest rotor specific energy is about three times higher than that for a moldboard plow in the same soil. However, a rotary tiller may produce the same degree of soil pulverization as obtained by one pass with a moldboard plow, two passes with a disk harrow, and one pass with a spike tooth harrow. These factors must be kept in mind while comparing rotary tillers with other tillage tools.

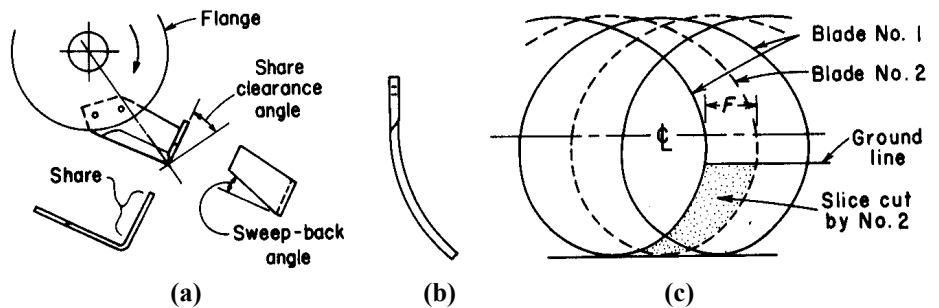


Figure 8.53 – (a) Three views of an L-shaped blade for a rotary tillage, (b) curved blade, (c) paths of cutting edges or tips for two blades 180° apart, in relation to forward speed (reprinted from Kepner et al., 1978).

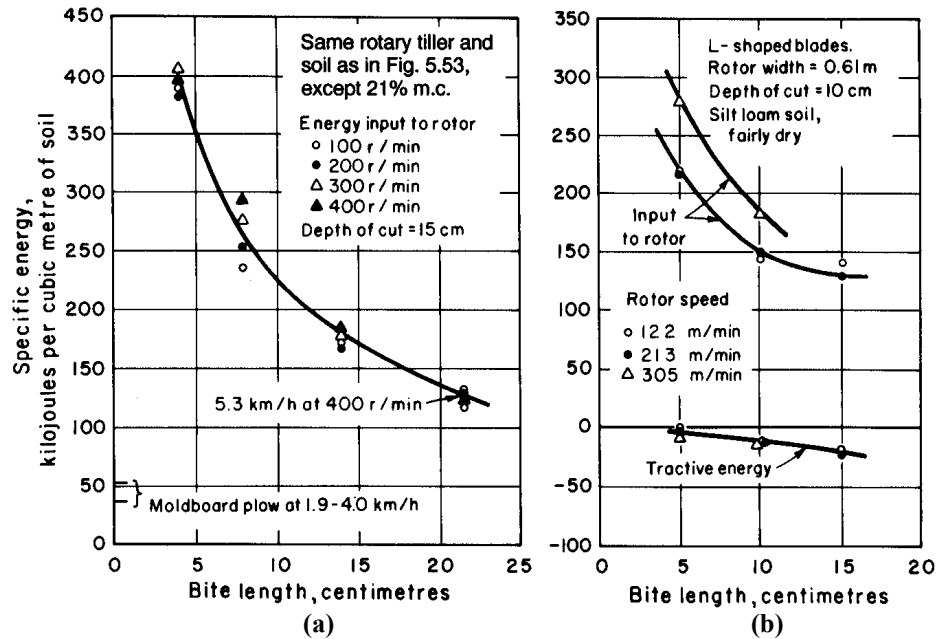


Figure 8.54 – Effect of bite length upon specific energy requirements for a conventional rotary tiller (reprinted from Kepner et al., 1978).

8.4 HITCHING OF TILLAGE IMPLEMENTS

The material presented in this section has been taken from Kepner (1978) and reorganized.

8.4.1 Forces on tillage tools

A tillage tool moving through the soil is subjected to the following forces:

- Implement weight,
- Soil reaction forces, and
- Forces exerted by the prime mover.

Implement weight determines the operating depth in case of the disk implements. Often weight is added to improve penetration in hard soils. The soil reaction forces are divided into *useful* and *parasitic* forces. Useful soil forces are those needed to cut, break up, and move soil. Parasitic forces are due to friction and rolling resistance and act on the stabilizing surfaces such as the landside and the furrow wheel. The useful forces are determined by soil condition and the parasitic forces are affected by tool design and adjustments. The resultant of forces exerted by the prime mover is the pull of the power unit upon the implement.

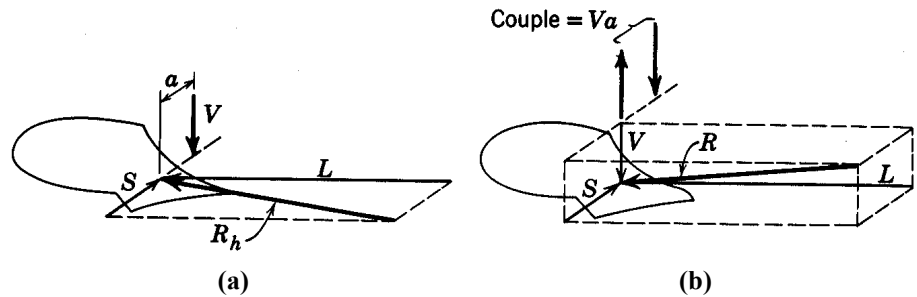


Figure 8.55 – Two ways of expressing the total soil reaction on a tillage tool when a rotational effect exists: (a) two non-intersecting forces, R_h and V , (b) one force R and a couple Va in a plane perpendicular to the line of motion (reprinted from Kepner et al., 1978).

When the tool is not symmetric, rotational effects are produced by the useful soil forces. There are several ways to represent these forces on a tillage tool. The method shown in Figure 8.55 consists of three mutually perpendicular force vectors and a moment. On tillage equipment with multiple soil engaging tools, resultants of forces acting on individual bottoms is computed. The resultant forces acting on the entire implement are used in hitching. The objective of proper hitching is to minimize parasitic forces and to obtain a stable operation.

The useful soil force components L , S , and V (or resultants R_h and R_v) and the implement gravitational force (W) are the independent force variables involved in analyzing either a simple drawbar hitch arrangement or an integral hitch system. The parasitic soil forces (Q) and the pull (P) are dependent variables that may be influenced by the hitch arrangement. The analysis procedures in this section assume that W and the components of the useful soil force are known or can be estimated. Another approach for determining the force relations between the implement and the tractor is to actually measure the magnitude and direction of the pull (or its components).

The following notations will be used while analyzing hitching of tillage implements:

- R = resultant of all useful forces acting on the plow
- L = longitudinal component of R
- S = lateral component of R
- V = vertical component of R
- Q = resultant of all parasitic forces acting on the plow
- P = resultant pull exerted by the tractor
- W = implement weight

Subscripts:

- h = horizontal component of a force
- v = vertical component of a force

8.4.1.1 Forces on a moldboard

Figure 8.56 shows a typical representation of the useful soil force component (R_h), parasitic force component (Q_h), and the horizontal component of the pull (P_x), as suggested by Clyde (1944). Force (R_h) consists of a lateral component (S) and a longitudinal component (L). Generally, the S/L ratios varies from 0.35 to 0.45 for sand (Randolph and Reed, 1938); 0.25 to 0.45 for sandy loams (Getzlaff, 1953; Nichols et al, 1958; Randolph and Reed, 1938); and 0.2 to 0.3 for clay loams (Cooper and McCreery, 1961); all with the coulter removed (Clyde, 1944). From these ratios the orientation of R_h can be determined. The component Q_h of the parasitic force consists of a landside reaction force equal to S but in the opposite direction and the frictional force that acts on the surface of the landside opposite to the direction of travel. The friction force is determined by multiplying the reaction force by the coefficient of soil metal friction. The soil metal friction determines the orientation of Q_h . Having established the parasitic and the useful force vectors, the magnitude of the draft force (P_x) along the line of pull may be determined by summing these force vectors. The point of convergence of the vectors is called the center of resistance and is located midway along the length of the landside and about one-third of the width from the landside shown as point H in the figure. As shown in Figure 8.56c, increasing the landside length moves the center of resistance towards the rear of the plow bottom. It should also be noted that H moves closer to the landside since the line of R_h does not change. Figure 8.56b shows the effect of an angled pull on the draft (P_x) and the parasitic force (Q_h). Because the line of pull is not the same as the direction of travel, the plow pulls harder against the furrow wall. This causes a larger reaction force (the lateral component of Q_h) and consequently a larger frictional force. The net result is an increase in the draft force.

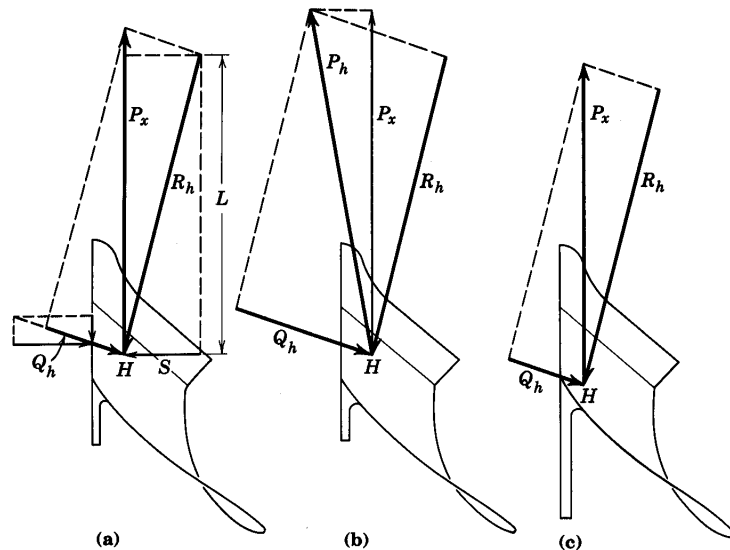


Figure 8.56 – Typical location of R_h and its relation to the landside force and pull: (a) straight pull, (b) angled pull, (c) long landside (reprinted from Kepner et al., 1978).

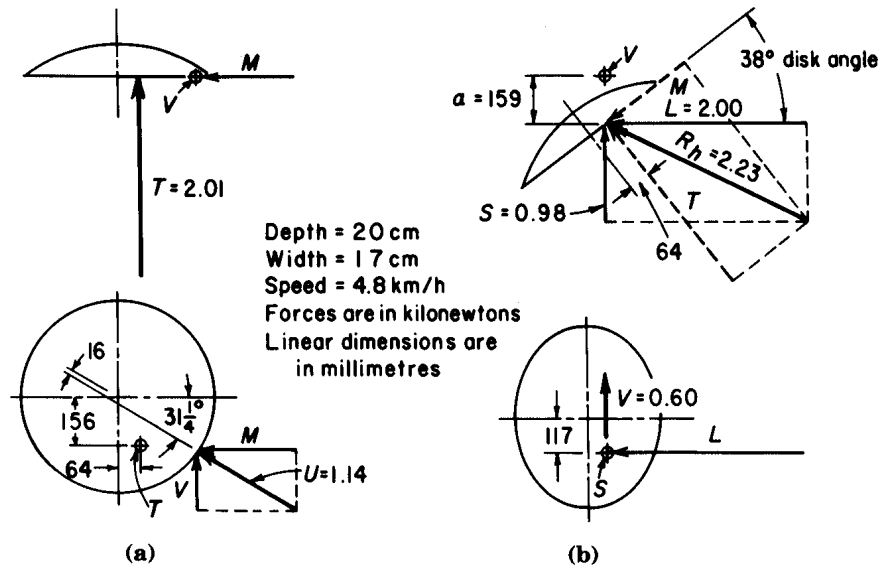


Figure 8.57 – Example of resultant soil forces acting upon a vertical disk blade. The total effect is represented by two non-intersecting forces: (a) a thrust force T and a radial force U , (b) a horizontal force V (reprinted from Kepner et al., 1978).

8.4.1.2 Forces on a disk blade

The net effect of all soil forces acting on a disk blade as a result of soil cutting, pulverizing, elevating, and inverting the furrow slice, plus any parasitic forces acting on the disk, can be expressed in many ways. In Figure 8.57a, the resultant effect is expressed by two non-intersecting forces, one being a thrust force (T) parallel to the disk axis, and the other being a radial force (U). This method is particularly advantageous in calculating loads on disk support bearings. The thrust force is always below the disk centerline because the soil acts against the lower part of the disk face. The radial force, which includes the vertical support force on the disk blade, must pass slightly to the rear of the disk centerline to provide the torque necessary to overcome the bearing friction and cause rotation of the disk.

The resultant effect can also be represented in terms of the longitudinal, lateral, and vertical components (L , S , and V), and resultants of these components as shown in Figure 8.57b. This representation is more useful when considering the soil forces on the whole implement. In Figure 8.57b, S and L are combined into R_h so that the entire effect is represented by two non-intersecting forces. Because the forces don't intersect, they constitute a couple Va that causes the disk to rotate.

8.4.1.3 Forces on a disk harrow

Figure 8.58b shows forces on an offset disk harrow without wheels when it is operating with no side draft. The location of the horizontal center of resistance H is determined by the intersection of R_{hr} and R_{hr} . For no side draft the hitch linkage of the disk harrow must be adjusted so the hitch point F_o is directly in front of H .

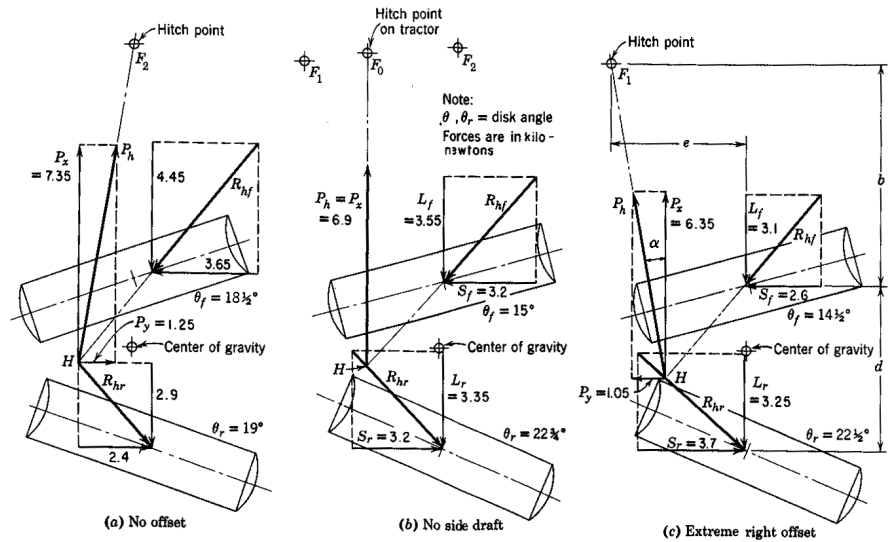


Figure 8.58 – Horizontal force relations for a pull-type, right-hand offset disk harrow without wheels (reprinted from Kepner et al., 1978).

If the hitch linkage is changed to move the implement either to the right or to the left from the no-side-draft position, side draft is introduced and the operating conditions of the harrow are changed. For example, if the hitch point in Figure 8.58a is moved from F_0 to F_2 , the force equilibrium is momentarily destroyed and the side component of the new pull, acting at point H, rotates the implement counterclockwise about F_2 . Rotation continues until the disk angle of the two gangs have readjusted themselves so that the difference between their lateral force components S_f and S_r become equal to the side draft P_y . Note that the magnitude of L_f and L_r and the position of H also change during this readjustment.

The force relations for a tandem disk harrow are symmetrical about the implement centerline because both front gangs are operating under the same soil condition (untilled), with the side components equal and opposite to each other, and both rear gangs are in tilled soil.

Amount of offset available. Let e be the amount of offset from the hitch point to the center of cut, α = the horizontal angle of pull, d = the longitudinal distance between the centers of the two gangs, and b = the longitudinal distance from the center of the front gang to the hitch point (Figure 8.58c). Taking moments about F_1 yields the following relationship assuming that the R_{hf} and R_{hr} pass through the centers of the gangs:

$$eL_f + eL_r + b S_f - (b + d) S_r = 0$$

from which:

$$e = \frac{b(S_r - S_f) + dS_f}{L_f + L_r} = b \tan \alpha + \frac{dS_r}{L_f + L_r} \tag{8.46}$$

For the condition of no side draft, $S_f = S_r = S$ and $\alpha = 0$. Then, from Equation 8.46, the offset with no side draft is:

$$e_o = \frac{dS}{L_f + L_r} \quad (8.47)$$

Equation 8.47 states that the amount of offset obtainable without side draft is a function only of the distance between gangs and of the relative magnitudes of the lateral and longitudinal soil reactions. The soil force relations, however, are affected by soil condition, disk angle, disk blade size and concavity, and other factors. S/L increases as the disk angle is increased and, according to Clyde (1944), is greater in firm soils than in soft soils.

Couples acting on disk harrow gangs. It is a well known fact that the concave end of a disk-harrow gang tends to penetrate more deeply than the convex end. This condition exists because the soil-force component (T), perpendicular to the disk blade, is applied well below the axle (Figure 8.59) while the balancing force (T') is applied at axle height, thus forming a couple (Tf).

With uniform penetration, V will act approximately at the center of the gang. To obtain uniform penetration with a single gang, the resultant downward force (W' minus the implement weight minus the upward component of pull) must act at a distance h from the center of the gang (toward the convex end) such that:

$$W' h = T f \quad (8.48)$$

It is a relatively simple matter with single-acting and tandem disk harrows to obtain uniform penetration by having the couples of the laterally opposed gangs counteract each other through the frame. The design problem is more complex in the case of an offset disk harrow because the opposing couples subject the frame between the gang to torsion. Adequate torsional stiffness and appropriate adjustments for lateral leveling of one gang with respect to the other are important.

It is a common practice in analyzing force relations for hitching tillage implements to give separate consideration to horizontal components of R , Q , and P , and to W and the components of these forces in a vertical plane (or planes) parallel to the line of motion. These considerations are referred to as horizontal hitching and vertical hitching. The following sections consider force relations involved in hitching pull-type and mounted implements.

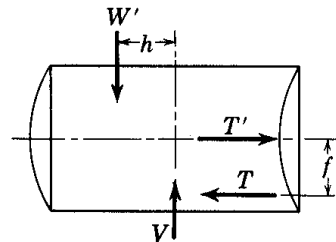


Figure 8.59 – Vertical and thrust forces acting upon a disk-harrow gang (reprinted from Kepner et al., 1978).

8.4.2 Pull-type implements

It is necessary to establish the locations and/or magnitudes of the resultant parasitic support force (Q_h or Q_v) and the pull (P_h or P_v) that are the most desirable from the standpoints of their effects on the pulling force upon the tractor and the magnitude and distribution of parasitic forces acting upon the implement.

8.4.2.1 Vertical hitching

Pull-type tillage implements generally fall into one of the following three categories in regard to vertical-hitching arrangements and the effects of hitching upon the force system:

1. Implements with hinged pull members that have support wheels or support runners to gage the depth. The pull member acts as a free link in the vertical plane. Examples are moldboard plows, disk plows, and drag-type spring-tooth harrows.
2. Implements with hinged pull members that do not have support wheels or runners. The only support is through the soil-working units, and parasitic forces cannot be separated from the useful soil forces. Examples are disk harrows without wheels, spike-tooth harrows, and tandem-gang rotary hoes.
3. Single-axle implements with rigid pull members. Examples are field cultivators and chisels, subsoilers, and disk harrows that have wheels for transport and depth gaging.

Force relations are shown in the following sections for one example of each type, and hitch adjustment recommendations are included for some other types. One must remember that in all the force analyses, the direction and magnitude of R_v may vary widely from those shown, even within one field.

Implements having hinged pull members and support wheels or runners. Figure 8.60 shows the vertical force relations for a pull-type moldboard plow. For uniform motion, W , R_v , and Q_v must be in equilibrium. Knowing the magnitudes and locations of the implement gravitational force W and the useful soil force R_v under the particular operating conditions involved, the first step in analyzing the hitch is to combine these forces graphically into the resultant AB .

The line of pull is established next. It must pass through the hitch point F on the tractor and the hitch hinge axis selected at E , since the pull member acts as a free link in the vertical plane. The line of pull and the resultant AB intersect at G . The line of action of the support force Q_v is now drawn through G , although its magnitude is not yet known. In Figure 8.60, Q_v is shown with some backward slant to include the rolling resistance of the wheels furnishing the vertical support. If the support were mostly on sliding surfaces, more slant would be needed to include the friction force. Since P_v must be in equilibrium with AB and Q_v , the magnitudes of Q_v and P_v can be determined by moving AB along its line of action to DG and then completing the force parallelogram as indicated.

The top example in Figure 8.60 represents a desirable hitch adjustment for a moldboard plow, with Q_v located well behind the front wheels so there is enough load on the rear wheel for stable operation. The lower example illustrates an extreme condition in which the hitch point E is so high on the plow that Q_v is about under the front

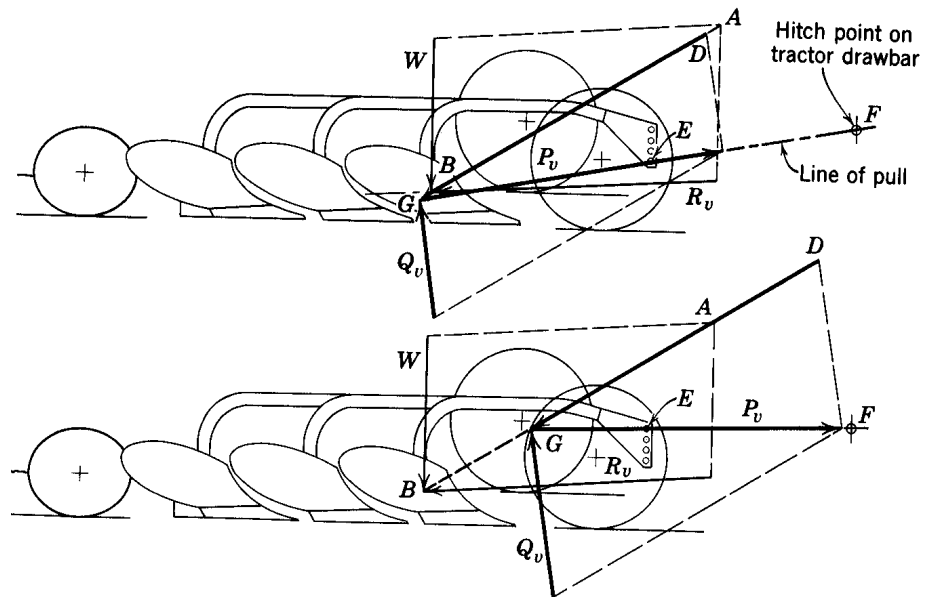


Figure 8.60 – Vertical force relation for a pull type implement having support wheels and a hinged pull member (reprinted from Kepner et al., 1978).

wheels, with practically no load being carried on the rear wheel. The rear of the plow will be very unstable, particularly when momentary variations in the direction and magnitude of R_v are considered.

Hitching at too low a point on the implement has the opposite effect. The resultant support force (Q_v) is moved toward the rear, thus reducing the load on the front wheels. Increasing or decreasing the slope of P_v without changing the location of G decreases or increases Q_v but does not change its location. Having too great a slope for P_v can cause difficulty in maintaining the desired depth, particularly with a relatively high implement that has little or no suction, such as a spring-tooth harrow.

Clyde (1944) recommended that for moldboard plows the preliminary adjustment of the hitch height on the plow frame be such that P_v passed through a point slightly below the ground surface and directly above the average location of all share points. For disk plows the suggested trial point for establishing the line of pull is at the ground surface midway between the centers of the front and rear disks. If the rear furrow wheel of a disk plow has the proper amount of lead toward the plowed ground and still tends to climb out of the furrow, the hitch point on the plow frame should be lowered, thus putting more of Q_v on the rear wheel.

Implements with hinged pull members but without support wheels or runners. Vertical force relations for an offset or tandem disk harrow without wheels are shown in Figure 8.61. The only support from the soil is through the disk blades. The position of point G is established by the intersection of W and the line of pull (P_v). The soil forces R_{vf} and R_{vr} automatically adjust themselves, by means of depth changes, so their resultant R_v passes through point G and is in equilibrium with W and P_v .

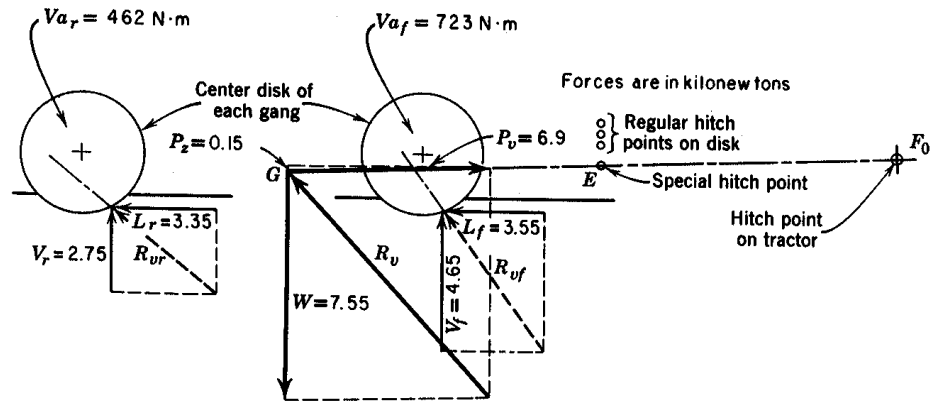


Figure 8.61 – Vertical force relation for a pull type offset or tandem disk harrow without wheels and no hinge axis between the front and the rear gangs (reprinted from Kepner et al., 1978).

Raising the hitch on the implement frame raises G and moves R_v closer to the front gang, thus increasing R_{vf} and decreasing R_{vr} . The result would be increased depth of penetration for the front gang and decreased depth for the rear gang. In the example shown, R_{vf} is greater than R_{vr} because the front gang is operating in firm soil and the rear gang is in loosened soil.

Single-axle implements with rigid pull members. When a single-axle implement receives vertical support only through its wheels, the location of Q_v is fixed. The line of Q_v must pass slightly behind the axle centerline (Figure 8.62) in order to supply torque to overcome wheel-bearing friction and cause rotation of the wheels. Point G is fixed by the intersection of AB and Q_v , and the line of pull is through G and the vertical hitch point F at the tractor drawbar. The only possible hitch adjustment is changing the height of the drawbar at F, which would change the slope of P_v . In the example shown, with R_v having a downward slope, moving the wheels rearward with respect to the soil-engaging tools would increase the slope of P_v and reduce the magnitude of Q_v .

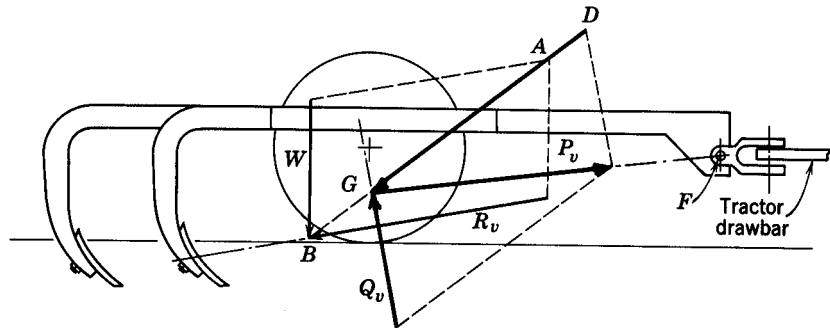


Figure 8.62 – Vertical force relations for a single-axle, pull-type implement receiving vertical support only through its wheels (reprinted from Kepner et al., 1978).

The force relations for a disk harrow having wheels to gage the depth would be basically the same as the relations shown in Figure 8.62, but R_v would have a steep upward slope as shown in Figure 8.61. The fore-and-aft location of R_v would be determined by the relative depths and soil resistances of the front and rear gangs. The relative depths would be related to the attitude of the frame, as established by the vertical adjustment of the rigid pull member.

8.4.2.2 Horizontal hitching

Most tillage implements, with the exceptions of moldboard plows, disk plows, and offset disk harrows, are symmetrical about their longitudinal centerline. The side components of the soil forces are balanced, the horizontal center of resistance is at the center of the tilled width, and the horizontal line of pull is in the direction of travel. In this section we will analyze all forces in a horizontal plane, thus the name “horizontal hitching.”

Plows and offset disk harrows can withstand substantial amounts of side draft (lateral component of pull), and proper hitching is necessary to minimize adverse effects on the tractor and the implement. Moldboard plows absorb side forces through the landsides, disk plows through the furrow wheels, and offset disk harrows by automatically changing the disk angles to create a difference between the soil-force side components for the front and rear gangs. Pull-type disk plows have essentially free-link pull members, whereas moldboard plows and disk harrows have laterally rigid pull members. Horizontal hitching for moldboard plows and disk plows is discussed in the following sections.

It is not always possible to have the horizontal center of resistance of an implement directly behind the center of pull of the tractor, particularly for narrow implements and wide-tread tractors. If the implement can withstand side forces, the alternatives are a *central angled pull*, in which the pull force passes through the geometric center of the implement at an angle, or an *offset angled pull*, in which the pull force is at an angle but does not pass through the geometric center, creating a rotational couple on the implement. If the implement cannot withstand side draft, the only alternative is an *offset straight pull* where the pull force is parallel to the line of travel but does not pass through the geometric center. The center of pull of the tractor is generally considered to be midway between the rear wheels and slightly ahead of the axle.

A central angled pull does not affect tractor steering, whereas the offset pulls do. An angled pull (either central or offset) introduces a side force on the tractor rear wheels that is sometimes of sufficient magnitude to be objectionable. An angled pull is undesirable with some implements, even though the implement can resist the side forces. Usually, some compromise in hitching is best, with part of the adverse effect being absorbed by the tractor and part by the implement. When the pull force is not parallel to the line of travel and/or does not pass through the geometric center of the implement, a torque is created which must be counterbalanced. This counterbalance torque or couple can be created by implement geometry or by the tractor via the hitching configuration.

Horizontal hitching of pull-type moldboard plows. The location of the horizontal center of resistance H for a moldboard plow bottom is determined by the point of

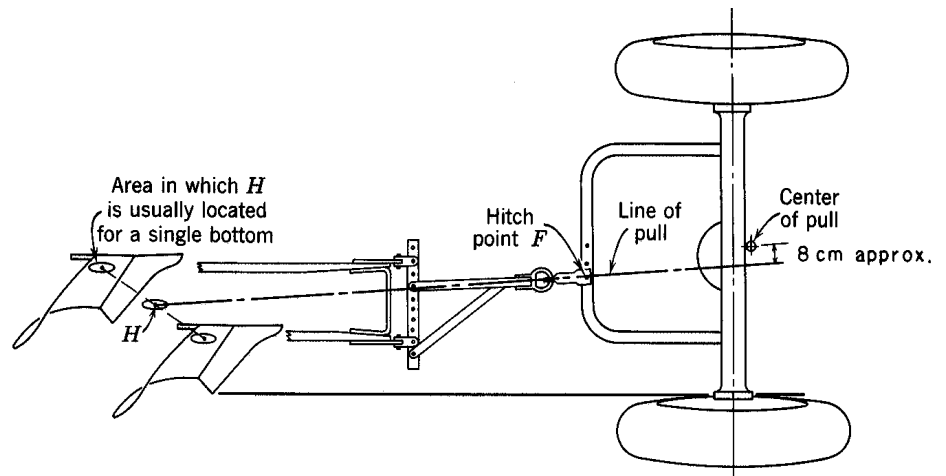


Figure 8.63 – Recommended horizontal hitching for a moldboard plow pulled by a wide tractor (reprinted from Kepner et al., 1978).

intersection of the parasitic force (Q_h) acting upon the landside and by R_h . The lateral location of H varies somewhat, depending upon soil conditions, length of landside, amount of side force taken by the rear furrow wheel, etc. For hitching purposes the location is often assumed to be about one-fourth of the width of cut over from the landside and a little behind the rear edge of the share. The line of pull is determined by the location of H and the location of the drawbar hitch point F (Figure 8.63) since the pull member is laterally rigid.

The ideal hitch is obtained when the tractor tread can be adjusted so the center of pull is directly ahead of the horizontal center of resistance. In some cases, however, a sufficiently narrow wheel tread cannot be obtained or is not practical, even with one rear wheel in the furrow. With large plows, the tractor is sometimes operated with both wheels on unplowed ground, primarily to reduce soil compaction from the wheel in the furrow. When a central straight pull cannot be obtained, it is common practice to divide the effects of the offset, as indicated in Figure 8.63, so that the line of pull passes a little to the right of the center of pull but not enough to cause steering troubles. Fortunately, a moldboard plow will operate satisfactorily even when the line of pull is at a considerable angle from the line of travel.

Horizontal hitching of pull-type disk plows. The horizontal force relations (Figure 8.64) are somewhat different for a disk plow than for a moldboard plow, because all the side thrust must be taken through the wheels and because the pull member on a disk plow (DF in Figure 8.64) is essentially a free link in regard to horizontal forces, whereas the horizontal line of pull on a moldboard plow must pass through the hitch point on the tractor and through a center of resistance established primarily by the plow and soil characteristics. The horizontal line of pull for a disk plow is determined by the location of hitch points D and F . The position of the horizontal center of resistance H and the location of the resultant side force Q_h and R_h are shown in Figure 8.64.

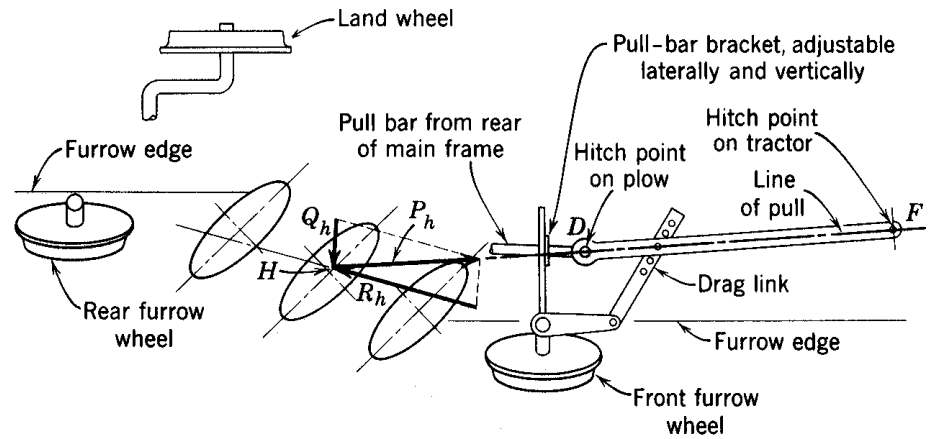


Figure 8.64 – Horizontal force relation and hitching for pull-type disk plow (reprinted from Kepner et al., 1978).

For the side force to be divided equally between the front and rear furrow wheels, the line of Q_h must pass midway between them. With most pull-type disk plows, this condition will be approximated if the hitch is adjusted so the line of pull passes through a point slightly to the left of the average position of all disk centers (thus establishing H in the desired location). If hitch point D in Figure 8.64 is moved to the left on the plow frame, H and Q_h will be moved toward the rear of the plow, and the rear furrow wheel will carry a greater proportion of the side thrust. Moving D to the right (or F to the left) puts more of the side thrust on the front wheel.

8.4.3 Mounted implements

Two types of hitch linkages, *free-link operation* and *restrained-link operation*, are common on modern tractors, regardless of the type of hitch. Practically all rear-mounted hitches are of the three-point, converging-link type. Parallel-link hitches are employed extensively for front-mounted cultivators. Single-axis hitches have been superseded by three-point hitches in new designs. Any of these three hitch types can be operated with the hitch members acting as free links in the vertical plane or with the implement supported through the lift mechanism of the tractor, i.e., as restrained links.

8.4.3.1 Free-link operation of three-point hitches

With free-link operation, depth is controlled by gage wheels or other supporting surfaces on the implement. Although depth control for mounted moldboard plows can be obtained through vertical support from the rear furrow wheel and the heel of the rear landside, gage wheels running on the unplowed ground are more common when free-link operation is desired.

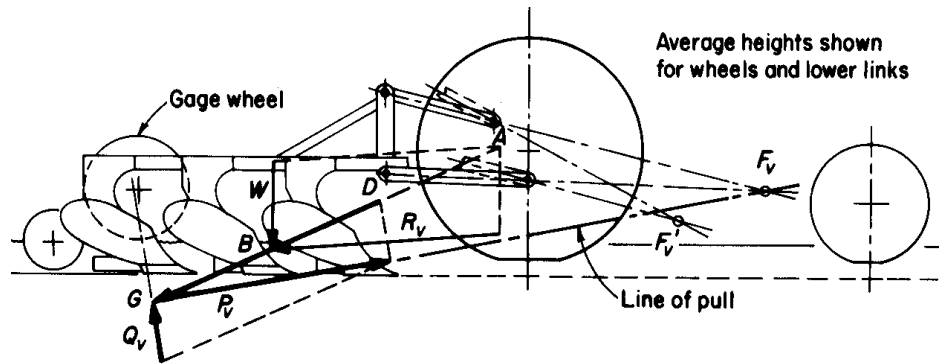


Figure 8.65 – Vertical force relations for a three-point hitch when operated as a free-link system (reprinted from Kepner et al., 1978).

The vertical force relations for free-link operation with a moldboard plow having a gage wheel are shown in Figure 8.65. In free-link operation, the convergence of the links in a vertical plane provides a vertical hitch point or instantaneous center of rotation as shown at F_v . The location of F_v can readily be changed by modifying the arrangement of the links and it shifts automatically as the implement is raised or lowered. The broken-line position of the links in Figure 8.65 illustrates how F'_v is lower than F_v and farther to the rear when the tool is entering the ground. This shift promotes more rapid entry of tools that have appreciable bottom support surfaces (such as a moldboard plow).

The force analysis is basically the same as for a single-axle, pull-type implement except that the line of pull P_v must pass through the virtual hitch point F_v rather than through a real hitch point. All the vertical support in this example is assumed to be on the gage wheel, thus establishing the line of action of Q_v . The slope represents the coefficient of rolling resistance. W and R_v are first combined into the resultant AB , and the location of G is established by the intersection of AB and Q_v . P_v then passes through G and F_v .

Raising F_v , by modifying the linkage, would reduce Q_v and increase the load on the tractor rear wheels. However, Q_v must not be reduced to the point where the implement becomes unstable due to momentary variations in R_v . Increasing the plow length by adding more bottoms would move W , R_v , Q_v , and G farther to the rear. P_v would then have less slope but would be higher above the ground at the tractor wheels.

Gaged, free-link operation gives more uniform depth than either automatic position control or automatic draft control when the field surface is irregular and the soil resistance varies substantially, particularly with the larger sizes of mounted moldboard plows. Gage wheels are sometimes used in preference to the other systems in light soils where the draft is relatively low. Wide field cultivators and chisels often have gage wheels to minimize depth variations across the width of the implement.

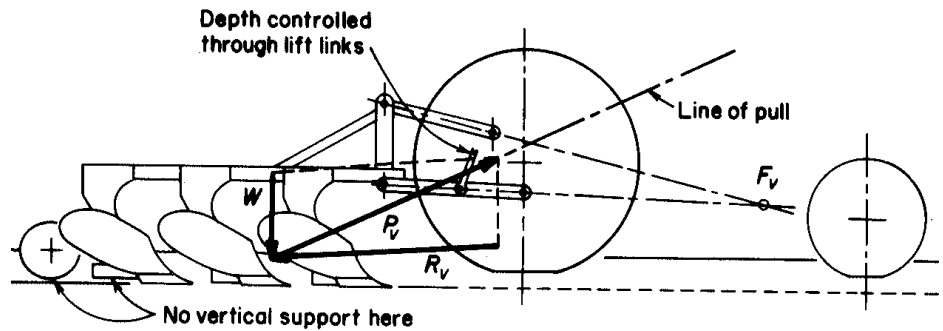


Figure 8.66 – Vertical force relations for a mounted implement when supported by restrained links (reprinted from Kepner et al., 1978).

8.4.3.2 Restrained-link operation of three-point hitches

In restrained-link operation, the implement gets all or most of its vertical support from the tractor, the hitch links being free only when the tool is entering the ground. As soon as a moldboard plow, for example, reaches its working depth, it is held by the hydraulic system. Its landside and rear furrow wheel must have clearance above the furrow bottom so the plow can go deeper when the controls call for greater depth.

Since the implement obtains no support from the soil, P_v is merely the vector sum of W and R_v as indicated in Figure 8.66. The lift links are in tension and the implement exerts downward bending moments on the portions of the lower links behind the lift links.

With restrained-link operation, the effect of the implement upon the tractor when the implement is at its operating depth is independent of the hitch linkage arrangement. The only significance of the virtual center of rotation (F_v) is that, with single-acting lift mechanisms (the usual arrangement for integral systems), the line of pull cannot pass below this point. However, when the tool is entering the ground, the location of the virtual center of rotation affects the pitch of the tool, just as it does with full free-link operation.

Operating with restrained links rather than free links increases the vertical load on the tractor rear wheels and thereby provides greater tractive ability. This is because the support forces that would act upon the gaging units in a free-link system are transferred to the tractor rear wheels when the links are restrained and because the higher location of P_v at the rear wheels increases the load transfer from the front wheels to the rear wheels.

PROBLEMS

- 8.1 A specimen of soil has a water content of 30%, a unit weight of 1.8 g/cm^3 , and a specific gravity (of solids) of 2.70. Find the void ratio and the degree of saturation.
- 8.2 A compacted soil sample weighs 1903 g and its volume is 930 cm^3 . The water content of the specimen is 10%. The specific gravity of solids is 2.7. Determine the wet density, dry density, void ratio, and the degree of saturation.
- 8.3 A soil sample has a water content of 25% and dry density of 1.1 g/cm^3 . (a) Find the void ratio and wet density. (b) The compaction is the same but assume the water content is 50%; find the void ratio and the wet density.
- 8.4 A specimen of cohesionless sand was subjected to the direct shear test under a normal stress of 100 kPa. The specimen failed when the shear stress reached 60 kPa. Plot the stresses and find the value of internal friction. At what value would the soil fail if the normal stress is 250 kPa?
- 8.5 In the consolidated-undrained triaxial test, two specimens were loaded to failure after consolidation under all around pressures of 200 and 400 kPa, and the results are shown below:

Sample No.	α_3 (kPa)	α' (kPa)	u_b (kPa)
1	200	150	140
2	400	300	280

Calculate (a) the values of c and ϕ for total stress, (b) the values c and ϕ for effective stress, (c) maximum shear stresses for both specimens, and (d) the shear and the normal stress on the failure planes for both cases

- 8.6 A cohesionless soil with a 30° angle of internal friction is subjected to a consolidation pressure of 150 kPa. At what value of the major principal stress will the specimen fail?
- 8.7 Consolidated-undrained triaxial tests were performed on two clay soil samples. The following are the stresses and pore water pressures at failure:

Sample No.	α' (kPa)	α_3 (kPa)	u_a (kPa)
1	40	100	30
2	80	200	60

Find the expression for the effective soil shear strength.

- 8.8 Derive an expression for the total vertical force (V) acting on an inclined blade tillage tool. Follow a procedure similar to that used in this chapter to develop the horizontal force expression.
- 8.9 Determine the draft on a plane tillage tool inclined at 45° , operating at 25 cm depth in a cohesionless soil. The tool forward speed is 5 km/h. The soil density

is 1.2 g/cm^3 and the angle of internal friction (ϕ) is 37° . The tool is 10 cm long and 25 cm wide and the soil-metal friction is 0.3. Neglect adhesion, the cutting resistance, and the effects of the tool supports.

- 8.10 Repeat Problem 8.9 but vary the tool depth from 10 cm to 25 cm in intervals of 5 cm. Plot the draft force against the tool depth. (Use of a spreadsheet is recommended.)
- 8.11 Repeat Problem 8.9 but vary the tool speed from 1 to 10 km/h in 1 km/h intervals. Plot the draft force against the tool speed. (Use of a spreadsheet is recommended.)
- 8.12 Repeat Problem 8.9 but vary the soil-metal friction from 0.1 to 0.5 in 0.05 intervals. Plot the draft force against soil metal friction. (Use of a spreadsheet is recommended.)
- 8.13 The line of pull on an implement is 15° above the horizontal and is in a vertical plane which is at an angle of 10° with the direction of travel. (a) Calculate the draft and side-draft forces for a pull of 11 kN. (b) What drawbar power would be required at 5.5 km/h?
- 8.14 Referring to Figure 8.56 of the text, determine (a) the percent increase in the draft of a plow bottom if the pull is at 10° to the left from the direction of travel. Assume that R_h is at 15° to the right and the soil-metal friction is 0.3. (b) The percent increase in the perpendicular force on the landside. (Hint: A graphical solution is recommended.)
- 8.15 The total draft of a four-bottom 41 cm moldboard plow when plowing 18 cm deep at 6 km/h was 15 kN. (a) Calculate the specific draft. (b) What is the actual power requirement?
- 8.16 Each gang of an offset disk harrow without wheels has thirteen 61 cm blades spaced 24 cm apart. The total mass is 1400 kg. In operation, $V_f = 8.7 \text{ kN}$ and $V_r = 5.3 \text{ kN}$. The disk angles are 16° for the front gang and 22° for the rear gang. Based on Figures 8.58 and 8.61, the estimated L/V is 0.9 for the front gang and 1.2 for the rear gang, and the estimated S/V 0.7 for the front gang and 1.1 for the rear gang. Calculate (a) draft, (b) side draft, and (c) draft per unit mass (N/kg).
- 8.17 A right hand offset disk harrow is operating with disk angle of 15° and 21° , respectively, for the front and rear gangs. The centers of the two gangs are 2.45 m and 4.25 m behind a transverse line through the hitch point on the tractor drawbar. The horizontal soil force components are: $L_f = 3.1 \text{ kN}$, $S_f = 2.65 \text{ kN}$, $L_r = 3.35 \text{ kN}$, $S_r = 3.8 \text{ kN}$. Calculate (a) the horizontal angle of pull, (b) the horizontal pull, and (c) the amount of offset of the center of cut with respect to the hitch point.
- 8.18 Assume that $P_v = 9.9 \text{ kN}$ in Figure 8.65. Determine the force in the top link and the total force in the bottom two links, indicating whether tension or compression. Scale the dimensions and angles from the text and solve by graphical methods. Also, determine the draft.

CROP PLANTING

INTRODUCTION

The growth of a new crop begins with the planting of seed or transplanting of seedlings. After planting, seeds must survive on energy stored within the seed until germination occurs and a seedling emerges through the soil surface. Usually not all of the seeds are able to survive through *germination* and *emergence*; thus the number of seeds planted per unit area must be greater than the final desired *plant population*. The most important factors affecting germination and emergence include seed viability (percent germination under controlled laboratory conditions), soil temperature, availability of moisture and air to the seeds, and soil strength and resistance to seedling emergence. An ideal seed environment is one in which the seed depth and soil firmness provide adequate moisture, oxygen, and temperature to the seed but without excessive soil firmness that retards root development and seedling emergence. While transplanted seedlings are already emerged, their survival and initial rate of growth are also dependent upon soil moisture and temperature. A planter can exert a strong influence on the rate of germination and emergence of seeds through control of planting depth and firming of soil around the seeds or roots of seedlings. In addition, the planter must meter seeds at the proper rate and, in some cases, must control the horizontal placement of seeds in a desired pattern.

9.1 METHODS AND EQUIPMENT

Three different planting methods can be distinguished by the horizontal pattern of seed placement. *Broadcasting* refers to random scattering of seeds on the soil surface. *Drilling* is the random placement of seeds in furrows that are then covered; the seeds thus emerge in rows. In *precision planting*, the seeds are planted in rows and the spacing of seeds within the rows is uniform. A fourth method of planting is the *transplanting* of plant seedlings into a field. Mechanisms and machines have been developed to permit each of these planting methods.

9.1.1 Broadcast seeding

A *centrifugal broadcast seeder* is shown in Figure 9.1. The seed is metered from a hopper through a *variable orifice*. An *agitator* is provided above the orifice to prevent bridging of the seed over the gate and to assure continuous feeding. Sometimes a fluted wheel is used to meter the seed. The metered seed drops onto a *spinning disk*



Figure 9.1 – A centrifugal broadcast seeder (courtesy of Vicon Corporation).

that accelerates and throws it, usually horizontally. The width of coverage depends upon the size, shape, and density of the seeds. Two counter-rotating spinning disks may be used to increase the width of coverage. The seeding rate is controlled by the size of the gate opening, the speed of travel, and the width of coverage. Centrifugal broadcasters are flexible in that they can be used for broadcasting seed, dry fertilizer or pesticides, or other granular materials. After broadcast seeding, a secondary tillage operation may be performed to cover the seeds with soil.

9.1.2 Drilling

A *drill seeder* is illustrated in Figure 9.2. Typically, for each row, the seeds are metered from a *hopper* by a ground-driven *fluted wheel* past an *adjustable gate* that controls the seeding rate. The seeds then enter a tube and fall by gravity to a furrow that has been opened by a disk. Typical row spacings range from 150 to 400 mm. A common method of covering the seeds is to pull a small *drag chain* behind each *furrow opener*. Figure 9.2 is an example of a *wheel drill*, in which the weight of the machine is carried on transport wheels. In the *press drill* illustrated in Figure 9.3, much of the

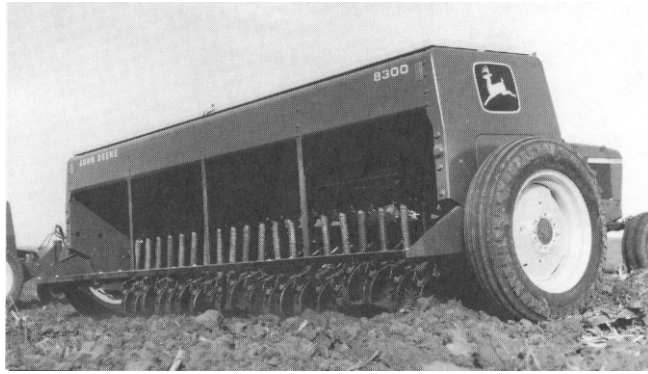


Figure 9.2 – A drill seeder (courtesy of Deere and Co.).

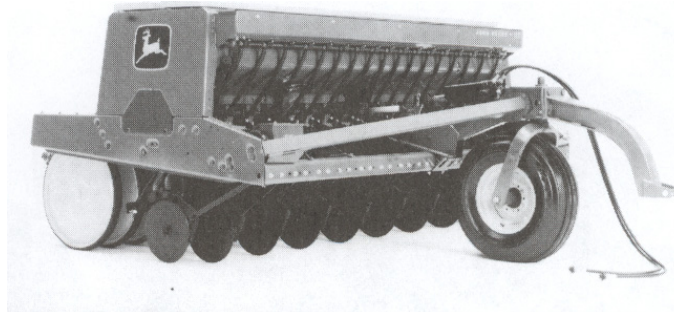


Figure 9.3 – A press drill (courtesy of Deere and Co.).

weight of the drill is carried on press wheels that follow each row. Press drills thus provided firmer soil around the seeds compared to wheel drills. The term *fluid drilling* has been used to describe a planting technique in which germinated seeds are sown using a protective gel. The gel and seed mixture can be pumped through a hose for transport to the furrow if seed spacing is not critical. For more uniform seed placement, Shaw (1985) was issued a patent for a device to singulate and meter seeds from a liquid gel or suspension.

9.1.3 Precision planting

Precision planters provide accurate placement of single seeds at equal intervals within rows; the rows are usually spaced widely enough to allow cultivation (Figure 9.4). Precision planters are available in many variations, but four functions are always included. These are: opening a furrow of controlled depth, metering seeds into the furrow at uniform intervals, covering the furrow, and firming the soil against the seeds. On some planters, a pair of inclined wheels accomplish both the covering and the soil firming. Until the mid-1960s, most precision planters included *seed plates* for metering seeds. Pockets along the periphery of the plates were sized to match the seed dimensions, so that only one seed could fit in each pocket. As each pocket passed the

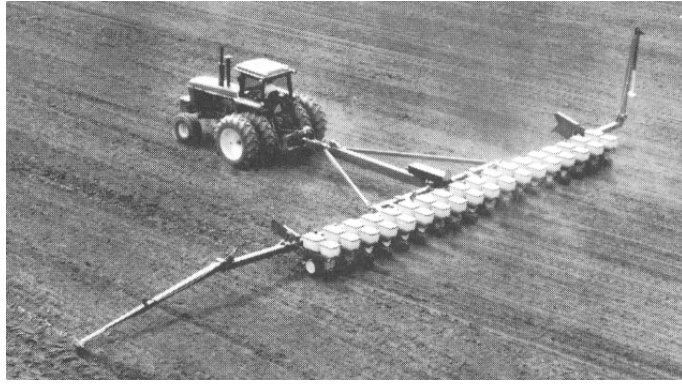


Figure 9.4 – A precision planter (courtesy of Deere and Co.).

seed tube, a spring-loaded knockout device would push the seed into the tube. Plates were easily replaceable, and farmers kept sets of plates to match each size of seed that was to be planted. “Plateless” planters were developed in the late 1960s and now there are a wide variety of mechanisms available for metering seed. The term *punch planting* is used to describe planting in *dibbles* created by a spaded wheel rather than planting in furrows. When vegetable crops are to be grown in soil covered by a plastic sheet, punch planting is especially useful in planting through the plastic cover.

9.1.4 Transplanting

A number of crops, including cabbage, lettuce, rice, strawberries, sweet potatoes, tobacco, and tomatoes, may be grown from seed in special beds and then transplanted into fields. Trees grown for commercial purposes are nearly always transplanted. The transplanting operation has not been fully mechanized, but a *transplanter* machine (Figure 9.5) can greatly increase the rate at which workers can do the transplanting.



Figure 9.5 – A seedling transplanter (courtesy of Deere and Co.).

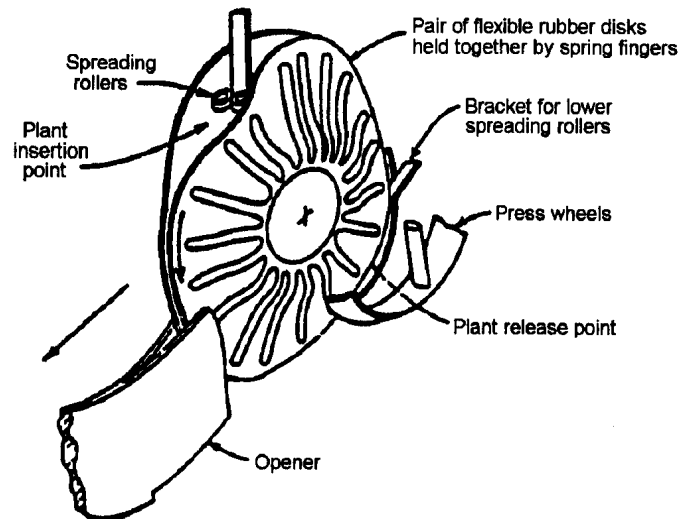


Figure 9.6 – Key elements of a seedling transplanter (courtesy of Deere and Co.).

One or more seats are included on transplanters to position the workers conveniently for doing the transplanting. The transplanter also includes a hopper for the seedlings, provision for opening a furrow, means for accepting seedlings from a worker (see Figure 9.6) and placing them in the furrow, and means for closing the furrow and firming the soil around the seedlings. Runner-type furrow openers are usually employed, while a pair of press wheels tilted outward at the top accomplish furrow closing and soil firming. A water supply tank and suitable plumbing is often included to water the newly planted seedlings, and some signaling device may be provided to help the workers achieve correct spacing of the seedlings along the furrow.

9.2 FUNCTIONAL PROCESSES

9.2.1 Seed metering

Seed metering has two aspects. The first, *metering rate*, refers to the number of seeds that are released from the hopper per unit of time. Metering rate is important in any planter to insure that the desired final plant population will be achieved. In addition, seeds must be *singulated* in precision planters to allow placement of seeds at uniform spacing in each row.

9.2.1.1 Seed metering mechanisms

The oldest principle for metering seeds is the *variable orifice* and its simple principle is still in use. The volumetric flow rate of seeds is regulated by changing the orifice size. An agitator is used above the orifice to prevent bridging of the seeds (Figure 9.7).

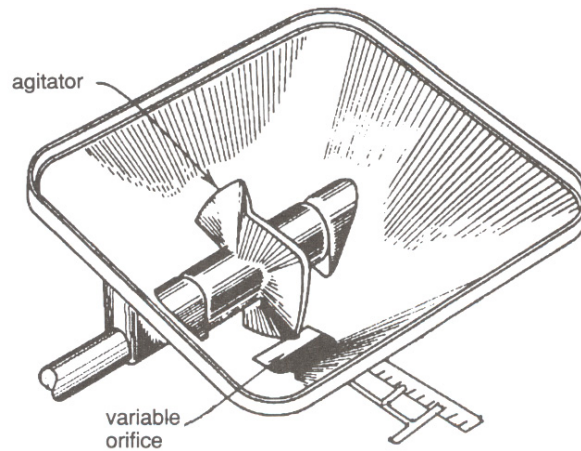


Figure 9.7 – Metering seeds with a variable orifice.

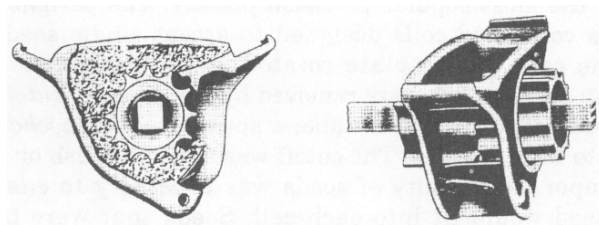


Figure 9.8 – Metering seeds with a fluted wheel.

The most popular system for seed metering in a drill is the *fluted wheel* (Figure 9.8). The fluted wheel assemblies are positioned at the bottom of the seed hopper so that seed can flow into the openings by gravity. The fluted wheel provides quasi-positive-displacement metering, i.e., seeds in the flute openings are carried toward an adjustable gate as the fluted wheel rotates. The gate opening is set to match the seed size. The fluted wheel can be moved endwise to control the volumetric flow rate of seeds. Maximum flow rate occurs when the fluted wheel covers the entire width of the gate, while zero flow rate occurs when the non-rotating cutoff covers the full gate width. The flow rate also varies with the rotational speed of the fluted wheel.

The *internal double-run seed metering* mechanism is used on some drills (Figure 9.9). As with the fluted wheel, the internal run is a quasi-positive-displacement metering device but the seed spaces are formed by fins on the inside of the wheel. It is called a double run because two wheels are positioned back to back. One has much smaller seed spaces and is used for small seeds, while the side with large spaces is used for large seeds. The internal double-run units are positioned at the bottom of the seed hopper so that seeds can flow in by gravity. Only one side of the internal double-run is used at a time; a removable feed cover is used to block off the side that is not being used. An adjustable feed gate is provided for each side of the unit. The distance between the gate edge and the internal fins can be regulated to control the feed rate.

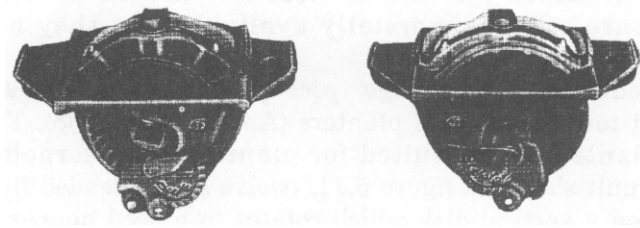


Figure 9.9 – Internal double-run metering.

Mechanisms previously mentioned in this section have metered seeds by volume. The remaining mechanisms to be discussed all meter individual seeds for precision planting.

Until the mid-1960s, the horizontal *seed plate planter* (Figure 9.10) was by far the most popular precision planter. The periphery of the seed plates contained cells designed to accept single seeds. Seeds entered the cells as the plate rotated in the bottom of the seed hopper. Any excess seeds were removed by a stationary *cutoff* and, as each cell passed over the seed tube, a spring-loaded *knockout* forced the seed into the drop tube. The cutoff was either a brush or a spring-loaded scraper. Uniformity of seeds was necessary to ensure that only one seed would fit into each cell. Seeds that were naturally non-uniform, such as corn kernels, had to be graded into uniform lots prior to planting. A wide variety of replaceable seed plates were available to match the various sizes and shapes of seeds. Plate planters are still commercially available, but they no longer dominate the market.

Introduction of the *finger pickup planter* in 1968 started a movement toward plateless planters (*Agricultural Engineering*, 1968). The finger pickup planter is best suited for planting corn kernels. In the metering unit shown in Figure 9.11, twelve spring-loaded fingers are mounted on a vertical disk that rotates in a seed hopper. As they travel on their circular path, the fingers ride on a stationary disk that is concentric with

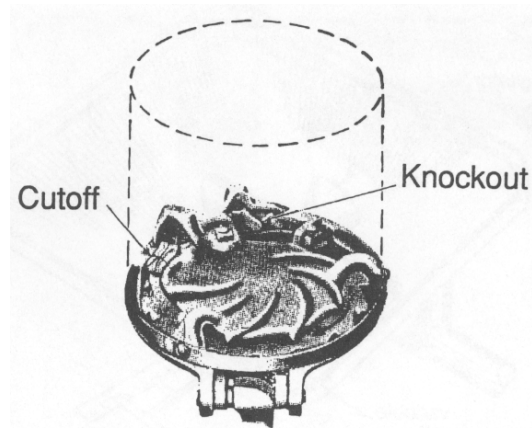


Figure 9.10 – Metering with gravity-fed seed plates.

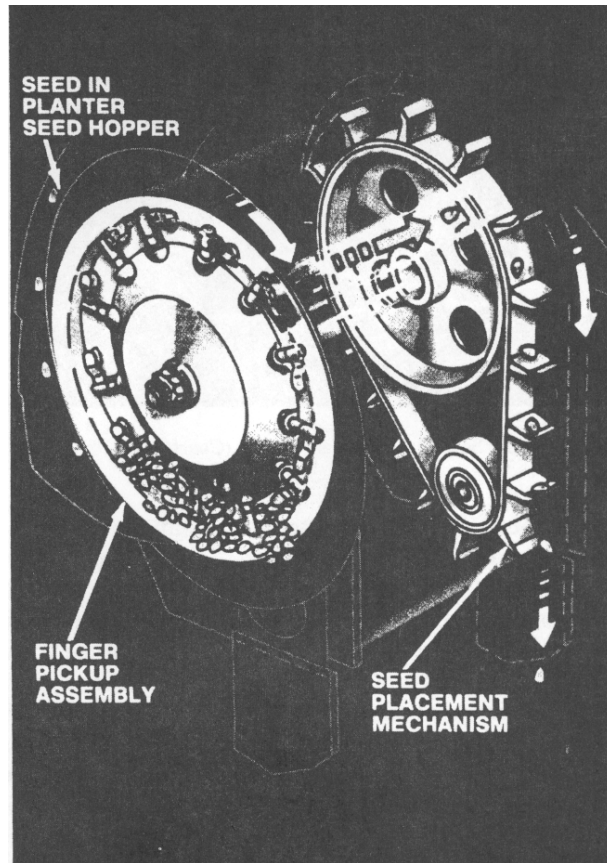


Figure 9.11 – Seed metering by finger pickup (courtesy of Deere and Co.).

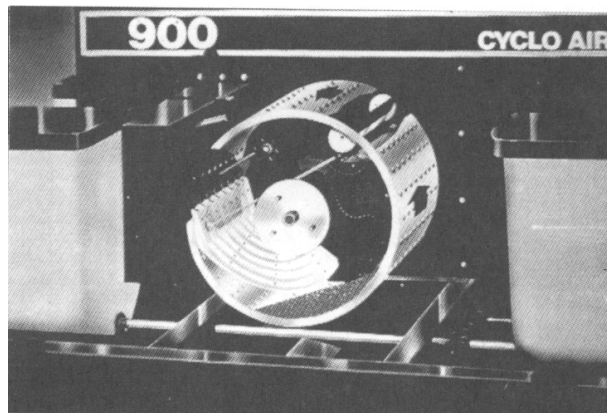


Figure 9.12 – Seed drum in an air planter (courtesy of CNH).

the rotating disk. As each finger passes through the bottom of the hopper, it picks up one or more seeds. With continued movement, the finger passes over an indentation in the stationary disk, causing it to grip one seed while any others fall back into the seed hopper. With further movement, the finger passes across an opening in the stationary disk and the seed is ejected into the seed placement belt for transport to the seed tube. The entire seed metering unit is ground driven to provide controlled spacing of the seeds along the rows.

The next innovation in plateless planting was the *air planter* (*Agricultural Engineering*, 1971). A ground-driven *seed drum* (Figure 9.12) is pressurized to about 4 kPa by a PTO-driven fan. Maximum practical drum speed is approximately 35 rev/min. Seeds flow by gravity from a central hopper to maintain a shallow reservoir of seed in the bottom of the drum. Each drum can be designed to serve 4, 6, or 8 rows, depending upon the number of rows of perforated holes that are provided. The drum shown in Figure 9.12 has eight rows of holes and thus meters seeds to eight rows in the field. Each hole terminates in a seed pocket at the inner face of the drum. As the drum rotates, air escapes through the holes and, when seeds enter the seed pockets, differential

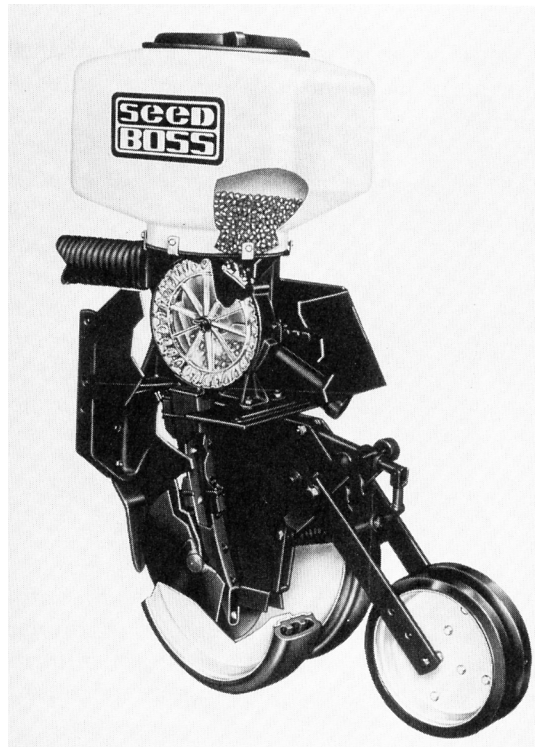


Figure 9.13 – Pressure-disk metering of seeds (courtesy of White Farm Equipment Co.).

pressure holds each seed in its pocket until drum rotation brings the seed close to a seed tube. A row of external wheels near the seed tubes blocks the holes momentarily, thus removing the differential pressure and allowing the seeds to fall into the seed tubes. Air escaping through the seed tubes carries the seeds to the planting units and deposits them in the rows. Crops that can be planted with the air planter include beans, corn, delinted cotton seed, and sorghum. The seed drums are easily replaceable and are changed to suit the seed being planted. A key advantage of the air planter is that it has only one seed hopper to be refilled, thus permitting faster refilling.

The *pressure-disk planter* (Figure 9.13) is similar to the air planter in that positive pressure in the seed reservoir is used to hold seeds in the pockets of the rotating seed plate. Unlike the air planter, however, the pressure-disk planter has a separate seed reservoir and plate for each row. Gravity moves the seeds from the hopper to the metering unit, where differential pressure holds a seed in each cell. As each cell nears the drop tube, a soft brush cuts off the air supply to the cell and the seed falls into the seed tube by gravity. Unlike the air planter, the seed tubes are not a conduit for escaping air. As with all precision metering units, the seed plate must be ground driven. Seed disks are replaceable and disks are available for corn, soybeans, edible beans, delinted cotton seed, pelleted or segmented sugar beet seeds, sunflowers, and sorghum.

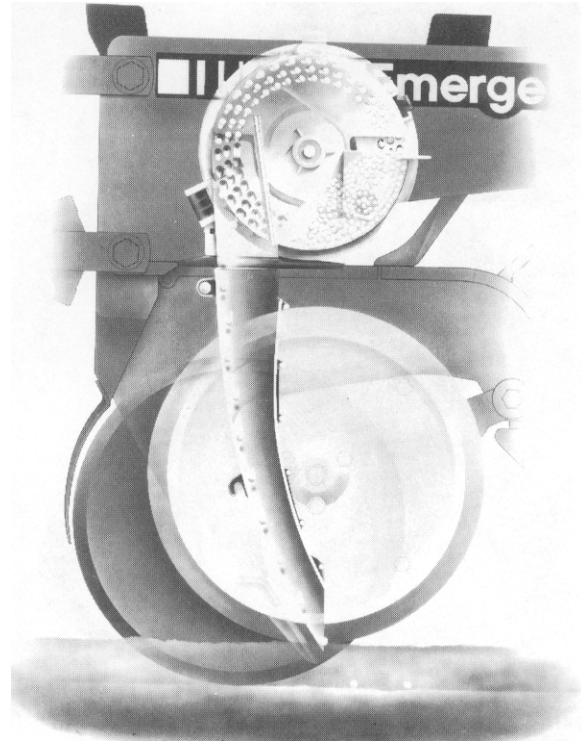


Figure 9.14 – Vacuum-disk metering of seeds (courtesy of Deere and Co.).

Vacuum-disk metering (Figure 9.14) is similar to pressure-disk metering, except that the pressure differential is supplied by creating a vacuum on the side of the seed disk opposite the seeds. Seed from the hopper enters the seed reservoir, where vacuum created by a pump holds the seeds in the seed cells on the rotating seed disk. The vacuum is blocked as the cells reach a point above the seed tube and the seeds fall into the tube by gravity. A vacuum of 15 kPa was used for holding seeds in a vacuum-disk planter designed by Giannini et al. (1967). In commercially available vacuum-disk planters, seed disks are available for metering edible beans, soybeans, corn, delinted cotton seed, edible peas, peanuts, sorghum, sugar beets, and sunflowers.

9.2.1.2 Seed metering theory

The two classes of seed metering mechanisms are those that meter by volume and those that meter individual seeds. When planting with metering by volume, the application rate can be expressed in number of seeds per hectare or in kilograms of seed planted per hectare. The application rate can be calculated by using the following equation:

$$R_s = \frac{10,000 Q \rho_b}{w v} \quad (9.1)$$

where R_s = seeding rate, kg/ha or seeds/ha

Q = flow rate of seeds from the metering unit, L/s

ρ_b = seed bulk density, kg/L or number of seeds/L

w = width of coverage of the planter, m

v = travel speed of planter, m/s

It is impractical to count the number of very small seeds per unit volume and seeding rates are thus given in kg/ha. For larger seeds, the seeding rate can be given either in kg/ha or in seeds/ha. If the planter plants in rows and has a separate metering device for each row, Q is the flow rate from one device and W is the row spacing. The method of controlling Q varies with type of metering device.

The variable orifice is the simplest and oldest method for volume metering of seeds. In studying the flow of grain through orifices, Moysey et al. (1988) reported that the flow rate is independent of the depth of grain above an orifice in the bottom of a hopper. The following equation was adapted from their data:

$$Q = -0.0342 + 770A_n \sqrt{gD_e} \quad (9.2)$$

where Q = volume flow rate, L/s

A_n = net effective area of orifice, m²

g = acceleration of gravity = 9.801 m/s²

D_e = hydraulic diameter of orifice, m

The equation is valid for circular or rectangular orifices that are centered at the bottom of the hopper. The volume flow rate is about 15% greater for a given orifice when the orifice is at the edge of the hopper. Both the effective diameter and the effective net area are smaller than the physical opening because seeds overhanging the edge reduce the effective opening size. To account for this effect, each linear dimension of

the orifice should be reduced by k times the seed size. For a circular orifice of diameter D , the hydraulic diameter is $D_e = D - kd$, where d = seed effective diameter and k is a constant. For a rectangular orifice with physical length a and width b , the effective opening is $a' = a - kd$ and $b' = b - kd$. The area is $A_n = 0.25 \pi D_e^2$ for the circular orifice or $A_n = a' b'$ for the rectangular orifice. The hydraulic diameter for a rectangular orifice is $D_e = (0.5 a' b') / (a' + b')$. Moysey et al. (1988) reported kd values of common seeds as 7.5 mm for barley, 5 mm for wheat, 3.3 mm for flax, and 1.8 mm for rapeseed, where $k = 1.4$ for all seeds. The flow through the orifice became irregular when D_e was less than $6d$ and was independent of grain size when D_e was more than $20d$. The hopper shape had little effect on flow rate when D_e was greater than $12d$. Equation 9.2 was developed for stationary hoppers without agitation. In a seeder, an agitator is used to prevent bridging and the vibration of the hopper due to rough terrain could influence the flow rate. Thus, Equation 9.2 only provides a starting point for design and accurate flow rates must be determined through calibration of a prototype. Example Problem 9.1 illustrates the use of Equation 9.2.

Example Problem 9.1

Calculate the flow rate of sweet clover seed from a seed hopper on a centrifugal spreader. The rectangular orifice with dimensions of 30 mm by 80 mm is located at the edge of the hopper. (Seed properties are given in Table 9.1, in the Problems section at the end of this chapter.)

Solution

The seed properties table indicates the diameter of sweet clover seeds is 1.41 mm. The effective orifice dimensions are:

$$a' = a - kd = 0.03 - 1.4(0.00141) = 0.0280 \text{ m}$$

$$b' = b - kd = 0.08 - 1.4(0.00141) = 0.0780 \text{ m}$$

$$A_n = a' b' = (0.0280)(0.0780) = 0.00218 \text{ m}^2$$

$$D_e = 0.5a' b' / (a' + b') = 0.5(0.028)(0.078) / (0.028 + 0.078) = 0.0103 \text{ m}$$

Then, from Equation 9.2, the flow rate for a centered orifice would be:

$$Q = -0.0342 + 770(0.0218)(9.801 \times 0.0103)^{0.5} = 0.499 \text{ L/s}$$

The flow rate for an orifice on the edge is 15% greater, that is:

$$Q = 0.499(1.15) = 0.574 \text{ L/s}$$

Both the fluted wheel and the internal run metering mechanisms are quasi-positive-displacement devices. For such devices, the following equation is useful for estimating the volume flow rate of seeds:

$$Q = \frac{V_c \lambda_c n}{60 \times 10^6} \quad (9.3)$$

where Q = volumetric flow rate, L/s

V_c = cell volume = volume of each cell, mm^3

λ_c = number of cells on periphery of fluted wheel or internal run

n = rotational speed of fluted wheel or internal run, rev/min

The flow rate is controlled by changing of the speed ratio between the ground drive wheels and the metering device and/or by changing V_c . As noted in Section 9.2.1.1, V_c is changed by sliding the fluted section endwise (Figure 9.8) or by changing the gate setting on a double internal run device (Figure 9.9). The term *quasi-positive* was used to describe the displacement of the fluted wheel or the internal double run because the void space between seeds results in not all of the cell volume being occupied by seeds. Also, some seeds will typically project beyond the edge of the cells. Thus, the volume of seeds delivered each time a cell passes the seed tube is not precisely equal to the cell volume. Equation 9.3 can be used for design purposes, but accurate determination of the flow rate for any given type of seed requires calibration using a prototype machine.

For any of the planters that meter individual seeds, the theoretical seeding rate can be calculated by using the following equation:

$$R_{st} = \frac{10,000}{w x_s} \quad (9.4)$$

where R_{st} = theoretical seeding rate, seeds/ha

w = row width, m

x_s = seed spacing along the row, m

The seed spacing along the row can be calculated by using the following equation:

$$x_s = \frac{60v}{\lambda_c n} \quad (9.5)$$

where λ_c = number of seeds delivered per revolution of the metering device

n = rotational speed of metering device, rev/min

v = travel speed of planter, m/s

Note that, for a given row spacing, the theoretical seeding rate can be changed only by changing the seed spacing in the rows. The seed spacing is changed by changing the speed ratio between the ground drive wheels and the metering device.

9.2.1.3 Performance of seed metering mechanisms

Of the various types of planters discussed in this chapter, the broadcast seeder is least accurate in holding to a desired rate for three reasons. The first is that the variable orifice is not a positive-displacement metering device. The second is that, since the

metering unit does not have positive displacement, the metering rate is not linked to the travel speed of the seeder; rather, operator skill is required to coordinate the travel speed with the metering rate. Finally, the swath width of the broadcast seeder is not as precisely determined as the swath width of the other seeders mentioned in the chapter. Thus, the broadcast seeder is best suited to situations in which precise control of the seeding rate is not important. Broadcast seeders are capable of fast application, with spreading widths up to 15 m and travel speeds of 5m/s or more.

Drilling provides more precise control of seeding rates because the swath width can be controlled precisely and the metering rate is automatically linked to the travel speed. Through calibration, the volumetric flow rate of any given seed from the metering device can be determined with good accuracy. Seed spacing within the row is not uniform because the seeds are delivered to the seed tube in cells. Seeds began to trickle into the seed tube as a cell approaches the tube and, after the cell empties into the tube, seeds again began to trickle in as the next cell approaches the tube. Thus, although the average seeding rate may be accurate, the seed tends to be deposited in bunches along the row. Field slope may affect the flow rate from fluted wheel metering. The tendency is for flow rates to increase as the drill travels down slope; in one case, flow rate increased 44% on a 15% down slope. Since the metering device is ground driven, the inflation pressure of the ground drive wheels can affect seeding rate; if the tires are under-inflated, the wheel radius will be reduced, thereby causing more rotations of the wheels per distance traveled and increasing the seeding rate. Slippage of the drive wheels reduces the seeding rate, so wheel slippage must be considered in calculating the seeding rate. Typical travel speeds for drills are in the range from 1 to 3 m/s. Power requirements for pulling a drill are typically in the range from 1.0 to 1.4 kW per row.

Planters that meter individual seeds provide the most precise control of seeding rates. The actual seeding rate will equal the theoretical rate if and only if every finger pickup or seed cell carries exactly one seed. Some cells may fail to fill for various reasons, and then the actual seeding rate will be less than the theoretical rate. Conversely, if some cells contain more than one seed due to a poor fit between seed size and cell size, the actual rate can be higher than the theoretical rate. The metering device on precision planters is ground driven and, as with drills, drive wheel slippage and/or inflation pressure therefore affect the seeding rate. Electronic seed monitors have been developed for precision planters. A sensor in each seed tube senses the passage of seeds. Some monitors can be programmed to sound an alarm if the seed passage rate is too high or too low. Travel speeds for precision planters are typically in the range from 1 to 3 m/s. Power requirements for pulling a row-crop planter are typically in the range from 1 to 2.4 kW per row.

9.2.1.4 Monitoring and control of seed metering

For crops that require metering of individual seeds, malfunctioning of the metering system can cause unacceptable planting performance. Monitors have been developed to warn the operator when the metering system is malfunctioning. Early monitors included mechanical switches that were tripped by passage of seeds in the seed delivery tubes, but the mechanical devices disrupted the natural trajectory of the seeds. Current monitoring devices are non-contacting. For example, seeds can be made to interrupt

the light transmission path between a light source and a photocell, resulting in an electrical pulse each time a seed passes. Simple monitors use each electrical pulse to flash a light on the operator console (there is a separate light for each row) each time a seed passes. Operation is satisfactory as long as the light for each row continues to flash. In more advanced systems, the amount of forward travel between the electrical pulses is measured. The seeding rate (in seeds/ha) is computed and displayed for the operator. Feedback control permits automatic control of metering rates. With feedback control systems, the operator sets the desired seeding rate. The seeding rate detected by the counters is compared with the desired rate and, if the desired and actual rates differ, an actuator is signaled to readjust the variable-speed drive of the metering device to correct the seeding rate.

9.2.1.5 Variable rate seeding

As discussed in Chapter 6, fields are not uniform but vary in natural productivity. Variable rate seeding involves increasing the plant density for higher-yielding areas of a field and reducing it for lower-yielding areas. Some initial research has shown that, if a producer has full information about the yield response to seeding rate for every part of a field and has access to a variable rate seeder, variable rate seeding can be profitable in that field. The difficulty is that few producers have such detailed information about their fields.

Variable rate corn planters are available for those producers who choose to use variable rate seeding of corn. The seed metering system on conventional planters is ground driven; thus the seed flow rate, Q , varies directly with v , the planter travel speed (see Equation 9.1). One variable rate planter on the market uses a hydraulic motor to drive the seed metering unit for each row. While a speed sensor inputs planter travel speed, an on-board computer consults a field map giving the desired seeding rate for each row, then computes the hydraulic motor speeds needed to obtain the desired seeding rate at each row. The resolution (see Section 6.4.3) of such a planter is thus one row width.

9.2.2 Seed transport

9.2.2.1 Seed transport mechanisms

After the seeds are metered, they must be transported to the soil surface or into a furrow. Most transport systems rely primarily on gravity for vertical movement of seeds. Horizontal movement, if it is needed, must be generated by the transport device. Friction is always present in seed transport and may have an effect on the path traveled by the seeds. Some seeders use pneumatic conveying to transport seeds.

9.2.2.2 Seed transport theory

For broadcast seeders, typically one or more spinning disks (Figure 9.15) are used to transport the seed. Seeds traveling down through a central seed tube enter the spinner through gates. Only one gate is shown on Figure 9.15. The following equations governing seed movement on the disk assume that the seeds slide along the disk and vane surfaces rather than rolling (Cunningham, 1963). The analysis below is for a cone-shaped spinner with radial blades, i.e., with $\delta = 0$. The angle (θ) through which

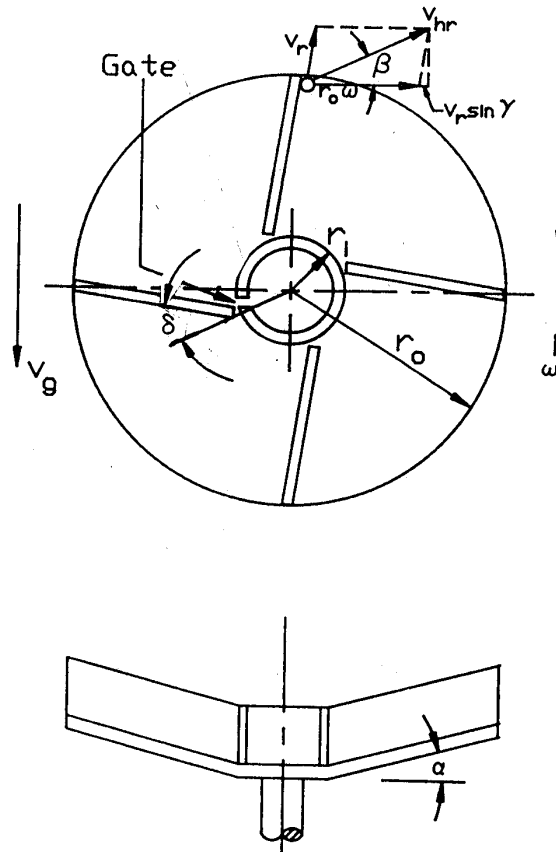


Figure 9.15 – A centrifugal spreader.

the disk turns while a seed is in contact with a vane can be calculated by solving the following equation:

$$\frac{(C_1 + f)e^{C_2(C_1 - f)\theta} + (C_1 - f)e^{-C_2(C_1 + f)\theta}}{2C_1} = \frac{r_o - \frac{C_3g}{C_4\omega^2}}{r_i - \frac{C_3g}{C_4\omega^2}} \quad (9.6)$$

After θ is calculated, the following equation can be used to calculate the velocity of seeds relative to a blade:

$$v_r = \frac{C_4\omega}{C_2} \left(\frac{r_i - \frac{C_3g}{C_4\omega^2}}{2C_1} \right) \left(e^{C_2(C_1 - f)\theta} - e^{-C_2(C_1 + f)\theta} \right) \quad (9.7)$$

where v_r = velocity of seeds relative to a blade, m/s
 f = coefficient of friction between spinner and seeds
 g = acceleration of gravity = 9.801 m/s²
 $C_1 = (f^2 + C_4/C_2)^{0.5}$
 $C_2 = \cos \alpha$
 $C_3 = \sin \alpha + f \cos \alpha$
 $C_4 = \cos \alpha - f \sin \alpha$
 r_i = radius to inner ends of blades, m
 r_o = outer radius of disk, m
 ω = rotational speed of disk, rad/s
 Angles θ , δ and α are all in radians.

Angles α and δ are shown on Figure 9.15. The spinning disk is a flat disk when $\alpha = 0$ and a cone-shaped disk when $\alpha > 0$. The cone-shaped disk increases the range of the seed trajectory by giving the seeds an upward component of velocity, $v_v = v_r \sin \alpha$. Angle δ is positive when the blades are forward pitched as shown in Figure 9.15, zero when the blades are radial, and negative when the blades have backward pitch.

Equation 9.6 cannot be solved explicitly for θ , so an iterative solution is required. As an alternative, Figure 9.16 has been prepared to solve Equation 9.6 graphically. The three variables on the left side of Equation 9.6 are f , α , and θ . In Figure 9.16, the value of the left side of Equation 9.6 has been plotted on the y-axis versus values of θ on the x-axis; curves are shown for three values of α . Although $f = 0.33$ was used in plotting the graph, the solution is only weakly dependent on f and would be useable for any $0.2 < f < 0.45$. The coefficient of sliding friction falls within that range for virtually all seeds sliding on steel. To use Figure 9.16, the value of the right side of Equation 9.6 is calculated for the specific situation and entered on the y-axis of Figure 9.16. A line is drawn to the right to the curve for the appropriate α , and then a vertical line is drawn to the x-axis to find the corresponding value of θ . Then, as previously mentioned, Equation 9.7 can be used to calculate the sliding velocity of the seed relative to the blade at the outer end of the blade.

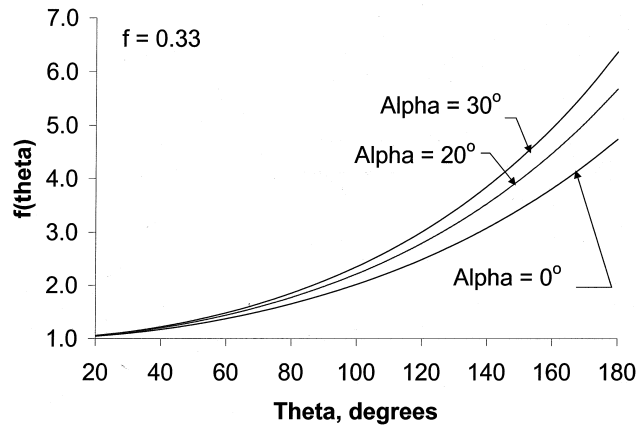


Figure 9.16 – Graphical solution of Equation 9.6.

The magnitude (v_{hr}) and direction (β) of the horizontal component of velocity as the seeds leave the disk can be calculated by using the following equations:

$$v_{hr} = \sqrt{(v_r \cos \alpha \cos \gamma)^2 + (r_o \omega + v_r \cos \alpha \sin \gamma)^2} \quad (9.8)$$

and

$$\beta = \arctan\left(\frac{v_r \cos \alpha \cos \gamma}{r_o \omega + v_r \cos \alpha \sin \gamma}\right) \quad (9.9)$$

where $\gamma = \arctan(r_1 \tan \delta / (r_o - r_1))$. The velocity at which the spreader moves over the ground, v_g , is shown in Figure 9.15. By adjusting the parameters in Equation 9.6, the direction of the seed trajectory relative to the direction of travel can be adjusted. Usually, several gates must be provided in the central seed tube to generate good coverage of seeds over the swath. Example Problem 9.2 illustrates the calculations.

Example Problem 9.2

A centrifugal spreader is to be used to seed sweet clover seed. The following data are available:

Blade inner radius, $r_1 = 0.05$ m

Blade outer radius, $r_o = 0.20$ m

Dish angle, $\alpha = 10^\circ$

Blade direction angle, $\delta = 0^\circ$

Rotational speed, $\omega = 78.5$ rad/s (750 rev/min)

Coefficient of friction, $f = 0.28$

Determine (a) the angle θ through which the spinner turns while the seed is in contact with the blade, (b) the velocity of each seed relative to the blade at the outer end of the blade, (c) the magnitude and direction of the horizontal component of velocity as the seeds leave the spinner, and (d) the vertical component of velocity as the seeds leave the spinner.

Solution

The first step is to calculate values for constants in Equation 9.6.

$$C_2 = \cos(10^\circ) = 0.985$$

$$C_3 = \sin(10^\circ) + (0.28) \cos(10^\circ) = 0.449$$

$$C_4 = \cos(10^\circ) - (0.28) \sin(10^\circ) = 0.936$$

$$C_1 = (0.28^2 + 0.936 / 0.985)^{0.5} = 1.014$$

$$C_3 g / (C_4 \omega^2) = (0.449 \times 9.801) / (0.936 \times 78.5^2) = 0.0007627$$

(a) The value of θ can now be determined. The value of the left side of Equation 9.6, $f(\theta)$, is:

$$f(\theta) = (0.20 - 0.0007627) / (0.05 - 0.0007627) = 4.046$$

By consulting Figure 9.16, a value of $f(\theta)$ corresponds to $\theta = 146.1^\circ$ or 2.549 radians when $\alpha = 10^\circ$.

(b) Next, Equation 9.7 can be used to calculate v_r . The lengthy equation will not be rewritten, but when the values are inserted the result is:

$$v_r = 11.38 \text{ m/s}$$

(c) Next, angle γ must be calculated for use in Equations 9.8 and 9.9:

$$\gamma = \arctan[(0.05 \tan(0^\circ)/(0.20 - 0.05)] = 0^\circ \text{ or } 0 \text{ radians}$$

Then, from Equation 9.8, the seeds leave the disk with a horizontal velocity of:

$$\begin{aligned} v_{hr} &= [(11.38 \cos(10^\circ) \cos(0^\circ))^2 + (0.20 \times 78.5 + 11.38 \cos(10^\circ) \sin(0^\circ))^2]^{0.5} \\ &= 19.3 \text{ m/s} \end{aligned}$$

From Equation 9.9, the departure angle is:

$$\begin{aligned} \beta &= \arctan[11.38 \cos(10^\circ) \cos(0^\circ)/(0.2 \times 78.5 + 11.38 \cos(10^\circ) \cos(0^\circ))] \\ &= 22.6^\circ \end{aligned}$$

(d) Finally, the vertical component of velocity of the seeds is:

$$v_v = 11.38 \sin(10^\circ) = 1.97 \text{ m/s (upward)}$$

Upon leaving the spinner, the seeds enter ballistic trajectories with absolute velocity v_v and velocity v_{hr} relative to the moving spreader. While the absolute horizontal velocity is the vector sum of v_{hr} and v_g , the contribution of v_g is usually negligible and v_{hr} can be used as the absolute initial horizontal velocity of the seeds. The following equations can be used to calculate the trajectory of a particle in still air (Goering et al., 1972; Pitt et al., 1982):

$$\ddot{h} = -C_6 \dot{h} [\dot{h}^2 + \dot{z}^2]^{0.5} \quad (9.10)$$

and
$$\ddot{z} = g - C_6 \dot{z} [\dot{h}^2 + \dot{z}^2]^{0.5} \quad (9.11)$$

where h = horizontal direction, m

z = vertical direction, m, positive downward

g = acceleration of gravity, m/s^2

$C_6 = 0.5C_D \rho_a A_p/m$

where A_p = projected frontal area of particle, m

m = mass of particle, kg

ρ_a = mass density of air, $\text{kg/m}^3 = 29p_b/(8.314 \Theta_a)$

where p_b = barometric pressure, kPa

Θ_a = ambient air temperature, $^\circ\text{K} = ^\circ\text{C} + 273$

The single dot over h or z indicates the first derivative with respect to time (velocity) while two dots represents the second derivative (acceleration). The drag coefficient,

C_D , varies with the Reynolds number. The following equations give a good approximation to drag coefficients first measured by Eisner (1930):

$$C_D = \frac{24}{N_{Re}} \quad \text{for } N_{Re} \leq 1 \quad (9.12)$$

or
$$C_D = (26.38N_{Re}^{-0.845} + 0.49) \quad \text{for } N_{Re} \geq 1 \quad (9.13)$$

where the Reynolds number is given by the following equation:

$$N_{Re} = \frac{\rho_a v_p d_p}{\mu_a} \quad (9.14)$$

where N_{Re} = dimensionless Reynolds number

v_p = velocity of particle, m/s = $(\dot{h}^2 + \dot{z}^2)^{0.5}$

d_p = effective diameter of particle, m

μ_a = dynamic viscosity of air, N's/m²

Over a wide range of barometric pressures, the air viscosity is a function only of air temperature, i.e.:

$$\mu_a = 4.79 \times 10^{-6} e^{0.678 + 0.00227\theta_a} \quad (9.15)$$

Equations 9.10 through 9.15 do not have a general closed solution but, by use of a computer, they can be solved iteratively to calculate the trajectory of a seed. The required parameters are the seed mass, effective diameter and frontal area, the air temperature and barometric pressure, and the initial velocity of the seed as it leaves the spinner. For a cone-shaped disk, the initial velocity in the z-direction is $-v_v$. The initial velocity in the z-direction is v_{hr} . The trajectory equations are based on the assumption of wind-still conditions.

Pitt et al. (1982) made further simplifying assumptions to enable calculation of trajectories without iteration. The first assumption is that the particle is launched horizontally, that is, the initial vertical velocity is zero. Also, the vertical velocity was set equal to zero in Equation 9.10 while the horizontal velocity was set equal to zero in Equation 9.11. Finally, the drag coefficient was assumed to be constant. Under those simplifying assumptions, the time required for the particle to fall distance z can be calculated by using the following equation:

$$t = \frac{\ln[\text{Arg} + (\text{Arg}^2 - 1)]}{2C_6 C_7} \quad (9.16)$$

where $\text{Arg} = 2e^{2C_6 z} - 1$

$C_7 = (g/C_6)^{0.5}$

The horizontal distance traveled during that fall time can be calculated from:

$$h = \frac{\ln(C_6 \dot{h}_0 t + 1)}{C_6} \quad (9.17)$$

where t = time for particle to fall distance z

\dot{h}_0 = initial velocity in h -direction, m/s

Equations 9.6 through 9.17 provide a means for evaluating the various transport factors that influence the uniformity of the pattern created by a broadcast seeder. Example Problem 9.3 illustrates the use of Equations 9.16 and 9.17 to calculate the end point of a seed trajectory.

Example Problem 9.3

Alfalfa seeds leave a centrifugal spreader horizontally with an initial velocity of 20 m/s. If the spreader disk is 2 m above the land surface, calculate the horizontal distance traveled by each seed before it reaches the ground. The barometric pressure is 100 kPa and the air temperature is 20°C.

Solution

Before Equation 9.16 can be used, values must be calculated for constants C_6 and C_7 . For a spherical particle, it can be shown that:

$$C_6 = 0.75 C_D \rho_a / (\rho_p d_p)$$

where ρ_p is the particle density in kg/m^3 . From Table 9.1 in the Problems section at the end of the chapter, $d = 0.00153$ m and $\rho_p = 1184$ kg/m^3 . The Reynolds number must be calculated for use in calculating a drag coefficient. The air density is:

$$\rho_a = 29 \times 100 / (8.314 \times 20 + 273) = 1.19 \text{ kg/m}^3$$

From Equation 6.15, at 20°C, the air viscosity is 1.835×10^{-5} $\text{N}\cdot\text{s/m}^2$. Although the particle velocity changes throughout the trajectory, we will use the initial velocity of 20 m/s in computing the Reynolds number, that is:

$$N_{Re} = 1.19 \times 20 \times 0.00153 / (1.835 \times 10^{-5}) = 1984$$

Then, from Equation 9.13, the drag coefficient is:

$$C_D = 26.38 \times 1984^{-0.845} + 0.49 = 0.533$$

Now, values for C_6 and C_7 can be calculated, that is:

$$C_6 = 0.75 \times 0.533 \times 1.19 / (1184 \times 0.00153) = 0.263$$

$$C_7 = (9.801 / 0.263)^{0.5} = 6.10$$

For a seed fall distance of 2 m, the value for Arg is 4.727 and, from Equation 9.16, the fall time is 0.697 s. Finally, from Equation 9.17, the horizontal distance traveled by the seed in 0.697 s is 5.86 m.

By comparison, a computer simulation of the trajectory of Example Problem 9.3 using Equations 9.10 through 9.15 indicated that the time for a 2 m fall would be 0.82 s and the horizontal travel in that time would be 6.05 m. Thus, the simplified approach using Equation 9.16 under-predicted the fall time by 15% but Equation 9.17 under-predicted the horizontal distance by only 3%. A plot of the entire trajectory showed that the seed was moving almost vertically near the end of the trajectory and thus the under-prediction of fall time had only a small effect on horizontal distance traveled. Using typical parameters for broadcasting of seeds, Equations 9.16 and 9.17 can generally predict the horizontal distance within 10% of the value calculated by Equations 9.10 through 9.15. If Equations 9.16 and 9.17 are used to calculate and plot a complete trajectory, inserting a factor in Equation 9.16 to increase each fall time by approximately 10% would improve the accuracy of the calculated trajectory.

Drills and precision planters include drop tubes for transporting seed from the metering device to the furrow. The drop tubes are nearly vertical and, if friction between the seed and the tube walls is neglected, Equation 9.11 can be used to calculate the time required for the seed to pass through the drop tube and the vertical velocity at the exit point. Since the tube is nearly vertical, at least at the seed entry point, the velocity in the x-direction can be set equal to zero in Equation 9.11. If C_D is variable, as in Equations 9.12 and 9.13, a computer is required to solve Equation 9.11. If C_D is assumed to be constant, the approximate transit time in the seed tube can be calculated using Equation 9.16 with z equal to the length of the tube. Also, by solving Equation 9.16 for z and differentiating with respect to time, the following equation can be obtained for seed velocity in the drop tube:

$$\dot{z} = \frac{C_7 \sin h(2C_6 C_7 t)}{1 + \cos h(2C_6 C_7 t)} \quad (9.18)$$

When t is taken as the transit time in the drop tube, then Equation 9.18 gives the z -direction velocity at the exit. Often the tube is curved toward the rear near the exit (see Figure 9.14) to give the seed a rearward velocity component near the exit. If the exit velocity is at an angle θ_e from the vertical, then the x -component of velocity at the exit, relative to the planter, is:

$$\dot{x}_r = \dot{z} \tan \theta_e \quad (9.19)$$

Seed bounce in the furrow disrupts the spacing of uniformly metered seeds. Seed bounce can be minimized or eliminated if the x -component of seed velocity relative to the planter is equal to the forward velocity of the planter. Then the seed will drop with zero horizontal velocity relative to the ground.

In the air planter, seeds are pneumatically conveyed from the metering point to the furrow through flexible hoses. It can be shown that the seeds must quickly attain the velocity of the air flowing through the hoses. Thus, the transit time in a hose can be calculated if the length of hose and the air velocity in the hose are known. v_a is the velocity of the air in the hose and if the exit velocity is at an angle θ_e from the vertical, then the horizontal component of the exit velocity relative to the planter will be:

$$\dot{x}_r = v_a \sin \theta_e \quad (9.20)$$

Again, seed bounce can be eliminated by insuring that the horizontal component of exit velocity relative to the planter is equal to the forward speed of the planter. Example Problem 9.4 illustrates the calculation of velocities in drop tubes.

Example Problem 9.4

A precision planter is to plant soybean seeds. The seeds leave the metering device with zero velocity relative to the planter and fall through a vertical distance of 0.5 m through a drop tube to reach the furrow. The barometric pressure is 100 kPa and the air temperature is 20°C. Calculate (a) the vertical velocity of the seed at the exit and (b) the exit angle required if the seed is to have zero horizontal velocity relative to the furrow when the planter speed is 1.8 m/s.

Solution

(a) As in Example Problem 9.3, values are needed for C_6 and C_7 before the fall time can be calculated. The air density is 1.19 kg/m^3 and the air viscosity is $1.835 \text{ N}\cdot\text{s}/\text{m}^2$, as in Example Problem 9.3. From the table of seed properties (Table 9.1 in the Problems section at the end of this chapter), the soybean seed diameter is 0.00676 m and the seed density is 1176 kg/m^3 . However, values are needed for the Reynolds number and drag coefficient before C_6 can be calculated. The fall velocity increases from zero to some as yet unknown value. To permit a solution, we will use the terminal velocity of 13.11 m/s for soybeans (Table 9.1). Then the values for Reynolds number and drag coefficient are:

$$N_{re} = 1.19 \times 13.11 \times 0.00676 / (1.835 \times 10^{-5}) = 5747$$

$$C_D = 26.38 \times 5747^{-0.845} + 0.49 = 0.507$$

The resulting values for C_6 and C_7 are:

$$C_6 = 0.75 \times 0.507 \times 1.19 / (1176 \times 0.00676) = 0.057$$

$$C_7 = (9.801 / 0.057)^{0.5} = 13.11$$

The value for Arg is 1.117 and, from Equation 9.16, the calculated fall time is 0.321 s. Then, from Equation 9.18, the vertical velocity at the exit is 3.09 m/s.

For comparison, a computer simulation using Equations 9.10 through 9.15 gave an exit velocity of 3.0 m/s. Note that this exit velocity is much less than the 13.11 m/s terminal velocity that was used in calculating the Reynolds number. The solution could be repeated while using a velocity of 3.09 m/s to calculate the Reynolds number. At high Reynolds numbers, however, the drag coefficient is so weakly dependent on Reynolds number that a second iteration would change the drag coefficient very little.

(b) From Equation 9.19, the required exit angle to give the seed zero horizontal velocity relative to the furrow is:

$$\theta_e = \arctan(1.8/3.09) = 30^\circ \text{ from vertical}$$

9.2.2.3 Air seeders

The time required to fill seed boxes on individual row units tends to degrade the field efficiency (see Chapter 15) of a planter. Fill time with air seeders is reduced by storing the seeds in a central bin and transporting them to the individual row units pneumatically. The reduction in fill times allows air seeders to have high field efficiency. Theory for doing calculations for pneumatic seed transport is given in Chapter 14.

9.2.2.4 Performance of seed transport mechanisms

Of the seed transport mechanisms discussed in the previous section, the spinning disk provides the least accurate control of seed transport. Since the seeds travel on ballistic paths, wind can disrupt the pattern of coverage. As can be seen from Equations 9.6 and 9.7, both the swath width and the uniformity of the pattern are affected by the rotational speed of the spinning disk. Pattern is affected because the disk speed influences the angle at which the seed departs from the spinner (Equation 9.6); swath width is affected because the disk speed controls the launch speed of the seeds. Spinner speeds typically are in the range from 500 to 600 rev/min. Some typical distribution patterns from centrifugal spreaders are shown in Figure 9.17. By proper overlapping of adjacent swaths, it is theoretically possible to achieve uniform distribution using either the pyramid or flat top patterns.

Seeds are transported through drop tubes when drilling or precision planting. Since drilling does not require precise placement of seeds, drop tubes have only to remain open for acceptable performance. In the usual case in which the furrow openers can move vertically relative to the seed hopper, the drop tubes must accommodate the vertical movement. In precision planting, precise metering is of little value unless the transport process also distributes the seeds uniformly in the rows. Horizontal bounce of the seeds can be eliminated if the seeds are released with zero horizontal velocity relative to the ground (Equations 9.19 and 9.20). Vertical bounce can be reduced by releasing the seeds close to the bottom of a narrow furrow. It is also important that each seed should have the same transit time in the drop tube. Thus, all seeds should have the same initial velocity upon entering the drop tube and random bouncing within

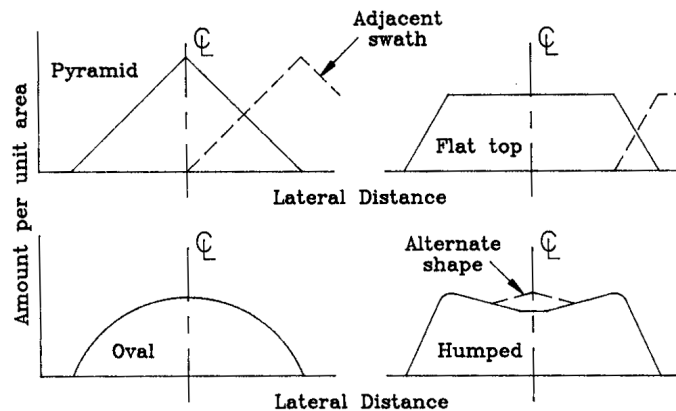


Figure 9.17 – Typical lateral distribution patterns from centrifugal spreaders.

the tube must be minimized. A tube with smooth interior will minimize seed-to-wall friction forces and a tube of small diameter will minimize bouncing within the tube.

9.2.3 Furrow opening and covering

9.2.3.1 Furrow opening and covering mechanisms

Hoes, runners, and single and double disks can be used to open furrows for planting seeds (Figure 9.18). Drills (Figures 9.2 and 9.3) normally employ the single-disk opener to open a furrow. Runner openers were widely used with plate-type planters and are still used on some precision planters. The double-disk opener is now used on many precision planters, either alone or in combination with a runner-type opener. For precision planting, the seeds must be placed at the proper spacing and also at the proper depth. Thus gage wheels (Figure 9.19) are located in close proximity to the furrow opener and seed release point to insure controlled, uniform planting depth. Use of a V-shaped tool to further shape the furrow provides a furrow cross section that minimizes seed bounce (Figure 9.20a and Figure 9.20b). After the seeds are deposited, covering disks (Figure 9.20c) or a scraper may be used to close the furrow. A press wheel (Figure 9.20d) may be used to firm the soil to assure good moisture transfer to the seeds. Alternatively, both covering and soil firming can be accomplished by a set of soil firming wheels (Figure 9.19) which move and firm the soil horizontally and without vertical pressure. A continuous furrow is not opened when the punch planter is used. Rather, spade-shaped wedges on the wheel (Figure 9.21) open holes or “dibbles” in the soil into which the seeds are dropped. Then the press wheel closes the soil over the seeds. The punch planter eliminates the non-uniform seed spacing that results from seed bouncing in a furrow. The spade wheel can roll over and punch through surface residue or other cover. It is the only type of planter that can plant through the plastic covers that are sometimes used in growing high value crops.

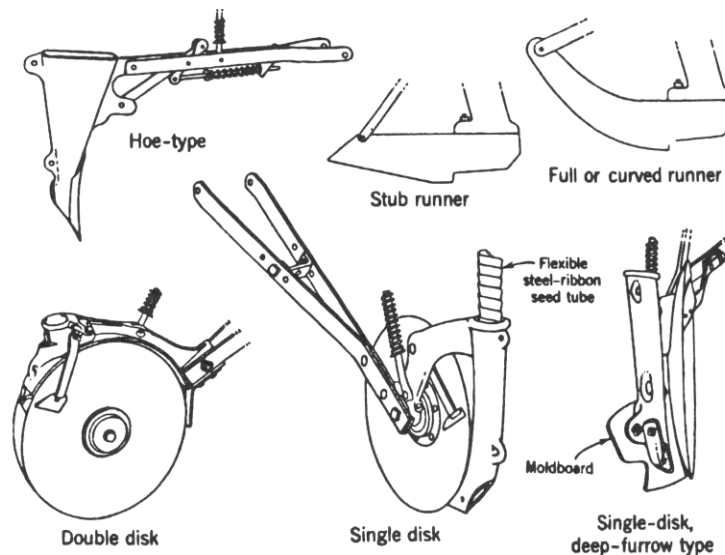


Figure 9.18 – Some common types of furrow openers.

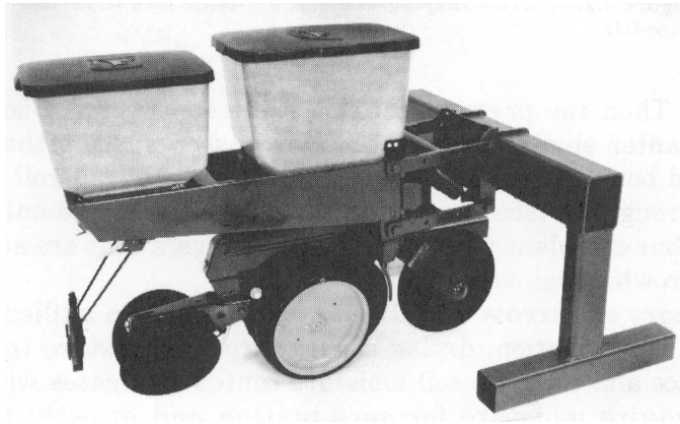


Figure 9.19 – A complete precision planter unit (courtesy of Deere and Co.).

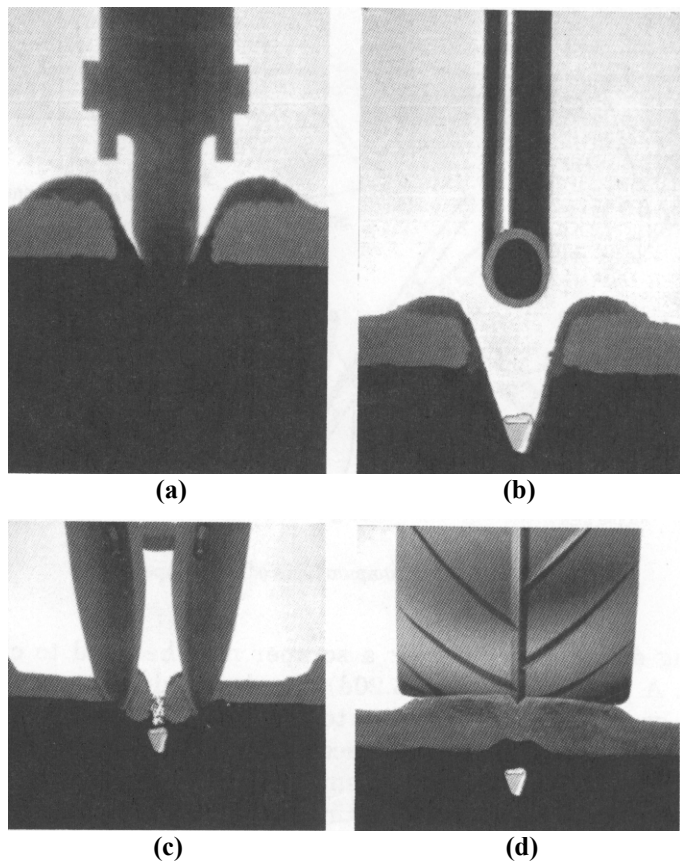


Figure 9.20 – Furrow-shaping and closing techniques (courtesy of CNH).

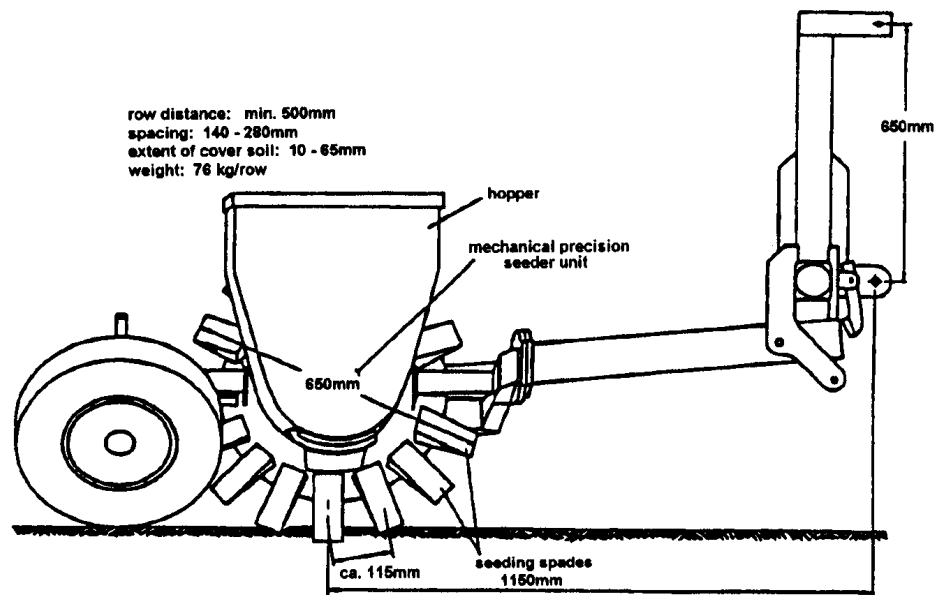


Figure 9.21 – A punch planter
 (courtesy of L.N. Shaw, University of Florida, Gainesville).

9.2.3.2 Theory of furrow opening and covering

In a tilled soil that is devoid of vegetation, drying occurs through moisture transfer to the surface and thus the soil moisture content increases with depth. Seeds require moisture for germination and growth; moisture transfer from soil to seed is promoted by placing the seeds in firm contact with moist soil. Increased depth of planting thus promotes better moisture transfer to the seeds. Choice of an optimum seed depth is a compromise, however, because two factors favor shallower planting. The first is that soil is normally warmer near the surface at planting time and warmer soil promotes seed germination. The second is that a seedling may not have sufficient strength to emerge if the seed is planted too deep in firm soil. Thus there is an optimum depth of planting which varies with type of crop and other factors (Morrison and Gerik, 1985). Typical planting depths, in mm, are: corn, 40-65; cotton, 25-50; grass seeds, 5-10; sorghum, 19-25; soybeans, 25-50; and wheat, 25-50. Theory relating to soil-seedling relationships is beyond the scope of this book, but the reader is referred to publications of a number of researchers who have investigated these relationships (Stapleton and Meyers, 1971; Vaughn and Bowen, 1977; Phene et al., 1978; and Goyal et al., 1980).

9.2.3.3 Performance of furrow opening and covering mechanisms

The most important criterion for judging the success of a furrow opening and covering mechanism is the percent emergence of the seeds that are planted in the furrow. Since percent emergence varies with soil and weather factors that vary from year to year, it is not possible to judge the effect of any given mechanism on emergence based

on data from only one season. However, there are other performance criteria which can be judged based on more limited testing. Many farmers are now using tillage techniques which leave crop residues on the soil surface in order to reduce soil erosion. The furrow openers must be able to cut through these crop residues. Disk-type openers are much better than runner-type openers (Figure 9.18) in cutting through surface residues. In addition, special notched disks may be attached ahead of the furrow opener to clear a path through the residue. The ability of the planter to maintain the desired, uniform depth of planting is an important criterion that may be evaluated using short-term tests.

9.2.4 Transplanting

9.2.4.1 Mechanisms for transplanting seedlings

A successful transplanting system includes the following elements:

1. Planting the seeds in a seedbed or greenhouse trays,
2. Removing the seedlings from the seed bed with or without retaining soil on the roots,
3. Storage of singulated seedlings in a carrier on the transplanter,
4. Feeding the seedlings to the planting mechanism one at a time,
5. Opening a furrow or hole for insertion of the seedlings, and
6. Firming the soil around the roots of the seedlings.

Elements 1 and 2 are not part of the transplanter machine, can be labor intensive, and, if the system is to be successful, must be coordinated with the design of the transplanter. The transplanter itself includes elements 3 through 6 and can also include provision for watering and fertilizing the newly planted seedlings.

On early transplanters (Figures 9.5 and 9.6), only elements 5 and 6 were mechanized; one or more seats were provided on the transplanter for human workers to accomplish item 4. Automated transplanting refers to a system in which element 4 is also accomplished mechanically (Brewer, 1988). One promising method is to grow the seedlings in paper pockets attached to Z-folded strands which, when the seedlings are ready, are loaded into a carrier on the transplanter. Figure 9.22 shows a *Ferris wheel transplanter* in which wheel-mounted grippers grasp each cell (segment of the strand containing one seedling), tear it from the strand, and carry it to the release point in the furrow. A strand restrainer holds the strand so that only one cell is torn away by each set of grippers. The *roll-feed transplanter* of Figure 9.23 also uses Z-folded strands for seedling storage. A pair of feed rolls feeds the strand into a pair of high-speed acceleration rolls that tear away the cells one by one and drop them into a drop chute. The seedlings fall through the chute to the furrow. A pair of firming wheels (see Figure 9.19) can be used to push soil laterally in closing the furrow and firming the soil around the seedlings. The paper cells are biodegradable, leaving only the transplanted seedlings. Transplanters based on the principles illustrated in Figures 9.22 and 9.23 are in commercial production (Suggs et al., 1987).

The dibble transplanter (Munilla and Shaw, 1987) illustrated in Figure 9.24 is similar to the spade planter in that it does not require a furrow. Rather, a seedling bucket dabbles holes in the soil and places a seedling in each hole. Each bucket is pivotally connected to a pair of arms such that the top of each bucket must remain horizontal. At

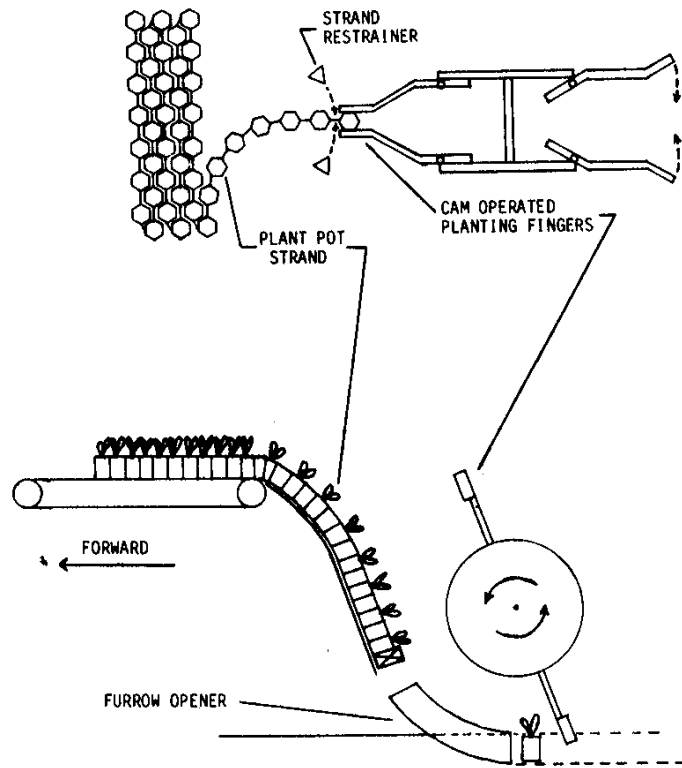


Figure 9.22 – A Ferris wheel feeding mechanism for automatic transplanting (Suggs et al., 1987).

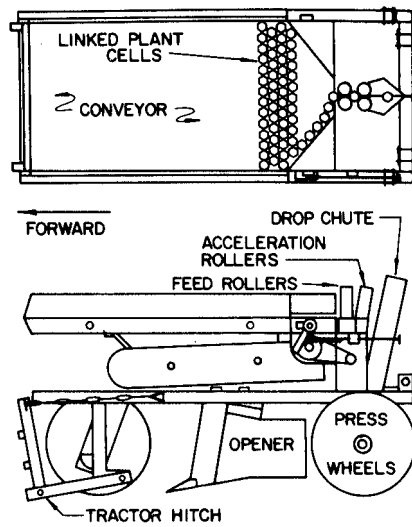


Figure 9.23 – A roll-type feeding mechanism (Suggs et al., 1987).

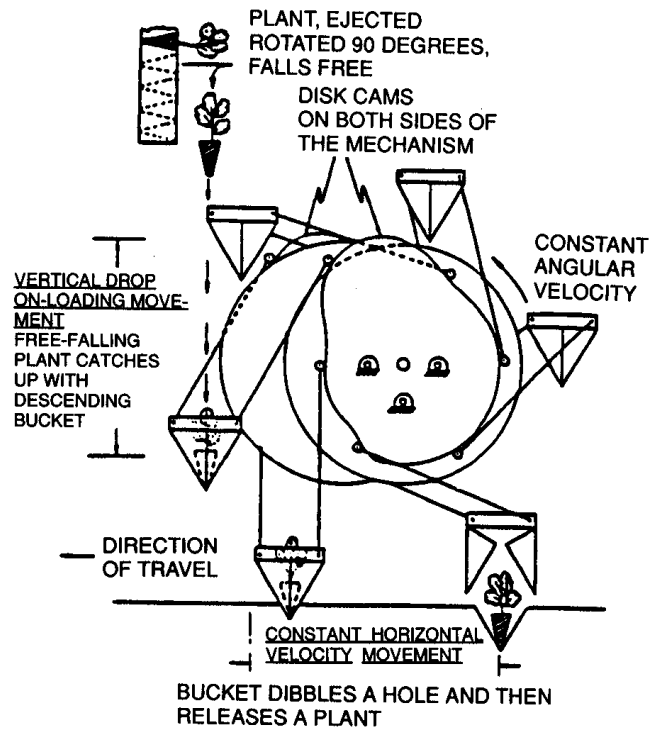


Figure 9.24 – A dibble transplanter (Munilla and Shaw, 1987).

their midpoints, the arms are pivotally connected to rotating disks so that the midpoints of the arms travel on circular paths. The remaining end of each arm follows a cam which is specially shaped to control the movement of the buckets. The rotating disks should be ground driven so that the movement of the buckets is automatically coordinated to the forward motion of the transplanter. The cams are shaped to cause the buckets to descend with zero horizontal velocity relative to the ground. Seedlings released from a carrier fall vertically into the descending buckets. As the dibbles enter the soil, the cams cause the dibbles to continue zero horizontal movement relative to the ground. Just before a dibble is raised from the soil, the bucket opens at the bottom to release the seedling into the hole. The bucket closes as it rises to accept the next seedling, thus completing the cycle.

9.2.4.2 Theory of transplanting machines

Just as precision planters meter individual seeds, transplanters plant individual seedlings. Thus, Equation 9.4 is valid for transplanters if the word seedlings is substituted for seeds. A key limiting factor in the capacity of transplanters is the feed rate, i.e., the rate at which seedlings can be fed into the transplanter. The required feed rate is:

$$R_{st} = \frac{60v\lambda_r}{x_s} \quad (9.21)$$

where R_{st} = required feed rate of seedlings, seedlings/min

v = forward speed of transplanter, m/s

λ_r = number of rows planted simultaneously by transplanter

x_s = seedling spacing along the row, m

Kinematics theory must be used in designing the transplanters shown in Figures 9.22, 9.23, and 9.24. In Figure 9.22, the grippers must close and open at the proper times to grab a seedling cell, carry it to the furrow, and release it in the furrow. The acceleration rolls in Figure 9.23 must tear away a cell and convey it to the chute. The kinematics of these transplanters is beyond the scope of this book. For a complete kinematic analysis of the transplanter shown in Figure 9.24, the reader is referred to the publication by Munilla and Shaw (1987).

9.2.4.3 Performance of transplanters

Seedlings suffer physiological damage when the roots are exposed to air as a part of the transplanting operation. Such seedling shock can be prevented by growing the seedlings in paper, peat, or other biodegradable containers that can be planted with the seedlings. For acceptable capacity, the feed rate of transplanters (Equation 9.21) should be at least 100 seedlings/min. Feeding capacities up to 140 seedlings/min have been observed. Maximum travel speeds have ranged from 0.9 to 1.8 m/s. For a feed rate of 100 seedlings/min, that speed range would accommodate seedling spacings from 0.93 to 1.85 m in a one-row machine or twice that spacing in a two-row machine. For a given feed rate, seedling spacing can be reduced only by reducing the travel speed. Thus, for reasonable seedling spacing, the feed rate clearly limits the maximum allowable travel speed of transplanting machines. A disadvantage of the dibbling transplanter of Figure 9.24 is that the seedling spacing can be changed only if the shape of the cams is changed.

An important performance criterion for transplanters is that the seedlings must be oriented properly and in good contact with the soil. A successful planting has been defined as one in which the seedling is inclined less than 30° from the vertical (Munilla and Shaw, 1987). The transplanters in Figures 9.23 and 9.24 allow the seedlings to be in free fall for a period of time. In the transplanter of Figure 9.24, the seedling then impacts with the descending bucket and the impact must be minimized to prevent shattering of the root clump. Because the seedling was falling into a descending bucket, it was possible to achieve impacts corresponding to only a 50 mm free fall. When the seedling falls into a properly shaped furrow, impacting can be useful in providing more intimate contact between the seedling root clump and the soil in the furrow. Soil firming wheels are usually used on these machines to improve the soil-to-root contact.

9.3 EVALUATING PLANTER AND TRANSPLANTER PERFORMANCE

The rate of application is of interest in the evaluation of any planter and, in addition, the uniformity of seed or seedling placement is often important. ISO Standard 7256, Sowing Equipment—Test Methods, provides detailed guidelines for evaluating planter performance. The statistical formulas provided below are also given in ISO Standard 7256.

9.3.1 Broadcast seeders

Broadcast seeders distribute seeds on the surface of the soil. Two aspects of performance require evaluation. The first is metering accuracy and the second is uniformity of distribution.

Seeders must be calibrated to allow the seeder operator to obtain desired seeding rates. Calibration charts can be prepared based on Equations 9.1 and 9.2. A separate chart is required for each type of seed and travel speed combination. Specifying the type of seed and travel speed fixes the values for ρ_s and v in Equation 9.1. Equations 9.6 through 9.17 can be used in estimating the swath width but, for best accuracy, the swath width should be measured experimentally. With ρ_s , w , and v held constant, the seeding rate then varies proportionally with Q (Equation 9.1) and Q varies proportionally with orifice area (Equation 9.2). The lever that controls the orifice area should be positioned near a numerical scale (Figure 9.7) to allow repeatable orifice settings. Then the numerical scale values can be included in the calibration charts. Although Equation 9.2 can be used to predict the volume flow rate, it is more accurate to measure the flow rate experimentally by collecting a measured volume of seed discharged through the orifice and measuring the time required to collect that volume. The measurements should be repeated for several different orifice openings to obtain an experimentally verified relationship between the orifice setting and the flow rate for each type of seed.

In assessing uniformity of seed distribution, variability can be assumed to exist across the width of the swath. ASAE Standard S341.2, for measuring swath uniformity when broadcasting granular materials, offers guidance in evaluating broadcast seeders. To assess seed distribution uniformity across the swath, a row of shallow trays is arrayed across the swath and the seeder discharges into the trays (Figure 9.25). If q_i is the quantity of seed caught in tray i and there are λ_t trays, then the following equations can be used to assess the uniformity of distribution:

$$\bar{q} = \sum_{i=0}^{i=\lambda_t} q_i \quad (9.22)$$

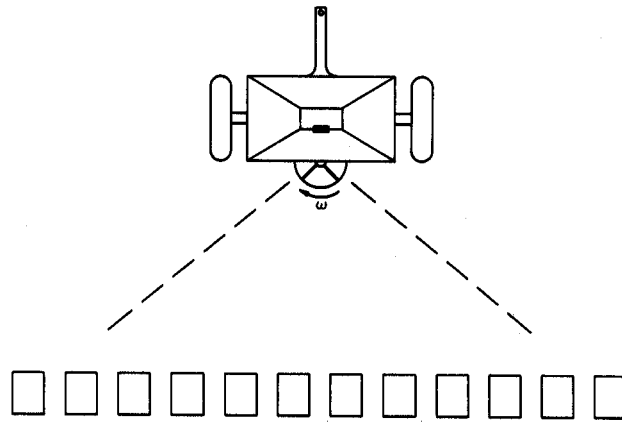


Figure 9.25 – Evaluation of uniformity of broadcast seeding.

and

$$sd = \left[\frac{\sum_{i=0}^{i=\lambda_t} (q_i - \bar{q})^2}{\lambda_t - 1} \right]^{0.5} \tag{9.23}$$

and

$$CV = \frac{100 \, sd}{\bar{q}} \tag{9.24}$$

- where q_i = quantity of seed in tray i , either mass or volume
- λ_t = number of trays
- \bar{q} = average amount in trays
- sd = standard deviation of amounts in trays
- CV = coefficient of variation, percent

The simplest method of testing pattern uniformity is to drive the seeder across the lateral row of trays while the seeder is operating. Since the spinning disk tends to deposit seeds in a circular pattern until the seeder begins moving forward, it is necessary to insure that the full pattern has passed over the seed trays before measuring the quantities in the trays. A perfectly uniform distribution would have a CV equal to zero. With good design, broadcast seeders can achieve a CV in the range from 20% to 30%. Since broadcast seeders cannot produce a rectangular distribution pattern (Figure 9.17), it is reasonable to calculate the CV based on the uniformity created by multiple, properly overlapped passes of the seeder.

9.3.2 Drills

Both the calibration and the distribution of drills require evaluation. The calibration procedure is similar to that for broadcast seeders, except that W is equal to the row spacing. Although Equation 9.3 can be used to predict the volume flow rate, it is more accurate to measure the flow rate experimentally by collecting a measured volume of seed discharged through each metering unit and measuring the time required to collect that volume. The measurements should be repeated for several different cell volumes to establish a calibration chart. Uniformity can be checked in a stationary test in the laboratory by placing the drive wheels of the drill on a treadmill, placing a collection tray under each drop tube, and operating the drill for a fixed time period to accumulate seed in each tray. Then, if q_i is the quantity of seed in tray i , Equations 9.22, 9.23, and 9.24 can be used to calculate the CV as an indication of uniformity. Uniformity can be assessed based on a single pass of the drill, since the patterns are not ordinarily overlapped. Seed metering can be assessed quantitatively, but other aspects of performance are assessed qualitatively. An example of qualitative assessment is the ability of the furrow openers to cut through surface residue in making a furrow.

9.3.3 Precision planters

Precision planters are designed to meter one seed at a time and to place the seeds in a furrow at a desired spacing. It is common practice to check metering accuracy in the laboratory using stationary tests. The drive wheels of the planter are placed on a treadmill and turned at the speed that simulates the desired travel speed. An elongated seed collection device is pulled under the drop tube at the desired travel speed. The collection device must be able to capture the seeds as they exit from the drop tube; in the greased-board technique, sticky grease is placed on a board that is pulled under the drop tube. The grease prevents seed bounce in capturing each seed as it exits the planter. Spacing of the seeds on the greased board can then be assessed, either manually or by an automatic counter. The numbers of skips or multiples can be determined by observation. A skip is created when a cell fails to deliver a seed to the drop tube. Multiples are created when more than one seed is delivered by a cell. Skips and multiples can be reported as a percentage of the total number of cells that passed the drop point during the run. After skips and multiples are removed from the data, the average spacing can be calculated using the remaining data and the average can be compared to the desired average seed spacing. Finally, using Equations 9.22, 9.23, and 9.24, the CV of the seed spacings can be calculated. Perfect metering is achieved when there are no skips or multiples, the CV of the spacings is zero, and the seed spacing is equal to the desired spacing.

Uniformity of planting depth and firming of soil around the seeds are important considerations for precision planters and are assessed during field tests. Futral and Verma (1973) suggest that, ideally, seeds should be placed in a narrow trench of uniform width which has a firm bottom. For many crops, the seed should be covered with approximately 12 mm of compacted soil and the remainder of the furrow should be filled with loose soil. The compacted soil aids moisture transfer to germinate the seed, while the loose soil inhibits moisture transfer and loss through the soil surface. Uniformity of depth can be measured by careful digging to expose planted seeds. Other

observations, such as ability of the furrow openers to cut through surface residue and degree soil firming around the seed, are usually reported qualitatively.

9.3.4 Transplanters

ASABE has not yet established standard procedures for evaluating automatic transplanters. Since seedlings are planted in rows and uniform spacing is desirable, Equations 9.22, 9.23, and 9.24 can also be used to quantify the ability of the transplanter to provide the desired spacing and the uniformity of spacing. In an analogy with precision planting of individual seeds, multiples are very unlikely to occur during transplanting. Skips could occur if the feeding mechanism ruins a seedling or fails to deliver it to the furrow. In successful transplanting, the seedlings should be planted with stems within a specified angle relative to a vertical line, e.g., within 15° of vertical. By measuring these angles for a number of plants, the average angle and standard deviation of the angle can be reported. Depth of planting may also be important; if the seedlings are uniform, depth of planting can be assessed by measuring the length of seedling protruding above the soil and subtracting from the total seedling length. The gentleness of the transplanter in handling the seedlings is also a consideration. Gentleness may be difficult to quantify except through study of survival rate of seedlings. In using survival rates for comparative evaluation of transplanters, it is important to ensure that all transplanters are evaluated under the same environmental conditions, since moisture, temperature and other factors can markedly influence survival rates of seedlings.

PROBLEMS

- 9.1 A centrifugal seeder is to be able to seed any of the top six crops listed in Table 9.1 (next page) at the maximum rate while traveling at a speed of 16 km/h with a swath width of 10 m. (a) What is the largest required flow rate of seeds through the metering orifice? (b) Calculate the required dimensions of the orifice if the orifice is square when open to the maximum. (c) The seeder must also provide the minimum flow rate required for any of the same six seeding jobs in the table. Calculate the minimum flow rate assuming no change in the travel speed or swath width. (d) Assuming the orifice size is reduced by partially covering the orifice, the reduced orifice will be rectangular. Calculate the dimensions of the rectangular orifice for to provide the flow rate of part c.
- 9.2 Similar to Problem 9.1, except now a drill is used to do the planting. The row spacing is 0.18 m and the travel speed is 7 km/h. The seeds are to be metered with a fluted wheel with 12 cells on the periphery (see Figure 9.8). (a) What is the maximum flow rate each fluted wheel must deliver to provide the maximum seeding rate as described in Problem 9.1? (b) How fast must the fluted wheel turn to deliver this flow rate if the maximum volume of individual cells is 155 mm^3 ? (c) Assuming that the fluted wheel speed is the same for all seeding jobs, what fraction of the length of the fluted wheel must be covered to accommodate the minimum flow rate as described in Problem 9.1?
- 9.3 Same as Problem 9.2, except that wheat is to be drilled.
- 9.4 Same as Problem 9.2, except that soybeans are to be drilled.

Table 9.1. Seed properties. Typical data in the table below are for illustrating the design of planters; seed properties may vary from listed values depending on varieties, growing conditions, etc.

Crop	Bulk Density, kg/L	Seed Count, seeds/L	Germ. Rate, %	Seed Rate, kg/ha	Mean ^[a] Diam., mm	Seed Density, kg/m ³	Term. Vel., m/s ^[b]
Alfalfa	0.77	339,000	72-94	8-13	1.53	1184 ^[c]	5.69
Sweet clover	0.77	441,000	73-94	7-11	1.41 ^[d]	1184 ^[c]	5.39
Red clover	0.77	446,000	73-94	7-11	1.41 ^[d]	1184 ^[c]	5.39
Brome grass	0.18	53,800	53-86	17-22	2.08	550 ^[c]	4.55
Orchard grass	0.18	259,000	53-81	9-11	1.59	440 ^[c]	3.37
Tall fescue	0.31	154,000	68-92	13-17	1.82	430 ^[c]	4.64
Wheat	0.68	22,500	80-97	100	4.10	1120	9.81
Sorghum	0.64	21,200	67-77	3-6	3.88 ^[d]	985 ^[c]	8.91
Soybeans	0.77	5,100	85-89	50-90	6.76	1176	13.11
Corn	0.72	2,370	85-95	10-15	7.29	1170	13.61

^[a] Geometric mean = $(\text{length} \times \text{width} \times \text{depth})^{0.333}$.

^[b] Calculated terminal fall velocity in still air at 20°C and 100 kPa.

^[c] Estimated values.

^[d] Calculated based on bulk density, seed count and seed density.

- 9.5 Soybeans are to be planted with a precision planter that meters 54 seeds per revolution of a metering disk; the row width is to be 75 cm and the planter speed is to be 7 km/h. A plant population of 480,000 plants per hectare is desired. Calculate (a) the required seeding rate assuming the lowest seed germination from the above table, (b) the required seed spacing along the row, and (c) the required rotational speed of the metering device. If the rolling radius of the planter wheels is 0.38 m, also calculate (d) the rotational speed of the wheels assuming 10% slip and (e) the ratio of the metering disk speed to the planter wheel speed.
- 9.6 Same as Problem 9.5, except that corn is to be planted for a plant population of 50,000 plants per hectare and the metering device meters 12 seeds per revolution.
- 9.7 Soybeans are to be planted using an air planter (Figure 9.12). Drums are available with 24, 36, 72, 96, 144, and 240 holes per row and rotate at 35 rev/min. If the planter travels at 2 m/s and the row spacing is 0.75 m, calculate (a) the seed spacing and (b) the theoretical seeding rate in seeds/ha for each of the available drums. (c) From data in the seed properties table above, calculate the normal range of seeding rates (in seeds/ha). (d) Which of the drums should be used in this planting application, i.e., how many holes should be in the drum?
- 9.8 Same as Problem 9.7, except that corn is to be planted.
- 9.9 A centrifugal spreader similar to Figure 9.15 is to be designed. The known specifications of the spinner are:

$$\begin{array}{lll} r_i = 0.05 \text{ m} & \delta = 0 \text{ radians} & \omega = 50 \text{ rad/s} \\ f = 0.28 & \alpha = 0.25 \text{ radians} & r_o = 0.15 \text{ m} \end{array}$$

- Using the spreadsheet “Spinning Disk Spreader Design” (on the CD-ROM), calculate (a) the angle of disk rotation during which the seeds will be in sliding contact with the disk (note that angle also specifies the gate location if the seed is to leave the disk at the point shown in Figure 9.15), (b) the velocity of the seeds relative to the blades at the outer edge of the disk, (c) the horizontal component of velocity, v_{hr} , as the seed leaves the spinner, and (d) the vertical component of velocity, v_g , relative to the disk as the seed leaves the spinner.(e) Compute and plot the trajectory of an alfalfa seed launched from the spinner.
- 9.10 Using the spreadsheet of Problem 9.9, determine the spinner rotational velocity needed to result in a horizontal trajectory of 5 m when spreading brome grass.
 - 9.11 Same as Problem 9.9, except that the coefficient of friction is 0.15.
 - 9.12 Same as Problem 9.9, except that the disk speed is 40 rad/s.
 - 9.13 Same as Problem 9.9, except that $\alpha = 0.1$
 - 9.14 Same as Problem 9.9, except that $\alpha = 0$.
 - 9.15 Equation 9.11 can be used to calculate the terminal velocity of seeds, i.e., the value of fall velocity that gives zero vertical acceleration when the velocity is zero in the x-direction. Typically, the terminal velocity and Reynolds number for seeds are sufficiently large that Equation 9.13 must be used to calculate drag coefficient and the solution for terminal velocity must be done iteratively. Using data from the above table of properties for seeds, use Equations 9.11 and 9.13 to verify that the listed terminal velocities are correct, i.e., that they give negligibly small vertical accelerations.
 - 9.16 Calculation of a seed trajectory requires a value for drag coefficient. The drag coefficient can be calculated from Reynolds number using Equation 9.12 or 9.13, but note that Reynolds number changes with seed velocity. The seed velocity begins losing velocity at point of release from the spreader, at which point it may be traveling 15 m/s or more, but never slows below its terminal velocity. Therefore, for each of the seeds listed in the above table, (a) calculate and plot Reynolds number versus seed velocity for velocities ranging from 15 m/s down to terminal velocity. (b) Also calculate and plot the corresponding drag coefficient versus velocity for each seed. (c) Note that the drag coefficient will vary as the seed moves through its trajectory. For each seed, estimate the average height of the seed curve, i.e., the best value of drag coefficient to represent the entire trajectory of the seed.
 - 9.17 Assuming that a centrifugal seeder releases alfalfa seeds at a height of 0.9 m and at an initial velocity of 9 m/s horizontally, calculate (a) the time of flight and (b) the horizontal distance traveled. Use data from Table 9.1 and a drag coefficient as discussed in Problem 9.16. Note that sweet clover and red clover have properties similar to alfalfa and should have similar trajectories.
 - 9.18 The situation is the same as in Problem 9.17, except that you are to develop a computer program based on Equations 9.10 and 9.11 to simulate the flight of the seed. The program should be designed to accept input data that will allow it to simulate the trajectory of any of the seeds in the table.
 - 9.19 Same as Problem 9.17, except use brome grass. Note that orchard grass and tall fescue have somewhat similar properties to brome grass.

- 9.20 Same as Problem 9.17, except use sorghum.
- 9.21 Same as Problem 9.17, except use soybeans.
- 9.22 After seeds are released by the metering unit in a precision planter (Figure 9.14), they fall through a drop tube whose vertical length is 0.6 m and which curves rearward to give the exiting seeds a rearward velocity relative to the planter. Assuming that the seeds being planted are corn, calculate (a) the time required for the seeds to fall through the drop tube, (b) the vertical fall velocity at the exit of the tube, and (c) the required exit angle, θ_e , to give the seeds zero horizontal velocity relative to the ground if the planter speed is 2 m/s. (Use a drag coefficient as discussed in Problem 9.13).
- 9.23 Same as Problem 9.22, except soybeans are being planted.
- 9.24 Same as Problem 9.22, except sorghum is being planted.
- 9.25 Seeds from an air planter (Figure 9.12) are transported through hoses to the furrow. If the 4 kPa pressure in the seed drum produces a seed velocity of 3.5 m/s at the exit of the hose and the planter is moving forward at 12 km/h, at what angle from the vertical, θ_e , should the tube be directed rearward to produce zero horizontal velocity of the seed relative to the ground?
- 9.26 Same as Problem 9.25, except planter speed is 8 km/h.
- 9.27 A one-row transplanter is to transplant strawberry plants at a spacing of 0.15 m within the row and with a 0.75 m row spacing. (a) If the feeding mechanism can deliver up to 100 seedlings/min, what is the maximum allowable travel speed of the transplanter? (b) What is the maximum allowable speed if the transplanter is a two-row machine? (c) Calculate the area (in m^2) covered by the one- and two-row machines. (d) Is there any advantage in using a two-row machine in this case if only one feeder serves both rows?
- 9.28 A row of 10 square trays, each 15 cm by 15 cm in size, are arrayed across the 20 m swath of a centrifugal seeder which is seeding alfalfa. After passage of the seeder, the following amounts of seed (in mg) are found in trays one through ten, respectively: 20.0, 32.8, 32.0, 30.5, 29.3, 29.1, 30.3, 31.5, 32.7, 23.5. Calculate (a) the mean, (b) the standard deviation, and (c) the coefficient of variation of the amounts of seed in the trays. (d) Also calculate the average seeding rate across the swath in kg/ha. (e) Compute a 95% confidence interval for the seeding rate in kg/ha.
- 9.29 Same as Problem 9.28, except orchard grass is being seeded and 18 cm by 18 cm trays are arranged across a 14 m swath. The amounts of seed in the trays are as given in Problem 9.28.

Relevant websites

(Warning: The following websites were relevant at time of publication of the book, but webmasters are free to change or eliminate websites at any time).

<http://www.pioneer.com/usa/agronomy/Precision.htm>

<http://www.ext.vt.edu/pubs/bse/442-456/442-456.html>

http://www.deere.com/en_US/ProductCatalog/FR/series/planting_seeding_air_seeders.html

CHEMICAL APPLICATION

10

INTRODUCTION

The purpose of applying agricultural chemicals is to provide nutrients for plant growth and to control weeds, insects and other crop pests, and plant diseases. Proper application of agricultural chemicals is crucial in successful modern agriculture. Agricultural chemicals, over the years, have become more sophisticated but also more expensive, so good methods avoid over-application. The major classifications of agricultural chemicals are fertilizers, pesticides (including insecticides, which kill insects), herbicides (which kill plants), fungicides (which kill fungi), growth regulatory hormones, and pheromones for biological control of insects. These chemicals may be either dry or liquid. The chemicals may be applied before planting during seed bed preparation, during planting, and/or after germination during the active growth period.

In this chapter we will discuss the chemical application methods and related equipment, their functional components and operating principles, equipment calibration, testing, and other related topics.

10.1 APPLICATION OF GRANULAR CHEMICALS

Dry chemicals in agricultural use are primarily fertilizers, herbicides, and insecticides. Technically many of these are powders; however, powders that are large in particle size and flow easily—as is the case with these agricultural chemicals—are referred to as granular material. That is the term used in this book. There are some agricultural chemicals that are non-granular powders of small size, such as insecticide powders applied by dusters. Because of drift and poor coverage these are of limited use in commercial farming. Better choices include liquid pesticides or granular pesticides that are liquid chemicals impregnated on inert granular carriers such as clay, sand, or corncobs.

Application of dry granules has certain advantages. It eliminates the need to haul water and the mixing required with liquid chemicals. Chemical drift, i.e., droplets that do not land on the intended target, is generally not as great a problem as it can be with liquids. The application equipment is less expensive and more trouble-free since no mixing, pumping, and agitation is involved. While practicing conservation tillage, better control is possible with granules than sprays since granules filter through the foliage onto the soil. Also, granules are generally safer to use than liquid formulations.

However, granular material is generally more expensive than the liquid chemicals. Granular material has poor metering characteristics and uniform distribution is a problem. The use of granules is limited to soil applications as they require moisture to become activated. Granular pesticides must be kept in a dry place and they are more bulky to store and transport.

Traditional granular pesticide rates have been 12 to 24 kg/ha (15 to 30 lb/acre) with 5% to 15% active ingredient. With the availability of granular pesticides that are 20% to 50% active ingredient there is a trend toward lower rates of application. Some new formulations have 75% to 90% active ingredient with a recommended application rate as low as 1.12 kg/ha (1 lb/acre). With increases in the concentration of active ingredients, there has been a shift toward smaller granular particles. Smaller particles tend to give better coverage by increasing the number of particles per unit area, but they are more prone to drift.

10.1.1 Methods for application of granular chemicals

Granular fertilizer may be spread uniformly over the entire field, in a *broadcast application*, or it may be applied in narrow rows, which is called a *banded application*. It may be applied before planting, during planting, or in established crops.

Pre-planting applications include applying the material either on the soil surface or placing it below the surface using an appropriate tillage attachment. Material applied on the surface may be incorporated into the soil using an appropriate tillage tool (generally a field cultivator or a disk harrow) as part of normal seed bed preparation. Fertilizers may be placed deep into the soil with a chisel type cultivator. A fertilizer distributor may be used as an attachment to a plow that places it in the furrows below the surface at plowing depth.

Application during planting is commonly done by fertilizer drills. Hoppers, tubes, and furrow openers are built in the drills to place the fertilizer below and to the side of the seed rows. Similarly, row-crop planters have attachments to place fertilizers in a narrow band on either side of the seed row. The furrow openers for fertilizer are separate from the seed furrow openers and they can be adjusted independently in the vertical and horizontal directions.

Application in established crops puts chemicals either on the surface or below the surface of the soil. The method of application depends upon the crop and the planting type. In solid-planted crops, fertilizers may be surface applied using either a drop-type or a rotary spreader. In row crops, granular chemicals may be banded between the rows or applied on either side of the rows as *side dressing*.

10.1.2 Equipment for application of granular chemicals

The equipment for applying granular material includes drop-type (gravity), rotary (centrifugal), and pneumatic (air) spreaders. Equipment may be drawn behind tractors or mounted on trucks or aircraft.

Drop-type spreaders may be either for broadcast application or for banded application. A truck-mounted drop-type spreader for broadcast application with a 15.24 m (50 ft) boom is shown in Figure 10.1. Tractor drawn units have 2.4 to 3.7 m (8 to 12 ft) long hoppers with narrowly spaced openings in the bottom. The openings are gener-



Figure 10.1 – A drop-type fertilizer distributor (courtesy of Ag-Chem Equipment Co.).

ally 150 mm apart. A ground-wheel-driven shaft located inside the hopper near the bottom carries agitators to help flow the material. A slide gate is used to control the openings and to shut off flow during turnaround. A drop-type applicator for banded application is shown in Figure 10.2. This applicator utilizes several small hoppers as compared to one long one. The material is metered and dropped through a tube and is spread in a wide band by a diffuser. Some fertilizer distributors have furrow openers to place the material below the surface. This type of spreader is most commonly used as an attachment to planting equipment.

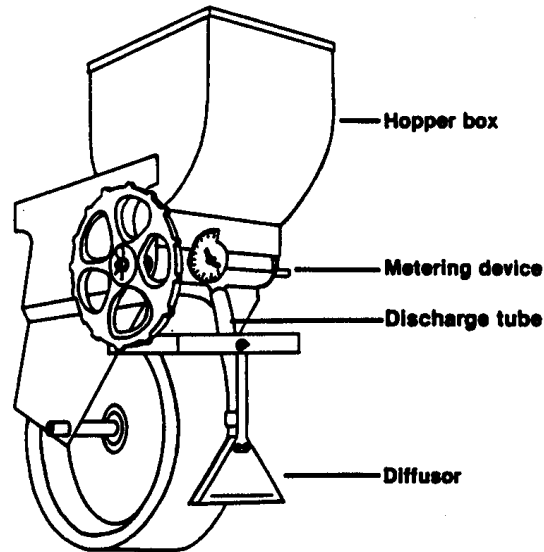


Figure 10.2 – A drop-type applicator for banded application (reprinted from Bode and Pearson, 1985).



Figure 10.3 – A truck-mounted commercial rotary applicator (courtesy of Ag-Chem Equipment Co.).

Rotary spreaders are used for broadcast application. These spreaders have one or two rotating disks with multiple vanes to impart energy to the granules. The material is metered onto the disks and is thrown wide due to the centrifugal force. Rotary spreaders are generally tractor mounted, but some of the larger commercial units are truck mounted with twin spinners as shown in Figure 10.3. The trucks used for chemical application use high flotation tires.

Pneumatic applicators can be used for either broadcast or banded application. They have a centrally located hopper from which granules are metered, delivered by air through tubes across the width of the machine, and spread by being impinged onto deflector plates. Pneumatic applicators allow central tank filling, easier installation on tillage implements, improved distribution, and easier transporting of trailer mounted applicators. A pneumatic applicator is shown in Figure 10.4.

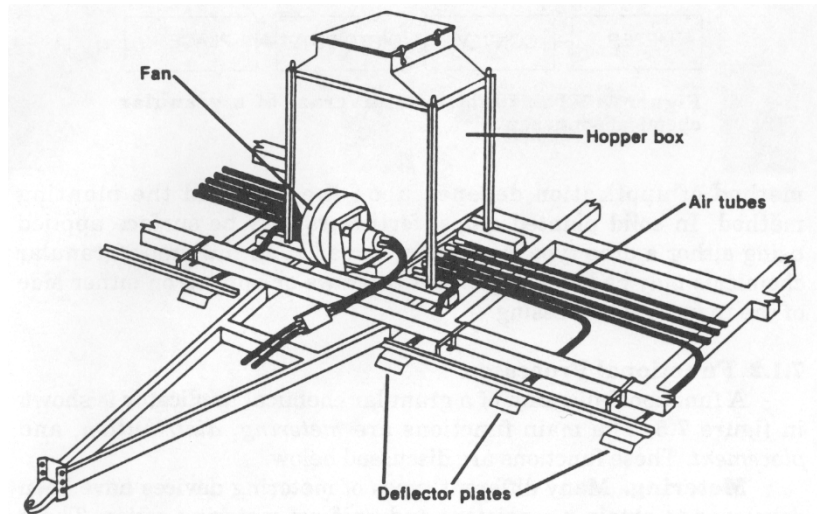


Figure 10.4 – A pneumatic applicator (reprinted from Bode and Pearson, 1985).

Aircraft are used to broadcast fertilizers in areas that are either too large or too difficult (rough terrain, flooded rice fields) for ground rigs. Airplanes carry a maximum payload of 500 to 1100 kg at working speeds of 130 to 190 km/h. The height of application usually varies from 9 to 15 m. *Ram-air spreaders* located underneath the fuselage consist of an air scoop, a venturi or restricted-throat section where the material is introduced, and a diverging section with dividers to give the proper lateral velocity components to the material being carried by the air streams. The air stream is generated by the propeller blast. Many ram-air spreaders give a trapezoidal distribution pattern that allows for a fairly uniform application with proper overlap at swath widths of 12 to 14 m. At application rates above 280 kg/ha (250 lb/acre) the particles are not accelerated properly and the distribution is not very uniform. The uniformity of application is also severely affected by crosswinds. Rotary spreaders are also used in aircraft applications. The spinners used in aerial applications rotate at a much faster speed as compared to the ground rigs in order to cover a much broader swath. Helicopters are used in areas where fixed-wing aircraft are not suitable, such as rugged, hilly terrain that is far away from a suitable landing site. The operating cost of helicopters is 2 to 3 times higher compared to fixed-wing aircraft.

10.1.3 Functional processes of granular chemical applications

A functional diagram of a granular chemical applicator is shown in Figure 10.5. The main functions are *metering*, *conveying*, *distribution*, and *placement*. These functions are discussed below.

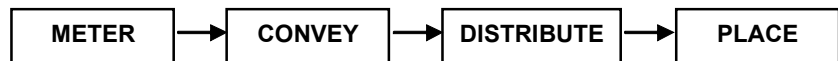


Figure 10.5 – The functional diagram of a granular chemical applicator.

10.1.3.1 Metering

Many different types of devices have been developed to obtain a consistent and uniform metering of granular chemicals. These devices are generally driven by a ground wheel that stops metering when the implement is stopped or lifted off the ground. Metering devices may be divided into *positive flow* and *gravity flow*. Positive flow metering devices provide for more accurate metering because a cavity is used to meter a certain volume of fertilizer (or other material). The rate of movement of the cavity determines the metering rate. Gravity flow devices rely on the orifice size to meter the flow rate. These differences are discussed in the following sections.

The *star-wheel feed* metering device (Figure 10.6) is used on some grain drills and a few row crop side-dressing attachments. Fertilizer, carried between the teeth of the feed wheel, falls into the delivery tube by gravity while material carried on top of the wheel is scraped off into the delivery opening. The discharge rate is controlled by raising or lowering a gate above the wheel.

Metering devices for some row-crop attachments have horizontal *rotating bottom plates* that fit up against the stationary bottom ring of the hopper base (Figure 10.7). The discharge rate is controlled by an adjustable gate over a side outlet. Sometimes there are two outlets permitting two bands from one hopper.

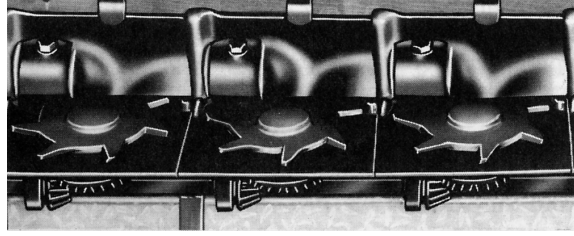


Figure 10.6 – Star wheel metering mechanism of a grain drill (reprinted from Kepner et al., 1978).

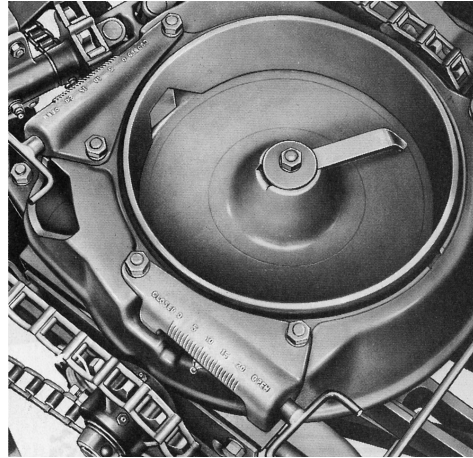


Figure 10.7 – A rotating bottom metering device (reprinted from Kepner et al., 1978).

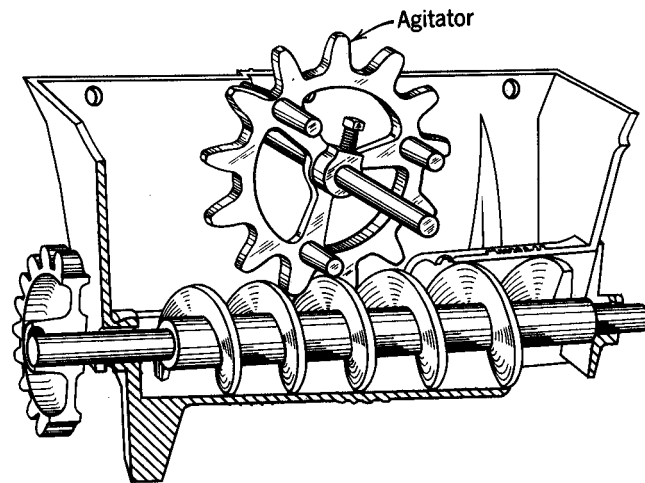


Figure 10.8 – A metering device with close fitting auger (reprinted from Kepner et al., 1978).

Auger-type metering devices are illustrated in Figures 10.8 and 10.9. The type shown in Figure 10.8 has a close-fitting auger tube and the auger has relatively large displacement per revolution. The loose-fitting or floating-auger arrangement shown in Figure 10.9a is widely used on row-crop attachments. The inside diameter of the tube is about 12.5 mm greater than the auger diameter. Each of the two auger sections move the material toward one end of the hopper, where it is discharged from the end of the tube or dropped through an outlet opening. One hopper serves two rows. Augers are easily removed for cleaning.

Figure 10.9b shows a variation of the *loose-fitting auger* principle in which the material enters the auger tube from the top instead of from the end, is transported a short distance through the chute, and is then discharged from a bottom outlet. The tube assembly forms the bottom of the hopper and is removable. A series of openings along the tube provide multiple outlets for row crop use or for drop-type broadcasters. With any of the auger-type metering devices, the discharge rate is adjusted by changing the speed ratio between the auger and the ground wheel.

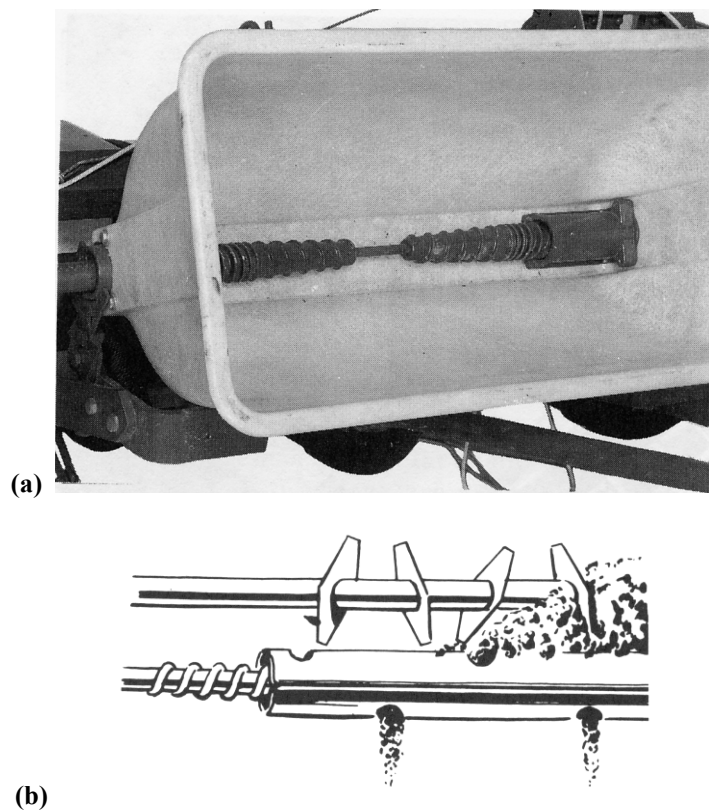


Figure 10.9 – Metering devices with loose-fitting auger (a) for row-crop attachments, (b) for row-crop attachment or drop-type broadcasters (reprinted from Kepner et al., 1978).

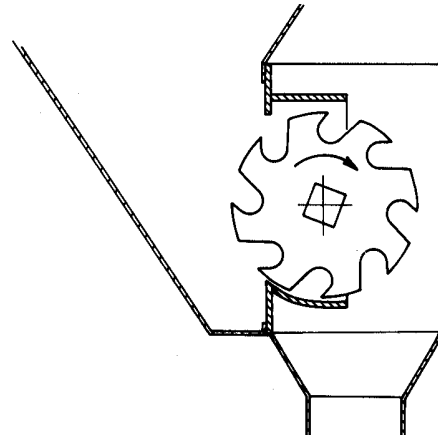


Figure 10.10 – An edge-cell vertical rotor metering device (reprinted from Kepner et al., 1978).

An *edge-cell, positive-feed metering device* is shown in Figure 10.10. Metering wheel assemblies are spaced as required along the hopper and are driven by a common shaft. Rotor widths ranging from 6 mm to 32 mm are employed for different rate ranges. The discharge rate for a given rotor is controlled by changing the rotor speed.

Belt-type metering devices are sometimes employed where relatively large application rates are required, as on rotary broadcasters with large hoppers. Some units have a flat wire belt (usually stainless steel) that drags the material along the hopper bottom (Figure 10.11) and others employ rubberized fabric belts. The discharge rate is controlled by an adjustable gate above the belt. The discharge can be split into two or more streams if desired.

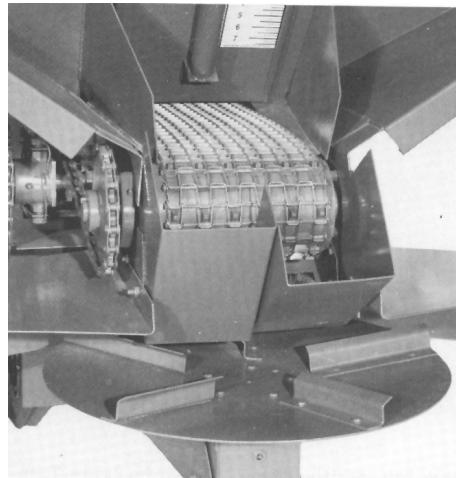


Figure 10.11 – A wire-belt metering device on a centrifugal broadcaster (reprinted from Kepner et al., 1978).

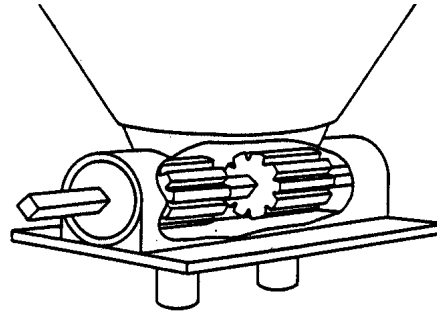


Figure 10.12 – A positive feed fluted roll type metering device (reprinted from Bode and Pearson, 1985).

Fluted metering devices are used for most granular-pesticide applicators. They consist of a ground-driven *vaned* or *fluted rotor* above an adjustable discharge opening (Figure 10.12). Hoppers for row crops sometimes have two or four openings whose outputs can be used separately or combined. Rotors fit closely in the hopper bottoms thus providing positive shut-off when the rotor is not turning.

Ideally, the discharge rate should be proportional to the rotor speed so that the application rate will not be affected by the forward speed. Tests have shown that this is not the case. Also, discharge rates are not proportional to the forward speed. This is due to incomplete filling of the inter-vane cavities, which is affected by the material flow characteristics. Fluted metering devices, like many other devices, produce a cycle variation in the uniformity of the application rate.

Gravity flow metering devices are common on drop-type broadcasters (Figure 10.13). In gravity flow devices, as opposed to the various positive flow metering devices discussed above, the metering rate is controlled by adjusting the size of the openings. A rotating agitator breaks up lumps and moves the material across the opening to assist in feeding. Rotating broadcasters have hoppers of a size that can be tapered down to a small bottom area and usually employ stationary-opening metering devices. Gravity metering devices are sensitive to ground speed.

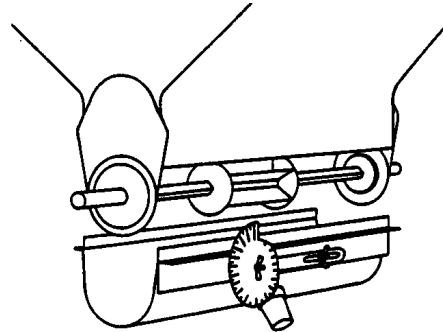


Figure 10.13 – A gravity flow metering device (reprinted from Bode and Pearson, 1985).

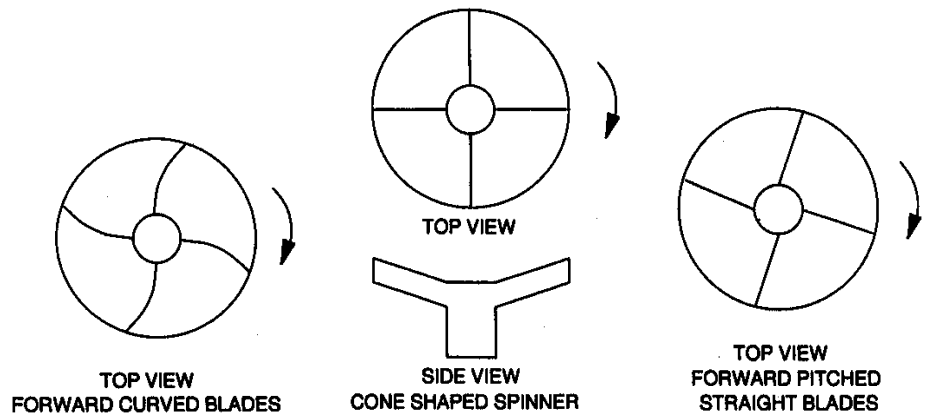


Figure 10.14 – Different types of spinners for rotary spreaders.

10.1.3.2 Distribution

Devices to distribute dry chemicals are of three main types: rotary, gravity, and ram-air spreaders.

Rotary spreaders usually consist of a single or a double counter-rotating horizontal spinner. The direction of rotation is such that the adjacent sides in the counter-rotating spinners move the material rearward. The spinners have blades that may be radial, forward pitched, or rearward pitched with respect to the radius. The blades may be either straight or curved. Forward-pitched blades give greater carrying distances for free-flowing materials, while rearward-pitched blades unload sticky material (e.g., moist lime) more readily. These spinners are shown in Figure 10.14. Rotary spreaders are used with broadcast types of applicators. A stream of granular material is dropped on the spinner and is thrown out by the action of centrifugal force. For a double spinner the stream is usually split in two by an inverted v-shaped splitter.

Gravity diffusers are made of an inverted v-shaped housing made of either plastic or sheet metal at the bottom of the drop tube. The housing has distributing vanes or other parts that take the stream of granular material and distribute it evenly into a wide band. Unlike rotary spreaders, the gravity type diffusers apply chemicals in more controlled manner and, therefore, they are more suitable as attachments to row-crop planters and cultivators. They are also available in open field fertilizer drills for full coverage of the field. Figure 10.15 shows various gravity type diffusers.

Ram-air spreaders are found in aircraft equipment. These are located in the propeller blast beneath the fuselage. A spreader of this type consists of an air scoop, a venturi or restricted-throat section where the material is introduced, and a diverging section with dividers to give the proper lateral velocity components to the material being carried by the air streams. Many different designs of the ram-air distributors have been developed. Most of those for spreading fertilizers or seeds are 910 to 1140 mm long, have a throat 610 to 760 mm wide and 150 to 200 mm high, and have a discharge area at least twice the throat area. The discharge angle for the outer sections is usually at least 45° from the line of travel.

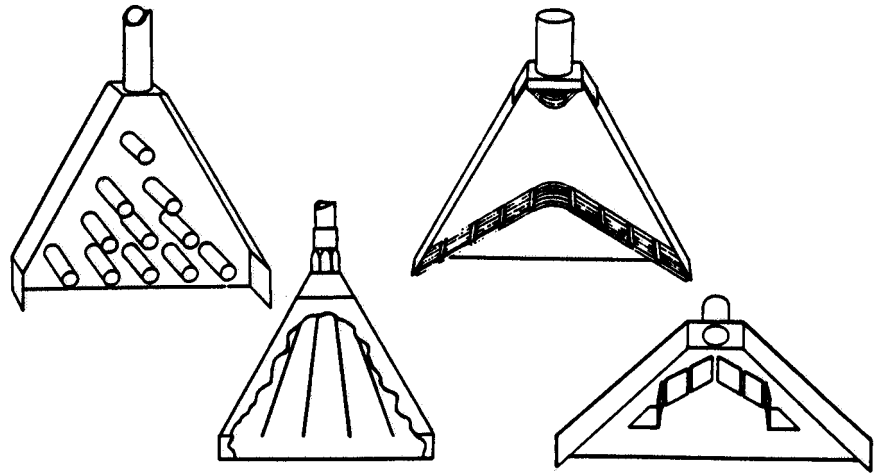


Figure 10.15 – Various types of diffusers used in drop-type applicators (reprinted from Bode and Pearson, 1985).

Many of the ram-air spreaders give a trapezoidal distribution pattern with a fairly flat top so that reasonably uniform distribution can be obtained with proper overlap at swath width of 12 to 14 m. However, as the material flow rate increases, the air velocity through the spreader is decreased and there is less energy available to accelerate the particles. Consequently, distribution patterns are poor for discharge rates greater than 900 kg/min. Another limitation of the ram-air distributors is the high aerodynamic drag and power requirement (Yates and Akesson, 1973).

Uniformity of coverage is one of the most important performance criteria. The horizontal distance through which the particles are thrown is affected by the particle size, density, and shape in addition to the spinner speed and geometric configuration. The components of a dry blend tend to separate as the larger particles of the same density travel farther. Wind also affects the carrying distance, and hence, the distribution pattern.

Uniformity of application is influenced by the shape of the pattern from the spreader and by the amount of overlap. Most patterns from rotary spreaders can be approximated by one of the shapes shown in Figure 9.17 (Chapter 9). Theoretically, pyramid, flat-top, and oval patterns give a uniform distribution if they are symmetrical, straight-sided, and overlapped as shown. The pyramid pattern allows more leeway for driving error. Humped patterns are undesirable from the standpoint of uniformity, but of the shapes shown would give reasonably uniform distribution, if the swath width were not over 40% of the overall pattern width, or if there were 60% overlap.

10.1.3.3 Placement

Placement devices may apply the chemical on the surface or below the surface. Surface applications are often incorporated into soil by a tillage tool if done before planting. On growing crops, especially solid-planted crops, a chemical is nearly always applied as top dressing and not incorporated into the soil. Fertilizer may be placed below the surface by a planter or a cultivator, or placed deep in the soil using chisel plows, or drilled into established pastures and other sods with special equipment.

Banded placement during row-crop planting is accomplished with applicators that are independent from the seed furrow opener. Double-disk, single-disk, and runner-type openers, similar to seed furrow openers, are often used.

Fertilizer grain drills often deliver the fertilizer through the seed tube, placing it in direct contact with the seeds in furrow. Separate disk openers are sometimes provided in front of the seed openers so that the seed row is not disturbed.

10.2 APPLICATION OF LIQUID CHEMICALS

Liquid chemicals include fertilizers, herbicides, pesticides, and growth-regulating hormones. These may be water emulsions, solutions, or suspensions of wettable powders. Liquid pesticides may be either *contact* or *systemic* type. Contact pesticides kill insects, fungi, etc., by coming in contact. To be effective, full coverage of the target, normally achieved by smaller droplets, is necessary. Systemic pesticides are taken in by the plant and they translocate within the plant. Full coverage of the plant is not required and larger droplets that are less prone to drift are acceptable.

10.2.1 Methods for application of liquid chemicals

Liquid chemical application methods vary depending on whether they are applied pre-planting, during planting, or post-planting. Pre-planting applications generally are fertilizers and herbicides and may include subsurface or surface application. Applications of aqua ammonia and anhydrous ammonia fertilizers are usually subsurface. Their application is accomplished by means of specially designed knives or chisel injectors. Liquid chemicals applied during planting generally include fertilizers and herbicides. Post-planting chemical applications may include fertilizers and all types of pesticides.

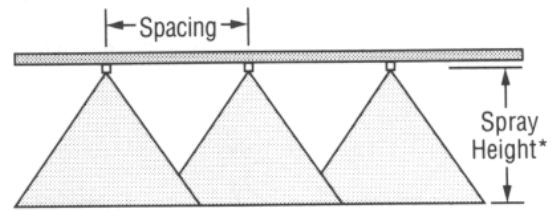
Liquid chemical application methods may be further divided based on the area covered. This may be *broadcast*, *banded*, and *directed spray*. In a broadcast application the chemical is applied uniformly on the ground or on the crop. In banded application the chemical is applied in narrow bands or strips. Several nozzles are used in directed spray for row-crop applications for a more complete coverage of the plants. Figure 10.16 shows the three methods of application.

10.2.2 Equipment for application of liquid chemicals

10.2.2.1 Sub-surface application

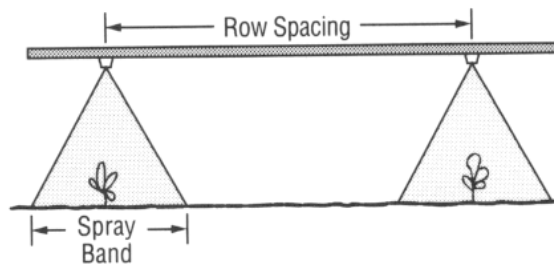
Sub-surface application is generally used for liquid chemical fertilizer in the form of anhydrous ammonia or aqua ammonia. These are called *pressure liquids* because they have a high vapor pressure that is used to create flow. *Anhydrous ammonia* contains 82% nitrogen and its boiling point is -28° F. When water is added to anhydrous ammonia to reduce the vapor pressure it is called *aqua ammonia*. It contains only 20% to 25% nitrogen, has a higher boiling point, and is termed *low pressure liquid fertilizer*.

With anhydrous ammonia, aqua ammonia (as well as other liquids with high vapor pressures), it is essential that the material be released in narrow furrows and

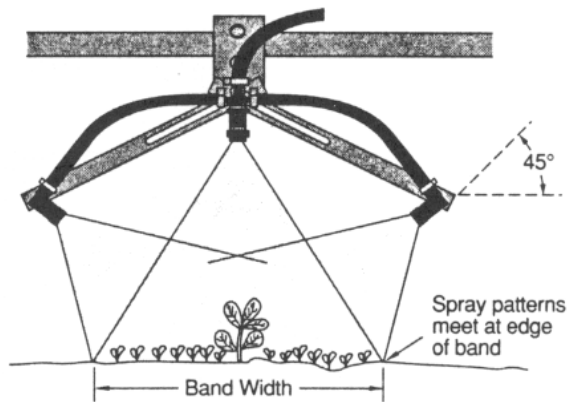


* Adjust spray height in the field to overlap approximately 30% of each edge of pattern.

Broadcast



Banded



Directed

Figure 10.16 – Methods of liquid chemical application (courtesy of Spraying Systems Co., 1991).

covered immediately to prevent escape. Anhydrous ammonia should be released at a depth of at least 10 to 15 cm. Aqua ammonia is applied about 5 cm below the surface since it is not as volatile. A loose, friable soil with adequate moisture is important for good sealing and for absorption of ammonia on the soil particles. Under some conditions press wheels or some other covering devices follow immediately behind the applicators.

Figure 10.17 shows a schematic of a trailing ammonia applicator. Note that there is no pump in the system, as the vapor pressure of the ammonia is used to pump the liquid. A regulator valve is needed to control the flow as the vapor pressure varies with the amount and concentration of ammonia in the tank and with temperature. For example, at 15.6° C the vapor pressure is 620 kPa (93 psi) but at 37.8° C the pressure rises to 1.3 MPa (197 psi). For subsurface application of aqua ammonia a pump is necessary because of its lower vapor pressure.

A typical narrow applicator blade for sub-surface applications is shown in Figure 10.18. The liquid is discharged from holes in the sides of the delivery tubes near the lower end. The spacing of the knives depends on the crop being grown.

Ground driven, variable stroke pumps are also employed to meter ammonia. Both mounted and pull-type implements are available for applying pressure liquids.

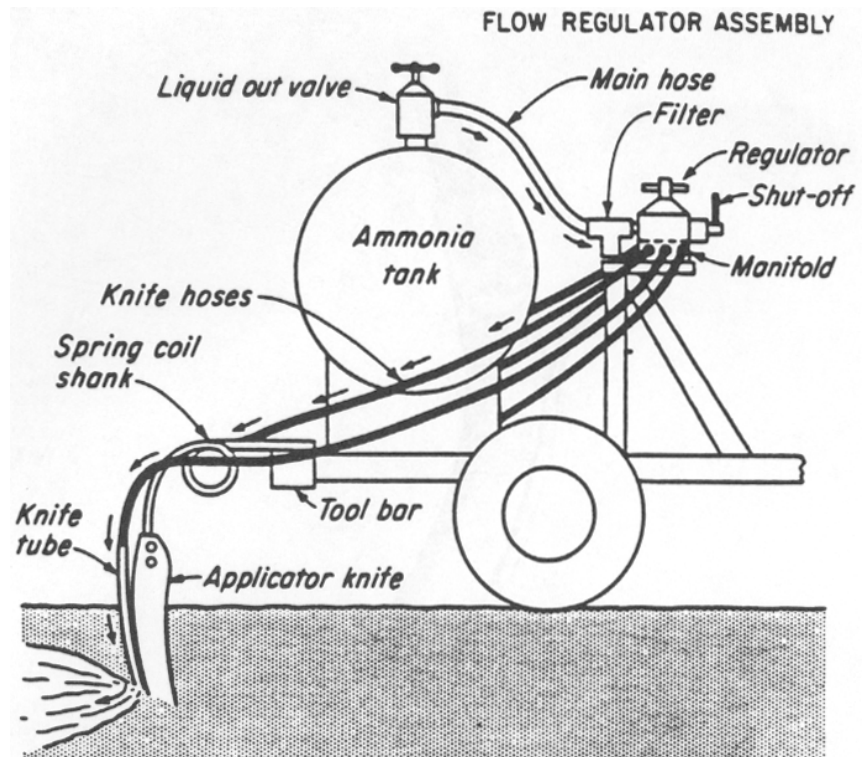


Figure 10.17 – A schematic of a trailing ammonia applicator (reproduced from Smith, 1964, by permission of McGraw-Hill Book Co.).

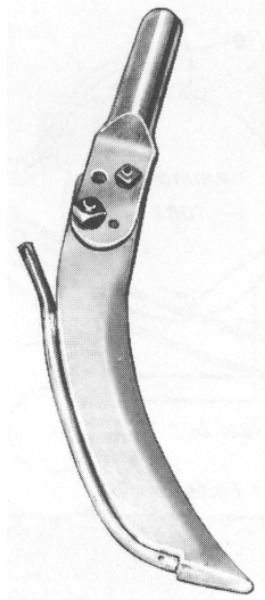


Figure 10.18 – An applicator blade for anhydrous ammonia (reprinted from Kepner et al., 1978).

10.2.2.2 Application of non-pressure liquids

In *non-pressure-liquid applicators*, the flow of liquid is due to gravity and the flow rate is controlled by fixed orifices. The attachments generally have a sediment bowl, a filter, one or two orifice disks with a range of orifice sizes, and a quick shut-off valve. Unless the tank elevation is large in relation to its depth, or bottom venting is employed, head changes will cause appreciable variations in flow rate. Bottom venting (inverted siphon) is obtained by having the tank sealed such that air can enter only through an open tube that runs from the top of the tank to a point inside the tank near the bottom. The height of the bottom end of the tube in relation to the orifice then establishes the liquid head. This tube may be attached to a sealing-type filler cap. With a given orifice size and head, the application rate per hectare is inversely proportional to the forward speed.

A simple squeeze pump as shown in Figure 10.19 has been developed for many non-pressure-liquid applicators. Units are available with as many as 20 tubes, each serving one applicator outlet. The positive-displacement, ground-wheel-driven pump produces flow rate proportional to ground speed. The application rate is adjusted by changing the speed ratio between the reel and the ground wheel.

Non-pressure liquids can be applied directly to the soil surface, as well as on pasture and other solid-planted crops. Banded application of non-pressure liquids are sometimes made during a row-crop planting operation or as later side dressing. Non-pressure liquid chemicals are available for many planters. Usually one tank is provided for each two rows. Liquid is discharged close to the furrow through small tubes.

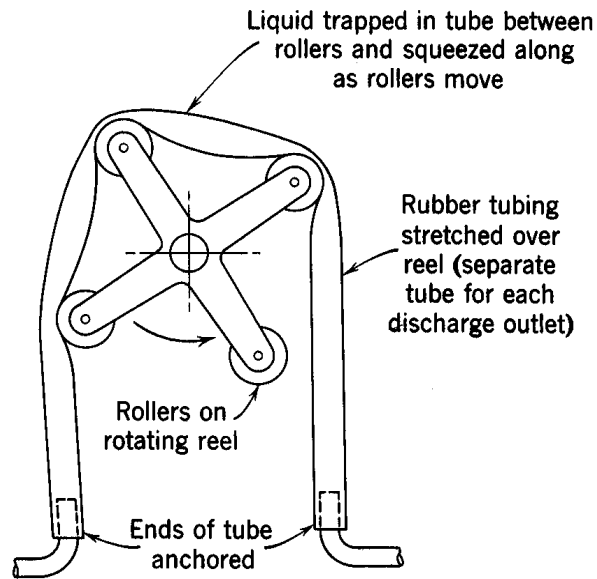


Figure 10.19 – A squeeze pump (reprinted from Kepner et al., 1978).

10.2.2.3 Low-pressure sprayers

Low-pressure sprayers are used to apply pre- and post-emergent chemicals to control weeds, insects, and diseases. Boom-type sprayers are used on tractors, trucks, or trailers; a tractor-mounted boom-type of field sprayer is shown in Figure 10.20. Low-pressure units usually operate in 150 to 350 kPa range and apply 50 to 200 L/ha. However, in some ultra low volume (ULV) applications, the rates may be as low as 10 L/ha to a few mL/ha. Tank-on-tractor mounted sprayers hold from 575 to 1000 L. For application in the standing row crop, high-clearance sprayers have been developed. They have a frame high enough to clear corn, cotton, and other tall crops. The spray boom may be raised or lowered depending upon the crop height. The sprayer may be mounted on a trailer or wheels and pulled through the field by a tractor. Tank capacity may be as high as 3750 L. The boom width may vary from 4 to 12 m. Skid-mounted sprayers may be placed on a pickup truck or a flatbed truck. The tank size may be up to 10,000 L and the boom width up to 18 m. The trucks are fitted with flotation tires so they can operate in wet conditions.

Aircraft-mounted low-pressure sprayers have the advantage of rapid coverage and applying chemicals when conditions are otherwise unsuitable for ground rigs. Because of the limited weight carrying capacities, aircraft-mounted sprayers are most suited for low application rates of less than 50 L/ha. The aircraft speed varies between 50 to 125 km/h for helicopters and 175 to 250 km/h for airplanes as they fly about 1 to 8 m above the crop height.



Figure 10.20 – A boom-type field sprayer (reproduced by permission of Deere and Co., © 1991. All rights reserved).

10.2.2.4 High-pressure sprayers

High-pressure sprayers are similar to low-pressure sprayers except they operate under much higher pressure, up to 7000 kPa, and generally do not have a boom with multiple nozzles. High-pressure sprayers are used in orchards where it is necessary to spray to the top of the trees and to penetrate the thick tree canopy. High-pressure sprayers are more expensive because the parts are made to withstand higher pressures.

10.2.2.5 Air-carrier sprayers

Air-carrier sprayers are sometimes called *air-blast sprayers* or *mist blowers*. The liquid is atomized either by pressure nozzles or rotary atomizers in a high velocity air stream. The atomized liquid is then carried to the target by the air stream. The sprayers are capable of generating air flow rates in the range of 2.5 to 30 m³/s with air speeds ranging from 125 to 240 km/h. Since air is used to carry the pesticide to the target, concentrated pesticides can be used resulting in a substantial savings in the amount of water needed and the time required for refilling. Two different types of air-carrier sprayers are shown in Figures 10.21 and 10.22.

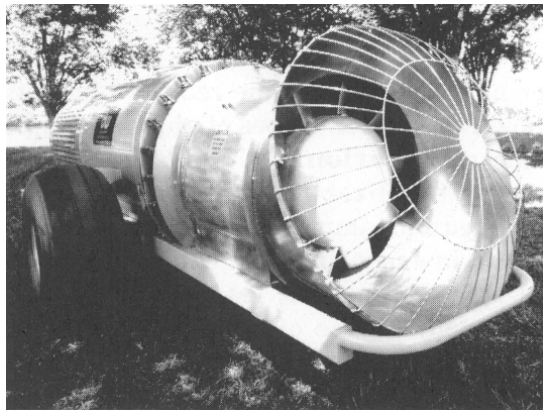


Figure 10.21 – An air-blast sprayer (courtesy of Durand-Wayland, Inc.).

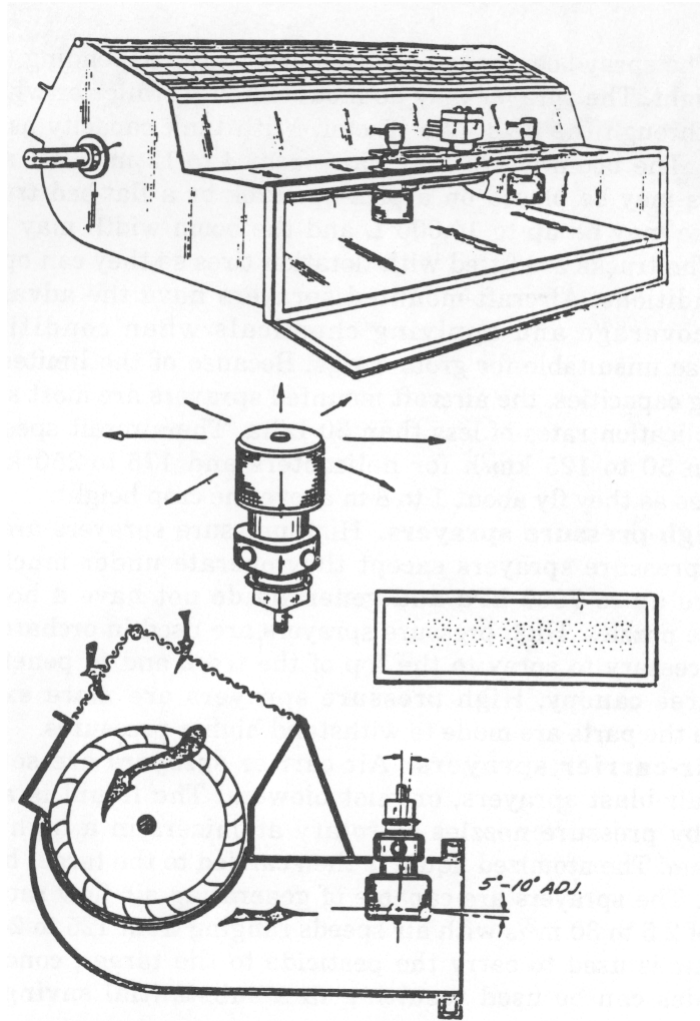
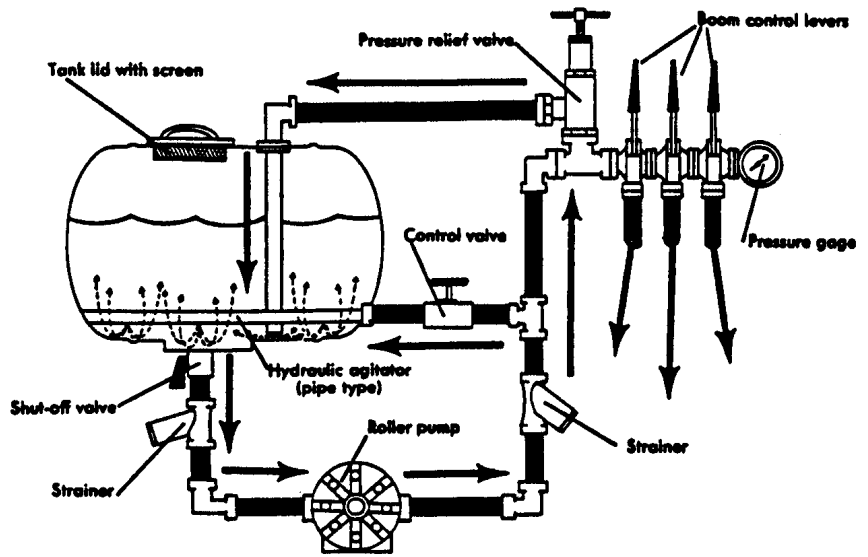


Figure 10.22 – An air-curtain sprayer utilizing a cross-flow fan and a rotary controlled droplet atomizer (Van Ee and Ledebuhr, 1987).

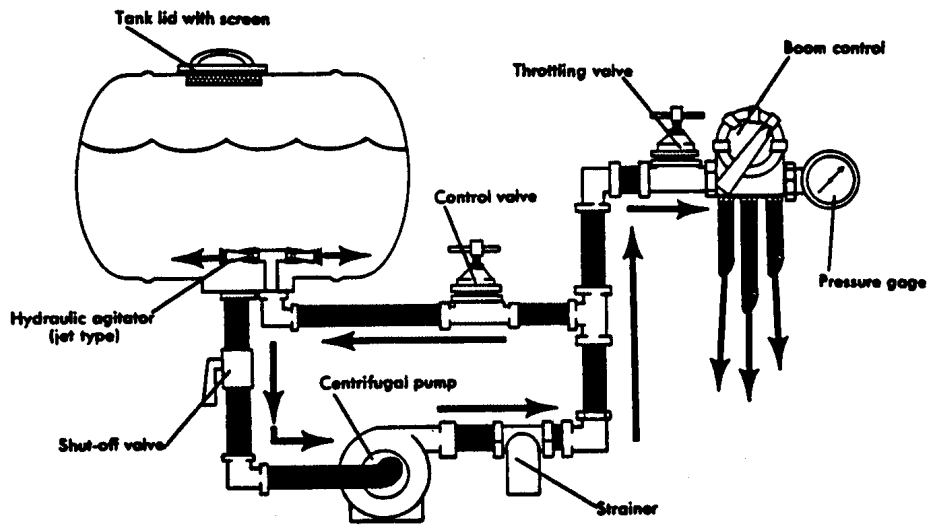
10.2.3 Functional processes of applying liquid chemicals

Figure 10.23 shows two typical arrangements for a hydraulic sprayer. A hydraulic sprayer consists of a tank to hold the liquid chemical, an agitation system to keep the chemical well mixed and uniform, a pump to create flow, a pressure regulator valve to control rate of flow, a series of nozzles to atomize the liquid, and miscellaneous components such as boom, shut-off valves, fittings and strainers.

The main functional processes—pumping, agitation, and atomization—are discussed below.



(a)



(b)

Figure 10.23 – Schematic diagrams of low-pressure hydraulic sprayers utilizing (a) a roller pump, (b) a centrifugal pump (reprinted from Bode and Butler, 1981).

10.2.3.1 Pumping

Positive-displacement pumps. With *positive-displacement pumps*, the output is not affected by the output pressure and the flow is created by positively displacing a volume by a mechanical means such as a piston or plunger. In contrast, with a *centrifugal pump*, flow is created by the action of centrifugal force. The output drops as the output pressure is increased.

Positive-displacement pumps found on sprayers include piston (plunger), rotary, and diaphragm types. These are self-priming, and they all require automatic (spring-loaded) bypass valves to control the pressure and to protect the equipment against mechanical damage if the flow is shut off.

Piston (plunger) pumps are a kind of positive-displacement pump that is well suited for high-pressure applications such as high-pressure orchard sprayers and multipurpose sprayers designed for both high- and low- pressure spraying. They are more expensive than other types, occupy more space, and are heavy, but they are durable and can be constructed so they will handle abrasive materials without excessive wear.

The volumetric efficiency of a piston pump in good condition is generally high (90% or more), and the discharge rate is essentially a direct function of crank speed and volumetric displacement. Crank speeds on the smaller piston sprayer pumps [38 L/min (10 gpm) and less] are mostly 400 to 600 rev/min. High-pressure piston sprayer pumps [4.1 to 5.5 MPa (600 to 800 psi)] are usually operated at 125 to 300 rev/min have capacities of 75 to 225 L/min (20 to 60 gpm). Mechanical efficiencies may range from 50% to 90%, depending on the size and condition of the pump.

Rotary pumps, another type of positive-displacement pump, are popular for low-pressure sprayers, the most common types being roller pumps (Figure 10.24a). Roller pumps have a slotted rotor that rotates in an eccentric housing. Rollers in each slot seal the space between the rotor and the wall of the case. The rollers are held against the case by centrifugal force during pump operation. As the rollers go past the inlet the space expands creating low pressure and causing the liquid to be drawn in toward the housing. The liquid trapped between the rollers is moved towards the outlet as the rotor turns. Now the cavity between the rollers contracts, expelling the liquid out through the outlet port. Pump output is determined by the length and diameter of the housing, its eccentricity, and the speed of rotation.

Teflon is a common material for the rollers, although rubber, steel, and carbon are also used. Rotary pumps are compact and relatively inexpensive, and can be operated at speeds suitable for direct connection to the tractor PTO. Although they are classed as positive-displacement pumps, leakage past the rollers causes a moderate decrease in flow as the pressure is increased. Normal output of roller pumps ranges from 19 to 114 L/min (5 to 30 gpm) and maximum pressures range from 1 to 3 MPa (150 to 300 psi). However, pressures above 690 kPa (100 psi) are not generally recommended for rotary pumps when pumping non-lubricating liquids. Roller pumps wear rather rapidly under abrasive conditions, but the rollers can be replaced economically.

Diaphragm pumps are another type of positive-displacement pump. They are becoming more widely used and are available with flow rates up to 19 to 23 L/min (5 to 6

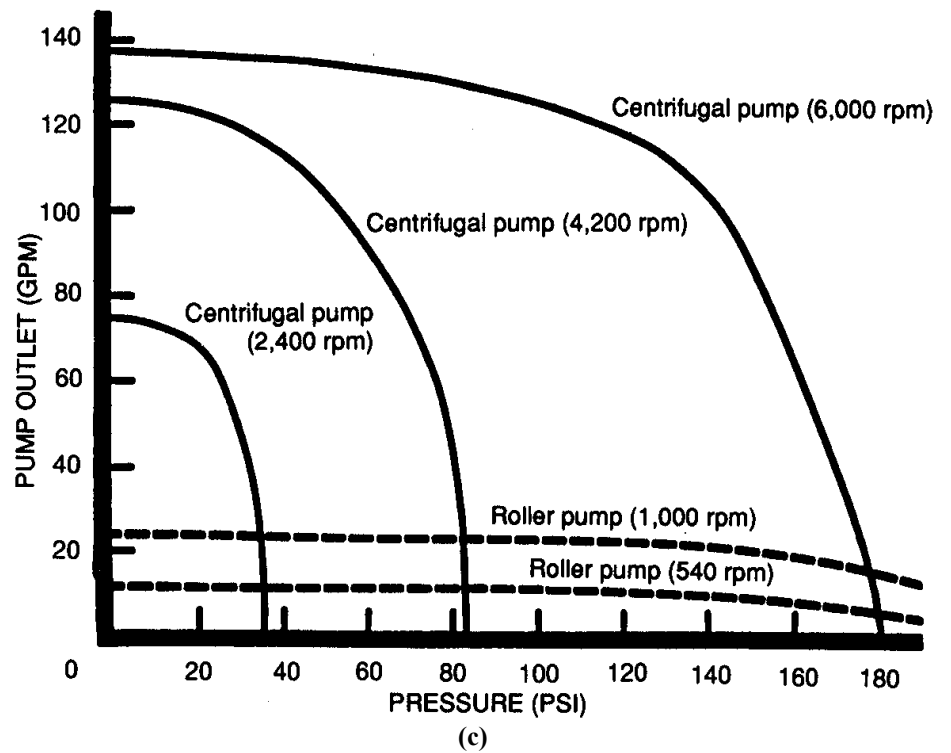
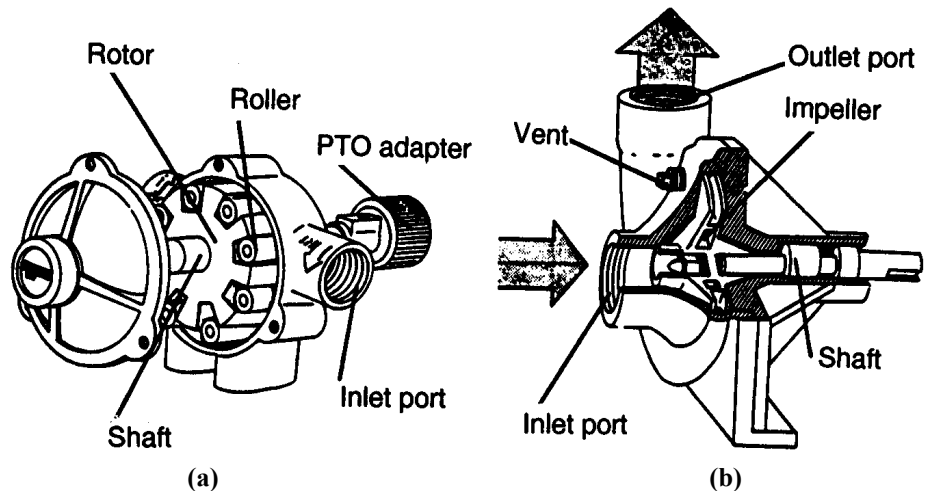


Figure 10.24 – (a) A typical roller pump, (b) a typical centrifugal pump, and (c) performance curves of roller and centrifugal pumps (reprinted from Bode and Butler, 1981).

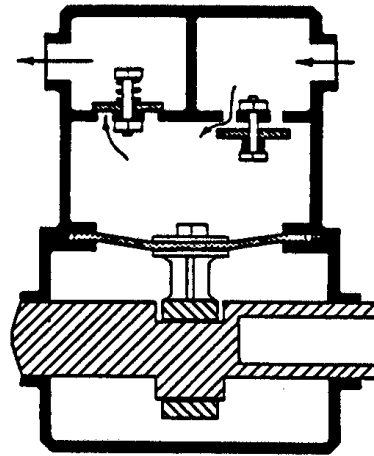


Figure 10.25 – A positive displacement diaphragm pump. (Reproduced by permission of Deere and Co. © 1991. All rights reserved.)

gpm) and pressures up to 3.4 MPa (500 psi). Since the valves and the diaphragm are the only moving parts in contact with the spray material, these pumps can readily handle abrasive materials (Figure 10.25).

Centrifugal pumps. *Centrifugal pumps* (Figure 10.24b) do not create flow by mechanically displacing a volume, as do positive-displacement pumps. Instead, they depend upon centrifugal force for their pumping action. They are essentially high-speed (3000 to 4500 rev/min), high-volume (70 to 130 gpm) devices not suitable for high-pressure applications because the pump output drops off rapidly when the outlet pressure is above 206 to 275 kPa (30 to 40 psi). The pressure or head developed by a given centrifugal pump at a particular speed is a function of the discharge rate, as indicated by the typical performance curves in Figure 10.24c. Note that the peak efficiency, which occurs at a relatively high flow rate, is well above 70% for this particular unit, whereas efficiencies at small flows are low.

For a given centrifugal pump and a given point on the efficiency curve, the discharge rate varies directly with the speed, the head varies as the square of the speed, and the power varies as the cube of the speed. If two or more stages are connected in series, the head and power at a given discharge rate are increased in proportion to the number of stages. Thus, multi-staging provides increased pressures without increasing the capacity range.

Centrifugal pumps are popular for certain types and sizes of sprayers because of their simplicity and their ability to handle abrasive materials satisfactorily. They are well suited to equipment such as air-blast sprayers and aircraft sprayers, for which high flow rates are needed and the required pressures are relatively low, and are used on many low-pressure field sprayers. The high capacities are advantageous for hydraulic agitation and for tank-filling arrangements. Speeds in these applications are generally in the range between 1000 and 4000 rev/min, depending upon the pressure required and the diameter of the impeller.

Since centrifugal pumps do not have positive displacement, they are not self-priming and do not require pressure relief valves for mechanical protection. Priming is usually accomplished by mounting the pump below the minimum liquid level of the tank or providing a built-in reservoir on the pump that always retains sufficient liquid for automatic priming.

Power requirements. Power requirements of pumps are determined by flow rate, operating pressure, and mechanical efficiency. The mechanical efficiency used for estimating the power requirements is 50% to 60%. The pump input power can be calculated using the following formula:

$$P = \frac{Qp}{60,000\eta_m} \quad (10.1)$$

where P = power, kW

Q = flow rate, L/min

p = pressure, kPa

η_m = mechanical efficiency, decimal

10.2.3.2 Agitation

Many spray materials are suspensions of insoluble powders or are emulsions. Consequently, most sprayers are equipped with agitating systems, either mechanical or hydraulic.

Mechanical agitation is commonly accomplished by flat blades or propellers on a shaft running lengthwise in the tank near the bottom and rotating at a speed of 100 to 200 rev/min (Figure 10.26). The following relations apply to round-bottom tanks with flat, I-shaped paddles sweeping close to the bottom of the tank. They are based on results originally reported by French (1942) as cited in Kepner (1978).

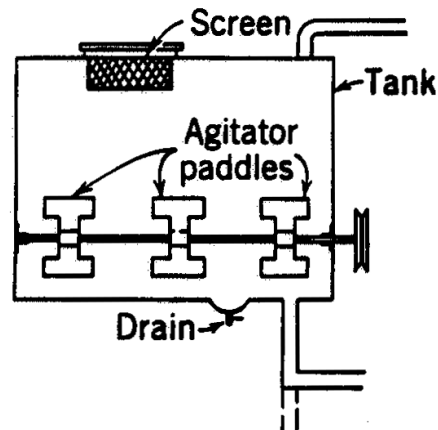


Figure 10.26 – Mechanical agitation (reprinted from Kepner et al., 1978).

$$s_m = 5.39A^{0.422}R^{-0.531}F_e^{0.293} \quad (10.2)$$

$$P_s = 3.26 \times 10^{-11} R^{0.582} s_m^{3.41} L \quad (10.3)$$

where s_m = minimum peripheral speed of paddles, m/min

A = depth of liquid above agitator shaft center line, mm

R = total combined width of all paddles divided by tank length

F_e = agitation factor indicating relative difficulty of agitating a given oil-water emulsion, either hydraulically or mechanically

P_s = shaft input power at any peripheral speed, s kW

L = length of tank, mm

Values of F_e for various oil-in-water emulsions are shown in Table 10.1. These were established during tests with hydraulic agitation but are assumed to apply reasonably well for mechanical agitation. French's tests were conducted with an emulsion containing 1% to 2% oil. No data are available to indicate mechanical agitation requirements for suspensions of wettable powders.

Paddle tip speeds in excess of about 150 m/min may cause significant foaming of some mixtures. For mechanical agitation of emulsions in flat-bottom tanks with rounded corners, the minimum tip speed from Equation 10.2 must be multiplied by the factor 1.11. This increase in minimum speed causes the minimum power requirement to be approximately doubled (Equation 10.3).

For *hydraulic agitation*, a portion of the pump's output is discharged into the spray tank through a series of jet nozzles or orifices located in a pipe along the bottom of the tank. The energy and turbulence from the jets provide the mixing action. Figure 10.27a shows different hydraulic agitator nozzles. In tests with various sizes of cylindrical tanks, Yates and Akesson (1963) found that best results were obtained when the jet nozzles were mounted as shown in Figure 10.27b. The location shown for wettable powders was satisfactory for an emulsion containing 40% oil and 60% water only when a suitable emulsifier was included in the formulation. Nozzle spacings from 75 to 710 mm were satisfactory for oil-water emulsions but not to exceed 305 mm for wettable powders.

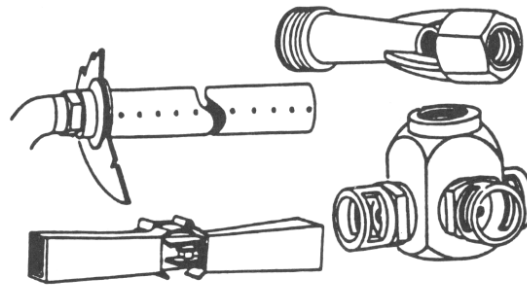
Table 10.1. Values of agitation factors (F_e) for oil-in-water emulsions (Kepner et al., 1978).

Oil, %	Water, %	Emulsifier, %	Jet Position (Figure 10.27b)	Agitation Factor, F_e
60	40	0	emulsion	0.83
50	50	0	emulsion	1.00
40	60	0	emulsion	1.00
10	90	0	emulsion	0.89
1 – 2	99 – 98	0	emulsion	0.50
40	59.9	0.1	emulsion	0.50
40	59.9	0.1	wettable powders	0.68

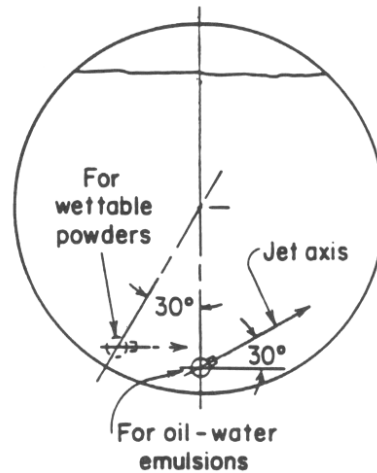
The minimum total recirculation rates for hydraulic agitation in a cylindrical or round-bottom tank, based on complete mixing of a full tank of material in 60 s, were found to be as follows:

$$\text{For oil-water emulsions, } Q_m = 3830 \frac{VF_e}{p^{0.56}} \quad (10.4)$$

$$\text{For wettable powders, } Q_m = 1380 \frac{VF_e}{p^{0.3}} \quad (10.5)$$



(a)



(b)

Figure 10.27 – (a) Various types of nozzles for hydraulic agitation (Bode and Butler 1981), and (b) locations of nozzles in the tank for agitation (reprinted from Kepner et al., 1978).

where Q_m = minimum total recirculation rate, L/min

V = tank volume, m^3

p = pressure at the agitation jet nozzle, kPa (ordinarily this will be essentially the same as the spray nozzle pressure)

The value of F_e was arbitrarily taken as 1.00 for a mixture of 120 g wettable sulfur per liter of water (1 lb/gal), since this is a difficult material to keep in suspension. Values of F_e for concentrations of 60, 12, and 6 g/L (0.5, 0.1, and 0.05 lb/gal) were found to be 0.87, 0.43, and 0.27, respectively. Table 10.1 indicates that adding an emulsifier to an oil-water mixture reduces the agitation requirements and also shows that F_e is greater when the jets are in the wettable powder optimum position (Figure 10.27b) instead of the emulsion position.

From basic hydraulic relations, the hydraulic useful power output required for any recirculation rate and pressure is:

$$P_h = \frac{Q_m p}{60,000} \quad (10.6)$$

where P_h = hydraulic power, kW

Q_m = total recirculation rate, L/min

The principal advantage of hydraulic agitation is its simplicity as compared with the mechanism and drive required for mechanical agitation. With hydraulic agitation, however, the spray pump must have additional capacity and the power requirements will be considerably greater than that for mechanical agitation, especially at high pressures. For high-pressure sprayers, mechanical agitation is definitely the more economical system.

Example 10.1

Determine the power requirements of a boom-type orchard sprayer if the spray gun pressure is 1.375 MPa and the flow rate is 15 L/min. The hose has an inside diameter of 2.54 cm, and it is 50 m long. The volume of the tank is 375 L and contains wettable powder. It is also recommended that a 20% over-capacity of flow should be designed to compensate for normal pump wear. The mechanical efficiency of the pump ranges from 50% to 60%. Assume the viscosity of the chemical is the same as that of water at 21° C or 0.98 MPa·s.

Solution

First we determine the pressure loss in the hose. Determine the flow regime by calculating the value of the Reynolds number as follows:

$$N_{Re} = \frac{4C_p Q}{4\mu d} = \frac{4(16.67)1000(15)1.2}{\pi(0.98)25.4} = 15,348$$

Note that $Q = 15 \times 1.2$ to account for 20% over-capacity as desired in the problem statement. The flow is fully developed turbulent flow since the Reynolds number is above 4000. To calculate the pressure drop, we use Equation 5.19:

$$\begin{aligned} \frac{\Delta p}{L} &= \frac{0.0333\mu^{0.25}\rho^{0.75}Q^{1.75}}{d^{4.25}} \\ &= \frac{0.0333(0.98)^{0.25}(1000)^{0.75}(15 \times 1.2)^{1.75}}{(25.4)^{4.25}} \\ &= 0.922 \text{ kPa/m} \end{aligned}$$

and $\Delta p = 0.992(50) = 49.59$ kPa. Thus, the total pressure required at the pump is:

$$p = 1375 + 49.59 = 1424.59 \text{ kPa}$$

Now, determine the flow rate required for hydraulic agitation using the following equation for wettable powder:

$$Q_m = 1380 \frac{VF_e}{p^{0.35}} = \frac{1380(0.375)0.68}{(1425)^{0.35}} = 27.7 \text{ L/min}$$

Thus, the total flow that the pump must generate is:

$$Q = 15(1.2) + 27.2 = 45.2 \text{ L/min}$$

Pump output power is, from Equation 10.14:

$$P = 1.667 \times 10^{-5} QP = 1.667 \times 10^{-5} (45.2)(1424.59) = 1.07 \text{ kW}$$

Considering the lowest efficiency of 50%, the input power is:

$$P_{\text{input}} = 1.07/0.5 = 2.14 \text{ kW}$$

10.2.3.3 Atomization

The main objective of atomization is to increase the surface area of the liquid by breaking it into many small droplets for effective coverage of plant and soil surfaces. During atomization, energy is imparted to the liquid to break it into small droplets by overcoming surface tension, viscosity, and inertia.

Types of atomizers. Based on the form of energy applied to produce atomization, the atomizers may be categorized as *pressure*, *rotary*, or *pneumatic* atomizers. Pressure atomizers are the most common type used in agriculture; use of the pneumatic kind is virtually non-existent.

In *pressure atomizers*, pressure energy is used to breakup a liquid jet. Pressure atomizers (but not rotary atomizers), often referred to as *nozzles* (Figure 10.28), produce several different spray patterns (Figure 10.29), described below.

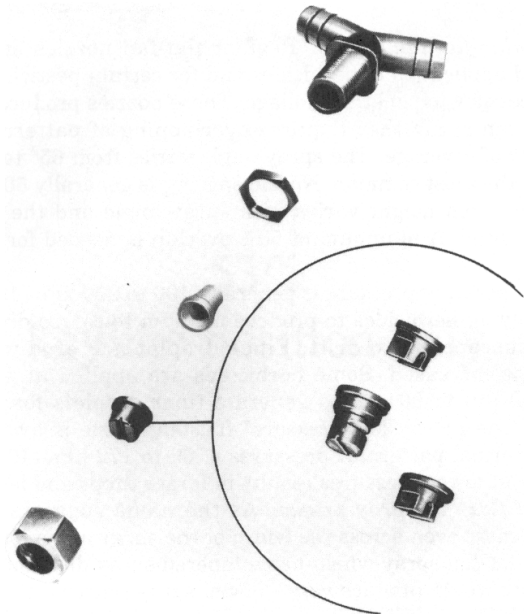


Figure 10.28 – A typical nozzle assembly. (Reproduced by permission of Deere and Co. © 1991. All rights reserved.)

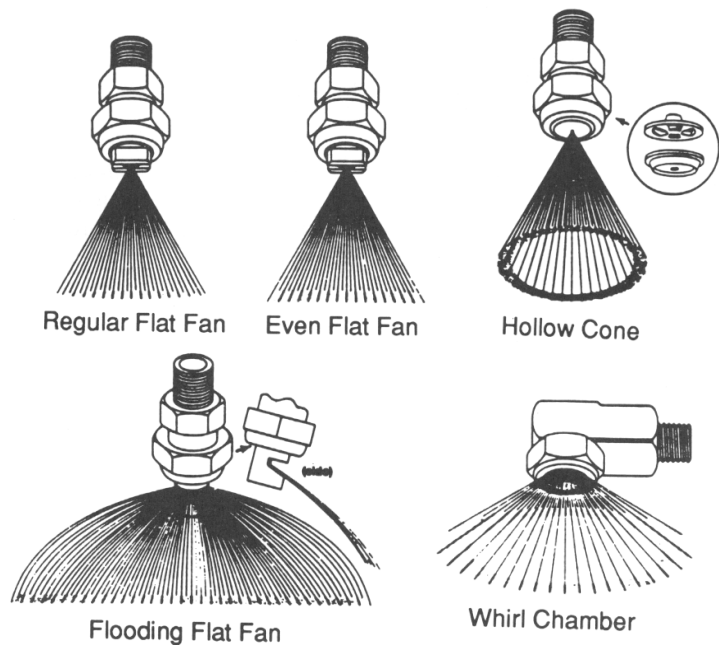


Figure 10.29 – Various types of spray nozzles and spray patterns (reprinted from Bode and Butler, 1981).

Regular flat-fan nozzles are used for most solid applications of herbicides and for certain pesticides when it is not necessary to penetrate foliage. These nozzles produce a tapered-edge flat-fan spray that requires overlapping of pattern to obtain uniform coverage. The spray angle varies from 65° to 110° with 80° being the most common. Nozzle spacing is generally 50 cm on the boom. The boom height varies with spray angle and the amount of overlap desired. A minimum of 50% overlap is needed for uniform coverage.

The operating pressure is generally 100 to 200 kPa (15 to 30 psi) when applying herbicides to produce medium to coarse droplets that are not susceptible to drift. Finer droplets are produced as the pressure is increased. Some herbicides are applied at pressure of 275 to 413 (40 to 60 psi) to generate finer droplets for maximum coverage. The LP or “low pressure” flat-fan nozzle develops normal pattern at pressures of 69 to 172 kPa (10 to 25 psi). Operating at lower pressures results in larger drops and less drift.

Even flat-fan spray nozzles provide a spray density that is more even across the width of the spray, as compared to the standard flat-fan spray with its tapered spray distribution. Since overlapping would produce a very uneven spray pattern, these nozzles are only for band application over or inbetween rows. The band width is determined by adjusting the boom height. The common spray angles are 80° and 95° and the operating pressures range from 100 to 200 kPa (15 to 30 psi).

Flooding flat-fan nozzles produce a wider spray pattern than the other flat-fan nozzles. They are most suited for broadcast applications where uniform surface application is critical. Uniform spray application is obtained by 100% overlap of individual spray patterns. These nozzles produce large droplets and reduce drift, when operated at 55 to 170 kPa (8 to 25 psi) pressure. Pressure changes affect the uniformity of spray pattern more with flooding flat-fan nozzles than with regular flat-fan nozzles.

Hollow-cone spray nozzles (both disk and core types) utilize a two-piece, disk-core, hollow-cone spray tip. The core gives the fluid a swirling action before it is metered through the orifice disk, resulting in a circular, hollow-cone, spray pattern. These nozzles are most suited for directed spray in row-crop applications when drift is not a concern, as these nozzles are operated at 275 to 550 kPa (40 to 80 psi) pressures. Since the droplets are small, these nozzles are most suited for contact herbicides, insecticides, and fungicides where full coverage of plant foliage is essential.

Whirl-chamber hollow-cone nozzles have a whirl-chamber above a conical outlet that produces a hollow-cone pattern of cone angles up to 130° . These nozzles are best suited for broadcast surface applications of herbicides. For best results the nozzle is tilted towards the rear at a 45° angle. Since the droplets tend to be larger, these nozzles are most suited for systemic herbicides and where drift may be a problem. The operating pressure ranges from 35 to 138 kPa (5 to 20 psi).

In *rotary atomizers*, as opposed to the various pressure nozzles listed above, the energy to produce droplets comes from a rotating wheel, disk, or cup. As the speed increases, smaller droplets are produced. Rotary atomizers (Figure 10.30) are not as common in agricultural applications as are pressure nozzles. Rotary atomizers are also called *controlled droplet atomizers* (CDA) for their ability to produce droplets that are more uniform in size compared to other atomizers.

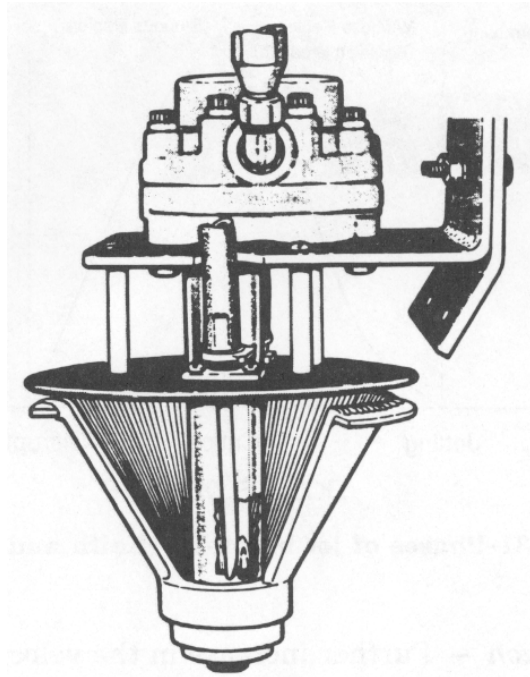


Figure 10.30 – A rotary or controlled droplet atomizer (courtesy of Farm Fans, Inc.).

Theory of pressure atomization. Atomization is a very complex process and depends highly upon the type of atomizer. To get a better understanding of the process we will discuss breakup of *liquid jets*, *liquid sheets*, and *liquid droplets*.

Liquid jet breakup. As the liquid flow rate is increased through a horizontal nozzle, it goes through the following four phases based on the Reynolds number (Figure 10.31). Think of N_{Re} as an indicator of flow rate. With everything else being the same, as flow rate increases, N_{Re} also increases. There are generally two flow regimes: laminar and turbulent. Two very different flow behaviors exist in these regimes.

1. *Drop formation.* At low flow rates drops form individually at the tip of the nozzle and grow in size until the weight overcomes the interfacial tension and the drop is released (Figure 10.32).

2. *Varicose region.* As the jet velocity is increased, symmetrical bulges and contractions appear and the jet lengthens. The drops become smaller and less uniform.

3. *Sinuuous region.* Further increase in the velocity results in the transverse oscillations of the jet. The jet waves irregularly in an S-curve fashion. The jet becomes shorter and the drops become larger.

4. *Atomization.* Finally, the jet breaks down into small droplets, usually within a distance of 15 times jet diameter of the orifice. The breakup is highly chaotic. The ligaments shed at the crest as the jet oscillates further break down into droplets. This occurs when a simple orifice is employed for atomization.

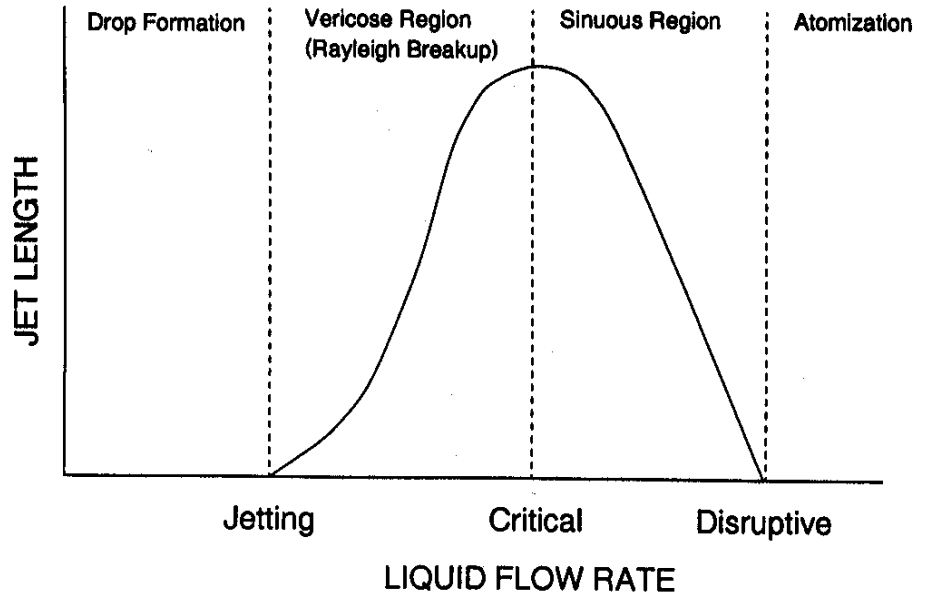


Figure 10.31 – Phases of jet breakup (Keith and Hixon, 1955).

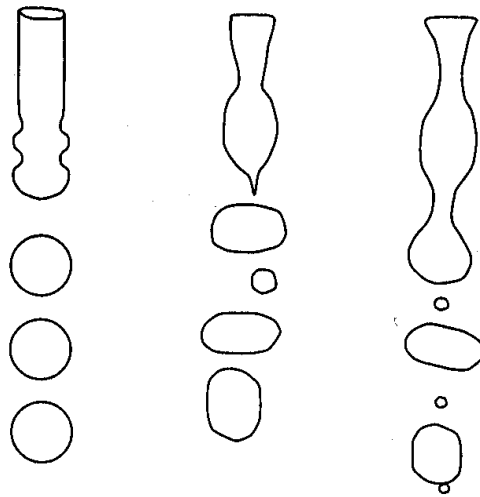


Figure 10.32 – Idealized and actual jet breakup (Marshall, 1954).

The jet is moving from the sinuous region to the atomization region when the following equation is true:

$$\left(\frac{d_j v_j \rho_l}{\mu_l} \right) \geq 280 \left[\frac{\mu_l}{(\sigma \rho_l d_j)^{0.5}} \right]^{-0.82} \quad (10.7)$$

where d_j = jet diameter, m

v_j = jet velocity, m/s

ρ_l = liquid density, kJ/m^3

μ_l = liquid viscosity, $\text{Pa} \cdot \text{s}$

σ = surface tension (N/m)

The jet velocity can be computed as follows once flow through the nozzle is known:

$$v_j = C_v \left(2 \frac{\Delta p}{\rho_l} \right)^n \quad (10.8)$$

where C_v = velocity coefficient, dimensionless

Δp = total pressure drop, Pa

$n = 0.5$ for turbulent flow

The discharge coefficient represents the ratio of the actual liquid discharge rate to that theoretically possible. The volumetric flow rate is determined by:

$$Q = v_j C_A A \quad (10.9)$$

where C_A = area coefficient, dimensionless

A = nozzle orifice area, m^2

C_A takes into account the vena contracta effects. Combining Equations 10.8 and 10.9 we obtain:

$$Q = C_v \left(\frac{2 \Delta p}{\rho_l} \right)^{0.5} C_A A \quad (10.10)$$

Now, if we let discharge coefficient $C_D = C_v C_A$, the above equation becomes:

$$Q = C_D A \left(\frac{2 \Delta p}{\rho_l} \right)^{0.5} \quad (10.11)$$

The average jet velocity may be computed from the above equation as follows:

$$v_j = \frac{Q}{C_D A} \quad (10.12)$$

The discharge coefficient (C_D) varies depending upon the size of the orifice and the nozzle design. For a given nozzle, if we plot flow rate against the square root of the pressure drop, the slope of the line will be $C_D A \sqrt{2/\rho_l}$ from which the discharge coefficient (C_D) may be computed.

Example 10.2

A spray nozzle manufacturer has provided the following pressure-flow rate data for a hollow-cone nozzle spraying water.

Nozzle flow rates at various pressures for an orifice diameter of 2.39 mm.

Pressure, kPa	207	276	345	414	552	689	862	1034	1379	2068
Flow, L/min	1.17	1.63	1.82	2.00	2.31	2.57	2.95	3.14	3.71	4.54

For the above nozzle determine the flow required to produce atomization phase of a jet of water issuing from the nozzle.

Solution

Equation 10.7 is to be used to determine the jet velocity required to produce atomization. This equation can be rewritten as:

$$v_j \geq 280 \frac{\sigma^{0.42} \mu_1^{0.18}}{\rho_1^{0.59} d_j^{0.59}}$$

For water, $\sigma = 0.0728 \text{ N/m}$
 $\mu_1 = 1 \text{ mPa} \cdot \text{s}$
 $\rho_1 = 1000 \text{ kg/m}^3$
 $d_j = 2.39 \text{ mm}$

Using the above values, $v_j > 16.06 \text{ m/s}$.

Equation 10.12 may be used to calculate the flow corresponding to the minimum jet velocity of 16.06 m/s as:

$$Q = C_D A v_j$$

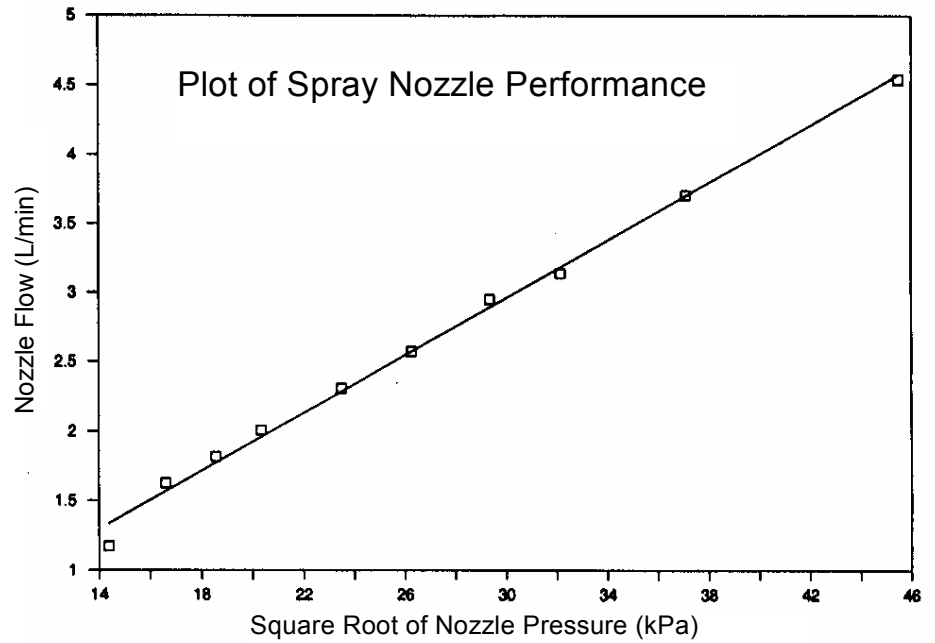
However, the discharge coefficient (C_D) is to be determined from the data given by the manufacturer. If we plot the nozzle flow against the square root of the nozzle pressure as shown on the next page, we find the slope as:

$$0.104 \frac{\text{L/min}}{\sqrt{\text{kPa}}} \quad \text{or} \quad 10^{-6} \frac{\text{m}^3/\text{s}}{\sqrt{\text{kPa}}}$$

Using Equation 10.11 we get:

$$\frac{C_D A \sqrt{2}}{\sqrt{\rho_1}} = 5.48 \times 10^{-8} \frac{\text{m}^3/\text{s}}{\sqrt{\text{Pa}}} \quad (\text{note conversion from kPa to Pa})$$

or
$$C_D = \frac{\sqrt{\rho_1}}{A \sqrt{2}} \times 1.735 \times 10^{-6}$$



Substituting the values of ρ_1 and A , C_D is found to be 0.274. Note that this value is considerably less than 0.611 normally used for turbulent orifice flow. This is due to the inserts and screens used in a working nozzle.

Once C_D is known, the flow is calculated as:

$$\begin{aligned}
 Q &= 0.274 \left[\frac{\pi}{4} (2.39 \times 10^{-3})^2 \right] \times 16.06 \\
 &= 19.7 \times 10^{-6} \text{ m}^3/\text{s} \\
 &= 1.18 \text{ L/min}
 \end{aligned}$$

It should be noted that this value corresponds to a pressure drop of 207 kPa. If the nozzle is operated at pressure less than 207 kPa, complete atomization will not occur. It should also be noted that this value corresponds to the minimum value of pressure given by the manufacturer. If lesser flow is desired, a smaller orifice should be used.

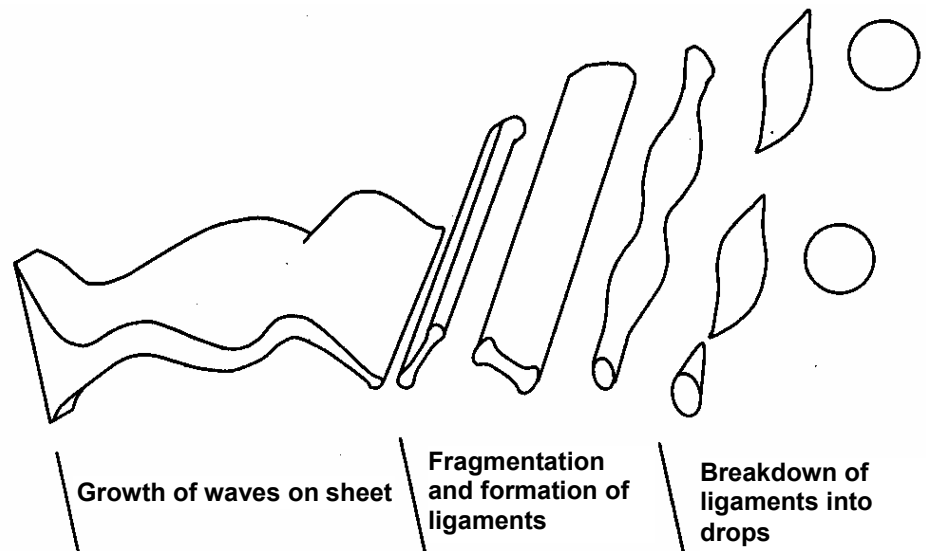


Figure 10.33 – Breakup of a liquid sheet (after Dombrowski and Johns, 1963).

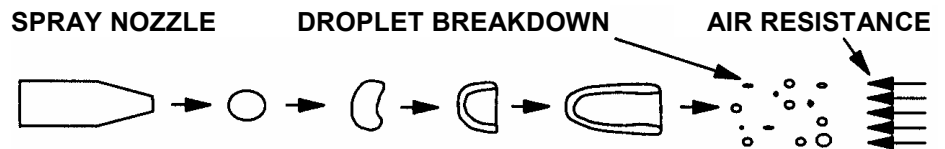


Figure 10.34 – Breakup of a droplet.

Liquid sheet breakup. When the liquid is pumped through a pressure nozzle, either a flat-fan (fanjet) nozzle or a whirl-chamber (swirl) nozzle, a sheet of liquid is formed. The liquid sheet breaks up into droplets of many sizes. The mechanism of sheet breakup is complex and depends upon many factors. However, four main mechanisms have been observed (Figure 10.33):

1. *Rim disintegration.* The free edge of the sheet contract into a cylinder, that then breaks from the surface as large drops followed by their liquid fingers.
2. *Sheet perforations.* Perforations appear in the sheet that expand under the influence of surface tension until ligaments remain.
3. *Unstable waves* are formed in the sheet at a right angle to the direction of flow of liquid. The amplitude increases until the sheet breaks up.
4. *Thick sheet breakup.* The crests of sheet are shed as ligaments.

Liquid droplet breakup. Droplets further break down in an air stream if the aerodynamic forces exceed the surface tension force. This may occur in air carrier sprayers. A sequence of droplet breakup is shown in Figure 10.34.

Droplet size and size distribution. When liquid is atomized, droplets of various sizes are formed. The spray droplets are classified by their diameters, typically measured in microns (μ).¹ The performance and effectiveness of an atomizer depends upon the droplet size and size distribution. Table 10.2 shows some of the characteristics of various size droplets. The area covered and the volume of liquid in individual droplets is important in achieving effective and efficient application. Smaller droplets of the same volume provide more coverage. For example, one 200 μ droplet when broken into 64 droplets of 50 μ diameter will cover four times more area than the 200 μ droplet. The droplet distribution is also important from the point of view of spray drift. As seen in Table 10.5 the smaller the droplet size the longer it takes for it to settle and the higher the probability of drift. Note also that droplets evaporate in flight, becoming smaller and thereby increasing the chances of drift.

Droplet size distribution can be represented by a plot of the number of particles of a given diameter, as in Figure 10.35. This kind of plot is called a histogram. A smooth curve through the center points of the maxima of each size class gives the distribution curve. This curve represented by a function, $f(x)$, is commonly called a distribution function. If the distribution function is known explicitly, then only a few parameters (e.g., mean diameter and standard deviation) are needed to define a given distribution. Minimum and maximum size are additional parameters, often associated with a distribution. Sometimes, the surface area or the volume of a droplet is more relevant in certain applications rather than the diameter. If this is used as the ordinate then the curve in Figure 10.35 would skew to the right because of the weighting effect of the surface area or volume associated with a droplet diameter.

Table 10.2. Spray droplet size and its effect on coverage for a 10 L/ha application rate (Bode and Butler, 1981).

Droplet diameter, μ	Type of droplet	Area relative to a 10 μ droplet	Volume relative to a 10 μ droplet	No. of droplets per cm^2	Coverage relative to 1000 μ droplet
5	Dry fog	0.25	0.125	1,524,647	200
10	Dry fog	1	1	190,581	100
20	Wet fog	4	8	23,822	50
50	Wet fog	25	125	1,525	20
100	Misty rain	100	1000	191	10
150	Misty rain	225	3375	56	6.7
200	Light rain	400	8000	24	5
500	Light rain	2500	125,000	1.5	2
1000	Heavy rain	10,000	1,000,000	0.2	1

¹ Microns are also called micrometers and may be abbreviated μm . One micron is one millionth of a meter or 1/25,400 of an inch. A person with normal eyesight can see 100 μm without any magnification.

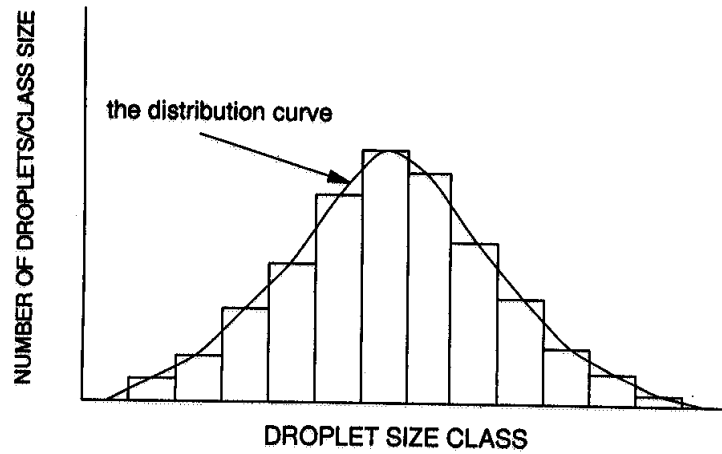


Figure 10.35 – A histogram of droplet sizes and associated frequency.

A more convenient method of representing a particle size distribution is to plot the cumulative fraction of the total number smaller than a given size against that given size. This plot is called a cumulative frequency plot and is shown in Figure 10.36. A more convenient way is to plot the data on a probability paper is shown in Figure 10.37. The droplet diameter is plotted on the ordinate (y-axis) and the abscissa is the cumulative percentage of droplet number, length, surface area, or volume. In pesticide application the cumulative number and cumulative volume are the most commonly used plot. The slope of the curve is an indication of the uniformity of the droplet size distribution.

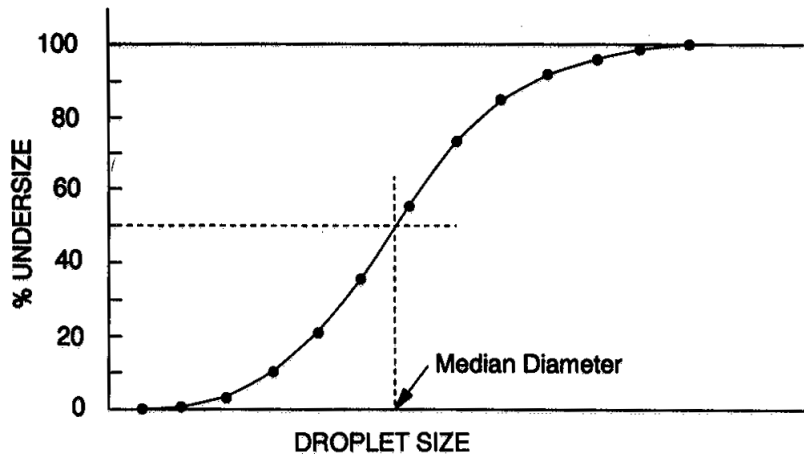


Figure 10.36 – A cumulative frequency plot.

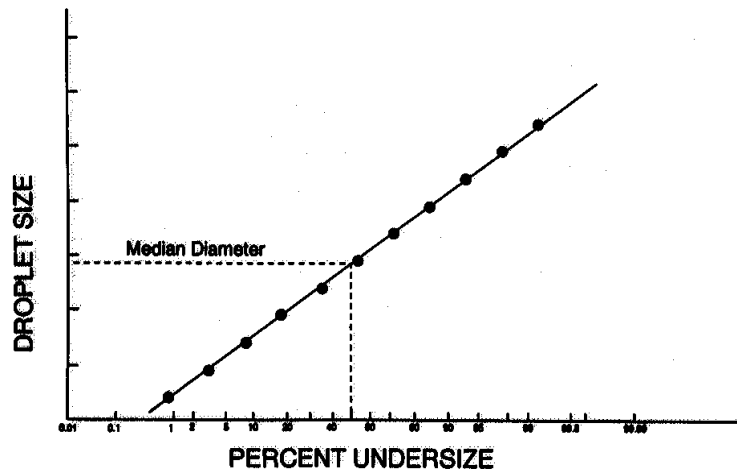


Figure 10.37 – A cumulative frequency plot on a normal probability paper.

The *median drop diameter* divides the spray into two equal parts by number, length, surface area, or volume. Number and volume median diameters are determined from the cumulative probability plots such as shown in Figure 10.38. A uniform method has been proposed to express the median diameters as $D_{x,f}$. The subscript, x , can be V for volume, A for area, L for length, or N for number, and the subscript, f , is the fraction on the cumulative distribution plot. Thus, $D_{v,5}$ = volume median diameter (VMD) indicates that 50% percent of liquid volume is in droplets smaller than this diameter and 50% in droplets larger than this diameter.

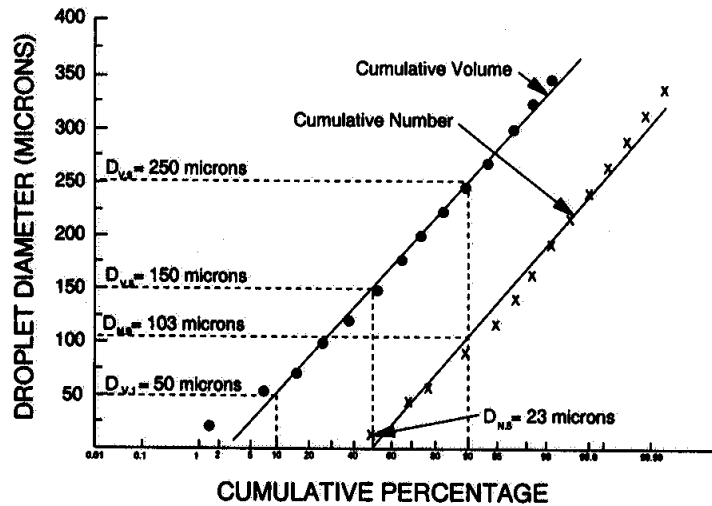


Figure 10.38 – Cumulative number and volume curves for a typical spray nozzle (after Bode and Butler, 1981).

Mean droplet diameters are weighted averages. Their names depend on the method used to compute the average. The following equation can be used to calculate the mean diameters:

$$\bar{D}_{pq}^{p-q} = \left(\frac{\sum_{i=1}^n N_i D_i^p}{\sum_{i=1}^n N_i D_i^q} \right)^{1/(p-q)} \quad (10.13)$$

where $p, q = 1, 2, 3, \text{ or } 4$ and $p > q$

D_i = droplet diameter for the i th size class

N_i = number of droplets in the i th size class

i = number of the size class

n = total number of size classes

Various weighted averages may be computed based on the number of droplets in each class size. Commonly used means include: arithmetic mean (\bar{D}_{10}), surface mean (\bar{D}_{20}), volume mean (\bar{D}_{30}) and Sauter mean (\bar{D}_{32}). The arithmetic mean is computed by letting $p = 1$ and $q = 0$ in the above equation and it is the weighted average of all droplet diameters in the spray. Volume mean diameter ($p = 3$ and $q = 0$) is the diameter of the droplet whose volume times the number of droplets in the spray equals the total volume sprayed. Sauter mean diameter is calculated by equating $p = 3$ and $q = 2$ and it is an indicator of the volume to surface ratio of droplets in the spray. Similarly, the surface mean diameter, with $p = 2$ and $q = 0$, is the diameter of the droplet whose surface area times the number of droplets in the spray equals the total surface area of all droplets.

There is no general agreement as to which method of specifying droplet diameters is the best in agricultural chemical application. However, volume mean and Sauter mean diameters are most commonly used. Median diameters have a better physical significance in that they divide the droplet spectra equally based on the count, area, volume, etc.

Example 10.3

For the droplet size data given on the next page, determine the mean and median droplet diameters.

Class size range, μ	Number of droplets in each class size range
19 – 46	699
46 – 72	326
72 – 99	282
99 – 125	286
125 – 152	243
152 – 178	201
178 – 204	150
204 – 231	88
231 – 259	50
259 – 284	43
284 – 310	13
310 – 336	12
336 – 363	5
363 – 389	2
389 – 415	1

Solution

Mean droplet diameters are computed from the table below (Bode and Butler, 1981).

Size (diameter) class range, μ	Midpoint diameter, μ	No. in each size class, N	ND, μ	ND ² , μ^2	ND ³ , μ^3
19 – 46	32	699	22,368	715,776	22,904,832
46 – 72	59	326	19,234	1,134,806	66,953,554
72 – 99	85	282	23,970	2,037,450	173,183,250
99 – 125	112	286	32,032	3,587,584	401,809,408
125 – 152	138	243	33,534	4,627,692	638,621,496
152 – 178	165	201	33,165	5,472,225	902,917,125
178 – 204	191	150	28,65	5,472,225	1,045,180,650
204 – 231	217	88	19,096	4,143,832	899,211,544
231 – 259	245	50	12,250	3,001,250	735,306,250
259 – 284	272	43	11,696	3,181,312	865,316,864
284 – 310	297	13	3,861	1,145,717	340,574,949
310 – 336	323	12	3,876	1,251,948	404,379,204
336 – 363	349	5	1,745	609,005	212,542,745
363 – 389	376	2	752	282,752	106,314,752
389 – 415	402	1	402	161,604	64,964,808
Totals		2401	246,631	36,826,178	6,880,181,431

$$\text{Mean droplet diameters are: } \bar{D}_{10} = 102.7\mu \quad \bar{D}_{30} = 142.0\mu$$

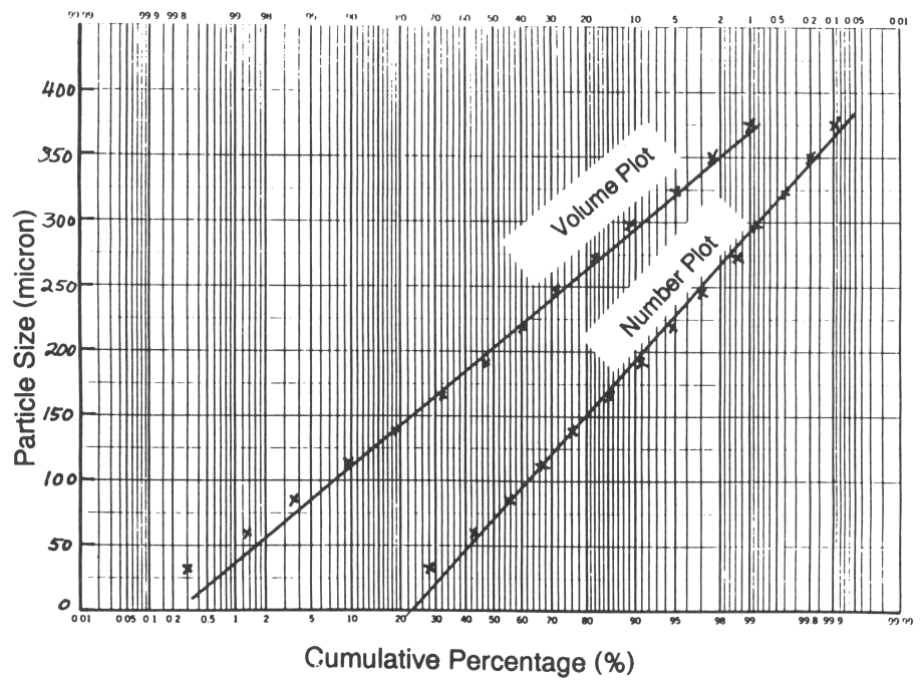
$$D_{20} = 123.8\mu \quad \bar{D}_{31} = 167.0\mu$$

$$\bar{D}_{21} = 149.3\mu \quad \bar{D}_{32} = 186.8\mu$$

To determine median diameters, complete the table as shown below and then plot the data on a probability paper as shown. Mean diameters are determined from the plot.

Size class midpoint, μ	No. in each size class	No. in each size class, %	Cum. % by number	Vol. in each size class, %	Cum. % by volume
32	699	29.1	29.1	0.3	0.3
59	326	13.6	42.7	1.0	1.3
85	282	11.7	54.4	2.5	3.8
112	286	11.9	66.3	5.8	9.6
138	243	10.1	76.4	9.3	18.9
165	201	8.4	84.8	13.1	32.0
191	150	6.2	91.0	15.2	47.2
217	88	3.7	94.7	13.1	60.3
245	50	2.1	96.8	10.7	71.0
272	43	1.8	98.6	12.6	83.6
297	13	0.5	99.1	4.9	88.5
323	12	0.5	99.6	5.9	94.4
349	5	0.2	99.8	3.1	97.5
376	2	0.1	99.8	1.6	99.1
402	1		99.9	0.9	100

$D_{N,1}$ = not applicable $D_{V,1}$ = 50 μ
 $D_{N,5}$ = 75 μ $D_{V,5}$ = 195 μ
 $D_{N,9}$ = 188 μ $D_{V,9}$ = 300 μ



10.3 PERFORMANCE EVALUATION

10.3.1 Uniformity of coverage of granular chemical application

The performance of a dry chemical applicator is measured by the uniformity of coverage and the calibration accuracy. The uniformity of coverage is based on the uniformity of metering and on the spreading or distribution. Field variables affect the uniformity and calibration accuracy. Bumpy and sloping fields result in undesirable performance. The material being applied also affects the performance. Free-flowing materials produce a more uniform application, as opposed to the materials that tend to form clumps and do not meter well.

A typical metering uniformity for 24 outlets across the width of the applicator is shown in Figure 10.39. The coefficient of variation (C.V.) was 9.5%. The C.V. is a measure of the scatter in a data set and it is computed by dividing the standard deviation by the sample mean. The higher the C.V., the greater the scatter in the data.

The uniformity of spreading is expressed in terms of application rate at a given location across the width of the applicator. The distribution and C.V. shown in Figure 10.40 is typical.

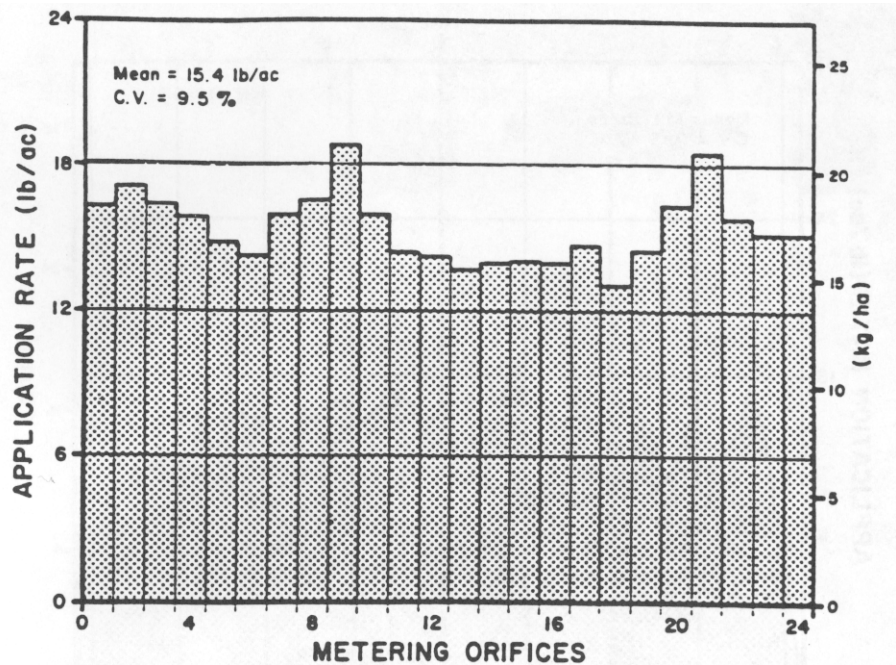


Figure 10.39 – Typical variation in delivery rates from individual outlets with the original set of hopper bottoms while applying Avadex BW at 17.3 kg/ha (15.4 lb/ac) and 8 km/h (5 mph) (courtesy of Prairie Agricultural Machinery Institute, Canada).

In addition to the lateral uniformity of application, longitudinal uniformity also affects the applicator performance. The longitudinal uniformity usually is in the form of cyclic variations that are caused by the design of the metering mechanisms. Figure 10.41 shows different lateral distribution patterns for centrifugal spreaders. The overall uniformity is based on the individual pattern and the amount of overlap for each swath.

The performance of rotary broadcast-type fertilizer distributors is affected by the speed of the spinning disk and the size of fertilizer granules, among other factors. Crowther (1958) conducted a study of these effects. A commercial fertilizer was used in the study with size distribution such that 92% of particles pass through sieve opening 3353 μ , 36% at 2411 μ and 4% at 1190 μ . Figure 10.41 shows that as the speed of the disk increased the particles were thrown farther, which was expected. However, distribution of the spread density across the width of the distributor was also affected. Figure 10.42 shows the segregation of the particles at 400 rev/min. There is some segregation of particles according to their size; however, it is not likely to affect the overall distribution pattern.

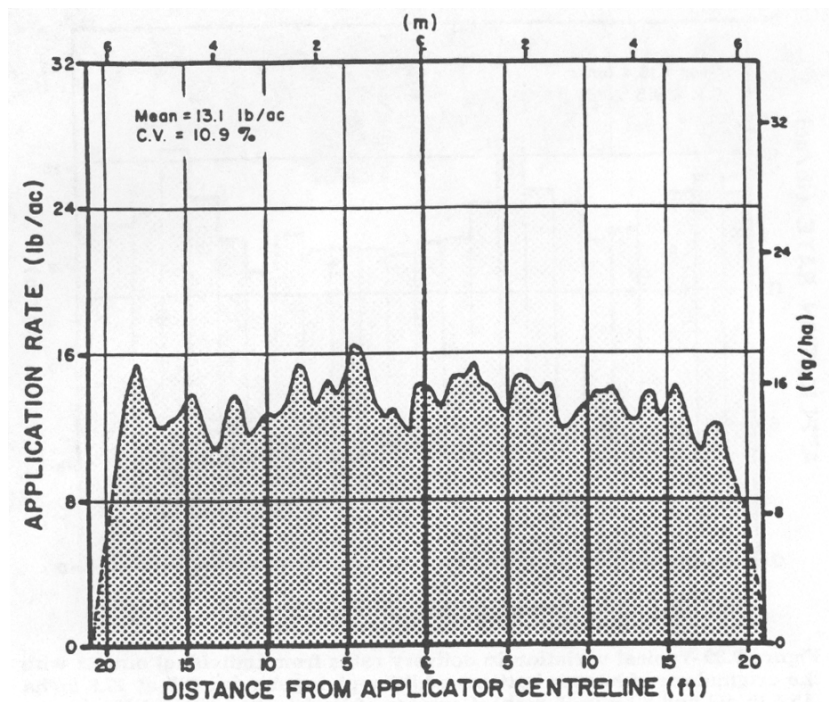


Figure 10.40 – Typical distribution pattern using the original hopper bottoms when applying 14.7 kg/ha (13.1 lb/ac) of Avadex BW at 8 km/h (5 mph) using 610 mm (24 in.) deflector spacing and a 610 mm (24 in.) deflector discharge height (courtesy of Prairie Agricultural Machinery Institute, Canada).

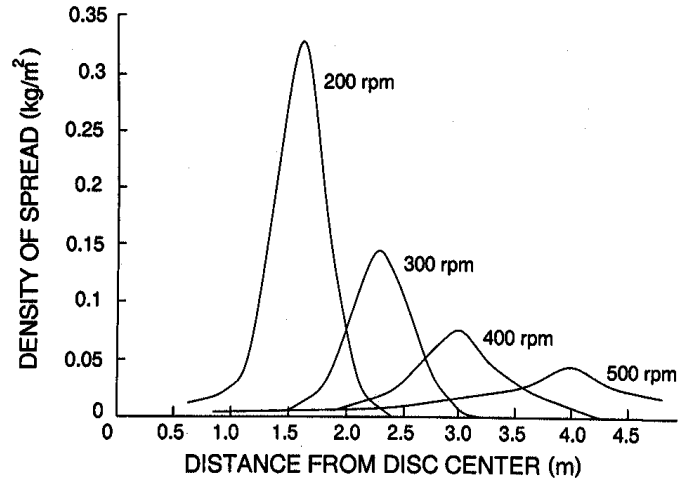


Figure 10.41 – The effect of disk speed on the distance the particles are thrown by the distributor (Crowther, 1958).

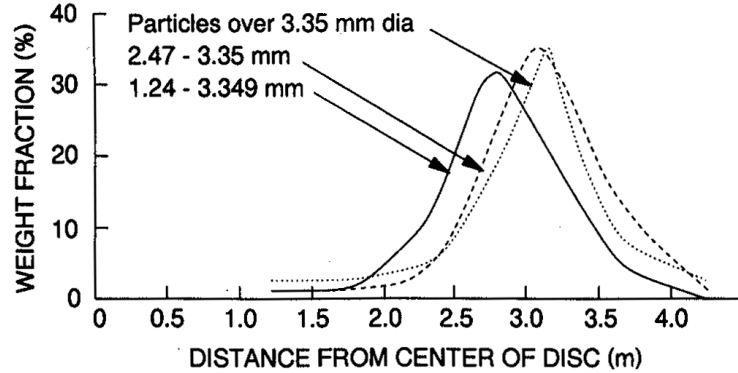


Figure 10.42 – Segregation of particles due to their size by the spinning disk (Crowther, 1958).

10.3.2 Calibration of fertilizer spreaders

10.3.2.1 Gravity spreaders

Calibration refers to the amount of chemical applied per unit area and is usually expressed as kilograms per hectare (kg/ha). The fertilizer (or other product) label indicates the recommended application rate. Sometimes the application rate is specified in terms of the amount of active ingredient to be applied per unit area since agricultural chemicals, particularly pesticides, are available in different formulations. In this case the product application rate can be computed using the following formula:

$$AR = \frac{AR_{ai}}{FR_{ai}} \quad (10.14)$$

where AR = product application rate, kg/ha

AR_{ai} = application rate of the active ingredient in the formulation

FR_{ai} = fraction of the active ingredient in the formulation

The rate of application is independent of the ground speed of the applicator as the metering rate is proportional to the rate of travel. This is accomplished by driving the metering mechanism by the ground wheel. Different fertilizers and pesticides require different application rates, so the applicator should be calibrated to the desired rate of application. The manufacturers of the applicators provide for the adjustment of the orifice to vary the application rate.

An applicator may be calibrated in the laboratory, although field calibration is recommended because ground roughness affects the rate. If the application rate is not correct, the applicator should be adjusted and the calibration should be performed again.

To calibrate in the field, fill the hopper with material and adjust the gage to the recommended setting. Pull the applicator forward until a steady stream is flowing from the tubes. Mark a distance at least 200 m. Remove the tubes and attach bags to collect the material. After traveling the marked distance at the desired speed, collect and weigh the material. The following formulas may be used to determine the application rate:

$$A = \frac{d w}{10,000} \quad (10.15)$$

$$AR = \frac{m}{A} \quad (10.16)$$

where A = treated area, ha

d = distance traveled, m

w = swath width, m

AR = application rate, L/ha

m = amount of material collected, kg

For laboratory calibration, the applicator is jacked up and the ground wheel is turned several times to simulate field travel. The granules are collected and weighed. The distance traveled in Equation 10.15 is then determined by:

$$d = \pi D_w N \quad (10.17)$$

where D_w is the ground wheel diameter (m) and N is the number of revolutions.

For banded applications, the rate of application in the band is the same as the recommended field application rate. Less total product is applied since the treated area is less than the total area. The following formula is used to compute the treated area in banded applications:

$$A_b = \frac{d_b A}{d_r} \quad (10.18)$$

where A_b = band treated area, ha

d_b = band width, m

d_r = row spacing, m

Table 10.3. Pan spacing for collecting samples to determine spread pattern.

Swath width (m)	Pan spacing, m,	
	9 pans	11 pans
9.144	1.143	1.066 on each side of center pan 0.991 between all other pans
10.668	1.321	1.066
12.192	1.524	1.219
13.716	1.727	1.372
15.240	1.905	1.524

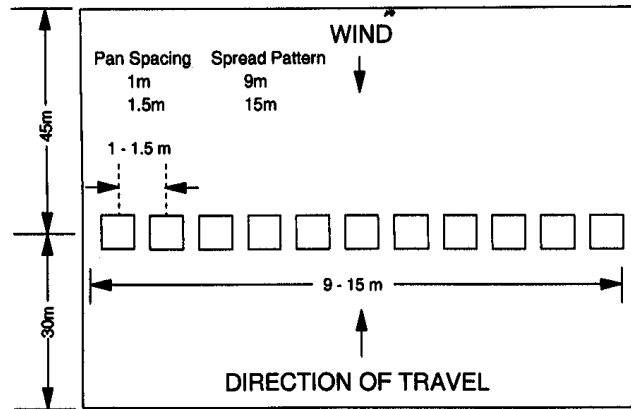


Figure 10.43 – Diagram showing the minimum requirements for a spread pattern test area.

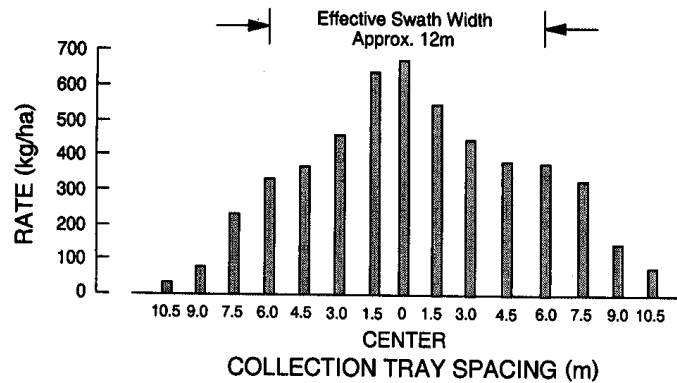


Figure 10.44 – Diagram showing the experimentally obtained distribution pattern and the effective swath width.

10.3.2.2 Rotary spreaders

The objective of calibrating a rotary spreader is to apply fertilizer at a desired application rate (kg/ha) and to obtain a uniform coverage. It is essential to establish the effective swath width and the spread pattern as they affect the amount of overlap. There are three acceptable spread patterns, flat-top, pyramid, and oval, that result in a uniform coverage if proper overlap is maintained.

Most spreaders come with a calibration kit and a set of instructions to establish spread pattern and swath width. These instructions should be followed carefully. Generally, a test area is set up as shown in Figure 10.43. Collection pans are placed according to the spacing as shown in Table 10.3. Position the row of pans so that the spreader is running at least 100 ft before it reaches them and continues to spread at least 150 ft beyond. Select the desired application rate for the fertilizer to be applied and perform the test. The application rate for each pan is then calculated based on the area of the pans and the weight of material collected in each pan. These data are then plotted in a manner similar to that shown in Figure 10.44. The effective swath width is computed from this data by locating the point on either side of the center where the application rate is one-half of that found in the center. The distance between these points is the effective swath width. The spread pattern can be visualized from the data given in Figure 10.44. If this pattern is not acceptable, necessary adjustments must be made according to the manufacturer's instructions. Finally, the application rate can be determined in field by keeping track of the amount of material applied and the area covered.

10.3.3 Liquid chemical application

Sprayer performance is evaluated by the uniformity of coverage and spray patterns, droplet size and size distribution, and target deposition and drift.

Uniformity of coverage. The uniformity of coverage is determined by (a) the type of nozzle, (b) the nozzle spacing, (c) the boom height, and (d) the angle of the spray nozzle. As shown in Figure 10.45, the most uniform coverage is produced with a flat-fan nozzle with a wide angle, with the boom height set at the minimum recommended height. Raising or lowering the boom results in over- or under-application. The figure also shows the effect of spray angle on the uniformity of the spray pattern. For narrow spray angle nozzles, the spray pattern is much more sensitive to changes in boom height. It is generally recommended that for flat-fan spray nozzles a 60% overlap should be obtained by adjusting the boom height. (The overlap is defined as the width covered by two adjacent nozzles divided by the width covered by a single nozzle, expressed in percent.) The boom height can be calculated for a given amount of overlap and nozzle spacing. However, manufacturers' recommended minimum boom height should be used because the actual spray width is somewhat less than the theoretical value as calculated by the spray angle and the boom height. The recommended amount of overlap for flooding flat-fan nozzles and some wide-angle hollow-cone nozzles is 100%.

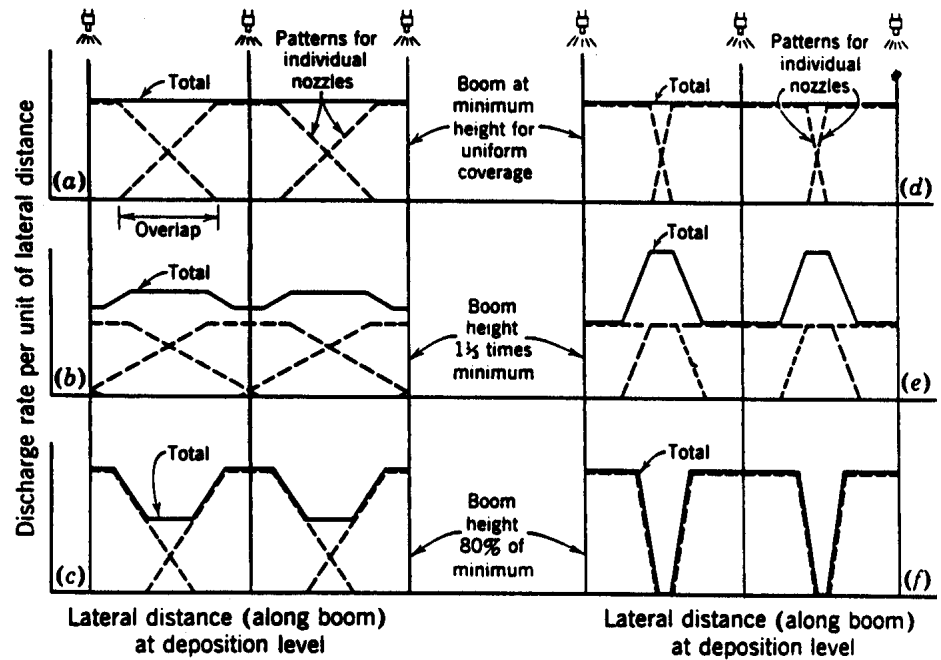


Figure 10.45 – Effect of nozzle distribution pattern and boom height on uniformity of coverage. Broken-line curves indicate distribution patterns (at the deposition level) for individual nozzles; the solid curve in each case shows the combined discharge pattern for all nozzles (i.e., the sum of the broken-line curves) (reprinted from Kepner et al., 1978).

According to the tests conducted at the Prairie Agricultural Machinery Research Institute (PAMI), Humboldt, Saskatchewan, Canada, the uniformity is affected by the nozzle pressure. Figure 10.46 shows a poor distribution pattern along the boom at low nozzle pressure corresponding to a forward speed of 8.3 km/h. The distribution became more uniform when the pressure was increased to maintain the same application rate for a forward speed of 14.6 km/h, as shown in Figure 10.47.

Other factors that result in unacceptable spray distributions include worn and damaged nozzles. Also, uneven ground causes boom height to vary thereby resulting in a non-uniform spray distribution.

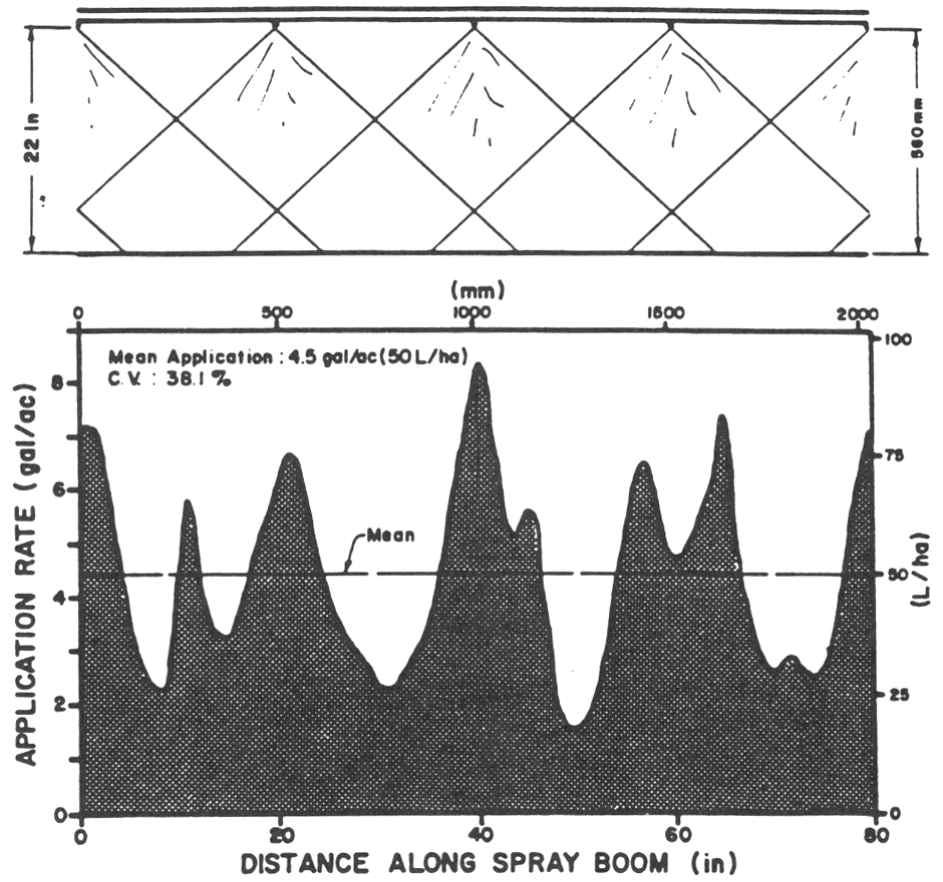


Figure 10.46 – Typical distribution pattern along the boom using number 3 nozzles at 8.3 km/h at a 560 mm nozzle height (courtesy of Prairie Agricultural Machinery Institute, Canada).

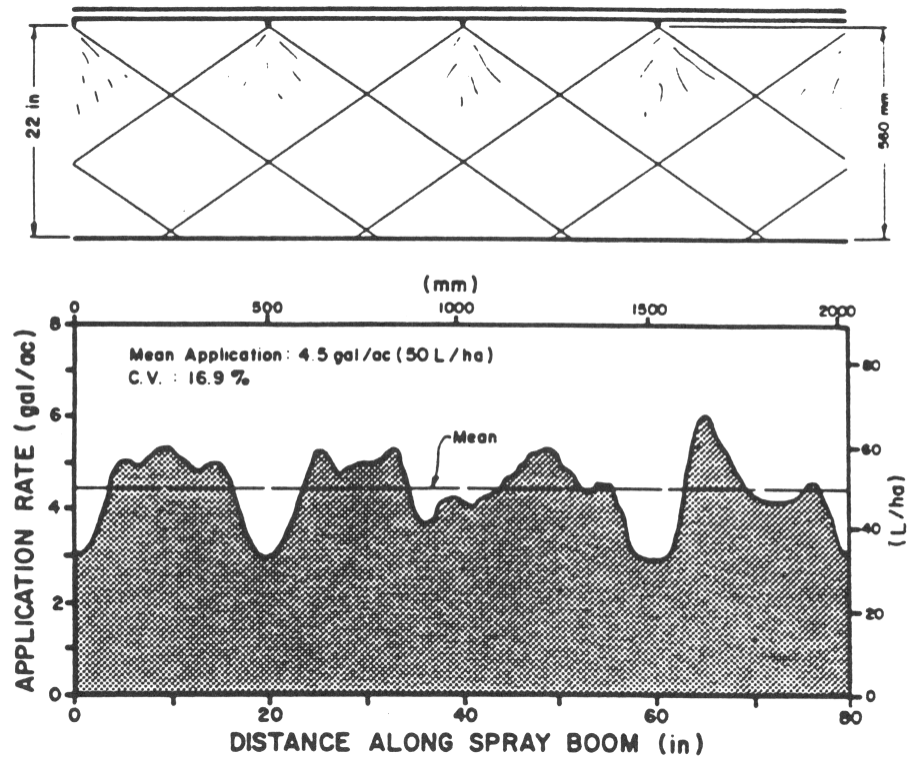


Figure 10.47 – Typical distribution pattern along the boom using number 3 nozzles at 14.6 km/h at a 560 mm nozzle height (courtesy of Prairie Agricultural Machinery Institute, Canada).

Droplet Size. Droplet size, often expressed as $D_{v,5}$ (volume median diameter), is affected by nozzle type, spray angle, flow rate, and operating pressure. Generally, the hollow-cone nozzles produce the finest droplets, flat-spray nozzles the next-finest, while the full-cone nozzles produce the coarsest spray. The droplets become finer as the width of spray increases, due to spreading of the liquid sheet to a greater angle, which produces more fines at the edges. For a given type of nozzle the smallest capacity nozzle produces smaller droplets and vice versa. Table 10.4 shows the effects of spray angle and flow rate on droplet size. As the operating pressure increases the droplet size decreases. It is, therefore, important to realize that while increasing the application rate by increasing pressure, the droplet size would decrease and may result in higher drift. Liquid viscosity and density have very little effect on droplet size in the range commonly found in agricultural application. Increasing the surface tension increases the volume median diameter (VMD).

Table 10.4. Effect of spray angle and flow rate on droplet size (Spraying Systems Co., 1991).

Spray Angle (°)	Nozzle Type (1.89 L min @ 275 kPa)	Volume Median Diameter (μ) (@ nozzle pressure of) (kPa)		
		103	275	550
40	4005 flat spray	900	810	780
65	6505 flat spray	600	550	530
80	8005 flat spray	530	470	450
110	11005 flat spray	410	380	360
Nozzle Type (275 kPa)		Volume Median Diameter (μ) (@ nozzle flow rate of) (L / min)		
		0.75	1.89	3
Std. TeeJet 80° Flat spray tip		390	470	560
XR TeeJet 80° Flat spray tip		360	460	560
TK-FloodJet Flat spray tip		370	450	540
FL-FullJet Full cone tip		—	680	770
TX ConeJet Hollow cone tip		220	360	—

Often manufacturers of spray nozzles give droplet VMD for a nozzle at a given pressure while spraying water. Droplet diameter may be estimated for a different pressure by the following equation:

$$\frac{D_{vm1}}{D_{vm2}} = \left(\frac{p_2}{p_1} \right)^{1/3} \quad (10.19)$$

where D_{vm1} , D_{vm2} = VMD at pressures p_1 and p_2 , respectively.

For similar nozzles and at constant pressure, the effect of different orifice size can be estimated from the manufacturers' data using the following equation:

$$\frac{D_{vm1}}{D_{vm2}} = \left(\frac{d_1}{d_2} \right)^{2/3} \quad (10.20)$$

where D_{vm1} , D_{vm2} = VMD at orifice diameters d_1 and d_2 , respectively.

Often surfactants are added to increase the surface tension thereby increasing the droplet size and reducing drift. The effect of changing surface tension can be estimated from the following equation:

$$\frac{D_{vm.chemical}}{D_{vm.water}} = \left(\frac{\sigma_{chemical}}{73} \right)^{1/2} \quad (10.21)$$

where $\sigma_{chemical}$ = surface tension of the chemical, mN/m (dyne/cm).

Table 10.5. Spray droplet size and its effect on drift (Bode and Butler, 1981).

Droplet diameter, μ	Steady state fall rate, m/s	Time to fall 3.04 m in still air, sec.	Drift distance in 3.04 m fall with 4.82 km/h wind, m	Lifetime of evaporating water droplet, sec ^[a]	Fall distance of evaporating droplet in life-time, m ^[a]
5	0.00075	3960	4815	0.04	<0.025
10	0.003	1020	1372	0.2	<0.025
20	0.012	230	338	0.7	<0.025
50	0.076	40	54.25	4	0.076
100	0.122	11	14.63	16	2.44
150	0.457	8.5	7.62	36	12.2
200	0.9274	5.4	4.57	65	38.4
500	1.158	1.6	2.13	400	>380
1000	2.133	1.1	1.52	1620	>380

^[a]Air temperature, 30°C; relative humidity, 50%.

Drift and coverage. Spray drift poses a significant hazard to the environment, as most pesticides, herbicides, and fertilizers are toxic or have other undesirable effects on unintended targets. Smaller droplets tend to drift more than larger ones, because smaller droplets take longer to settle (Table 10.5). Note that as the droplet size decreases settling time increases in a logarithmic manner. Droplets that take longer to settle are very prone to drift. Every nozzle produces droplets of different sizes, but if the size distribution is very wide, a lot of droplets will be undersize and be prone to drift. It is, therefore, best to produce a narrow distribution of droplet sizes near the desired size. Generally, a balance has to be struck between the large droplets and the small droplets. Large droplets give greater penetration of the plant canopy while smaller droplets give greater coverage. Table 10.2 shows the effects of droplet size on coverage. As the droplets become smaller the coverage increases for the same application rate. For systemic herbicides larger droplets would be acceptable, but for contact herbicides or fungicides, full coverage made possible by smaller droplets is more desirable. In addition, although smaller droplets give better coverage they evaporate at a faster rate adding to the drift. Table 10.5 shows evaporation rates for different size droplets.

Research is under way to improve sprayer efficiency and reduce drift. Electrostatic charging and air-curtain sprayers are two results of the efforts in this direction. Droplets are electrostatically charged to improve their tendency to adhere to the plants thereby increasing efficiency of coverage and reducing drift. In air-curtain sprayers, the droplets are introduced in a fast moving air stream to increase penetration into the plant canopy.

10.3.4 Sprayer calibration

Sprayer calibration refers to adjusting the chemical application rate in terms of L/ha. The application rate depends on the sprayer forward speed, effective sprayer width, and the nozzle flow rate. The following formula can be used to determine the required nozzle flow rating for broadcast applications:

$$Q_n = \frac{AR d_n S}{600} \quad (10.22)$$

where Q_n = nozzle flow rate, L/min
 AR = application rate, L/ha
 d_n = nozzle spacing, m
 S = sprayer speed, km/h

Once the desired nozzle flow rate is determined an appropriate nozzle may be selected from the manufacturers' catalog. The next step is to adjust the system pressure to obtain the desired flow rate. The following formula may be used to determine the desired pressure (p):

$$p = \left(\frac{Q_n}{Q_r} \right)^2 p_r \quad (10.23)$$

where Q_r = rated nozzle flow rate (L/min)
 p_r = rated nozzle pressure (kPa)

For banded application, use the spray-band width or swath width for spacing in Equation 10.22. For multiple-nozzle directed spray, the value to be used for spacing is the row width divided by the number of nozzles per row. Keeping a sprayer calibrated properly is very important to maximize chemical effectiveness and to minimize environmental hazards. Sprayer controllers are now available that monitor the tractor/sprayer speed and the flow rate, and continuously adjust flow to the desired application rate.

Example 10.4

Determine the nozzle flow rate for a hollow-cone nozzle for an application rate of 200 L/ha. The sprayer speed is 10 km/h and the nozzle spacing is 50 cm. The available 0.787 mm orifice diameter nozzle is rated at 0.473 L/min at 275 kPa pressure. Determine what pressure would be required to produce the desired nozzle flow. If the nozzle produces a VMD of 200 μ at 1000 kPa, determine the droplet size at the desired flow rate. If a VMD of 350 μ is needed, determine the surface tension that should be achieved by adding surfactants.

Solution

Determine the nozzle flow rate as:

$$Q_n = \frac{200(0.5)7.5}{600} = 1.24 \text{ L/min}$$

Now determine the desired pressure for the given nozzle as:

$$p = \left(\frac{1.24}{0.473} \right)^2 275 = 1889 \text{ kPa}$$

VMD at the above pressure is calculated next:

$$d_{vml} = \left(\frac{1000}{1889} \right)^{1/3} 200 = 162 \text{ } \mu$$

Surface tension has to be increased to get the desired droplet size of 350 μ . The necessary surface tension is calculated as:

$$\sigma_{\text{chemical}} = \left(\frac{350}{200} \right)^2 73 = 223.5 \text{ dynes/cm}$$

Manufacturers of surfactants should be consulted to determine the appropriate compound and its proportion to achieve the desired surface tension.

PROBLEMS

- 10.1 A side-dressing fertilizer unit is to place two bands per row on a crop with a 1-m row spacing. It is desired to apply a fertilizer having an apparent specific gravity of 0.85 at a rate of 560 kg/ha. If the distributor is calibrated by driving the machine forward a distance of 30 m, what mass of material should be collected from each delivery tube when the distributor is properly adjusted?
- 10.2 A distributor for liquid fertilizer has gravity feed through fixed orifices. The tank is 460 mm deep and is top-vented. The bottom of the tank is 610 mm above the ground and the ends of the delivery tubes are 75 mm below ground level. The metering heads (including orifices) are just below the tank, but the delivery tubes are small enough so each one remains full of liquid between the orifice and the outlet end (thereby producing a negative head on the orifice). (a) Calculate the ratio between flow rates with the tank full and with a depth of only 25 mm remaining in the tank. (b) List three possible changes in the system that would reduce the variation in rates.
- 10.3 A 0.95-m³ round-bottom sprayer tank is 1.5 m long and has a depth of 0.9 m. Mechanical agitation is to be provided with four paddles 280 mm long (tip:

- diameter) and 200 mm wide mounted on a shaft 150 mm above the bottom of the tank. (a) Calculate the minimum rev/min for agitating a mixture of 10% oil and 90% water. (b) If the mechanical efficiency of the power transmission system is 90%, what input power would be needed for agitation?
- 10.4 Under the conditions of Problem 10.3, (a) what recirculation rates would be required for hydraulic agitation at 400 kPa and 2.75 MPa? (b) If the pump efficiency is 50%, what pump input power would be needed for hydraulic agitation at each pressure? (c) Prepare a table to summarize and compare the results of Problems 10.3 and 10.4. Note the decreased recirculation rate and increased power requirement when the hydraulic-agitation pressure is increased.
- 10.5 A field sprayer having a horizontal boom with 20 nozzles spaced 46 cm apart is to be designed for a maximum application rate of 750 L/ha at 520 kPa and 6.5 km/h. (a) Determine the required pump capacity in liters per minute, assuming 10% of the flow is bypassed under the above maximum conditions. (b) If mechanical agitation requires 375 input watts and the pump efficiency is 50%, what should be the engine rating if the engine is to be loaded to not more than 80% of its rated power? (c) What discharge rate per nozzle (L/min) is required under the above conditions? (d) If the nozzles have 70° spray angles and the pattern is such that 50% overlap is needed for uniform coverage (i.e., spray pattern 50% wider than nozzle spacing), at what height above the tops of the plants should the boom be operated?
- 10.6 A field sprayer is equipped with nozzles having a rated delivery of 0.42 L/min of water at 275 kPa. The nozzle spacing on the boom is 51 cm. Each kilogram of active ingredient (2,4-D) is mixed with 80 L of water and the desired application rate is 0.95 kg of chemical per hectare. What is the correct forward speed for a nozzle pressure of 200 kPa?
- 10.7 A hollow-cone spray nozzle deposits most droplets between two concentric circles. Assume the diameter of the inner circle is 70% of the diameter of the outer circle and that the distribution of droplets is uniform between the circles. Plot the theoretical distribution pattern that would be expected as the nozzle is moved forward past a transverse line. Graphical solution is acceptable.
- 10.8 At a deposition level 410 mm below the tip of a particular fan-spray nozzle, the discharge rate-across a 20-cm width at the center of sprayed strip is essentially constant at 15 mL/min per centimeter of width and decreases uniformly to zero at a lateral distance of 36 cm from the nozzle centerline. (a) Plot the distribution curve to scale. (b) On the same graph, draw a curve for this nozzle at a deposition level 585 mm below the nozzle tip. (c) Calculate the nozzle spray angle. (d) If nozzles having this pattern are 50 cm apart on the boom, what tip height above the deposition level would give uniform coverage?
- 10.9 An airblast sprayer is to be operated at 4 km/h and the desired application rate is 19 L per tree. The tree spacing is 9 × 9 m and each nozzle delivers 4.0

- L/min at the operating pressure of 415 kPa. (a) If one-half row is sprayed from each side of the machine, how many nozzles will be needed? (b) How many hectares can be covered with a 2-m³ tank full of spray?
- 10.10 A manufacture of pressure nozzles specifies that a volume median diameter of 135 μ m is obtained at 345 kPa using water. The same nozzle is to be used for a chemical whose surface tension is 50 dynes/cm. Determine the volume median diameter droplet size if the nozzle is to be operated at 525 kPa.
- 10.11 One hundred droplets from an atomizer were determined to have diameters in microns as shown below. Determine (a) arithmetic mean, surface, volume, and Sauter mean diameters. (b) Complete a probability distribution plot and determine number, surface, and volume median diameters.

70	250	490	160	150	370	370	330	210	500
340	210	150	340	290	110	580	760	350	290
260	270	1130	730	650	470	130	380	760	190
210	870	650	310	150	340	340	190	970	660
340	390	640	640	750	1140	450	280	160	270
250	620	150	200	520	190	440	700	280	360
140	470	470	180	1010	170	210	410	800	390
340	460	230	630	1070	570	460	550	310	170
150	150	490	100	780	370	330	520	350	250
470	540	330	150	170	370	270	370	160	190

HAY AND FORAGE HARVESTING

11

INTRODUCTION

Domesticated animals have been used as power sources and/or as food during the entire recorded history of agriculture. Through grazing, animals are able to make use of grasses, legumes, and other forage crops that people cannot consume directly. The climate permits year-around grazing in some parts of the world. Because grazing is selective and management intensive, however, *forages* are generally machine harvested and stored for later feeding. The two most common methods of preserving forage crops are as *direct-cut* or *field wilting*. With direct-cut harvest, silage is stored at the moisture level of the cut crop; field wilting allows the moisture content to decrease. *Ensilage* involves cutting the forage at 70% to 80% moisture, allowing it to field dry to 50% to 65% moisture, chopping it into short lengths to obtain adequate packing, and preserving it by fermentation in an airtight chamber. For *hay* harvest, the forage must be cut and allowed to dry to a moisture content of 15% to 23% before it can be stored. Hay has low bulk density and does not flow readily; *silage* has the same limitations, plus it will spoil if it is not fed soon after removal from storage. Thus, both hay and silage are often fed close to the point of production. There are, however, commercial hay farms that produce high-quality hay, bale it, and ship it considerable distances—even internationally—to customers.

Forages are unique because they are harvested with high moisture content levels. Because of the large volume of water that must be removed and the limited crop value, it is generally not feasible to dry forages by artificial means. Losses and storage properties are highly dependent on crop moisture (Figure 11.1).

11.1 METHODS AND EQUIPMENT

Figure 11.2 illustrates common activities for harvesting forage. For harvesting as silage, the standing or wilted crop is cut, field cured, and then chopped into short lengths by a forage harvester (Figure 11.3). The same machine conveys the chopped forage into a wagon or truck for transport to the silo. There, the chopped forage is dumped directly into a bunker or trench silo, bagged into horizontal bags, or blown into a tower silo with a forage blower (Figure 11.4). Most grass and legume forage is

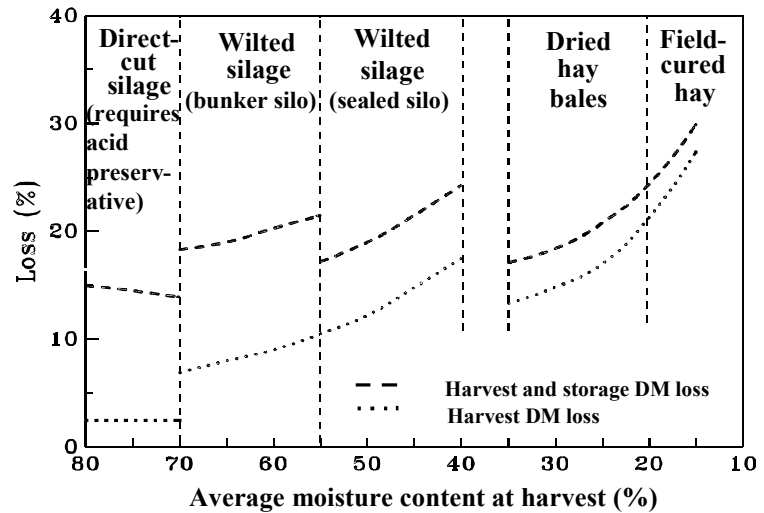


Figure 11.1 – Typical dry matter losses of forage during haycrop harvest and storage (Rotz et al., 1990).

allowed to partially dry by wilting before chopping; silage stored too wet produces effluents and causes poor fermentation. Silage that is too dry packs poorly and spoils. Therefore, once the crop has reached the proper moisture content (Figure 11.1), the forage harvester and its complementary equipment must provide for a rapid harvest. Direct-cut corn (maize) can be ensiled without drying, since the fermentation process prevents spoilage.

Forages are field dried in either a *swath* or a *windrow*. A swath approaches the width of the cut strip, generally leaving enough stubble uncovered to permit wheel traffic during subsequent operations. Swaths dry more rapidly due to greater area exposed to solar radiation, but they must be raked into a windrow for harvesting. A windrow is a narrow strip of forage that dries at a slower rate but does not require further manipulation before harvest. Forages to be made into dry hay are usually placed in a swath while those to be made into silage are placed directly into a windrow to control the drying rate. Tedding is sometimes used to spread the crop uniformly to increase the drying rate.

Leaves dry faster than stems with legume and grass-type forages. The leaves, especially in legumes, are higher in nutritional value than the stems. Brittle, dry leaves may be lost during raking and harvesting. To reduce such losses, the forage will be conditioned so that the stems dry at a rate approaching that of the leaves. *Conditioning* is a physical process of crushing or abrading the stems, or a chemical process that dissolves the waxy cutin layer of the stems. Either process increases the stem-drying rate by reducing the natural resistance to moisture removal from the stems.

Grass and legume forages are usually cut with a machine that combines the cutting and the conditioning process (Figure 11.5). The mower-conditioner can place the forage into either a wide swath or a narrow windrow. A windrower can be used to harvest either forages or small grains, but can only place the material into a narrow windrow.

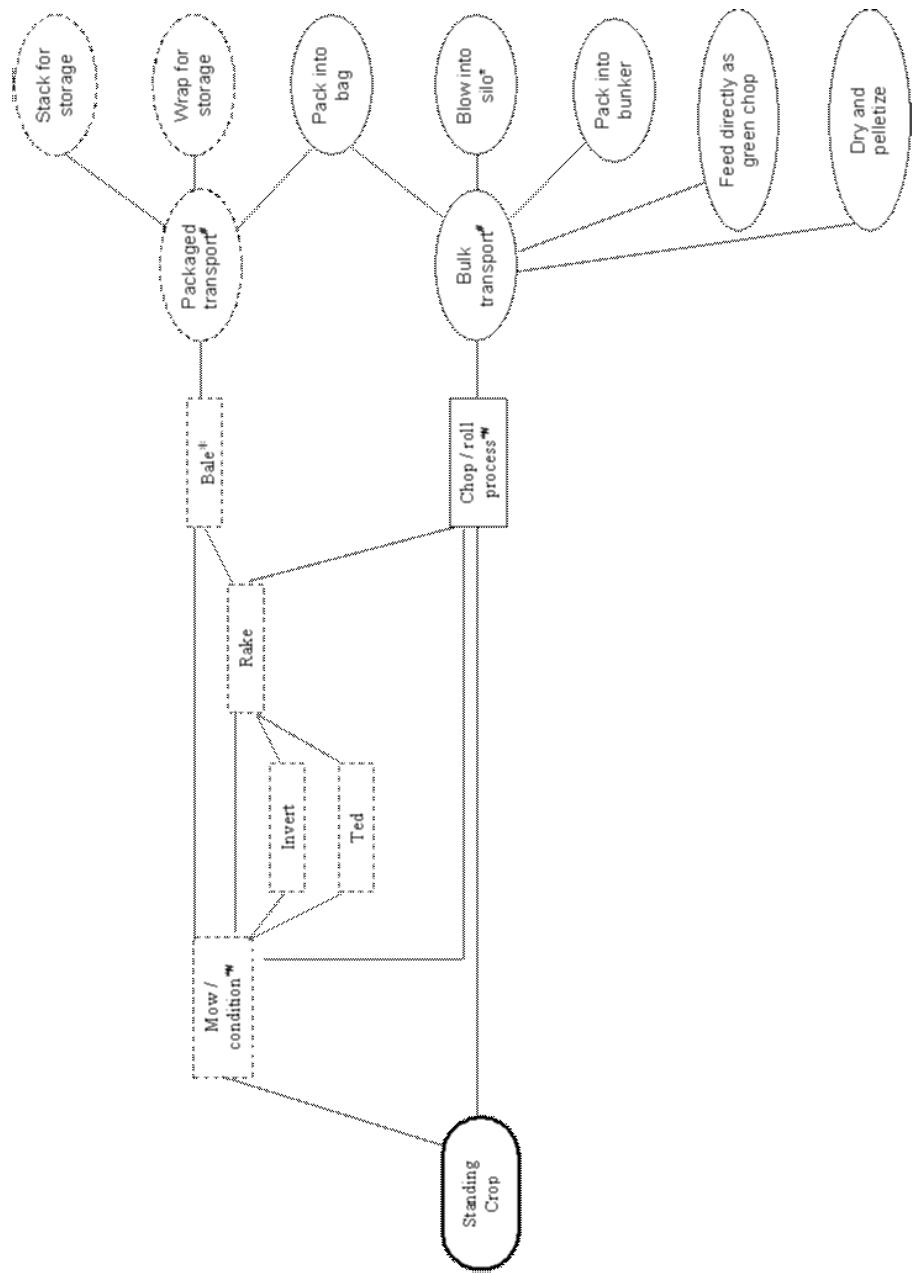


Figure 11.2 – Primary operations of forage harvest systems sequenced left to right (rectangles – harvest operations; ovals – non-harvest operations; dashed enclosures – wilted crops only; solid enclosures – wilted or direct-cut crops; * common points of chemical application; # sometimes self-propelled).



Figure 11.3 – Forage harvesters (Courtesy of CNH).

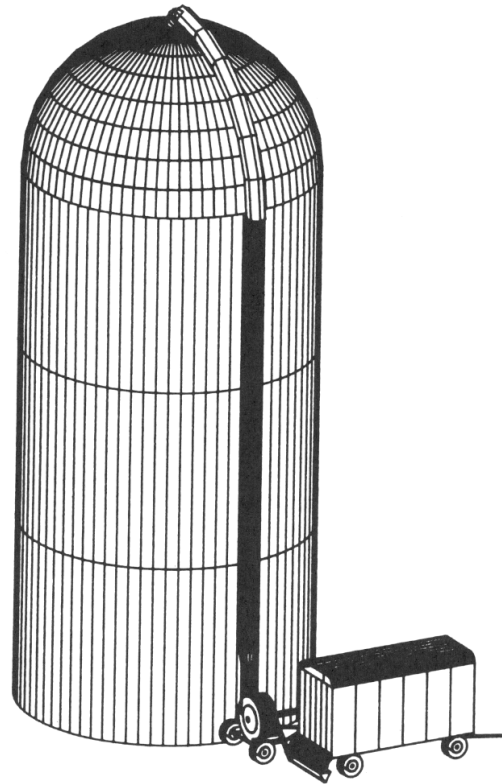


Figure 11.4 – Conveying forage into a tower silo.

After the forage dries to 23% moisture or less, it is usually compressed to some degree before being transported to storage. Baling the hay into small rectangular bales of 25 to 40 kg mass (Figure 11.6) provides hay packages that can be convenient to store and can be lifted by a single person or by machine. Because they do not resist water penetration very well, rectangular bales are usually transported and stored under a roof soon after baling. In another alternative, the hay is rolled into large round bales of 100 to 500 kg mass (Figure 11.7) that are more resistant to water penetration, especially if plastic wrapped, and are sometimes stored outdoors, although storage losses will be higher. The large round bales are too heavy to be handled by hand, so specialized powered equipment has been developed for handling and transporting such bales. Another approach is to package the hay into large rectangular bales that are similar in weight and density to large round bales. The large rectangular bales will not shed water and thus cannot be stored outdoors, but are better suited to shipping by truck than are large round bales.

In addition to those mentioned above, numerous other methods have been developed for harvesting hay. These include pelleting, stacking the hay into stacks in the field, compressing the hay into large loaves, and other methods. Specialized equipment has been developed to support each of these methods. Space does not permit an engineering analysis of all of this diverse equipment, so such analyses will be confined to mowing, conditioning, raking, forage chopping, and baling.

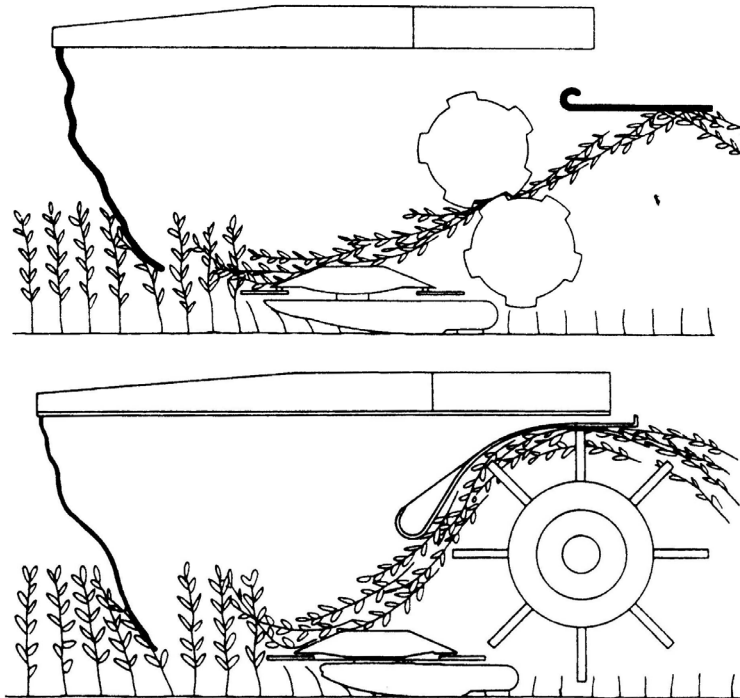


Figure 11.5 – Schematic, cross-sectional view of disk mower-conditioners (a) with roll conditioning, (b) with flail conditioning (Courtesy of CNH).

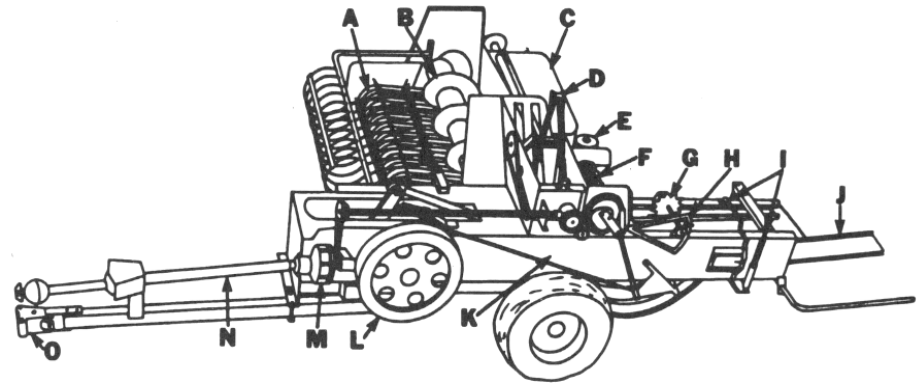


Figure 11.6 – A baler that compresses hay into rectangular bales: A = pickup, B = feed auger, C = twine box, D = feed fork, E = hydraulic pump for density control, F = knotter, G = metering wheel, H = metering arm, I = density control rams, J = bale chute, K = bale chamber, L = flywheel, M = slip clutch, N = PTO drive, O = hitch (courtesy of Prairie Agricultural Machinery Institute, Canada).

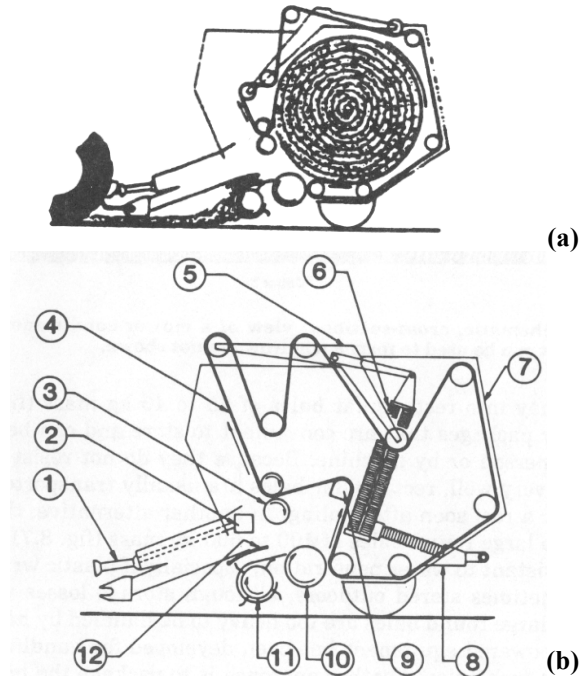


Figure 11.7 – Baler for large round bales showing (a) operation and (b) construction details: 1 = drive shaft, 2 = gear box, 3 = stripper roll, 4 = chamber belt, 5 = tensioning arms, 6 = tensioning springs, 7 = tailgate, 8 = bale ejector, 9 = core-forming cam idler, 10 = floor roll, 11 = pickup, 12 = wind guard (courtesy of Prairie Agricultural Machinery Institute, Canada).

11.2 FUNCTIONAL PROCESSES

11.2.1 Cutting mechanics and plant structure

Mowing and forage chopping involve the cutting of plant materials and cutting will be subjected to engineering analyses in this chapter. Those same analyses have wider application. For example, sickle bar mowers are used for cutting hay and forage, but similar sickle bars are included on the combines that harvest wheat, soybeans, and other crops. Thus theory learned in this chapter will be useful in understanding Chapter 12 and perhaps in analyzing machines not covered in this textbook.

11.2.1.1 Cutting geometry

In many agricultural machines, a knife is used to sever plant material. Often severing is accomplished by shearing the material between a moving knife and a stationary countershear. In designing equipment to accomplish the severing, the objectives are to maintain the quality of the harvested product while minimizing the force and energy needed to accomplish the task. The characteristics of both the cutting device and the plant must be considered in pursuing these objectives.

Figure 11.8 illustrates the geometry associated with a mower in which a knife (sickle section) moves with reciprocating motion. The plant material is sheared as the sickle section reaches and passes over the countershear (ledger plate) on the right. At the instant illustrated in Figure 11.8, the knife is just leaving the left end of its stroke and moving toward the ledger plate. Guards direct the plant material between the knife and ledger plate and also shield the blunt ends of the sickle sections while they reverse directions at the ends of their stroke.

Typically, in cutting theory, the x-axis of the coordinate system is in the direction of knife movement relative to the plant material. In Figure 11.8, the knife has a velocity component, v_{km} , relative to the mower and a component, v_f , due to the forward speed of the mower. The vector sum of these two components gives the knife velocity, v_{kg} , relative to the ground. Since the plants to be cut are attached to the ground, v_{kg} is also the knife velocity relative to the uncut plants. Therefore, the x-axis is in the direction of v_{kg} , the y-axis is in the plane of the paper but perpendicular to x, and the z-axis is perpendicular to the plane of the paper and points upward. Note that the orientation of the coordinate system in Figure 11.8 is for only one instant in time, since the magnitude of v_{km} varies during the cutting stroke and thus the coordinate system rotates about the z-axis as the direction of v_{kg} varies.

It is common knowledge that a sharp knife aids cutting. It is important, however, to distinguish between *sharpness* and *fineness*. A fine knife has a small bevel angle, ϕ_{bk} , while a blunt knife has a large bevel angle. Sharpness is defined by the edge radius, r_{ek} , of the knife, i.e., a sharp knife has a small radius while a dull knife has a larger radius. Initial penetration of the knife into the plant material is aided if the knife rake angle, ϕ_{rk} , is large. The knife clearance angle, ϕ_{ck} , is the angle formed between the bottom edge of the knife and the x-y plane. In general, the following relationship holds between the rake, bevel, and clearance angles:

$$\phi_{rk} + \phi_{bk} + \phi_{ck} = 90^\circ \quad (11.1)$$

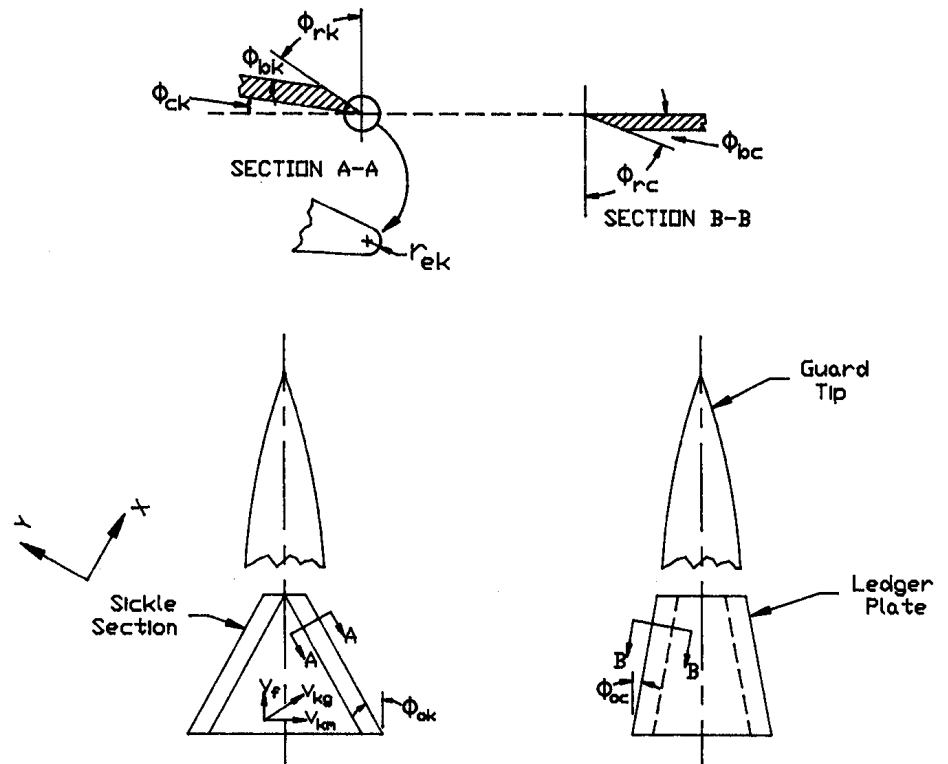


Figure 11.8 – Illustration of geometry of a knife and countershear.

The chip angle on the knife, ϕ_{chk} , is defined as follows:

$$\phi_{chk} = \phi_{bk} + \phi_{ck} \quad (11.2)$$

The oblique angle of the knife, ϕ_{ok} , is the angle between the y-axis and the cutting edge. The ϕ_{ok} illustrated in Figure 11.8 is for the special case where $v_f = 0$. A straight cut is one in which $\phi_{ok} = 0$. Conversely, an oblique cut is one in which ϕ_{ok} is not equal to zero. Oblique cutting reduces the peak cutting force because the plant material is sheared progressively rather than all at once as in a straight cut.

The bevel, rake, clearance, and oblique angles all have their counterparts on the countershear, as shown in Figure 11.8. For each of these angles, the subscript k indicates that it relates to the knife, while a subscript c indicates the corresponding angle on the countershear. The clip angle, ϕ_{cl} , is the angle formed between the knife and countershear, i.e.:

$$\phi_{cl} = \phi_{ok} + \phi_{oc} \quad (11.3)$$

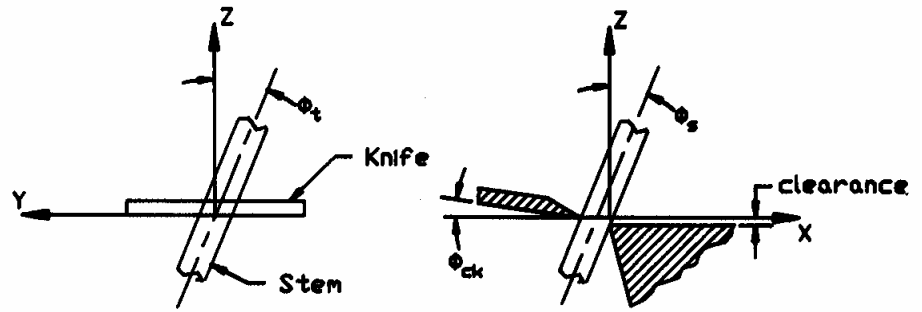


Figure 11.9 – Illustration of stem misalignment.

Frequently, plant stems are not parallel to the z-axis. Figure 11.9 illustrates the tilt angle, ϕ_t , and the slant angle, ϕ_s , which are used to define the orientation of such stems. The tilt angle is the angle between the stem axis and the z-axis projected into the y-z plane, while the slant angle is the angle between the stem axis and the z-axis projected into the x-z plane. Figure 11.9 also illustrates a positive clearance angle on the knife and the clearance that may be present between the knife and the counter-shear.

When ϕ_{ok} is not zero and the plant material is not yet in contact with the counter-shear, the possibility exists that the plant material may slide along the edge of the knife before or while being cut. The sliding is expected if the oblique angle is greater than the following maximum angle:

$$\phi_{ok,max} = \arctan f_{ek} \tag{11.4}$$

where f_{ek} = knife edge friction coefficient. The knife edge friction coefficient is the lateral force (parallel to the knife edge) imposed by the plant on the knife edge divided by the normal force imposed by the plant. When the plant is in contact with both the knife and countershear, sliding is expected if the clip angle is greater than the following maximum:

$$\phi_{cl,max} = \arctan \frac{f_{ek} + f_{ec}}{1 - f_{ek}f_{ec}} \tag{11.5}$$

where $\phi_{cl,max}$ = maximum value of ϕ_{cl} that will prevent sliding
 f_{ek} = friction coefficient for knife edge
 f_{ec} = friction coefficient for countershear edge

Since the forward motion of the mower helps to push the plants toward the rear of the knife sections, sliding is most likely to occur when v_f is small. To increase friction and thus prevent sliding, serrations may be cut into the edge of the knife and/or countershear. For example, values of $f_{ek} = 0.306$ for a smooth knife edge and $f_{ec} = 0.364$ for a serrated ledger plate were observed during cutting of flax straw.

11.2.1.2 Plant structure

Cutting is a process that causes mechanical failure of plant stems and/or leaves and thus the structure and strength of plant materials are of interest. The engineering properties of plant parts are not as well understood as those of more common engineering materials such as steel, but some engineering studies of plant materials have been made. Living plants consist of solid material that surround air- and liquid-filled cavities. Fiber cells, with diameters of 10 to 50 μm and lengths exceeding 30 mm, provide the main strength of the plant material. Fiber cell walls include three basic layers: the middle lamella, the primary wall, and the secondary wall, with combined thicknesses on the order of 500 nm. The secondary wall lies inside the primary wall and provides the strength and flexibility of the structure. Cellulose chains, the main ingredient of the secondary wall, are bound together in parallel microfibrils of considerable length and with cross-sectional dimension of 2.5 to 20 nm (Figure 11.10). The microfibrils are oriented in spirals, and the angle of the spiral relative to the cell axis determines the elasticity of the cell wall. The cell wall density is approximately 1.45 g/mm^3 , but makes up only a small proportion of the cross section. Some cell walls have strength approaching that of steel, but the numerous cavities greatly reduce the average strength of the plant cross section.

Plant stems and leaves consist of large numbers of similar cells. Structurally, the stems can be viewed as materials with fibers of high tensile strength oriented in a common direction and bound together by material of much lower strength. The softer cells make use of their turgor (liquid pressure) to connect and support the fibers. Grasses, including small grains and corn (maize), and legumes are the materials most commonly involved in agricultural cutting processes, so their structure and strength

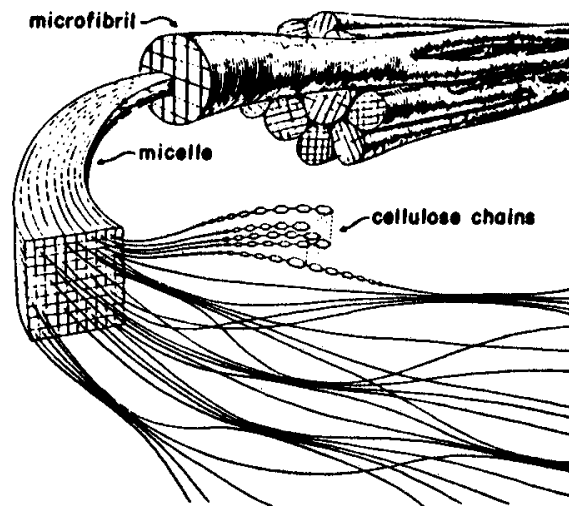


Figure 11.10 – Arrangement and structure of microfibrils (reprinted from Persson, 1987).

are of special interest. Many grass stems have hollow internode sections joined by solid nodes (Figure 11.11). The internode sections are much weaker than the nodes and thus determine the stem strength. The corn stalk has internode sections which are not hollow but have a more uniform cross section. Figure 11.12 shows simplified models that were drawn to represent the actual cross section of a hollow stem for analyzing stem strength in bending. The strength is determined by the amount of structural fibers and their locations in the plant, rather than by the outside dimensions.

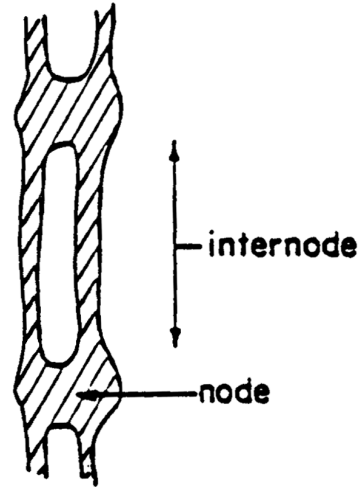


Figure 11.11 – Longitudinal section through a stem showing nodes and internodes (reprinted from Persson, 1987).

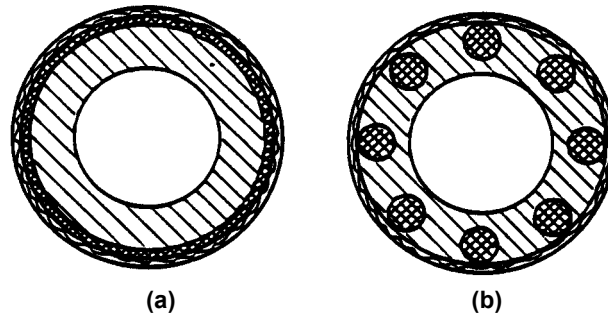


Figure 11.12 – Mechanical equivalents stem cross sections, showing the main structural components arranged as (a) a concentric cylinder, and (b) eight reinforcement rods. Drawn to approximate scale with regard to area and moments of inertia in bending (reprinted from Persson, 1987).

Secondary cell walls in their natural position have ultimate tensile strengths ranging up to 1100 N/mm², a modulus of elasticity (E) in the range from 10,000 to 100,000 N/mm², and ultimate strain (S_u) of 0.5% to 5%. Those subject to compression in the growing plant have lower tensile strength but greater elasticity. Other cell walls have much lower strength; for example, tensile strength of the outer layer (skin) ranges from 2 to 14 N/mm². Ultimate tensile strength of the solid portions of timothy or alfalfa stems ranges from 90 to 470 N/mm²; when the entire cross section of the alfalfa stem is used, the ultimate strength is only 8 to 35 N/mm².

The bending strength of a plant stem may be important during cutting. For example, some devices cut a plant in the absence of a countershear; the plant stem below the cutting plane is loaded as a cantilever beam. In other situations, the stem may be loaded as a simply supported beam. In either case, the direction of loading is radial (perpendicular to the longitudinal axis of the plant stem). The radial load that would cause failure in bending can be calculated using the following equation:

$$F_{bu} = \frac{I S_u}{c L} \quad (11.6)$$

where F_{bu} = ultimate load at bending failure, N

I = moment of inertia of the cross section, mm⁴

c = radius from neutral axis of stem to most distant load-carrying fiber, mm

or, alternately, I/c = section modulus, mm³

S_u = ultimate stress of plant fibers, N/mm²

L = distance from concentrated load to point of support, mm

The deflection of the stem is given by:

$$\delta_r = \frac{F_r L^3}{C_b EI} \quad (11.7)$$

where δ_r = radial deflection, mm

F_r = radial concentrated load, N

E = modulus of elasticity of stem fibers, N/mm²

C_b = constant (3 for cantilevered stems, 48 for simply supported stems).

The moment of inertia of a homogeneous solid, circular section is:

$$I = \frac{\pi d^4}{64} \quad (11.8)$$

where d = diameter of the section, mm. For a hollow, thin-walled section, the moment of inertia is:

$$I = \frac{3\pi d^3 t}{32} \quad (11.9)$$

where t = wall thickness, mm. From comparing Equations 11.8 and 11.9, we note that the moment of inertia of a natural stem should be proportional to the section diameter raised to an exponent between 3 and 4. Similarly, assuming that the neutral axis is

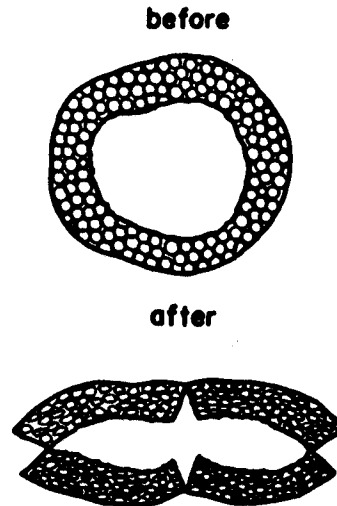


Figure 11.13 – Cross section of a stem before and after compression bending (reprinted from Persson, 1987).

centered in the stem, the section modulus should be proportional to the diameter raised to an exponent between 2 and 3. The appropriate section diameter is determined by the location of the cell wall fibers rather than the outside diameter (see Figure 11.12) and thus, if the outside diameter is used, the bending strength will be somewhat over estimated. If loading crushes a stem prior to cutting (see Figure 11.13), the circular cross section no longer exists; the moment of inertia and section modulus must then be calculated for the new geometry of the cross section.

The size and bending strength of plant stems increases with plant maturity (Persson, 1987). For example, the stem dry mass of timothy increased from 0.6 to 1.4 mg/mm of length as the plant matured; the corresponding stiffness (EI) increased from 1260 to 3900 $N \cdot mm^2$. For red fescue (which has a much finer stem) at 67% moisture content, the corresponding figures were stem dry mass increasing from 0.017 to 0.083 mg/mm as the plant matured, while the stem stiffness increased from 0.53 to 5.7 $N \cdot mm^2$. The stiffness of timothy stems was found to vary with diameter raised to an exponent between 2.66 and 2.99. For cotton stalks ranging in diameter from 7 to 16 mm, the stiffness varied with diameter to the 3.0 power. The modulus of elasticity of cotton stalks ranged from 600 to 3500 N/mm^2 . Moisture content affects the strength of plants, since the turgor pressure in the cells affects stem rigidity and strength. Since plants must resist wind loading, strength also varies with height on the plant, i.e., most plants are larger and stronger near the ground than at the top. Near the base of rice straw at 62% moisture content, for example, the stems were 3.5 to 4 times heavier per unit length than near the top. Calculation of plant strength and deflection is illustrated in Example Problem 11.1.

Example Problem 11.1

A living alfalfa stem of 2.5 mm diameter is loaded horizontally at a distance 30 mm above the soil surface (as a cantilever beam). Based on the entire stem cross section, the modulus of elasticity is 1500 N/mm² and the ultimate tensile strength is 35 N/mm². (a) Calculate the horizontal force that would cause bending failure. (b) Calculate the horizontal deflection of the stem at point of failure.

Solution

(a) Before using Equation 11.6 to calculate the ultimate load, it is necessary to calculate the section modulus, I/c , of the stem. The value of c is half the stem diameter, or 1.25 mm. From Equation 11.8, the moment of inertia is:

$$\pi 2.5^4/64 = 1.92 \text{ mm}^4$$

The $I/c = 1.92/1.25 = 1.53 \text{ mm}^3$. Then, from Equation 11.6, the ultimate bending load is:

$$F_{bu} = 1.53 \times 35/30 = 1.79 \text{ N}$$

(b) Now, Equation 11.7 can be used to calculate the stem deflection:

$$\delta_r = 1.79(30)^3/(3 \times 1500 \times 1.92) = 5.6 \text{ mm}$$

For this example, the stem would deflect 5.6 mm before the stem fibers failed in bending.

11.2.1.3 Mechanics of cutting

Several different modes of tissue failure can occur during cutting, depending upon the knife characteristics. Initial penetration of the knife results in localized plastic deformation (flow) of the plant material. In moist stems and with high knife speeds, turgor pressure in the stems limits initial compression of the plant. With further knife movement, considerable stem buckling and compression occurs (see Figure 11.13); depending on knife sharpness and speed, the compression can advance well ahead of and to the sides of the knife edge. The precompression before failure results in a gradual buildup of force on the knife and the energy for precompression can consume 40% to 60% of the total cutting energy. As the fibers are deflected ahead of the knife edge, the shear strength of the material is mobilized to produce fiber tensile stresses. These stresses become sufficiently large to cause the fibers to fail in tension, whereupon loading is transferred to fibers further ahead of the knife edge. For common crop materials, cutting occurs when the pressure exerted ahead of the knife edge exceeds 9 to 30 N/mm².

Figure 11.14a illustrates a knife and countershear cutting a bed of plant material. Forces on the knife are illustrated in Figure 11.14b. The force, F_x , in the direction of

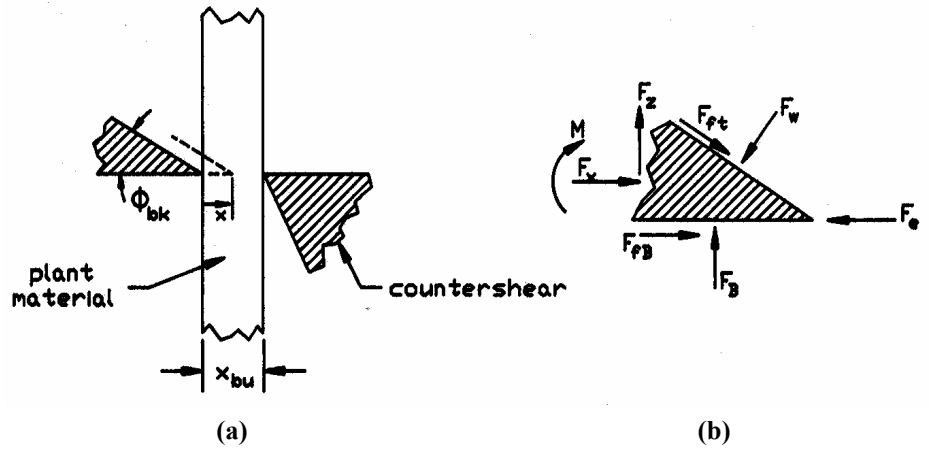


Figure 11.14 – Illustration of knife forces during cutting.

knife motion is the sum of the knife edge force plus x-components of forces imposed on the top and bottom surfaces of the knife as it compresses and penetrates the plant material. By assuming that only the material directly ahead of the knife is compressed and by use of the bulk modulus for the plant material, the following equation for knife force was derived:

$$\frac{F_x}{w} = \frac{F_{ek}}{w} + \frac{B_f x^\lambda}{2X_{bu}} (\tan \phi_{bk} + 2f) \tag{11.10}$$

- where F_x = knife driving force in x direction, N
- F_{ek} = force imposed by plant on the knife edge, N
- w = width of knife, mm
- B_f = bulk modulus of forage, N/mm²
- x = knife displacement after initial contact, mm
- λ = exponent
- X_{bu} = uncompressed depth of material between knife and countershear, mm
- ϕ_{bk} = bevel angle of knife edge
- f = coefficient of friction of forage on knife

Theoretically, $\lambda = 2$ in Equation 11.10. However, a smaller exponent gives a better fit to some experimental cutting data. In an experiment in which a thin ($X_{bu} = 8.9$ mm) bed of timothy at 20% moisture was cut at a very low (0.42 mm/s) knife speed, Equation 11.10 fit the data when $\lambda = 1.46$ and $B_f = 10$ N/mm². The knife edge force is calculated as the product of the projected frontal area of the knife edge times the pressure imposed on that edge by the forage. The approximate frontal area can be calculated from the following equation:

$$A_{ek} = r_{ek} [1 + \cos(\phi_{bk} + \phi_{ck})] \tag{11.11}$$

- where A_{ek} = frontal area of knife edge per mm of width, mm²
- r_{ek} = radius of knife edge, mm

Figure 11.15 shows the typical shape of the force-displacement curve when plant material is cut by a knife and countershear. In Section A, only compression occurs as the knife edge force is not yet high enough to cause cutting. After initial stem failure, some compression continues in Section B along with cutting. In section C, the material is fully compressed; cutting continues and then the force drops rapidly as the knife edge crosses the edge of the countershear. With suitable choice of parameters, the force in Sections A and B could be calculated using Equation 11.10. Section C does not involve compression so Equation 11.10 does not fit that section. The diagram in Figure 11.15 is for a straight cut, i.e., with $\phi_{cl} = 0$. For an oblique cut, the peak cutting force would be reduced and the duration of cut would be extended compared to Figure 11.15.

Figure 11.15 is useful in calculating the power requirement for cutting with a knife and countershear. The energy per cut is equal to the area under the cutting force curve; multiplying by the cutting frequency gives the power. The following equation can be used to compute the power requirement for cutting:

$$P_{\text{cut}} = \frac{C_f F_{\text{max}} X_{\text{bu}} f_{\text{cut}}}{60,000} \quad (11.12)$$

where P_{cut} = power for cutting, kW

F_{xmax} = maximum cutting force, kN

X_{bu} = depth of material at initial contact with knife, mm (see Figure 11.15)

f_{cut} = cutting frequency, cuts/min

C_f = ratio of average to peak cutting force

C_f is always between 0 and 1 and, for a typical force-displacement curve as illustrated in Figure 11.15, it is approximately equal to 0.64.

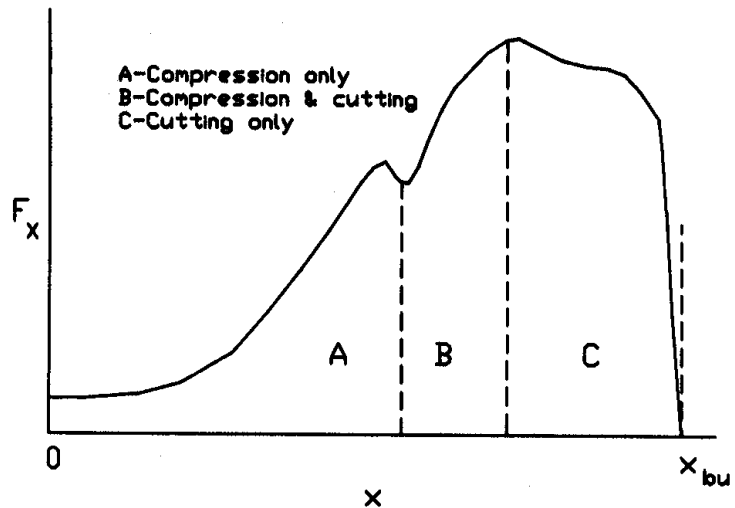


Figure 11.15 – Knife force-displacement curve for a straight cut against a countershear.

The cutting force, F_x , must be supported. If a countershear is present and clearance is small, the support force can be provided entirely by the countershear. When no countershear is present, the support force must be provided entirely by the plant itself through the bending strength of the stump below the cut and the inertia of the plant above the cut. The resulting cut is called, alternatively, an impact cut, an inertia cut, or a free cut. As clearance with a countershear increases, the plant strength and inertia come increasingly into play; thus, impact cutting is similar to countershear cutting with very large clearance. Figure 11.16 illustrates the forces and moments on the plant during impact cutting. The soil and the plant root system provide a force, F_B , and a moment, M_r , which tend to keep the stump upright. Acceleration of the stump is considered to be negligible. Force F_B represents the combined effects of the root system and stalk strength in providing bending resistance at the height of the cut. The center of gravity of the cut portion of the plant is at a height, z_{cg} , above the cut. The impact shown in Figure 11.16 tends to accelerate the cut plant to the right and counterclockwise; consequently, an inertia force and inertia moment appear on the plant at the center of gravity. The following equation results from summing moments about the center of gravity of the cut plant:

$$I_p \alpha_p = (F_x - F_b) z_{cg} \tag{11.13}$$

where α_p = angular acceleration of plant, radians/s²

F_x = cutting force, N

F_b = bending resistance of stump, N

z_{cg} = height of center of gravity of cut plant, m (see Figure 11.16)

I_p = centroidal moment of inertia of plant, kg m²

= $m_p r_g^2$ where m_p = mass of cut portion of plant, kg

r_g = radius of gyration of cut portion of plant, m

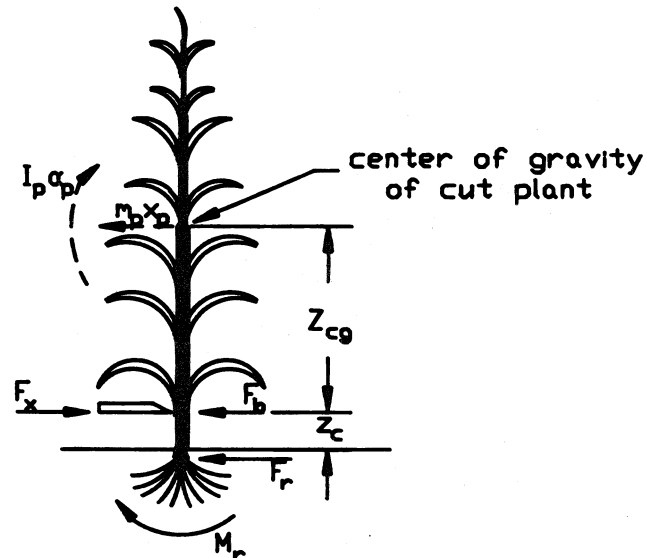


Figure 11.16 – Forces and moments in impact cutting.

An analysis of the kinematics (motions) of the plant gives the following equation for angular acceleration:

$$\alpha_p = \frac{a_c - a_{cg}}{z_{cg}} \quad (11.14)$$

where a_c = acceleration of plant at plane of cut, m/s^2

a_{cg} = acceleration of plant center of gravity, m/s^2

By assuming that the plant acquires knife velocity at the plane of cut, the following equation was derived:

$$a_c = \frac{1000v_k^2}{d_s} \quad (11.15)$$

where v_k = knife velocity, m/s

d_s = stalk diameter at plane of cut, mm

Equations 11.13 through 11.15 can be combined to give the following equation for minimum knife velocity for impact cutting:

$$v_k = \left[d_s \frac{(F_x - F_b)}{1000m_p} \left(1 + \frac{z_{cg}^2}{r_g^2} \right) \right]^{0.5} \quad (11.16)$$

When values for r_g and z_{cg} are not readily available, a simpler approximate equation can be obtained by assuming that $r_g = z_{cg}$. The simpler equation illustrates the key variables involved in impact cutting. If the stump bending resistance, F_b , is large enough to support the entire cutting force, F_x , the minimum required knife velocity is zero and cutting is equivalent to cutting with a countershear. Lowering the height of cut to increase F_b and reducing F_x by maintaining a sharp knife will both reduce the minimum required knife velocity. Tests of impact cutting of timothy, for example, have shown that cutting could be accomplished at knife velocities as low as 25 m/s but velocities of 45 m/s were required for reliable cutting of all stems. To assure reliable cutting over a wide range of knife sharpness and stem stiffness, minimum knife velocities of 50 to 75 m/s are generally recommended. Example Problem 11.2 illustrates the calculation of minimum knife velocity for impact cutting.

Example Problem 11.2

Impact cutting is to be used to cut the alfalfa stem of Example Problem 11.1 at a height 30 mm above the ground. The mass of the plant above the cut is 0.01 kg . Assume that cutting occurs when the pressure ahead of the knife edge reaches 25 N/mm^2 . The knife has a bevel angle of 20°, zero clearance angle, and an edge radius of 0.3 mm . Calculate (a) the force imposed by the knife edge to achieve cutting, and (b) the minimum knife speed required for impact cutting.

Solution

(a) The frontal area of the knife edge can be calculated using Equation 11.11:

$$A_{ek} = 0.3[1 + \cos(20 + 0)] = 0.582 \text{ mm}^2/\text{mm width}$$

The width of knife is not known, but since only a single stem is being cut, the width will be assumed equal to the stem diameter, 2.5 mm. Then, using the critical pressure of 25 N/mm², the force required to initiate cutting will be:

$$F_{ek} = 0.582 (2.5) 25 = 36.4 \text{ N}$$

(b) Equation 11.16 is available for calculating the minimum knife velocity for impact cutting. Values for r_g and z_{cg} are not available, but we will assume $r_g = z_{cg}$. No value for F_b is given but we will assume it is equal to the ultimate bending load calculated in Example Problem 11.1, that is, $F_b = 1.79 \text{ N}$. Then the minimum velocity is:

$$v_k = [2 \times 2.5 \times (36.4 - 1.79) / (1000 \times 0.01)]^{0.5} = 4.2 \text{ m/s}$$

Note: In this idealized cutting of a single stem, the minimum velocity was low. Typically, to allow for interaction of multiple stems during cutting, velocities of 50 to 75 m/s are recommended.

11.2.2 Cutting and chopping

11.2.2.1 Cutting with a countershear

The construction of a typical cutterbar is illustrated in Figure 11.17. Terminology for the cutting elements is shown on the detailed cross-sectional view in Figure 11.17. The knife sections and sometimes the ledger plates are replaceable. Knife section edges can be smooth or serrated and either type of sickle can be removed for sharpening. Ledger plate edges are usually serrated on the underside and are not resharpened. The knife clips maintain correct clearance between the knife sections and ledger plates. The wear plates support the rear edges of the knife sections and must be replaced when vertical clearance becomes excessive. In addition to guarding the blunt ends of the knife sections from the oncoming material at each end of the stroke, the guards also help to protect the sickle from being damaged by rocks. Typical guard spacing is 76.2 mm; the sickle stroke can be equal to or up to about 15 mm less than or greater than the guard spacing.

Most forages are harvested with a machine that combines the mowing and conditioning process, hence the name, mower-conditioner. The cutterbar and associated reel (Figure 11.5) are mounted on a separate framework which is connected to the machine by a spring-loaded four-bar linkage. Adjustable shoes are placed at each end of the separate assembly to adjust the cutting height, typically in the range from 25 to 100 mm. The floatation springs are adjustable to provide from 0.3 to 0.4 kN of vertical ground reaction on the shoes. The cutterbar assembly should “float” easily over the ground without bouncing.

The type of pickup reel that is used on a mower-conditioner is also used on other machines, for example, forage harvesters and combines. Figure 11.18 illustrates three

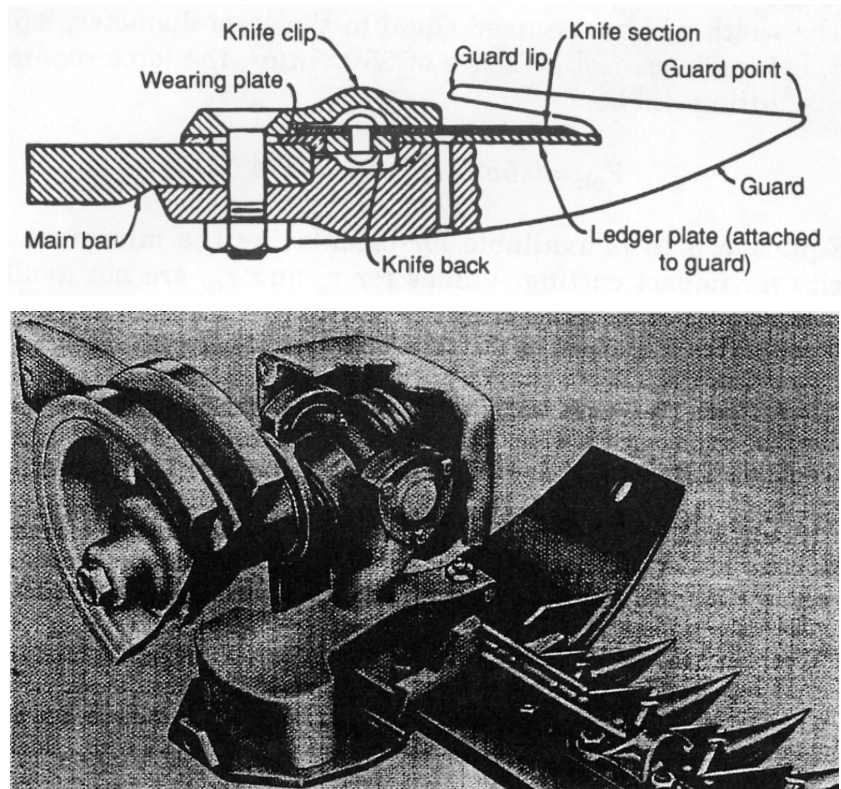


Figure 11.17 – A mower cutterbar with drive unit (reprinted from Kepner et al., 1978).

different types of mechanisms used in pickup reels. The mechanisms in Figures 11.18a and 11.18c keep all of the reel teeth parallel at all times, but, because eccentric spider control is simpler and less expensive, it has supplanted the planetary gear control that was previously used. By adjusting the location of the center of the bearing control plate (Figure 11.18a), the pitch of the teeth can be adjusted. Although cam control (Figure 11.18b) is more complex than eccentric spider control, the cam does permit changing the pitch of the teeth on each tooth bar as the bar progresses through its cycle. Thus, the teeth can be given a greater lifting action as they pass near the cutterbar.

The cutterbar should have proper tilt, register, and alignment. Tilt is adjusted by rotating the cutterbar about an axis parallel to the sickle to raise or lower the guard tips. Proper register is achieved by moving the cutterbar in or out relative to the drive mechanism until the knife stroke is in symmetry with the guard spacing. The cutterbar is in proper alignment when it is perpendicular to the direction of travel while mowing. Alignment is generally not a problem when the cutterbar has horizontal support on both ends. On mowers that have the cutterbar extending outward from one side of

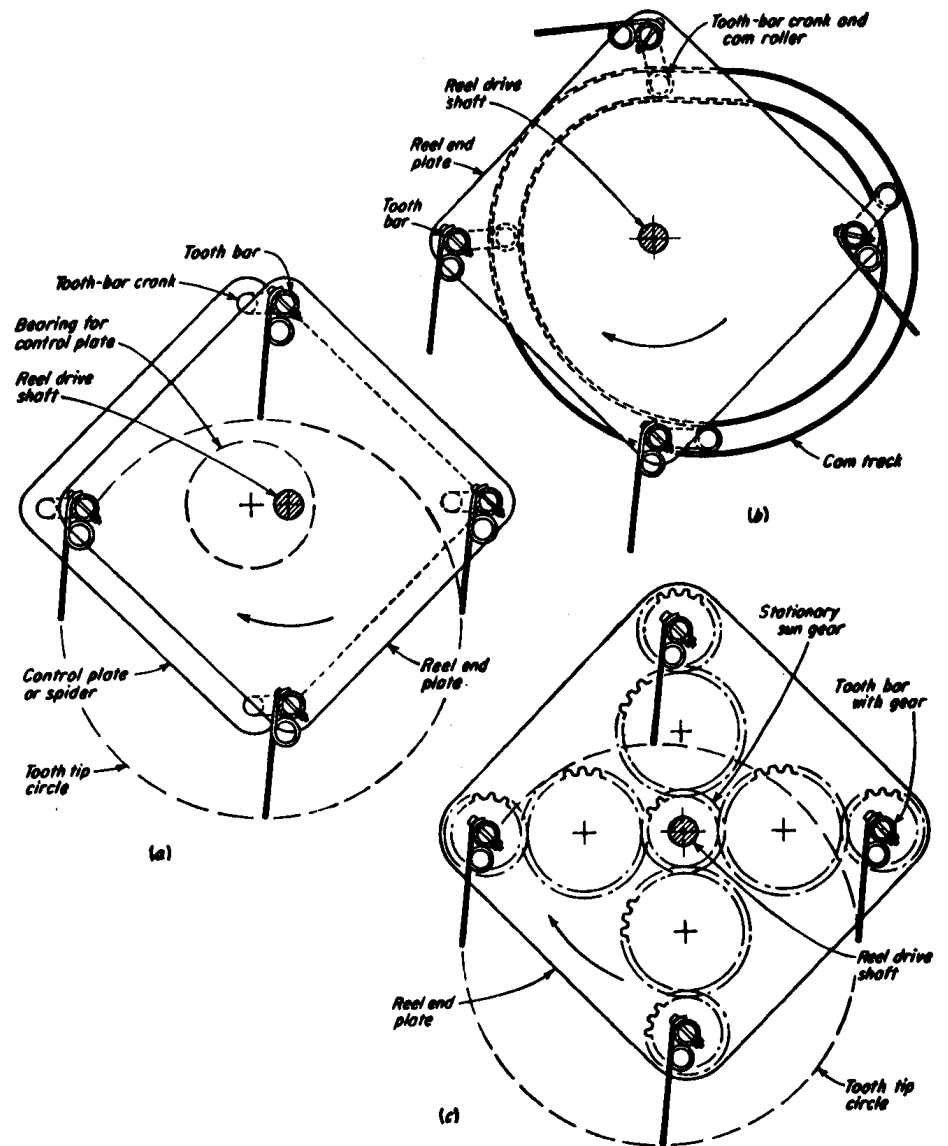


Figure 11.18 – Feathering actions used in pickup reels with
 (a) concentric spider control, (b) cam control, (c) planetary gear control
 (reprinted from Richey et al., 1961).

the machine, however, the horizontal forces on the cutterbar create a moment and the resulting deflection causes the outer end to lag behind the drive mechanism. To offset the lag, the outer end must lead the drive mechanism by about 20 mm per meter of bar

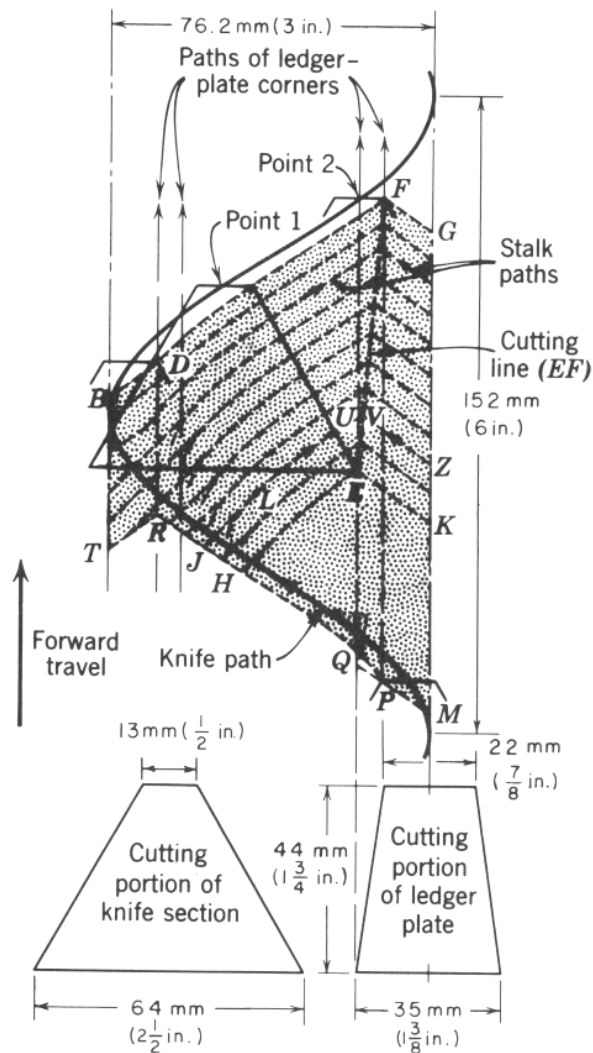


Figure 11.19 – Cutting pattern of a conventional sickle bar mower (reprinted from Kepner et al, 1978).

length when the mower not operating. The driveline to the cutterbar should be protected to prevent damage if the sickle becomes jammed. A v-belt in the drive can provide overload protection, but if there is no belt in the drive, a slip clutch or jump clutch should be included in the drive line.

The cutting frequency is a key variable in the operation of a sickle bar mower. A higher cutting frequency aids cutting by increasing v_{km} (see Figure 11.8) and also allows higher travel speeds. Figure 11.19 shows typical dimensions of a sickle section

and ledger plate, as well as a typical cutting pattern. Note that plants growing in the area bounded by points KMPQHE on the diagram must be deflected forward and cut ahead of point E. In Figure 11.19, that area is equal to 25% of the total area cut per stroke; such bunching is undesirable because it leads to increased cutting forces and uneven stubble height. To avoid excessive bunching with a conventional mower, the forward travel of the mower should not exceed 150 mm per knife cycle; thus increasing the cutting frequency also increases the maximum allowable travel speed. Since the mowing capacity of the mower varies with the product of the cutterbar width and the forward speed, the maximum mowing capacity is proportional to the cutting frequency. Because the sickle must be reversed in direction at each end of its stroke, vibration imposes an upper limit on cutting frequency. The mower shown in Figure 11.17 includes a counterweight that moves opposite in direction to the sickle to reduce the vibrations. Double sickle mowers are available; such mowers have no guards but have two reciprocating sickles moving in opposite directions. Double sickle mowers permit up to 220 mm of forward travel per cycle with out excessive bunching and the opposite-moving sickles provide automatic balancing. A major limitation has been that the absence of guards has led to rock damage to the unprotected sickles. Also, some vibration of the cutterbar is desirable because it helps to keep the cut material flowing over the cutterbar.

Two well-known mechanisms are available for converting rotary motion into the reciprocating motion required to drive a sickle, a slider-crank and a spatial-crank mechanism. The spatial-crank mechanism is more common because of its compact size and the ease with which it can be integrated into the drive train of a machine.

The spatial-crank oscillator is a mechanism from the spherical mechanism group. Another well-known member of this group is the Cardan universal joint which was described in Chapter 4. All of the joint axes in this group of mechanisms intersect at a common point. In the spatial-crank oscillator, the output shaft must be skewed with respect to the input shaft, and the angle γ must be smaller than the angle β (Figure 11.20). In the oscillator shown in Figure 11.20, angle β is 90° or 1.57 radians. The following three equations govern the displacement, velocity, and acceleration, respectively, of the oscillating shaft:

$$\tan \Gamma = \tan \gamma \sin \theta \quad (11.17a)$$

$$\dot{\Gamma} = \frac{\dot{\theta} \tan \gamma \cos \theta}{1 + \tan^2 \gamma \sin^2 \theta} \quad (11.18)$$

$$\ddot{\Gamma} = \frac{-\dot{\theta} \tan \gamma \sin \theta [1 + \tan^2 \gamma (\alpha + \cos^2 \theta)]}{(1 + \tan^2 \gamma \sin^2 \theta)} \quad (11.19)$$

where Γ = displacement of the oscillating shaft, radians

θ = rotational displacement of input shaft, radians

γ = input shaft angle, radians (see Figure 11.20)

The dot notation used in Equations 11.18 and 11.19 indicates time derivatives of the variables indicated.

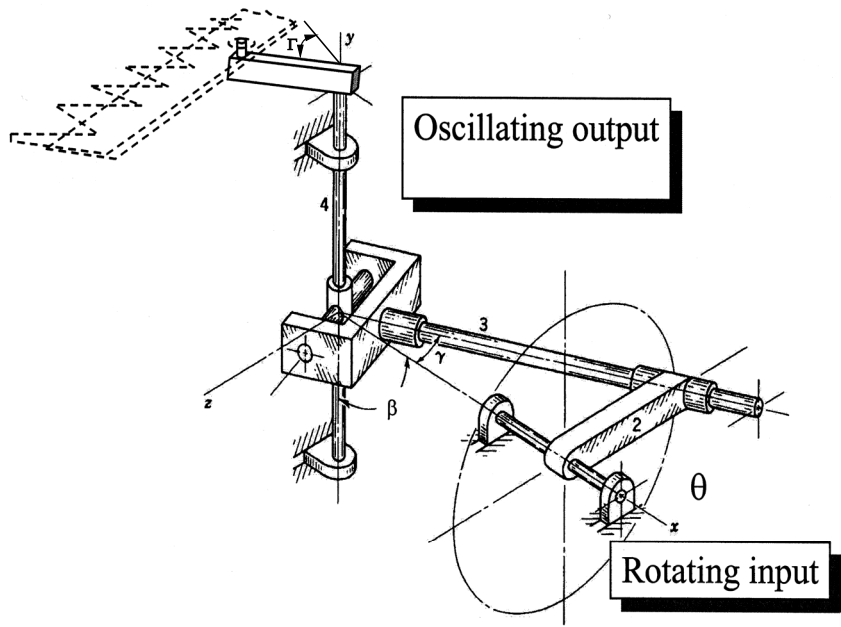


Figure 11.20 – Isometric view of a spatial-crank oscillator (Rotz et al., 1991).

If $\gamma < 0.33$ radians in Equation 11.17, the tangent functions in the equation are approximately equal to the value of the argument in radians and thus the following simplified equation gives the displacement of the oscillating shaft with less than 0.2% error:

$$\Gamma = \gamma \sin \theta \quad (11.17b)$$

An oscillating arm is generally attached to the oscillating shaft to convert the shaft rotational oscillation to the required rectilinear motion required by the sickle. Note, however, that the tip of the oscillating arm travels on an arc rather than in a straight line. The problem is overcome by using a flexible bushing to connect the arm to the knife and by keeping the oscillation angle small and the arm length long within reasonable limits.

Counterbalancing to reduce vibration caused by inertial forces is not generally required because the mass of the machine supporting the cutterbar is so large relative to the mass of the reciprocating knife. However, the vibrations generate stresses, increasing maintenance problems and the possibility of early fatigue failure of the moving parts. Essentially full dynamic balancing can be obtained by attaching a counterweight to the crank arm. For example, if a counterweight equal to the sickle mass was attached to the top of the crank arm in Figure 11.20 and if the sickle and counterweight were vertically equidistant from the output shaft, the horizontal oscillating forces would cancel. There would be a residual oscillating couple due to the vertical separation between the sickle and the counterweight.

The approximate velocity of the knife relative to the mower (v_{km}) can be calculated by assuming that the sickle moves with sinusoidal motion. This assumption neglects some higher-order harmonics that may be present depending upon the specific drive used to power the sickle. Assuming sinusoidal motion, the relative sickle speed is given by:

$$v_{km} = \frac{L_s \omega_c}{2000} \cos(\omega_c t) \quad (11.20)$$

where v_{km} = velocity of knife relative to mower, m/s

L_s = stroke length of knife, mm

ω_c = sickle frequency, radians/s

t = time measured from center of stroke, s

Equation 11.20 is useful in estimating the speed of the knife through the cutting zone. Also, as shown in Example Problem 11.3, Equation 11.20 is useful in determining the conditions under which plant material may slide forward on the knife and escape cutting.

Example Problem 11.3

The oblique angle of the sickle sections is 30° when $v_f = 0$, i.e., when the mower is not moving forward. If the stroke length is 76.2 mm and the cutting frequency is 105 radians/s, what is the minimum v_f at which, during the entire knife stroke, the plant material will move towards the rear of the knife sections rather than moving toward the knife tips to possibly escape cutting?

Solution

Insight can be gained by calculating the conditions under which the oblique angle is zero during cutting since, when the oblique angle is zero, there is no tendency for the material to move along the edge of the knife sections. The oblique angle is zero when the knife movement relative to the ground is perpendicular to the knife edge, i.e., when:

$$v_f/v_{km} = \tan 30^\circ$$

or, by making use of Equation 11.20, when:

$$v_f = \frac{L_s \omega_c}{2000} \cos(\omega_c t) \tan(30^\circ)$$

The most critical point is at midstroke ($t = 0$) when the cosine term has its maximum value of 1.0. Then, substituting in the given values of L_s and ω_c , the minimum forward travel speed is:

$$v_f = 76.2 (105/2000) \cos(0) \tan(30^\circ) = 2.31 \text{ m/s}$$

At $v_f = 2.31$ m/s, the material will have no y-component of velocity at midstroke but will tend to move towards the rear of the knife sections at all other parts of the stroke. At slower travel speeds, the material will tend to move towards the knife tips at midstroke. Of course, as Equation 11.4 indicates, edge friction may be sufficient to keep the material from moving along the edge of the knife sections.

Equation 11.12 can be used to calculate the theoretical power requirement for mowing with a cutterbar mower. However, that equation does not include friction between the knife and cutterbar or other losses. Interestingly, with no crop being cut, there is power required to accelerate and decelerate the mechanism. When there is crop being cut, the plant material automatically provides deceleration, yet demands power for cutting when accelerating the knife. By comparing PTO power delivered to a mower while not cutting and while cutting moderately heavy mixed forage, Elfes (1954) found that cutting used only about 30% of the total PTO power. Cutting frequency was 942 cycles/min and average total knife force was 1.2 kN/m of bar length. Harbage and Morr (1962) measured an average total knife force of 2.3 kN/m when mowing bluegrass at 1250 cycles/min. ASAE Data D497 suggests a PTO power requirement of 1.2 kW per meter of bar length for mowing alfalfa. To that must be added the tractive power required to overcome drag on the cutterbar, rolling resistance of the tractor and mower, and power for conditioning (if applicable). PTO power for cutterbar mowing and conditioning is approximately 4.5 kW/m (ASAE D497).

11.2.2.2 Impact cutting, horizontal axis

Impact cutting is used in flail mowers and rotary mowers. As shown in the schematic view of Figure 11.21a, the flails in flail mowers rotate about a horizontal, transverse axis. Hinging of the flails provides flexibility for the flails to swing back and minimize damage in rocky fields. Some of the various types of knives used on flail mowers are shown in Figure 11.21b. Staggering the flails in the successive rows provides complete coverage of the swath. Early flail mowers suffered excessive losses because short pieces of forage were lost in the stubble. Losses were reduced by designing the shroud to bend the plants forward to permit basal cutting and to provide clearance above the flail to reduce recutting. Bending the plants forward also permits lower knife velocities than calculated by Equation 11.16 and the lower knife velocities also reduce recutting. Knife peripheral speeds of 43 m/s or less have been found to be satisfactory. The full-width gage roller behind the flail (Figure 11.21a) provides accurate control of cutting height and prevents scalping of high spots. The hitch of pull-type flail mowers is offset so that the tractor wheels run on cut forage rather than on the standing crop. The lacerating effect of the knives on the stems provides a conditioning effect that helps to increase the drying rate. In upright crops, the flail mower typically recovers 5% to 10% less of the crop than sickle bar mowers. Conversely, the flail mower can recover substantially more of a severely lodged crop.

The tips of the knives on the flail mower trace out cycloidal paths as the mower moves forward over the land. The x,z-coordinates of the path can be calculated using the following equations:

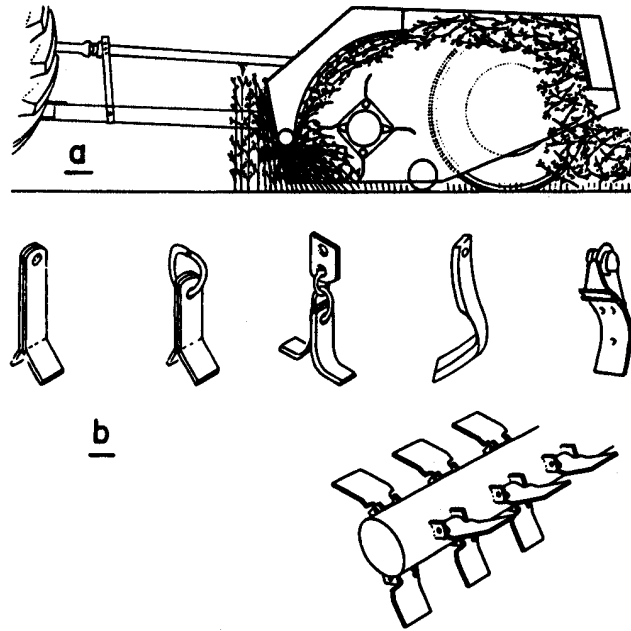


Figure 11.21 – A flail mower, showing (a) side view and (b) flail detail (reprinted from Persson, 1987).

$$\frac{x}{r_f} = \frac{v_f t}{r_f} + \sin \theta_r \tag{11.21}$$

$$\frac{z}{r_f} = 1 - \cos \theta_f \tag{11.22}$$

where x = displacement of the tip in the x-direction, m
 z = corresponding displacement of the tip in the z-direction, m
 r_f = radius to tip of flail, m
 v_f = forward velocity of mower, m/s
 t = time, s
 θ_r = angular displacement of rotor, radians (see Figure 11.22)

Theoretically, the stubble height can become uneven if v_f becomes too large in relation to the knife peripheral speed, v_p . The distance, z_d , in Figure 11.22 illustrates the uneven stubble height. The following equation can be used to calculate the approximate value of z_d :

$$\frac{z_d}{r_f} = 1 - \cos \left(\frac{\pi}{\lambda_r (1 + C_v)} \right) \tag{11.23}$$

where z_d = stubble height difference, m
 λ_r = number of rows of flails on the rotor
 C_v = velocity ratio = v_p/v_f

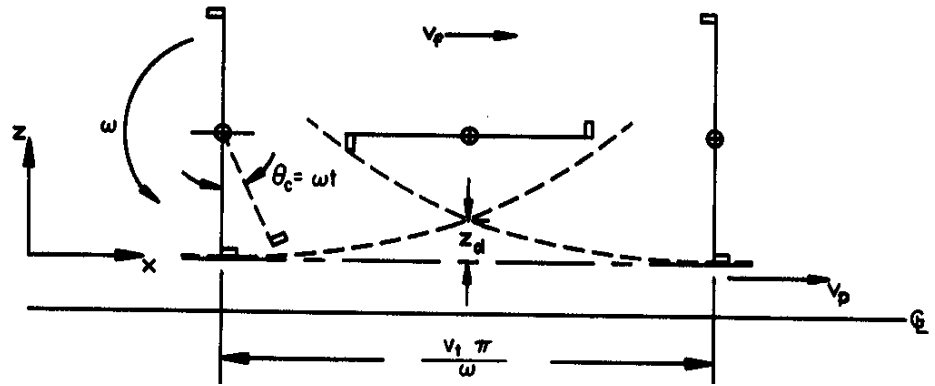


Figure 11.22 – Flail mower cutting analysis.

Equation 11.23 includes the assumption that the sine of the rotor angle is approximately equal to the value of the angle in radians. For realistic values of C_v , that assumption is valid. Note in Figure 11.21b that alternate rows of flails are staggered to assure cutting over the entire swath width. Because of the staggered arrangement and the lateral gaps between the flails, $\lambda_r = 2$ for the rotor shown in Figure 11.21. Given that a typical v_p for flail mowers is about 43 m/s, C_v is 10 or greater for reasonable travel speeds. Equation 11.23 shows that the flail mower can produce good stubble uniformity under such conditions.

The power requirement of a flail mower is considerably higher than for a sickle bar mower of the same width, because impact cutting requires greater power than cutting with a countershear and because of the air pumping done by the rotor. Therefore, Equation 11.12 is not valid for flail mowers because of the lack of a countershear. ASAE Data D497 suggests the following equation for calculating the power requirement of a flail mower mowing alfalfa:

$$P_{\text{mow}} = 10 + 4.0 m_f \quad (11.24)$$

where P_{mow} = PTO power required for flail mower, kW

m_f = feed rate, kg/s

The feed rate of any mower can be calculated from the following equation:

$$m_f = \frac{Y w_s v_f}{10} \quad (11.25)$$

where Y = forage yield, wet basis, Mg/ha

w_s = swath width cut by mower, m

v_f = travel speed, m/s

Combining Equations 11.24 and 11.25 shows that, as expected, the PTO power requirement increases with the speed and cutting width of the flail mower. Since the mower must convey the material (see Figure 11.21) as well as cut it, the PTO power requirement also increases with crop yield. The PTO power requirement with zero

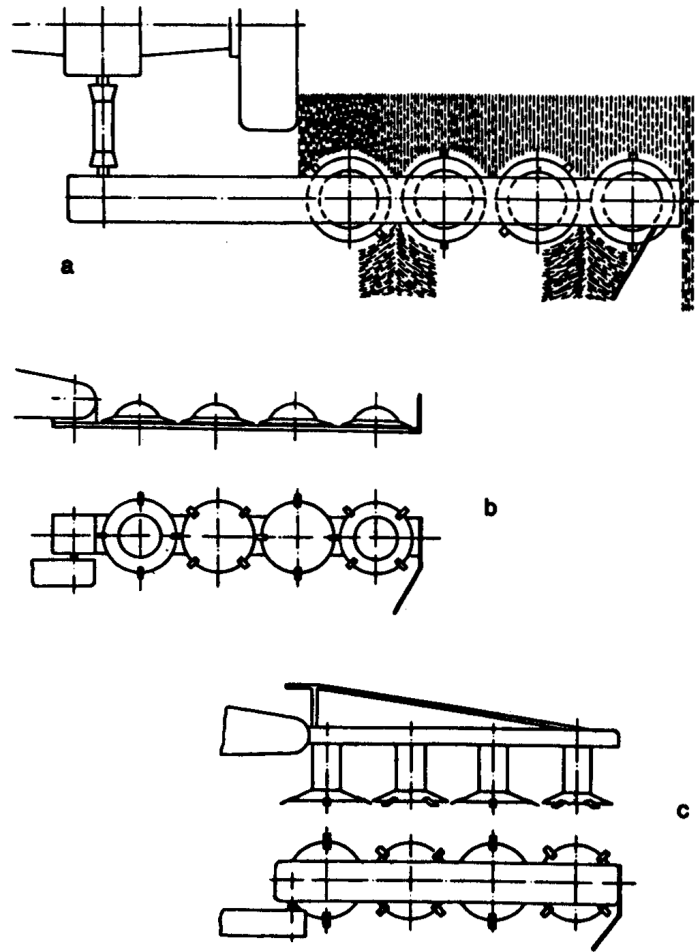


Figure 11.23 – Rotary mowers, showing (a) cutting action, (b) disk-type mower, and (c) drum-type mower (reprinted from Persson, 1987).

yield or travel speed is an indication of the power needed to pump air and to overcome friction in the mower. Drawbar power needed to overcome rolling resistance of the mower must be added to PTO power to obtain the full power requirement.

11.2.2.3 Impact cutting, vertical axis

A rotary disk mower for mowing forage (Figure 11.23) is an example of impact cutting using a vertical axis. Figure 11.23b shows the disk-type mower in which the drive mechanism is below the cutting blades. In the drum-type mower shown in Figure 11.23c, the drive is above the cutting blades and adjacent drums are counter-rotating so that the cut crop falls in distinct bands rather than being uniformly distributed across the cutting width. Mowers are also available in which all blades rotate in the

same direction. Blades of adjacent disks or drums are designed to overlap to assure complete cutting. As each blade rotates about its center with velocity ω_b while the center moves forward with velocity v_f , the blade tip follows a cycloidal path over the ground (Figure 11.24). The velocity of a blade tip relative to the ground is the vector sum of the forward velocity and the peripheral velocity of a blade tip, i.e.:

$$v_{bg} = v_f + v_p \quad (11.26)$$

where v_{bg} = velocity of blade tip relative to ground, m/s

v_f = forward velocity of mower, m/s

v_p = peripheral velocity of blade tip, m/s

= $r_b \omega_b$, where r_b = radius out to blade tip, m

ω_b = rotational speed of blade, radians/s

Since the x-direction is defined as the direction of the blade relative to the material, it is in the direction of v_{bg} and constantly changes in direction as the blade rotates. In the non-rotating u,v coordinate system shown in Figure 11.24, the mower moves in the u-direction. The u and v components of blade tip velocity are:

$$v_u = v_f - r_b \omega_b \sin(\omega_b t) \quad (11.27)$$

$$v_v = r_b \omega_b \cos(\omega_b t) \quad (11.28)$$

where v_u = component of blade tip velocity in u-direction, m/s

v_v = component of blade tip velocity in v-direction, m/s

t = time, s, measured from point where $\theta = 0$

θ = angle between blade and direction of travel = $\omega_b t$ (see Figure 11.24)

The oblique angle, ϕ_{ob} , can be calculated using the following equation:

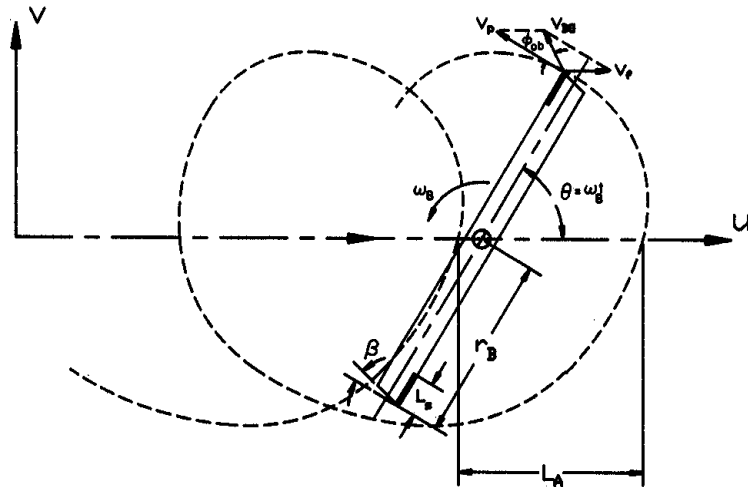


Figure 11.24 – Analysis of cutting action of a rotary mower.

$$\tan \phi_{ob} = \frac{1}{C_v \sec \theta - \tan \theta} \quad (11.29)$$

where $C_v = v_p/v_f$. If $v_f = 0$, then $\phi_{ob} = 0$. Since v_f is always much smaller than v_p , the oblique angle is always close to zero in a rotary mower and sliding of plant material along the blade is not a problem.

The crescent shaped area between two successive passes of a blade (Figure 11.24) defines the area cut by each pass of a blade. The advance per blade, L_a , is given by:

$$L_a = \frac{2\pi v_f}{\lambda_b \omega_b} \quad (11.30)$$

where L_a = advance per blade passage, m

λ_b = number of blades on each disk or drum

The width of the sharpened ends of the blades, L_s , must be greater than L_a . Because the blade velocity must be high for impact cutting (see Equation 11.16) and the blade peripheral velocity declines toward zero at the center, L_a must be limited to assure reliable cutting. The permissible L_a would be considerably less than is shown in Figure 11.24, where L_a was enlarged for clarity. To avoid crop drag against the ends of the blades (which are not sharpened), the ends must be tapered at angle β (see Figure 11.24). The most critical point for crop drag is at $\theta = 0$, when the blade is aligned with the direction of travel. The minimum required angle β is:

$$\beta = \arctan\left(\frac{v_f}{r_b \omega_b}\right) \quad (11.31)$$

The maximum width cut by each disk or drum is $2r_b$, but, to assure complete cutting, some overlap is necessary and the disks or drums must be spaced less than the maximum cutting width. The drive provides timing such that knives on any disk (or drum) do not strike those on adjacent units. Example Problem 11.4 illustrates design considerations for a vertical-axis mower.

Example Problem 11.4

In a rotary mower as shown in Figure 11.23b, each disk carries four blades and rotates at 3000 rpm. Each disk is to cut a 0.4 m swath. If the maximum travel speed is 15 km/h, (a) calculate the minimum required length of each knife. (b) Select an actual blade length and (c) base diameter of each disk onto which the knives are to be attached. (d) Finally, calculate the minimum taper angle on the end of each blade.

Solution

(a) Equation 11.30 can be used to calculate the minimum length of each of the four blades on each disk. The travel speed is 15 km/h (4.17 m/s); the disk rotation speed is 3000 rpm (314 radians/s). Then the minimum blade length is:

$$L_a = 2\pi(4.17)/(4 \times 314) = 0.021 \text{ m or } 21 \text{ mm}$$

(b) Such short blades would leave little room for accumulation of cut plants to be carried from the front to the side of the disk for discharge. Thus, we will select a longer blade length, 0.05 m or 50 mm. (c) The base disk diameter will then be:

$$\text{disk diameter} = 0.4 - 2(0.05) = 0.3 \text{ m or } 300 \text{ mm.}$$

(d) Equation 11.31 can be used to calculate the minimum taper of the ends of the blades:

$$\beta = \arctan [4.17/(0.2 \times 314)] = 3.8^\circ$$

Several design features are included on rotary mowers for safety purposes. The knives are hinged to the disk or drum so that they can swing back if they hit a rock or other obstruction; centrifugal force keeps the knives in cutting position during normal operation. Since the rotating cutters have appreciable inertia, an over-running clutch is usually provided in the drive to allow the mower to coast to a stop when power is interrupted. When rocks are encountered, the high-speed knives are capable of launching them as projectiles that could injure the operator or bystanders. Thus, for safety reasons, the entire cutterbar is covered by a canvas or flexible plastic shroud.

The power requirement of a rotary mower is much higher than that of a sickle bar mower of the same width, because the forage is not only cut but also accelerated by the knives during impact. Tests at the NIAE (National Institute of Agricultural Engineering) (Persson, 1987, p. 176) in England suggest the following equation for calculating power requirements of a rotary mower:

$$P_{mt} = (P_{Ls} + E_{sc}v_f)w_c \quad (11.32)$$

where P_{mt} = total PTO power to mower, kW

P_{Ls} = specific power losses due to air, stubble, and gear-train friction, kW/m of width

E_{sc} = specific cutting energy, kJ/m²

w_c = width of mower, m

The NIAE data suggest that P_{Ls} ranges from 1.5 to 4 kW/m for disk and drum-type rotary mowers; disk mowers are at the lower end of the range, while drum mowers are at the upper end. Values of E_{sc} ranged from 1.5 kJ/m² for sharp blades to 2.1 kJ/m² for mowers with worn blades. ASAE Data D497 suggests 5 kW/m for PTO power requirement. Power to run a conditioner and propel the mower and tractor must be added to obtain the total power requirement for mowing. A more recent survey of rotary mowers on the market indicated total PTO power requirements ranging from 11 to 16 kW per meter of cutting width while mowing and conditioning at 15 km/h. Disks on typical mowers rotate at 3000 rpm while cutting a 0.4 m swath per disk. Typical peripheral knife speeds are between 60 and 70 m/s. Mowers are available with from 3 to 7 disks to provide a range of swath widths.

11.2.2.4 Chopping

Forage harvesters include means for gathering the crop into the machine, chopping it into short pieces, and conveying the chopped forage into a wagon or truck. ASAE Standard S472 defines two basic types of forages harvesters, precision-cut and non-precision-cut. A cylindrical cutterhead and stationary countershear are used for chopping in most precision-cut forage harvesters. Nonprecision-cut forage harvesters, to be discussed later, make use of a flail cutter for cutting and chopping the standing crop. Precision-cut forage harvesters can be further subdivided into cut-and-throw and cut-and-blow types. Cut-and-throw harvesters utilize energy imparted to the forage during cutting to transport the chopped material from the harvester. Cut-and-blow configurations use an auxiliary blower for material transport. An auger conveyor is often used between the cutterhead and blower on some pull-type forage harvesters. The cut-and-blow configurations allow the blower and wagon to be placed directly behind the tractor, thus eliminating side draft. The cut-and-throw configuration requires fewer components and can require less energy.

Figure 11.25 shows two types of feeding mechanisms for precision-cut forage harvesters. In either type, the upper feed rolls are spring-loaded to pre-compress the forage before it reaches the cylinder. The length of cut is controlled by the peripheral speed of the feed rolls relative to the speed of the cutterhead. A smooth feed roll is placed near the shear bar to maintain the grip on the forage as close to the shear bar as possible. In determining peripheral speeds of fluted feed rolls, the pitch (effective) diameter is slightly less than the outside diameter.

Several different types of headers are available for the precision-cut harvesters. Pickup headers (Figure 11.26a) are for chopping hay crops that have been allowed to partially dry in windrows. Row-crop headers (Figure 11.26b) are used when maize or other row crops are to be chopped. Reciprocating sickles on earlier row crop headers have given way to a pair of rotating cutting disks for cutting each row. Non-direction-sensitive heads (Figure 11.26c) can be used in row crops but do not require travel down the row. Direct-cut headers (Figure 11.26d) are for harvesting standing crops.

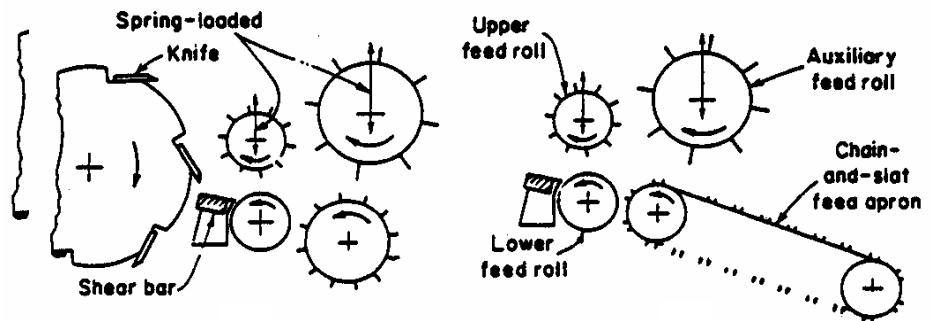


Figure 11.25 – Two types of feed mechanisms for a forage harvester (reprinted from Kepner et al., 1978).





Figure 11.26 – Gathering units for forage harvesters: (a) pickup, (b) row-crop, (c) non-direction-sensitive, and (d) direct-cut (courtesy of Claas).

The theoretical length of cut can be calculated using the following equation:

$$L_c = \frac{60,000v_f}{\lambda_k \omega_c} \quad (11.33)$$

where L_c = theoretical length of cut, mm

v_f = feed velocity, m/s = peripheral speed of feed rolls

λ_k = number of knives on the cutterhead

ω_c = rotational speed of cutterhead, rpm

Some particles will be longer than the theoretical length when stems are not oriented parallel to the direction of feed. Others will be shorter than the theoretical length when the arrival of the ends of stems does not coincide with the arrival of a cutterhead knife. Theoretical lengths of cut typically range from 3 to 90 mm. The actual length of cut is usually close to the theoretical length for row crops because the stalks are oriented nearly perpendicular to the shear bar. For direct-cut forages, actual average lengths of cut are generally about 50% longer than the theoretical length. When wind-rowed crops are being chopped, the average actual length of cut is much longer than the theoretical length due to the random stem alignment. Figure 11.27 illustrates particle size distributions for wilted alfalfa chopped with varying theoretical lengths of cut. Note that for each length of cut, approximately 70% of the chopped silage is particles

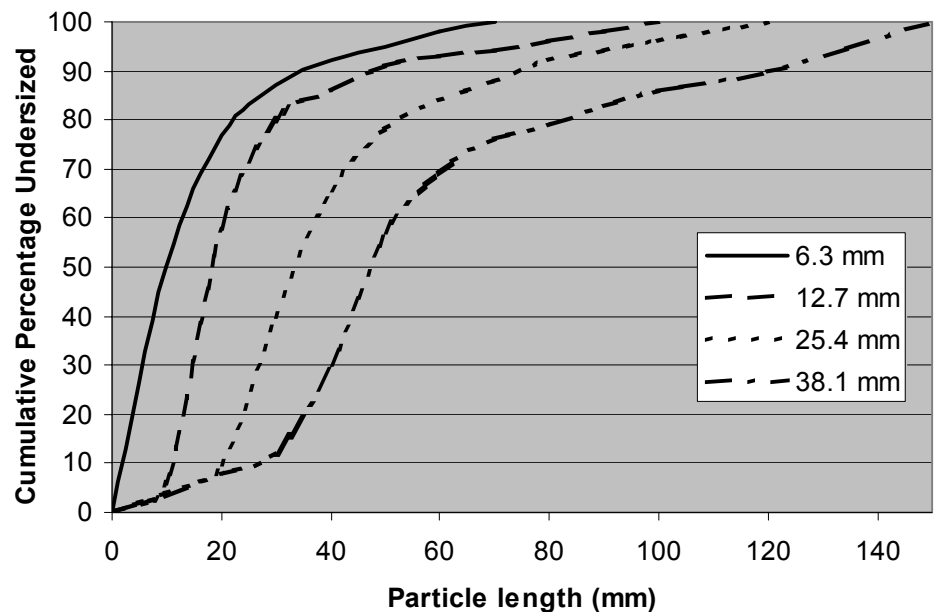


Figure 11.27 – Particle size distribution of wilted alfalfa chopped with various theoretical lengths of cut (Savoie et al., 1989).

longer than the theoretical length of cut. On a specific forage harvester, large increases in theoretical length of cut are made by removing knives from the cutterhead. For example, by going from 12 to 6 to 3 knives, the length of cut can be doubled twice. Another popular pattern is 8 to 4 to 2 knives. Smaller changes in length of cut are made by adjusting the feed velocity. The feed rolls will separate further to accommodate the reduced feed velocity until the maximum separation distance is reached; further reductions in feed velocity will then reduce the capacity of the harvester. The cutterhead speed is normally maintained at its maximum design value, typically 850 to 1000 rpm, and thus is not adjusted. Cutterhead diameters normally range from 520 to 770 mm and widths range from 450 to 620 mm.

The theoretical capacity of a precision-cut forage chopper can be calculated using the following equation:

$$m_f = \frac{\rho_f A_t L_c \lambda_k \omega_c}{6 \times 10^8} \quad (11.34)$$

where m_f = theoretical capacity or feed rate, kg/s

ρ_f = density of forage in the throat, kg/m³

A_t = throat area, cm²

Throat areas vary considerably among forage harvesters, but usually are within the range from 770 to 1350 cm². Based on research at the University of Wisconsin, typical forage densities between the feed rolls range from 56 kg/m³ for hay at 26% moisture to 340 kg/m³ for green corn (maize). If the forage yield changes during any given pass through a field, the corresponding change in capacity is accommodated through changes in the depth of forage between the feed rolls. Thus, the top feed rolls must be spring loaded to permit such changes in depth. The throat area is equal to the product of cylinder width times maximum forage depth between the upper and lower feed rolls. Maximum depths are typically in the range from 140 to 180 mm.

After the forage is chopped by the cutterhead, centrifugal force holds it against the housing as the cutterhead moves it toward the exit; the housing terminates at the bottom or rear of the cutterhead to allow the chopped material to escape. In a cut-and-throw machine, the cutterhead imparts sufficient energy to throw the chopped material to a trailing wagon or truck. Alternatively, in a cut-and-blow machine, a separate impeller-blower is used to convey the chopped material. Sometimes a recutter screen is installed at the exit of the cutterhead housing. Working against the recutter screen, the cutterhead further reduces the average length of cut of the exiting material (Figure 11.28). On machines with a recutter, an impeller-blower must be used to convey the chopped material. Electric motors or a hydraulic actuator controllable from the operator's seat permit swiveling the spout and/or tipping the end deflector to direct the forage to completely fill the truck or wagon. Figure 11.28 illustrates one method for providing access to the cutterhead and recutter screen. The impeller-blower is hinge-connected to the forage harvester. Swinging the impeller-blower away from the cutterhead permits access for installing or removing a recutter screen or for servicing the cutterhead.

Roll processors are often used after a cutterhead to crush and crack kernels and cobs of corn silage (Figure 11.29 and Figure 11.30). Rolls have adjustable clearance and typically have a 15% to 30% peripheral speed differential. Since roll processing

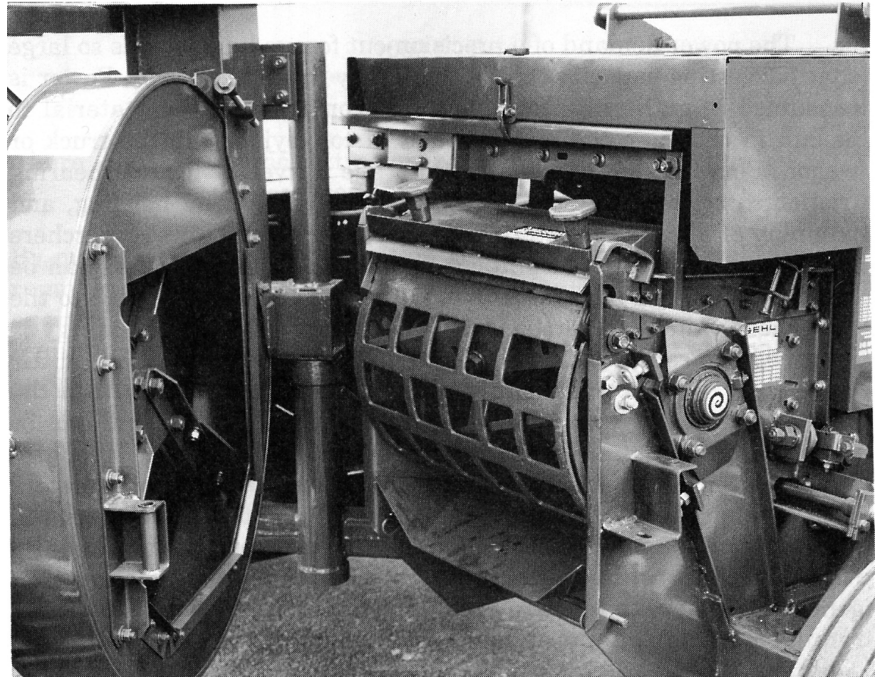


Figure 11.28 – Recutter screen installed between cutterhead and impeller blower (courtesy of Gehl Equipment Co.).



Figure 11.29 – Roll processor used to crush kernels and cobs in chopped corn silage (courtesy of Claas).

decreases particle size and consumes power, current recommendations are to set the theoretical length of cut to 20 mm when roll processors are used. The roll clearance would be adjusted for the crop moisture and kernel damage required. Shinnars et al. (2000) reported that specific energy and throughput capacity were similar between harvest with 9.5 mm theoretical length of cut and 19 mm theoretical length of cut with roll processing (clearance of 3 to 5 mm). With the longer cut length and roll processing, there was more coarse fiber, no intact cob pieces, and much more kernel damage. With a 1 mm roll clearance, capacity decreased and harvest energy increased.

The crop flow path through a harvester can have a significant effect on capacity and energy consumption. Figure 11.30 illustrates the crop flow and accompanying power transmission system for a large self-propelled harvester. With few direction changes in a processing stream such as this, kinetic energy imparted to the crop stream accumulates as each step increases particle velocity; this aids in reducing specific energy requirements. A fundamental concept in material flow is to remove it (any subsequent process) faster than it shows up (the preceding process). One aspect is actual particle speed; another aspect which is just as important and is directly related is volumetric and mass throughput. (This is also affected by the cross section of the process stream).

The power demand of a precision-cut forage harvester is so large that harvesting capacity can be limited by available power. Power is consumed in gathering, conveying, and compressing the material to be cut, in chopping the material, and in conveying it to the truck or wagon. Parasitic power losses in a forage harvester include bearing friction, friction of the cut material on the cutterhead housing, and pumping of air at the cutterhead and blower. Numerous researchers have found that power use in cut-and-blow forage harvesters can be divided roughly as follows: 20% to gathering and feeding, 40% to the cutterhead, and 40% for blowing. Within the cutterhead, energy is required for compressing and shearing, for acceleration and air movement, and for overcoming friction at the housing. Within the blower, energy is required for acceleration, for air movement and for overcoming friction. Material parameters such as shear strength, moisture content and friction coefficient, and machine parameters such as sharpness of the knife and length of cut will all affect the distribution of power in the harvester. However, cutting usually requires the greatest energy at the cutterhead, while friction generates the greatest energy requirement at the blower. The power requirement for chopping can be estimated using the following equation:

$$P_c = \frac{1000C_f F_{smax} \dot{m}_f}{\rho_f L_c} \quad (11.35)$$

where P_c = power required for chopping, kW

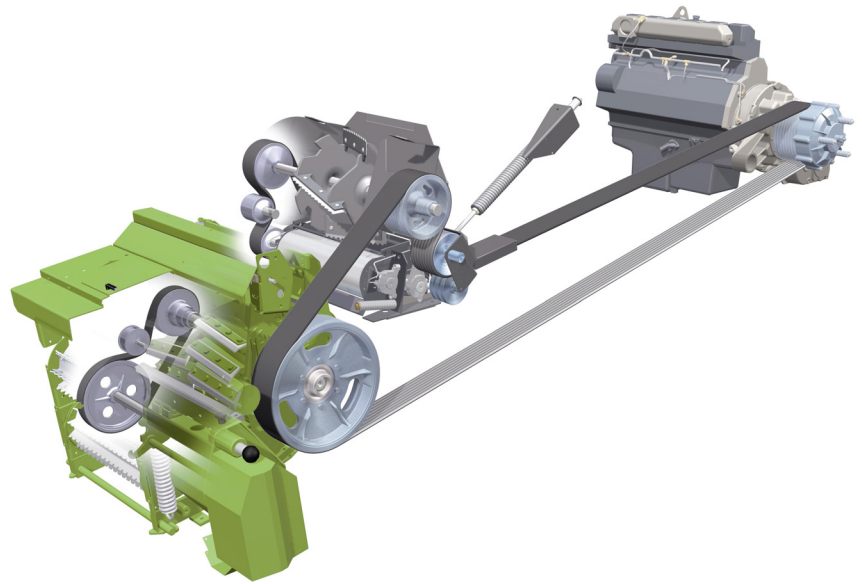
C_f = ratio of average to maximum specific cutting force

F_{smax} = maximum specific cutting force, N/mm of countershear length

The knives on the cutterhead in forage harvesters are normally helix-shaped; the resulting oblique cutting extends the duration of each cut while reducing the peak cutting force. Compared to the force-displacement diagram for a straight cut (Figure 11.15), oblique cutting would lengthen and lower the diagram without changing the area under the curve. Thus, as with straight cutting, C_f is about equal to 0.64 for typi-



(a)



(b)

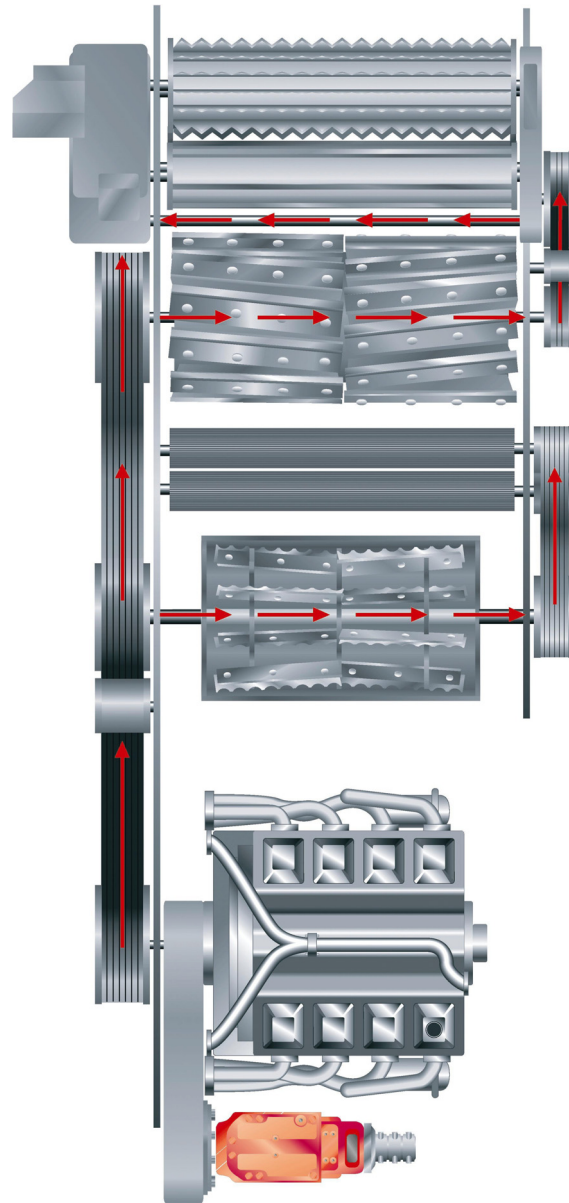


Figure 11.30 – Crop flow and associated power transmission diagrams for a self-propelled forage harvester: (a) crop flow through feedrolls, cutterhead, roll processor and crop accelerator; (b) power transmission illustration, and (c) power flow diagram (courtesy of Claas).

cal oblique cutting. Power for chopping varies with feed rate and length of cut; the specific cutting energy provides a better index for comparing forage harvesters of differing design. Specific cutting energy is defined as follows:

$$E_{sc} = \frac{1000C_f F_{max}}{\rho_f} \quad (11.36)$$

where E_{sc} = specific cutting energy per unit mass on the countershear, J m/kg.

By measuring power consumption while changing feed velocity and removing knives to change the theoretical length of cut and by assuming that such changes did not change other power requirements in the forage harvester, Richey (1958) estimated the specific energy requirements of two cylindrical cutterheads. For those tests, chopping alfalfa at 73% moisture and a 13-mm length of cut consumed 0.33 kW h/Mg, giving a value of $E_{sc} = 15.4$ J m/kg. Once a value of E_{sc} is known, the following equation can be used to calculate power:

$$P_c = \frac{E_{sc} m_f}{L_c} \quad (11.37)$$

Notice from Equation 11.36 that E_{sc} is proportional to the maximum specific cutting force. Thus, maintaining sharp knives and shearbar/knife clearance is very important to reduce the power requirement for forage chopping. As the knife edge wears from a 0.1 mm (sharp) to a 0.3 mm radius (dull), the cutting energy approximately doubles. The cutting energy also doubles as the clearance increases from 0.1 to 0.4 mm. The combined effect of dulling the knife and increasing the clearance as indicated above is approximately a tripling of the cutting energy. Dull knives and excessive clearance cause the crop to be torn rather than sheared and also accelerates wear due to wedging between the knife and shearbar. A sharpening stone with automatic traversing along the cutterhead is included as a standard feature of many forage harvesters. The automatic sharpener permits the operator to interrupt harvesting and sharpen the knives without leaving the field. The clearance should also be easy to adjust. The adjustment must be done with the cutterhead running at normal speed to accommodate the centrifugal expansion of the cutterhead.

Metal detectors are another valuable option on forage harvesters. Metal can damage the chopper and/or kill livestock that consumes the metal in the forage. When a magnetic sensor detects metal in the throat, the feed rolls are automatically stopped to prevent the metal from reaching the cutterhead. The feed rolls must be reversed to expel the metal-bearing forage before harvesting can be resumed.

Power to overcome friction between the cut forage and the cutterhead or blower housing can be calculated by using the following equation:

$$P_f = \frac{\beta \mu m_f v_{pc}^2}{1000} \quad (11.38)$$

where P_f = power absorbed by rubbing friction, kW

β = average arc of housing rubbed by chopped material, radians

μ = coefficient of friction between forage and steel housing

v_{pc} = peripheral velocity of cutterhead, m/s

Material leaving the cutterhead does not all strike the housing at the same place, so angle β is the average angle of contact. Manufacturers have realized that a short cutterhead housing is desirable to reduce friction power and thus have minimized arc β in most modern forage harvesters (Figure 11.29). ASAE Data D251.1 presents data on friction coefficients between chopped forages and metal surfaces. Friction coefficients for forage on steel range from 0.2 to 0.8 depending on type of forage, moisture content, peripheral velocity, and other factors. Peripheral velocities of cutterheads typically range from 20 to 28 m/s and, for such velocities, both chopped corn and chopped alfalfa have a coefficient of approximately 0.49 on polished stainless steel.

Power required to convey accelerate the forage at the cutterhead or blower is derived by assuming that the forage leaves the blades at about the peripheral speed of the blades:

$$P_{\text{accel}} = \frac{m_f v_p^2}{2000} \quad (11.39)$$

where P_{accel} = power to accelerate the forage, kW

v_p = peripheral velocity of the cutter or blower, m/s

Both the cutterhead and the blower move air, although the latter at a greater rate. According to well-established fan laws, fan power varies with the cube of the peripheral speed. Making use of data by Blevins and Hansen (1956), the following equation was derived for the approximate air power:

$$P_{\text{air}} = \frac{v_p^3}{16,600} \quad (11.40)$$

where P_{air} = power to move air, kW.

The header power, including power for the feed rolls, varies with the feed rate and is not large except at very high feed rates. The following equation can be used to estimate the header power:

$$P_h = C_{h0} + C_{h1} m_f \quad (11.41)$$

where P_h = power consumed by header, kW

C_{h0} , C_{h1} = constants for any given header, kW and kW s/kg

C_{h0} is the amount of power required to overcome friction when the harvester is running empty. Cutting, conveying, and compressing the forage between the feed rolls requires power in proportion to the feedrate.

By combining Equations 11.36 and 11.38 through 11.41, an equation for the total power consumption, P_{th} , of a forage harvester can be obtained. Note that air power is independent of feed rate, but power to all other components is proportional to feed rate. The form of the equation for P_{th} is thus similar to the following equation adapted from ASAE Data D497 for the total PTO power consumption of a precision-cut forage harvester:

$$P_{fh} = 6.0 + \frac{3.6 m_f (1 - M_{fwb}) C_c C_r}{(L_c / 9)^{0.32}} \quad (11.42)$$

where P_{fh} = total PTO power consumed by forage harvester, kW

C_c = crop factor = 3.3 for green corn, 4.0 for wilted alfalfa, or 5.7 for direct-cut forages, kW h/Mg dry matter

C_r = recutter factor = 1.0 with no recutter or 1.25 with recutter screen

M_{fwb} = moisture content of forage, wet basis, decimal

Engineers in industry use benchmarks for total (PTO plus drawbar) harvester power requirement, in good conditions, of approximately 2.1 kWh/Mg for corn and 3.3 kWh/Mg for hay crops. Equation 11.42 represents only average conditions and the equation is not useful for exploring the effect of various design variables. The design of a precision forage harvester is illustrated in Example Problem 11.5.

Example Problem 11.5

A cut-and-throw forage harvester has a cylindrical cutter head with width of 50 cm and diameter of 60 cm; it carries 8 knives and rotates at 950 rpm. The theoretical length of cut is to be 7 mm. The maximum height of the throat is 18 cm. When cutting corn, the compressed density of material in the throat is 320 kg/m³, and the specific cutting energy is 15 J m/kg. The coefficient of friction between the forage and the housing is 0.49, and the material is in contact with the housing through 2.5 radians of arc. Assume the power coefficients for the header are 0.6 kW and 0.3 kW s/kg. Calculate (a) the required feed velocity into the cutterhead, (b) the maximum allowable feedrate into the harvester, (c) the total PTO power requirement of the harvester, and (d) compare this to an estimate based on Equation 11.42 if the corn is at 70% moisture.

Solution

(a) The required feed velocity can be calculated by solving Equation 11.33 for v_f :

$$v_f = L_c \lambda_k \omega_c / 60,000 = 7(8)(950) / 60,000 = 0.887 \text{ m/s}$$

(b) Before using Equation 11.34 to calculate the maximum allowable feedrate, the maximum throat area must be calculated. It is:

$$A_t = (\text{cutterhead width})(\text{throat height}) = 50(18) = 900 \text{ cm}^2$$

Then the maximum allowable feedrate is:

$$\dot{m}_f = 320(900)(7)(8)(950) / (6 \times 10^8) = 25.5 \text{ kg/s or } 92 \text{ Mg/h}$$

(c) The various component power requirements must be calculated using Equations 11.37 through 11.41 to get the total power requirement. The peripheral velocity of the

cutterhead is needed to calculate the power used in friction, in accelerating the forage and in moving air. The radius of the cutterhead is 0.3 m and the rotation speed is 99.5 radians/s. Then the peripheral velocity is:

$$v_{pc} = v_p = 0.3(99.5) = 29.9 \text{ m/s}$$

Now the various power requirements can be calculated:

$$P_c = 15(25.5)/7 = 54.6 \text{ kW}$$

$$P_f = 2.5(0.49)(25.5)(29.9)^2/1000 = 27.9 \text{ kW}$$

$$P_{\text{accel}} = 25.5(29.9)^2/2000 = 11.4 \text{ kW}$$

$$P_{\text{air}} = 29.9^3/16,600 = 1.6 \text{ kW}$$

$$P_h = 0.6 + 0.3(25.5) = 8.3 \text{ kW}$$

$$P_{\text{th}} = 54.6 + 27.9 + 11.4 + 1.6 + 8.3 = 103.8 \text{ kW}$$

$$(d) \quad P_{\text{th}} = 6.0 + \frac{3.6(25.5)(1 - 0.70)(3.3)(1)}{(7/9)^{0.32}} = 104 \text{ kW}$$

In this example of a cut-and-throw harvester, the power delivered to the shaft of the cutterhead would be the sum of P_c , P_f , P_{accel} , and P_{air} . Thus, 95.5 kW, or 92%, of the total power requirement would be delivered to the shaft of the cutterhead.

Forage harvesters with nonprecision cut represent a lower-cost alternative to precision-cut harvesters. A flail-type forage harvester has a nonprecision cut and uses flails similar to those in a flail mower (Figure 11.21) to cut the standing crop and deliver it into a cross auger. Rotor speeds are usually in the range from 1100 to 1600 rpm, giving flail peripheral speeds in the range from 45 to 60 m/s. The auger conveys the cut forage to an impeller-blower to be conveyed to the trailing wagon. On some flail harvesters, a flywheel-type cutterhead is substituted for the impeller-blower. The cutterhead recuts the forage and conveys it to the wagon. Recutters generally have 2, 3, or 6 knives to provide varying lengths of cut. The average recut lengths are comparable to those from precision-cut forage harvesters except that the lengths are less uniform. Power requirements of a flail-type forage harvester with recutter are typically double or greater compared to those of a precision-cut forage harvester. Thus, the lower initial cost of the flail-type harvester are partially offset by higher operating costs. The flail-type harvesters are also less versatile because they cannot be used to harvest row crops.

11.2.3 Curing and preservation of forage

Losses of dry matter and quality can be very large during harvest of hay, especially for leafy hay such as alfalfa or other legumes. In alfalfa, for example, crude protein accounts for about 28% of the leaf dry matter but only 11% of the stem dry matter. Protein and nonstructural carbohydrates provide most of the nutritional value from the forage; NDF (nondetergent fiber) is less digestible and serves primarily as roughage (a coarse substance, usually high in cellulose, whose bulk stimulates peristalsis in the intestines). Dry matter and quality losses occur due to plant respiration, rain, and machine losses during harvesting. Typically, 3% to 5% of the plant dry matter, consisting primarily of nonstructural carbohydrate, is lost through respiration after cutting. Respiration losses thus increase the concentration of crude protein and NDF in the forage. Respiration ceases when the plants dry to 40% moisture. Rain causes leaf shatter and leaching losses. Leaf losses readjust the leaf to stem ratio, resulting in an overall loss in crude protein concentration and increased fiber concentration. Leaching losses from both leaves and stems consist of nonfiber; the leaching loss of crude protein is typically 20% greater than leaching loss of other dry matter. Machine losses include both leaves and stems but leaves are lost more readily; thus the reduction in the leaf-stem ratio caused by machines can reduce the overall protein concentration in the forage. Since fast drying of forage reduces respiration losses and also the opportunity for rain to fall on the cut forage, losses of dry matter and of quality are decreased by faster drying.

Leaves of legume crops dry much faster than the stems because the surface-volume ratio of leaves is much greater than that for stems. Also, a waxy cutin layer on the surface of stems acts as a natural moisture barrier and reduces their drying rate. *Conditioning* is a process in which the stems are crushed, cracked, or abraded such that they dry at approximately the same rate as the leaves. Magnified cross sections of conditioned and unconditioned stems are shown in Figure 11.31. Conditioning of legumes is usually accomplished by running the forage between a set of rolls, either of the corrugated crimper type or the intermeshing crushing type. The corrugated crimper, which has deep flutes that feed aggressively, is less likely to plug but can cause excessive leaf loss. Conditioning occurs through splitting each stem as it is bent to pass through the rolls. Intermeshing crushing rolls are less aggressive and thus less likely to cause leaf loss. These accomplish conditioning by crushing the stems. The peripheral speed of conditioners should be 3 to 4 times the travel speed of the machine to maintain a thin layer of forage between the rolls, since thin layers are conditioned more effectively and uniformly than thick layers. Thin layers are also facilitated when the reel provides a uniform feed rate to the conditioner and by use of the widest possible rolls; however, stiffness limitations place a practical limit on roll width. Roll spacing must automatically vary to accommodate different crop yields. Springs are used to maintain pressure between the rolls and the spring force is adjustable to control the degree of conditioning. An adjustable minimum clearance is also provided between the rolls; minimum clearance is increased for crops with larger stems, since excessive roll pressure or insufficient clearance can cause excessive leaf loss. Rolls are usually constructed from steel, neoprene, or tire carcasses. Shinnars et al. (1990) found no difference in leaf loss or drying rate of alfalfa due to type of rolls. ASAE Data D497 suggests the power requirement of mechanical conditioners is approximately 3 kW per m of mower width.

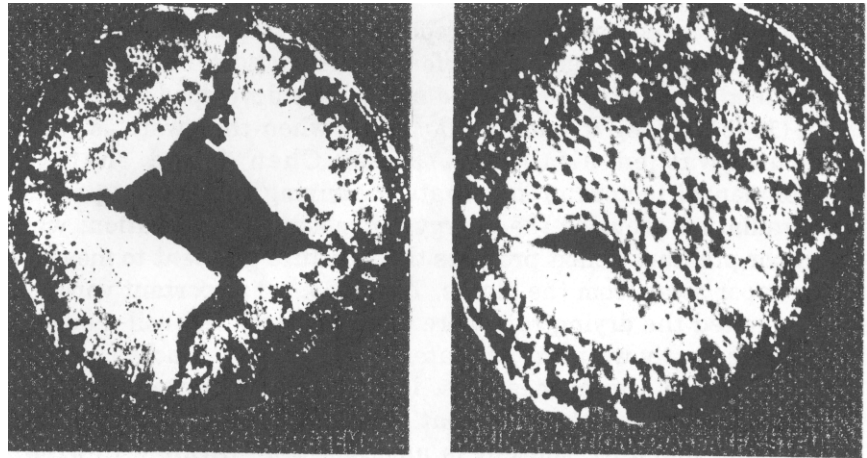


Figure 11.31 – Magnified compression of conditioned and unconditioned alfalfa stems (courtesy of Deere and Co.).

Using conventional techniques for harvesting, hay curing in the field required from 3 to 5 days depending on weather conditions. Use of crop conditioners to crush the stems (Figure 11.5) accelerated the drying and reduced curing time to 2 to 4 days. Use of chemical agents to accelerate drying of crushed hay can reduce curing time by an additional day. Spraying an aqueous solution of potassium and/or sodium carbonate on the forage increases the permeability of the waxy cutin surface of the plants, thus allowing faster escape of moisture (Rotz et al., 1990).

With severe conditioning, also called *maceration*, alfalfa or grass is shredded before being pressed into a mat; with maceration and mat making, forage may dry to baling moisture in as few as 4 hours (Rotz et al., 1990). Figure 11.32 illustrates different maceration techniques; commonly serrated rolls are used to crush, tear, and shred the plant; this is most effective when the plant is high in water content (fresh cut and 75% to 80% water by weight). The resulting material has much more surface area and many ruptured cells; maceration results in faster field drying as well as more rapid fermentation if silage is the product. Maceration requires additional energy of 2 to 4 kWh/Mg DM (Savoie, 2001).

A model of drying of swathed alfalfa was developed by Rotz and Chen (1985); drying dynamics may differ when the swath is raked. For the swathed alfalfa, Rotz and Chen found that two environmental factors predominate in driving the drying process: solar radiation provides the energy for moisture evaporation, while the vapor pressure deficit provides the moisture gradient to move the water vapor away from the plants. The two most important variables that limited the drying rate were swath density and soil moisture. Drying theory shows that, as material density approaches infinity, the drying rate approaches zero. Drying is also slowed when soil moisture keeps a wet surface at the bottom of the swath. The equilibrium moisture content is an important variable in drying theory. However, the model of Rotz and Chen best described actual

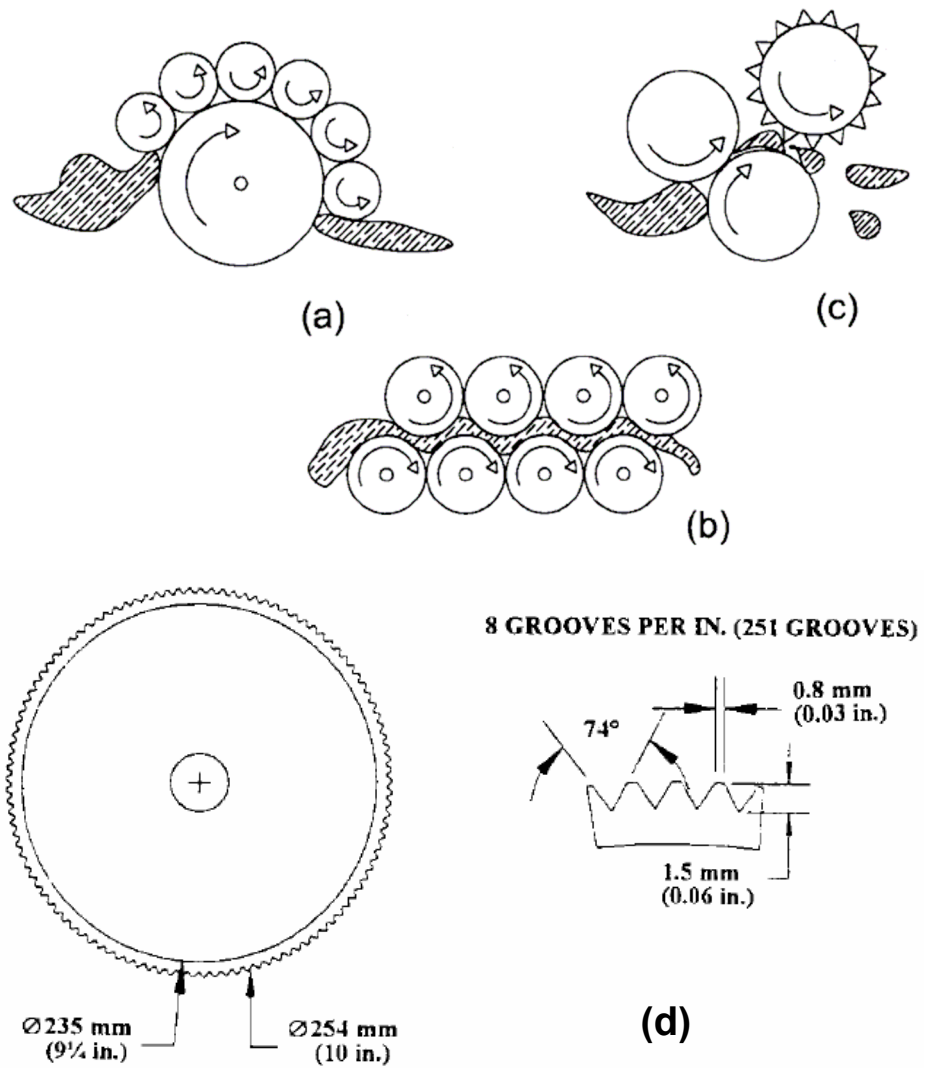


Figure 11.32 – Different configurations for intensive forage conditioning with typical roll characteristics: (a) peripheral roll macerator; (b) staggered roll macerator; (c) crushing-impact macerator (d) typical roll characteristics (Savoie et al., 1999, and Savoie, 2001).

drying when the equilibrium moisture content was assumed to be zero. Then the following equation gives the moisture content at any time during daylight drying:

$$M_f = M_{f_0} e^{-C_{dr}t} \quad (11.43)$$

where M_f = moisture content (dry basis) at end of time t

M_{f_0} = moisture content (dry basis) at $t = 0$.

t = drying period, h

C_{dr} = drying rate constant, 1/h.

On the basis of 5000 experimental observations on the drying of alfalfa, the following two empirical equations were developed for the drying rate constant:

$$C_{dr} = \frac{S_{rad}(1 + 9.30R_c) + 5.42\Theta_{db}}{66.4M_s + \rho_s(2.06 - 0.97\lambda_d)(1.55 + 2.19R_c) + 3037} \quad (11.44)$$

or

$$C_{dr} = \frac{S_{rad}(1 + 9.03R_c) + 43.8p_{vd}}{61.4M_s + \rho_s(1.82 - 0.83\lambda_d)(1.68 + 24.8R_c) + 2767} \quad (11.45)$$

where S_{rad} = solar radiation, W/m^2

R_c = application rate of chemical drying agent or conditioner, g of solution/g of dry matter

M_s = soil moisture content, % dry basis

ρ_s = swath density, g/m^2

λ_d = 1 on day of cutting, else 0

Θ_{db} = dry bulb temperature, $^{\circ}C$

p_{vd} = vapor pressure deficit, kPa

The above equations apply only to daytime drying; rewetting by rain or dew will slow the drying process. Both models gave realistic prediction of alfalfa daytime drying rates in the East Lansing, Michigan area and also in the semi-arid regions of California; the models have not yet been validated for other areas. Solar insolation rates typically range from 0 to $950 W/m^2$. It is easier to measure dry bulb temperature than vapor pressure deficit and thus Equation 11.44 may be best in areas of relatively high relative humidity. In very dry areas, Equation 11.45 may give more realistic predictions of drying rate of alfalfa. The factor, λ_d , is in the model because drying is faster on the day of cutting when the moisture is still uniformly distributed through the swath. The top of the swath dries first and later moisture removal from the bottom of the swath occurs more slowly. Swath densities range from 150 to $1500 g/m^2$, with $450 g/m^2$ being a typical value; it is determined from crop yield and percentage of land area covered by the cut swath. Note that the model makes no reference to the concentration of chemical in the drying solution; tests have shown that the effectiveness was nearly independent of the concentration of the chemical in the solution but was very dependent on the rate at which the solution was applied to the forage. Rates range from 0 to 0.25 grams of solution per gram of forage dry matter, with 0.075 g/g being a typical rate. Higher rates provide more complete coverage of the plant surfaces and thus promote drying. Example Problem 11.6 illustrates the calculation of alfalfa drying.

Example Problem 11.6

On a day when the dry bulb temperature is 20°C, the solar radiation is 650 W/m², and the soil moisture is 18%, alfalfa is cut at 80% moisture in a humid area. Alfalfa yielding 3 Mg/ha was cut with a 2.7 m wide mower and laid into a 1.8 m swath. Potassium carbonate drying agent is applied at the rate of 0.075 g/g. Estimate the moisture content of the hay after 1 h and 2 h of drying.

Solution

The hay was cut in a humid area, so Equation 11.44 applies.

Swath density is determined from yield and swath width:

$$(3 \text{ Mg/ha}) (2.7\text{m cut}/1.8\text{m swath})(1\text{ha}/10,000 \text{ m}^2)(10^6\text{g/Mg}) = 450 \text{ g/m}^2$$

Substituting values into Equation 11.44, the drying rate constant is:

$$C_{\text{dr}} = \frac{650(1 + 9.3 \times 0.075) + 5.42 \times 20}{66.4 + 450(2.06 - 97.1)(1.55 + 2.19 \times 0.075) + 3037} = 0.234\text{h}^{-1}$$

Initial moisture was 80% wet basis. 80 g water in a 100 g sample means there would be 80 g water for every 20 g dry matter. Therefore, initial moisture content, dry basis was 80/20 or 400%. Then, from Equation 11.43, the crop moisture at the end of the first hour is:

$$M_f = 400 (e^{-0.234 \cdot 1}) = 318\% \text{ dry basis} = 68.5\% \text{ wet basis}$$

At the end of the second hour, the crop moisture is:

$$M_f = 400 (e^{-0.234 \cdot 2}) = 318 (e^{-0.234 \cdot 1}) = 252\% \text{ dry basis} = 60\% \text{ wet basis}$$

Thus, the forage lost 11.5 points of moisture in the first hour and 8.5 points in the second hour. Since the moisture loss during any hour is proportional to the beginning moisture, the hourly moisture loss continues to decline as the forage dries.

11.2.4 Windrowing

In some methods of forage harvesting, the forage is formed into windrows that can then be picked up directly by the harvester. This is common practice when harvesting forage for silage or where the climate is very dry. When dry hay is desired in humid climates, the forage is placed in a swath and then raked into a windrow. Tedders are sometimes used to spread swaths to fully and uniformly cover the field area. A side-delivery rake can be used to roll swaths left by the mower, or tilled forage, into windrows. Rakes can also be used to invert previously-formed windrows to promote faster drying, especially after rain has wetted the windrows. Dry matter losses during raking typically range from 3% to 6% and more leaves than stems are usually lost. Thus, gentle handling is an important goal in rake design. Popular types of side delivery rakes are the finger-wheel and rotary.

Definitions of symbols in Equations 11.46 through 11.54 are as follows:

- α_1 = angle before bottom at which raking begins, radians (see Figure 11.33)
- α_2 = angle at which raking ends, radians
- β = angle between tooth bars, radians
- γ = Acute angle between raking front and direction of travel, radians
- θ_{tr} = angle between direction of travel and planes of reelheads, radians
- θ_t = angle between v_t and direction of travel, radians
- x_2 = horizontal distance traveled by teeth during nonraking, m
- y_2 = vertical distance from lowest position of rake teeth to top of windrow, m
- $L_1 + L_2$ = horizontal distance traveled by teeth during raking, m
- r = reel radius, m
- v_f = forward velocity of rake, m/s
- v_{tr} = reel component = average horizontal velocity of teeth during raking, relative to rake, m/s
- v_p = peripheral speed of reel, m/s
- v_t = resultant tooth velocity = vector sum of v_f and v_{tr} , m/s
- v_{hr} = average horizontal velocity of hay relative to rake, m/s
- v_h = average resultant hay velocity = vector sum of v_f and v_{hr} , m/s
- L_h = maximum theoretical distance travelled by hay during raking, m
- w_r = width of rake, m

A parallel-bar (oblique-reelhead) rake is illustrated in Figure 11.33. The two reelheads are parallel but at an acute angle with the tooth bars. Thus, when one of the reelheads is driven, either by PTO power or by a ground wheel, every rake tooth follows a circular path in a plane parallel to the reelheads. All teeth automatically maintain parallel positions, usually vertical, but the pitch of the teeth can be changed by changing the tilt of the reelhead axes. Pitching the bottoms of the teeth forward gives a more vigorous raking action in heavy crops.

Figure 11.33 was used in deriving velocity relationships for a parallel-bar rake. Rake teeth contact the hay at angle α_1 from the lowest tooth position and release it at angle α_2 at the top of the windrow. Teeth are in contact with the hay during forward travel x_1 and out of contact during forward travel x_2 . One expression for x_2 can be derived from Figure 11.33a, i.e.:

$$x_2 = (L_1 + L_2) \left(\cos \theta_{tr} + \frac{\sin \theta_{tr}}{\tan \gamma} \right) \quad (11.46)$$

Another expression for x_2 can be derived from Figure 11.33b, i.e.:

$$x_2 = r \frac{v_f}{v_p} (\beta - \alpha_1 - \alpha_2) \quad (11.47)$$

Then, since $L_1 = r \sin(\alpha_1)$ and $L_2 = r \sin(\alpha_2)$, Equations 11.46 and 11.47 can be combined into the following equation:

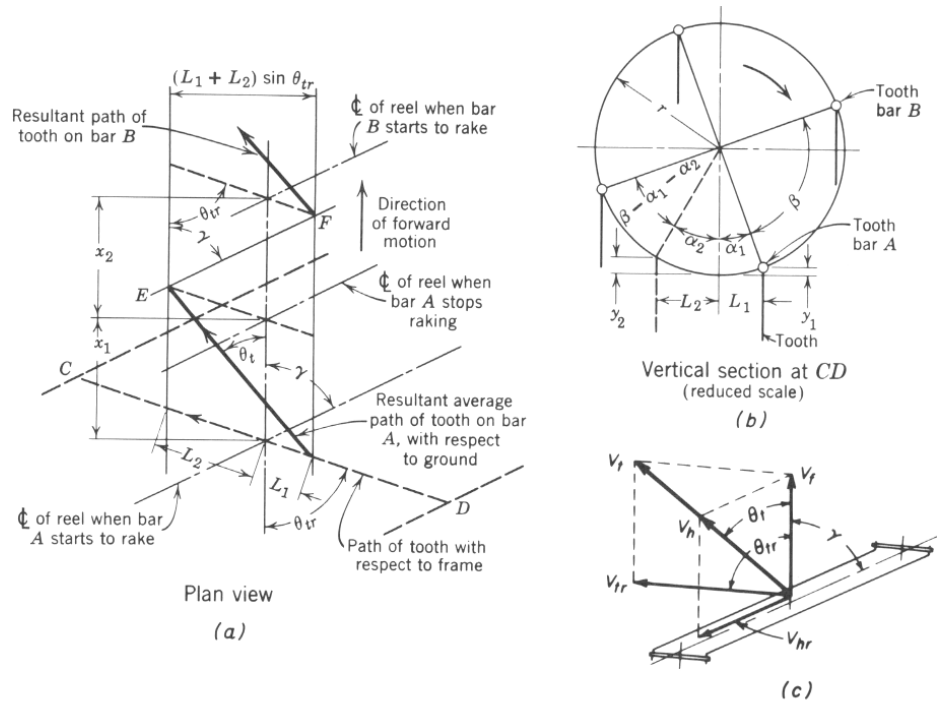


Figure 11.33 – A side-delivery parallel bar rake (courtesy of CNH).

$$\frac{\beta - \alpha_1 - \alpha_2}{\sin \alpha_1 + \sin \alpha_2} = \frac{v_p}{v_f} \left(\cos \theta_{tr} + \frac{\sin \theta_{tr}}{\tan \gamma} \right) \quad (11.48)$$

All terms in Equation 11.47 are design variables except α_1 and α_2 , which are unknowns depending upon operating conditions. From Figure 11.33b:

$$\alpha_2 = \arccos \left(1 - \frac{y_2}{r} \right) \quad (11.49)$$

Distance y_2 can be determined as the height of the top of the windrow relative to the lowest position of the rake teeth. Then Equation 11.49 can be solved for α_2 and Equation 11.48 can be solved (iteratively) for α_1 . Note that α_1 can be negative if the effective raking stroke begins beyond the lowest point of tooth travel. After α_1 and α_2 are known, the magnitude of vector v_{tr} can be calculated using the following equation:

$$\frac{v_{tr}}{v_p} = \frac{\sin \alpha_1 + \sin \alpha_2}{\alpha_1 + \alpha_2} \quad (11.50)$$

The direction of v_{tr} is parallel to the planes of the reelheads. After vector V_{tr} is determined, the direction and magnitude of v_t can be calculated. Angle θ_t can be calculated from:

$$\theta_t = \arctan \left(\frac{v_{tr} \sin \theta_{tr}}{v_f + v_{tr} \cos \theta_{tr}} \right) \quad (11.51)$$

and the magnitude, v_t , can be calculated from:

$$v_t = \frac{v_{tr} \sin \theta_{tr}}{\sin \theta_t} \quad (11.52)$$

The direction of v_h is coincident with v_t . The magnitude of v_h can be calculated using the following equation:

$$v_h = \frac{v_f}{\cos \theta_t + \sin \theta_t + \cot \gamma} \quad (11.53)$$

The theoretical maximum distance traveled by the hay during raking is given by the following equation:

$$L_h = \frac{w_r}{\sin \theta_t} \quad (11.54)$$

A finger-wheel side-delivery rake is illustrated in Figure 11.34. The action of one raking wheel is illustrated in Figure 11.34a, while velocity relationships for the complete rake are shown in Figure 11.34b. Raking teeth are carried on wheels whose planes of orientation allow each wheel to be ground driven. Thus, no separate drive train is required. As was true for the parallel-bar (oblique-reelhead) rake, the vector v_{hr} is parallel to the raking front and v_{tr} is parallel to the planes of the raking wheels.

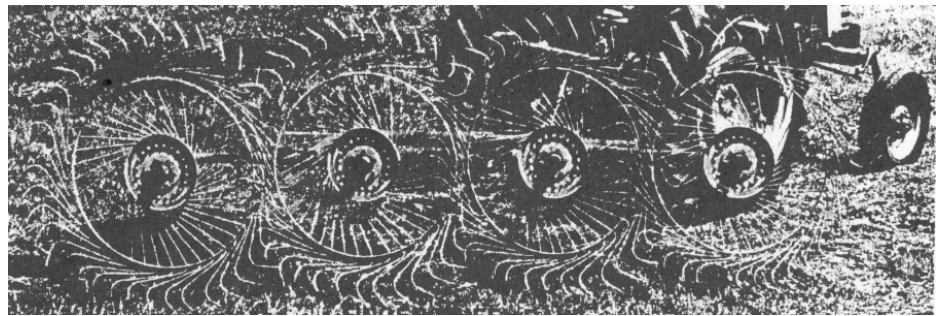
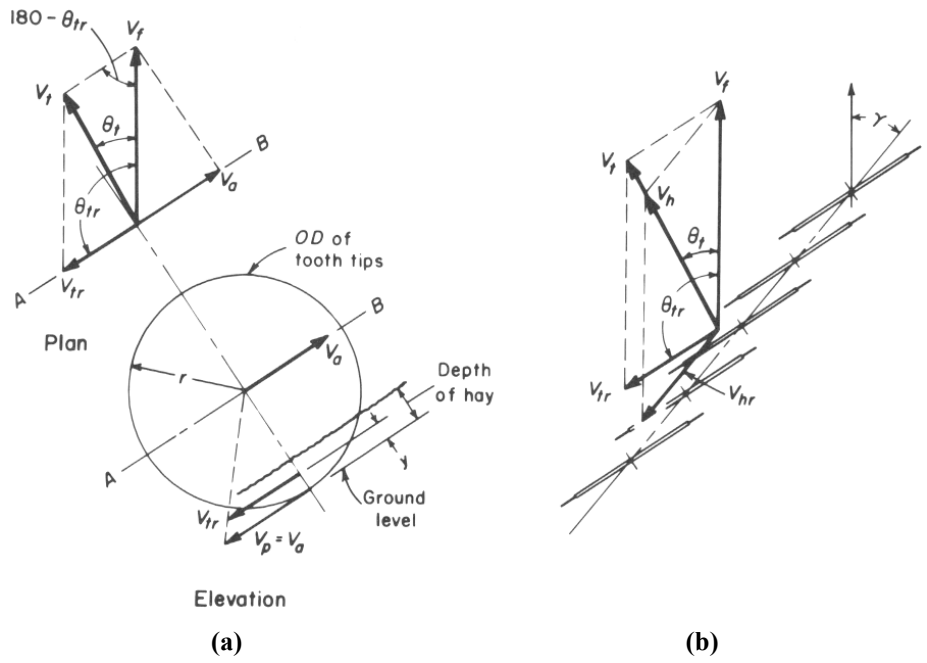


Figure 11.34 – A finger-wheel side-delivery rake (courtesy of Deere and Co.).

Since the tooth wheels are each ground driven, the magnitude of v_p can be calculated from the following equation (see Figure 11.34a):

$$\frac{v_p}{v_f} = \cos(\pi - \theta_{tr}) = \cos \theta_{tr} \tag{11.55}$$

The reel component, v_{tr} , is proportionally less than v_p as shown in the following equation:

$$v_{tr} = \frac{r - y}{r} v_p \tag{11.56}$$

where y = half of the windrow height, m (see Figure 11.34a)

r = radius from center of tooth wheels to tooth tips, m

The angle, θ_t , of the resultant tooth and hay path is given by the following equation:

$$\theta_t = \arctan\left(\frac{v_{tr} \sin \theta_{tr}}{v_f}\right) \quad (11.57)$$

The magnitudes of v_t and v_h can be calculated using Equations 11.52 and 11.53, respectively. The theoretical maximum length of hay travel for the finger wheel rake can be calculated using Equation 11.54.

The gentleness with which the hay is handled during raking is influenced by rake design variables. Gentleness is promoted by maintaining low hay velocity, v_h , by keeping v_t as close as possible to v_h to reduce tooth impacting on the hay, and by keeping hay travel, L_h , as small as possible. The ratio of v_h/v_t is closer to unity for the finger-wheel rake, thus providing a smoother raking action than for the parallel-bar rake. However, the finger-wheel rake has a somewhat longer hay path (compare Figures 11.33c and 11.34a). For the parallel-bar rake, reducing the ratio v_p/v_f lengthens the hay path but reduces the frequency of tooth impacts on the hay and also reduces the ratio v_t/v_h . Reducing v_f also provides gentler handling of the hay but decreases the raking capacity. The theoretical effects of the various raking parameters were determined analytically, but there is little published information on the effect of raking parameters on losses. Example Problem 11.7 illustrates calculations for a side delivery rake with oblique reel head.

Example Problem 11.7

A five-bar side delivery rake with an oblique reel head has a raking front angle, $\gamma = 65^\circ$ (6.81 radians) and a raking width of 2.4 m. The reel radius is 0.3 m and the head angle is $\theta_{tr} = 72^\circ$ (7.54 radians). The reel is ground driven with a speed ratio $v_f/v_p = 0.8$. When the rake is traveling at 8 km/h while raking a windrow of height 0.45 m, calculate the (a) direction and (b) magnitude of the resultant tooth path, (c) the average hay velocity, (d) the maximum theoretical distance travelled by the hay during raking, and (e) the ratio, v_h/v_t , of the average hay velocity to the resultant tooth velocity.

Solution

(a) Angles α_1 and α_2 must be calculated to begin the analysis. Since the angles and their trigonometric functions will be used, radians will be used instead of degrees in all of the trigonometric calculations. The value of α_2 can be calculated using Equation 11.49:

$$\alpha_2 = \arccos(1 - 0.45/0.3) = 2.09 \text{ radians}$$

then all variables in Equation 11.48 are known except for α_1 . Because the reel has 5 bars, $\beta = 2\pi/5 = 1.26$ radians. Then:

$$\frac{1.26 - \alpha_1 - 2.09}{\sin \alpha_1 + \sin 2.09} = \frac{1}{0.8} \left(\cos 7.54 + \frac{\sin 7.54}{\tan 6.81} \right)$$

Solving the above equation by iteration gives $\alpha_1 = 5.45$ radians. The forward speed of the rake is $8/3.6 = 2.22$ m/s and the peripheral speed of the reel is $v_p = 2.22/0.8 = 2.78$ m/s. Equation 11.50 can be used to calculate the reel component, v_{tr} :

$$v_{tr} = 2.78 (\sin 5.45 + \sin 2.09) / (5.45 + 2.09) = 1.53 \text{ m/s}$$

Next, the direction of the resultant tooth path can be calculated using Equation 11.51:

$$\theta_t = \arctan[(1.53 \sin 7.54) / (2.22 + 1.53 \cos 7.54)] = 2.97 \text{ radians or } 28.4^\circ$$

(b) From Equation 11.52, the magnitude of the resultant tooth velocity is:

$$v_t = 1.53 \sin(7.54) / \sin(2.97) = 3.06 \text{ m/s}$$

(c) Next, from Equation 11.53, the average hay velocity is:

$$v_h = 2.22 / [\cos(2.97) + \sin(2.97) + \cot(6.81)] = 1.22 \text{ m/s}$$

(d) The maximum length of the hay path, from Equation 11.54, is:

$$L_h = 2.4 / \sin(2.97) = 5.1 \text{ m}$$

(e) Finally, the ratio of hay velocity to tooth velocity is:

$$v_h/v_t = 1.22/3.06 = 0.40$$

The maximum hay path length is over twice the swath width and the average travel speed of the hay is only 40% of the tooth velocity. The teeth impact the hay repeatedly in moving it into the windrow and thus the leaves of legumes can be lost if the hay is very dry during raking.

Power requirements for side delivery raking are small and data are sparse. ASAE Data D497 suggests the following power requirement for hay rakes:

$$P_{\text{rake}} = C_1 W_{\text{rake}} \quad (11.58)$$

where P_{rake} = PTO power requirement for raking, kW

W_{rake} = rake width, m

$C_1 = 0.4$ kW/m for side delivery rakes, 2.0 kW/m for rotary rakes

11.2.5 Baling

Hay can be harvested as loose hay in stacks or as chopped hay, but baling is the most popular method of hay harvest. The two types of balers in popular use are *rectangular balers* (Figure 11.6) and *round balers* (Figure 11.7). Although the discussion in this chapter relates to baling of hay, the same machines are used for baling straw and other fibrous materials. The principles of compression and packaging are applicable to many non-forage materials.

11.2.5.1 Rectangular balers

Virtually all rectangular balers have the baling chamber oriented in the direction of travel of the baler. A windrow pickup unit feeds the windrow into a cross conveyor which, in turn, feeds the hay into the baling chamber. There are three types of cross conveyors. In one type, an auger conveys the hay to a set of packer fingers that sweep the hay into the bale chamber. In a second type, linear moving packer fingers travel the full width of the pickup in conveying the hay into the bale chamber. In the third type, rotating finger wheels move the hay laterally to the packer fingers. The bale chamber is fed from the side or from below in current balers. Feeding from the bottom allows the baler to travel directly behind the tractor. In all feeder designs, the packer fingers must be timed to the movement of the reciprocating plunger so that the fingers are out of the bale chamber except when the plunger is in a forward position.

As the feeder delivers each charge of hay, a knife on the edge of the plunger and a countershear at the rear edge of the feed opening shear off the charge of hay as the plunger moves rearward. Continued movement of the plunger compresses the charge of hay and pushes previously accumulated compressed hay through the bale chamber. Controlled convergence of the bale chamber (Figure 11.35) provides resistance to bale movement and thus controls bale density. Fixed wedges and spring-loaded dogs extend into the bale chamber and minimize re-expansion of the compressed hay during forward movement of the plunger. During compression, a star wheel at the top of the bale chamber (the leftmost star wheel in Figure 11.35a) is driven by the moving bale to trigger the tying mechanism when a bale of sufficient length has been formed. When the plunger reaches its rearmost position after the tying mechanism has been triggered, needles (visible at bottom of Figure 11.35a) move through slots in the plunger face to deliver twine or wire to the knotter. The knotter completes the knots and the needles retract as the plunger begins moving forward.

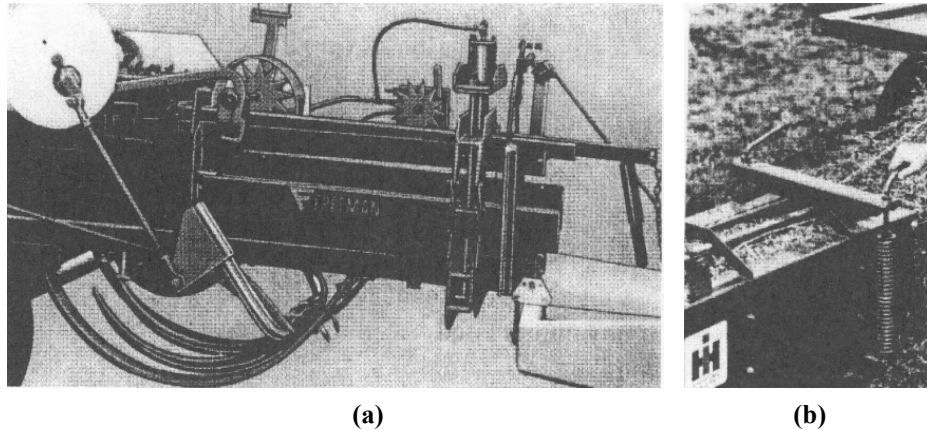


Figure 11.35 – Control of bale density (a) hydraulically and (b) with manually adjustable springs (reprinted from Kepner et al., 1978).

The density of hay in the bales is determined by the type of material being baled, its moisture content, and by the resistance provided by the convergence of the bale chamber. The convergence causes the hay to be compressed laterally as the bale moves through the chamber. Assuming the hay is an elastic material, the plunger force generated by convergence can be calculated using the following equation:

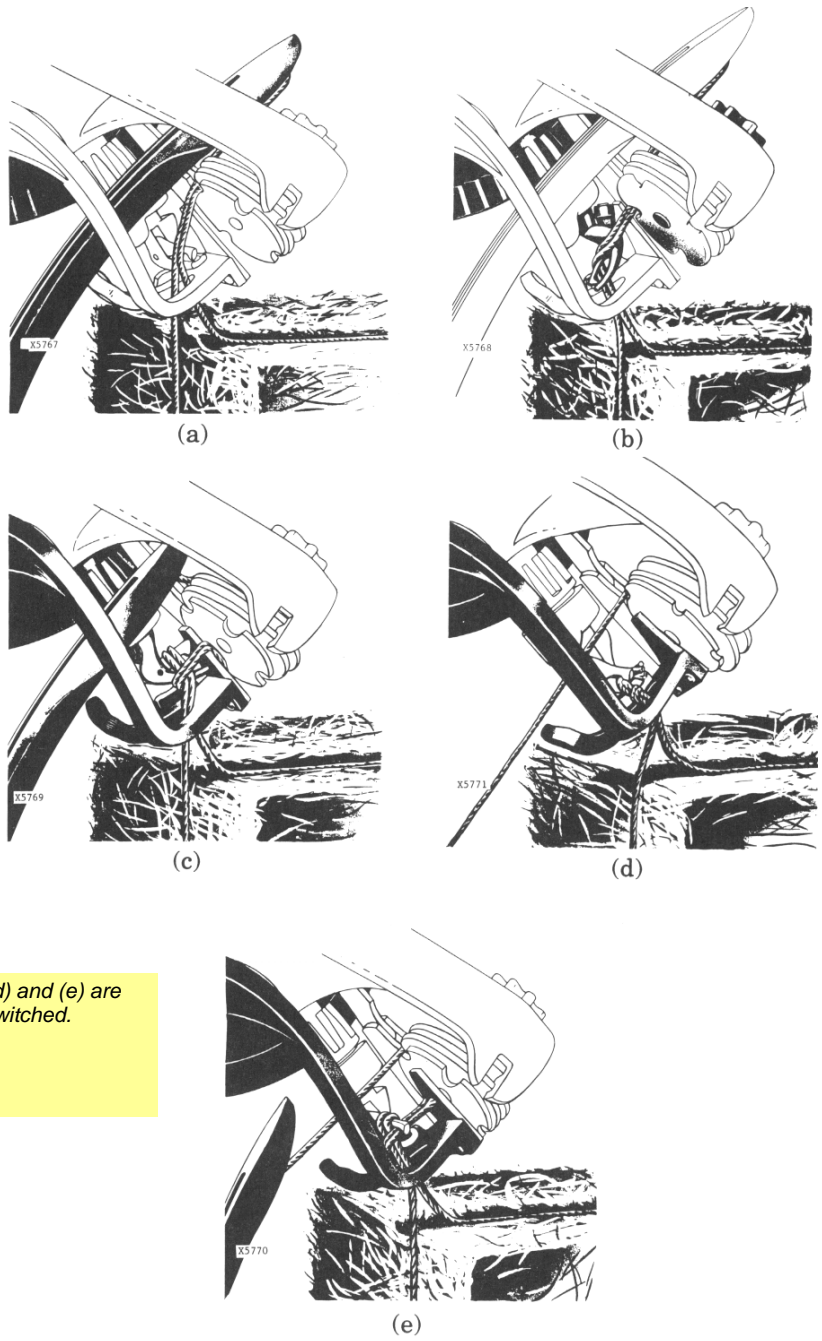
$$F_c = \frac{E_h y}{d_c} L_c w_c f_h \quad (11.59)$$

where F_c = compressive force supplied by plunger, N
 E_h = effective modulus of elasticity of the hay, kPa
 y = total convergence in converging section, mm
 d_c = depth of bale chamber, m
 L_c = length of converging section, m
 w_c = width of bale chamber, m
 f_h = coefficient of friction between hay and bale chamber

The quantity $E_h y/2d_c$ is the lateral pressure to compress the hay a distance y , and $2L_c w_c$ is the total area on which the lateral pressure acts assuming only two sides converge. Multiplying by the coefficient of friction gives the contribution of convergence to the plunger force. There will be some friction against the nonconverging sides. If all four sides converge, convergence of each pair of sides is usually controlled independently. In either case, the friction against all sides should be included in calculating F_c . Equation 11.59 is difficult to use to compute actual forces because of difficulty in determining values for E_h . However, the equation does provide insights into the problems of density control. Both E_h and f_h increase with moisture content of the hay, thus increasing the plunger force and the bale density. The tension-control springs in Figure 11.35b provide the lateral force for squeezing the bales in the convergence section. Hand cranks are provided to adjust the amount of spring tension and the tension must be adjusted to compensate for changes in moisture and crop. During operation, the springs extend when E_h increases and, although y declines, the lateral force increases. Zero-rate springs would be preferable and the equivalent effect is achieved by substituting a hydraulic cylinder to provide the convergence force (Figure 11.35a). The hydraulic pressure can be adjusted from the operator's station but remains at the set value, thus providing constant force. One large rectangular baler uses several load cells placed on the plunger face to monitor the compression force. The signals from the load cells are sent to a microprocessor. The microprocessor controls bale density by sending output signals to electrohydraulic valves that control oil pressure in hydraulic cylinders which regulate bale chamber convergence. The microprocessor system ensures uniform, constant bale density as crop conditions change.

Both twine-tie and wire-tie balers are available but the twine-tie balers are much more popular. ASAE Standards S229 and S315 provide specifications for baling wire and twine, respectively.

Figure 11.36 shows a twine knotter tying a bale. In a popular-sized baler, each bale is tied by two loops of twine and thus two knotters are included on the baler. When tying a bale, each knotter grips the cut end of its twine as the needles retract. As the



Note (d) and (e) are switched.

Figure 11.36 – Operation of a twine knotter (courtesy of Deere and Co.).

next bale advances through the chamber pushing the twine strands on its leading edge, twine is pulled from two twine balls through the needle eyes. When the bale tying mechanism is triggered by the star wheel through a limited-motion pawl clutch, the needles rise through the plunger slots, carrying the twine strands to the respective knotters. Figure 11.36a shows the start of the tying cycle. The needle has brought the twine around the bale and placed it in the twine holder. The two outside disks of the holder have rotated through the angle between adjacent notches while the center disk remained stationary, thus pinching the twine between the spring-loaded disks to hold it when the needle withdraws. The knotter-bill assembly in Figure 11.36b has begun rotating to form a loop in the string about the knotter bills. The loop is completed in Figure 11.36c, the knotter bills have opened and, with continued rotation, the bills close over the strings held by the twine holder. As the bills grip the strings, the knife attached to the stripper arm cuts the twine between the knotter and the twine holder, thus releasing the formed bale. The bills have gripped the strings and the knife has completed the cutting in Figure 11.36d and, in Figure 11.36e, the wiper has completed the knot by moving forward to push the loop from the bills over the twine held by the twine holder. Note that, in Figure 11.36d, the twine holder has already gripped the twine end for the next bale and continues to hold it while the current bale is being tied and the next bale is being formed.

Wires are tied around bales in a manner similar to that described above, except that the wire ends are twisted, not knotted. Thus a wire-tie baler has a wire twister instead of a twine knotter. Because of the greater tensile strength of wires, wire-tied bales can have greater density than string-tied bales.

The baling rate (in kg/s) can be limited by the rate at which forage is fed into the baler, by the design of the baler, or by available power. The following equation relates the first of these possible limits:

$$m_f = \frac{d_c w_c \delta_s \rho_c \omega_c}{60} \quad (11.60)$$

where m_f = baling rate or material feed rate, kg/s

d_c = depth of bale chamber, m

w_c = width of bale chamber, m

δ_s = thickness of each compressed hay slice, m

ρ_c = compressed density of hay in bale, kg/m³

ω_c = crank speed, rpm

A popular chamber size is $w_c = 0.46$ m and $d_c = 0.36$ m. However, much larger balers with chambers 1.2 m by 1.2 m are on the market and several intermediate sizes are also available. Densities of hay in bales, including moisture at time of baling, range from 130 to 225 kg/m³ with the lower end of that range being the most popular. Use of low crank speeds limits capacity and increases stress loads. Tests by Burroughs and Graham (1954) have shown that, for a given feed rate and bale density, peak plunger force fell 20% as crank speed increased from 40 to 50 rpm but showed little decline with further increases in speed. Use of high speeds generates excessive inertia forces in the reciprocating plunger and causes greater losses of hay from the bale chamber. Practical crank speeds range from 45 rpm for some large balers to 100 rpm for smaller

balers. Each time the baler plunger moves rearward, it shears off the incoming hay and compresses the hay charge into a flake or slice. The flake thickness varies with the rate at which hay can be fed into the bale chamber. Typically, flake thickness is less than 20 cm. From Equation 11.60, for a baler with chamber dimensions of 36 by 46 cm, crank speed of 50 rpm, bale density of 225 kg/m³, and flake thickness of 20 cm, the baling capacity would be 6.21 kg/s or 22.4 Mg/h. In NIAE (1965) tests of balers with the 36 by 46-cm bale chamber, rates as high as 22 Mg/h were recorded for short time periods, but maximum rates fell to 16.3 Mg/h for continuous tests.

Instantaneous crank torque varies widely on a baler and a flywheel is used to maintain a relatively constant crank speed; this also steadies the torque demand from the tractor PTO. Figure 11.37 shows two typical force-deflection curves for a baler plunger working with two different feed rates. The curves are similar except that compression starts earlier with the larger hay charge and the peak force is higher. The small peaks near 300 to 400 mm displacement are knife forces for shearing the hay charge; on most hay charges, these cutting peaks occur later and closer to the force

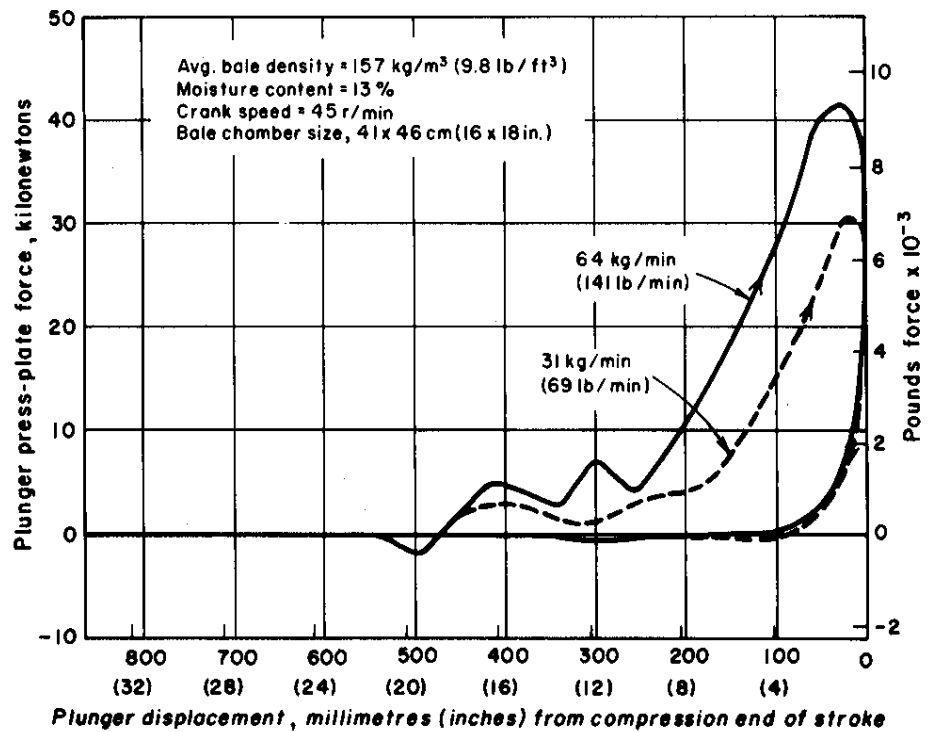


Figure 11.37 – Plunger work diagrams for two feed rates in alfalfa (Burroughs and Graham, 1954).

peak. The force reaches a peak and begins declining when the hay compressed on earlier strokes begins moving in the chamber; the decline occurs because the sliding friction is less than the static friction in the chamber. Both force curves merge after the plunger starts forward. The force is greater than zero during the first 100 mm of return travel only because the compressed hay re-expands somewhat. During the re-expansion, a small amount of potential energy in the compressed hay is returned to the plunger in the form of kinetic energy. A force-displacement curve (Figure 11.37) can be converted to a torque versus angular displacement curve for the crank. For any given crank angle, θ_c , the plunger displacement, x_p , can be calculated using the following equation from slider-crank theory (Figure 11.38):

$$x_p = r_c(1 - \cos \theta_c) + L_{cr} - \left(L_{cr}^2 - r_c^2 \sin^2 \theta_c \right)^{0.5} \quad (11.61)$$

where x_p = plunger displacement, m (see Figure 11.38)

r_c = crank radius, m

L_{cr} = length of connecting rod, m

θ_c = crank arm displacement, radians

For the x_p corresponding to each θ_c , a force-displacement curve similar to the one in Figure 11.37 can be used to find the corresponding plunger force. Then the instantaneous torque at that crank angle is given by the following equation:

$$T_c = \frac{-\dot{x}_p}{\dot{\theta}_c} F_p \quad (11.62)$$

where T_c = torque in crank arm, N·m

F_p = force on plunger, N

$$\text{and} \quad \frac{\dot{x}_p}{\dot{\theta}_c} = r_c \sin \theta_c \frac{r_c \sin \theta_c \cos \theta_c}{\left(\frac{L_{cr}^2}{r_c^2} - \sin^2 \theta_c \right)^{0.5}} \quad (11.63)$$

where \dot{x}_p = plunger speed, m/s

$\dot{\theta}_c$ = crank speed, radians/s (note: $\dot{\theta}_c = \omega_c 2\pi/60$)

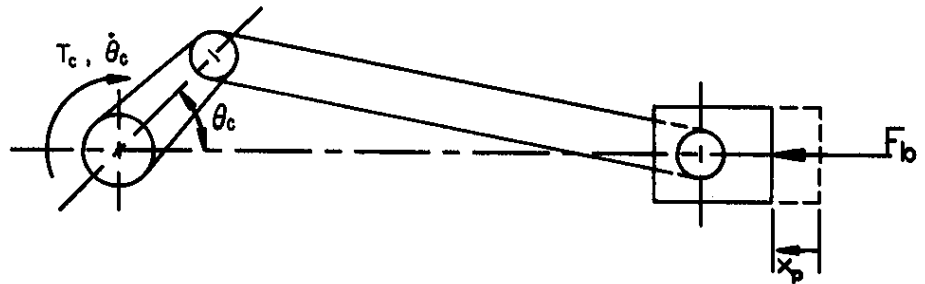


Figure 11.38 – Diagram of a slider-crank mechanism in a baler.

Figure 11.39 is an illustration of instantaneous crank torque. The small peak on the left is the cutting peak. The data representing instantaneous torque as a function of crank angle can be integrated numerically to obtain the average torque. The average torque, T_{cave} , that must be supplied by the engine is shown by the dashed line across the peak. The cross-hatched area represents energy that must be supplied by a flywheel when the instantaneous torque exceeds the torque output supplied by the engine. The required flywheel size can be calculated using the following equation:

$$I_f = \frac{\Delta E_k}{R_s \theta_{cave}} \quad (11.64)$$

where I_f = mass moment of inertia of flywheel, $kg\ m^2$

ΔE_k = kinetic energy required from flywheel, J (see Figure 11.39)

R_s = speed regulation = (max speed – min speed)/average speed

θ_{cave} = average crankshaft speed, radians/s, = (max speed – min speed)/2

The average power required to operate the plunger can be calculated from the product of the average torque and speed at the crankshaft. It can be shown that the average torque is proportional to the area within the plunger force-displacement diagram (Figure 11.37). Note that the average torque and thus the average power requirement increase with the feed rate. The power required by the pickup, conveyors, and packer also increase with feed rate (see Figure 11.40). The equation for the PTO power requirement of a baler thus has the following form:

$$P_{baler} = C_0 + C_1 m_f \quad (11.65)$$

where P_{baler} = PTO power requirement of baler, kW

m_f = feed rate, kg/s

C_0, C_1 = constants that vary with baler design, type and moisture content of material being baled. Units are kW for C_0 and kW s/kg for C_1 .

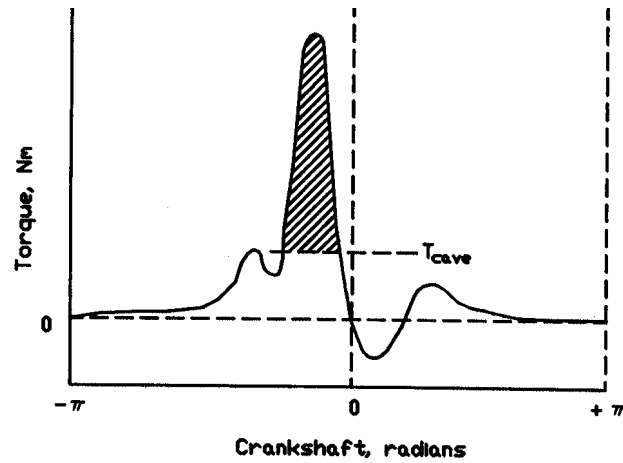


Figure 11.39 – Instantaneous torque in the crank arm.

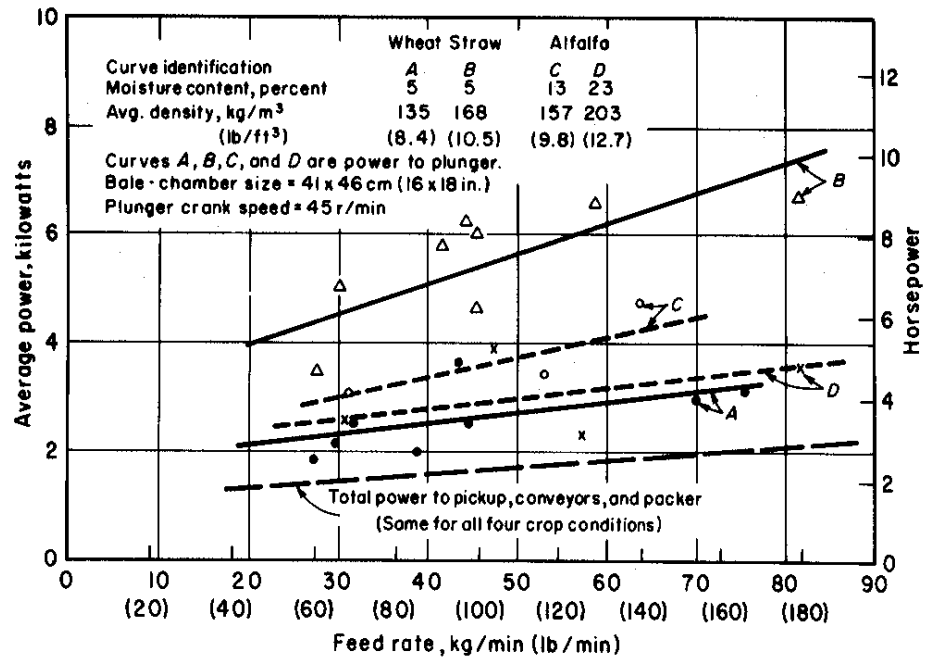


Figure 11.40 – Relation of average power requirements to baling rate (Graham, 1953).

Values for constants C_0 and C_1 can be determined from field tests of balers. From Figure 11.40, for example, values for (C_0, C_1) are (1.75, 1.17), (2.84, 3.37), (1.88, 2.23), and (1.97, 1.23) for curves A, B, C, and D, respectively. ASAE Data D497 suggests values of (2, 3.6) and (4, 4.7) for small and large rectangular balers baling hay, respectively. Calculation of baler capacity and power are illustrated in Example Problem 11.8.

Example Problem 11.8

A rectangular baler with chamber cross section of 0.36 m by 0.46 m is operated at a crank speed of 70 rpm. The feed rate is such that the thickness of each compressed slice is 0.15 m and slice density is 180 kg/m³. Power constants are $C_0 = 2$ kW and $C_1 = 3.6$ kW s/kg. Calculate (a) the baler capacity and (b) the power requirement.

Solution

(a) From Equation 11.60, the capacity is:

$$m_f = 0.36(0.46)(0.15)(180)(70)/60 = 5.2 \text{ kg/s or } 19 \text{ Mg/h}$$

(b) The baler conforms to varying feed rates by changing the slice thickness. For example, if the feed rate is increased by increasing the travel speed along the windrow, the slice thickness increases accordingly. The power requirement for the entire baler is:

$$P_{\text{baler}} = 2 + 3.6(5.2) = 21 \text{ kW}$$

Most of the power is used in driving the plunger.

11.2.5.2 Round balers

Machines to make large round bales (Figure 11.7) entered the marketplace in 1971. Early machines employed a variety of techniques for forming bales, including use of variable-geometry chambers (Figure 11.41), fixed-geometry chambers (Figure 11.42), and chambers without a floor (not shown) in which the forming bale is rolled on the ground. A pickup similar to those on rectangular balers but smaller in diameter is used to convey the windrow into the baler. When the windrow is narrower than the bale chamber, a certain amount of weaving is required by the operator to deliver hay to the full width of the chamber.

The variable-geometry chamber of Figure 11.41 is the most widely used design; it creates a bale of nearly uniform density whereas the other types create bales with a low-density core. In the design of Figure 11.41, a group of parallel, flat belts form the chamber. Typically, the belts are each 100 to 150 mm wide and have 50 to 100 mm wide spaces between them. The rollers on spring-loaded idler arms retract and allow the chamber to enlarge as the bale grows to full size. Power must be supplied to the chamber belts so that the moving periphery of the chamber will rotate the incoming

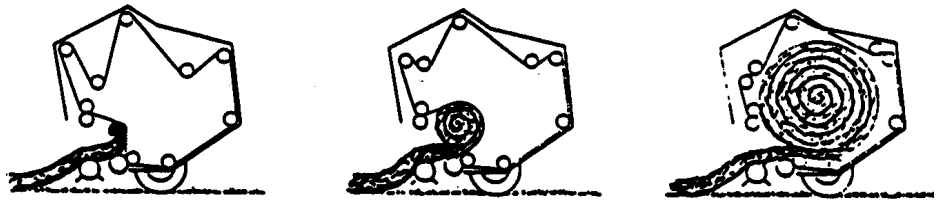


Figure 11.41 – A round baler with variable geometry
(courtesy of Prairie Agricultural Machinery Institute, Canada).

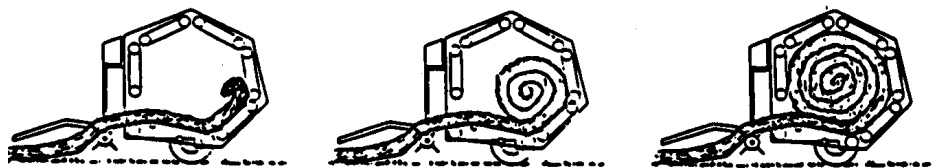


Figure 11.42 – A round baler with fixed geometry
(courtesy of Prairie Agricultural Machinery Institute, Canada).

hay and cause it to form into a tight roll. Peripheral speeds of the belts and floor conveyor typically range from 1.3 to 2.8 m/s. The chamber forms a bale with a low-density core. As additional layers are added, the density increases and is controlled by the belt tension. When the bale reaches the desired diameter, the operator stops forward motion and engages a wrapping mechanism as the bale continues to rotate. A manual or powered traversing guide spaces twine wraps at 150 to 200 mm intervals across the face of the bale. The twine is not tied; the twine end is inserted into the chamber, wraps on the bale as it rotates, is cut and left with a free end when the bale is completed. On some balers, dual-tying mechanisms allow both ends of the bale to be tied simultaneously for faster tying. As an alternative to tying with twine, the baler may be equipped with facilities for wrapping the bales in a full-width plastic netting. Only 1.5 to 2.5 turns of the bale are needed to wrap with netting, compared to 10 to 20 turns to wrap with twine. The netting gives the exterior of the bale a more closed structure, thus reducing leaf loss and improving weatherability compared to twine-wrapped bales. Although the netting is more expensive than twine, the improved productivity from faster wrapping, coupled with the reduced losses and improved weatherability, generally offset the higher cost of the netting. After tying, the operator backs the baler approximately 6 m and raises the tailgate to eject the completed bale onto the ground. The baler is moved ahead 6 m before lowering the tailgate to allow the gate to clear the discharged bale and then baling resumes.

Typical bale dimensions are 1.22 to 1.52 m in width and 1.22 to 1.83 m in diameter. Average densities range from 100 to 240 kg/m³, giving bale masses ranging from 320 to 1050 kg per bale. Bale density varies with belt or chain tension and with belt-to-ground speed ratio. Increasing the belt speed relative to the ground speed causes thinner layers to enter the chamber and thus produces more dense bales. Good judgment must be used when ejecting bales on sloping land; ejecting bales while traveling up or down slope can allow the bales to roll downhill with great destructive potential.

Maximum instantaneous harvesting capacity of a large round baler is a product of the size of the windrow (in kg/m) and the allowable forward speed of the baler. Forward speed is typically limited by the pickup, i.e., pickup losses become excessive at very high speeds. Average travel speeds are generally in the range from 5 to 13 km/h, but speeds up to 19 km/h have been observed. Average capacity is reduced by the time lost in tying and discharging a bale. Depending upon the windrow size, formation of a bale can take from 1 to 15 or more minutes. The tying and unloading cycle typically requires about 1 minute with twine wrapping. Baling rates, accounting for the wrapping and unloading cycle, can reasonably reach 15 to 20 Mg/h. Since power requirements stay relatively high throughout the bale-forming process, the energy use per bale increases with the time required to form a bale (Figure 11.43). Thus, to save energy, it is advantageous to form the bales as quickly as possible.

Power requirements for operating a large round baler include PTO power to form and discharge the bales, and drawbar power to propel the baler. The PTO requirements follow the characteristic curve of Figure 11.44, in which point A is the end of the bale-forming cycle and point B is the end of the tying cycle. The PTO power requirements when the baler is running empty are typically 2 to 4 kW, but increase as the bale forms as shown in Figure 11.44. With a full bale in the chamber, PTO power requirements

range from 12 kW to 55 kW depending on bale density and baler design. Drawbar power requirements depend heavily on field conditions as well as bale size. On firm, level fields, drawbar requirements typically range from 2.5 to 10.5 kW but the requirements can increase by 50 kW in soft, hilly fields.

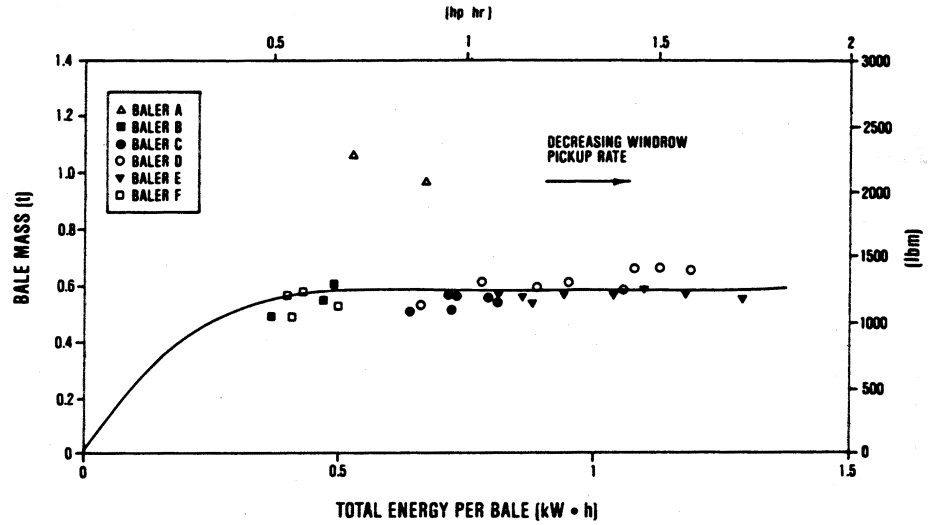


Figure 11.43 – Cumulative bale mass versus energy required to form a bale (Freeland and Bledsoe, 1988).

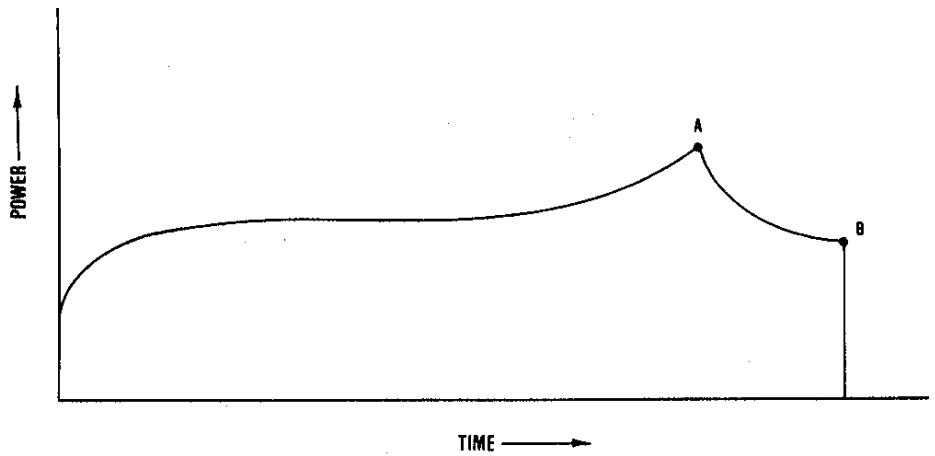


Figure 11.44 – Characteristic power curve of a variable-geometry baler (Freeland and Bledsoe, 1988).

11.3 PERFORMANCE EVALUATION

Techniques for evaluating performance can be specific to a particular machine and a wide variety of machines are used in hay and forage harvesting. For any machine, however, three types of evaluation are generally included. These are measurement of capacity, power requirements, and quality of the finished product. The Prairie Agricultural Machinery Institute (PAMI) of Humboldt, Saskatchewan, Canada, conducts independent tests of various farm machines under sponsorship of several Canadian provinces. The PAMI reports are an excellent source of performance data on selected hay and forage harvesting equipment.

Capacity measurements can be on the basis of area covered per unit time (in ha/h) or of material processed per unit time (in Mg/h). The amount of area that can be covered in unit time is called *field capacity* and is a product of the processing width and speed of the machine. Since width and speed are easily measured, field capacity measurements are not complex. For machines such as mowers, rakes, mower-conditioners, or windrowers, where the forage receives a minimum of processing, the material handling capacity is not important and only the field capacity is measured. Conversely, the *material handling capacity* is very important for forage harvesters or balers. Material handling capacity is the maximum feed rate that can be accommodated on a sustained basis. Forage harvester feed rate is the product of mass processed per unit travel distance (for example, in kg/m) times the forward speed of the harvester. The mass per unit distance can be measured before the material enters the harvester or as it leaves. As indicated by Equation 11.25, the former method involves measuring the crop yield and effective width processed by the harvester. In the latter method, the chopped material can be caught in a container for a given travel distance and then weighed. Baler feed rate can be determined by measuring the average time required to produce a bale and weighing to determine the mass in an average bale.

Power requirements of a machine include rotary power transmitted through the PTO shaft and drawbar power to propel the machine. Rotary power is the product of shaft speed and shaft torque. Accurate measurement of shaft speed can be accomplished by positioning a magnetic pickup to detect passage of teeth on a gear attached to the shaft in question. Digital data loggers are available for recording the tooth passage frequency, from which the shaft speed can be determined. Measurement of torque generally involves measurement of the deflection in a given length of shaft; since shafts are designed to work within their elastic range, the deflection is proportional to the shaft torque. From strength of materials theory, shaft torque causes both tensile and compressive strains to appear on the shaft surface (see Figure 11.45). Electric resistance or semiconductor strain gages can be attached to measure these strains and thus to measure the shaft torque. By proper positioning of the speed and torque transducers, the power demand of the various components of the machine can be measured during operation. When measuring power, it is important to simultaneously measure the other variables that affect the power requirement. Since feed rate affects the power requirement of forage harvesters and balers, the feed rate should always be measured and reported with power measurements. The moisture content of the forage should

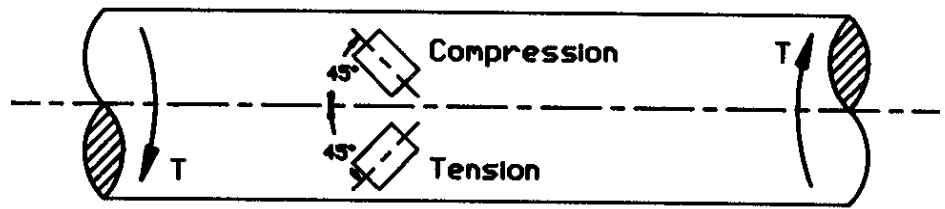


Figure 11.45 – Use of strain gages to measure shaft torque.

also be reported. Finally, values for all relevant machine parameters should be reported. In the case of a forage harvester, for example, the condition of the cutter knives has a large influence on the power requirement of the cutterhead. Drawbar power required to propel hay and forage machinery is usually much less than PTO power and is not always reported. If drawbar power is to be reported, it can be determined by measuring travel speed and drawbar pull. Radar units are available as optional or standard equipment on many tractors and can be used to determine travel speed. As in the case of torque measurement, strain gages can be used to make a drawbar force transducer and such transducers are commercially available.

Relevant measures of quality vary with the type of machine. As examples, uniformity of stubble height may be measured for sickle bar mowers, while length of cut is important for forage harvesters. ASAE Standard S424, which has been adopted by ISO as a technical report, provides methods for determining and expressing particle sizes of chopped forage. ISO Standard DP8909-1 deals with procedures for testing forage harvesters.

Forage loss is an important parameter for all of the machines. Koegel et al. (1985) used rolled plastic to evaluate losses. Plastic sheets 3.7 m in width by 30 m in length were folded along the length to a width of 2.2 m and rolled onto spindles. A spindle was attached to a mower-conditioner and, as the plastic was unrolled during operation, the swath was deposited on the plastic. Hedge shears were used to cut and a pitchfork was used to carefully remove sections of the swath. Material remaining after the swath was removed was gathered and weighed to determine mower-conditioner loss. Next, the part of the plastic sheet that was folded underneath was pulled out and the plastic was staked at its full 3.7 m width to provide space for raking on plastic. Again, hedge shears were used to cut and a pitchfork was used to remove sections of the windrow. Material remaining after windrow removal was gathered and weighed to determine mowing plus conditioning plus raking losses. Finally, a baler was used to bale the windrows from the plastic. Additional materials deposited on the plastic were attributed to baler losses. The technique did not permit separation of pickup and chamber losses from the baler. Minor damage sustained by the plastic during raking and baling was repaired with tape. The above method used by Koegel et al. (1985) may overestimate losses. One alternative to using plastic is to hand-pick losses from the ground in small (0.25 to 0.5 m²) sampling frames placed in representative areas of the field. Buckmaster (1993) used artificial stubble put in place after mowing to measure subsequent harvester loss.

Length of cut is often measured when evaluating forage harvesters. Since 1 kg of chopped forage may contain over 500,000 pieces, a mechanical means of length analysis is essential (O'Dogherty, 1982). Sieving is the most common method used for length analysis, i.e., the chopped forage is passed through a series of sieves with increasingly smaller openings. A given sieve contains those lengths that passed through the sieve above but would not pass the given sieve, and the mass of that fraction is determined by weighing. The sieves must be able to size pieces which are long in relation to their cross-sectional dimensions, i.e., length to diameter ratios range up to 50:1. Sieves are oscillated to promote movement of the material; by keeping the screens horizontal and using a horizontal oscillation, the possibility of endwise movement of forage through the sieves is minimized. ASAE Standard S424 gives specifications for a lab standard sieving device. Kononoff et al. (2003) developed a simpler device commonly used on farms to determine forage and total mixed ration particle size distribution (Figure 11.46)



Figure 11.46. – Sieve set used to assess particle size distribution in forages and total mixed rations (Kononoff et al., 2003).

PROBLEMS

- 11.1 A certain knife has a rake angle of 85° and a clearance angle of 2° . Calculate (a) the bevel angle and (b) the chip angle of the knife.
- 11.2 A rotary mower is cutting grass which leans 30° from the vertical in the direction the mower is traveling (the U-direction in Figure 11.24). Assume the forward speed of the mower is negligibly small compared to the peripheral speed of the blade. For the condition where the angle between the blade and direction of travel is 0, calculate the (a) tilt and (b) slant angles. Next, calculate the (c) tilt and (d) slant angles when the blade is perpendicular to the direction of travel.
- 11.3 In Figure 11.8, the oblique angle of the sickle section is 30° when the forward velocity of the mower is zero, so that the velocity of the knife relative to the plants coincides with the velocity of the knife relative to the mower. When the forward speed is 2.2 m/s, what knife velocity yields an oblique angle of zero?
- 11.4 Refer to Figure 11.8. Consider a smooth sickle section with an oblique angle of 30° , a coefficient of friction of 0.306, and a forward speed of the mower is zero (so that the velocity of the knife relative to the plants coincides with the velocity of the knife relative to the mower). (a) Will the plant material slide along the edge when the knife moves toward the countershear? (b) What is the minimum coefficient of edge friction that will prevent sliding?
- 11.5 Assume in Figure 11.8 that the leading corner of the sickle section has reached the ledger plate and the forward velocity of the mower is essentially zero. The oblique angle of the sickle section is 30° , while the oblique angle of the ledger plate is 8.4° . (a) If both the sickle section and the ledger plate have smooth edges with a coefficient of friction of 0.306, is the clip angle small enough to prevent the plant material from sliding forward along the edges? (b) Repeat part (a), except that the ledger plate is now serrated and has an edge coefficient of friction of 0.364. (c) Repeat part (a), except that both the section and ledger plate have serrated edges with coefficients of friction of 0.364. (d) Suppose that the forward speed of the mower has reduced the oblique angles of both the knife and the countershear by 10° and both edges have the same coefficient of friction. What is the minimum coefficient of friction that would prevent sliding?
- 11.6 Assume an alfalfa plant with a stem diameter of 3 mm, stem modulus of elasticity of $1,800 \text{ N/mm}^2$, and ultimate tensile strength of 35 N/mm^2 is being cut at a height of 60 mm above the ground, i.e., the plant roots fix the stem to the ground and the knife loads the stem as a cantilever beam. (a) How large must the knife force be to load the plant fibers to their ultimate stress? (b) How far would the stem deflect when the plant fibers reached their ultimate stress?

- 11.7 Same as Problem 11.6, except use a cotton plant with a stem diameter of 12 mm, ultimate fiber stress of 70 N/mm^2 and modulus of elasticity of 2000 N/mm^2 .
- 11.8 Use Equations 11.10 and 11.11 to generate a curve of knife force versus knife displacement (ranging from 0 to 9 mm) during the cutting of forage. The knife width is 10 mm, the bevel angle is 20° , the radius of the knife edge is 0.15 mm, and initial penetration occurs when the knife edge pressure on the forage reaches 20 N/mm^2 . The uncompressed depth of the forage is 9 mm, the bulk modulus is 10 N/mm^2 , and the coefficient of friction between forage and knife is 0.3. Assume the exponent $\lambda = 2$ in Equation 11.10.
- 11.9 Same as Problem 11.8, except that the radius of the knife edge is 1.5 mm and the coefficient of friction is 0.4.
- 11.10 A forage harvester with 8 knives on the cutterhead rotates at 900 rpm. The depth of forage at initial contact of the knife is 150 mm and the maximum cutting force is 8 kN. Estimate the power required for cutting (Equation 11.12).
- 11.11 Same as Problem 11.10, except that the cutterhead has only 4 knives.
- 11.12 Use Equation 11.16 to study the effect of stem diameter on the theoretical minimum velocity required for impact cutting. Assume the radius of gyration of the cut portion of the plant equals the height of the center of gravity of the cut plant to simplify the equation. Use Equation 11.6 to calculate the bending resistance of the solid (not hollow) stem, assuming that the roots fix the stem as a cantilever beam which is struck by the knife at a distance 100 mm above the soil and the ultimate bending strength of the stem is 50 N/mm^2 . Use Equations 11.10 and 11.11 to estimate the knife force. Let the knife width, the uncompressed depth of material, and the total knife displacement all be equal to the stem diameter; assume the exponent $\lambda = 2$, forage bulk modulus is 10 N/mm^2 , the coefficient of forage on the knife is 0.25, and the bevel angle of the knife edge is 20° . Also, assume that the edge radius of the knife is 0.1 mm (a sharp knife) and the pressure ahead of the knife edge is 30 N/mm^2 to initiate cutting. Finally, note that the mass, m_p , will vary with stem diameter, i.e., more massive plants must have larger stems to support gravitational and wind loads on the plant. Assume that $m_p = 5 \times 10^{-6} d^4$, where d is the stem diameter in millimeters and m_p is the plant mass in kilograms. Plot the required knife velocity versus stem diameter for diameters from 1 to 25 mm.
- 11.13 Same as Problem 11.12, except use a duller knife (edge radius of 1 mm).
- 11.14 Same as Problem 11.12, except the cut is made 2 mm above the ground.
- 11.15 Assuming that the input shaft angle (γ) is 0.3 radians for the spatial-crank oscillator, calculate and plot values of oscillator angular displacement (Γ), velocity, and acceleration versus rotational displacement of the input shaft (θ) for values of θ ranging from 0 to 2π , i.e., for one full cycle.
- 11.16 Same as Problem 11.15, except that the input shaft angle is 0.5 radians.
- 11.17 (a) Differentiate Equation 11.17b to derive an expression for the velocity of the oscillating arm. (b) Plot velocity versus input angle for one full cycle for

both your derived equation and for Equation 11.18 using an input shaft angle of 0.33 radians.

- 11.18 (a) Derive the following equation for the knife velocity (v_{km}) assuming that knife is driven by a spatial-crank oscillator whose oscillating arm has radius r_{oa} :

$$v_{km} = \frac{r_{oa} \omega \tan \gamma \cos \gamma}{(1 + \tan^2 \gamma \sin^2 \theta)^{1.5}}$$

(b) Compare the above equation to Equation 11.20 in the text, which is an approximate equation for knife velocity. Note that, from the comparison,

$$r_{oa} \tan \gamma = L_s/2000, \text{ approximately}$$

- (c) Further compare the two equations by plotting knife velocity versus crank angle for one full revolution of the crank. Use an input shaft angle of 0.3 radians in the plots. (d) How closely do the curves from the two equations match?
- 11.19 Same as Problem 11.18, except use an input shaft angle of 0.5 radians.
- 11.20 Assume that the movement of the knife in Figure 11.19 is governed by Equation 11.20. The stroke length is 76.2 mm and the sickle frequency is constant at 105 radians/s (1000 rpm). (Note that time, t , in Equation 11.20 is measured from when the knife is in midstroke, i.e., halfway between its position as shown in Figure 11.18 and the position when it is centered on the ledger plate.) Cutting is improved by maintaining a high knife speed through the cutting zone, i.e., from when the leading edge of the knife reaches the ledger plate until the trailing edge reaches the ledger plate. (a) Obtain an equation for knife displacement by integrating Equation 11.20. Use the displacement equation to find the times when (b) the leading edge of the knife reaches the ledger plate (beginning of cutting) and (c) when the trailing edge of the knife reaches the ledger plate (end of cutting). Then, calculate the knife speed relative to the ledger plate at (d) start and (e) end of cutting. (f) Finally calculate the percent of the stroke during which cutting occurs.
- 11.21 Same as Problem 11.20, except that the stroke length is 87 mm (i.e., the knife travels beyond the center of the ledger plate at each end of the stroke) and the sickle frequency is 84 radians/s.
- 11.22 Calculate the maximum inertia force on the sickle for the situation of Problem 11.20 if the sickle mass is 5 kg. (Hint: differentiate Equation 11.20 to obtain an equation for knife acceleration.)
- 11.23 Calculate the maximum inertia force on the sickle for the situation of Problem 11.21 if the sickle mass is 5 kg. (Hint: differentiate Equation 11.20 to obtain an equation for knife acceleration.)
- 11.24 Consider a sickle cutterbar with standard cutting geometry as shown in Figure 11.19. Let the depth of material at initial contact with the knife be equal to the effective length of stroke (i.e., the distance traveled by the knife from

- when the leading until the trailing edge of the knife reaches the ledger plate). Use Elfes (1954) data that average total knife force was 1.2 kN/m of bar length when cutting frequency was 942 cycles/min and that cutting used only 30% of the total PTO power. (a) Estimate the power required for cutting. (b) Estimate the total required PTO power per meter of bar length. (c) Compare the answer of part (b) with ASAE Data D497, which suggests a PTO power requirement of 1.2 kW/m for mowing alfalfa. (d) What are some of the factors that could account for differences between answers of parts b and c?
- 11.25 Repeat Problem 11.24, except use Harbarger and Morr (1962) data that the total average knife force was 2.3 kN/m of bar length when the cutting frequency was 1250 cycles/min.
- 11.26 A flail mower has a total of four rows of flails but, because of offsetting the flails as in Figure 11.21b, there are effectively only two rows from the standpoint of stubble uniformity. The rotor radius is 250 mm. (a) Calculate and plot the ratio of stubble height difference over rotor radius (z_d/r_f) versus velocity ratio (v_f/v_p) for velocity ratios ranging from 0 to 0.1. (b) On the same graph, plot a similar curve except for a six-row rotor with offset flails. What is the maximum stubble height difference for the (c) four-row rotor and (d) six-row rotor? (e) Is a six-row rotor needed to achieve adequate stubble uniformity?
- 11.27 A flail mower with a rotor width of 2 m is used to mow alfalfa which has a yield of 3.2 Mg/ha. Plot the PTO power requirement for the flail mower versus travel speed for travel speeds ranging from 0 to 15 km/h.
- 11.28 Same as Problem 11.27, except that the rotor width is 3 m.
- 11.29 The path of a rotary mower blade is as shown in Figure 11.24. If the forward velocity, v_f , is 4% of the blade peripheral velocity, determine the maximum oblique angle (ϕ_{ob}) and the blade angle (θ) at which it occurs. (Hint: you may find the answer either by differentiating Equation 11.29 with respect to blade angle or by plotting oblique angle versus blade angle.)
- 11.30 A rotary mower has a single blade with both ends sharpened as shown in Figure 11.24. The radius of the blade is 300 mm and the blade rotates at 1900 rpm. (a) What is the minimum width of the sharpened portion of each end of the blade, L_s , if the forward speed of the mower can be up to 4% of the peripheral speed of the blade? (b) Calculate the minimum taper of the end of the blade to prevent crop drag against the end of the blade.
- 11.31 Same as Problem 11.30, except the blade radius is 250 mm and the blade rotates at 2200 rpm.
- 11.32 Consider a disk-type rotary mower that has six disks, each cutting a 0.4 m width; the mower is traveling at 15 km/h. Stating other assumptions: (a) Estimate the PTO power requirement if the blades are sharp. (b) Estimate the PTO power requirements for the same mower after the blades become worn.
- 11.33 Same as Problem 11.32, except the mower is a drum-type mower.

- 11.34 A forage harvester has a cylindrical cutterhead 600 mm in width and 700 mm in diameter. It has 8 knives and rotates at 900 rpm. It is to harvest corn at a feed rate of 65 Mg/h while producing an average length of cut of 5 mm. The specific cutting energy can be held to 14 J m/kg when the knives are sharp. The forage is in contact with the housing for 2.36 radians of arc and the coefficient of friction between the corn and the steel housing is 0.49. Crop density between the feed rolls is 300 kg/m³. Calculate (a) the required peripheral speed of the feed rolls, (b) the maximum height of the throat area, and the PTO power requirements for (c) chopping, (d) friction, (e) impelling (assume the impeller peripheral velocity equals that of the chopper), (f) moving air, and (g) the total power requirement. (h) For comparison, calculate the total PTO power requirement using Equation 11.42. (i) What length of cut would cause the answers for parts h and i to agree?
- 11.35 Same as Problem 11.34, except only 4 knives are used. Also (j) calculate the new length of cut when only 4 knives are used if feed roll and cutterhead speeds are unchanged.
- 11.36 Same as Problem 11.34, except that dull knives have allowed the specific cutting energy to rise to 28 J m/kg.
- 11.37 Same as Problem 11.34, except alfalfa is being harvested at a rate of 50 Mg/h, the length of cut is to be 10 mm, the density in the throat is 55 kg/m³ and the specific cutting energy is 16 J m/kg.
- 11.38 Alfalfa is cut at 80% moisture on a day when the dry bulb temperature is 30° C, the solar radiation is 700 W/m², and the soil moisture is 17%. The density of alfalfa in the swath is 450 g/m². Assume the hay is cut in a humid area, so that Equation 11.44 applies. (a) Plot the moisture content of the hay versus time for 8 hours of drying on the day the hay is cut with no drying agent. (b) Add a second curve to the graph, but with 0.08 g/g of drying agent used. (c) Add a curve to the graph with a drying agent application rate that results in hay reaching 20% moisture, wet basis, after 8 drying hours.
- 11.39 Same as Problem 11.38, except that the temperature is only 20°C and the solar radiation is only 350 W/m²; i.e., it is a poorer drying day.
- 11.40 Same as Problem 11.38, except use Equation 11.45 with a vapor pressure deficit of 2.5 kPa.
- 11.41 Same weather, soil, and crop conditions as Problem 11.38, except swath density is different. Crop yielding 3 Mg/ha is cut with a 2.7 m mower and laid into a swath covering 100% of land area (a 2.7 m swath).
- 11.42 A side-delivery rake with five bars in its oblique reel head has the following parameters:
- raking width is 2.59 m
 - reel radius is 0.30 m
 - angle between direction of travel and planes of reel heads is 72°
 - acute angle between raking front and direction of travel is 65°

The reel is ground driven such that the ratio of forward velocity and reel peripheral speed (v_f/v_p) is 0.82. Assume the vertical distance from the lowest position of rake teeth to the top of the windrow is 0.2 m. For travel speeds ranging from 3 to 11 km/h, calculate and plot (a) the ratio of resultant hay velocity to forward velocity (v_h/v_f) and (b) the ratio of maximum theoretical distance traveled by hay to rake width (L_h/w_r).

- 11.43 Same as Problem 11.42, except that the vertical distance from the lowest position of rake teeth to the top of the windrow is 0.1 m.
- 11.44 Same as Problem 11.42, except the rake is a finger-wheel rake with the following parameters:
 raking width is 3.20 m
 reel radius is 0.74 m
 angle between direction of travel and planes of reel heads is 130°
- 11.45 Estimate a value for effective modulus of hay elasticity (E_h) by using Equation 11.59, data from Figure 11.37 and assumed values as follows (chosen to be realistic values for the baler used to develop Figure 11.37):
 bale chamber depth = 0.46 m, from Figure 11.37
 bale chamber width = 0.41 m, from Figure 11.37
 plunger compressive force = 42 kN, from Figure 11.37
 converging section length = 0.70 m, assumed
 total convergence in converging section = 75 mm, assumed
 coefficient of friction between hay and the bale chamber = 0.25, assumed
- 11.46 (a) Normalize the high feed rate data from Figure 11.37 by tabulating and plotting plunger compressive pressure (on the y-axis) versus percent of plunger stroke (on the x-axis). The compressive pressure is the plunger force divided by the cross-sectional area of the plunger (bale chamber cross-section dimensions are given on Figure 11.37). Percent of stroke is the actual plunger displacement divided by the maximum displacement (547 mm in Figure 11.37). (b) Repeat part (a) but use the plunger retracting data. (c) Repeat part (a) but use the low feed rate data. (d) Generalize using data from Figure 11.37 and Equation 11.60 to compute slice thickness for each feed rate.
- 11.47 Scale up the baler represented by Figure 11.37 to a chamber that is 0.36 m wide and 0.46 m high. Let crank radius be 0.38 m, connecting rod length be 1.12 m, and crank speed be 79 rpm. Note that Equation 11.58 can be used to compute the dimensionless plunger displacement for each crank angle through the full cycle. Equations 11.62 and 11.63 can be used to calculate torque at each crank angle.
 (a) Generate cubic polynomial models of normalized data from parts a and b of Problem 11.46 to get equations for pressure exerted by the plunger as a function of percent of stroke. (b) Use the cubic polynomial models from part (a) to generate a torque-displacement curve similar to Figure 11.39. (c) Numerically integrate the torque-displacement curve from part (b) to find the average torque through the cycle. (d) Compute the required flywheel inertia

- to provide 20% speed regulation. (e) Estimate the power required to operate the plunger. (f) Calculate the baling rate in kg/s.
- 11.48 Same as Problem 11.47, except use the low feed rate data of Figure 11.37 (refer to Problem 11.46b and 11.46c)
- 11.49 A large round baler is making alfalfa bales with a width of 1.5 m, diameter of 1.75 m, and average density of 200 kg/m³. The speed of the baler while making bales is 8 km/h and the windrows contain 0.9 kg of hay per meter of length. The peripheral speed of the chamber belts is 2.75 m/s. The PTO power is 3 kW when the baler is running empty, and 30 kW when a bale reaches full size. Calculate (a) the time required to form a full bale, (b) the mass of a full bale, (c) the rotational speed of the bale in the chamber when full size, (d) the torque and (e) peripheral force that must be supplied by the belts to turn the full bale, (f) the number of rotations of the bale required to wrap twine at 150 mm spacing across the full width of the bale, and (g) the time required to wrap the twine. (h) Calculate the time savings per bale if each bale is wrapped with 1.5 turns of net wrap instead of twine.
- 11.50 Same as Problem 11.49, except that the peripheral speed of the chamber belts is 1.5 m/s.
- 11.51 Re-derive or confirm Equation 11.42 based on ASAE Data D497 which gives the following information for forage harvester power requirement:

$$P_{th} = C_0 + C_1 m_{fdm}$$

where P_{th} = PTO power requirement for forage harvesters, kW

C_0 = 6 kW

C_1 = 3.3 kWh/Mg for corn

= 4.0 kWh/Mg for wilted alfalfa

= 5.7 kWh/Mg for direct-cut forage

m_{fdm} = feed rate, Mg dry matter/h

Accompanying notes are: Throughput (m_{fdm}) is units of dry matter per hour with a 9 mm theoretical length of cut. A 50% reduction in length of cut setting or use of a recutter screen increases power by 25%.

- 11.52 Obtain data from Figure 11.27 for the 12.7 mm theoretical length of cut. (a) Plot the data on Weibull or lognormal paper. (b) Per ASAE S424 guidelines, estimate the geometric mean particle length assuming the average length of material on the top sieve was 50 mm.

GRAIN HARVESTING

12

INTRODUCTION

The purpose of grain harvesting is to recover grains from the field and separate them from the rest of the crop material in a timely manner with minimum grain loss while maintaining highest grain quality. The methods and equipment used for harvesting depend upon the type of grain crop, planting method, and climate. The major grain crops are rice, wheat, corn, soybeans, barley, oats, sorghum, and dry beans (navy beans, pinto beans, etc.). Many other grain crops, such as oil-seed crops, are harvested using the methods and equipment described in this chapter.

12.1 METHODS AND EQUIPMENT

The entire harvesting operation may be divided into cutting, threshing, separation, and cleaning functions. *Threshing* is breaking grain free from other plant material by applying mechanical force that creates a combination of impact, shear, and/or compression. It is important to avoid damaging grain during threshing—a challenging task under certain crop conditions. For example, at high moisture content it is harder to break grain away from the crop material but easier to damage grain. The operation of *separation* refers to separating threshed grains from bulk plant material such as straw. The *cleaning* operation uses air to separate fine crop material such as chaff from grain.

Depending upon the method employed for harvesting, these functions are performed by different machines, often with time allowed for windrowing or curing between the cutting and the threshing functions, or all the functions may be performed by one machine in a single pass over the field. The modern grain harvesters that combine all of these operations in one field-going machine are commonly called *combines*.

12.1.1 Direct harvesting

In the direct harvesting method, all functions, from cutting to cleaning, are performed by one machine called the combine (Figure 12.1). All major crops mentioned above can be harvested directly. There are two main kinds of combines, conventional types and rotary types. Either of these types may be self-propelled or pulled by a tractor and powered by the PTO drive as shown in Figure 12.2.

Figure 12.3 is a schematic diagram of a conventional combine showing the functional components. Different manufacturers have different designs but the functional components are similar. During combine operation the uncut standing crop is pushed



Figure 12.1 – A modern grain combine (courtesy of Ford/New-Holland).



Figure 12.2 – A typical pull-type combine drawn by a tractor (reproduced by permission of Deere and Co. © 1991).

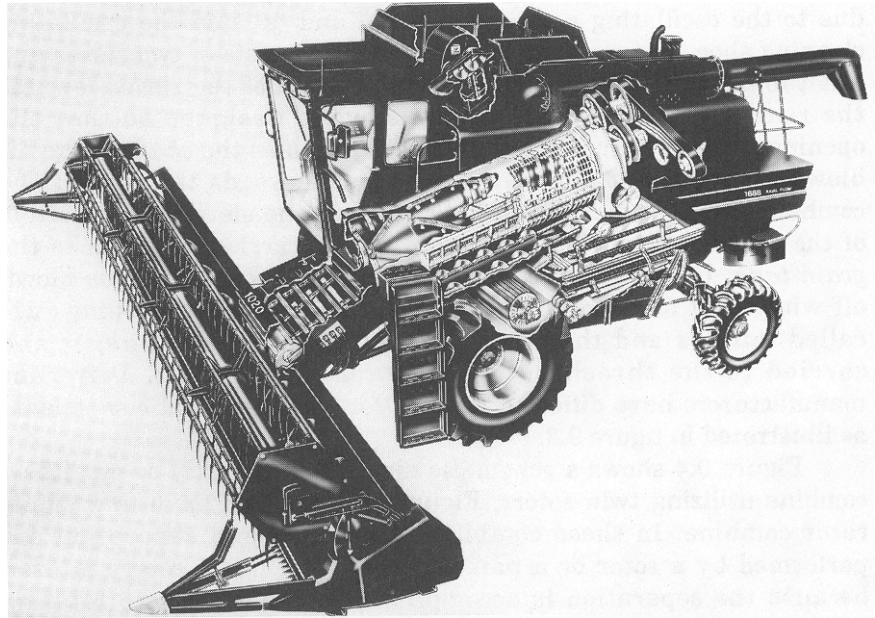


Figure 12.3 – Internal construction of a modern self-propelled grain combine (courtesy of Case-IH Co.).

by the *reel* against the *cutterbar* and onto the *platform*. The cut crop is conveyed towards the center of the platform from either side by the *platform auger* and conveyed to the threshing cylinder by the *feeder conveyor*. The crop is threshed by the *threshing cylinder*. The threshing cylinder rotates at a very high speed (about 30 m/s peripheral speed). About 80% of the grain, along with some chaff and small pieces of straw, is separated through the *grate*. The bulk of the straw, chaff, and the remaining grains pass through the concave-cylinder gap where the *beater* causes it to slow down. Then this material is delivered to a *separator*. In a conventional combine the separator is made of oscillating channel sections called the *straw walkers*. Since early 1970s separator design has changed to a rotary design. Rotary types of combines are discussed below. The separated material falls into the channels, moves towards the front of the combine, and is delivered on top of an oscillating *grain pan* where it is combined with the grain-chaff mixture separated at the cylinder-concave. This mixture of chaff and grain moves rearward due to the oscillating action of the pan and falls on the oscillating *cleaning shoe*. The cleaning shoe generally consists of two sieves and a fan to blow air upwards through the bottom of the sieves towards the rear of the combine. The top sieve is designed so that the openings may be adjusted. It is referred to as the *chaffer*. The air blows the chaff and the straw pieces off towards the rear of the combine while the clean grain falls through the sieves to the bottom of the cleaning shoe. The *clean-grain auger* carries the grain to the *grain tank*. Unthreshed grain heads that are too heavy to be blown off with chaff and too large to escape through sieve openings are called *tailings* and they are collected by the *tailings auger* and carried to the threshing cylinder for rethreshing.

In some combine designs multiple conventional threshing cylinders are used as shown in Figure 12.4. Each cylinder rotates faster successively to thresh out increasingly hard-to-thresh grains. Figure 12.5 shows yet another arrangement. A transversely mounted conventional threshing cylinder is used in conjunction with a rotary tine separator. This design is especially suited for crops such as rice that have tough straw.

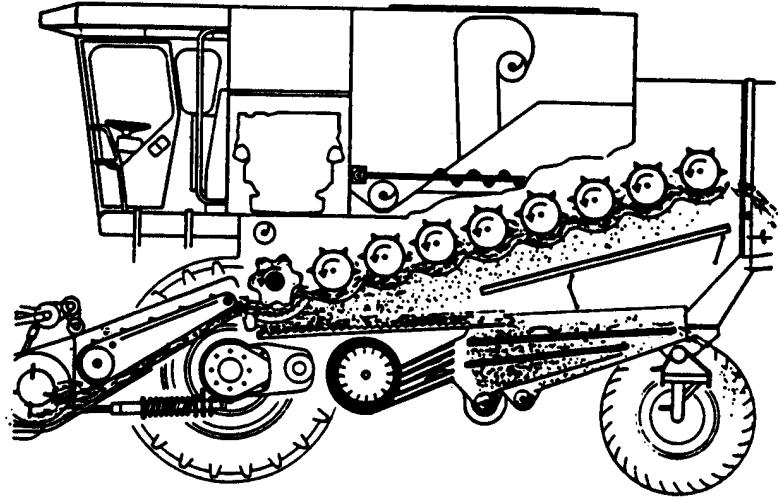


Figure 12.4 – A combine design utilizing a conventional threshing cylinder and multiple separation cylinders (courtesy of Prairie Agricultural Machinery Institute, Canada).

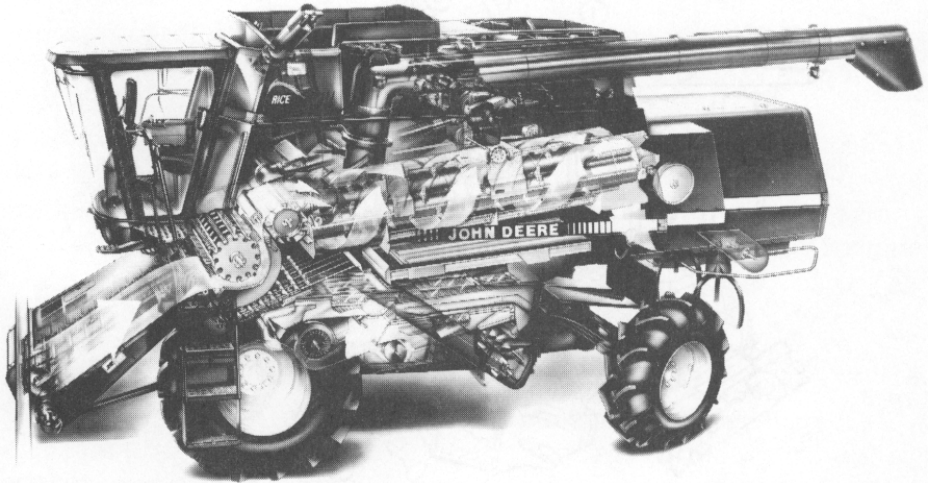


Figure 12.5 – A combine configuration utilizing a transversely mounted conventional threshing cylinder and a rotary tine separator (courtesy of Deere and Co.).

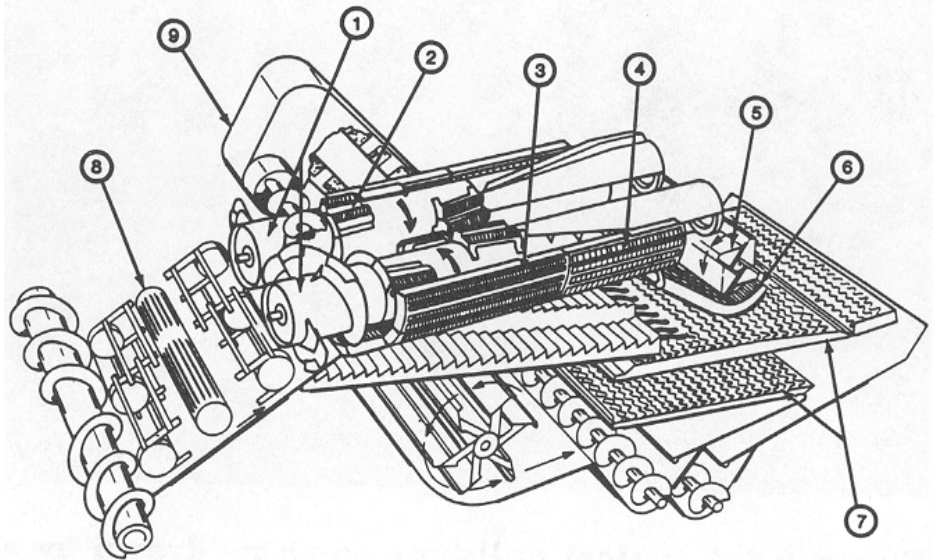


Figure 12.6 – An axial flow rotary combine utilizing twin rotors: (1) rotor, (2) rasp bars, (3) threshing concave, (4) separating concave, (5) discharge beater, (6) beater grate, (7) cleaning shoe, (8) feeder housings, (9) tailings auger (courtesy of Prairie Agricultural Machinery Institute, Canada).

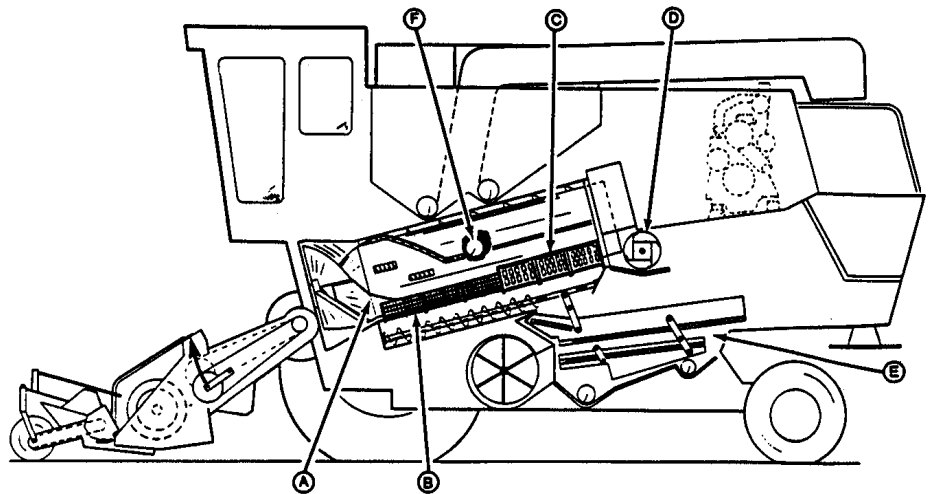


Figure 12.7 – An axial flow rotary combine utilizing a single rotor: (a) rotor, (b) threshing concave, (c) separating concave, (d) back beater, (e) cleaning shoe, (f) tailings return (courtesy of Prairie Agricultural Machinery Institute, Canada).

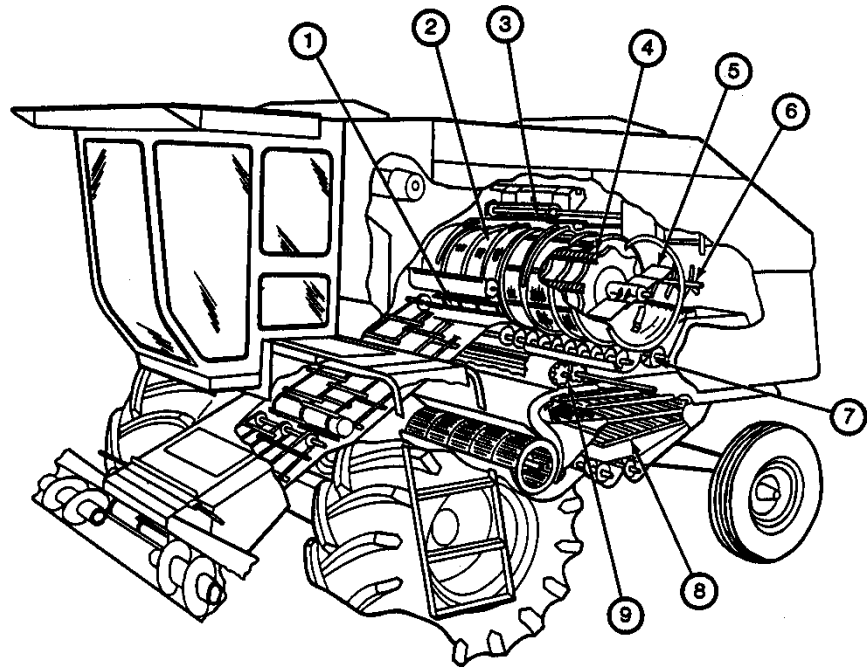


Figure 12.8 – A rotary combine utilizing a single transversely mounted rotor:
 (1) threshing concave, (2) cage, (3) cage sweeps, (4) rotor, (5) discharge paddles,
 (6) straw choppers, (7) distribution auger, (8) cleaning shoe, (9) accelerator rolls
 (courtesy of Prairie Agricultural Machinery Institute, Canada).

Combines that do not use the oscillating action of a straw walker use rotary action to accomplish threshing and separation, and are thus called *rotary combines*. Figure 12.6 is a diagram of a rotary or axial flow combine utilizing twin rotors. Figure 12.7 shows an axial flow single-rotor combine. In these combines, threshing and separation are performed by a rotor or a pair of rotors. The name *axial flow* is used because the axis of the rotor is parallel to the line of travel. The threshing cylinder is located transversely in some rotary combines, such as that shown in Figure 12.8, as well as in conventional combines.

12.1.2 Cutting and windrowing

Some crops that do not lend themselves to direct harvesting are better harvested by cutting and windrowing before threshing, separating, and cleaning. When the crop does not ripen evenly or (as in some northern climates) does not mature fully, cutting and windrowing allows for the crop to cure in the field before threshing. Some crops, such as edible beans, are cut below-ground and windrowed to avoid cutting bean pods.

Generally, cutting is accomplished by a cutterbar and windrowing is done by a draper. A draper is a flat horizontal belt that runs perpendicular to the line of travel. As the crop is cut by the cutterbar, it falls onto the draper and is carried to the side and



Figure 12.9 – A windrow pickup attachment and its operating principle (reproduced by permission of Deere and Co. © 1991).

dropped in a windrow. The crop material in a swath width is placed in a narrow windrow for the purpose of drying. If the crop was planted in rows, several rows are combined to form a windrow. The reel and cutterbar header is replaced by a pickup attachment in the combine as shown in Figure 12.9. The windrow is gently picked up by the pickup header and taken into the combine where the subsequent harvesting operations are completed.

12.2 FUNCTIONAL PROCESSES

A modern grain combine performs many functional processes. These are gathering and cutting (or in case of windrows, picking up), threshing, separation, and cleaning. Figure 12.10 shows a process diagram of a combine.

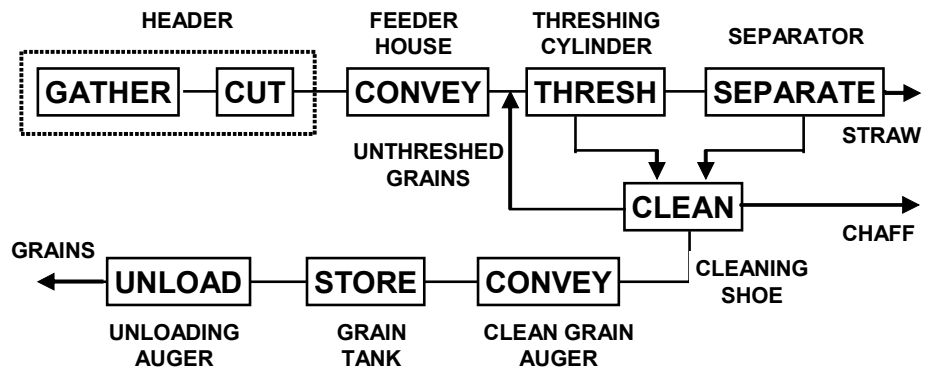
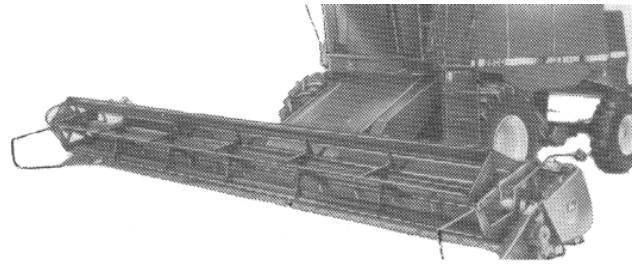
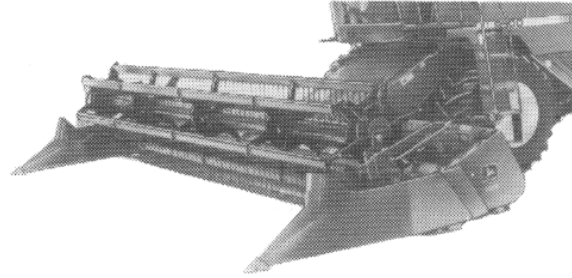


Figure 12.10 – Process diagram of a combine.



SLAT-TYPE REEL



PICKUP REEL

**Figure 12.11 – Slat (or bat) and pickup reels
(reproduced by permission of Deere and Co. © 1991).**

12.2.1 Gathering, cutting, pickup, and feeding

12.2.1.1 Grain header

Mechanisms to gather and cut the crop are located in the *header*, which is also called the *cutting platform*. Slat-type (bat) and pickup reels, as shown in Figure 12.11, are commonly used for gathering most small grain crops. Pickup reels are used for lodged crops (crops that have fallen over due to heavy rains, winds, etc.), because they have fingers that reach into the lodged crops and help pick them up for cutting. The orientation of the fingers is controlled by either cam guides or a parallel bar mechanism.

Proper operation of the reel is critical to minimize header losses, which include shatter losses and cutterbar losses. Shatter losses are grain heads or pods that fall to the ground due to the action of the reel. Cutterbar losses are grain heads or pods that are cut by the cutterbar but fall to the ground. If the crop is windrowed, there are windrowing losses as well as combine gathering losses in the pickup and conveying operations. In direct-cut cases, all header losses are considered gathering losses.

Factors affecting header losses are (1) cutting height, (2) reel position with respect to the cutterbar, and (3) reel speed with respect to the forward speed.

For optimum combine operation the crop should be cut just below the grain heads. If the crop height is uneven or if the crop is lodged it may not be cut in some places, which will contribute to losses. Optimum reel position is determined by the crop

height, amount of straw cut, and the condition of the straw. Normally, the reel should be set so the slats, when in their lowest position, will strike the straw 15 to 25 cm above and slightly ahead of the cutterbar. For lodged crops the reel should be set farther back. Proper reel speed is important to minimizing shattering and gathering losses. A reel turning too fast will result in excessive shatter loss, whereas too slow a speed will result in the cut grain head falling off the platform, a cutterbar loss.

It is recommended that the peripheral speed of the reel should be about 25% to 50% faster than the forward speed of the combine, or in other words, that the reel index be between 1.25 to 1.5. The reel index is defined as:

$$\text{Reel Index} = \frac{v_r}{v_c} \tag{12.1}$$

where v_r = peripheral speed of the reel
 v_c = forward speed of combine

The reel is powered by either a V-belt drive or a hydraulic motor. Many manufacturers provide control of the reel speed from the operator’s station. The position of the reel axis with respect to the cutterbar is adjustable and must be adjusted properly for satisfactory gathering operation. For example, in heavily lodged crops the reel is set well ahead of the cutterbar to improve lifting. Figure 12.12 shows the effect of reel position and reel index on cutterbar losses for slat and pickup reels.

For most small grain crops the cutting is accomplished by a cutterbar consisting of oscillating knife sections that shear the crop stems. The cutterbar operation was discussed in detail in Chapter 11. To minimize cutterbar losses for crops with grains close to the ground a flexible cutterbar has been designed. The flexible cutterbar follows the ground profile across the width of cut for a uniform cutting height and minimum losses.

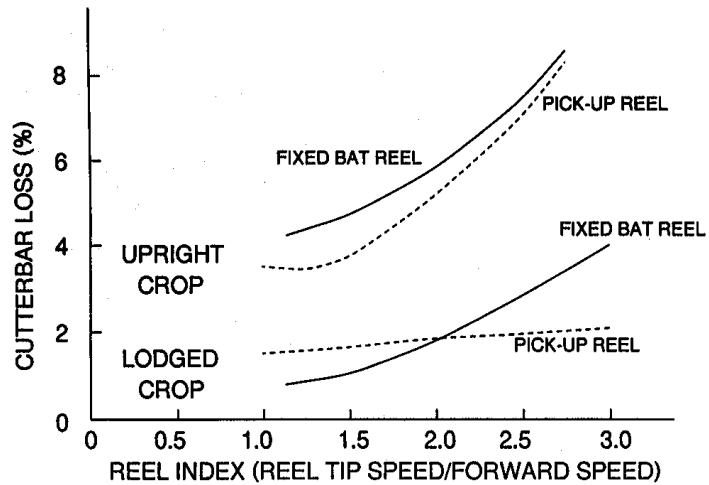


Figure 12.12 – Losses associated with reel adjustments (Wilkinson and Braumbeck, 1977).

12.2.1.2 Corn header

The gathering and cutting of seed corn is accomplished by a corn header, as shown in Figure 12.13. A corn header can harvest three to twelve rows at a time. The row spacing is designed to match the planter row spacing. During the operation, the gatherer points are positioned between the corn rows. The corn head on a combine primarily performs *gathering*, *snapping*, and *trash removal*. The gathering units are fitted with gathering chains equipped with finger links that assist in moving stalks into and through the snapping zone and prevent loose ears from sliding forward to be lost. When stalks are upright, the chain speed is adjusted to be approximately equal to the forward speed of travel.

The breaking of corn ears from stalks is called *snapping*. Snapping is performed by snapping rolls that grab the cornstalks and pull them between the snapping bars. The spacing between the snapping bars is such that the corn ears cannot go through. As corn ears reach the snapping bars they are snapped off and carried into the machine by the gathering chains, as shown in Figure 12.14. The entire cornstalk is pulled through, causing all ears to snap off.

One design of snapping rolls has fluted rollers (Figure 12.14). Straight-fluted rolls are more aggressive than spiral-ribbed rolls. Stripper plates located above the rolls prevent ears from contacting the rolls. Roll lengths of the fluted part are generally 40 to 60 cm and diameters are usually 9 to 12.5 cm. Because of their positive action, fluted rolls permit faster capacities and higher ground speeds.

Another design of snapping roll is referred to as a spiral-ribbed or spiral-lugged roll (Figure 12.15). As the name suggests, these rolls have spiral ribs on them. They are closer together than fluted snapping bars. The ears snap off as they reach the rolls and the spiral is such that the stalks move rearward. Roll lengths generally range from 1 to 1.25 m and the diameters from 7.5 to 10 cm.

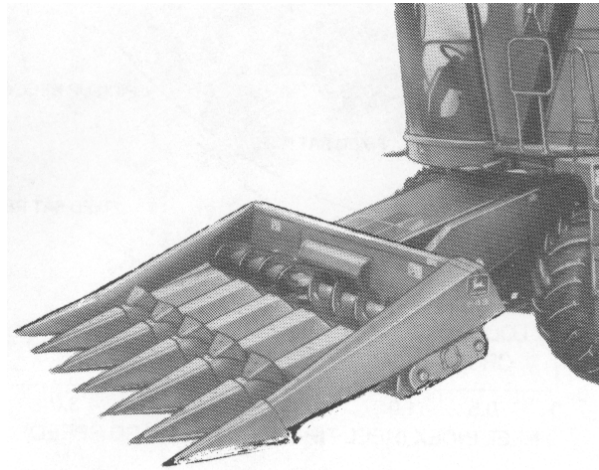


Figure 12.13 – A six-row corn header
(reproduced by permission of Deere and Co. © 1991).

Peripheral speeds of snapping rolls are usually 180 m/min. Proper speed is important for adequate operation. Faster speeds result in shelling of cobs at the point of attachment to the stalk, while slower speeds result in stalk slippage and trash buildup on the rolls. It is also important to operate snapping rolls at a speed proportional to the forward speed of the combine. If the snapping rolls operate too slowly, the combine would run the stalks down before they are pulled through. Too high a velocity would cause the stalks to bounce off the snapping bars and fall to the ground. Roll spacing is also important to satisfactory roll operation. It is generally kept between 6 and 13 mm. Larger spacing may cause stalk slippage, and narrower spacing, stalk breakage.

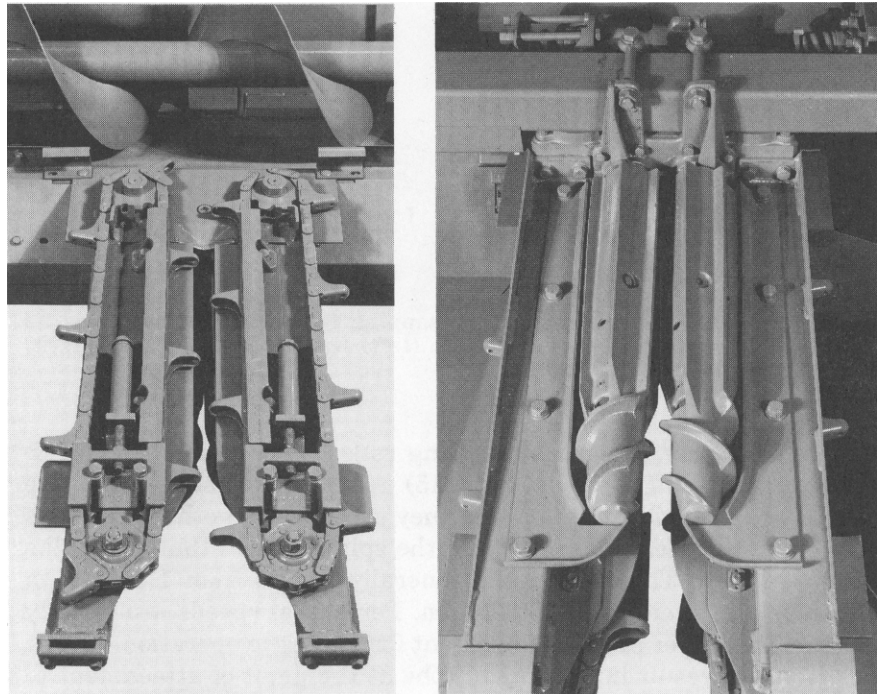
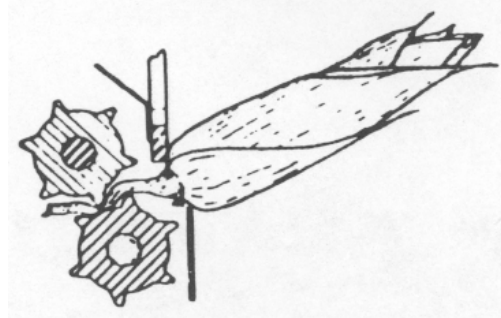


Figure 12.14—Fluted snapping rolls of a corn header, showing operating principles. Top, reprinted from Wilkinson and Braumbeck (1977); bottom, from Kepner et al. (1978).

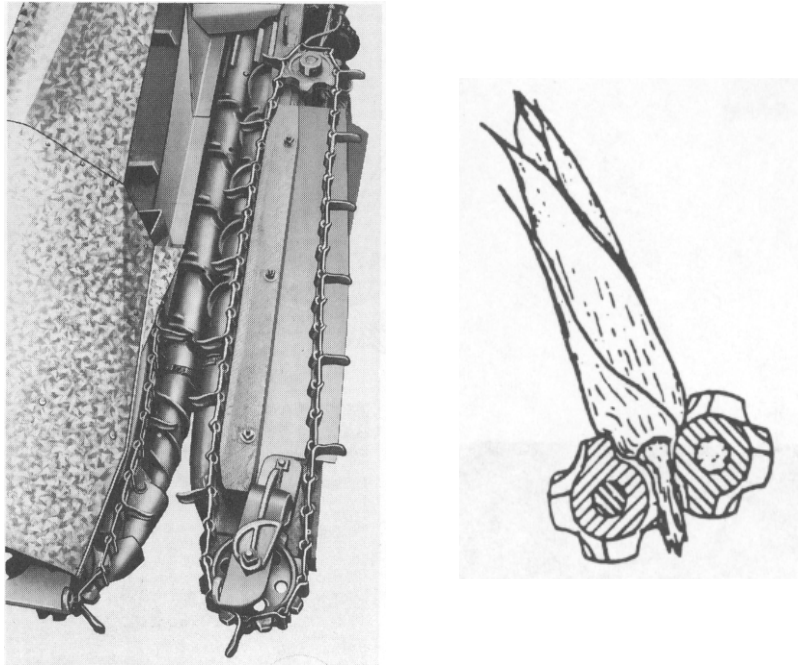


Figure 12.15 – Spiral-ribbed snapping rolls of a corn header, showing operating principles. Left, reprinted from Kepner et al. (1978); right from Wilkinson and Braumbeck (1977).

Special trash rolls are often provided on corn pickers to remove trash and broken stalks not expelled by spiral-ribbed snapping rolls. Fluted sections may be incorporated on the upper end of the snapping rolls as shown in Figure 12.16.

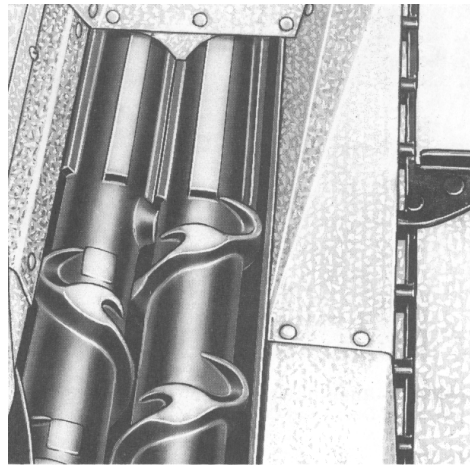


Figure 12.16 – Fluted trash rolls on the upper ends of snapping rolls (reprinted from Kepner et al., 1978).

12.2.2 Threshing

12.2.2.1 Threshing mechanisms

Threshing is accomplished by a rotating cylinder and a concave grate in both conventional and rotary combines. As the cylinder rotates, crop is forced through the gap between the concave and the cylinder and is subjected to impact and rubbing action that cause grains to be detached. In a rotary combine the crop flow is parallel to the axis of rotor, whereas in a conventional combine the crop flow is transverse to the axis of rotation.

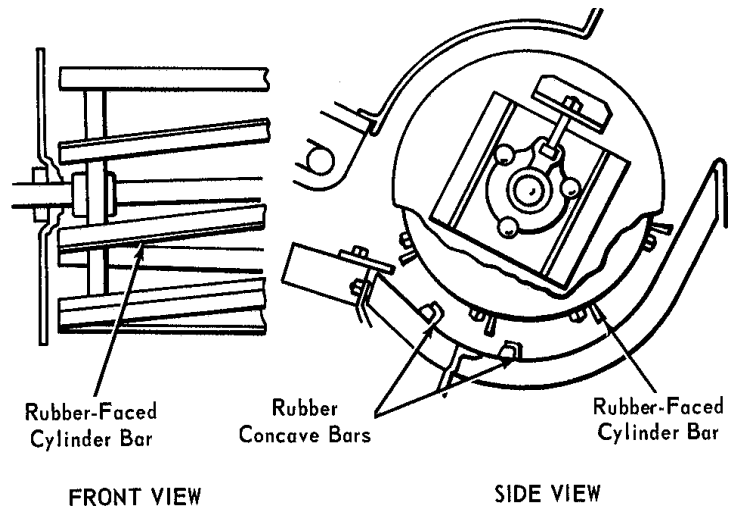
In rotary (axial flow) combines, threshing cylinders are part of the separator. The front part of the rotor has helical rasp bars mounted at equal distance. The twin-rotor model has two helical bars mounted 180° apart (Figure 12.4). A single-rotor design has three helical bars with a staggered straight section between them (Figure 12.3). The rotor diameter for the twin-rotor is 43.2 cm; in the single-rotor design the diameter ranges from 61 to 76.2 cm. The crop takes a helical path while being threshed in a rotary combine. The rotor speed is less and the concave gap is higher than in conventional combines; that results in more thorough threshing with less damage under most harvesting conditions.

In conventional combines, there are three primary types of threshing cylinders and associated concaves: the rasp-bar cylinder and concave, the angle-bar cylinder and concave, and the spike-tooth cylinder and concave.

The *rasp-bar cylinder* consists of a number of steel bars that are mounted on several star-shaped hubs to form a cylinder. The hubs are mounted on a common shaft that is supported by bearings and driven by means of V-belts. The outer surfaces of the bars are corrugated. The concave is made of parallel bars that are held together by parallel curved bars as shown in Figure 12.17. As the cylinder rotates the crop is forced through the gap between the concave and the rasp bars, and is subjected to a combination of impact and rubbing action to accomplish threshing. The rasp-bar is most commonly used cylinder type because most crops can be threshed by the action it produces.



Figure 12.17 – Rasp-bar thresher
(reproduced by permission of Deere and Co. © 1991).



FRONT VIEW SIDE VIEW
 Figure 12.18 – An angle-bar threshing cylinder and concave
 (reproduced by permission of Deere and Co. © 1991).

The *angle-bar cylinder* is made of helical rubber-coated angle irons in place of rasp bars (Figure 12.18). The concave is also rubber-coated. The threshing action is primarily that of flailing that results in a gentler threshing action. The angle-bar design is commonly used for crops such as clover and alfalfa seed.

The *spike-tooth cylinder* has spikes on the bars in place of the rasps. The concave has matching spikes, as shown in Figure 12.19. The threshing action in this design is that of tearing and shredding. Compared to other cylinders, there is less damage to the grain. However, the tearing and shredding action has the undesirable effect of breaking up the straw that must be removed from the grain. Thus, the spike-tooth cylinder is used for rice, which has tough straw, and often for edible beans because beans are easily damaged.

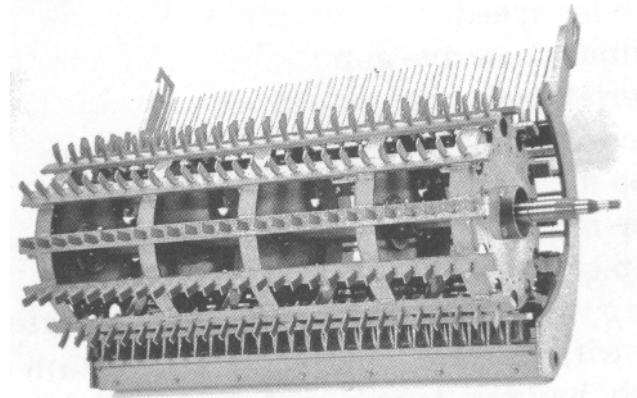


Figure 12.19 – A spike-tooth threshing cylinder and concave
 (reproduced by permission of Deere and Co. © 1991).

The threshing cylinders in conventional combines vary from 38 to 56 cm in diameter and rotate between 150 to 1500 rev/min. The cylinder speed is determined by the crop type and condition. Wet, hard-to-thresh conditions require higher speeds, but grain damage increases as cylinder speed is increased. Another factor affecting the quality of threshing is the cylinder-concave gap. If the gap is too large, the crop is not threshed completely. Too narrow a gap results in excessive power and grain damage. The length of the threshing cylinder is proportional to the width of the combine header. Multiple threshing cylinders arranged in series have been utilized to thresh edible beans and peanuts. Each successive cylinder rotates at a higher speed.

12.2.2.2 Threshing performance

The performance of threshing mechanisms is measured by threshing efficiency, separation efficiency, the amount of grain damage and the amount of straw breakup. Threshing performance parameters are affected by the following factors:

- Design factors: cylinder diameter, concave length, number of rasp bars;
- Operating parameters: cylinder speed, cylinder-concave gap, material feed rate;
- Crop condition: crop moisture content, crop maturity, crop type.

Threshing efficiency is the percentage of the threshed grains calculated on the basis of the total grains entering the threshing mechanism. It increases asymptotically with concave length up to a certain point. Increasing concave length beyond this point does not increase threshing efficiency and might even decrease it under certain conditions. However, experiments show that under easy threshing conditions there is little advantage of increasing the concave length beyond 33 cm (Arnold, 1964). Increasing the diameter of the conventional threshing cylinder increases threshing losses at a rate of about 0.9% for each 7.5 cm increase in the diameter. The number of rasp bars and their spacing do not seem to have any effect on the threshing efficiency. Cylinder speed is one of the most important variables affecting threshing losses. For hard-to-thresh crops and/or conditions, threshing losses can be significantly reduced by increasing the cylinder speed. In one set of experiments increasing the speed from 23 to 33 m/s reduced losses from 8% to 4%. The cylinder-concave gap affects threshing losses adversely. An increase of $\frac{1}{8}$ in. increased the unthreshed loss from 0.6% to 2.0%. Changing the concave clearance ratio (the ratio of the gap at the front to that at the rear of the cylinder) is done to facilitate crop feeding into the cylinder, but the effect of this variable on the threshing efficiency is not consistent.

Threshing losses increase with material feed rate, which is generally expressed in terms of tons/h of material-other-than-grain (MOG). The other ways of expressing material feed rate are grain feed rate and total feed rate. Threshing losses also increase with the MOG-to-grain ratio. Moisture content also affects threshing efficiency. Generally, the crop becomes hard to thresh at higher moisture content and as a result the threshing losses become higher. Also, if the crop is not fully mature and if there is a lot of green material in the crop, threshing becomes difficult and losses increase.

The *separation efficiency* of the threshing cylinder is defined as the percent of grains separated through the concave grate of a conventional combine, or at the threshing part of a rotary combine, to the total grain in the crop entering the threshing mechanism. A major portion of the total grain separation is done at the threshing

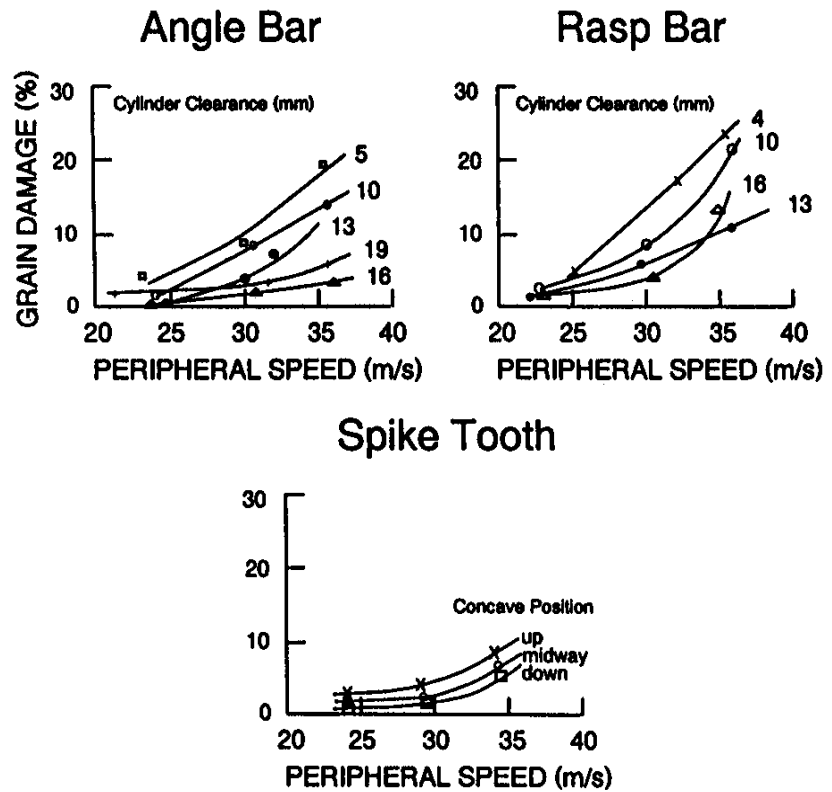


Figure 12.20 – Effect of cylinder speed and clearance on visible damage to barley having a moisture content of 12% to 15% (redrawn from Wilkinson and Braumbeck, 1977).

cylinder, and a high cylinder separation efficiency generally translates into higher separation and cleaning efficiencies of the combine. Cylinder separation efficiency varies from 60% to 90%. Increasing the concave length increases the separation efficiency but at a diminishing rate. Grain separation increases with cylinder speed. The number of rasp bars has little effect, while increasing the cylinder diameter or the cylinder-concave clearance tends to reduce the separation efficiency. Increasing the feed rate has a negative effect on the separation efficiency.

Grain damage refers to mechanical damage to grain during the process of threshing. It includes broken kernels, kernels with skin damage, and kernels with internal damage. Mechanical damage to grain results in poor germination, poor storability, and poor processing characteristics. There are many methods of measuring grain damage, including visual inspection of a sample of grain, sieving through a standard sieve, and germination testing. Cylinder speed has the most profound effect on grain damage during threshing, as increasing cylinder speed increases damage exponentially. Increasing concave length tends to increase grain damage slightly. Increasing cylinder

diameter and cylinder concave gap reduces grain damage. Increasing feed rate provides more cushioning that may reduce grain damage. The effect of cylinder type, cylinder speed, and clearance on visible damage to barley is given in Figure 12.20. Increasing grain moisture increases grain damage, however at very low moisture content the kernels tend to crack and increase grain damage. For shelling corn the optimum moisture content was reported by Byg (1968) to be around 20%.

Excessive *straw breakup* during threshing results in an increased load on the cleaning shoe, which causes additional cleaning losses. Increased straw breakup also increases power requirements of the threshing cylinder.

Figure 12.21 shows the effect of the various factors, except for straw breakup, on threshing performance of a combine. Typical cylinder threshing speeds and concave clearances are given in Table 12.1.

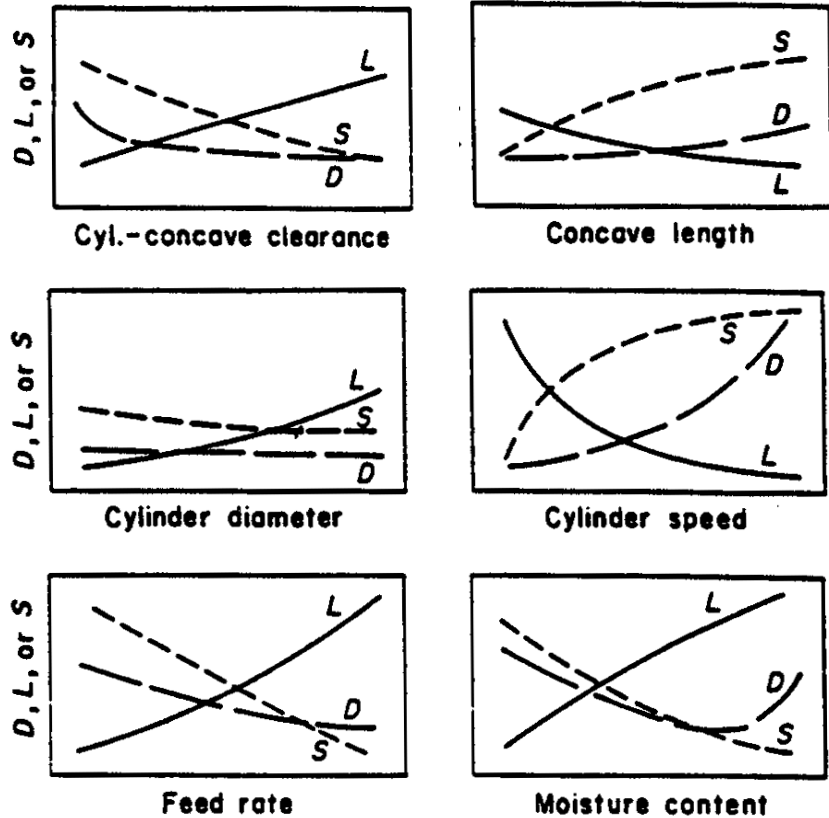


Figure 12.21 – Graphical characterization of some of the performance relations for a rasp-bar cylinder with an open-grate concave. L = cylinder loss; D = grain damage; and S = percent of grain separated through concave grate (Wieneke, 1964).

Table 12.1 Typical cylinder peripheral speeds and clearances for various crops (Kepner et al., 1978)

Crop	Peripheral Speed (rasp-bar or spike-tooth), m/s	Mean Clearance (rasp-bar cylinders), mm
Alfalfa	23–30	3±10
Barley	23–28	6–13
Edible beans	8–15	8–19
Beans for seed	5–8	8–19
Clovers	25–33	1.4–6
Corn	13–22	22–29
Flax	20–30	3–13
Grain sorghum	20–25	6–13
Oats	25–30	1.5–6
Peas	10–15	5–13
Rice	25–30	5–10
Rye	25–30	5–13
Soybeans	15–20	10–19
Wheat	25–30	5–13

12.2.3 Separation

12.2.3.1 Separation mechanisms

Grain separation in combines refers to the separation of grains from straw after threshing. A large percentage (70% to 90%) of grains are separated during the threshing process. Two types of grain separators are commonly used in combines: conventional combines use straw walkers and rotary combines use rotary separators.

Straw walkers consist of several long channel sections mounted on a crankshaft. As the shaft turns the channel sections follow an elliptical or circular path that causes the straw to bounce on top of the channels and move toward the rear of the combine due to the design of the sawtooth shape of the top of the channel sections. The oscillating action causes the grains and some chaff to be sifted down and be separated from the straw. There are three to eight sections in a combine depending upon its size. The sections are about 20 to 30 cm wide and the crank throw is about 5 cm. It rotates at approximately 200 rev/min. Figure 12.22 shows the straw walker movement. The crankshaft used to create the oscillatory action of the channel sections is shown in Figure 12.23.

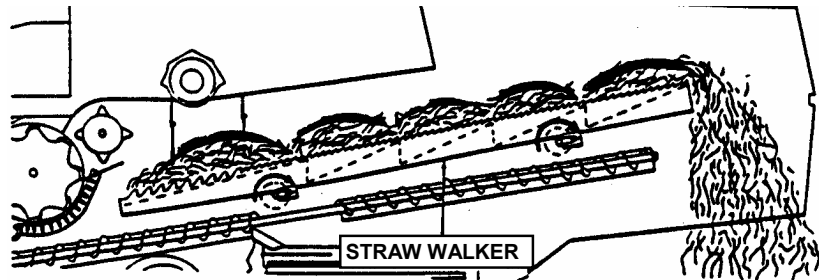


Figure 12.22 – Straw walker action in a conventional separator, side view (reproduced by permission of Deere and Co. © 1991).

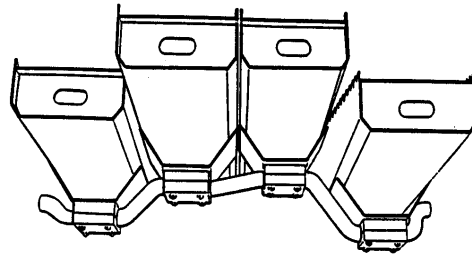


Figure 12.23 – Straw walkers and the driving crankshaft, end view (reproduced by permission of Deere and Co. © 1991).

Rotary separators. The main force causing the grain to move through a mat of straw is the centrifugal force caused by rotation of the straw mat by the rotor, as compared to the gravity force in the straw walkers. The rotor, which rotates inside of a stationary cylindrical screen, generates a centrifugal force field which is several times that of gravity. The paddles mounted on the rotor surface cause the crop to take a helical path in the annular space defined by the rotor and the screen. In rotary separators the crop motion is forced rather than induced (as in the case of straw walkers). This results in higher capacity per unit grate area, but requires higher power. Since the separation is not gravity dependent, irregularity of the ground surface has no effect on the separation process. Figure 12.24 shows a rotary separator that utilizes two rotors. The diameter of the front feed section of the rotor is 464 mm and the separator section is 502 mm providing a total separation area of 1.2 m². The rotors turn at 700 rev/min.

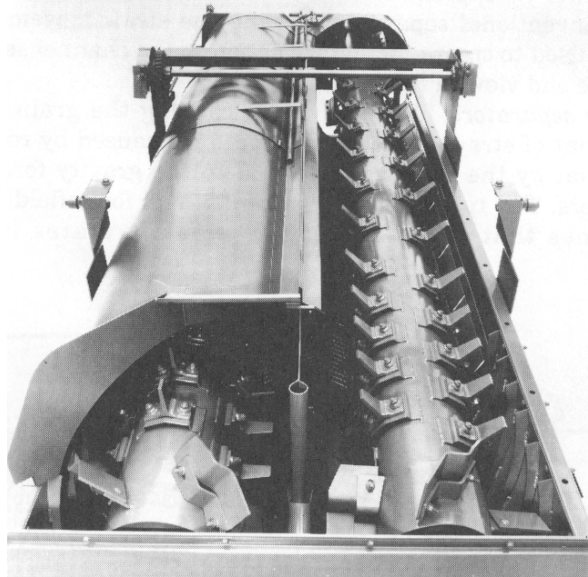


Figure 12.24 – A cylinder and tine rotary separator (courtesy of Deere and Co.).

12.2.3.2 Theory

The grain separation theory presented here is based on the research conducted by Gregory and Fedler (1987). They compared grain movement through a mat of straw with the process of diffusion to develop a separation model. The model, based on Fick's Law, is given as follows:

$$Q_g = -D \frac{A}{L_d} (C_2 - C_1) \quad (12.2)$$

where Q_g = volumetric grain flow rate, m^3/min

A = cross-sectional area, m^2

D = coefficient of diffusion, m^2/min

C_2 = concentration of grain on straw walkers

C_1 = concentration of grain below straw walkers

L_d = length through which diffusion is occurring, m

For the straw walker, the grain flow rate is defined as the change in grain volume with time. The grain concentration under the straw walker is zero. The above equation becomes:

$$\frac{dV_g}{dt} = -D \frac{A}{L_d} (C_2 - C_1) \quad (12.3)$$

where V_g = volume of grain on straw walker, m^3

t = time, s

The concentration of grain, C_2 , on the straw walker is defined as the volume of grain divided by the total volume of material. Since the grain is contained in the volume of MOG, the total volume is equal to the volume of MOG. The area is defined in terms of the width and length of the straw walker. Equation 12.3 is then expressed as:

$$\frac{dV_g}{dt} = -D \frac{WL}{L_d} \left(\frac{V_g}{V_{MOG}} \right) \quad (12.4)$$

where W = width of separator area, m

L = length of separator area, m

V_{MOG} = volume of material-other-than-grain on the straw walker

The equation after rearranging and integrating becomes:

$$\ln \left(\frac{V_{gf}}{V_{gi}} \right) = -D \left[\frac{WL}{L_d V_{MOG}} \right] t \quad (12.5)$$

Taking the exponential of both sides of the above equation gives:

$$\frac{V_{gf}}{V_{gi}} = e^{-[DWL/(L_d V_{MOG})]t} \quad (12.6)$$

The grain volume can be replaced by grain mass divided by grain density. The above equation is rewritten in terms of grain masses as follows:

$$\frac{G_f}{G_i} = e^{-[DWL/(L_d V_{MOG})]t} \quad (12.7)$$

where G_f = final grain mass, kg

G_i = initial grain mass, kg

Replacing V_{MOG}/t by the MOG feed rate divided by MOG density:

$$\frac{G_f}{G_i} = e^{\left[\frac{DW\rho_{MOG}}{L_d \dot{m}} \right] L} \quad (12.8)$$

where ρ_{MOG} = bulk density of MOG, kg/m³

\dot{m} = MOG flow rate, kg/min

If all the variables, except for L , in the exponent on the right hand side of the above equation were held constant (= K_L) the resulting equation will be a decaying function of straw walker length as shown below. The values of K_L were found to be dependent on the MOG feed rate.

Reed et al. (1974) and Wang (1987) studied grain straw separation in conventional and rotary combines. They found that grain separation is an exponential function of the separator length as shown in Figures 12.25 and 12.26. Reed suggested the following relationship for grain loss in a conventional combine:

$$GL = e^{-bL} \quad (12.9)$$

where GL = grain loss

b = constant

L = straw walker length

Comparing Equation 12.8 with 12.9, we find that the two equations are identical and that K_L has the same meaning as b . Therefore, K_L may be determined using the data reported by Reed. The separator efficiency is determined by subtracting the grain loss from one and expressing the number in percentage. The walker length corresponding to 50% efficiency is determined as follows:

$$0.5 = e^{-bL_{0.5}}$$

or

$$\ln(0.5) = -bL_{0.5}$$

or

$$b = \frac{0.693}{L_{0.5}} \quad (12.10)$$

The value of b can be determined from the data given in Figure 12.25. It depends on the MOG feed rate and MOG/grain ratio. The following relationship was developed to estimate the value of b :

$$b = 648.4 \dot{m}^{-1.296} \left(\frac{MOG}{Grain} \right)^{-0.662} \quad (12.11)$$

where \dot{m} = MOG feed rate, kg/min

MOG/Grain = MOG-to-grain ratio in the crop

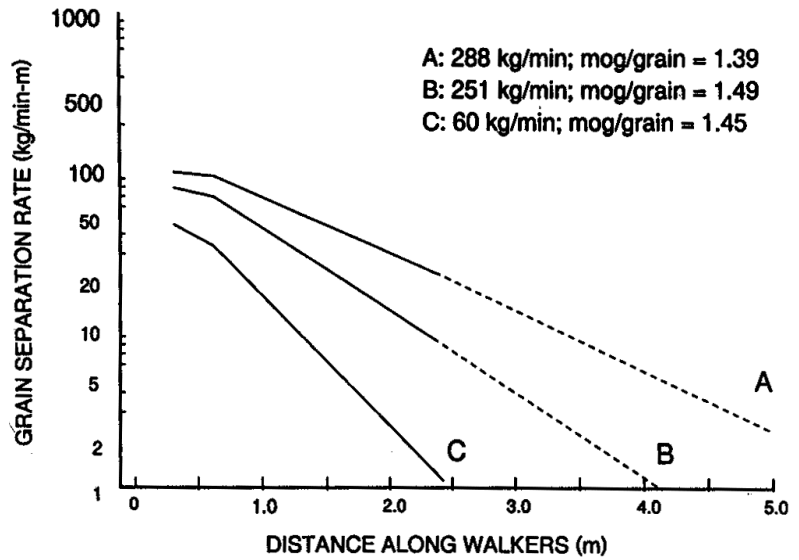


Figure 12.25 – Distribution of grain separated along straw walkers at three different feed rates. The number at each foot interval indicates the percentage of total separated at that foot of length (redrawn from Reed et al., 1974).

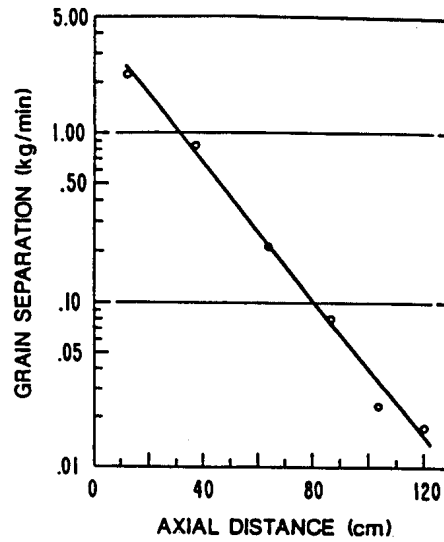


Figure 12.26 – Typical separation distribution along and beneath the central region of the threshing and separation concave of a rotary combine in wheat (Wang et al., 1987).

Example 12.1

A combine fitted with a 2.44 m long straw walker is harvesting wheat at a MOG feedrate of 9 t/h. The MOG/grain ratio is 0.8. Determine the expected grain loss from the separator. Assume that 75% of the grain was separated at the cylinder concave.

Solution

The grain loss is determined from Equation 12.9. Estimate the value of b from Equation 12.11 as follows:

$$b = 648.4 (150)^{-1.296} (0.8)^{-0.662} = 1.137 \text{ m}^{-1}$$

Substituting in Equation 12.9 we get:

$$\text{grain loss} = e^{-1.137(2.44)} = 0.0624 \text{ or approximately } 6\%$$

Since only 25% of the total grain reaches the separator, 6% of which is lost, the grain loss on the total grain basis would be $0.25 \times 0.06 = 0.015$ or 1.5%. This is a reasonable amount for separation loss.

12.2.3.3 Separation performance

The performance of the separator is measured in two ways: *walker efficiency*, measured in percent grain loss, and *walker capacity*, measured in tons/h of MOG feed rate corresponding to a given grain loss (usually 1% to 2%). The *walker efficiency* is calculated by dividing the amount of grains separated by the amount of grains entering the separator and expressed as percentage. The amount of grain still in the straw as it leaves the combine is considered the separator loss. This method is preferred for comparing the separation performance of different combines.

The separation performance parameters for conventional combines are affected by the following factors:

- Design factors: walker length, crank throw and speed;
- Operating parameters: material feed rate, walker slope;
- Crop properties: grain-to-MOG ratio, crop physical and mechanical properties.

Effect of design factors. The effect of separator length on the performance has been presented earlier. The size and speed of straw walker crank are designed to obtain an optimum combination of the straw agitation and crop throughput rate. Increasing the crank throw would increase the agitation but at a higher power requirement. Increasing the speed would increase the throughput rate but may not allow all grains to sift out before the straw escapes through the rear of the combine.

Effect of operating parameters. Increasing the MOG feed rate of the crop increases grain loss exponentially. A reasonable balance between capacity and grain loss has to be maintained. Figure 12.27 shows the effect of uphill and downhill ground slope on the separator performance; downhill slope results in better performance. Hill

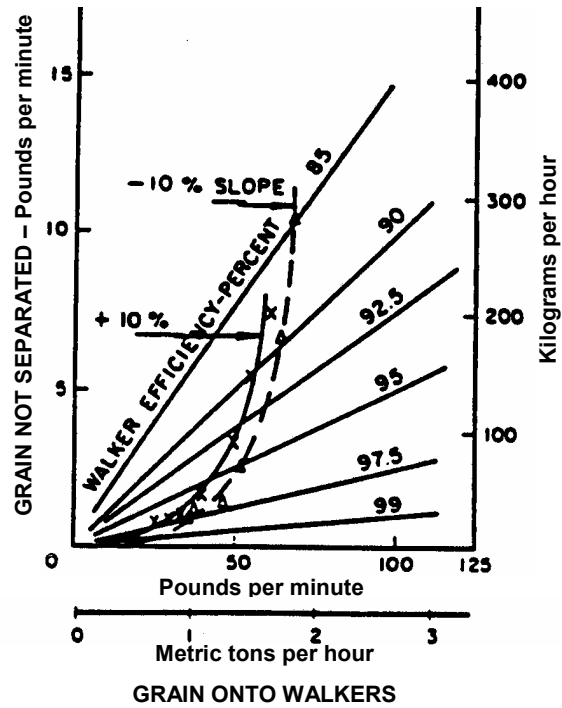


Figure 12.27 – The effect of 10% slope on walker efficiency (Reed et al., 1974).

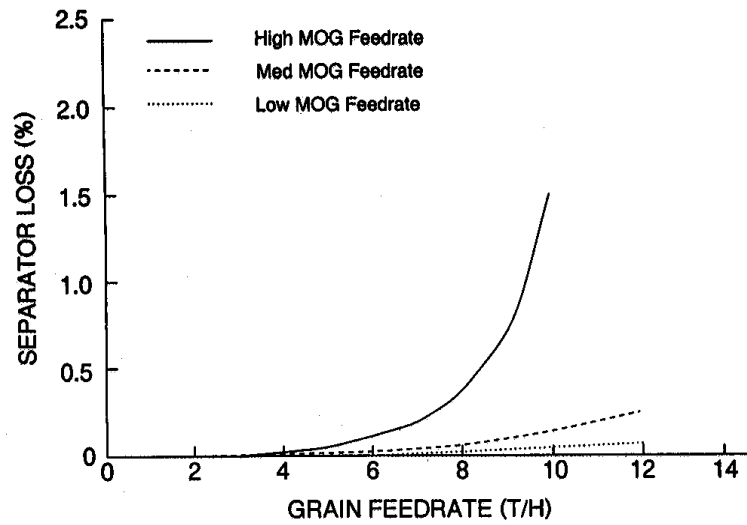


Figure 12.28 – Typical effect of MOG/G ratio on straw walker loss for wheat crop (redrawn from Hill and Frehlich, 1985).

and Frehlich (1985) reported that as the MOG/grain ratio increases, separator losses increase somewhat exponentially in wheat and barley as shown in Figure 12.28. In wheat, reducing the MOG/grain ratio from maximum (1.2) to medium (0.85) reduced the average straw walker losses from 0.73% to 0.48%. Reducing the MOG/grain ratio from 1.2 to 0.64 reduced losses to less than 0.3%. This suggests that an accurate header height control to cut the stalks just below the grain heads would improve separator performance.

Effect of crop properties. Srivastava (1990) reported that grain bulk density, grain angle of repose, and straw bulk density are related to separator performance while harvesting wheat and barley. Increasing grain density increases separator capacity while increasing the grain angle of repose has the opposite effect. Higher straw density reduces separator capacity.

12.2.4 Cleaning

Cleaning refers to the final separation of grain from other crop material, which consists mainly of chaff and broken straw pieces. The grain separated at the threshing cylinder and the separation unit is combined on an oscillating conveyor or a set of augers that feed the mixture of grain and chaff to the cleaner, often referred to as the *cleaning shoe*.

12.2.4.1 Cleaning mechanisms

A common cleaning shoe arrangement is shown in Figure 12.29. The separation is accomplished due to aerodynamic and mechanical actions. The cleaning shoe design consists of two or three oscillating adjustable-opening sieves and a paddle-type fan to blow air through the sieve openings. The crop is dropped on the top sieve (*chaffer sieve*) near the front of the shoe. The chaff gets blown off by the air and the grain falls through the openings onto the lower sieve (*cleaning sieve*). The process is repeated once more as the clean grain passes through to the *clean grain auger* and conveyed to the *grain tank*. The separation occurs due to difference in the terminal velocities of grain and chaff material. For example, the terminal velocity of wheat, oat, and barley

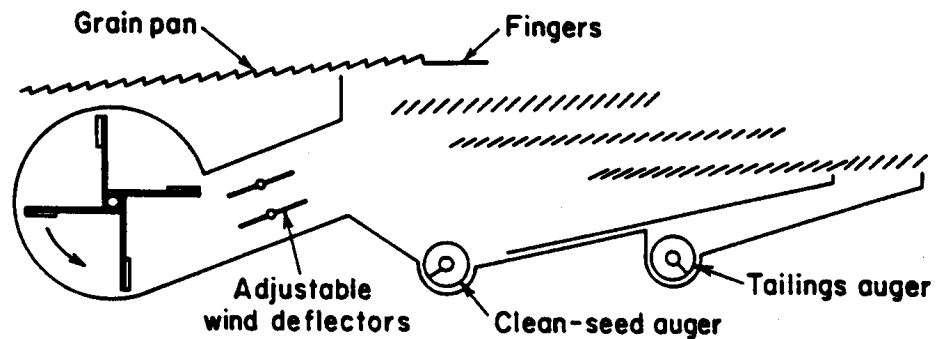


Figure 12.29 – A schematic diagram of a cleaning shoe showing an auger bed for feeding the grain-chaff mixture.
(Reproduced by permission of Deere and Co. © 1991. All rights reserved.)

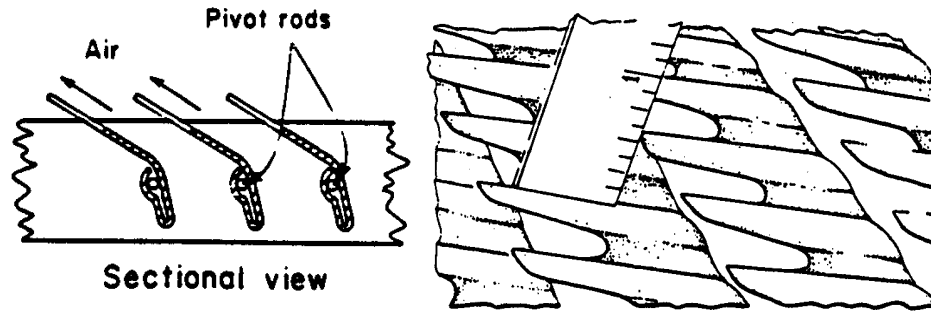


Figure 12.30 – An adjustable chaffer sieve (reprinted from Kepner et al., 1978).

grains range from 5 to 10 m/s whereas the terminal velocity for short pieces of straw is from 2 to 6 m/s and from 1.5 to 2.5 m/s for chaff.

The two sieves may oscillate in the same direction or opposite to each other for better balance. The rate of oscillation varies from 250 to 325 cycles per minute. The sieve area depends on the width of the threshing cylinder. Generally, the chaffer sieve area varies from 114 to 147 cm² per cm of the cylinder width for models having two sieves. Figure 12.30 shows the adjustable opening sieve design. The lips rotate to open or close the openings. The bottom sieve has smaller openings. For small grain the bottom sieve is replaced by round-hole sieve. The unthreshed grain that is too small to go through the sieves and too heavy to be blown off by the fan is commonly referred to as the *tailings*. The tailings travel on top of the chaffer towards the rear of the combine due to the oscillations and are collected by an auger and conveyed to the threshing cylinder for rethreshing.

Rotary combines utilize the same cleaning shoe design as conventional combines. There are augers placed longitudinally under the rotor to carry the grain-chaff mixture to an oscillating grain pan that feeds the mixture to the cleaning shoe. Some rotary designs create air flow through the rotor to remove chaff. This may be considered a form of pre-cleaning.

12.2.4.2 Theory

To understand the theory that applies to the cleaning shoe it would be worthwhile to examine what happens to the crop material during the process of cleaning. The mixture of grain, chaff, and small pieces of straw falls from the oscillating grain pan or an auger bed on to the front part of the chaffer sieve. As the mixture falls, a blast of air is directed at about a 45° angle towards the rear of the combine. The air velocity is such that it carries most of the chaff with it while the grain and some chaff fall on the chaffer sieve. The remaining mixture of crop material is subjected to air movement as well as mechanical oscillations. The mat of crop material moves towards the rear of the combine on the chaffer sieve due to the oscillations. The air moving through the mat causes the mat to lose chaff as it is carried by the air stream while the grain sifts down through the mat of chaff and small pieces of straw due to gravity and passes through the openings in the chaffer. The grain and a small fraction of chaff fall on the cleaning sieve where the process is repeated.

Thus, the theoretical principles applicable to the cleaning process are (1) aerodynamic separation based on the terminal velocities, (2) movement of the crop material on the chaffer, (3) movement of the grain through the mat, and (4) escape of the grain through the openings in the chaffer. *Aerodynamic separation* is based on the pneumatic conveying of chaff and straw which in turn depends upon the terminal velocities and the drag coefficients of the different components in the crop mixture. The crop movement on the chaffer is based on the theory of oscillating conveyors. Grain motion through the chaff and straw mat is due to gravity and the resistive force caused by the straw mat. The escape of grain through the sieve opening is based on the theory of sieving which is based on the theory of probability.

Aerodynamic model. The *aerodynamic model*, based on the research reported by Rumble and Lee (1970) on aerodynamic separation, is presented here. This model applies to the separation process that occurs as the crop falls from the grain pan and is subjected to an air blast and as it moves over the upper screen. The following assumptions apply:

1. The drag coefficient is independent of the air velocity.
2. The particles are accelerated as free bodies and not as a mat.
3. The velocity of air through the upper screen is constant.
4. Air flow above the upper screen is streamlined parallel to the orientation of the chaffer lips.

Summing forces acting on the particles in the vertical direction we get:

$$m a = F_g - F_d \quad (12.12)$$

where m = particle mass, kg

a = particle acceleration, m/s^2

F_g = force of gravity acting on the particle, N

F_d = aerodynamic drag acting on the particle, N

The aerodynamic drag force is expressed as:

$$F_d = C_d v_y^2 \quad (12.13)$$

where C_d = drag coefficient

v_y = relative velocity between the particles and air in the vertical direction, m/s

At terminal velocity the drag force equals the weight of the particles, or:

$$F_d = m g = C_d v_t^2 \quad (12.14)$$

where v_t = terminal velocity of the particle.

From the previous two equations the drag force can be computed as follows:

$$F_d = m g \left(\frac{v_y}{v_t} \right)^2 \quad (12.15)$$

Substituting Equation (12.15) in (12.12) the following equation is obtained:

$$\frac{d^2y}{dt^2} = g - g \left(\frac{v_y}{v_t} \right)^2 \quad (12.16)$$

Acceleration in the horizontal direction is given by:

$$\frac{d^2x}{dt^2} = g \left(\frac{v_x}{v_t} \right)^2 \quad (12.17)$$

where v_x = velocity of the particles relative to the air in the horizontal direction. Note that v_x and v_y are $dx/dt - v_{ax}$ and $dy/dt - v_{ay}$, respectively, where v_{ax} and v_{ay} are the horizontal and the vertical components of the air velocity.

The above two equations are non-linear and require numerical solution. The equations were solved using an analog computer by Rumble and Lee (1970). The solution was obtained in two parts. The first part was related to the free fall of the particles from the grain pan and the second part consisted of the particle motion on the chaffer. The vertical motion would come to a stop when the particles reached the chaffer sieve. After the particles fall 17.78 cm (7 in.), the second condition applies. It was considered, based on the experimental studies, that excessive loss would occur if the grain travelled 7.62 cm (3 in.) towards the rear of the combine without landing on the chaffer. Using this as the criterion, they developed the results as shown in Figure 12.31. The horizontal axis is the initial downward velocity of the grain. If the initial downward velocity is too low grain would travel farther toward the rear and will end up in grain loss. Very high values would result in excessive chaff landing on the screen which will also result in the grain loss. An optimum zone is shown in the figure.

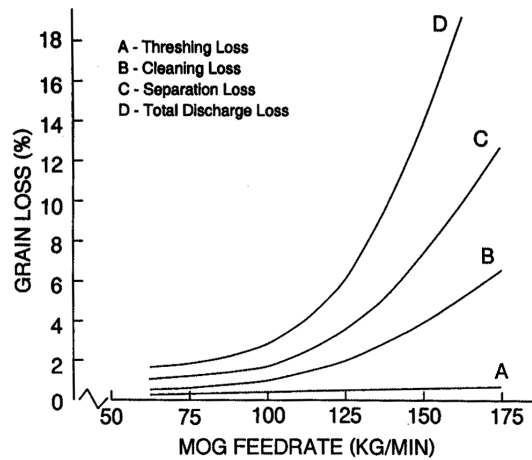


Figure 12.31 – Computer-simulated results of a cleaning shoe showing the combination of grain and air velocity for acceptable performance (redrawn from Rumble and Lee, 1970).

12.2.4.3 Cleaning performance

The performance of a cleaning shoe is expressed in terms of (1) grain loss or cleaning efficiency, (2) cleaner capacity, and (3) grain dockage. *Grain loss* is calculated by determining the percentage of lost grain on the basis of the total grain entering the cleaning shoe. The *cleaning efficiency* is the percentage of grain recovered by the shoe. The *cleaner capacity* is determined by first plotting a curve of grain loss against the material other than grain (cleaner MOG) feed rate passing through the cleaning shoe. A curve is fitted to the data, usually an exponential function, and the capacity of the cleaning shoe is determined corresponding to a given grain loss level. *Grain dockage* is the amount of chaff that is separated with grain. It is determined by taking a sample of grain from the grain tank of the combine and cleaning the sample to determine the percentage of chaff in the sample.

The cleaning shoe performance is affected by the following factors:

- Design factors such as sieve size, oscillation amplitude and frequency.
- Operating conditions including material feed rate, cleaning shoe slope, air flow, and chaffer openings.
- Crop properties including grain to MOG ratio, chaff and grain properties.

Design factors. Longer sieves would allow longer dwell time for more complete separation of grain. However, physical considerations limit the size of the cleaning shoe. Studies have indicated that the initial sieve length does not contribute much to the cleaning action. A cascade arrangement permits a more complete cleaning while keeping the length of the sieves short. The frequency and the amplitude determine the level of acceleration imparted on the crop. This determines the level of agitation necessary to provide the least resistance to grain separation. The material flow rate is also determined by these parameters. German and Lee (1969) reported on the effects of the frequency of oscillation on the shoe performance. The range of frequencies used were 260 to 460 cpm. Increasing the frequency of oscillation at 90 kg/min input rate reduced the grain loss significantly. However, they did not recommend increasing the frequency because of the increased mechanical vibrations.

Operating conditions. German and Lee (1969) also studied the effect of air volume on cleaning performance. The air volume has to be matched with the feed rate. They developed a relationship between the air volume and the debris found in the grain sample as follows:

$$Z = 2 - 50 \times 10^{-6} V + 0.4 \times 10^{-9} V^2 \quad (12.18)$$

where Z = amount of debris, kg/min

V = air flow rate, m^3/min

Bottinger and Kutzbach (1987) reported on the effect of fan speed and feed rate. Their results are shown in Figure 12.32. As shown in the figure, the grain loss increases somewhat exponentially with the fan speed and feed rate. Nyborg et al. (1969) found that the cleaning losses increase with MOG feed rate and with grain/straw ratio. The results are shown in Figure 12.33. As shown in the figure, the effect of feed rate becomes more significant at high grain/straw ratios and vice versa. Increasing the lip angle from 30° to 36° reduced grain loss according to a study reported by Lee and Winfield (1969). The lip angle effect is highly dependent on other factors such as the material feed rate.

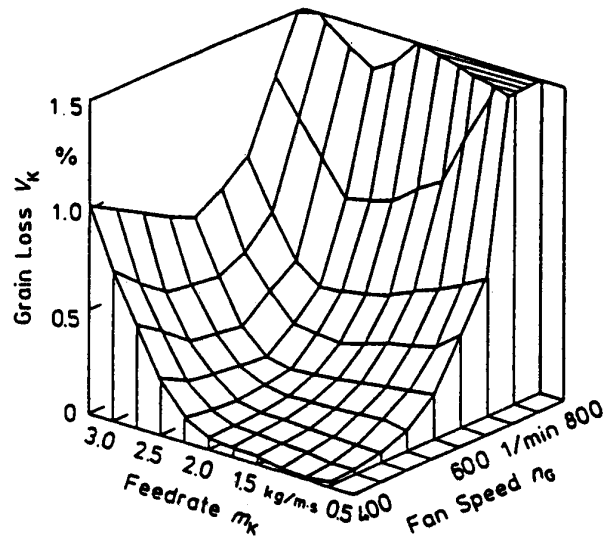


Figure 12.32 – Performance characteristics of a cleaning shoe (Bottinger and Kutzbach, 1987).

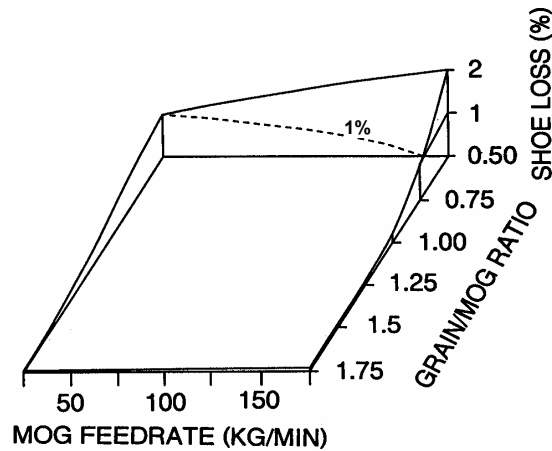


Figure 12.33 – Shoe-loss surface for a standard combine in wheat (Nyborg et al., 1969).

Crop properties. Srivastava et al. (1990) studied the effect of chaff and grain properties of wheat and barley on the capacity of the cleaning shoe. They found that the grain angle of repose had a negative effect on the cleaner capacity. Increasing the chaff friction also decreased the capacity. Increasing grain density increased the cleaner capacity. Increasing chaff mean length tended to reduce the cleaner capacity. Both grain and chaff moisture tended to decrease the cleaner capacity. Increasing grain-to-MOG ratio decreased cleaner capacity.

12.2.5 Power requirements

Rotz et al. (1991) reported a simplified method for estimating rotary power requirements for agricultural machines by the following equation:

$$P_r = a + c F \quad (12.19)$$

where P_r = rotary power required, kW

F = material throughput rate, t/h

a, c = machine-specific parameters

Use $a = 20$ kW and $c = 3.6$ kWh/t for small grain self-propelled combines. The material flow rate is based on MOG flow rate. To estimate power for grain corn use $a = 35$ kW and $c = 1.6$ kWh/t. The throughput rate for corn is based on grain flow rate. For PTO-driven combines the value of parameter a should be reduced by 10 kW. A variation of as much as 50% can be expected in the value of b depending on the crop and the harvesting conditions.

If F is set equal to zero, Equation 12.19 can be used to estimate no-load or propulsion power. The cylinder generally accounts for a large portion of the total power. Power requirements for the separation and cleaning units are small and relatively independent of material flow rate. Short-time peak power requirements for the cylinder may be two to three times as great as the average requirement.

12.3 COMBINE TESTING

Combine testing is performed in the field as well as in the laboratory. Laboratory testing has the advantage of uniform crop and better control on test conditions. However, the crop has to be stored and that may cause changes in its properties, which affect the performance characteristics of the component being tested. The test engineer has to be aware of this.

The objectives of combine testing are to determine the performance characteristics of its functional components, power requirements, and durability. Only functional testing is discussed in this book. The objective of functional testing is to determine grain losses and capacity. Grain losses are expressed as percentages of total grain entering the combine. The capacity of a functional component is expressed as the MOG feed rate (t/h) through that component at a certain grain loss level.

Combine losses are divided into (1) header losses, (2) threshing losses, (3) separation losses, and (4) cleaning losses.

Header losses include lodging, shatter, and cutterbar loss. Lodged crop not cut by the cutterbar is considered lodging loss. Shatter loss is the grain that falls to the ground as the grain head is shattered due to the impact by the reel. Cutterbar loss is the cut grain heads that fail to land on the platform. The header losses may be expressed as kg/ha or as percentage of the crop yield. To determine the header losses, the combine is driven in the field and when the steady state operation is achieved, the combine is stopped. The combine is backed up a distance less than or equal to the longitudinal distance between the cutterbar and the discharge chute at the rear of the combine. A sample area is marked off in front of the combine and the losses collected from that area. Uncut grain heads still on the crop are considered lodging losses. Loose grain is considered shatter losses and the cut grain heads are considered cutterbar losses.

Threshing or cylinder losses are those unthreshed grain heads that escape the combine at the rear with straw and are expressed as the percentage of total grain entering the combine.

Separation losses, also called walker losses in conventional combines, are lost grain with straw expressed as the percentage of total grain entering the combine.

Cleaning losses, also called shoe losses, are the grain lost with chaff expressed as the percentage of the total grain entering the combine.

Discharge losses are the sum of threshing, separation, and cleaning losses. These losses are affected by the material-other-than-grain (MOG) flow rate through the machine. The plot of these losses at different MOG feed rates is referred to as the *machine performance curve*. The capacity of a functional component is the MOG feed rate at a certain loss level. This loss level is 1% to 2% for the separator capacity and 0.5% to 1% for the cleaner capacity.

To determine the discharge losses in field material, discharges from the separator and the cleaner are collected separately. A simple method of collecting the sample is to hang a canvas bag at the appropriate discharge chute at the rear of the combine. The combine is run in the field and when the steady state operation is reached the bag is opened to collect the material. At the same time, grain coming out of the clean grain auger is collected at the grain tank. When the bag is full it is closed and the sampling time is recorded. The material is weighed and the MOG flow rate is established. The grains are separated from the collected MOG and their percentage is computed. The procedure is repeated several times at different combine forward speeds and a curve is plotted as in Figure 12.34. To determine threshing losses the MOG collected from the separator is re-threshed in a stationary thresher after determining separator losses. Re-threshed grains are then separated to find cylinder losses. The separator and cleaner losses are often plotted against their own MOG feed rate rather than the total machine MOG feed rate. In this case it is necessary identify it as the separator MOG (primarily straw) and the cleaner MOG (primarily chaff). Various manufacturers have developed automated methods that save time and increase accuracy in developing loss curves.

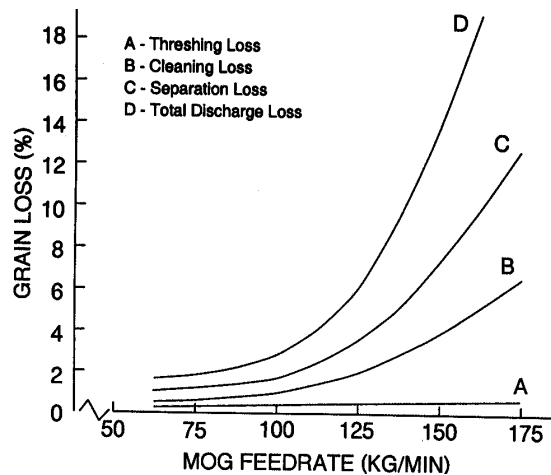


Figure 12.34 – Typical combine performance curves.

PROBLEMS

12.1 The following data were collected in a field test while harvesting barley with a 4-m self-propelled combine:

total material over walkers = 9.4 kg total material over shoe = 4.4 kg
free seed over walkers = 76 g free seed over shoe = 289 g
unthreshed seed over walkers = 60 g unthreshed seed over shoe = 81 g
total seed collected at grain tank = 17.6 kg

The length of test = 12 m, the time = 21.3 s, and the average gathering loss = 10.2g/m^2 . Calculate (a) cylinder, walker, shoe, and total processing losses as percentage of total grain feed rate; (b) gross yield, gathering loss, and processing losses in kg/ha; (c) gathering loss as percentage of gross yield; and (d) walker, shoe, and total MOG feed rate in t/h.

12.2 For the case as described in Example 12.1, what would be the separator length if the separation loss was to be under 1%? Is it practical? What other means do you have at your disposal to reduce the losses if the same separator length was used?

12.3 List possible causes and cures for each of the following combining losses: (a) excessive header loss, (b) excessive amount of unthreshed seed, (c) broken kernels of grain, (d) excessive seed loss over the separator, (e) excessive amount of chaff in the grain tank, and (f) excessive cleaner seed loss.

12.4 Suppose you are the test engineer in charge of comparative functional performance testing of a new combine against a reference combine. Develop a detailed testing program that you would follow.

FRUIT, NUT, AND VEGETABLE HARVESTING

13

INTRODUCTION

To appreciate the engineering complexities of fruit, nut, and vegetable field harvesting systems, one needs only to walk the aisles of a modern supermarket. In the fresh produce section, fruits, nuts, and vegetables are either recently harvested or have been maintained in a fresh condition by special extended shelf-life storage means. The canned goods section contains fruits and vegetables processed to assure shelf-lives of a year or more. The glass-packed aisles display a large array of products. Frozen fruits and vegetables are available in many fresh-frozen and preprocessed forms. Interestingly, some commodities can be found in more than one section. This fact is not unusual from the consumer's point of view, but, depending upon which section of the store the commodity is marketed, often requires an entirely different harvesting system. For example, peaches in the fresh produce section were probably harvested by hand, but peaches are usually mechanically harvested for fresh-frozen sliced peaches, canned peach halves, and peach jam.

In this chapter the underlying principles of mechanical harvesting of fruits, vegetables, and nuts will be explained by examining a sampling of recent U.S. patents in the field of mechanical harvesting. While only selected patent figures will be used, the student will be introduced to the unique format of these drawings. The complete specifications of the patents are not presented here. All patents cited in this chapter are listed in the Patent Reference section in Appendix A. Students wishing to study any of these patents in more detail can use the internet to search the text collection of patents at the U.S. Patent and Trademark Office (PTO), Washington, D.C. The PTO has maintained text of all patents issued since 1972 in a searchable collection. A second collection of FAX images of virtually every patent issued by the PTO is also available, but is searchable only by title and patent number. The URL for the PTO is <http://www.uspto.gov>. Thus, the secondary educational objective of Chapter 13 is to introduce the student to the patent literature and to the unique value of this literature in providing a functional understanding of harvesting machines.

Natural constraints

Not only has the consumer demanded a wide selection of produce in different forms, but nature has further complicated harvesting by imposing size and stage-of-maturity variables. Some varieties of grapes, for example, will continue to flower throughout the growing season so that late in the growing season, at the time of harvest, the vines will have flower buds still opening, green fruit in various stages of development, and large grapes at several stages of ripeness. Sweet potatoes will also continue to grow and increase the root size until the tops are destroyed by mowing or a heavy fall frost. Harvesting systems must be able, in some cases, to accommodate a considerable variation in product size and maturity.

It is important to realize that the choice of one-time harvesting or multiple harvests is often a basic natural commodity constraint. In some cases, such as the tomato, genetic modifications to achieve uniform maturation have been introduced to facilitate field mechanized harvesting (Hightower, 1972). Plant materials are selected for their ability to synchronize the maturation process, thus producing a higher percentage of ripe product for one-time harvest. Also, traits that enhance mechanical harvestability, such as firmness and bruise-resistance, are selected by plant breeders.

Often food production results from crops produced only once per year on the natural yearly cycle of nature. Some food crops can be produced in repeated cycles in a given year. U.S. food production, by virtue of climatic differences, and world food production, by virtue of climatic and seasonal differences, tend to produce food more or less continuously throughout the year. However, in any given location, every commodity commercially produced results in an intense harvest activity of limited duration. Timing of harvest to ensure peak product quality may further intensify the harvest activity. This intense harvesting period requires high capacity harvesting systems that are very reliable.

Economic constraints

Harvesting of fruits, nuts, and vegetables can be viewed as a value-added operation. In other words, a grower must look at the market opportunities for the crop at harvest to attempt to ensure maximum economic return to the enterprise. Sometimes this evaluation results in a choice between fresh or processed markets. The complex inter-relationship between the harvesting system used and the resulting fresh product shelf-life often dictates that hand harvest methods be used for products destined for the fresh market. Hand harvesting is an important component of the food production system and will continue to be employed in food production enterprises as long as consumers are willing to support the resulting value-added pricing.

It is important to realize that the mechanized harvesting of any fruit, nut, or vegetable commodity results only after a commodity has been produced (and harvested by hand) in sufficiently large quantities. Once the importance (and volume) of a commodity increases, there is often economic justification to replace hand harvesting with mechanical means, assuming product quality and market potential remain unchanged. Philosophically, this releases the hand labor to move to some other minor commodity and the cycle is repeated. It is most important to understand that many successful mechanical harvesting systems in use today were originally developed to “mimic” the hand harvesting system.

13.1 THE FUNCTIONAL PROCESSES

Before developing a detailed understanding of the important functional harvesting processes, it is important to consider their interrelationships. While *removal*, *control*, *selection*, and *transportation* are the four required functional operations for a harvester, the order in which these functions are achieved is determined by the harvest requirements of the specific commodity. For example, hand harvesting almost always begins with selection. The hand is guided to the visually selected object after which control is achieved. Removal (detachment) is then accomplished by a cutting, pulling, twisting, or rolling motion to remove the object from the host plant. After removal, the hand-harvested object is carefully placed (hopefully) into a suitably selected transportation receptacle. In mechanical harvesting systems, as another example, detachment is seldom as selective as desirable, thus the selection function is achieved after detachment in the form of a sorting operation, either as part of the field harvesting operation or at some later processing, sorting, cleaning, grading, or packaging operation.

Given the four functional processes listed above, it is clear that there are mathematically 24 (i.e., 4!) ways in which to order the functions to effect the field harvesting operation. While certain of these combinations may appear to be impractical, the fact that the combinations exist offer an experienced engineer with the opportunity to explore non-obvious design alternatives. This checklist of design alternatives can be an important tool in understanding and classifying existing harvesting machines.

13.1.1 Removal

As defined earlier, removal is the actual separation of the harvested portion from the host plant. Application of energy is necessary to do this. The method in which this energy is applied is an important consideration, depending upon the commodity in question. Severing the attachment requires that the ultimate fatigue, tensile, or shear strength limits must be exceeded. Application of removal energy can affect one or more of these properties simultaneously. The necessary removal energy can be delivered by application of direct force to the harvested portion, or delivered indirectly as an inertial force response to the attachment as a result of a difference in relative acceleration. Hand and robotic harvesting effect control of the harvested portion and then exert the necessary force to cause detachment. In contrast, inertial removal methods cause detachment by accelerating the attachment support away from the harvest object. In some cases, cutting may be the preferred method of removal. The direct application of the necessary cutting forces is the most energy efficient method of removal (Persson, 1987). Cutting is usually employed only after achieving control. In most cases this control is explicit in that machine elements are in contact with plant materials such that the location of the attachment point or region is known. In some cases control is implicit since non-uniformity from plant to plant is negligible and the location of attachment can be assumed with a high degree of certainty.

Inertial application of energy usually results from accelerating plant materials with machine elements in a pattern and frequency that has been selected for a specific commodity. If the point of application of the inertial energy is the trunk or branch of a tree, then care must be exercised to minimize the possibilities of damage to the under-

lying plant tissues. When the machine elements interact directly with the commodity to be harvested, there is always the possibility of product damage.

Inertial shakers are commonly constructed as a slider-crank mechanism, two counter-rotating masses with a common center of rotation, or a compound counter-rotating two-mass pendulum. It is possible to construct shakers with three synchronously rotating masses to effect a wide variety of shaking patterns. The kinematic analysis of the rotating mass shaker will be an example problem.

13.1.2 Control

Catching surfaces are often required to gain or maintain product control during harvesting operations. While padding is desirable to reduce the possibilities of product damage, careful selection of these padding materials is necessary. Good padding materials absorb the impact energy of the product, are easy to keep clean, and are durable. Specialized catching surfaces and systems are used in the harvest of many bush, trellis, and tree crops.

If the product can be engaged by machine elements before separation, then subsequent operations are often simplified. In grape harvesting, for example, the row of plants enter the harvester where the engagement, separation, and control of the product occur more or less simultaneously and in the same area. By directing the separation energy in the grape harvester, the harvested product flow can be controlled into the conveyors that will move the product to the transportation function.

Harvesting functions often interact with each other. For example, if inertial separation is used by interacting with the plant material, then the separated fruit usually has an associated kinetic energy. Now, the harvested product is unattached and moving, thus making it difficult to reestablish its control. Had inertial separation not been used, better opportunities for gaining and maintaining product control might have been achieved.

13.1.3 Selection

Selection is the process, in general, in which only the ripe, correctly sized, or desirable product is obtained from the entire product population on the plant, while the remainder is rejected. In principle this seems trivial. However, developing machines that are capable of implementing complex selection algorithms is neither simple in practice nor economically attractive. Often, a simple air-blast selection means will provide a high degree of functionality while minimizing implementation complexities. This is not surprising when large aerodynamic property differences exist between the harvested product and leaves, for example. Effective design of these air separation subsystems can be achieved with an understanding of terminal velocities, usually within a turbulent air flow field.

Size or uniformity of size is often associated with product quality. Seldom are harvesting systems equipped to achieve size grading in the field. This would unnecessarily complicate the harvesting operations with the resulting need for transportation of multiple sizes.

Product maturity is an important parameter that requires special attention, especially in multiple-pass harvest systems. Ideally, during any one harvest, all mature product (and only mature product) is harvested. This is important because the un-

harvested mature product will likely be harvested on a subsequent harvest, when it is over-mature. Harvest of immature product usually, and unnecessarily, reduces the available crop on subsequent harvests. Once harvested, both over-mature and immature product must be separated from the marketable product, and are liabilities to be avoided. Once-over harvest systems also need to consider these factors since the exact timing of the harvest is subject to horticultural and weather factors.

13.1.4 Transportation

Bulk handling systems are preferred where product considerations permit. In many cases, truckload lots for commodities such as tomatoes, field-packed lettuce, green beans, onions, sweet potatoes, wine and juice grapes, juice apples, and potatoes are handled from the field through the wholesale or process marketing systems.

Standard pallet-sized containers (ASAE Standard S337.1) can be handled with forklift equipment and are desirable when on-farm operations are limited to pallet-sized lots. In small operations, the common means of transporting products in low volume has been the smaller-sized, hand lug that holds about 15 to 25 kg of product. Lugs are often constructed from wood or plastic and have provided an important mode of transportation for many years. Many harvesting systems provide for direct filling of the hand lug on the harvester.

13.2 METHODS AND EQUIPMENT

Given the diversity of fruit, nut, and vegetable crops grown for human consumption, it should not be surprising that classifying harvesting systems into a small number of categories is difficult. In general, the harvest methods will be categorized by the physical location in which the harvestable portion of the crop is located. Figure 13.1 illustrates the production zones of interest. Certainly the location of the soil surface is more or less precisely known, but the transition between the surface crop zone and the bush and trellis zone is not always so clear. For example, tomatoes are grown as a surface crop and also as a trellis crop supported on wooden stakes. Blueberries grow on the surface (low-bush varieties), as a bush (high-bush varieties), and as small trees (mature rabbiteye varieties).

Even though some commodities belong to more than one harvesting zone classification, it is important to realize that harvesting functionality generally conforms to the harvesting zone. Surface crops are usually harvested in a once-over operation. This is certainly true for most processing tomatoes and low-bush blueberries. Bush blueberries and trellis tomatoes for fresh market are usually harvested by hand several times throughout the season. Peanuts, although not botanically a root crop, are harvested with methods common to root crops. Thus, an overview of harvesting methods and equipment will be considered by class within the four general harvesting zones. Figure 13.1 shows the generally overlapping vertical root, surface, bush, and tree harvest zones.

Finally, it is beyond the scope of this text to present a complete and comprehensive engineering functional analysis of each and every harvesting system employed in the field for agricultural food production. Furthermore, the variation in the degree of

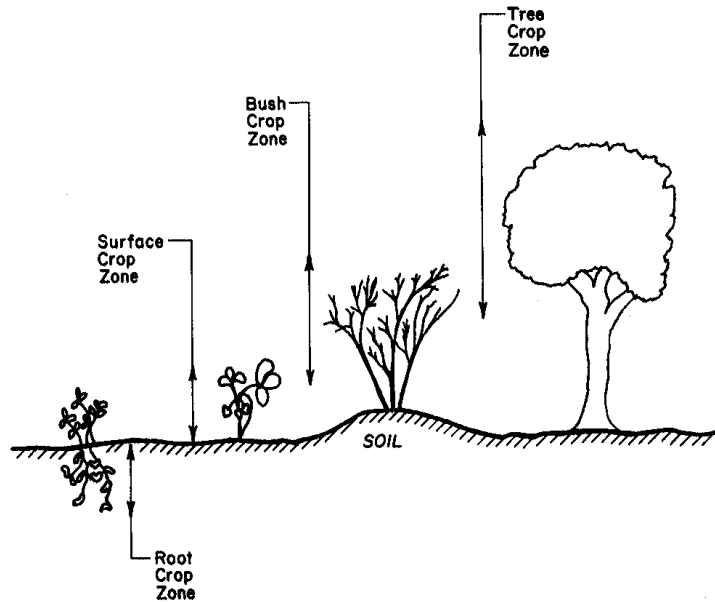


Figure 13.1 – Illustration of the generalized production zones of interest.

mechanization in specific commodities is based upon economic factors and the relative degree of difficulty in engineering machines to achieve the harvesting operations. However, several selected theoretical treatments of harvesting principles will be presented later in this chapter.

Recent U.S. Patent literature will be used to illustrate example harvesting systems and survey important harvesting components for each harvest zone. The principles utilized by these systems will be explained and functionally analyzed from an engineering perspective. O'Brien et al. (1983), ASAE (1984), Cargill and Rossmiller (1969), and Ag Eng 88 (1988) are four excellent references on the status of world wide mechanization in fruit, vegetable, and nut harvesting mechanization.

13.2.1 Root crops

Major root crops grown in the U.S. are carrots, beets for sugar, onions, peanuts, potatoes, and sweet potatoes. Minor root crops grown in the U.S. are radishes, rutabagas, and turnips. Each of these crops are grown in rows with the average in-row and between-row spacing being specific to each crop.

13.2.1.1 Bulk root crop harvesting

Potato harvesting is commercially achieved by bulk harvesting. Typically these machines unearth relatively large volumes of soil that contain the roots to be harvested. The machine, like that shown in Figure 13.2, is designed to separate these large volumes of soil from the potatoes. In principle this machine moves through a defined volume of soil and engages the product by virtue of the product position

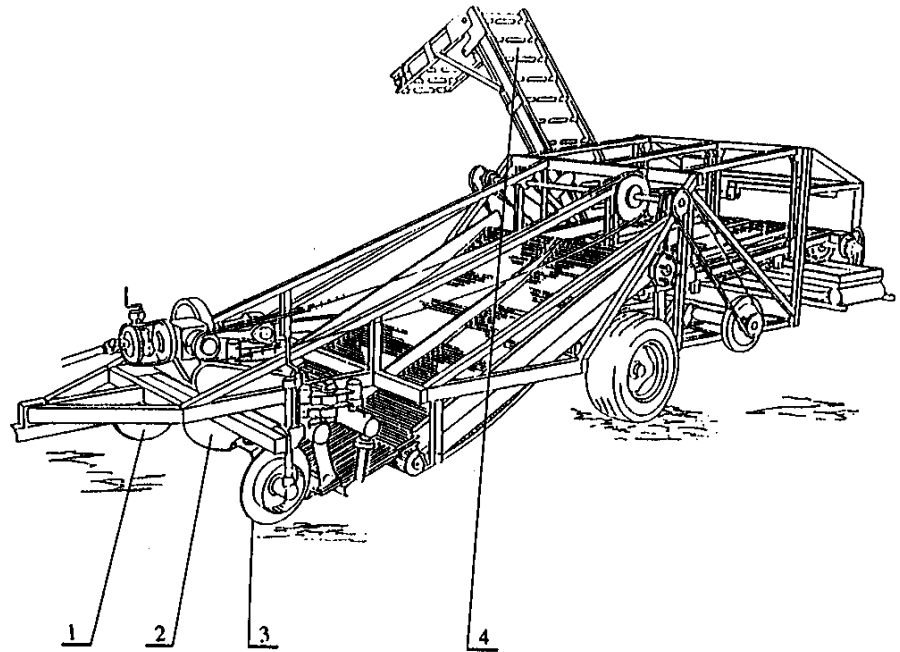


Figure 13.2 – Root crop harvester (U.S. Patent #4,560,008).

within the volume of soil being processed. The actual process volume in this two-row machine is defined by the horizontal shear plates (2) and the vertical shearing coulters (1 and 3). As the harvester moves forward, a defined mass of soil containing the potatoes to be harvested (as well as the surrounding soil and above-ground plant portions) enter the machine. In some cases the above-ground plant material is removed or harvested prior to the digging operation, similar to the method of green peanut harvesting illustrated later in this chapter.

Once in the machine, the primary function is to sort the potatoes from the soil, soil clods, and stones as gently and completely as possible. Machine elements are designed to remove the soil quickly with as little damage as possible and elevate (4) the clean potatoes into a storage and transport container (not shown) that is towed beside the machine.

13.2.1.2 Controlled root crop harvesting

Often root crops are harvested by initially engaging the above-ground portion of the crop prior to actually digging or engaging the root portion that is to be harvested. In Figure 13.3 the plants (P) with above-ground portions (F) and root portions (RC) are engaged before the soil lifter (1) uproots the crop. The concept is to gain control of the root crop by the tops and transfer that control to the elevator means (2) prior to actual digging. If the soil conditions are favorable at harvest, then the digger will fracture the soil such that the root crop is extracted free, or nearly free, of soil. In this machine the next function is to separate the unwanted tops from the desired root portion by the general means (4) shown in Figure 13.4.

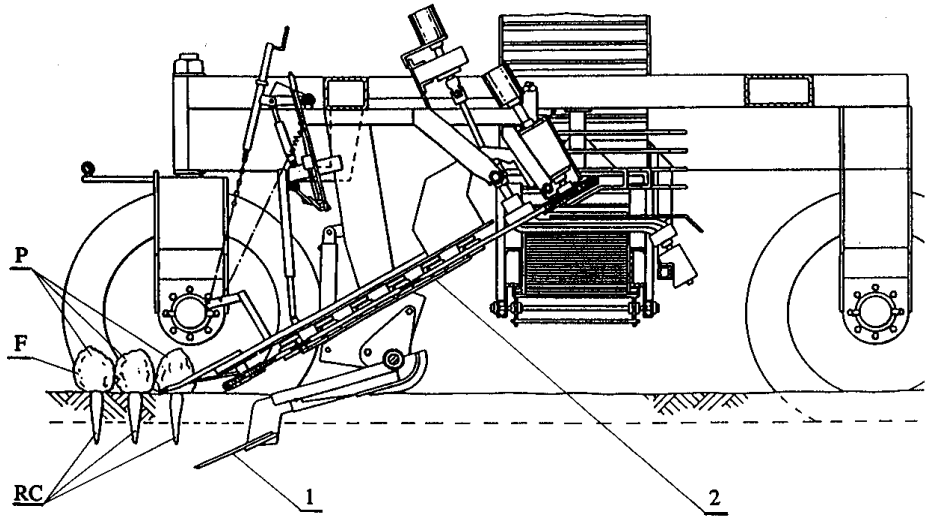


Figure 13.3 – Row crop harvester, side view (U.S. Patent #4,416,334).

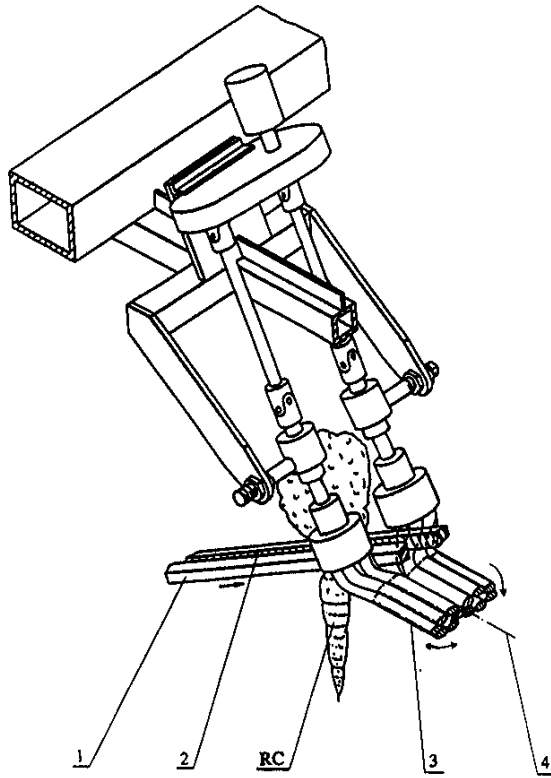


Figure 13.4 – Row crop harvester, side view (U.S. Patent #4,185,696).

In Figure 13.4 we see two important functions being implemented. Top removal is desired at the lowest point on the plant with respect to the top of the harvested root. The interior surfaces (2) of the elevating belts (1) grasp and continue to elevate the crop until the top portion of the root crop engages the counter-rotating toppers (3). This counter-rotation of the topper elements further ensures that the top of the plant is pulled up to the desired topping height. By adjusting the lateral clearance of the counter-rotating elements, top removal is achieved at a very uniform position with little top remaining on the root. This is the common method used for carrot harvesting.

13.2.1.3 Peanut harvesting

Peanuts are harvested commercially in a two-stage harvesting operation. At an optimum time the crop is dug from the ground and the complete plant with attached peanuts is inverted and left to air-dry on the soil surface. This operation is accomplished by a peanut digger/inverter as shown in Figure 13.5. The initial functions performed by the peanut digger/inverter are the same as the bulk potato harvester. A volume of soil, containing the peanuts with the attached above-ground portions, is engaged by a series of disk coulters that are strategically positioned. In Figure 13.5, the initial four coulters on each row serve to loosen and break the soil away from the peanuts. The final pair of opposing coulters (1) is designed to provide an elevation and inversion of the peanut plant while depositing the plant mass on windrowing and soil separating finger-like elements at the rear end of the machine. In this machine, the PTO (power-

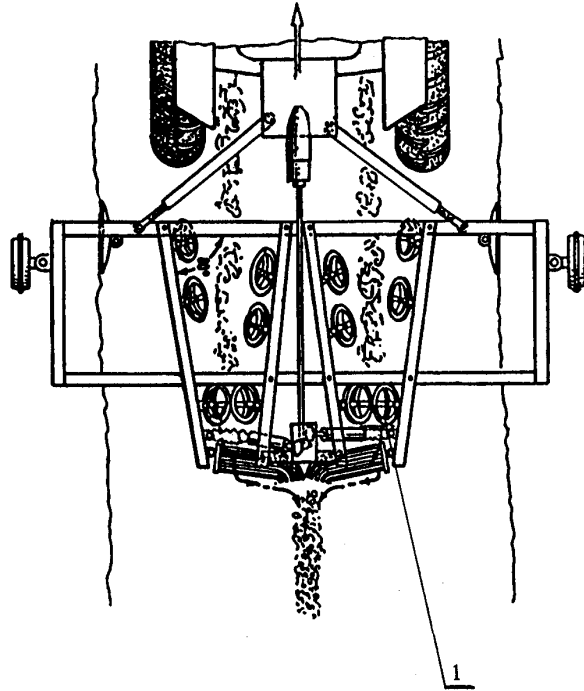


Figure 13.5 – Peanut digger/inverter, top view (U.S. Patent #4,934,461).

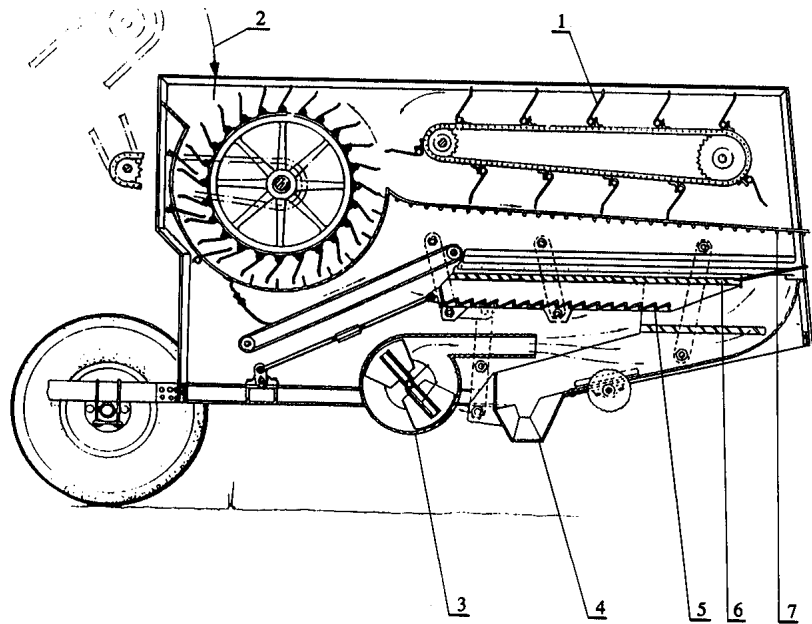


Figure 13.6 – Green peanut combine, side view (U.S. Patent #4,166,505).

take-off) is used as a source of energy to vibrationally excite the separating elements to increase their separation effectiveness and assist in moving the plant material toward the central windrow position. When the peanut moisture has been sufficiently lowered, a peanut combine (similar in function to a windrow grain combine) is used to move through the field and thresh (separate) the peanuts from the plant stem material. The functional elements of this combine are further illustrated in the green peanut harvester shown in Figure 13.6.

In some cases it may be desirable to harvest the green peanut tops for animal forage. A forage harvester is used to chop the tops and blow the chopped material into a trailing wagon. Without the tops, the peanuts must be dug immediately, since they will deteriorate rapidly if left in the ground. In this case, the green peanut combine must also possess the functionality of a root crop harvester in addition to the threshing and separation functions of a grain combine as shown in Figure 13.6. This detailed view shows how the dug plants with attached peanuts are introduced at the arrow (2) into the concave separation cylinder assembly that rotates about an axis. The tooth/tine arrangement of this threshing device is designed to remove the green peanut containing pods from the plant peg material while minimizing damage to the pods. The entire mass of threshed material is moved across a stationary screen grid (7) by the positive action of tines (1). Further separation is achieved with shakers (5 and 6), similar to straw walkers in grain combines, and a fan (3). Finally the cleaned pods are collected in conveyor means (4) where they are elevated to the storage and transport element of the machine.

13.2.2 Surface crops

Major surface crops grown in the U.S. are beans (bush and dried), low-bush blueberries, cabbage, celery, cranberries, cucumbers, lettuce, peas, strawberries, sweet corn, and tomatoes. Minor surface crops grown in the U.S. include artichokes, asparagus, broccoli, cauliflower, eggplant, peppers, spinach, squash, and several types of melons.

13.2.2.1 Cabbage harvesting

As seen earlier, root crop harvesting attempts to selectively remove the desirable root portion of the crop from the tops. In the case of cabbage harvesting, the reverse is true. The functional elements of the harvester are quite similar. Again the once-over harvest is initiated by the engagement of feed roller means (1 and 2) in Figure 13.7. These rollers have helical spiral elements on their surface to provide a component of controlled motion in the horizontal direction parallel to the forward travel of the machine. This requires synchronization between this forward motion component and the travel of the machine. This machine would normally be powered with a tractor that has a ground-synchronized PTO shaft or the feed roller elements could be driven by a ground wheel such as 3 or 5.

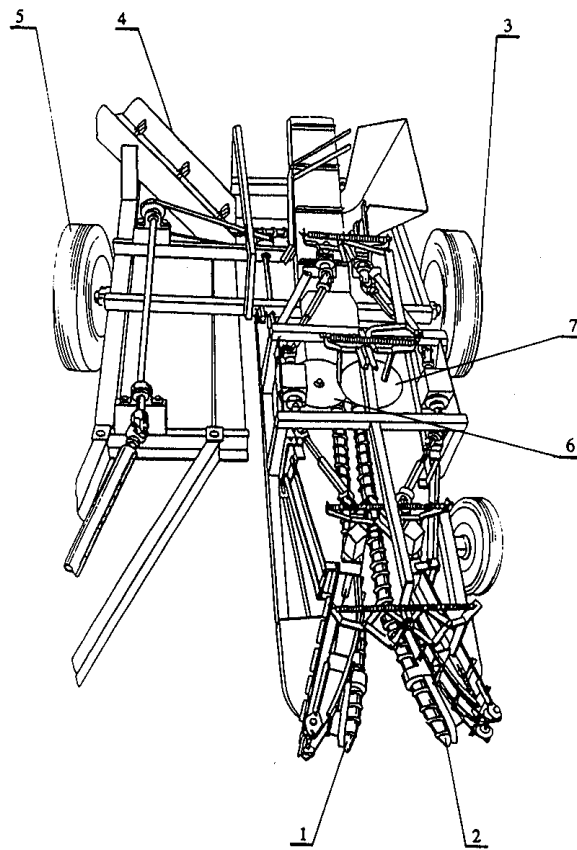


Figure 13.7 – Cabbage harvester (U.S. Patent #3,858,660).

The elevation of the rollers increases as the cabbage plant moves toward the rear of the machine. Two actions occur. The resistance of the plant to being pulled up by the roots causes the cabbage head and lower leaves to seat down against the rollers until the resulting seating force is sufficient to begin to remove the plant root system from the soil. Complete uprooting of the plant is undesirable since the restraining force of the roots is essential to maintaining proper head position. The counter-rotation of the engagement rollers with the stem contact surface moving downward also keeps the heads properly seated as they approach the disk cutters (6 and 7). The severed heads are transferred to the elevator (4) for transport to the storage and transportation means.

13.2.2.2 Tomato harvesting

Tomato harvesting by machines is a well-established practice in the industry for tomatoes that are destined to be processed into canned or frozen products. In general these harvesters will move over the crop only one time. The entire plant is harvested so uniform fruit maturation is very important. The harvest begins in Figure 13.8 with coulters (1) and a subsurface root cutter (2). Elevating means raise the harvested plants with the attached tomatoes while removing all remaining soil. At the top of the machine the pairs of counter-rotating rollers (4 and 5) pull the vines downward and rearward toward the walker-shaker assembly (6). The separated tomatoes are collected in a series of conveyors and deposited by conveyor (3) into the field bins.

On some field tomato harvesters the sorting is fully automated, with electronic systems that sort the tomatoes by color for stage of maturity. Immature tomatoes are left in the field.

Mechanically harvesting tomatoes for the fresh market is functionally identical to harvesting for the processed market, except that mechanical damage must be reduced. Designing machines that minimize bruising and scraping during the harvesting operations is much more difficult. On these harvesters all tomato contact surfaces must be covered with soft and resilient materials to protect the tomatoes from damage.

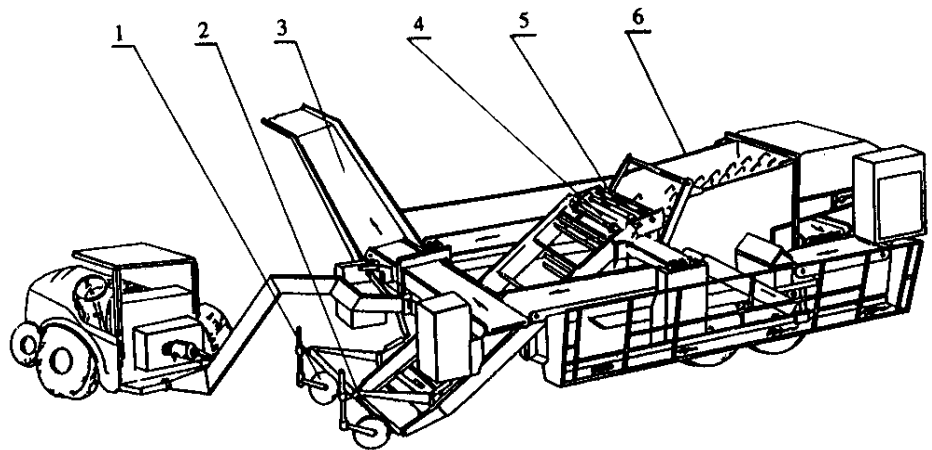


Figure 13.8 – Tomato harvester (U.S. Patent #4,584,826).

13.2.2.3 Strawberry harvesting

Mechanical harvesting of strawberries has received considerable attention over the years. Modification of cultural practices appears to be an important factor in moving towards mechanized systems. Figure 13.9 shows an integrated approach to strawberry production that begins with proper field site location. Postharvest practices are also important in preparing the plants for the next year's crop. Clearly the machine designed must rely on certain of these cultural practices to assure that the crop at the time of harvest will have the required properties. For example, the location of the strawberries will be greatly affected by site selection, weed control, variety selection, plant density, fertilization, irrigation, and moisture control. This machine must have a uniform, solid mass of plant and strawberry material to harvest at one time.

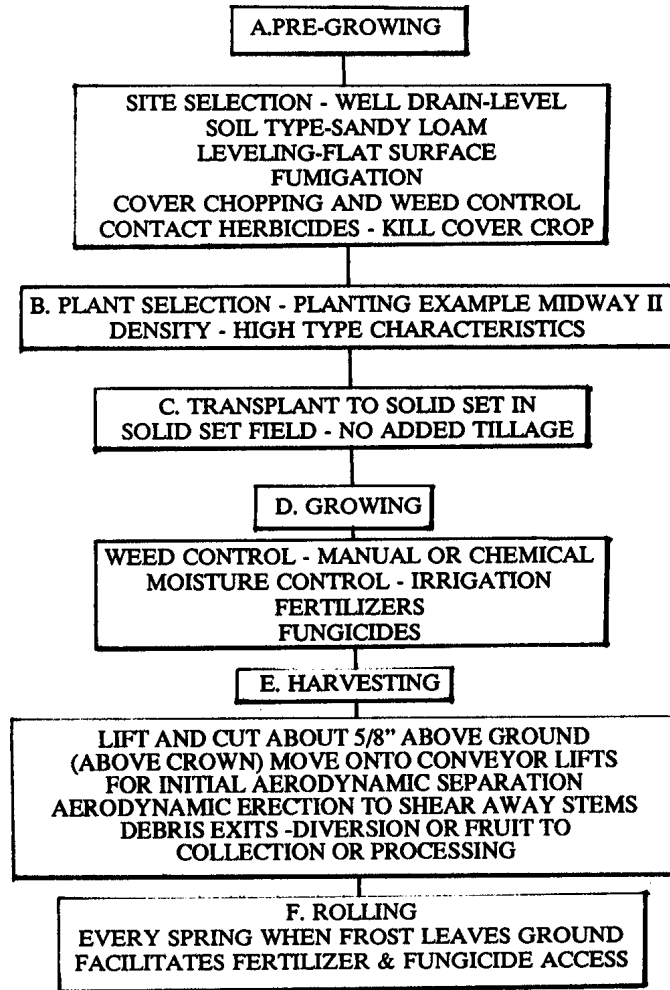


Figure 13.9 – Strawberry harvesting, cultural practices (U.S. Patent #4,519,191).

The powered reel and cutter means at the right end of the machine in Figure 13.10 cuts the plant material just above the surface of the ground (4). The entire mass of plant stems, leaves, and strawberries is elevated into the initial air separation means which are more clearly shown in Figure 13.11. The single leaves and lightest material are blown out the discharge chamber (1). The berries and attached material are heavier and fall to the conveyor means (5). This conveyor moves the plant material over two upwardly directed air blasts from fans (6) as shown in Figure 13.12. The upward air velocity is carefully selected to aerodynamically orient the berries and stems for the cutter assemblies (2 and 3) to clip the stem and leaf material from the berries.

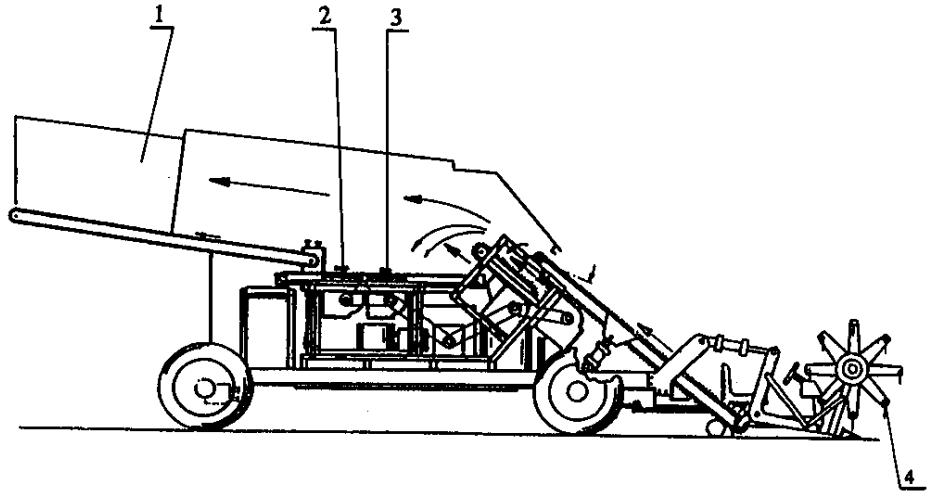


Figure 13.10 – Strawberry harvester, side view (U.S. Patent #4,519,191).

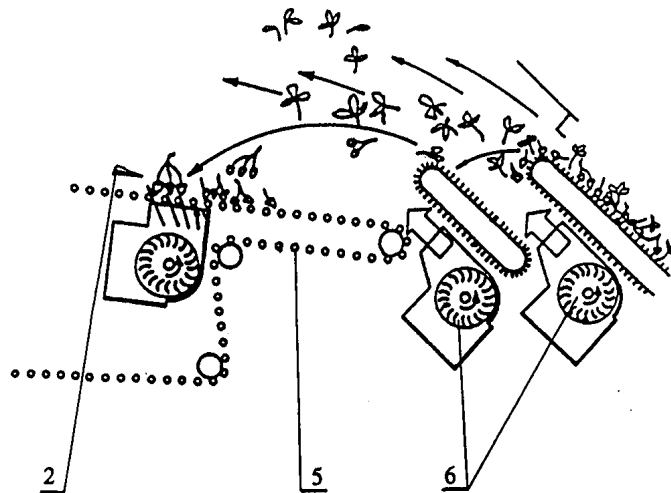


Figure 13.11 – Strawberry harvester, air cleaning (U.S. Patent #4,519,191).

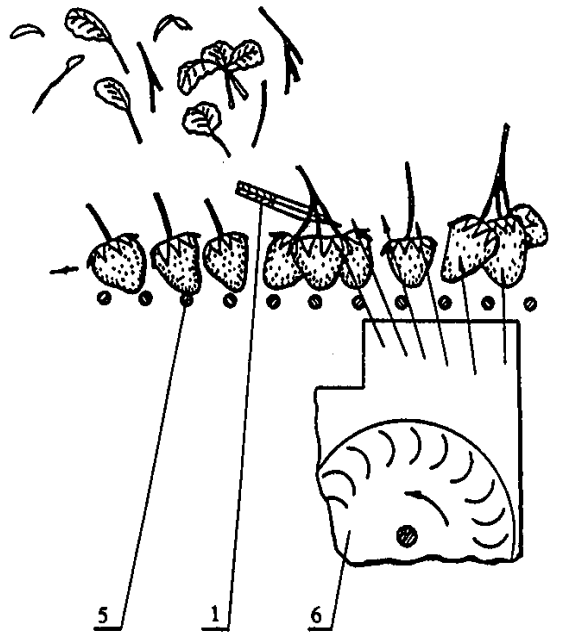


Figure 13.12 – Strawberry harvester, stem removal (U.S. Patent #4,519,191).

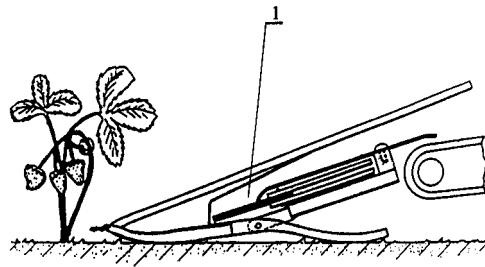


Figure 13.13 – Strawberry harvester, plant cutting (U.S. Patent #4,519,191).

The successful operation of a once-over harvester of strawberries (for that matter, any one-over harvester) is a function of many factors. Clearly the ability of the machine to engage and cut all the material as close as possible to the soil surface is crucial. This fact is shown in a relative way in Figure 13.13 where the relative distances are realistic and illustrate the need to sever each and every plant at the soil surface. The cutter knives (1) are often within 1 to 1.5 cm of the soil surface.

Another strawberry harvesting machine attempts to assist the lifting of the plant material into the cutters with opposed and intersecting air streams as shown in Figures 13.14 and 13.15. Again, the important aerodynamic properties of lift and drag influence the operational success of this harvesting principle.

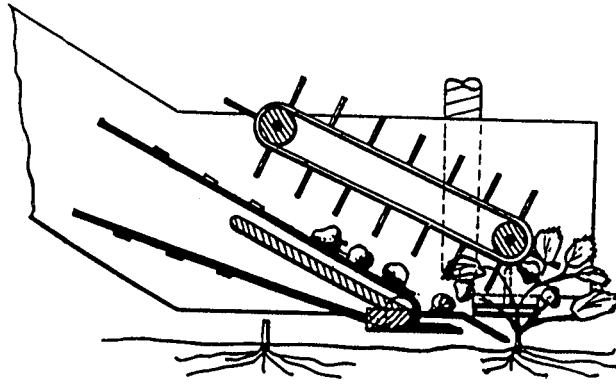


Figure 13.14 – Strawberry harvester, air pickup, side view (U.S. Patent #3,964,245).

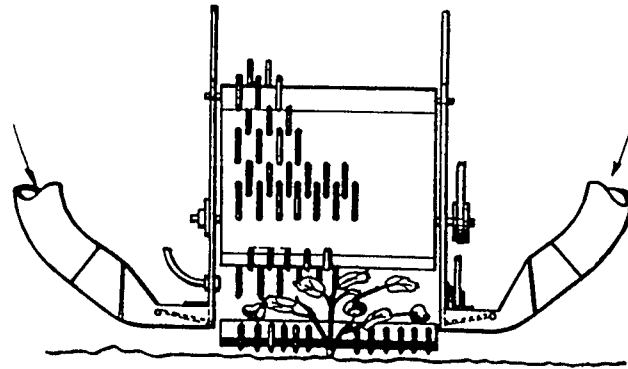


Figure 13.15 – Strawberry harvester, air pickup, front view (U.S. Patent #3,964,245).

13.2.3 Bush and trellis crops

Major bush and trellis crops grown in the U.S. are blueberries (high-bush), boysenberries, grapes, pineapples, and table grapes. Minor bush and trellis crops grown in the U.S. are blackberries, black raspberries, coffee, currants, dewberries, kiwifruit, loganberries, marionberries, okra, red raspberries, and youngberries.

13.2.3.1 Grape harvesting

Worldwide a large percentage of grapes harvested for processing purposes are harvested by machines. A number of types of trellises are used for different varieties and in different growing areas. Functionally, grape harvesting is a machine operation in which the fruit is shaken from the vines and caught as it falls. Conveyors transport the collected fruit from the catching surfaces to the air-blast cleaners and then into the field transport and storage bins. This basic functional harvesting approach has been used for many years. The design engineer is always interested in improving the performance or efficiency of these basic functional components, which is the subject of the remainder of this section.

The overall harvesting effectiveness of shake-catch method is adversely affected by the trailing grape vines that originate from the cordon (trellis) wires and generally overlay the grape bearing positions of the vines. One approach to reduce this effect is shown in Figures 13.16 and 13.17, in which the inclined rods (1) at the front of the harvester are positioned to lift the trailing vines up and out of the way of the subsequent beaters (2). This improves the effectiveness of the beaters. Furthermore, if the trailing vines are not lifted, then they have a tendency to form a shielding curtain that encourage the detached grapes to fall in a vertically downward direction. Ground losses are normally highest around the vine trunks and trellis support posts, as we will review in the next section.

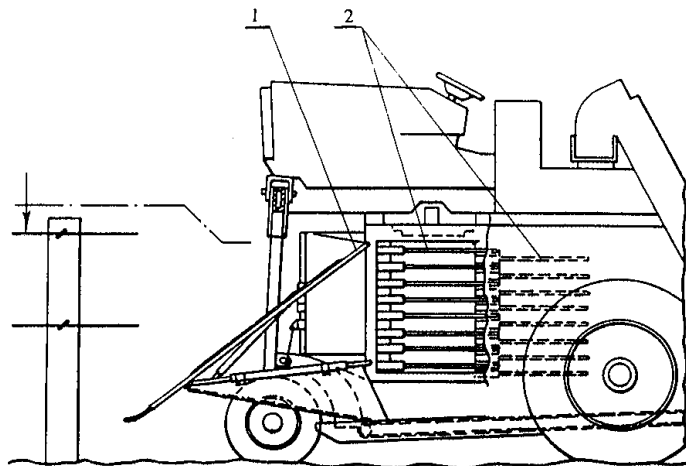


Figure 13.16 – Grape harvester with cane lifter, side view (U.S. Patent #4,251,983).

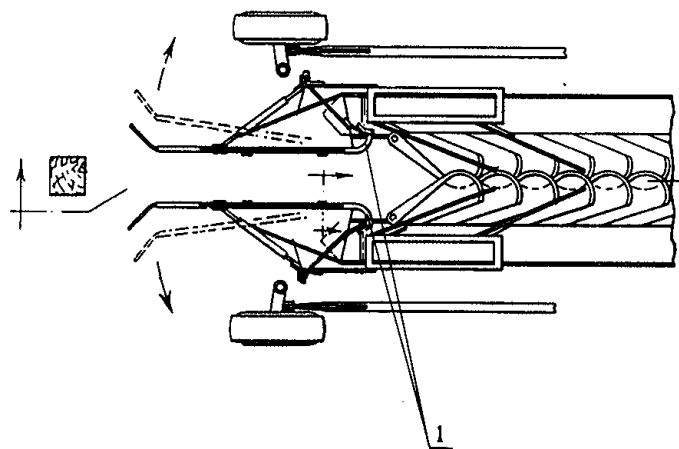


Figure 13.17 – Grape harvester with cane lifter, top view (U.S. Patent #4,251,983).

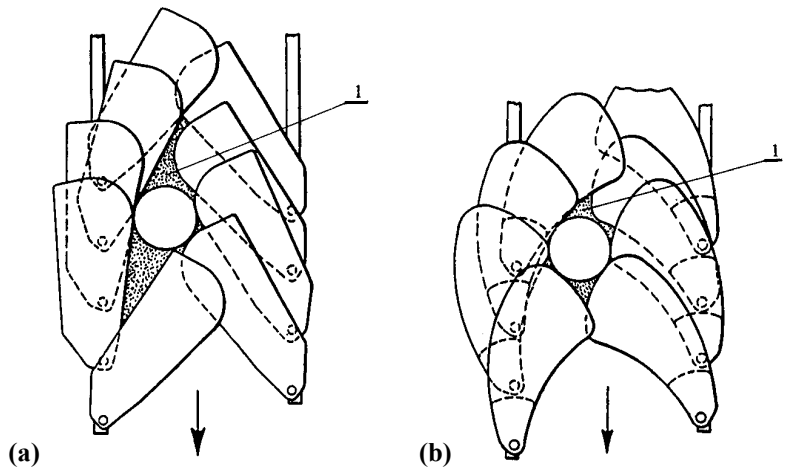


Figure 13.18 – Fruit collector construction, (a) prior art, (b) improvement (U.S. Patent #4,464,888).

13.2.3.2 Fruit catchers

Forming a catching surface below the shakers is normally accomplished with a series of overlapping plates as shown in Figure 13.18a. As the harvester moves forward, the spring-loaded plates, while maintaining contact with the stationary vine trunk or post, rotate open and closed to form a catching surface. Clearly the area (1) is not covered so falling fruit will be lost to the ground. It is possible to improve this functional arrangement by modifying the shape, or number of plates used as shown in Figure 13.18b. Here we see that the relative geometry of Figure 13.18a has been substantially improved by a reduction of the uncovered area (1) in the improved design.

13.2.3.3 Shakers

The interaction of machine elements with plant materials has many important results. Shakers or beaters that are used to remove grapes are subject to cyclic stresses that cause fatigue failures of the beater rods and drive components if not properly designed. It is important to realize that the plants are also subjected to mechanical and physiological stresses that result from the actions of the shakers or beaters. Tissue damage from impacts can reduce future crop productivity.

Shaking systems have been devised that are internally force-balanced to reduce machine element fatigue as shown in Figure 13.19 (see also Figure 13.20). In this embodiment, the shaker mechanism is located vertically above the single wire vertical cordon while the shaking action is imparted to the trellis/vine system by bars (4 and 5). Catching surfaces and conveyors (3) are strategically located below to receive the falling fruit. The entire arm assembly (2) with positioning means (6) is supported as a four-bar linkage by the two vertical links (1).

The isometric view (Figure 13.20) shows clearly the front and rear four-bar linkage assemblies. The horizontal component of force-balance shaking is achieved by synchronously rotating two masses (8 and 8') in one direction while simultaneously and synchronously rotating two additional masses (7 and 7') in the opposite sense. Thus, primary vertical force balance is achieved.

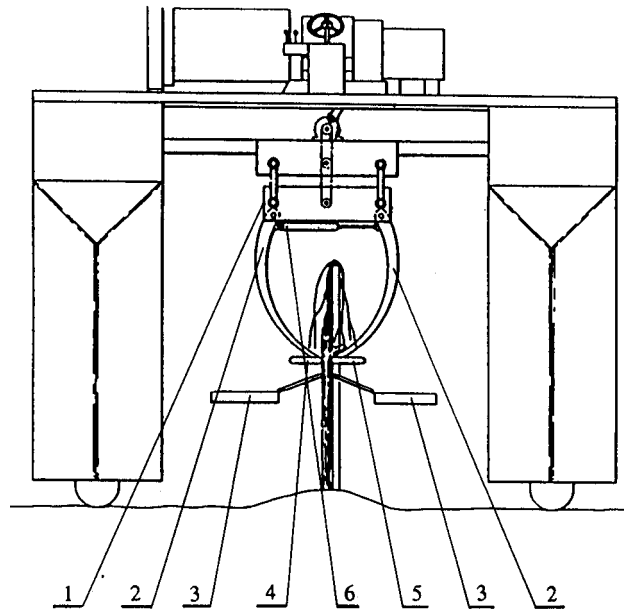


Figure 13.19 – Horizontal force-balanced shaker, front view (U.S. Patent #4,793,128).

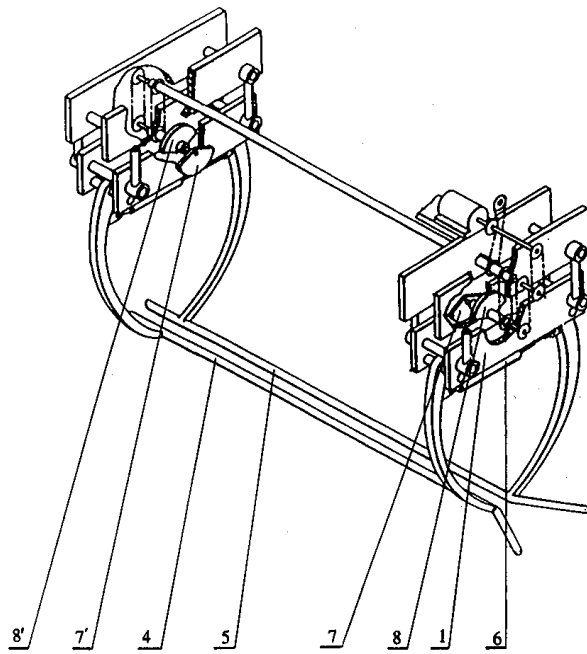


Figure 13.20 – Horizontal force-balanced shaker, detailed front view (U.S. Patent #4,793,128).

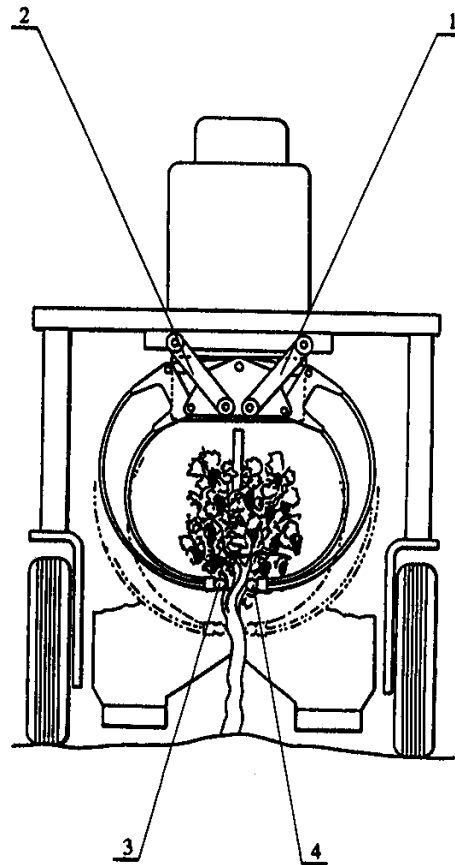


Figure 13.21 – Oscillatory shaker, general front view (U.S. Patent #4,621,488).

The concept of force balancing can be achieved by many mechanisms. A second example is shown in Figure 13.21. This shaker interacts with the vines in a manner functionally identical to the previous example. However, the four-bar linkage with non-parallel links (1 and 2) introduces a virtual rotation point for the shaker action. This has the effect of amplifying the displacement of the vine contact bars (3 and 4).

In this second example, the method of generating the force-balanced shaking component can be seen more easily by examining Figures 13.22 and 13.23 as orthographic top and left side views, respectively. Two masses (2 and 3) rotate on a common shaft in the counter-clockwise sense while at the other end, two masses (4 and 5) rotate on a common shaft in the opposite sense. The direction of travel is from the left of these figures to the right and the resulting unbalanced rocking force is imparted to the plant materials via the arm assemblies (1 and 6).

Shakers or beaters are often comprised of a rod-like structure that is fixed and actuated from one end like those shown in Figures 13.16 and 13.17 as pivotally mounted

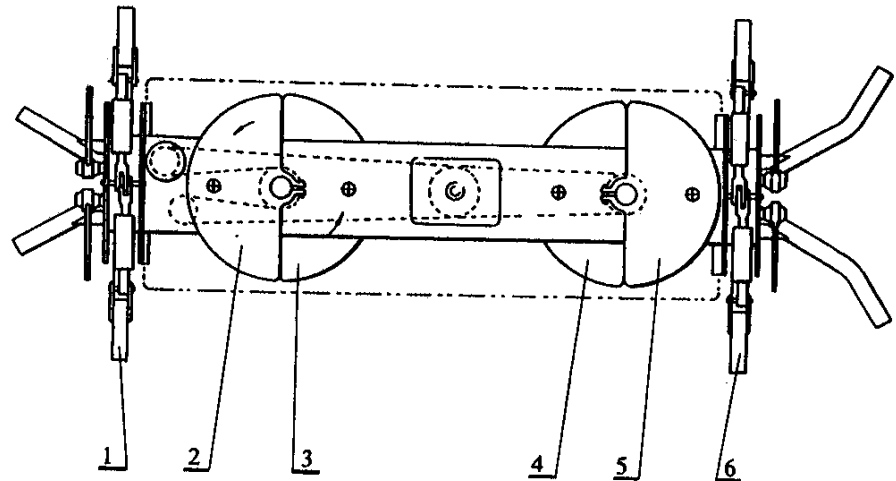


Figure 13.22 – Oscillatory shaker, detailed top view (U.S. Patent #4,621,488).

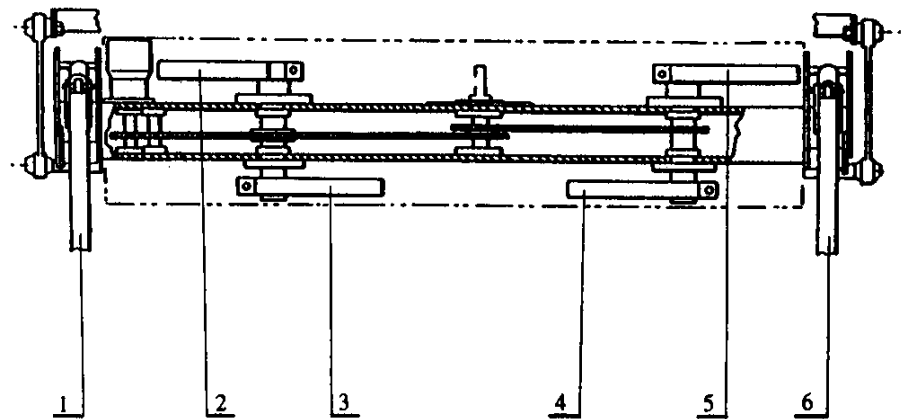


Figure 13.23 – Oscillatory shaker, detailed side view (U.S. Patent #4,621,488).

rods (1) that oscillate through a relatively small arc and strike the plant material. This type of mechanism will generate whip-like internal vibrations that may produce substantially higher impact velocities as indicated by harmonic design.

One side of a grape harvester shaker design that restrains the displacement of both ends of the impact rod, and overcomes this high whip-like impact velocity, is shown in Figure 13.24. The lead ends of the shaker rods are fixed in common to a member (2) that is pivotally mounted on an axis (3), which is, in turn, excited by a bell crank (1) four-bar linkage. The trailing ends of the beater rods (4) are restrained in displacement but not in moment. The eccentric drive (5) sets the beater rods into a standing wave oscillation pattern. This design reduces impact damage potential while increasing the forward travel speed of the harvester.

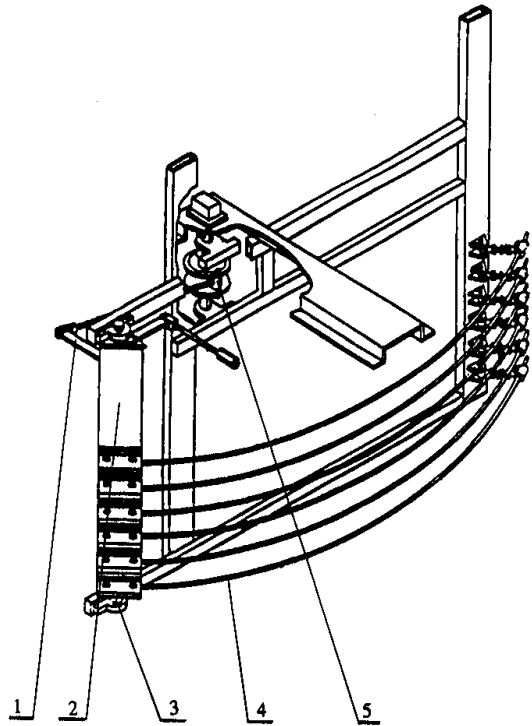


Figure 13.24 – Oscillatory shaker, top view (U.S. Patent #4,769,979).

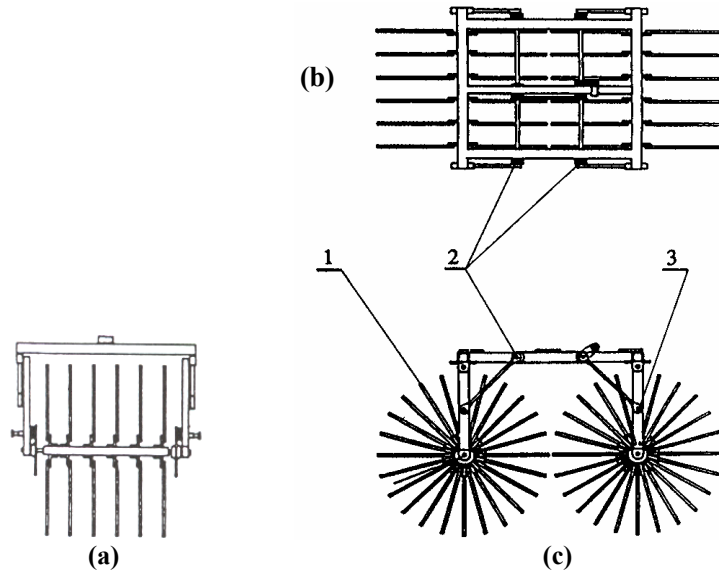


Figure 13.25 Shaking mechanism, (a) front view, (b) top view, (c) side view (U.S. Patent #4,860,529).

Three orthographic views of a bramble harvesting shaker are shown in Figure 13.25. Eccentrics on synchronously rotating shafts (2) cause the diagonal braces to oscillate the vertical support arms at point (3) as well as the spiked bush impact drum assemblies (1) in force-balance. The fruit harvesting spikes in the 4 o'clock-8 o'clock positions in Figure 13.25c are moving with relatively uniform horizontal displacement, a significant functional advantage of this mechanism. Each spike drum is free to rotate through the plant material as the harvester moves forward. A rotational ratchet system restricts any reverse rotational component thus ensuring that a positive displacement of impacted material will occur in one direction.

13.2.4 Tree crops

Major tree crops grown in the U.S. are apples, apricots, avocados, cherries, citrus of several types, peaches, pears, pecans, and plums. Minor tree crops grown in the U.S. are almonds, dates, figs, filbert nuts, macadamia nuts, olives, and walnuts of several types.

13.2.4.1 Tree harvesters

The mechanical harvest of edible tree crops has been of interest to engineers for a number of years. Many factors influence the degree of success of these attempts to harvest by machine. The structure, size, and shape of the tree is important. Apple trees are quite different from date palm trees. The relative durability of the harvested crop is no less important. Peaches are much more subject to bruising damage than pecans. Finally, the relative value of the individual harvested unit is indicative of the revenue that is available to mechanize the harvest. The value of a single red tart cherry for processing is small compared with the value of a freshmarket orange. In short, the revenue that can be applied towards mechanization of any commodity is a complex issue. The important feature is that the general trends outlined above can provide

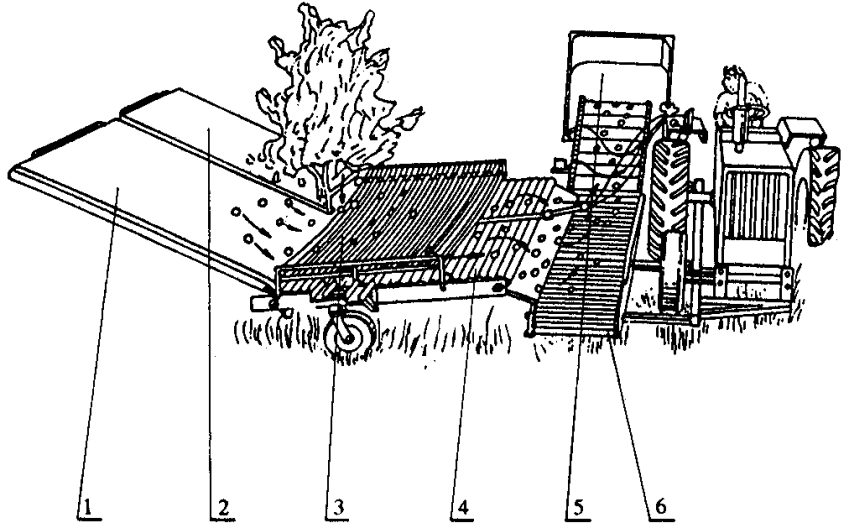


Figure 13.26 – Tree fruit harvester, extended (U.S. Patent #3,896,612).

initial insight and guidelines into the realistic expectations of providing mechanized harvesting systems.

Certain tree crops lend themselves to whole tree harvesting one or more times a season by mechanical means. Figure 13.26 illustrates a harvester for trees that provides for a catching surface (1 and 2) that can be positioned within the row by a tractor and deployed across the row to form a complete catching surface beneath the tree canopy. The inclined surfaces, after deployment, collect the harvested fruit by gravity means while the decelerator strips (3) protect the fruit from directly impacting the collector means (4) that transfers the fruit to the transport conveyor (6) and then into the bulk storage and transport bin (5). The mechanisms used for shaking the tree to cause fruit release will be addressed in the following sections.

13.2.4.2 Tree shakers

In general, harvesting tree fruits by shaking the tree requires the transfer of relatively large amounts of energy into the tree structure. Application of this energy is achieved with trunk or limb shakers that attach to the pertinent tree member. The nature of the connection between the tree and the vibrator has evolved over many years. The application of shear stress to the bark must be avoided since “slipping” the bark can cause sufficient damage to kill the tree outright, or may accumulate over the years if the tree survives in a weakened state. The importance of proper design and operation of the shaker assembly is essential if tree crops are to be harvested successfully.

Eccentric rotating masses are used almost exclusively in tree shaker designs. Since these are inertial shaker designs, it should be clear that the resulting amplitude of shake is related to the relative mass of the rotating inertial shaker mass and the mass of the shaken tree or branch. The frequency of shake is also important, but is usually much easier to monitor and control.

There is also a practical operational matter to be considered with tree shakers. If the eccentric displacement is fixed, then it is necessary for the shaking frequency to be zero while the shaker is attached or clamped to the tree. Additional time is required since the shaker must then be brought up to the desired operational shaking frequency. During this acceleration process, undesirable and potentially damaging low frequency structural harmonics may be excited within the tree. It is therefore important to have shakers that can be operated at one frequency with variable amplitudes of force.

Figure 13.27 shows a rotating mass (1) that, in the position shown in the figure, has its center of gyration coincident with the axis of rotation of the shaft (2). The eccentricity is controlled by a hydraulic cylinder (3). Synchronous combinations of this shaker can be used to force-balance in a manner similar to the grape-shaking systems examined earlier in this chapter.

In harvesting nuts and citrus for processing, it is common to shake the crop onto the ground for subsequent collection by a machine in a second field operation. Thus, tree shakers are used alone as shown in Figure 13.28. Of more interest, this shaker can produce different patterns of shaking displacement, subject to the understanding that the resulting displacement of all inertial shakers is a function of the mass and resonant structural vibrational characteristics of the tree being shaken. Figure 13.29 illustrates three co-axial mounted eccentric masses that can be rotated in either direction and at independently selected speeds.

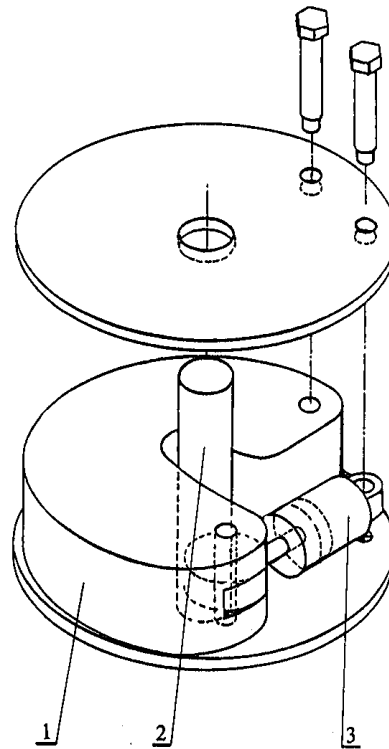


Figure 13.27 – Variable eccentricity mass shaker (U.S. Patent #4,776,156).

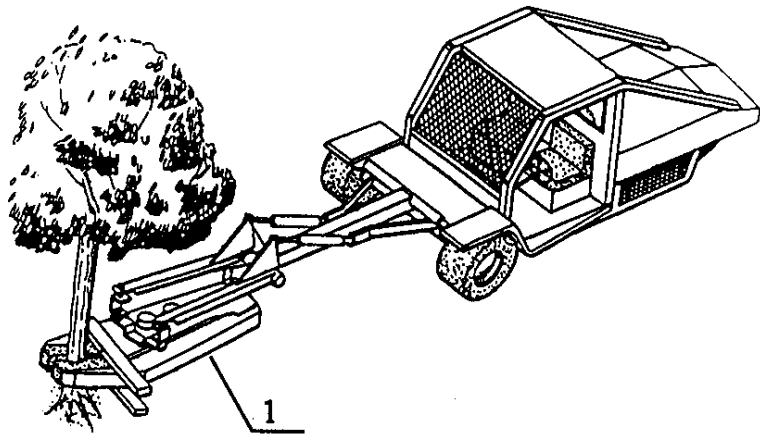


Figure 13.28 – Multi-pattern mass shaker (U.S. Patent #4,409,782).

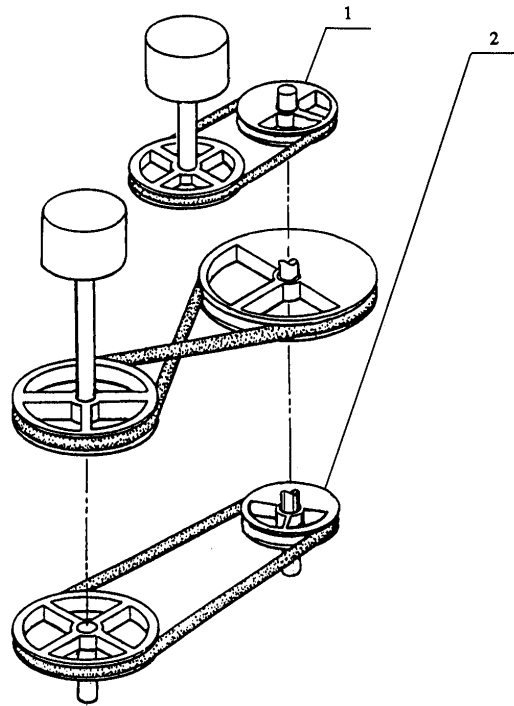


Figure 13.29 – Multi-pattern mass shaker, isometric (U.S. Patent #4,409,782).

13.2.4.3 Pick-up systems

The functional requirements of ground collection systems like the one shown in Figure 13.30 include product engagement and control elements. Once the product is elevated into the harvester, air is used to remove the lighter trash from the product. Careful attention to the mechanics of aerodynamic cleaning is shown in Figure 13.31. A combination of high air velocity in the principle flow path as well as an alternating gradient in the conveyor assures that all light material is removed. Products that are inadvertently entrained into the air stream have an opportunity to fall back out before entering the fan. This system has no means for separating stones or heavier material from the product.

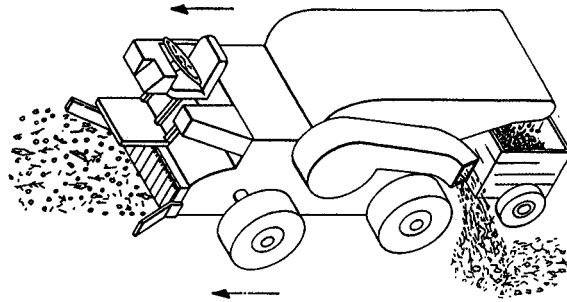


Figure 13.30 – Nut gathering machine (U.S. Patent #4,364,222).

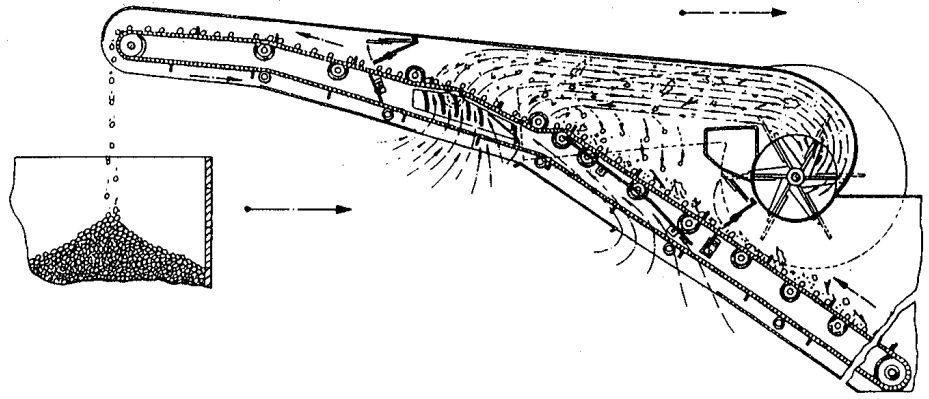


Figure 13.31 – Nut gathering machine, side view (U.S. Patent #4,364,222).

13.2.4.4 Automatic tree harvesters

The advances in computer technology and vision systems have led to the development of field systems that are functionally capable of unattended operation in well-established orchards, harvesting single fruits at a time and carefully placing the harvested fruit into the storage bin. Functionally, these systems are operationally similar to manual labor. Television cameras view the tree with harvestable fruit and computers process the images to determine which fruit to pick. As shown in Figure 13.32, the computers then control the robotic arm with a vacuum gripper (2) that rotates to detach the fruit (1). The machine is self-propelled between the tree rows. The machine senses the position of the tree and stops to pick the fruit. At the end of the rows, the machine is computer-controlled to loop back into the next row middle and continue fruit picking operations. The only human interaction would be a forklift operator who removes filled bins of fruit and replaces them with empty bins.

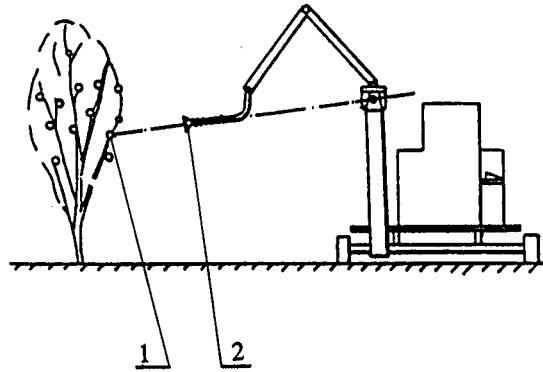


Figure 13.32 – Automatic fruit harvesting machine (U.S. Patent #4,975,016).

13.3 THEORETICAL CONSIDERATIONS

Several principles have been successfully utilized in solving mechanization problems in fruit, vegetable, and nut harvesting. Appropriate engineering analyses are often used to explore the feasibility of a possible design solution or understand why an existing machine element or process functions. In each section that follows, important problem conditions are stated along with the necessary assumptions for the theoretical analyses and definitions of all engineering variables.

13.3.1 Aerodynamic concepts

Often it is possible to effect an operational result based upon one physical parameter by implementing another. This concept is useful and effective as long as a high correlation exists between the operational property and the desired result. For example, the size of an object is often used to effect a separation of product by mass. Similarly, the color of product is used to indicate ripeness or maturity. The choice of physical property to utilize in the machine function is dependent upon several factors. First is the relative ease of implementation. It is much easier to subject products to sizing by falling through a dimensionally controlled opening, than to effect a mass balance measurement of each item. Secondly, the two properties must be in fact significantly related. In some cases this relationship is functional as in the case of physical size and weight where the product density is known to be constant or nearly constant. Thus, it is a common and accepted design practice to utilize a strongly related property to effect a unit operation based upon another property.

13.3.1.1 Aerodynamic properties of strawberries

Cleaning the leaves, severed stems, straw, and other lightweight trash from harvested strawberries depends upon being able to introduce the unsorted materials into an air flow field that has an average flow velocity component lower than the relative terminal velocity of the berries, but higher than the relative terminal velocity of the lighter materials.

Terminal velocity in air (V_t) is defined as the maximum free-falling velocity that is achieved by a body subject to gravitational acceleration. Relative terminal velocity in air (V_r) is defined as the velocity of air in a uniform flow field that, when directed vertically upward, will suspend or “float” a body that is subject to gravitational acceleration. Thus, the free-falling terminal velocity of a strawberry will be different from the average upwardly directed air velocity necessary to suspend a berry in mid-air within that flow field. The preferred units for both terminal and relative terminal velocities are meters per second.

In practice, terminal velocity can be measured by determining the time of free-fall from a given height as determined by Equation 13.1 (Bilanski et al., 1962):

$$S = \frac{V_t^2}{g} \ln \left[\cosh \left(\frac{g t}{V_t} \right) \right] \quad (13.1)$$

where S = free-fall distance, m

V_t = terminal velocity in still air, m/s

g = gravitational acceleration, 9.807 m/s²

t = time to free-fall a distance S , s

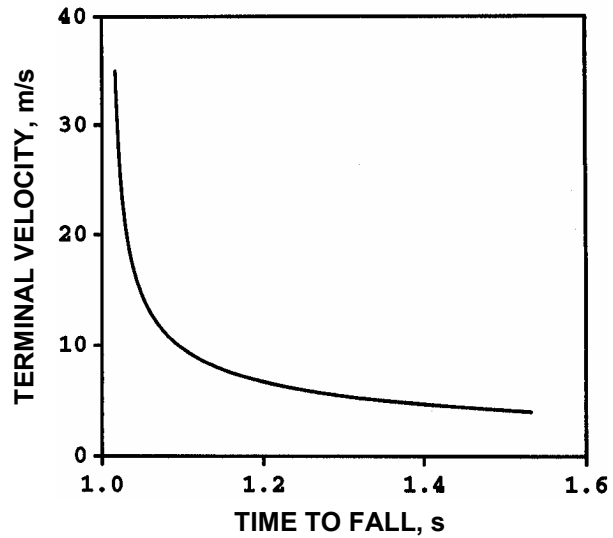


Figure 13.33 – Relationship between the terminal velocity of an object and the time to fall for a given drop height (Bilanski et al., 1962).

Equation 13.1, for a free-fall height of 5 m, is shown graphically in Figure 13.33. If the terminal velocity exceeds about 15 m/s, then the drop height must be increased above practical limits. Alternatively, the relative terminal velocity must be considered by establishing an airflow field with an average velocity that suspends the body. Often this process is complicated by the fact that the suspended body rotates or otherwise becomes unstable, thus making experimental observation of relative terminal velocities difficult.

The factors affecting the relative terminal velocity are the berry mass and the drag coefficient. The drag coefficient is a function of berry shape, size, and surface characteristics, as well as the Reynolds number of the fluid flow field. DeBaerdemaeker and Segerlind (1974) combined the technique of free-falling time measurement with a flow field that had an average upward velocity somewhat less than the terminal velocity of

Table 13.1. Regression analysis coefficients for relative terminal velocity (V_r) as a function of strawberry mass (m) for various maturities.

$V_r = a + b m^{0.5}$			
Maturity	Mass, g	a	b
Green	1–11	9.52	2.51
White	2–12	10.18	2.52
White-pink	2–16	10.43	2.39
Pink	2–16	11.18	2.16
Red	3–19	11.98	1.92
Overall	1–19	10.08	2.53

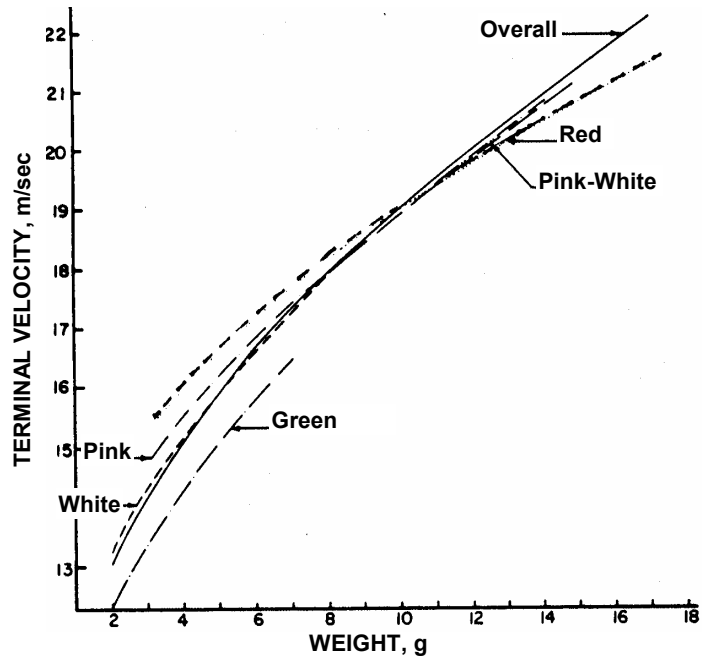


Figure 13.34 – Terminal velocity of strawberries by mass for five color groups (DeBaerdemaeker and Segerlind, 1974).

the body to be measured. Thus, they were able to experimentally determine the relative terminal velocities of strawberries as a function of mass as given by:

$$V_r = a + b m^{0.5} \quad (13.2)$$

where V_r = relative terminal velocity, m/s

a, b = coefficients from Table 13.1

m = mass of individual berry, g

Table 13.1 gives the values of the coefficients a and b that were derived from experimental data and these computational results are shown in Figure 13.34. Clearly seen in this figure, the stage of ripeness has much less effect on relative terminal velocity than does the berry mass. With the exception of the green berries, little effect can be seen due to stage of ripeness.

13.3.1.2 Aerodynamic properties of blueberries

Low-bush blueberries are harvested by stripping the plants using either hand-held rakes (combs) or by a mechanized system of rakes. Both methods require removal of trash and leaves, which is most often achieved with the use of a vertical, upwardly directed air stream. If the mean velocity of the air stream is somewhat less than the relative terminal velocity of the berries, then the lighter trash with a lower relative terminal velocity will be removed. Since blueberries are nearly spherical, the drag coefficient can be expected to be nearly constant at 0.44 for fully developed turbulent

flow ($N_{Re} > 103$). Soule (1970) reported mean drag coefficients (C_d) between 0.483 and 0.525, depending upon berry shape. Berry suspension occurs in the air stream when the drag force (F_d) is equal to the force due to gravity reduced by buoyant effects (F_g) as given by:

$$F_d = C_d A_b \rho \frac{V_r^2}{2} \quad (13.3)$$

and

$$F_g = g m_b \frac{\rho_b - \rho}{\rho_b} \quad (13.4)$$

Combining Equations 13.3 and 13.4, the general equation for the relative terminal velocity becomes:

$$V_r^2 = 2g m_b \frac{\rho_b - \rho}{\rho_b \rho A_b C_d} \quad (13.5)$$

where C_d = coefficient of drag, dimensionless

A_b = berry cross-sectional area perpendicular to the air flow direction, m^2

ρ = density of air, kg/m^3

ρ_b = density of berry, kg/m^3

m_b = mass of berry, kg

Example Problem 13.1

It is necessary to design a leaf removal station for a red tart cherry harvester using an upwardly directed vertical air stream. What is the maximum average air velocity needed to accomplish this function? Would you expect this cleaner to remove the very small cherries if they were also present, and why?

Solution

It is necessary to assume that all fruit and leaves are single, and that if stems are present their effects can be neglected. Furthermore, we assume that red cherries are similar enough in shape and surface characteristics that Equation 13.5 can be used after you determine appropriate numeric values for the variables in the equation.

The effect of small fruit can be determined by looking at the relative change in relative terminal velocity when the fruit size is, for example, reduced by 50%. Cross-sectional area is a function of radius squared, thus if the radius is reduced to $1/2$ its previous value, the area reduces by $(1/2)^2$, or $1/4$. Similarly, the mass is proportional to the volume which is a function of the radius cubed, thus volume (and mass) are reduced by $(1/2)^3$ or $1/8$. We see from Equation 13.5 that V_r^2 is proportional to m_b/A_b , or $1/8 \div 1/4 = 1/2$. Therefore, we conclude that reducing the cherry size to $1/2$ the original radius reduces V_r^2 to $1/2$ its original value, hence V_r is reduced to $1/(2)^{0.5}$ or $1/1.414$ or 0.707 times the original value. If the air velocity is set at 85% of the relative terminal velocity of the large cherries, then the small (50% size) cherries will be removed with the leaves.

13.3.2 Fundamentals of bush and tree shakers

Inertial vibrators have proven to be a simple and reliable means of imposing forced vibrational motion upon bush and tree structures. The purpose of transmitting the vibrational energy to the plant structure is to cause detachment of the harvestable material. In addition to the mechanics of the vibrator itself, there are additional questions of damage to the harvested product, damage to the remaining plant structure itself, and the actual mechanics of detachment. We shall treat each of these factors in subsequent sections.

13.3.2.1 A single moving mass shaker

A simple shaker with one moving mass (m) is shown in Figure 13.35. We assume that the axis of rotation ($0, 0$) is fixed in space and that the inertial shaker mass (m), rotates with constant angular velocity (ω) in a counterclockwise direction. The angle of rotation is equal to the product of time (t) and ω . At any time (t) the center of mass (m) is located at point (x, y) where:

$$x = r \cos(\omega t)$$

and

$$y = r \sin(\omega t) \quad (13.6)$$

where x, y, r are displacements, m

t = time, s

ω = angular frequency, radians/s

The centrifugal force (F) created by the circular motion of m about $0,0$ can be resisted by the two component forces:

$$F_x = m \frac{d^2x}{dt^2} = -m\omega^2 r \cos(\omega t)$$

and

$$F_y = m \frac{d^2y}{dt^2} = -m\omega^2 r \sin(\omega t) \quad (13.7)$$

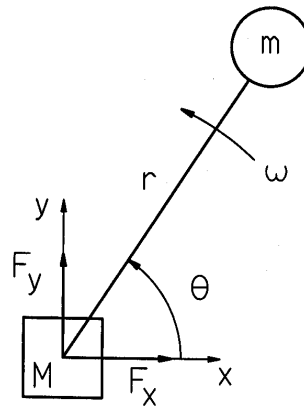


Figure 13.35 – A single rotating mass inertial shaker.

Power is the vector cross product of force times velocity. In this case, since the center of rotation has been assumed to be fixed, the power needed to operate the system is clearly zero. This model of a rotating mass is useful for predicting shaking forces, subject to the assumed limits. Another limitation of this model is that control of the direction of shaking force or the shaking pattern is not possible since the centrifugal force is constant in magnitude and its direction rotates uniformly.

Before proceeding, it is important to differentiate between the number of masses in a vibrational system and the number of degrees of freedom in that system. For each degree of freedom in the system, it is necessary to have one linearly independent equation in order to be able to solve the resulting system of equations. Each mass in the system is capable of producing six possible orthogonally independent motions, three mutually perpendicular linear displacements and three rotational displacements about axes that are at 90° to each other. Another way to consider the number of degrees of freedom of a system is to determine the number of independent engineering dependent variables needed to completely describe the system under consideration.

13.3.2.2 A double moving mass shaker

Control of both the direction and pattern of shaking can be achieved by the addition of a second rotating mass as shown in Figure 13.36. We also assume that the mass of the base, M, is very large such that the resulting “small” movements of M do not invalidate the inertial force summation calculations of F_x and F_y . Using the results of the single mass shaker, we have for Figure 13.36:

$$\Sigma F_x = M \frac{d^2x}{dt^2} = -m_1\omega_1^2r_1 \cos(\omega_1t) - m_2\omega_2^2r_2 \cos(\Theta - \omega_2t)$$

and $\Sigma F_y = M \frac{d^2y}{dt^2} = -m_1\omega_1^2r_1 \sin(\omega_1t) - m_2\omega_2^2r_2 \sin(\Theta - \omega_2t)$ (13.8)

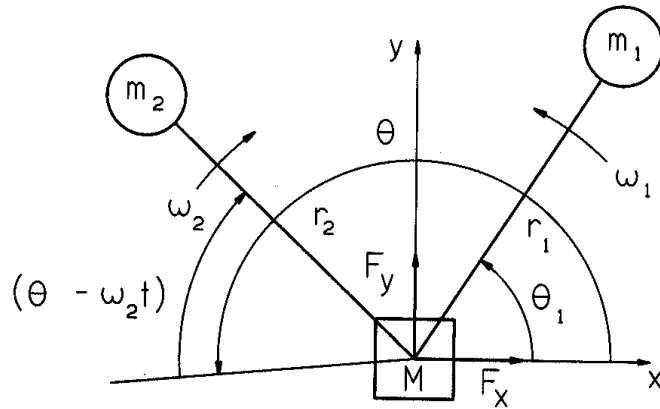


Figure 13.36 – A double rotating mass inertial shaker.

In the special symmetric case where $\omega_1 = \omega_2 = \omega$, $m_1 = m_2 = m$, $r_1 = r_2 = r$, and $\theta = \pi$, we have:

$$\sum F_x = 0$$

and
$$\Sigma F_y = -2m\omega^2 r \sin(\omega t) \quad (13.9)$$

Under these assumptions, the shaker is force-balanced in the x-direction with a pure sinusoidal excitation force in the y-direction.

If the y-direction force Equation 13.9 is divided by the mass (m) and twice integrated with indefinite limits of integration, then the y-direction displacement equation is given as:

$$y = (2 m r/M) \sin(\omega t) \quad (13.10)$$

The general Equations 13.8 can also undergo double indefinite integration to yield the general displacement equations for the center of mass (M) that is also assumed to be the center of rotation of masses m_1 and m_2 . These general equations of displacement are:

$$x(t) = (m_1/M) r_1 \cos(\omega_1 t) + (m_2/M) r_2 \cos(\theta - \omega_2 t)$$

and
$$y(t) = (m_1/M) r_1 \sin(\omega_1 t) + (m_2/M) r_2 \sin(\theta - \omega_2 t) \quad (13.11)$$

Example Problem 13.2

In the two rotating mass shaker analysis, the resulting motion was assumed to be “small.” What conditions are necessary for the maximum displacement to be no more than 10% of the radius of the rotating masses in the case of the force-balanced shaker?

Solution

The amplitude of the resulting motion can be obtained from Equation 13.10 in the y-direction. Thus:

$$2 m r/M < 0.10 r$$

or
$$m < 0.05 M \quad (13.12)$$

Therefore, if the rotating mass (m) is less than 5% of the shaken mass (M) the resulting maximum displacement of shaking will be less than 10% of the rotating mass radius (r).

Example Problem 13.3

Using Equations 13.11, subject to conditions of Equation 13.12, determine the values for m_1 , m_2 , ω_1 , ω_2 , r_1 , r_2 , and M that result in a three lobe shaking displacement pattern as shown in Figure 13.37.

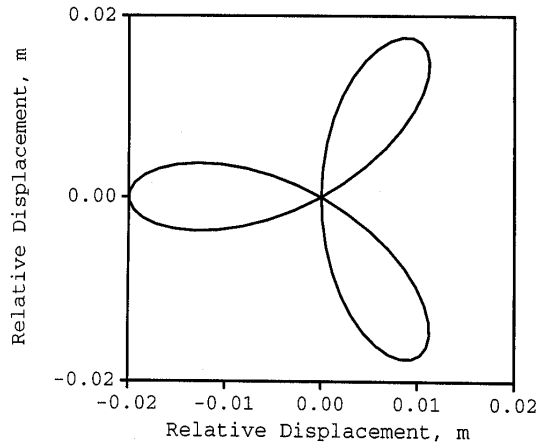


Figure 13.37 – Displacement of the center of a double rotating mass inertial shaker.

Solution

Equations 13.11 must be solved (by computer) for several incremental values of t between $t=0$ and $t=2\pi/\omega_1$ or $t=2\pi/\omega_2$, whichever is the greater value of time. In this example TK Solver™ was used and the rule and variable sheets are shown in Table 13.2.

Table 13.2. TK Solver™ output sheets for Figure 13.37.

RULE SHEET For Academic Use Only		VARIABLE SHEET For Academic Use Only				
$A1 = m1 \cdot r1 / M$		St	Input	Name	Output	Units
$B1 = m2 \cdot r2 / M$				A1	0.01	(m)
$x = A1 \cdot \cos(w1 \cdot t) + B1 \cdot \cos(\text{theta} - w2 \cdot t)$		10	m1	m1		(kg)
$y = A1 \cdot \sin(w1 \cdot t) + B1 \cdot \sin(\text{theta} - w2 \cdot t)$		0.2	r1	r1		(m)
				B1	0.01	(m)
		10	m2	m2		(kg)
		0.2	r	r		(m)
		200	M	M		(kg)
		L	x	x	0	(m)
		10	w1	w1		(rad / s)
		L	t	t		(s)
		0	theta	theta		(rad)
		3.1415927	w2	w2		(rad / s)
		20	y	y	1.225E-18	(m)
		L				

13.3.2.3 A triple moving mass shaker

Figure 13.29 shows a triple moving mass shaker. All three masses rotate about a common axis. To this point, we have assumed the two moving mass shaker as being force-balanced in every direction except one. This is true, if the centers of gravity of the two masses rotate in a common plane perpendicular to the axis of rotation. In practice it is not so simple to achieve this result. A practical solution is to “split” one mass into two, placing one half above and the other half below the third mass in the middle, as shown in Figure 13.29. If equal masses (1) and (2) are synchronized to be in phase with each other at the same rotational direction and frequency, it should be obvious from symmetry that the resulting shaker is force-balanced in the plane perpendicular to the axis of rotation, but also moment balanced such that there are no unbalanced moments “rocking” this plane. Furthermore this shaker is clearly capable of producing the two-dimensional shaking patterns in the tree shown in Figure 13.28 if the entire mass of the shaker head (1) combined with the tree has an effective center of mass at the centerline of rotation of the three moving masses.

13.3.2.4 Shaker power

Consider the force-balanced shaker shown in Figure 13.38 where the forcing function F_y is given by Equation 13.9. The resulting differential equation of motion in the y-direction is:

$$M \frac{d^2 y}{dt^2} + C \frac{dy}{dt} + Ky = 2mr\omega^2 \sin(\omega t) \quad (13.13)$$

where C = damping coefficient, N·s/m

K = stiffness, N/m

The transient (complementary) solution to Equation 13.13 is of little interest since it generally disappears relatively quickly. The steady state (particular) solution is of the form:

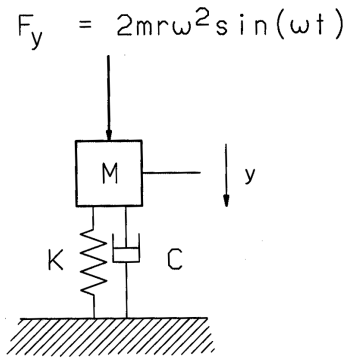


Figure 13.38 – Forced vibrational two-degree-of-freedom model excited with a force-balanced double rotating mass inertial shaker.

$$y(t) = \frac{2m r \omega^2}{\left[(K - M\omega^2)^2 + (C\omega)^2 \right]^{0.5}} \sin(\omega t - \alpha)$$

where

$$\alpha = -\tan^{-1} \left(\frac{C\omega}{K - M\omega^2} \right) \quad (13.14)$$

If we define the natural frequency, $\omega_n^2 = K/M$, and the damping ratio, $\xi = C/(2M\omega_n)$, then,

$$y(t) = \frac{2m r \omega^2 / K}{\left[\left(1 - (\omega / \omega_n)^2 \right)^2 + 2(\xi \omega / \omega_n)^2 \right]^{0.5}} \sin(\omega t - \alpha) \quad (13.15)$$

where

$$\alpha = \tan^{-1} \left(\frac{2\xi \omega / \omega_n}{1 - (\omega / \omega_n)^2} \right) \quad (13.16)$$

If the excitation frequency is much higher than the natural frequency, i.e., $\omega \gg \omega_n$, then Equation 13.15 reduces to:

$$y(t) = \left(\frac{2m r}{M} \right) \sin(\omega t - \alpha) \quad (13.17)$$

This result should be compared with Equation 13.10. The difference is that the damping effect has introduced a phase lag in the displacement with respect to the forcing function. The velocity is given by:

$$\frac{dy}{dt} = \frac{2m r \omega}{M} \cos(\omega t - \alpha) \quad (13.18)$$

Finally, the instantaneous power can be written as the product of the force times the velocity as:

$$P_{inst} = \left[2m r \omega^2 \sin(\omega t) \right] \left[\frac{2m r}{M} \right] \cos(\omega t - \alpha) \quad (13.19)$$

The average power can be obtained by integrating Equation 13.19 over the time required for one cycle of the slower rotating mass (T_f) as:

$$P_{avg} = 1/T_f \int_0^{T_f} P_{inst} dt$$

with the limits of integration being 0 to T_f . Thus, the average power is given by:

$$P_{avg} = \left[2m^2 r^2 \omega^3 / M \right] \sin(\alpha) \quad (13.20)$$

Adrian and Fridley (1965) investigated the shaker power requirements under actual field conditions.

13.3.2.5 LaGrange's equation

Complex, forced vibrational problems with damping are often treated from the point of view of energy. Simply stated, LaGrange's equation is an energy balance applied to the entire vibratory system. Multi-degree-of-freedom systems are conveniently treated, but the resulting systems of differential equations often require a computer to solve. Closed-form (analytic) solutions to real, non-linear systems of equations that represent practical problems are virtually impossible to obtain. LaGrange's equation in generalized orthogonal coordinates (q_i) has the general form of:

$$\frac{d}{dt} \frac{\partial(\text{K.E.})}{\partial \dot{q}_i} - \frac{\partial(\text{K.E.})}{\partial q_i} + \frac{\partial(\text{P.E.})}{\partial q_i} + \frac{\partial(\text{D.E.})}{\partial \dot{q}_i} = Q_i \quad (13.21)$$

where K.E. = kinetic energy of the system = $0.5 M (\text{dx}/\text{dt})^2$

P.E. = potential energy of the system = $0.5 K x^2$

D.E. = dissipation energy of the system = $0.5 C (\text{dx}/\text{dt})^2$

Q_i = generalized external force acting on the system

Example Problem 13.4

Apply the LaGrange equation to the forced vibrational of a single-degree-of-freedom damped mass shown in Figure 13.38. The parameters M , C , and K are defined in Equation 13.13. Neglect gravity.

Solution

The kinetic energy of the system is $\text{K.E.} = 0.5M \left(\frac{dy}{dt} \right)^2$ (13.22)

The potential energy of the system is $\text{P.E.} = 0.5 K y^2$ (13.23)

The dissipative energy of the system is $\text{D.E.} = 0.5C \left(\frac{dy}{dt} \right)^2$ (13.24)

The forcing function in the single degree-of-freedom direction of motion (y) is

$$Q = F_0 \sin(\omega t) \quad (13.25)$$

After calculating the appropriate partial derivatives and substitution, Equation 13.21 becomes (13.26)

$$\frac{d}{dt} \left[M \left(\frac{dy}{dt} \right) \right] - 0 + K y + C \left(\frac{dy}{dt} \right) = F_0 \sin(\omega t)$$

and finally reduces to $M \left(\frac{d^2 y}{dt^2} \right) + C \left(\frac{dy}{dt} \right) + K y = F_0 \sin(\omega t)$ (13.27)

13.3.3 Vibrational detachment during harvest

The LaGrange equation has been used to successfully analyze vibratory harvesting of olives (Tsatsarelis, 1987) and air-suspended strawberries (Ruff et al., 1980). A two-degree-of-freedom model for olives is shown in Figure 13.39a and a five-degree-of-freedom-model is shown in Figure 13.39b. Both of these studies looked at the resulting vibrational mode shapes that resulted from forced vibrations and confirmed with experimental observation that the tilting mode of vibration shown in Figure 13.40 is very important to fruit removal by causing detachment at the stem-fruit connection.

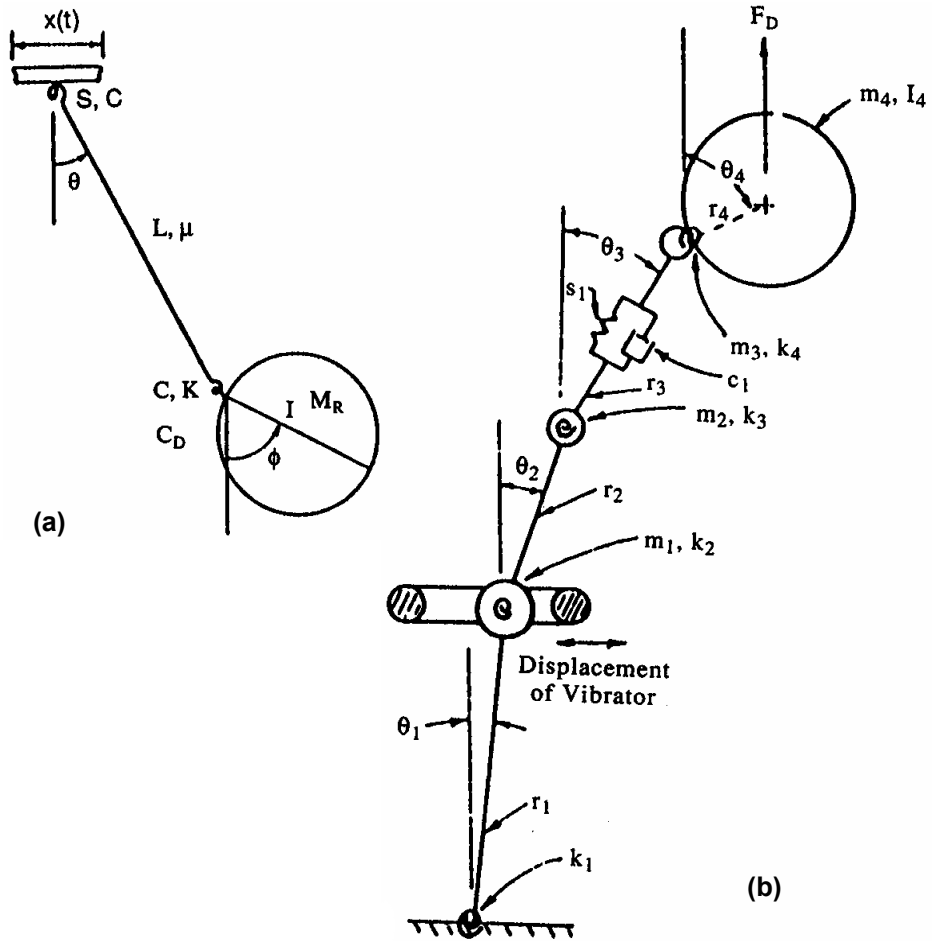


Figure 13.39 – (a) Two-degree-of-freedom fruit attachment vibrational model (from Tsatsarelis, 1987). (b) A five-degree-of-freedom vibrational model of an air-suspended depended, fruit-stem system (from Ruff et al., 1980).

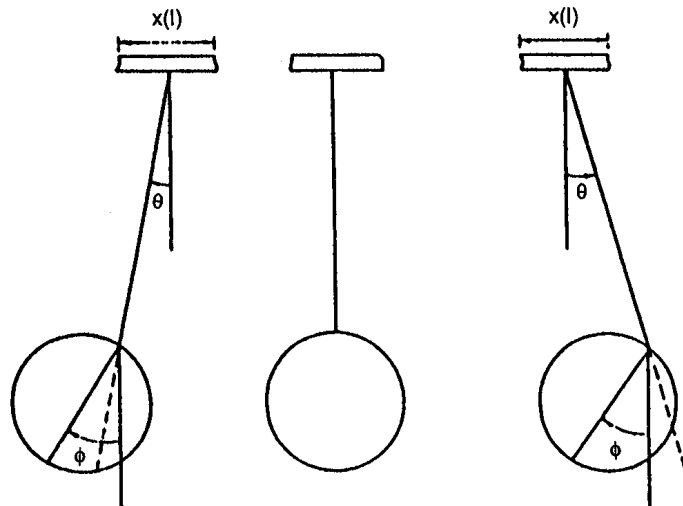


Figure 13.40 – Vibrational modes defined; pendular, left; rest, middle; and tilting, right (Tsatsarelis, 1987).

Three modes of vibration are important in understanding the mechanism of fruit detachment. The tilting mode is the most important and has been experimentally observed to be present at the time of detachment. This mode causes high tensile stresses to develop in the stem-calyx junction of the stem and the fruit. Under normal maturation processes this junction becomes weaker as the natural abscission layer develops. Furthermore, there is evidence that biological materials fatigue under repeated cycles of stress, each cycle of which is not individually capable of causing failure, but accumulatively will produce failure of the stem or stem-calyx junction.

The second important vibrational mode is the axial tension mode. This mode is the result of the application of forces directed along the axis of the stem itself. In the forced vibrational excitement of the plant structure, it is relatively easy to imagine how the vibrating fruit-stem could achieve a relative position such that the next cycle of vibration, by the assumed geometry, would result in a sudden imposition of a relatively high axial stem force. This situation can be recognized by the common expression of “crack the whip” which results in an amplification of tensile forces by sudden redirection of momentum forces.

The pendular mode is the third mode and is important to excite if the fruit is to be detached with the stem intact. It is much more difficult to excite this mode if the stems are relatively long than the tilting mode. In fact all three modes are present to varying degrees and as such combine to produce detachment.

13.3.4 Impact models and mechanical damage

Mechanical damage during harvesting operations can affect both the plant and the harvested product. In multiple-pick crops, unharvested product can also be damaged. The focus of this section will be on models that attempt to characterize damage to the harvested product. There are four principal components of failure in fruits and vegeta-

bles that contribute to reduced product value. These four components are compressive stress, shear stress, creep stress, and fatigue stress. Stress analysis in three dimensions in complex shapes with non-isotropic bodies is very difficult. The presence of a protective (usually tough) skin over a product is only one example of non-isotropic condition. Most loading conditions that are observed under practical conditions are a combination of the above four component loadings. For engineering purposes, useful information in equation form can be derived from empirical (physical) observations. Care should be exercised in applying empirical results to non-identical products or conditions.

13.3.4.1 Impact force response of a sphere on a flat plate

If a stationary flat plate is impacted with a spherically shaped object dropped under gravity, the resulting total force exerted on the plate is a function of the mass, impacting and rebounding velocities of the sphere. This results from the application of Newton's Second Law as given by:

$$I = \int_0^{t_c} f(t) dt = m(v_2 - v_1) \quad (13.28)$$

where I = impulse, $N \cdot s$

$f(t)$ = contact force as a function of time, N

t = time during contact, s

t_c = total contact time, s

m = mass of sphere, kg

v_1 = velocity of center of mass, m/s , before contact, i.e., $t = 0$

v_2 = velocity of center of mass, m/s , after contact, i.e., $t = t_c$

The coefficient of restitution (r) is defined as:

$$r = -v_2/v_1 \quad (13.29)$$

where velocities v_1 and v_2 are defined as above and the minus sign reflects the fact that the direction of rebound is opposite the impact direction.

If one assumes r is greater than zero and considers two successive bounces, then on the first impact:

$$I_1 = m(v_2 - v_1)$$

and on the second impact, neglecting air frictional losses:

$$I_2 = m(v_3 - v_2)$$

If one assumes that the coefficient of restitution is constant for both impacts, then it can be shown that:

$$r = I_2/I_1 \quad (13.30)$$

Hence, by measuring the impulse of two successive impacts, the coefficient of restitution can be determined experimentally.

It is also possible to determine the fruit mass from the impact response by:

$$I_1 = m(v_2 - v_1) = m v_1 (v_2/v_1 - 1)$$

or

$$m = -I_1/[v_1(1 - r)] \quad (13.31)$$

The pre-impact velocity (v_i) can be estimated by knowing the free-fall height under constant gravitational acceleration. Thus, it is possible to experimentally determine the coefficient of restitution and the mass of a sphere dropped from a known height onto a rigid flat surface provided two consecutive impulses are measured and analyzed.

Until this point, the actual shape of $f(t)$ has not been considered and, in fact, has no effect on the above equations. The shape of the impact force curve, $f(t)$, is a function of the fruit firmness and damping as shown in the next section.

13.3.4.2 Impact models with firmness and damping effects

For ordinary engineering purposes, it is often assumed that the impact force and contact deformations within a convex fruit or vegetable product and a rigid flat surface can be modeled with one or two degrees of freedom. Two models are shown in Figure 13.41. The Kelvin model has a single degree of freedom with lumped parameter mass, spring, and damping characteristics. The Maxwell model contains the same lumped physical elements as the Kelvin model, but is based upon a different physical arrangement. Lumped parameter models are defined by parameter constants that represent invariant conditions. For example, in these models all mass is assumed to be “lumped” together and moves without internal deformations, hence the motion of the center of mass is assumed to be the motion of all mass.

Each model provides useful insights and engineering information. However, each model is also subject to certain restrictions and limitations. In addition to the lumped parameter assumption, the development of initial conditions, while physically justifiable, sometimes results in mathematical consequences that are not physically realizable. As each model is developed, further examples of differences between the physical and mathematical representations will be identified.

Before considering the equations of motion for the two models in Figure 13.41, an understanding of initial conditions will be developed. The models are considered at rest, without the effects of gravity, at times prior to “impact.” This condition is assumed to exist for all time $t < 0$. At $t = 0^+$, the mass is considered to have an instantaneously achieved velocity of V_i in the direction noted in Figure 13.41. At this time, contact with the stationary surface exists and the initial displacements of all displacement variables are taken to be zero. Neither model is subjected to an external forcing function.

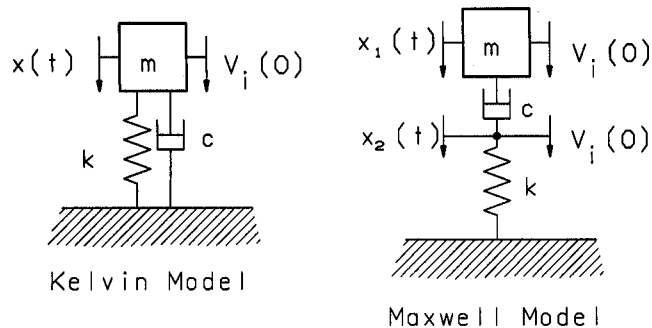


Figure 13.41 – Kelvin model and Maxwell model of a viscoelastic impact with a stationary surface.

Since contact continues to exist only if the contact force is positive, then the model equations of motion are only valid during the initial contact period. Once the contact force goes to zero, the initial impact event is considered to be complete and the velocity of the mass, if any, is considered to be the impact rebound velocity. The choice of units for the equations of motion can be made consistent with the equations themselves. Any consistent set of units may be used.

The Kelvin model, being a single-degree-of-freedom system, is described by the following equation of motion:

$$m \frac{d^2x}{dt^2} + c \frac{dx}{dt} + kx = 0 \quad (13.32)$$

while the general solution for this equation is of the form:

$$x = x_c + x_p \quad (13.33)$$

Only the complementary solution (x_c) is of interest since the particular solution (x_p) is, in this case, zero. The characteristic equation (or auxiliary equation) is:

$$m\lambda^2 + c\lambda + k = 0 \quad (13.34)$$

If $\omega_n^2 = k/m$ and $\zeta = c/(2m\omega_n)$, where ζ is called the damping factor, then,

$$\lambda_1 = \omega_n \left(-\zeta + \sqrt{\zeta^2 - 1} \right) \quad (13.35)$$

and

$$\lambda_2 = \omega_n \left(-\zeta - \sqrt{\zeta^2 - 1} \right) \quad (13.36)$$

The roots of the characteristic equation (λ_1 and λ_2) will be real and distinct, real and equal, or complex conjugates for ζ , being greater than one, equal to one, or less than one, respectively.

If ζ is greater than one the system is overdamped and oscillatory motion is not possible as given by the overdamped complementary solution:

$$x_c = Ae^{-\lambda_1 t} + Be^{-\lambda_2 t} \quad (13.37)$$

$$x_c = Ae^{-\lambda_1 t} + Be^{-\lambda_2 t}$$

where A and B are constants determined from the initial conditions.

Critical damping is a very special mathematical condition, seldom seen in the physical world, where $\zeta = 1$, and clearly $\lambda_1 = \lambda_2 = -\omega_n$. In this special case, the complementary solution is given by:

$$x_c = (C + Dt)e^{-\omega_n t} \quad (13.38)$$

again where C and D are constants determined from the initial conditions.

The underdamped condition, $\zeta < 1$, is often encountered in fresh, mature fruits and vegetables, and results in the complementary solution:

$$x_c = (A \cos \omega_d t + B \sin \omega_d t)e^{-\zeta \omega_n t} \quad (13.39)$$

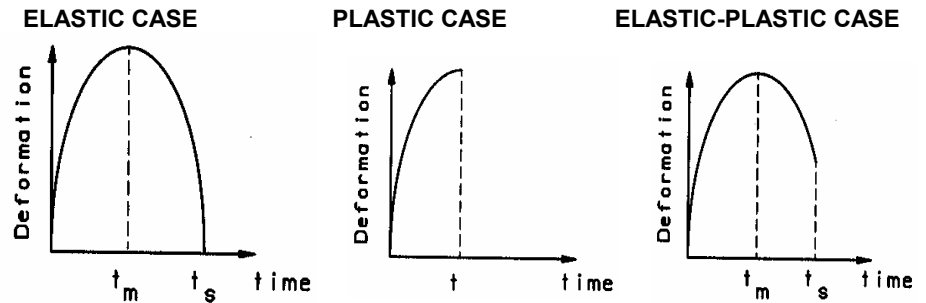


Figure 13.42 – Impact deformation curves for products with elastic, plastic, or elastic-plastic properties.

where the damped natural frequency $[\omega_d^2 = (1 - \zeta^2) \omega_n^2]$ is given by definition. If the initial displacement is taken as zero and the initial velocity is V_i , then $A = 0$ and $B = V_i/\omega_d$.

Maxwell's model is more complex because it has two degrees of freedom. By example problem, these equations will be derived using the LaGrange equations. The complementary solution can then be obtained by using a symbolic math package such as MAPLE™ resulting in rather than complex algebraic analytical solution. A TUTSIM™ computer solution to the differential equations could also be used.

Both the Kelvin and Maxwell models are useful in demonstrating the impact phenomena. Depending upon the relative mass, firmness, and internal energy absorption of the impacting body, elastic, plastic or elastic-plastic impact responses can be demonstrated as illustrated in Figure 13.42. The coefficient of restitution ($r = 1$ for elastic, $r = 0$ for plastic, and $0 < r < 1$ for plastic-elastic) characterizes the impact behavior.

Example Problem 13.5

Use LaGrange's equation to find the equations of motion for Maxwell's model shown in Figure 13.41. Neglect gravity.

Solution

The needed expressions and terms of the LaGrange's equations are written as follows:

$$\text{P.E.} = \frac{k x_2^2}{2} \quad (13.40)$$

$$\text{K.E.} = \frac{m}{2} \left(\frac{dx_1}{dt} \right)^2 \quad (13.41)$$

$$\text{D.E.} = \frac{c}{2} \left[\left(\frac{dx_2}{dt} \right)^2 - \left(\frac{dx_1}{dt} \right)^2 \right] \quad (13.42)$$

and $Q = 0$ since there is no generalized forcing function.

After calculating the appropriate partial derivatives and substitution, Equation 13.21 becomes:

$$m x_1 - c \left(\frac{dx_2}{dt} - \frac{dx_1}{dt} \right) = 0 \tag{13.43}$$

and

$$k x_2 + c \left(\frac{dx_2}{dt} - \frac{dx_1}{dt} \right) = 0 \tag{13.44}$$

subject to $x_1(0) = x_2(0) = 0$ and $\frac{dx_1(0)}{dt} = \frac{dx_2(0)}{dt} = v$

The solutions to Equations 13.43 and 13.44 are:

$$x_1(t) = -\frac{v m}{c} - 2 \frac{c v m^{0.5} e^{-kt/2c} \sinh(\beta)}{k^{0.5} (-4c^2 + m k)^{0.5}} + \frac{v m^{1.5} k^{0.5} e^{-kt/2c} \sinh(\beta)}{c (-4c^2 + m k)^{0.5}} + \frac{v m e^{-kt/2c} \cosh(\beta)}{c}$$

and

$$x_2(t) = -2 \frac{c v m^{0.5} e^{-kt/2c} \sinh(\beta)}{k^{0.5} (-4c^2 + m k)^{0.5}}$$

13.3.4.3 Impact models results and applications

A Kelvin model (Bower and Rohrbach, 1976) and a double Kelvin model in series (Glass and Rohrbach, 1980) have been used to model blueberry fruit impacts. For a blueberry, the mass ranges from less than 1 g to nearly 3 g, the damping constant between 0.1 and 0.8 N · s/m, and the spring constant can take values between 500 and 8000 N/m. Actual model parameters were selected to match individual berry coefficient of restitution or contact force and velocity mechanical impedance criterion. Model berry mass is often found to be slightly less than actual berry mass.

Table 13.3 summarizes the impact parameters used in computer solutions of blueberry impact results for the Kelvin model shown in Figure 13.43 and the Maxwell model shown in Figure 13.44. In both cases the coefficient of restitution is 0.414 with the model mass being 1.54 g. The damping constant and the spring constant values were empirically adjusted in the Maxwell model to obtain equal coefficients of restitution for the two different models.

Table 13.3. Impact parameters and results for the solution of Kelvin and Maxwell equations of motion for blueberry models.

Model	m, g	c, N · s/m	k, N/m	F _{peak} , N	t _s , ms	r	See figure	d _p , mm
Kelvin	1.54	0.75	797	0.713	3.60	0.414	13.43	0.40
Maxwell	1.54	12.0	1000	1.27	3.85	0.414	13.44	0.28

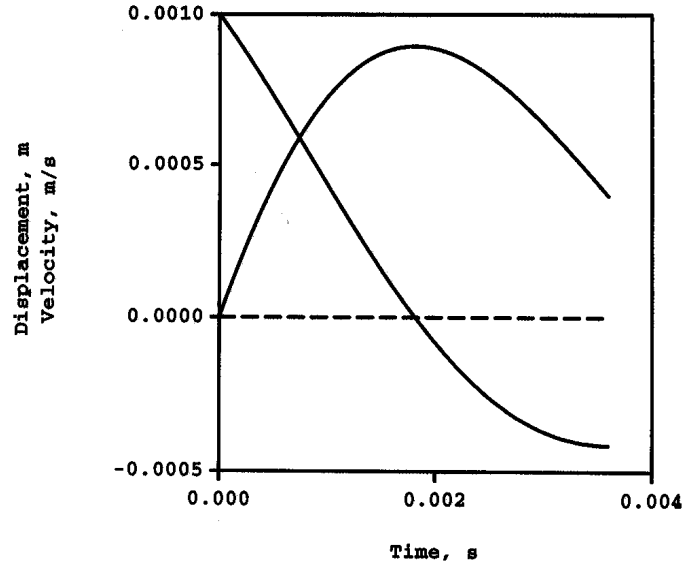


Figure 13.43 – Solution to Kelvin model of a blueberry. See Table 13.3 for model parameter values and results.

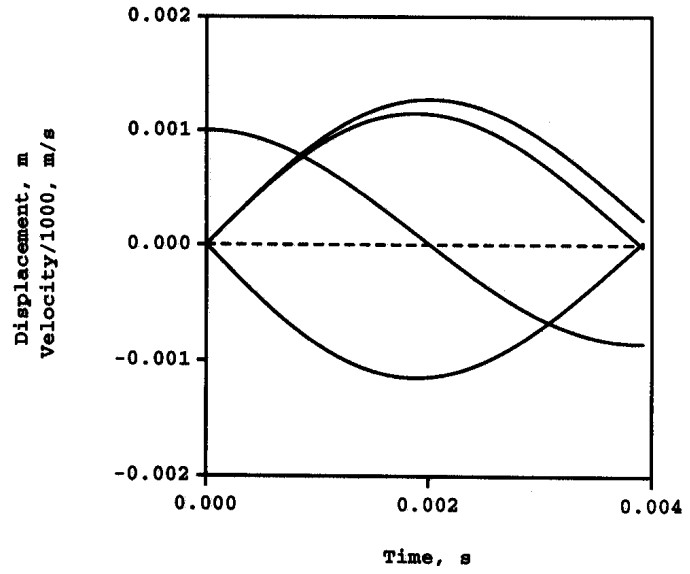


Figure 13.44 – Solution to Maxwell model of a blueberry. See Table 13.3 for model parameter values and results.

Once the deformations within the spring model elements have been calculated, $x_1(t)$ for the Kelvin model and $x_2(t)$ for the Maxwell model, the impact force $f(t)$ is easily calculated as the product of the deformation and the spring stiffness (k). However, the Kelvin model predicts a non-zero impact force at the time of rebound or separation, which is not particularly useful, but, results from the model's "attempt" to restore the initial free length of the unstressed spring element. If one attempts to "correct" for the non-zero contact force prediction at the time of rebound by subtracting the force component associated with the viscous damping element, then the initial contact force becomes a step at $t = 0^+$ with a magnitude of $c(dx_1/dt)$. The Kelvin model does predict a permanent fruit deformation after separation in the case where separation does indeed occur.

The Maxwell model comes closer to predicting an impact force that exists during rebound, which is consistent with physical observation as well as a permanent fruit deformation (d_p) with a magnitude of $x_2(t_s)$, where t_s is the time at separation. The comparative results of the two impact models, in Table 13.3, show some differences between the predicted contact time, peak impact force, F_{peak} , and permanent fruit deformations after impact for identical coefficients of restitution. It is important to remember that engineering models are very useful to the extent that they help the engineer understand the physical situation represented and the engineering parameters of interest, but not all physical aspects of the real situation are accurately modeled.

In practice, most values for k are obtained from empirical force-deformation tests (Instron Universal TesterTM) or drop test data, and are only valid for the size and conditions of that test. The development of tri-axial contact stress during a fruit impact is beyond the scope of this text. Additional theoretical aspects of food rheology and physical properties are presented in Mohsenin (1970). Goldsmith (1960) is an excellent reference for additional discussion of impact events.

The coefficient of restitution in peaches has been reported to be successfully measured and used to identify individual fruit firmness (Meredith, Leffler and Lyon, 1988). The coefficient of restitution was determined from data collected from two consecutive bounces on an instrumented load cell. Neither variety, fruit size, nor drop height affected the determination of the coefficient of restitution within the range of the investigated variables.

An impact probe for determining apple and pear firmness was developed and tested by Delwiche et al. (1991). A small air cylinder moved an impact surface towards the side of a "stationary" fruit. Impact force was sensed by an accelerometer attached to the impact surface. A strong correlation between peak impact deceleration and fruit firmness was obtained by testing.

13.4 PERFORMANCE FACTORS

The fundamental concepts useful in reducing or eliminating damage to harvested products involve a number of complex issues. Basically, bruising results from the undesirable absorption of energy in the product tissue. Product that free-falls onto a receiving surface results in the application of a deceleration or impact force. This force, when distributed over the impact area or region, will damage the product if the critical values of shear or compressive stress are exceeded for the product being harvested.

Often harvesting elements that are designed to transmit vibrational energy to the plant material cause bruising. Fruit impacts on other fruit during free-fall or at the collection surfaces are also a common source of damage.

13.4.1 Damage

Product bruising, cutting, scuffing, and direct damage to the remaining plant are all undesirable effects of field harvesting operations. Direct product damage reduces the value of the product in the market and the general desirability to the consumer. Plant damage, for multiple-harvest enterprises, is also undesirable since subsequent harvests are reduced.

Damage is often accumulative and proportional to the total energy absorbed by the fruit tissue. In blueberries, for example, sixteen 2-cm drops onto a rigid flat surface cause the same relative damage as eight 4-cm drops or four 8-cm drops. Clearly, the first and most important principle in minimizing bruising is to minimize the amount of kinetic energy that the fruit has at any time during machine operations.

The United States Department of Agriculture (USDA) oversees the development of quality standards for most of the more popular commodities grown or marketed in the U.S. as fresh or processed. In some cases these standards have evolved into an extensive collection of quality factors that are used to establish the marketing grade for a specific shipment of product. As an example, Figure 13.45 is a summary of the USDA apple grade standards. In the case of apples, combined grade classifications are permitted.

13.4.2 Efficiency

Field harvest efficiencies for multiple-harvest operations are only meaningful when compared with some existing or accepted standard. There is no single definition for field harvest efficiency. Usually it is defined as economic recovery of product as a percentage of total available harvest. Often this total available harvest is taken as the “hand harvest.” However, most “hand harvest” methods have a measurable component of loss as either ground loss or unharvested product.

Ground loss is an important component of machine harvesting systems. Ground loss is defined as a percentage of either the total harvest or the net harvest. This is not to be confused with preharvest ground loss that may result from preharvest weather conditions or ground losses due to other harvest delays.

13.4.3 Reliability

Since fruit, vegetables, and nuts are usually high-value commodities, harvesting systems should be designed for high mean times between failure (MTBF). Since the harvest period is often concentrated in a short time, harvesting systems must be serviced and have all preventative maintenance completed before the annual harvest season. In the design of these systems, standard parts should be used whenever possible to ensure local availability of repair parts in the event of a breakdown.

Since a food product for human consumption is being harvested, care should be exercised by the designer to avoid the possibility of product contamination with hydraulic oil or other machine fluids. Special consideration should be given to minimize the



UNITED STATES STANDARDS FOR GRADES OF APPLES



	U. S. EXTRA FANCY	U. S. FANCY	U. S. NO. 1	U. S. UTILITY
Maturity	Mature but not overripe	Mature but not overripe	Mature but not overripe	Mature but not overripe
Scab	Free from	Not over ¼ inch dia.	Same as Fcy.	Not over ¼ inch dia.
Russetting	1. Net-like (not over 10% of surface) 2. Smooth solid (not over 5% of surface) 3. Slightly rough (not over ½ inch) 4. Rough (not over ¼ inch)	Not over 15% of surface Not over 5% of surface Same as Ex. Fcy. Same as Ex. Fcy.	Not over 25% Not over 10% Same as Ex. Fcy. Same as Ex. Fcy.	Any amount allowed Not over ½ of surface Not to detract from appearance More than smooth solid
Sunburn & Sprayburn	Must blend with color	Skin not cracked and must blend with color	Same as Fcy.	Not seriously detracting from appearance
Limb Rub	Not over ¼ inch	Not over ½ inch	Same as Fcy.	Not more than one-tenth of surface
Hail Marks	1. When skin not broken 2. When surface not discolored 3. When not over 1/16 inch deep 4. One spot not over ¼ inch in diameter or aggregate not over ½ inch.	Unbroken skin, not over ½ inch in aggregate Not over ¼ inch deep Well healed, not over ¼ inch in diameter	Same as Fcy.	Unbroken, not more than 1/10 of surface in aggregate Well healed broken skin not more than ½ .inch in dia.
Stem & Calyx Cracks	When well healed or not over ¼ inch aggregate length	Same as Ex. Fcy.	Same as Ex. Fcy.	When well healed or not over ½ inch in length
Cedar Rust	Not over 3/16 inch in diameter	Not over ¼ inch in the aggregate	Same as Fcy.	Not more than 3/4 inch
Sooty Blotch or Fly Speck	Dark and heavy, not over ¼ inch Thin, not over 5% surface	Dark and heavy, not over ½ inch Not over 10% surface	Same as Fcy. Same as Fcy.	Not more than 1/3 of surface
Stings	Not over ¼ inch in diameter	Not over 3/16 inch in diameter	Same as Fcy.	Not more than ¼ inch in diameter
Worm Holes	None	None	None	None
Decay	None	None	None	None

Percent of Color Required By Variety And Grade				
Red Delicious	66	40	25	None
Delicious	50	25	15	None
Red Rome	66	40	25	None
Rome	50	33	15	None
Red Stayman	66	40	25	None
Stayman	50	33	15	None
Winesap	66	40	25	None
Golden Delicious	75% characteristic color	Same as Ex. Fcy.	characteristic ground color	None

COMBINATION GRADES PERMITTED

- Comb. U.S. Extra Fancy and U.S. Fancy
- Comb. U.S. Fancy and U.S. No. 1
- Comb. U.S. No. 1 and U.S. Utility

Note: At least 50% shall meet the higher grade to qualify as combination grade.

OTHER GRADES: U.S. No. 1 Early: Same as U.S. No. 1 except 2 inch min., no color requirements, need not be mature.
 U.S. No. 1 Hail: Must meet all requirements of U.S. No. 1 except unlimited well healed hail marks allowed provided apples are fairly well formed.

Figure 13.45 – Summary of USDA apple grade standards. The current standard is several pages, available at <http://www.ams.usda.gov/standards/apples.pdf>.

sites on the machine that can accumulate unwanted residue. The machine itself will need to be cleaned periodically to eliminate the buildup of microbes that could adversely affect harvested product quality.

The safety of the people that are working with the harvesting system needs special attention. Often machine elements that perform useful harvesting functions must be accessible to the commodity for proper operation and cannot be guarded by position from human access. All such hazards must be shielded to the maximum extent possible and all individuals warned to the greatest extent possible of the potential hazards. Standard operating procedures should require that power be disengaged for all maintenance and repair activities. All applicable engineering safety design standards must be applied to fruit, vegetable, and nut harvesting equipment.

PROBLEMS

- 13.1 For your state, determine the relative importance (rank among other states) of fruit, nut, and vegetable production. Which of these commodities is most important to your state's agricultural income?
- 13.2 For each of the possible 24 logical combinations of functional harvest operations, list at least one commodity example for as many combinations as possible. For example, hand harvesting of apples is the functional equivalent of selection, control, removal, and transportation.
- 13.3 Design a two-mass (coaxial and counter-rotating at equal angular speeds) inertial shaker that will develop a linear ± 4 cm stroke at 250 Hz operating on the shaker frame and plant material equivalent mass of 100 kg.
- 13.4 Modify (non-equal angular speeds) the linear shaker designed in Problem 13.3 above, to produce a six-directional shaking pattern, i.e., each successive stroke precesses 60° from the preceding stroke. Is it necessary to adjust the masses of the counter-rotating masses?
- 13.5 Visit a large fruit, vegetable, or nut grower near your location. Interview the grower with the following list of questions plus three of your own: What new harvesting equipment or features do you need? What existing machine harvesting functions need improvement? What are the safety concerns of the grower relative to harvesting equipment?
- 13.6 What is the effect of the relative direction of rotation of the two masses in the inertial shaker shown in Figure 13.36? What is the effect of the initial angular displacement?
- 13.7 Program Equations 13.11 on a computer in a manner to allow for evaluation of various combinations of values for mass, frequencies, rotational radii, etc. Determine empirically the relationship between the relative angular frequencies and the number of "lobes" in the displacement pattern. What is the importance of the relative magnitudes of the rotating masses in establishing the "lobe" shape?

- 13.8 It is assumed that the relative amplitude of displacement in the base mass (M) in Figure 13.36 should be only 1% of the minimum radius of rotation of either excitation mass. What is the maximum relative rotating mass that can be used compared with the base mass (M)? Does this result depend upon the resulting displacement pattern? Why?
- 13.9 The terminal velocity of a harvested product is believed to be in the range of 30 m/s. If you want to confirm this estimation by actual measurement of the free-fall time, what drop height should be used?
- 13.10 Integrate Equation 13.19 to obtain the average shaker power given by Equation 13.20. Show all steps.
- 13.11 What air velocity would you propose to be used to separate green strawberries from ripe (red) strawberries in an upwardly directed air-blast separator? Fully justify your answer.
- 13.12 Table 13.2 lists the model parameters for the inertial shaker displacements shown in Figure 13.37. With a computer model of Equations 13.11, determine one model parameter change that will result in the relative displacements shown in Figure 13.46.
- 13.13 With a computer model of Equations 13.11, determine one model parameter change from Problem 13.12 that will result in the relative displacements shown in Figure 13.47.
- 13.14 With a computer model of Equations 13.11, experiment and determine the model parameter changes needed that will result in the relative displacements shown in Figure 13.48.
- 13.15 With a computer model of Equations 13.11, experiment and determine the model parameter changes needed that will result in the relative displacements shown in Figure 13.49.

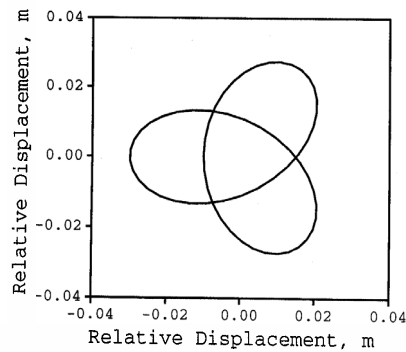


Figure 13.46 – Displacement of the center of a double rotating mass inertial shaker, for Problem 13.12.

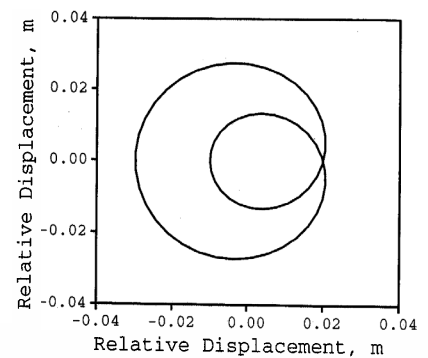


Figure 13.47 – Displacement of the center of a double rotating mass inertial shaker, for Problem 13.13.

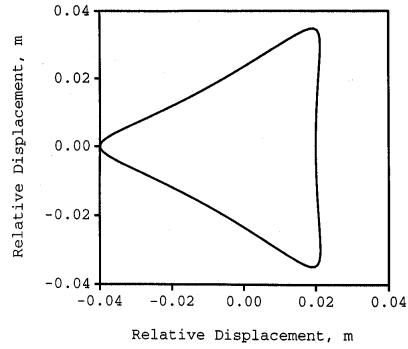


Figure 13.48 – Displacement of the center of a double rotating mass inertial shaker, for Problem 13.14.

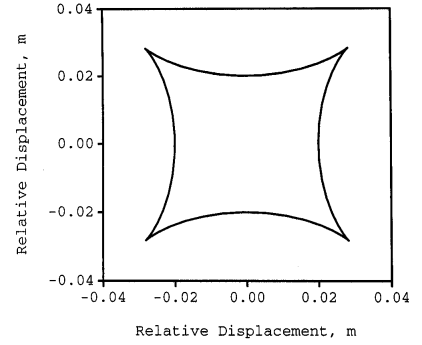


Figure 13.49 – Displacement of the center of a double rotating mass inertial shaker, for Problem 13.15.

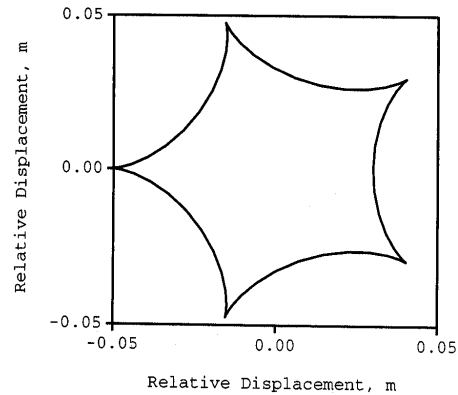


Figure 13.50 – Displacement of the center of a double rotating mass inertial shaker, for Problem 13.16.

- 13.16 With a computer model of Equations 13.11, experiment and determine the model parameter changes needed that will result in the relative displacements shown in Figure 13.50.
- 13.17 With a computer model of the equations for Maxwell's impact model, experiment and determine how the model parameters are related to the coefficient of restitution. Is there a simple relationship between the model parameters m , c , and k and the resulting coefficient of restitution (r)? What is it?
- 13.18 For a fruit, vegetable or nut crop grown in your location, obtain a copy of the USDA Grade Standards. Develop a concise tabular summary of the standard similar to the USDA Apple Grades in Figure 13.45.
- 13.19 For the Kelvin blueberry impact model shown in Figure 13.43, find the exact time of rebound, i.e., the time when the model predicts the maximum re-

bound velocity. Hint: Calculate the appropriate derivatives of the displacement and investigate the maximums of the velocity expression.

- 13.20 Use a computer to solve the Maxwell blueberry model and calculate the contact force during impact. Evaluate the coefficient of restitution using Equation 13.30. Compare this result with the coefficient of restitution from Equation 13.29, and explain any differences.
- 13.21 Based upon interest, select one of the patents from the “Patents Cited” list in Appendix A and obtain a complete copy. Study the patent carefully and report to the class the exact nature of the patent coverage. (You may wish to find another interesting patent, within the scope of your course, to study and report.)

CONVEYING OF AGRICULTURAL MATERIALS

14

INTRODUCTION

There are several methods used to convey agricultural materials. The selection of conveying method depends upon the nature of application and on the type of material being conveyed. The agricultural material may be liquid, granular, powder, fibrous, or any combination of these. This chapter does not cover conveying of liquid material.

Generally, conveying is accomplished by a combination of mechanical, inertial, pneumatic, and gravity forces. Conveyors utilizing primarily mechanical forces are screw, belt, and mass conveyors. Oscillatory conveyors rely on the inertial and the friction forces. Pneumatic conveyors employ aerodynamic drag to accomplish conveying. Conveying by throwing combines both inertial and aerodynamic forces. Forage blowers utilize these principles.

14.1 SCREW CONVEYORS

Augers are used to convey materials that are free flowing, such as grain, as well as difficult fibrous materials and powders. For example, in a grain combine, augers are used to move cut crop on the platform to the feeder housing, clean grain from the bottom of the cleaning shoe to the grain tank, and to unload the grain tank onto a wagon or a truck. Augers are used at grain elevators and farmsteads to load grain storage bins and on feedlots for feed distribution.

14.1.1 Screw conveyor methods and equipment

The *screw conveyor* consists of a shaft that carries helicoid flightings on its outer surface. These flighting are enclosed either in a trough for horizontal augers or in a tube for elevating augers. The tube or the trough is held stationary while the rotation of the flightings causes the material to move longitudinally. Figure 14.1 shows the essential components of a screw conveyor. At the inlet side, the auger flightings extend beyond the tube. Generally, a hopper is provided to hold the material while it is conveyed into the tube. Augers can be permanently installed in a machine, or at a site, or they can be portable. The augers are driven either at the intake side or the discharge side. There are some center-drive augers but they are not common in agricultural applications.

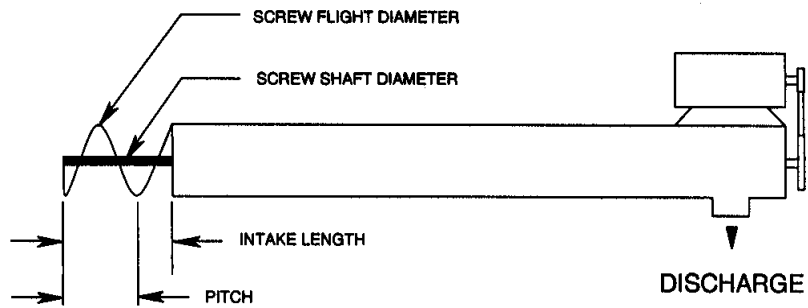


Figure 14.1 – A schematic diagram of a screw conveyor.

The auger length is defined as the length of the tube assembly including any intake but not including the intake hopper and/or the head drive. The intake length is the visible flighting at the intake of the auger. The outside diameter of the tube is referred to as the auger size. A standard pitch auger is the one whose pitch is approximately equal to the outside diameter of the helicoidal flighting. Generally, the pitch is not less than 0.9 and not more than 1.5 times the outside diameter. Standard pitch augers are used for horizontal and up to 20° inclination angles. For inclination angles greater than 20°, half-standard pitch screws are used. Double- and triple-flight, variable-pitch, and stepped-diameter screws are available for moving difficult materials and controlling feed rates.

14.1.2 Theory of screw conveyors

The *theoretical volumetric capacity* of an auger is expressed as:

$$Q_t = \frac{\pi}{4} (d_{sf}^2 - d_{ss}^2) l_p n \quad (14.1)$$

where Q_t = theoretical volumetric capacity, m^3/s

d_{sf} = screw flighting diameter, m

d_{ss} = screw shaft diameter, m

l_p = pitch length, m

n = screw rotational speed, rev/s

In reality the actual capacity of an auger is considerably less than the theoretical capacity. This results in loss of volumetric efficiency. The *volumetric efficiency* is defined as:

$$\eta_v = \frac{Q_a}{Q_t} \quad (14.2)$$

where η_v = volumetric efficiency

Q_a = actual volumetric capacity, m^3/s

Generally, the throughput rate in terms of mass (or weight) per unit of time, for example t/h or kg/min, is specified. The volumetric capacity is obtained by dividing the throughput rate by the bulk density of the material.

The power requirement of an auger is expressed by the *specific power*, defined as:

$$P' = \frac{P/L}{Q_a \rho_b} \tag{14.3}$$

where P' = specific power, W s/kg m
 P = power requirement, W
 L = auger length, m
 ρ_b = material bulk density, kg/m³

Thus, the specific power is the power required to convey a unit mass throughput rate per unit auger length.

The process of conveying by a screw conveyor is complex. It is difficult to develop analytical models to predict volumetric capacity and power requirements without making overly simplified assumptions. Purely empirical models, on the other hand, are not general enough in nature and cannot be used to predict auger performance in a variety of applications. Rehkugler and Boyd (1962) proposed the application of dimensional analysis as a tool to develop a comprehensive prediction model for screw conveyor performance. Table 14.1 shows a list of variables that are pertinent to the problem. These variables can be combined into ratios or dimensionless groups called the pi-terms using Buckingham's Theorem (see Chapter 1). The following equation includes the dimensionless terms:

$$\pi_1 = f \left(\frac{d_t}{d_p}, \frac{d_{sf}}{l_p}, \frac{d_{ss}}{l_p}, \frac{l_i}{l_p}, n \sqrt{\frac{l_p}{g}}, f(\theta), \mu_1 \mu_2 \right) \tag{14.4}$$

where
$$\pi_1 = \frac{Q_a}{\frac{\pi}{4}(d_{sf}^2 - d_{ss}^2) l_p n} \quad \text{or} \quad \frac{P/L}{Q_a \rho_b g} \tag{14.5}$$

Table 14.1. A list of variables affecting screw conveyor performance.

Symbol	Variable definition	Dimensions	Units
Q _a	actual volumetric capacity	L ³ /T	m ³ /s
P	power requirement	ML ² /T ³	W
d _t	tube inside diameter	L	m
d _{sf}	outside screw diameter	L	m
d _{ss}	screw shaft diameter	L	m
L	screw length	L	m
l _p	screw pitch length	L	m
l _i	exposed screw intake length	L	m
n	angular speed	1/T	rev/s
θ	angle of conveyor inclination	–	degrees
ρ _b	material bulk density	M/L ³	kg/m ³
μ ₁	material-metal friction	–	–
μ ₂	material-material friction	–	–
g	acceleration of gravity	L/T ²	m/s ²

The first term in the right hand side of Equation 14.5 is the ratio of the actual volumetric throughput rate to the theoretical volume swept by the screw per unit of time. This has been regarded as the volumetric efficiency of the screw conveyor. The second term in the right hand side of the above equation is the power required per unit length per unit mass flow rate of the material being conveyed. It has been defined as the specific power or the power efficiency of the conveyor. The conveyor length does not affect the volumetric efficiency.

The dimensionless terms of Equation 14.4 were used to develop prediction equations using experimental data. Published data on the performance of auger conveyors conveying wheat, oats, and shelled corn were used to develop the performance equations. These equations may be used to estimate conveyor performance for similar materials.

$$\frac{Q_a}{\frac{\pi}{4}(d_{sf}^2 - d_{ss}^2) l_p n} = (4.332 \times 10^{-4}) \left(2\pi n \sqrt{\frac{l_p}{g}} \right)^{-0.44} \left(\frac{l_i}{l_p} \right)^{0.31} (f_1(\theta))^{1.35} \mu_1^{-4.59} \mu_2^{-3.72} \quad (14.6)$$

$$\frac{P/L}{Q_a \rho_b g} = 3.54 \left(2\pi n \sqrt{\frac{l_p}{g}} \right)^{0.14} \left(\frac{d_{sf}}{l_p} \right)^{-10.12} \left(\frac{l_i}{l_p} \right)^{0.11} (f_2(\theta)) \mu_2^{2.05} \quad (14.7)$$

$$\text{where } f_1(\theta) = 1 + \cos^2 \theta \quad (14.8)$$

$$f_2(\theta) = 6.94 (1.3 - \cos^2 \theta)$$

θ = conveyor angle as measured from the horizontal, degrees

$$0.414 > \mu_1 > 0.374$$

$$0.554 > \mu_2 > 0.466$$

14.1.3 Screw conveyor performance

The performance of a screw conveyor, as characterized by its capacity, volumetric efficiency, and power requirements, is affected by the conveyor geometry and size, the properties of the material being conveyed, and the conveyor operating parameters such as the screw speed and the angle of inclination. The effect of these factors is discussed below.

14.1.3.1 Capacity

Screw length has no effect on the capacity of a screw conveyor. The effect of speed and inclination is given in Figure 14.2. As shown in the figure, there is a limiting value of speed beyond which the capacity does not increase. In fact, it may even decrease beyond a certain speed. It is also seen from this figure that the capacity decreases as the angle of inclination increases. The limiting value of speed is independent of the angle of inclination. It has been suggested that there may be two factors responsible for this behavior: (1) the maximum possible rate of grain flow through an orifice, and (2) the centrifugal force due to the rotation of the grain mass. Initially, the capacity increases directly with speed up to 250 rev/min. After this point the centrifugal force restricts the flow of grain at the intake and causes the slope to decrease. If the speed is increased sufficiently the centrifugal force may become so restrictive as to cause a decline in the capacity.

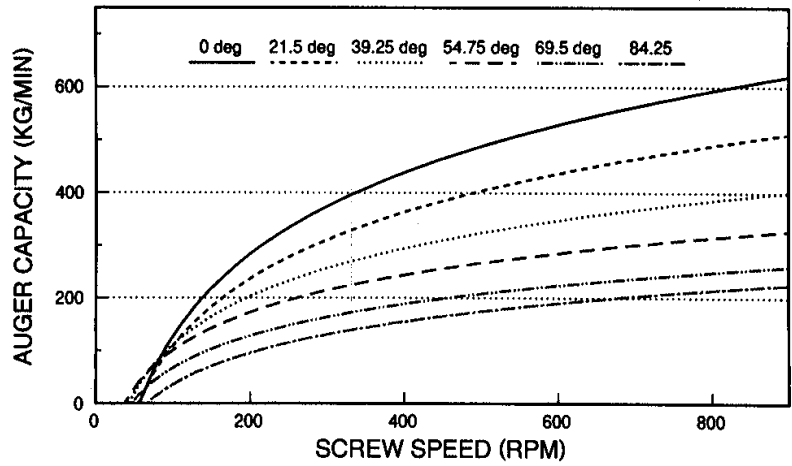


Figure 14.2 – Effect of screw speed and angle of auger inclination on conveying capacity (redrawn from Regan and Henderson, 1959).

Figure 14.3 shows the effect of screw angle of inclination on the capacity. The reduction in the capacity approximately follows the cosine function with two exceptions: (1) the capacity at higher speed is well below the cosine function, and (2) the capacity at 90° angle is about 30% of the horizontal capacity. This may be due to the restriction to grain flow into the intake of the conveyor at higher speeds and the fact that grain flows from a vertical orifice at one-third the rate from a comparable horizontal orifice.

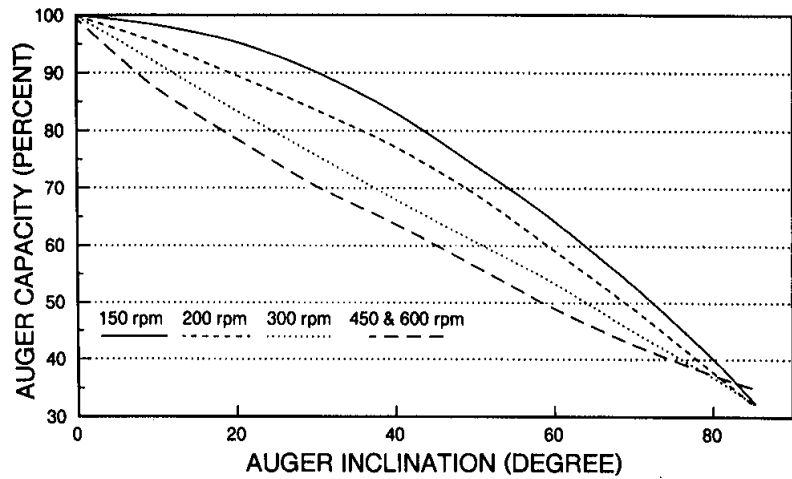


Figure 14.3 – Reduction in the auger conveying capacity as affected by the angle of inclination at different speeds (redrawn from Regan and Henderson, 1959).

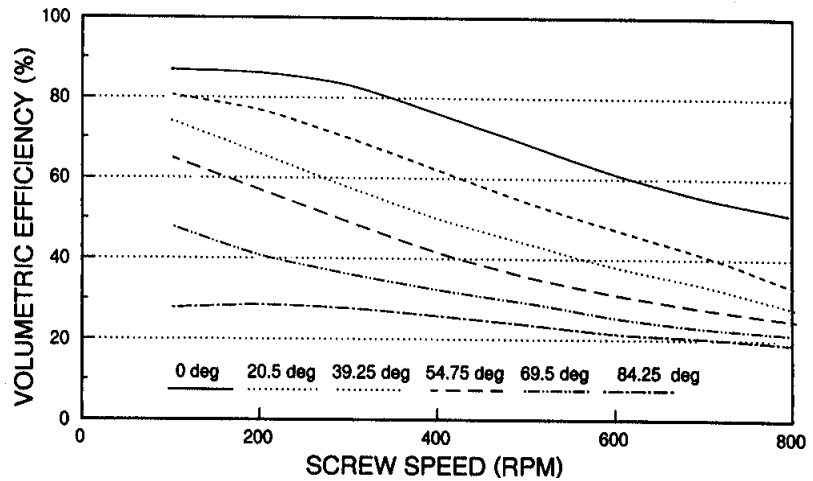


Figure 14.4 – Effect of screw speed on volumetric capacity at various angles of inclination (redrawn from Regan and Henderson, 1959).

14.1.3.2 Volumetric efficiency

Screw length has no effect on the capacity and volumetric efficiency of a screw conveyor. The effect of screw speed and inclination on volumetric efficiency is given in Figure 14.4. Generally, volumetric efficiency decreases as the screw speed and the angle of inclination increase. Brusewitz and Persson (1969) reported that the screw clearance affects the volumetric efficiency. As shown in Figure 14.5, the diametral

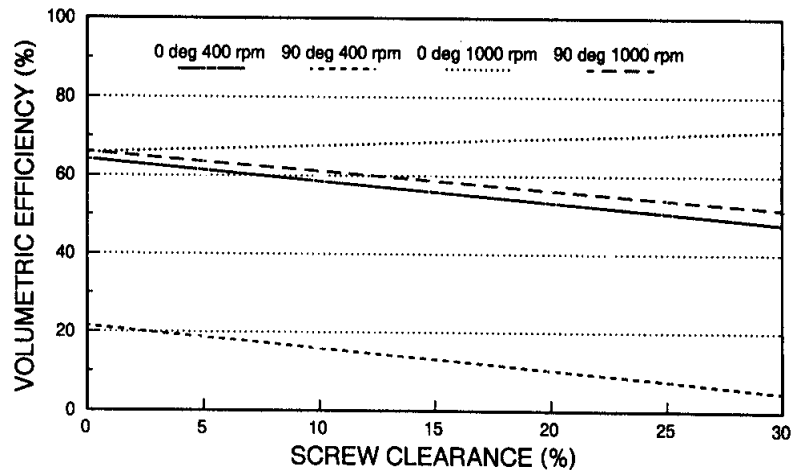


Figure 14.5 – Effect of the clearance between screw flightings and the tube inside diameter on the volumetric conveying efficiency (redrawn from Brusewitz and Persson, 1969).

clearances up to 5% to 7% have little effect on the volumetric efficiency, but a drop in efficiency of 0.7% per 1% increase in clearance can be expected. No interaction of the conveyor inclination and screw clearance is evident.

14.1.3.3 Power requirements

The effect of screw diameter on specific power, as defined earlier, is dependent on the speed of a screw conveyor. At low speeds there is a decrease in the specific power with increase in the screw diameter. The trend reverses with higher speeds. Screw length has no effect on specific power. There is a slight effect of the pitch on the specific power. An increase in pitch tends to reduce the specific power. For horizontal augers, an increase in the diametral clearance causes a slight decline in the specific power. However, for vertical augers, this results in a general increase in the power. An increase in screw speed results in an increase in the required power as shown in Figure 14.6. The hump in the power curve below 300 rev/min is due to the high torque value at lower speeds. Increasing the angle of inclination causes the power to increase initially but a decrease follows beyond a certain angle. This is due to the decline in the volumetric efficiency. Moisture content that is associated with increase in friction causes the specific power to increase significantly.

Presently, concise data are not available for individual design problems. The selection is based on data provided by the manufacturers. Most data provided by the manufacturers are for low-speed horizontal augers. However, the equations given above may be used for estimating auger capacity and power requirements for a given application.

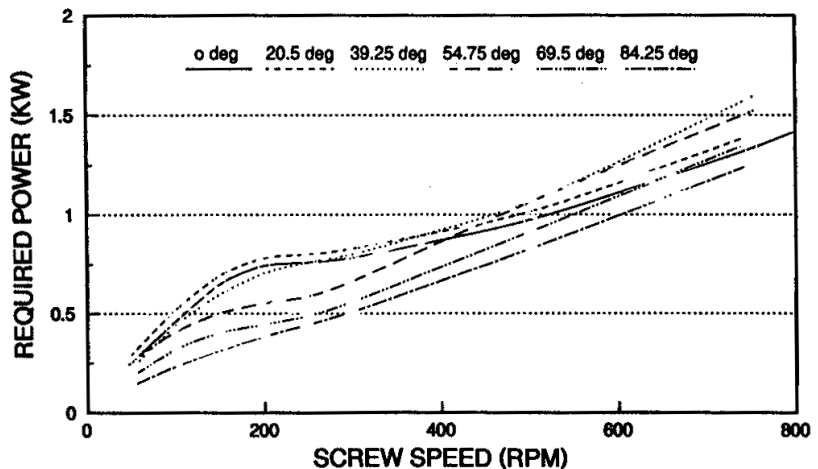


Figure 14.6 – Auger conveyor power requirements at different screw speeds and angles of inclination (redrawn from Regan and Henderson, 1959).

Example 14.1

Determine the efficiency, volumetric capacity, and power requirement of a horizontal standard pitch screw auger conveying wheat. The screw diameter is 15.24 cm (6 in.) and the shaft diameter is 2.54 cm (1 in.). The screw speed is 600 rev/min. The grain-metal friction may be taken as 0.414 while a value of 0.466 may be used for internal friction coefficient. The intake length of the screw is two times the pitch.

Solution

$$\begin{aligned} \text{Given: } d_{sf} &= 0.1524 \text{ m (6 in.)} & \mu_1 &= 0.414 \\ d_{ss} &= 0.0254 \text{ m (1 in.)} & \mu_2 &= 0.466 \\ l_p &= 0.1524 \text{ m (6 in.)} & n &= 10 \text{ rev/s (600 rev/min)} \\ l_i &= 0.3048 \text{ m (12 in.)} & \theta &= 0 \\ \rho_b &= 769 \text{ kg/m}^3 \text{ (Table 14.2)} \end{aligned}$$

Table 14.2. Grain properties related to pneumatic conveying (ASAE Data D241.2).

Material	Bulk density, kg/m ³	Particle density, kg/m ³	Equivalent particle diameter, mm
Wheat	769	1300	4.08
Oats	410	1050	4.19
Barley	615	1330	4.05
Soybeans	769	1180	6.74
Corn	718	1390	7.26

Use Equation 14.6 to determine the efficiency. The dimensionless groups are calculated as follows:

$$2\pi n \sqrt{\frac{l_p}{g}} = 2\pi(10) \sqrt{\frac{0.1524}{9/81}} = 7.83$$

$$\frac{d_{sf}}{l_p} = \frac{0.1524}{0.1524} = 1$$

$$f_1(\dots) = 2$$

$$\frac{l_i}{l_p} = \frac{0.3048}{0.1524} = 2$$

Substituting in Equation 14.6 we get:

$$\begin{aligned} \frac{Q_a}{\frac{\pi}{4}(d_{sf}^2 - d_{ss}^2) l_p n} &= (4.32 \times 10^{-4})(7.83)^{-0.44} (2)^{0.31} (2)^{1.35} (0.414)^{-4.59} (0.466)^{-3.72} \\ &= (4.32 \times 10^{-4})(0.4)(1.24)(2.55)(57.3)(17.12) \\ &= 0.53 \\ \eta_v &= 0.53 \text{ or } 53\% \end{aligned}$$

Volumetric capacity can be found as:

$$Q_a = 0.53 \frac{\pi}{4} [(0.1524)^2 - (0.0254)^2] (0.1524)(10) = 0.014 \text{ m}^3/\text{s} \text{ (or } 40.5 \text{ t/h)}$$

Use Equation 14.7 to determine the power requirement.

$$\begin{aligned} \frac{P/L}{Q_a \rho_b g} &= 3.54(7.83)^{0.14} (1)^{-10.12} (2)^{0.11} (3/23)^{1.0} (0.466)^{2.05} \\ &= 3.54(1.334)(1)(1.079)(3.23)(0.209) = 3.345 \\ P/L &= 3.345(0.014)(769)(9.81) = 368.4 \text{ W/m} \end{aligned}$$

14.2 PNEUMATIC CONVEYORS

Pneumatic conveyors move grain by imparting the kinetic energy of moving air to grain in conduits. Pneumatic conveyors are flexible in that they may be used to convey material to areas that are hard to reach by other mechanical conveyors. However, pneumatic conveyors require relatively higher specific power as compared to screw conveyors.

14.2.1 Pneumatic conveyor methods and equipment

14.2.1.1 Types of pneumatic conveying systems

The pneumatic conveying systems can be divided into three types: positive pressure, negative pressure, and combination negative/positive pressure systems. However, negative pressure systems are not common in agricultural applications.

Positive pressure systems. Material is introduced into the high-pressure stream of air by means of an air lock as shown in Figure 14.7. The material may be transported from a single point to many destination points. There is no need for a cyclone separator and a dust collector. High capacities may be obtained from a relatively smaller unit due to the higher operating pressures. The system is limited to 10 psig pressure.

Combination negative/positive systems. Some systems employ a combination of both vacuum and positive pressure. Vacuum is used to draw the material into the system and then the positive pressure is used to convey the material to its destination. The air mover for this system is larger than either of the above systems. A combination system is shown in Figure 14.8. The total range of pressure for the combination system is 33 cm (13 in.) Hg to 68.9 kPa (10 psig).

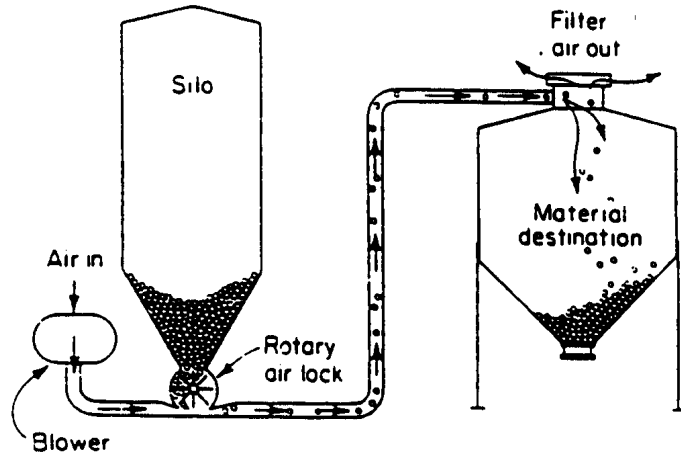


Figure 14.7 – A positive pressure pneumatic conveying system (reproduced from *Chemical Engineers' Handbook* by permission of McGraw-Hill Book Co.).

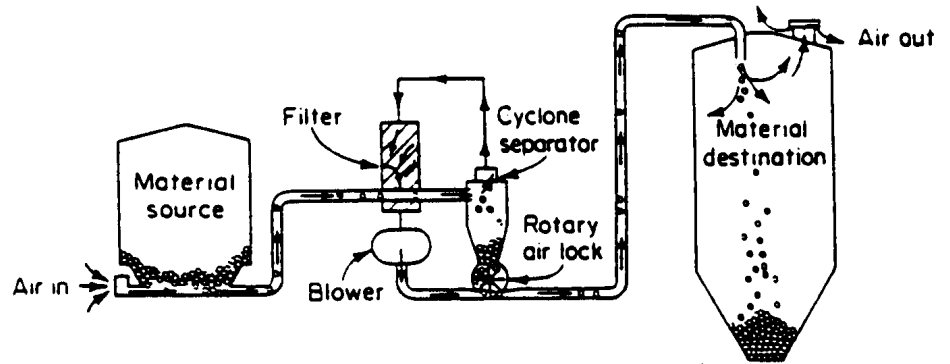


Figure 14.8 – A combination negative/positive pressure pneumatic conveying system (reproduced from *Chemical Engineers' Handbook* by permission of McGraw-Hill Book Co.).

14.2.1.2 Components of pneumatic conveying systems

The necessary components used to complete a pneumatic conveying system may be classified into the air moving system, the feeding system, the discharge system, and the piping and fittings.

Air moving system. The selection of the air mover depends upon the pressure and airflow requirements of the system. The air movers may be divided into low volume, high pressure or high volume, low pressure systems. Figure 14.9 shows a rotary posi-

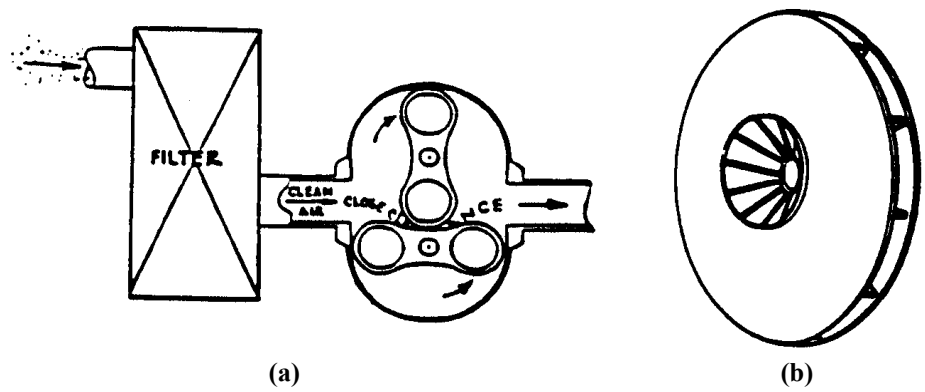


Figure 14.9 – (a) A rotary positive displacement blower, (b) a centrifugal blower (reprinted from Hellevang, 1985).

tive displacement blower and centrifugal blower. As shown in the figure, a pair of lobed rotors fitted inside a housing create the positive pumping action. These blowers are suitable for pressures up to 68.9kPa (10 psig). A pressure relief valve and an air filter are essential for a positive displacement blower. A centrifugal blower can generate a large volume of air but at relatively low pressures—usually less than 34.5 kPa (5 psig). However, the blowers may be connected in series to generate higher pressures. Centrifugal blowers are more tolerant of dirt which is an advantage when used in a negative pressure system.

Feeding system. The design of a feeding system depends upon the type of the conveying system used. For a pipeline under vacuum the material may be metered in

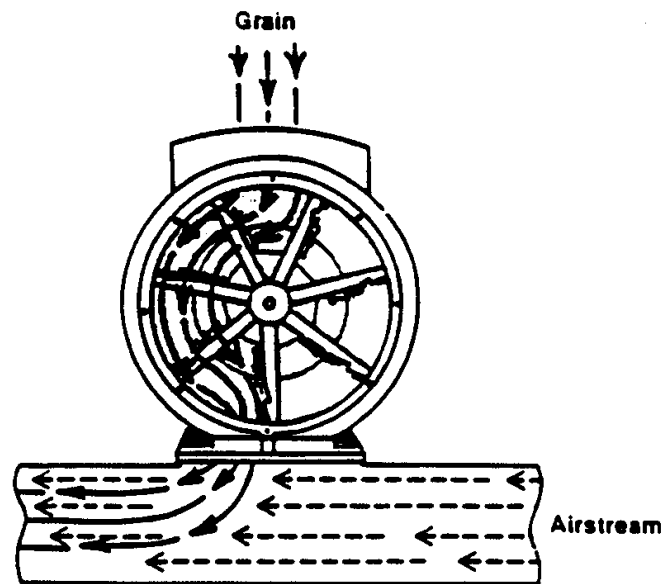


Figure 14.10 – A rotary air lock (reprinted from Hellevang, 1985).

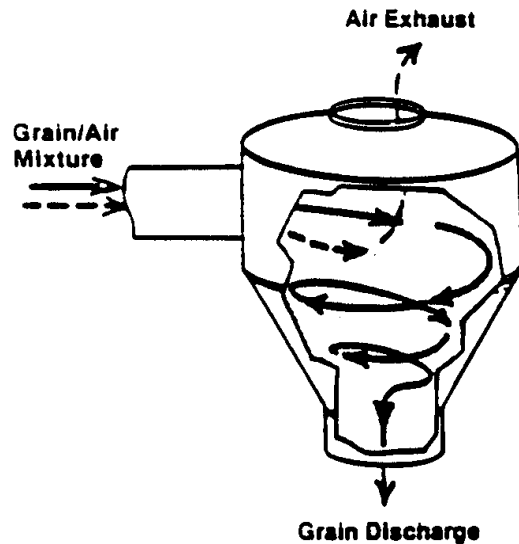


Figure 14.11 – A cyclone separator (reprinted from Hellevang, 1985).

through a rotary air lock, a controlled feed hopper, or a self-regulating pickup nozzle. For a pipeline under positive pressure the material must be metered in through a rotary air lock to keep back pressure to a minimum. A vent is provided in the feed hopper to relieve back pressure. Figure 14.10 shows a rotary air lock feeder. The speed of rotation is controlled to regulate the material flow rate.

Discharge system. For a pipeline under vacuum, the conveyed material must be separated from the conveying air. A *cyclone separator* is used to slow the grain in order for it to settle in the bottom and be separated from the air. A screen or a filter is needed to remove the dirt from the air before it enters the blower. For pipelines under pressure, the material may be discharged directly into the bins or silos. The discharge is tangential to create a cyclone effect. Often, in high velocity, low positive pressure systems, a cyclone separator is used to slow the material down to minimize damage to grain. A cyclone separator is shown in Figure 14.11.

Pipelines and fittings. Pipeline diameter, wall thickness, and the pipe material are to be determined while selecting a pipeline. The pipe material should be wear resistant. Most piping has smooth bores and couplings that butt the pipes to minimize grain damage. Long factory bends are preferred to minimize grain damage and pipe wear. It is recommended that the turning radius be six to eight times the tube diameter for bends of 45° or greater.

14.2.2 Theory of pneumatic conveyors

As solid particles are introduced in a flowing stream of air in a duct they are subjected to aerodynamic drag. If the air velocity is sufficiently high the particles accelerate and the drag is reduced, because the relative velocity between the particles and the

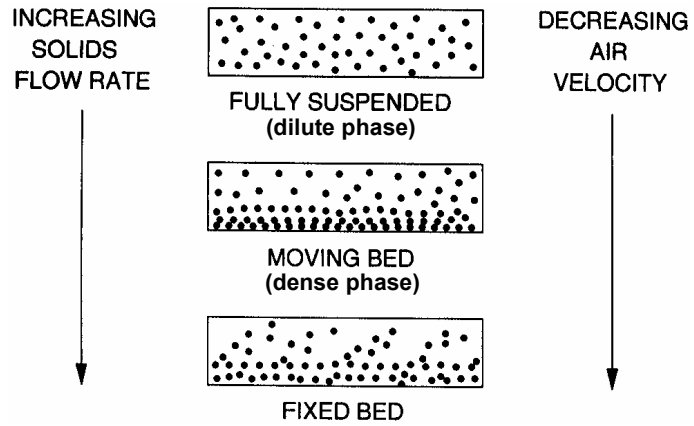


Figure 14.12 – Different phases of solids flow in pneumatic conveying.

air also is reduced. When the particles are being conveyed, the drag overcomes the forces of gravity, particle-to-particle interaction, and friction between the particles and the conduit wall. As the number of particles in the airstream are increased as a result of a higher conveying rate, the resistance to airflow increases. If the conveying rate of the solids continues to increase, there comes a point when the particles no longer behave as discrete particles. They may form clusters and eventually a plug if the flow rate of solids continues to increase. The phase when the solids are in a uniform suspension is called the *dilute phase* (also called the *lean phase*). The *dense phase* occurs when the particles begin to form clusters. Conveying of agricultural material is done in the dilute phase. Figure 14.12 shows the distribution of particles as the solids flow rate increases.

Figure 14.13 shows a plot of pressure drop per unit length versus superficial air-flow velocity at different material flow rates. In the initial part of the curve, the pressure drop decreases as the velocity increases. Then, after a certain velocity the pres-

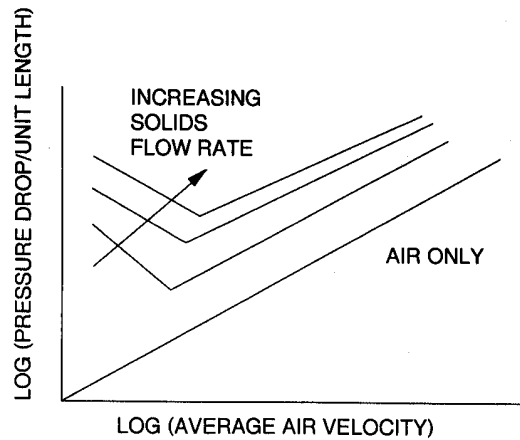


Figure 14.13 – A pneumatic conveying state diagram.

sure drop increases. The point of inflection of the curve essentially separates the dense phase from the dilute phase. The point that separates the two flow regimes is based on the mass flow rate of solids relative to that of the air. Generally, a solid/air mass flow ratio less than 15 would result in the dilute phase. The minimum point on the curve represents the minimum velocity required to produce the dilute phase for that mass flow rate.

During transport, the solid particles are in a suspension and may be treated as an aggregate of solids with void space. The void ratio (e) is defined as:

$$e = \frac{V - V_s}{V} = 1 - \frac{V_s}{V} \quad (14.9)$$

where V_s = volume occupied by solids, m^3
 V = total volume, m^3

The total volume occupied by solids is the sum of each solid particle and may be expressed as follows:

$$V_s = n V_p = \frac{\dot{m}}{\rho_p c} dL \quad (14.10)$$

where n = number of solids in the control volume

V_p = volume of each solid particle, m^3

\dot{m} = mass flow rate of solids, kg/s

ρ_p = density of solid particles, kg/m^3

c = velocity of solid particles, m/s

dL = elemental length of the conveyor tube, m

The density of solid particles may be determined from the data presented in Table 14.2. Substituting Equation 14.10 in Equation 14.9 we get:

$$e = 1 - \frac{\rho^*}{\rho_p} \quad (14.11)$$

where ρ^* = apparent bulk density of solids during transport, kg/m^3 , calculated as:

$$\rho^* = (\phi_m v \rho) / c$$

where ϕ_m = mass flow ratio = $\dot{m} / (\rho Q)$

where Q = volumetric flow rate of air, m^3/s

v = velocity of air, m/s

ρ = density of air, kg/m^3

c = solids velocity, m/s

Marcus et al. (1990) have reported the following equation for estimating the solids velocity (c):

$$\frac{c}{v} = 1 - 0.68d^{0.92} \rho_p^{0.5} \rho^{-0.2} D^{0.54} \quad (14.12)$$

where d = particle mean diameter, m .

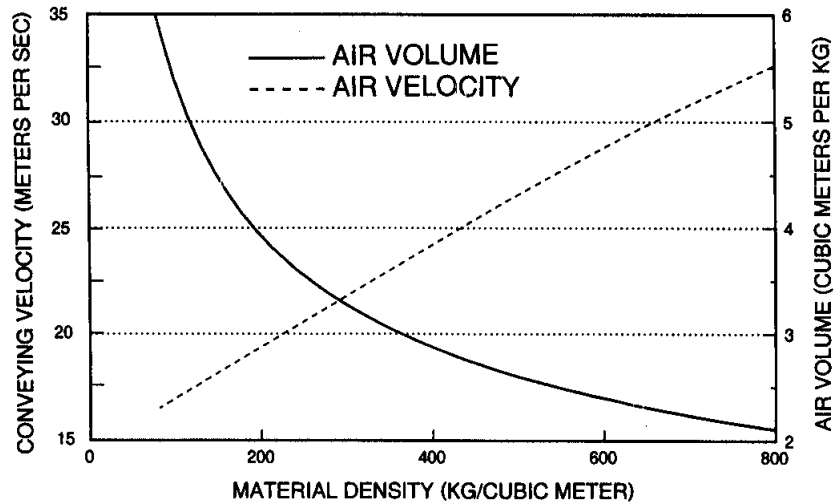


Figure 14.14 – Average velocities and air volume for low pressure pneumatic conveying of materials (redrawn from ASAE Data D273).

The design of a pneumatic conveying system involves determining the conveying air velocity, volume of conveying air, total pressure drop, and power requirement for the blower. The air velocity depends upon the size, shape, and density of the particles to be conveyed. The volume of air depends on the desired mass flow rate. Figure 14.14 shows the desired air velocity and volumetric flow rate that would produce dilute phase transport conditions. The pressure drop in the conveying system is a sum of many terms, as given by the following equation:

$$\Delta p = \Delta p_L + \Delta p_a + \Delta p_s + \Delta p_b + \Delta p_c \quad (14.13)$$

where Δp = total system pressure drop, Pa

Δp_L = line pressure loss due to air only, Pa

Δp_a = pressure drop due to particle acceleration, Pa

Δp_s = pressure drop due to solids friction, Pa

Δp_g = pressure drop due to vertical lift, Pa

Δp_b = pressure drop in bends, Pa

Δp_c = pressure drop in accessories, Pa

Line pressure loss. The line pressure loss is the pressure loss due to only air flowing through the conveying ducts. It can be estimated from the following equation:

$$\Delta p_L = \lambda_1 \frac{\rho}{2} v^2 \frac{L}{D} \quad (14.14)$$

where λ_1 = friction loss factor

L = length of the conveying duct, m

For turbulent flow the following equation given by Koo (as cited in Marcus et al., 1990) may be used to determine line friction loss factor:

$$\frac{\lambda_1}{4} = 0.0014 + 0.125 N_{Re}^{-0.32} \quad (14.15)$$

where the Reynolds number $N_{Re} = (\rho v D) / \mu$, and μ is the viscosity of air.

Acceleration pressure drop. As the solids are introduced into the air stream they are accelerated to the solids velocity (c). This acceleration requires an additional pressure drop. This pressure drop may be estimated from the following equation given by Marcus et al. (1990):

$$\Delta p_a = \phi_m v \rho c \quad (14.16)$$

Pressure drop due to solids. This pressure drop is due to solid particle interaction and wall friction. The following equation may be used to estimate this part of the total pressure drop:

$$\Delta p_s = \phi_m \lambda_s \frac{\rho}{2} v^2 \frac{L}{D} \quad (14.17)$$

Konno and Saito (Marcus et al., 1990) gave the following equation to determine the solids friction factor, λ_{ss} , needed in the above equation:

$$\lambda_s = \frac{0.0285 \sqrt{gD}}{c} \quad (14.18)$$

where g = acceleration due to gravity (9.81 m/s^2).

Pressure drop due to lift height. This pressure drop represents the potential energy change in lifting the solids through the desired height. The following equation is used to estimate this pressure drop:

$$\Delta p_g = \rho^* g \Delta z \quad (14.19)$$

where Δz = lift height, m.

Pressure drop due to bends. As the air/solid mixture goes around a bend, there is some loss of energy due to the friction of air and solids against the wall. The solids slow down as they go around the bend and an additional pressure is needed to accelerate them up to the conveying velocity. The pressure drop in a bend is computed separately for air and solids. The pressure drop due to air only is calculated by determining an equivalent length for the bend. An equivalent length is that length that produces the pressure drop in a straight pipe as that in the bend. The following equation is used to compute the equivalent length:

$$L_{eq} = \frac{K D}{\lambda_1} \quad (14.20)$$

where K = fitting loss coefficient.

The fitting loss coefficient (K) can be selected from Table 14.3. Equivalent length should be calculated for each bend and added to determine the total pressure loss due to the bends.

The pressure loss due to the solids can be calculated by the following equation:

$$\frac{\Delta P_{b, \text{solids}}}{\rho V^2} = 0.245 \left(\frac{m}{\rho v D^2} \right)^{1.267} \left(\frac{R}{D} \right)^{-0.260} \tag{14.21}$$

where $\Delta P_{b, \text{solids}}$ = pressure drop due to solids in bends, Pa
 R/D = bend radius to pipe diameter ratio

Pressure drop in accessories. The pressure loss in accessories is based on their design. No simple equations are available to estimate this pressure drop. Graphs are available in literature that can be used to determine Δp_c for different accessories. Often manufacturers provide pressure drop data which should be consulted. Table 14.4 gives pressure loss data for some common accessories.

Power requirements. The blower power requirement depends on the conveying air volumetric flow rate and total system pressure drop. The power requirement may be computed from the following equation for standard air. Correction should be made for altitude, temperature, and humidity.

$$P = \frac{\Delta p Q}{\eta_b} \tag{14.22}$$

where P = blower power requirement, W
 Δp = total system pressure drop, Pa
 Q = volumetric flow rate of air, m³/s
 η_b = blower efficiency, 0.5 to 0.7

The specific power or power per unit material flow rate may be calculated from:

Table 14.3. Some fitting loss coefficients, K, for turbulent flow (ASHRAE, 1972).

Fitting	Geometry	K
Entrance	Sharp	0.5
	Well-rounded	0.005
Contraction	Sharp ($D_2/D_1 = 0.5$)	0.38
90° elbow	Miter	1.3
	Short radius	0.9
	Long radius	0.6

Table 14.4. Pressure loss data for some common pneumatic conveying accessories (Noyes and Pfeiffer, 1985).

Accessory	Pressure drop, kPa
Blower suction	0.7
Inlet filter	0.7
Inlet filter and muffler	1.4
Outlet muffler and check plate	1.4
Discharge cyclone	0.7
Bin vent	1.4
In-line filter	1.4

$$P' = \frac{P}{\dot{m}} \quad (14.23)$$

where P' = specific power, W s/kg.

Example 14.2

Wheat is to be conveyed through a horizontal distance of 30 m horizontally and 10 m vertically at a rate of 30,000 kg/h. The transport line has four 90° bends and its diameter is 12.7 cm. Assuming standard air properties, determine total system pressure loss and blower power requirement.

Solution

From Table 14.2, wheat density, $\rho = 769 \text{ kg/m}^3$. Corresponding to this value, it is recommended that the conveying velocity be 32 m/s (Figure 14.14).

$$\text{Volumetric flow rate of air} = Q = (\pi/4)(0.127)^2(32) = 0.405 \text{ m}^3/\text{s}$$

$$\text{Mass airflow rate, } \rho Q = 1.2(0.405) = 0.486 \text{ kg/s}$$

Converting the 30,000 kg/h conveying rate to kg/s, we get 8.33 kg/s.

$$\text{Then, mass flow ratio, } \phi_m = 8.33/0.486 = 17.1$$

This ratio is higher than the required 15 for lean phase conveying. The velocity of air must be increased to decrease the mass flow ratio.

$$\text{Required air mass flow rate} = 8.33/15 = 0.56 \text{ kg/s}$$

$$\text{Required air velocity, } v = \frac{0.56}{1.2 \frac{\pi}{4} (0.127)^2} = 36.53 \text{ m/s}$$

Corresponding Reynolds number,

$$N_{Re} = \frac{\rho v D}{\mu} = \frac{1.2(36.53)(0.127)}{10^{-5}} = 5.57 \times 10^5$$

$$\text{Line pressure loss, } \Delta p_L = \lambda_1 \frac{\rho}{2} v^2 \frac{L}{D}$$

$$\lambda_1/4 = 0.0014 + 0.125(5.57 \times 10^5)^{-0.32}$$

$$\lambda_1 = 0.013$$

$$\text{So } \Delta p_L = 0.013 \frac{1.2}{2} (36.53)^2 \frac{(30+10)}{0.127} = 3240 \text{ Pa} = 3.24 \text{ kPa}$$

Acceleration pressure loss (use Table 9.1, p. 266, for d , particle diameter),

$$\Delta p_a = \phi_m v \rho c$$

$$c/v = 1 - 0.68 d p^{0.92} \rho_p^{0.5} \rho^{-0.2} D^{0.54}$$

$$= 1 - 0.68 (4.10 \times 10^{-3})^{0.92} (1300)^{0.5} (1.2)^{-0.2} (0.127)^{0.54} = 0.951$$

$$c = 0.951(36.53) = 24.74 \text{ m/s}$$

$$\Delta p_a = 15(36.53)(1.2)(24.74) = 22843 \text{ Pa} = 22.84 \text{ kPa}$$

Pressure drop due to lift height, $\Delta p_g = \rho^* g \Delta z$

$$\rho^* = \frac{\phi_m v \rho}{c} = \frac{15(36.53)(1.2)}{37.74} = 18.91 \text{ kg/m}^3$$

$$\Delta p_g = 18.91(9.81)(10) = 1860 \text{ Pa} = 1.86 \text{ kPa}$$

Pressure drop due to solids, $\Delta p_s = \phi_m \lambda_s \frac{\rho}{2} v^2 \frac{L}{D}$

$$\lambda_s = \frac{0.0285 \sqrt{g D}}{c} = \frac{0.0285 \sqrt{9.81(0.127)}}{34.74} = 0.92 \times 10^{-3}$$

$$\Delta p_s = 15(0.92 \times 10^{-3}) \frac{1.2}{2} (36.53)^2 \frac{40}{0.127} = 3460 \text{ Pa} = 3.46 \text{ kPa}$$

Pressure loss in bends, $L_{eq} = \frac{K D}{\lambda_1}$

$$\text{Assuming } K = 0.9 \text{ (Table 14.3), } L_{eq} = \frac{0.9(0.127)}{0.013} = 8.79 \text{ m}$$

$$\text{Total equivalent length for four bends, } L_{eq} = 4(8.79) = 35.2 \text{ m}$$

$$\text{Pressure loss, } \Delta p_{b,air} = 3.24(35.2)/40 = 2.85 \text{ kPa}$$

Pressure loss due to solids (assuming $R/D = 5$),

$$\begin{aligned} \frac{\Delta p_{b,solids}}{\rho v^2} &= 0.245 \left(\frac{m}{\rho v D^2} \right) \left(\frac{R}{D} \right)^{-0.260} \\ &= 0.245 \left(\frac{8.33}{1.2(36.53)(0.127)^2} \right) (5)^{-0.260} = 3.67 \end{aligned}$$

$$\Delta p_{b,solids} = 1.90(1.2)(36.53)^2 = 5870 \text{ Pa} = 5.87 \text{ kPa}$$

Thus, the total pressure drop is:

$$\Delta p = 3.24 + 22.84 + 1.86 + 3.46 + 2.85 + 5.87 = 40.12 \text{ kPa}$$

Note that the pressure drop is exclusive of the pressure drop due to the accessories, such as cyclones, etc.

$$\text{The power requirement is then } P = \frac{\Delta p Q}{\eta_b} = \frac{40.12 \frac{\pi}{4} (0.127)^2 36.53}{0.6} = 30.93 \text{ kW}$$

14.2.3 Pneumatic conveyor performance

The performance of a pneumatic conveying system depends on factors related to the equipment, the material being conveyed, and the operating conditions. Proper design is important for efficient operation. The selection of the type of conveying system would depend upon the given constraints on material feeding and discharge. Material properties and the desired feed rate would determine the airflow rate and the power requirements. Figure 14.15 presents performance data for corn for a 11.12 kW (15 hp) positive pressure system. The figure shows the effect of vertical lift and the horizontal conveying distance on the volumetric conveying rate. Table 14.5 gives a comparison of performance of an 60 kW (80 hp) positive/negative pneumatic unit with a 15.2 cm (6 in.) screw conveyor (PAMI, 1979). It is evident that a screw conveyor is considerably more efficient than the pneumatic unit.

Grain damage is an important performance parameter. According to a PAMI report (1977), 0.25% grain damage is caused for each pass through a pneumatic unit. It was also reported that the damage was comparable to that caused by a grain auger. Grain damage increases with conveying speed. Table 14.6 shows the effect of conveying speed on damage for white beans. Grain damage as caused by air lock is shown in Table 14.7 for two phases of conveying (Hellevang, 1985).

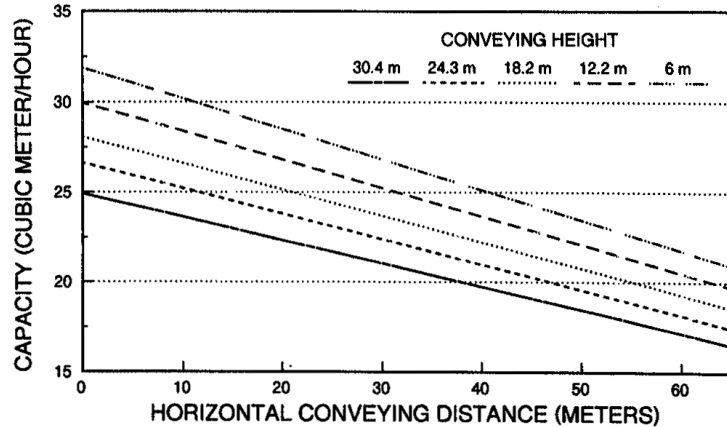


Figure 14.15 – Capacity of a pneumatic conveyor as affected by the vertical lift and the conveying distance (drawn using data by Hellevang, 1985).

Table 14.5. Comparison of 60 kW, positive/negative pressure 20.32 cm (8 in.) pneumatic unit to a 15.24 cm (6 in.) grain auger (Hellevang, 1985).

Grain type	Maximum conveying rates				Specific capacities	
	Pneumatic unit		Auger		Pneumatic unit, m ³ /kWh	Auger, m ³ /kWh
	t/h	m ³ /h	t/h	m ³ /h		
Wheat	25.1	28.5	37.6	42.7	0.87	10.60
Barley	24.2	34.4	27.9	39.7	1.04	11.77
Oats	33.5	67.1	21.8	43.8	1.79	16.00

Table 14.6. Damage in conveying white beans with a pneumatic conveyor (Hellevang, 1985).

Seed velocity, m/min	Germination, %	Visible seed damage, %
0 (control)	93.5	0.00
198	91.0	0.40
292	89.7	0.49
440	83.5	0.59
505	82.7	0.70
689	73.5	1.62

Table 14.7. Damage in conveying white beans with a pneumatic conveyor (Hellevang, 1985).

Breakage due to	Conveying Phase	
	Dense phase, %	Lean phase, %
Air lock	1.03	0.27
Transport	0.52	1.35
Total	1.55	1.62

14.3 BUCKET ELEVATORS

The bucket elevator is most commonly employed for vertical conveying of free-flowing materials such as small grain and pellets. A bucket elevator consists of equally spaced buckets mounted on a belt. The belt wraps around two pulleys located at the top and the bottom of a rectangular shaped housing as shown in Figure 14.16. As the belt rotates the buckets scoop some grain from the bottom and carry it up. At the top the buckets unload the material as they go around the top wheel and are made to turn upside down. Bucket size varies from 10.16 cm × 7.62 cm (4 in. × 3 in.) to as large as 35.56 cm × 20.32 cm (14 in. × 8 in.). Bucket spacing ranges from 11.43 cm (4.5 in.) to 30.49 cm (12 in.). The belt speed can vary from 1.2 m/s to 3.3 m/s. The capacity of the bucket elevator depends on the bucket size, bucket spacing, and belt speed. Commonly, the capacity of the elevators employed for agricultural applications is in the range of 7 m³/h to 350 m³/h.

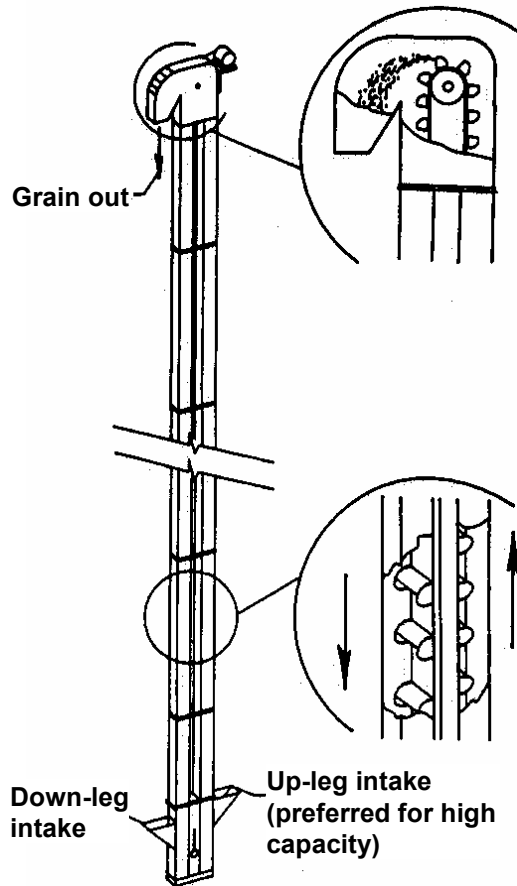


Figure 14.16 – Schematic diagram of a bucket elevator (reproduced with permission from *Grain Drying, Handling and Storage Handbook*, 2nd ed., 1987 © Midwest Plan Services).

14.3.1 Theory of bucket elevators

The relationship between head wheel speed and diameter is very important for satisfactory operation of this type of elevator. When the mass of grain in the bucket is moving around the head pulley it is subjected to the force of gravity acting vertically downward and the centrifugal force acting radially from the center of the head pulley. The resultant of these forces causes the material to be discharged from the bucket into the discharge chute. For clean emptying of the buckets, the start of the flow from the bucket must be delayed until after the bucket has passed its uppermost position on the head wheel. This situation will exist when the gravity and the centrifugal forces are equal. When the bucket reaches the top position on the head wheel, the resultant of the two forces will be zero, and there will be no discharging force on the material. It will neither be thrown vertically from the bucket nor fall out of the bucket.

Equating the weight of the grain to the centrifugal force acting on the grain, we get:

$$W = \frac{W}{g} \frac{v^2}{R}$$

or $v^2 = g R$

or $v = \sqrt{g R}$

Using $v = 2\pi Rn = (gR)^{0.5}$, the necessary wheel speed may be calculated as:

$$n = \frac{1}{2\pi} \sqrt{\frac{g}{R}} \quad (14.24)$$

where W = weight of material, N

v = velocity of material, m/s

g = acceleration of gravity, m²/s

R = radius to the center of gravity of material in the bucket, m

n = speed of head pulley, rps

Figure 14.17 shows the relationship between the head wheel speed and the radius of the path of the center of gravity of the material in the bucket about the center of the head wheel. To find the diameter of the head wheel, deduct from this radius the thickness of the belt and the distance from the belt to the center of gravity of the material in the bucket.

The trajectory of the material from the buckets is parabolic and can be determined from an equation of motion. It has been found that for high-speed elevators, those with head wheel diameters and speeds determined from the high-speed curve in Figure 14.17, the inner lip of the discharge chute should be located as close to the descending buckets as possible and at an angle of 15° to 20° below the center of the head wheel.

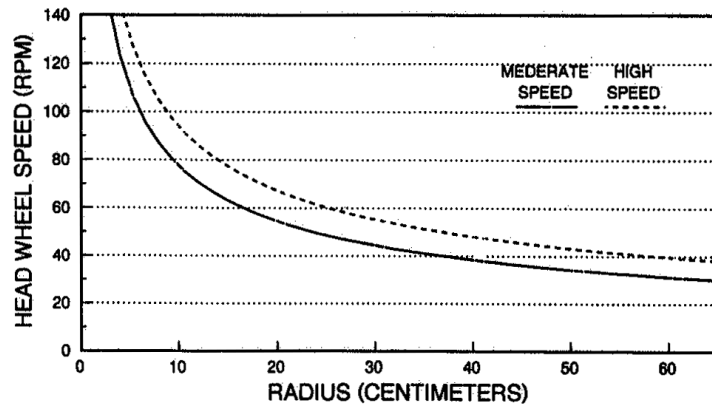


Figure 14.17 – Bucket conveyor vs. radius of the path of the center of gravity of the material in the bucket (redrawn from Millier, 1958).

14.3.2 Bucket elevator capacity

The capacity of bucket elevators depends upon the capacity of the individual buckets, the bucket spacing, and speed of the belt or chain carrying the buckets. Bucket spacing is governed by the shape of the bucket and its resulting discharge characteristics.

The capacity of a bucket is considered to be from 85% to 90% of the struck volume for high-speed elevators, if the feed is arranged to allow loading at or above the center of the foot shaft. If loading is below this point, the capacity may be reduced to 80% of the struck volume. On moderate speed elevators the bucket should be expected to fill 90% of its struck volume.

The following equation is used to determine elevator capacity:

$$Q = \frac{V v}{s} \quad (14.25)$$

where Q = elevator capacity, m^2/s

V = bucket volume, m^3

v = belt speed, m/s

s = bucket spacing, m)

14.3.2 Bucket elevator power

The horsepower required to operate a bucket elevator is that required to lift the material, to scoop the material into the buckets, to discharge the material, to move a small amount of air, and to overcome friction in the bearings and other drive components. In general the bucket elevator has a high elevating efficiency. In practice it has been found that theoretical horsepower required to lift the material needs to be increased only 10% to 15% to obtain the actual power requirement. The following equation is used to obtain the theoretical power requirement:

$$P = \rho_b g Q h \quad (14.26)$$

where P = theoretical power, W

ρ_b = material bulk density, kg/m^3

h = material lift height, m

It is advisable to use the struck volume of each bucket in determining the elevator capacity. This will eliminate power failures in instances where feed rate is high and the buckets are filling well above the center of the foot wheel.

Example 14.3

Find the velocity of the material being conveyed if the radius to the center of gravity of the material in the bucket is 30.48 cm (12 in.). Then, find the speed of the head pulley in rev/min. Determine the power requirement of this bucket elevator.

Given: bucket capacity = 0.25 kg bucket spacing = 20 cm
 belt speed = 1.25 cm/s height = 15 cm

$$\text{Velocity of material} = v = \sqrt{gR} = \sqrt{9.81 \times 0.3048} = 1.729 \text{ m/s}$$

$$\text{Speed of the head pulley} = n = \frac{60}{2\pi} \sqrt{\frac{g}{R}} = \frac{60}{2\pi} \sqrt{\frac{9.81}{0.3048}} = 54.17 \text{ rpm}$$

$$\begin{aligned} \text{Elevator capacity can be found as capacity} &= \frac{\text{bucket capacity} \times \text{belt speed}}{\text{bucket spacing}} \\ &= \frac{0.25 \times 1.250}{0.2} = 1.5625 \text{ kg/s} \end{aligned}$$

$$\begin{aligned} \text{Then, power requirement} &= \text{capacity} \times \text{height} \times g \\ &= 1.5625 \times 1.5 \times 9.81 = 22.845 \text{ W} \end{aligned}$$

14.4 FORAGE BLOWERS

Forage blowers are commonly used to convey chopped forage by imparting enough kinetic energy to the material to carry it through the conveying pipe. The blowers comprise of a feed hopper, a radial paddle blower, and a conveying pipe. Forage blowers are sometimes called forage throwers because of the throwing action caused by the blower paddles. A schematic of a forage blower is shown in Figure 14.18. The

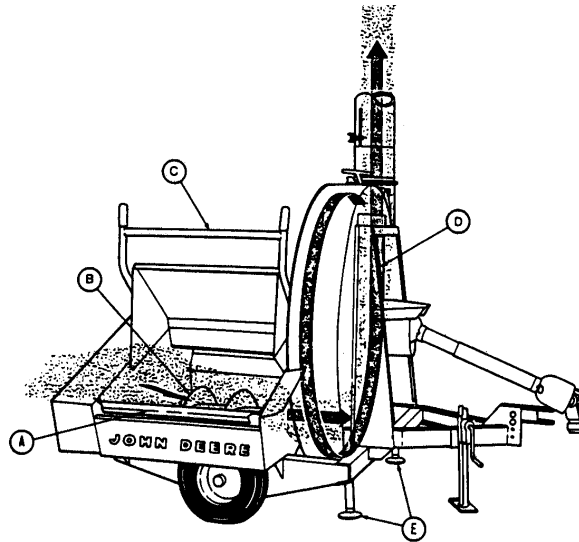


Figure 14.18 – A schematic of a forage blower: (a) shaker pan, (b) transfer auger, (c) clutch lever, (d) blower fan, (e) stabilizers (courtesy of Prairie Agricultural Machinery Institute, Canada).

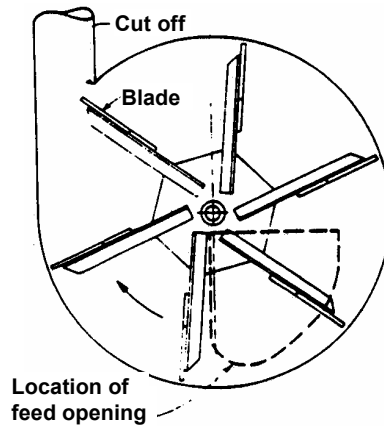


Figure 14.19 – Schematic diagram of an impeller blower (reprinted from Kepner et al., 1978).

material enters the blower housing through an opening in the side. The material is immediately accelerated by the rotating blades, as shown in Figure 14.19, and blown up the pipe that is located tangentially. As the material leaves the blades its velocity is higher than the airflow velocity. Consequently, the air provides a resistance to its movement upward. The material continues to slow due to the effects of the air drag, gravity, and friction with the pipe walls. After a time the material slows sufficiently so that its velocity is slower than the air velocity and the conveying is accomplished in a manner similar to that of a pneumatic conveyor. Therefore, the blower must impart enough kinetic energy to the material so that it will travel to the desired height in the conveying pipe.

Forage blowers are generally driven by the PTO shaft of a tractor. The blower impeller diameters are generally 1.2 to 1.4 m and peripheral speed about 35 m/s. Most discharge pipes have a 22.9 cm (9 in.) diameter. Capacities up to 100 t/h of corn silage are possible.

14.4.1 Theory of forage blowers

Chancellor (1960) completed an analysis of solid particles moving upward in a vertical pipe in an air stream. Based on the analysis and the experiments, he concluded that in the case of a blower, the solids impart energy to the air stream rather than the other way around. The result of air movement in the pipe is to reduce the effect of air resistance. He analyzed three possible cases as discussed below.

Phase 1. The particle is moving faster than the air stream velocity. The forces that act on the particle are inertia acting upward, air drag acting downward, and gravity also acting downward. The total height (H_1) that the material will rise until the particle velocity becomes equal to that of the air stream was developed by summing these forces and solving the resulting differential equation as:

$$H_1 = t_1 v_a - \left[\frac{v_s^2}{2g} \ln \left(\frac{v_s^2 + v_r^2}{v_s^2 + v_{ro}^2} \right) \right] \quad (14.27)$$

$$\text{where } t_1 = \frac{v_s}{g} \left(\tan^{-1} \frac{v_{ro}^2}{v_s} - \tan^{-1} \frac{v_r}{v_s} \right)$$

v_r = relative velocity of the particle in the air stream, m/s

v_{ro} = initial relative velocity, m/s

v_{ss} = terminal velocity of the particle, m/s

v_a = velocity of air stream, m/s

Phase 2. The particle will continue to decelerate until $v_r = v_s$. The height traveled in the second phase is as:

$$H_2 = v_a t_2 + \frac{v_s}{2g} \ln \left(\frac{v_s^2 - v_r^2}{v_s^2 - v_{ro}^2} \right) \quad (14.28)$$

$$\text{where } t_2 = \frac{v_s}{g} \left[\tan^{-1} \frac{v_r}{v_s} - \tan^{-1} \frac{v_r}{v_s} \right] \text{ and } v_r \text{ is negative.}$$

Phase 3. The final phase is when the relative velocity (v_r) is less than the terminal velocity (v_s) and the air is moving faster than the particle. For this case, the height traveled by the particle is H_3 .

$$H_3 = v_a t_3 - \frac{v_s}{2g} \ln \left(\frac{v_{ro}^2 - v_s^2}{v_r^2 - v_s^2} \right) \quad (14.29)$$

$$\text{where } t_3 = \frac{v_s}{g} \left[\coth^{-1} \frac{v_{ro}}{v_s} - \coth^{-1} \frac{v_r}{v_s} \right].$$

This phase is similar to that of pneumatic conveying of solids. If the air velocity (v_a), terminal velocity (v_t), and initial relative velocity (v_{ro}) are known or assumed, various values of t may be chosen and values of v_r computed and plotted (Figure 14.20). This plot is then used to construct a plot of total height (H_t) versus time (Figure 14.21).

As the particles travel upward in the pipe, the change in their velocity is caused by gravity and the air-particle interaction. The velocity change due to gravity is $\Delta v_g = g(\Delta t)$, where Δt is the time taken by the particle to travel between locations 1 and 2. The velocity change due to air interaction (Δv_f) is determined by equating the rate change of momentum to the force of the air in the pipe as follows:

$$F = \frac{dm}{dt} (\Delta v_f)$$

$$\text{or} \quad \Delta p = \frac{1}{A} \frac{dm}{dt} (\Delta v_f) \quad (14.30)$$

where $F = (\Delta p)A$

Δp = pressure drop in the pipe, Pa

dm/dt = mass flow rate, kg/s

Δv_f = total velocity change minus Δv_g , m/s

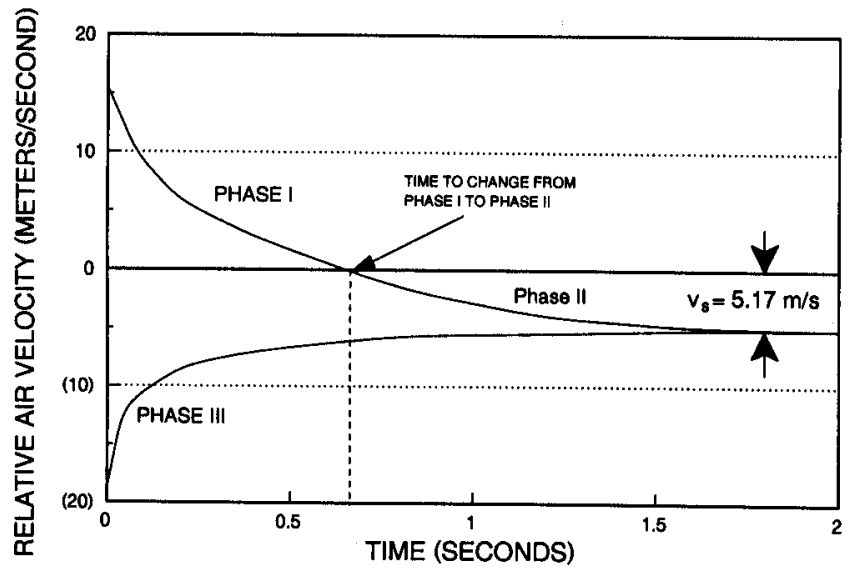


Figure 14.20 – Examples of particle velocity changes with time (redrawn from Chancellor, 1960).

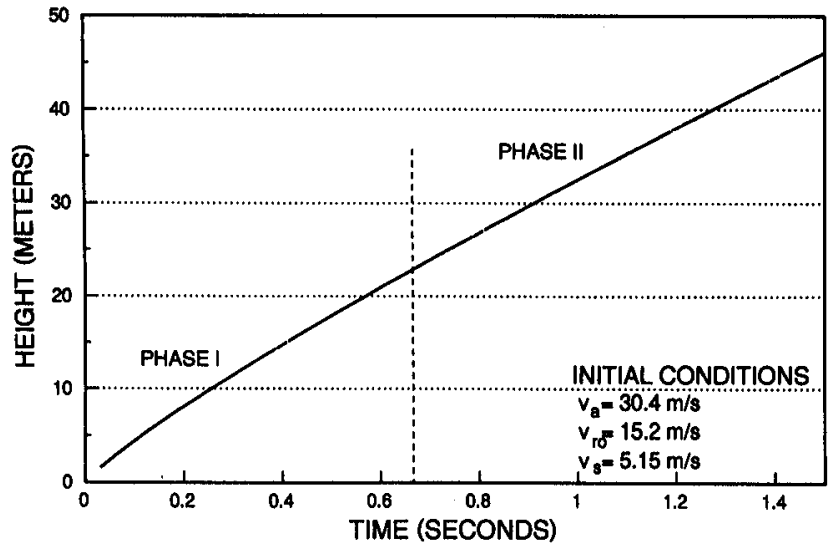


Figure 14.21 – Examples of particle height increase with time (redrawn from Chancellor, 1960).

Example 14.4

Find the total pressure drop in the pipe for a forage blower.

Given: $v_a = 30.4$ m/s $dm/dt = 4.54$ kg/s
 $v_{ro} = 15.2$ m/s pipe diameter = 0.228 m
 $v_s = 5.17$ m/s pipe height = 12.46 m

Solution

From Equation 14.27 (Phase 1 as plotted in Figures 14.20 and 14.21):

$$t = 0.33 \text{ sc (from 0 to 12.46 m)}$$

$$v_r = 2.8 \text{ m/s (at exit)}$$

$$\text{Particle velocity} = 30.4 + 2.8 = 33.2 \text{ m/s}$$

$$\text{Total velocity change} = 45.6 - 33.2 = 12.4 \text{ m/s}$$

$$\Delta v_g = 0.33 \times 9.81 = 3.24 \text{ m/s}$$

$$\Delta v_f = 12.4 - 3.24 = 9.16 \text{ m/s}$$

$$F = (4.54) 9.16 = 41.6 \text{ N}$$

$$\Delta p = 41.6/\pi (0.114)^2 = 1018.6 \text{ Pa}$$

The pressure loss due to pipe friction may be computed from Equation 14.14. The pipe Reynolds number is 8.3×10^5 . Using Equation 14.15, the line friction factor was computed as 0.012. These values result in $\Delta p_L = 364$ Pa for $v_a = 30.4$ m/s. The total pressure difference between the ends of the pipe will be $1018.6 - 364 = 654.6$ Pa. Since the top of the pipe is open to the atmosphere, the pressure at the bottom of the pipe will be 654.6 Pa below atmospheric pressure.

14.4.2 Energy requirements of forage blowers

Totten and Millier (1966) suggested that the total power requirements of a forage blower may be computed from the following equation:

$$P = \frac{1}{2\eta_b} \dot{m} r_f^2 \omega^2 \quad (14.31)$$

where P = power requirement, W

η_b = power efficiency of the forage blower

\dot{m} = mass flow rate, kg/s

r_f = paddle tip radius, m

ω = angular velocity, rad/s

A theoretical plot of efficiency as affected by the friction is given in Figure 14.22. According to this figure efficiency increases as the friction decreases.

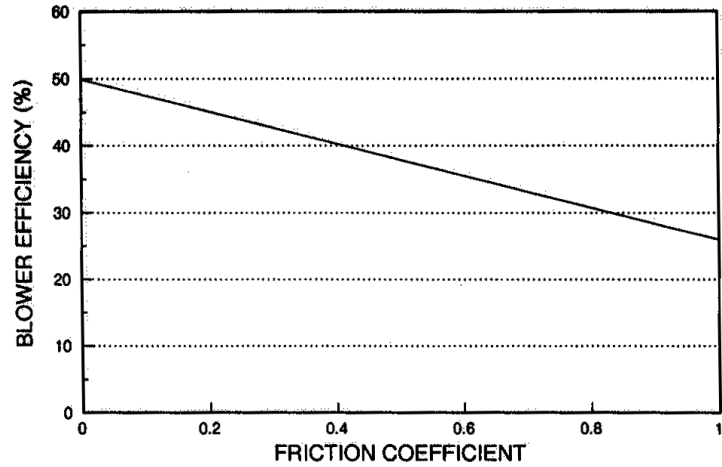


Figure 14.22 – Effect of friction on blower efficiency (redrawn from Chancellor, 1960).

Example 14.5

The material flow rate of a forage blower is 500 kg/min at 600 rev/min impeller speed. Determine the power requirement if the efficiency is 35%.

Solution

$$\dot{m} = \frac{500(\text{kg}/\text{min})}{60(\text{s}/\text{min})} = 8.34\text{kg}/\text{s}$$

$$\omega = \frac{600(\text{rpm})2\pi(\text{rad}/\text{rev})}{60(\text{s}/\text{min})} = 62.8\text{rad}/\text{s}$$

$$r_f = 0.6 \text{ m}$$

$$P = \frac{1}{2(0.35)}(8.34)(0.6)^2(62.8)^2 = 16.9\text{kW}$$

Table 14.8. Blower efficiency for various speeds, feed rates, and air inlet conditions (Pettingill and Millier, 1968).

Feed rate, kg/min	Blower speed, rpm	Air-door Conditions	
		Open	Closed
408	600	24.5	25.7
544	800	28.4	30.7
680	600	24.6	25.9
907	600	25.5	26.9

Table 14.9. Blower efficiency for various design changes (Pettengill and Millier, 1968).

Design condition	Blower efficiency (%) at air-door conditions	
	Open	Closed
Normal system	24.60	25.90
Inlet cutoff	24.63	25.22
Teflon paddles	24.08	24.17
Teflon paddles and housing	24.70	26.01

14.4.3 Forage blower performance

The blower efficiency is affected by the factors related to blower design, the operating conditions, and the material properties. Blower design factors include the blower size, number of blades, angle of paddle slant, clearance between paddle tip and the scroll, the location and size of the material inlet opening and the size of conveying pipe. The operating parameters include the conveying height, blower speed, and the material flow rate. The material parameters include bulk density and the coefficient of friction.

Pettingill and Millier (1968) conducted studies on the blower efficiencies that are summarized in Table 14.8. From the data presented in Table 14.8 they concluded that higher efficiency can be obtained in every case if the air door was closed. For a constant material flow rate, increasing the paddle speed increases the efficiency. Efficiency increases slightly with an increasing in paddle loading. Table 14.9 shows that the design changes have very little effect on the blower efficiency. Reducing friction increases efficiency.

14.5 MISCELLANEOUS CONVEYORS

14.5.1 Belt conveyors

Belt conveyors can carry different types of materials from easy flowing to hard-to-handle sticky material. They handle material gently with minimum damage. Belt speeds vary from very slow to a high of 300 m/min. Belt capacity can be as high as several tons per hour. Belts come in various widths. Generally, belt conveyors are not used at angles steeper than 30° while the most common inclination is around 20°. A general layout is given in Figure 14.23. The belts may be flat or troughed (Figure 14.24). Table 14.10 shows typical values for the capacity of horizontal conveyors. The capacity is affected by belt speed, width, and uniformity of loading.

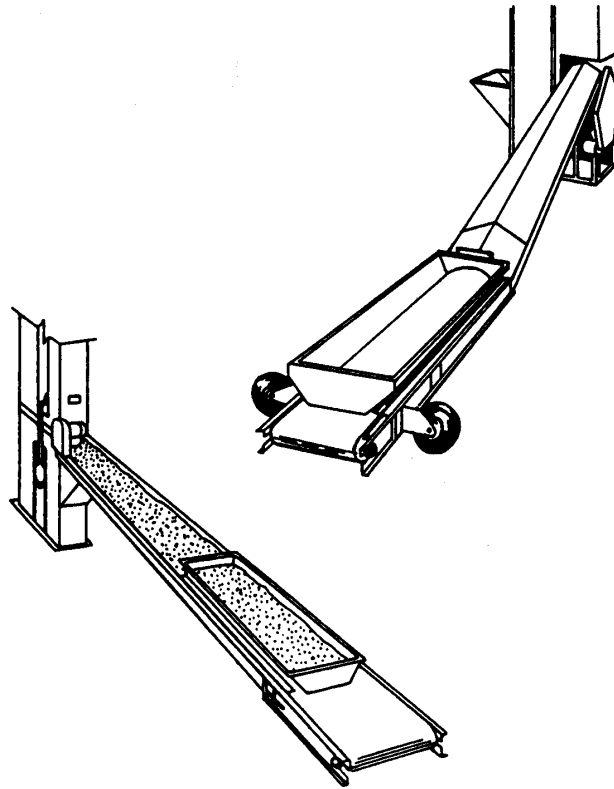


Figure 14.23 – Typical farm belt conveyors
(reproduced with permission from *Grain Drying, Handling and Storage Handbook*, 2nd ed., 1987 © Midwest Plan Service).

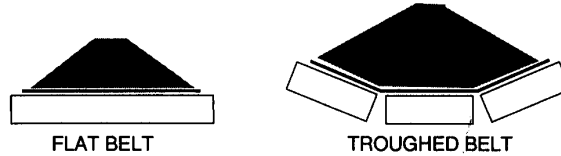


Figure 14.24 – Two types of belt conveyors.

Table 14.10. Typical bulk flow capacity and power (Midwest Plan Service, 1987).

Conveyor width and depth,		Capacity, M ³ /h	Power, kW/m
m	(in)		
0.203	(8)	130	0.245
0.228	(9)	164	0.294
0.254	(10)	202	0.343
0.279	(11)	245	0.392
0.304	(12)	291	0.441
0.330	(13)	342	0.515

14.5.2 Bulk or mass conveyors

Bulk flow or mass flow conveyors are paddles of various shapes attached to a chain at equal distance and housed in a rectangular or circular housing. As the chain moves, these paddles drag material along the bottom of the housing. These conveyors are common in commercial elevators. Figure 14.25 shows rectangular and round mass conveyors. The capacity of these conveyors may be estimated from the data given in Table 14.10.

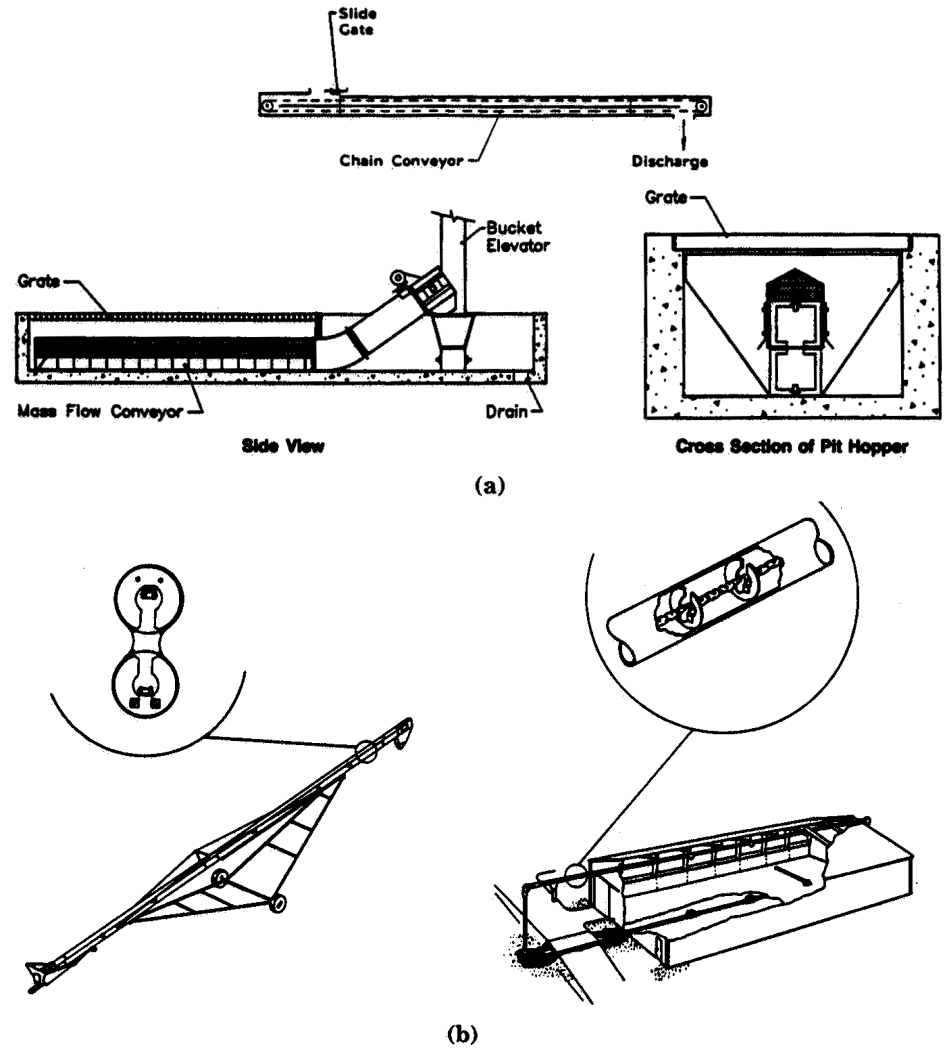


Figure 14.25 – Bulk or mass flow conveyors: (a) horizontal conveyors, and (b) inclined and vertical conveyors (reproduced with permission from *Grain Drying, Handling and Storage Handbook*, 2nd ed., 1987 © Midwest Plan Service).

PROBLEMS

- 14.1 The auger conveyor of Example 14.1 is to be used at an angle of 45° from the horizontal. If the desired capacity is to remain unchanged, what changes would you make to accomplish this? What power would be required?
- 14.2 For the conveyor of Problem 14.1 plot the volumetric capacity against the angle of inclination ranging from 0° to 90° . Also plot the power requirements.
- 14.3 If the material is shelled corn in Problem 14.1, determine the volumetric capacity and the power requirements for 0° and 45° .
- 14.4 If a half-pitch screw is used in Problem 14.1, determine the capacity of the conveyor. Is the capacity reduced? If yes, what would you do to achieve the same capacity? Is the specific power changed? Explain the results.
- 14.5 Soybeans are to be pneumatically conveyed in a 15 cm diameter tube at a rate of 10,000 kg/h. Determine the minimum air velocity needed to produce dilute phase transport conditions. Determine the apparent bulk density and void ratio during transport.
- 14.6 Same as Example 14.2, except use shelled corn data and determine the total system pressure drop exclusive of the accessories.
- 14.7 Same as Problem 14.6, except compute pressure drop for 10, 12.5, 15, 17.5, and 20 cm diameters. Plot the pressure drop and power requirements against the pipe diameter. What would you recommend as the most desirable pipe diameter and why?

MACHINERY SELECTION AND MANAGEMENT

15

INTRODUCTION

Because of the seasonal nature of farm work, farm machinery is used during relatively short periods of the year. With growth in average farm size, machines of high capacity are required to accomplish their task during these short periods. Unlike factory machines, whose costs can be amortized over thousands of hours of annual use, farm machines are typically amortized over hundreds of hours of annual use. The need to amortize machine costs over low hours of annual use puts tight constraints on the manufacturing costs of farm machines. At the same time, since lost time is very costly during the limited periods of annual use, farm machines must be designed to have high reliability and high field efficiency. As early as 1924, it was noted that “time is the essence of farming” and that whatever helps to shorten the time required for planting and harvesting will help overcome the effects of adverse weather (Mount, 1924). Thus, machinery selection and management techniques are of great interest to both the designer and user of farm machinery. ASAE (now ASABE) has fostered research on machinery selection and management for many years and currently has three related documents in its annual standards book. They are Standard S495 on uniform terminology, Engineering Practice EP496 on machinery management, and D497 on machinery management data.

15.1 FIELD CAPACITY AND EFFICIENCY

15.1.1 Field capacity

Field capacity refers to the amount of processing that a machine can accomplish per hour of time and was first calculated by McKibben (1930). Field capacity can be expressed on a material or area basis. On an area basis, the field capacity is:

$$C_a = \frac{v w \eta_f}{10} \quad (15.1)$$

On a material basis, the field capacity is:

$$C_m = \frac{v w Y \eta_f}{10} \quad (15.2)$$

where C_a = field capacity, area basis, ha/h (C_{at} when $\eta_f = 1.0$)

C_m = field capacity, material basis, Mg/h (C_{mt} when $\eta_f = 1.0$)

v = travel speed, km/h

w = machine working width, m

Y = crop yield, Mg/ha

η_f = field efficiency, decimal

The term *theoretical field capacity* is used to describe the field capacity when the field efficiency is equal to 1.0, i.e., theoretical field capacity is achieved when the machine is using 100% of its width without interruption for turns or other idle time. For cultivators and other machines that work in rows, the machine working width is equal to the row spacing times the number of rows processed in each pass. An operator with perfect steering skills would be required to use the full width of mowers and other machines that do not work in rows. Since operators are not perfect, less than the full width of such machines is used in order to ensure coverage of the entire land area, i.e., there is some overlapping of coverage.

The travel speed of balers, forage choppers, and other machines that process a product may be limited by the C_{mt} , i.e., by the theoretical field capacity of the machine on a materials handling basis. For a given C_{mt} , W , and Y , Equation 15.2 could be used with $\eta_f = 1.0$ to find the allowable forward speed. Equation 15.2 is not relevant to machines that do not process a product, e.g., tillage machines; the speed of such machines is limited by one or more other factors, including available power, quality of the work accomplished, safety, etc. Typical operating speeds for various machines are listed in Table 15.1.

15.1.2 Field efficiency

The theoretical time, τ_t , required to perform a given field operation varies inversely with the theoretical field capacity and can be calculated using the following equation:

$$\tau_t = \frac{A}{C_{at}} \quad (15.3)$$

where τ_t = theoretical time required to perform operation, h

C_{at} = theoretical field capacity, ha/h

A = area to be processed, ha

The actual time required to perform the operation will be increased due to overlap, time required for turning on the ends of the field, time required for loading or unloading materials, etc. Such time losses lower the field efficiency below 100%. The following equation can be used to calculate the field efficiency:

$$\eta_f = \frac{\tau_t}{\tau_e + \tau_h + \tau_a} \quad (15.4)$$

where $\tau_e = \tau_t / K_w$ = effective operating time, h

K_w = fraction of implement width actually used

τ_a = time losses that are proportional to area, h

τ_h = time losses that are not proportional to area, h

Table 15.1. Field efficiency, field speed, and repair and maintenance cost parameters (adapted from ASAE Data D497).

Machine	Effic. Range %	Typ. Effic. %	Speed Range, km/h	Typ. Speed, km/h	Est. Life, h	Total Life R & M ^[b] Cost, % of list price	RF1	RF2
Tillage and Planting								
Moldboard plow	70-90	85	5.0-10.0	7.0	2000	100	0.29	1.8
Heavy-duty disk	70-90	85	5.5-10.0	7.0	2000	60	0.18	1.7
Tandem disk harrow	70-90	80	6.5-11.0	10.0	2000	60	0.18	1.7
Chisel plow	70-90	85	6.5-10.5	8.0	2000	75	0.28	1.4
Field cultivator	70-90	85	8.0-13.0	11.0	2000	70	0.27	1.4
Spring tooth harrow	70-90	85	8.0-13.0	11.0	2000	70	0.27	1.4
Roller-packer	70-90	85	7.0-12.0	10.0	2000	40	0.16	1.3
Mulcher-packer	70-90	80	6.5-11.0	8.0	2000	40	0.16	1.3
Rotary hoe	70-85	80	13-22.5	19.0	2000	60	0.23	1.4
Row crop cultivator	70-90	80	5.0-11.0	8.0	2000	80	0.17	2.2
Rotary tiller	70-90	85	2.0-7.0	5.0	1500	80	0.36	2.0
Row crop planter	50-75	65	6.5-11.0	9.0	1500	75	0.32	2.1
Grain drill	55-80	70	6.5-11.0	8.0	1500	75	0.32	2.1
Harvesting								
Corn picker sheller	60-75	65	3.0-6.5	4.0	2000	70	0.14	2.3
Combine	60-75	65	3.0-6.5	5.0	2000	60	0.12	2.3
Combine (Sp) ^[a]	65-80	70	3.0-6.5	5.0	3000	40	0.14	2.1
Mower	75-85	80	5.0-10.0	8.0	2000	150	0.46	1.7
Mower (rotary)	75-90	80	8.0-19.0	11.0	2000	175	0.44	2.0
Mower-conditioner	75-85	80	5.0-10.0	8.0	2500	80	0.18	1.6
Mower-condition (rotary)	75-90	80	8.0-19.0	11.0	2500	100	0.16	2.0
Windrower (SP)	70-85	80	5.0-13.0	8.0	3000	55	0.06	2.0
Side delivery rake	70-90	80	6.5-13.0	10.0	2500	60	0.17	1.4
Rectangular baler	60-85	75	4.0-10.0	6.5	2000	80	0.23	1.8
Large rectangular baler	70-90	80	6.5-13.0	8.0	3000	75	0.10	1.8
Large round baler	55-75	65	5.0-13.0	8.0	1500	90	0.43	1.8
Forage harvester	60-85	70	2.5-8.0	5.0	2500	65	0.15	1.6
Forage harvester (SP)	60-85	70	2.5-10.0	5.5	4000	50	0.03	2.0
Sugar beet harvester	50-70	60	6.5-10.0	8.0	1500	100	0.59	1.3
Potato harvester	55-70	60	2.5-6.5	4.0	2500	70	0.19	1.4
Cotton picker (SP)	60-75	70	3.0-6.0	4.5	3000	80	0.11	1.8
Miscellaneous								
Fertilizer spreader	60-80	70	8.0-16.0	11.0	1200	80	0.63	1.3
Boom-type sprayer	50-80	65	5.0-11.5	10.5	1500	70	0.41	1.3
Air-carrier sprayer	55-70	60	3.0-8.0	5.0	2000	60	0.20	1.6
Bean puller-windrower	70-90	80	6.5-11.5	8.0	2000	60	0.20	1.6
Beet topper/stalk chopper	70-90	80	6.5-11.5	8.0	1200	35	0.28	1.4
Forage blower					1500	45	0.22	1.8
Forage wagon					2000	50	0.16	1.6
Wagon					3000	80	0.19	1.3

^[a] SP indicates self-propelled.

^[b] R & M is repair and maintenance.

τ_a and τ_h represent the two extremes for types of time losses and some losses may fall between these extremes. Examples of τ_a -type losses include unclogging of spray nozzles, adding filling fertilizer or seed boxes, or filling spray tanks. For a given yield, time spent in unloading harvested crop is proportional to area but unloading time also increases with yield. Many τ_h -type losses are proportional to effective operating time, τ_e ; these include rest stops, adjusting equipment, and idle travel at field ends if such travel is at normal operating speed. Field shape can have an important effect on τ_h , i.e., τ_h will be much smaller relative to τ_e if the field is long and narrow. Then the machine will make fewer turns at the end for a given field area. Time required to move a machine to or from a field is not included in field efficiency calculations; else the field efficiency would vary widely depending upon distance between fields and distance from the machine storage site. Calculation of field efficiency and capacity is illustrated in Example Problem 15.1.

Example Problem 15.1

A self-propelled combine with a 12-row corn head for 75 cm row spacing travels at 5 km/h while harvesting corn yielding 12 Mg/ha. Losses proportional to area total to 5.2 minutes per hectare and are primarily due to unloading grain from the combine. Neglecting any other losses, calculate (a) the field efficiency and the field capacity on (b) an area basis and (c) material basis.

Solution

(a) In calculating the field efficiency, consider the time uses while harvesting one hectare. From the given information, $\tau_a = 5.2$ minutes and $\tau_h = 0$. To determine τ_e , note that a row crop header uses the full width, so that $K_w = 1.0$ and thus $\tau_e = \tau_t$. From Equation 15.1, the theoretical field capacity on an area basis is:

$$C_{at} = 5(12 \times 0.75)1.0/10 = 4.5 \text{ ha/h}$$

Then, from Equation 15.3:

$$\tau_e = \tau_t = 1/4.5 = 0.222 \text{ h or 13.3 minutes}$$

Finally, from Equation 15.4, the field efficiency is:

$$\eta_f = 13.3/(13.3+5.2+0) = 0.72$$

(b) Now the actual field capacity on an area basis can be calculated:

$$C_a = 4.5(0.72) = 3.24 \text{ ha/h}$$

(c) Finally, by multiplying by the crop yield, the field capacity on a material basis can be calculated:

$$C_m = 3.24(12) = 38.9 \text{ Mg/h}$$

Machine breakdowns cause time losses and reduction of field efficiency if the breakdowns occur during planned working hours. The probability of machine downtime is equal to one minus the operational reliability of the machine. One useful way of expressing machine reliability is as the mean time between failures. As shown in ASAE EP456, the reliability of a group or components or machines with a serial relationship is the product of the individual reliabilities, i.e.:

$$R_m = \frac{100r_1r_2\dots r_\lambda}{100^\lambda} \quad (15.5)$$

where R_m = reliability of the entire machine, percent
 $r_1, r_2, \text{ etc.}$ = reliabilities of individual components, percent
 λ = total number of components in series

Components are said to be in series if the failure of any one of the components stops the operation of the entire machine. Conversely, reliability can be increased through redundancy, i.e., through use of components in parallel such that, when a component fails, a parallel component will take over the function. Equation 15.5 is valid for calculating the reliability of a single machine based on the reliabilities of its components, or for calculating the overall reliability of a group of machines based on their individual reliabilities. For example, if a successful hay harvesting operation requires the use of a mower, a rake, and a baler in sequence, the overall reliability of the harvesting operation is the product of the individual reliabilities of the mower, rake, and baler. The reliability probability for a machine or group of machines is essentially one for the next minute, but decreases with time. Thus, the probability that a large, complex machine will operate extensively over several seasons without a breakdown is essentially zero. Farmers repair machines during the off-season or trade old machines for new in order to maintain an acceptable level of reliability.

Careful consideration of Equation 15.4 leads to the conclusion that time losses are much more critical for a large machine than for a smaller one. As τ_c declines with increasing C_{at} , time losses τ_a and τ_h become larger relative to τ_c . Thus, as a company increases the theoretical field capacity of its combines, for example, it becomes essential to also increase the rate at which the grain tank can be unloaded, decrease the field time needed to service the machine, and decrease any other time losses. Similarly, in increasing a planter size from 4-row capacity to 12-row capacity, for example, it is important to provide a quicker means for refilling seed boxes on the larger planter. Otherwise, the field efficiency will decrease and the effective field capacity will increase less than the increase in theoretical field capacity. Table 15.1 provides a range of field efficiencies and a typical field efficiency for a variety of machines.

15.2 DRAFT AND POWER REQUIREMENTS

Draft and power requirements are important in selecting tractors and implements because tractors must be large enough to meet the implement draft requirements. Also, the engine in tractors or self-propelled machines must be large enough to supply the

power requirements of the field operations. The following equation can be used to estimate draft requirements:

$$D_i = F_i (A + Bv + Cv^2) wd \quad (15.6)$$

where D_i = implement draft, kN

F_i = dimensionless texture adjustment factor from Table 15.2

i = 1 for fine, 2 for medium, or 3 for coarse textured soils

A, B, and C = implement-specific constants from Table 15.2

d = tillage depth, cm (use 1.0 for minor tillage tools and seeders)

Draft estimates from Table 15.2 are averages and can vary by plus or minus the percentages shown in the right-most column of the table. After the implement draft is determined, the drawbar power can be calculated using the following equation:

$$P_{db} = \frac{D_i v}{3.6} \quad (15.7)$$

where P_{db} = drawbar power, kW

v = travel speed, estimated from Table 15.1.

Tractors are often rated by brake power or PTO power rather than drawbar power. After the drawbar power is calculated, the PTO power and/or net flywheel power can be estimated using Figure 15.1.

Table 15.2. Draft parameters for tillage and seeding implements (adapted from ASAE Data D497).

Implement	Width units	A	B	C	F_1	F_2	F_3	Range, \pm %
Major Tillage Tools								
Subsoiler/manure injector								
Narrow point	tools	226	0.0	1.8	1.0	0.70	0.45	50
30 cm winged point	tools	294	0.0	2.4	1.0	0.70	0.45	50
Moldboard plow	m	652	0.0	5.1	1.0	0.70	0.45	40
Chisel plow								
5 cm straight point	tools	91	5.4	0.0	1.0	0.85	0.65	50
7.5 cm shovel/35 cm sweep	tools	107	6.3	0.0	1.0	0.85	0.65	50
10 cm twisted shovel	tools	123	7.3	0.0	1.0	0.85	0.65	50
Sweep plow								
Primary tillage	m	390	19.0	0.0	1.0	0.85	0.65	45
Secondary tillage	m	273	13.3	0.0	1.0	0.85	0.65	35
Disk harrow, tandem								
Primary tillage	m	309	16.0	0.0	1.0	0.88	0.78	50
Secondary tillage	m	216	11.2	0.0	1.0	0.88	0.78	30
Disk harrow, offset								
Primary tillage	m	364	18.8	0.0	1.0	0.88	0.78	50
Secondary tillage	m	254	13.2	0.0	1.0	0.88	0.78	30
Disk gang, single								
Primary tillage	m	124	6.4	0.0	1.0	0.88	0.78	25

Secondary tillage	m	86	4.5	0.0	1.0	0.88	0.78	20
Coulters								
Smooth or ripple	tools	55	2.7	0.0	1.0	0.88	0.78	25
Bubble or flute	tools	66	3.3	0.0	1.0	0.88	0.78	25
Field cultivator								
Primary tillage	tools	46	2.8	0.0	1.0	0.85	0.65	30
Secondary tillage	tools	32	1.9	0.0	1.0	0.85	0.65	25
Row crop cultivator								
S-tine	rows	140	7.0	0.0	1.0	0.85	0.65	15
C-shank	rows	260	13.0	0.0	1.0	0.85	0.65	15
No-till	rows	260	13.0	0.0	1.0	0.85	0.65	15
Rod weeder	m	210	10.7	0.0	1.0	0.85	0.65	25
Disk Bedder	rows	185	9.5	0.0	1.0	0.88	0.78	40
Minor Tillage Tools								
Rotary hoe	m	600	0.0	0.0	1.0	1.0	1.0	30
Coil tine harrow	m	250	0.0	0.0	1.0	1.0	1.0	20
Spike tooth harrow	m	600	0.0	0.0	1.0	1.0	1.0	30
Spring tooth harrow	m	2000	0.0	0.0	1.0	1.0	1.0	35
Roller packer	m	600	0.0	0.0	1.0	1.0	1.0	50
Roller harrow	m	2600	0.0	0.0	1.0	1.0	1.0	50
Land plane	m	8000	0.0	0.0	1.0	1.0	1.0	45
Seeding Implements								
Row crop planter, prepared seedbed								
Mounted								
Seeding only	rows	500	0.0	0.0	1.0	1.0	1.0	25
Drawn								
Seeding only	rows	900	0.0	0.0	1.0	1.0	1.0	25
Seed, fertilizer, herbicides	rows	1550	0.0	0.0	1.0	1.0	1.0	25
Row crop planter, no-till								
Seed, fertilizer, her- bicides, 3 fluted coulters per row	rows	3400	0.0	0.0	1.0	0.94	0.82	35
Grain drill w/press wheels								
<2.4 m drill width	rows	400	0.0	0.0	1.0	1.0	1.0	25
2.4 to 3.7 m drill width	rows	300	0.0	0.0	1.0	1.0	1.0	25
>3.7 m drill width	rows	200	0.0	0.0	1.0	1.0	1.0	25
Grain drill, no-till								
1 fluted coulter/row	rows	720	0.0	0.0	1.0	0.92	0.79	35
Hoe drill								
Primary tillage	m	6100	0.0	0.0	1.0	1.0	1.0	50
Secondary tillage	m	2900	0.0	0.0	1.0	1.0	1.0	50
Pneumatic drill	m	3700	0.0	0.0	1.0	1.0	1.0	50

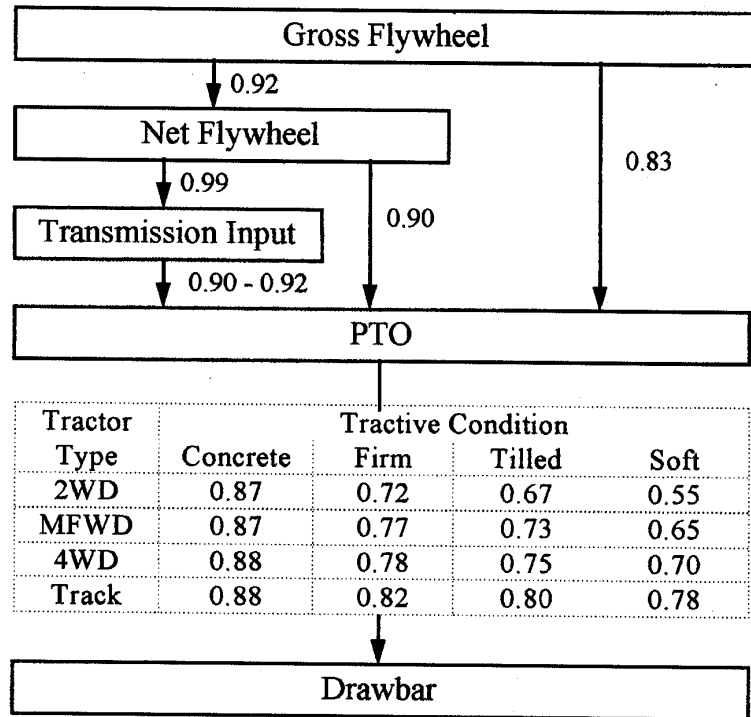


Figure 15.1 – Power relationships for agricultural tractors.

Some machines have a rotary power requirement, where the power is supplied via the tractor PTO or, in the case of self-propelled machines, from the engine on the self-propelled machine. Equation 15.8 can be used to estimate rotary power requirements.

$$P_{rot} = a + bw + cC_m \quad (15.8)$$

where P_{rot} = rotary power, kw

a, b, c = machine specific constants from Table 15.3

For some machines, a drawbar power requirement must be added to the rotary power requirement to obtain the total power requirement. For example, the potato harvester in Table 15.3 has such a requirement as indicated in the footnote in Table 15.3.

Table 15.3. Rotary power requirements. (Adapted from ASAE Data D497).

Machine Type	a, kW	b, kW/m	c, kW h/Mg	Range ^[a] , ± %
Baler, small rectangular	2.0	0	1.0 ^[b]	35
Baler, large rectangular bales	4.0	0	1.3	35
Baler, large round (var. chamber)	4.0	0	1.1	50
Baler, large round (fixed chamber)	2.5	0	1.8	50
Beet harvester ^[c]	0	4.2	0	50
Beet topper	0	7.3	0	30
Combine, small grains	20.0	0	3.6 ^[d]	50
Combine, corn	35.0	0	1.6 ^[d]	30
Cotton picker	0	9.3	0	20
Cotton stripper	0	1.9	0	20
Feed mixer	0	0	2.3	50
Forage blower	0	0	0.9	20
Flail harvester, direct-cut	10.0	0	1.1	40
Forage harvester, corn silage	6.0	0	3.3 ^[e]	40
Forage harvester, wilted alfalfa	6.0	0	4.0 ^[e]	40
Forage harvester, direct cut	6.0	0	5.7 ^[e]	40
Forage wagon	0	0	0.3	40
Grinder mixer	0	0	4.0	50
Manure spreader	0	0	0.2	50
Mower, cutterbar	0	1.2	0	25
Mower, disk	0	5.0	0	30
Mower, flail	0	10.0	0	40
Mower-conditioner, cutterbar	0	4.5	0	30
Mower-conditioner, disk	0	8.0	0	30
Potato harvester ^[c]	0	10.7	0	30
Potato windrower	0	5.1	0	30
Rake, side delivery	0	0.4	0	50
Rake, rotary	0	2.0	0	50
Tedder	0	1.5	0	50
Tub grinder, straw	5.0	0	8.4	50
Tub grinder, alfalfa hay	5.0	0	3.8	50
Windrower/swather, small grain	0	1.3	0	40

^[a] Range in average power requirement due to differences in machine design, machine adjustment, and crop conditions.

^[b] Increase by 20% for straw.

^[c] Total power requirement must include a draft of 11.6 kN/m ($\pm 40\%$) for potato harvesters and 5.6 kN/m ($\pm 40\%$) for beet harvesters. A row spacing of 0.86 m for potatoes and 0.71 m for beets is assumed.

^[d] Based on material-other-than-grain (MOG), throughput for small grains and grain throughput for corn. For a PTO driven machine, reduce parameter "a" by 10 kW.

^[e] Throughput is units of dry matter per hour with a 9 mm length of cut. At a specific throughput, a 50% reduction in the length of cut or cut setting or the use of a recutter screen increases power by 25%.

Example Problem 15.2

A farmer is using a tandem disk harrow for primary tillage in a medium texture soil. The disk width is 6 m, the travel speed is 10 km, and the tillage depth is 20 cm. Estimate the implement draft, the drawbar power and the equivalent PTO power of the MFWD tractor.

Solution

From Table 15.2, the draft parameters are $A = 309$, $B = 16.0$, $C = 0$ and $F_2 = 0.88$. Then the draft is:

$$D_1 = 0.88 [309 + 16 (10)] (6) (20) = 49,526 \text{ N} = 49.5 \text{ kN}$$

The drawbar power is:

$$P_{db} = \frac{49.5(10)}{3.6} = 138 \text{ kW}$$

From Figure 1, assuming the soil ahead of the disk and under the tractor is firm, the ratio between drawbar and PTO power is 0.77. Then the equivalent PTO power is $138 / 0.77 = 179 \text{ kW}$.

Example Problem 15.3

A farmer is using a 12-row corn head on a combine to harvest corn planted in 75-cm rows at a speed of 5 km/h. The corn is yielding 12 Mg/ha. Calculate the rotary power requirement.

Solution

The first step is to calculate the theoretical field capacity on a material basis using Equation 15.2 with $\eta_f = 1.0$. Theoretical field capacity is used because the combine engine must supply sufficient power during periods when the combine is moving through the field, i.e., not turning. Note that the header width is $w = 12(75)/100 = 9 \text{ m}$.

$$C_{mt} = \frac{5(9)(12)(1.0)}{10} = 54 \text{ Mg/h}$$

From Table 15.3, $a = 35 \text{ kW}$, $b = 0 \text{ kW/m}$ and $c = 1.6 \text{ kW h/Mg}$. Note from Table 15.3 that the combine throughput is based on only the grain as the stalks do not pass through the combine. Then the rotary power is:

$$P_{rot} = 35 + 0(9) + 1.6(12) = 54.2 \text{ kW}$$

Note that this estimate is for average conditions. The actual power requirement could be 30% higher or lower as indicated in Table 15.3.

15.3 MACHINERY COSTS

Machinery costs include costs of ownership and operation as well as penalties for lack of timeliness. Ownership costs tend to be independent of the amount a machine is used and are often called fixed or overhead costs. Conversely, operating costs increase in proportion to the amount the machine is used. Total machine costs are the sum of the ownership and operating costs. Ownership, operating, and total machine costs can be calculated on an annual, hourly, or per-hectare basis. Total per-hectare cost is calculated by dividing the total annual cost by the area covered by the machine during the year. A custom cost is the price paid for hiring an operator and equipment to perform a given task. A farm operator can compare total per-hectare costs to custom costs to determine whether it would be better to purchase a machine or to hire the equipment and an operator to accomplish a given task. Per-hectare ownership costs vary inversely with the amount of annual use of a machine. Therefore, a certain minimum amount of work must be available to justify purchase of a machine and, the more work available, the larger the ownership costs that can be economically justified.

15.3.1 Ownership costs

Ownership costs include depreciation of the machine, interest on the investment, and cost of taxes, insurance and housing of the machine.

15.3.1.1 Depreciation

Depreciation is the reduction in the value of a machine with time and use. It is often the largest single cost of machine ownership, but cannot be determined until the machine is sold. However, several methods are available for estimating depreciation. One of these is to estimate the current value using various price guides for used equipment. Annual depreciation is generally highest in the first year of the life of a machine and declines each year. The sum-of-the-year digits and the declining-balance methods both give rapid depreciation in the early years and lower depreciation as the machine ages (Thuesen et al., 1971). Rapid early depreciation is used by many machine owners to obtain the income tax advantages associated with such methods. For simplicity in machinery management calculations, straight-line depreciation can be used. With straight-line depreciation, the difference between the purchase price and the salvage value is divided by the machine life to obtain the annual depreciation. Alternatively, the cost of depreciation and interest can be recovered through use of a capital recovery factor. The capital recovery factor is discussed in the Total Annual Ownership Costs section.

15.3.1.2 Machine life

The life of a machine can be terminated by wear out or by obsolescence. Wear out does not occur at a definite point in time. Rather, the repair costs required to keep the machine operational gradually increase until it becomes uneconomical to continue making repairs. Obsolescence occurs when the machine is out of production and repair parts are no longer available, or when it can be replaced by another machine or method that will produce a greater profit. Table 15.1 gives the estimated life of a number of machines based on total number of hours until the machine is worn out. The number of years of life until wear-out can be obtained by dividing by the annual hours

of use. In many cases, because of limited annual use, machines will become obsolete before reaching the wear-out lives given in Table 15.1. The term *economic life* is defined as the length of time after purchase of a machine that it is more economic to replace the machine with another than to continue with the first, whether because of wear-out or obsolescence. The economic life is then the appropriate life to use in calculating ownership costs.

15.3.1.3 Interest on investment

The money spent to purchase a machine is unavailable for other productive enterprises. Therefore, the cost of ownership includes the interest on the money that is invested in the machine. If a loan is used to purchase a machine, the interest rate is known. If a machine is purchased for cash, the relevant interest rate is the prevailing rate that could have been obtained if the money had been invested instead of being used to purchase the machine. The principal on which the interest is assessed is equal to the remaining value of the machine in any given year. For simplicity, when the straight-line method of depreciation is used, the annual interest cost is assumed to be constant over the life of the machine. It is calculated on the average investment, i.e., the average of the new cost and salvage value of the machine. Alternatively, it can be included in the capital recovery factor.

15.3.1.4 Taxes, insurance, and shelter

Taxes include sales tax assessed on the purchase price of a machine and property tax assessed on the remaining value in any given year. For simplicity, both kinds of taxes are distributed over the life of the machine. Some states have neither a sales tax nor property tax and, in such states, no tax cost should be included. The machine designer may not know which tax rate to use, especially if a machine can be used in any of a number of different states. If actual taxes are unknown, it is reasonable to estimate the annual tax charge at 1% of the purchase price of the machine.

Machines may be insured against loss by fire or other causes, in which case the cost of insurance is known. If no insurance policy is purchased, the owner has elected to carry the risk himself but an insurance cost should still be included. Insurance costs should be based on the remaining value of a machine. If insurance costs are unknown, a reasonable estimate of annual insurance cost is 0.25% of the purchase price of the machine.

There are no conclusive data to prove the economic value of sheltering farm machines. Nevertheless, providing shelter is often associated with better care and maintenance of machines that can result in longer life, improved appearance, and better resale value. If shelter is provided, the cost of providing that shelter can be calculated. If no shelter is provided, there is probably an economic penalty associated with reduced machine life and/or resale value. Thus, a shelter cost should be included whether or not shelter is provided. The annual cost of shelter is considered to be constant over the life of the machine. If shelter cost data are unavailable, it is reasonable to estimate annual shelter cost as 0.75% of the purchase price of the machine.

The total cost of taxes, insurance and shelter can be estimated at 2% of the purchase price of a machine unless more accurate data are available. Although taxes, insurance, and shelter are small relative to total ownership costs, they should be included.

15.3.1.5 Total annual ownership costs

The total annual ownership costs, as discussed above, can be expressed in the following equation:

$$C_{os} = \frac{C_{oa}}{P_u} = (1 - S_v) \left[\frac{I_r(1 + I_r)^{\tau_L}}{(1 + I_r)^{\tau_L} - 1} \right] + \frac{K_{tis}}{100} \quad (15.9)$$

where C_{os} = specific annual ownership costs, 1/yr

C_{oa} = total annual ownership costs, dollars/yr

P_u = purchase price of machine, dollars

S_v = salvage value as fraction of purchase price

I_r = real annual interest rate, decimal

τ_L = economic life of machine, years

K_{tis} = annual cost of taxes, insurance and shelter as percent of purchase price

As noted above, K_{tis} may be assumed to be 2% unless better data are available. The factor in the square brackets in Equation 15.9 is the capital recovery factor. The need for capital recovery is reduced to the extent that the machine has a salvage value at the end of its economic life. In the absence of better data, S_v is often assumed to be 0.1, i.e., the salvage value is estimated at 10% of the purchase price.

The real interest rate, as defined by Bartholomew (1981) is:

$$I_r = \frac{I_p - I_g}{1 + I_g} \quad (15.10)$$

where I_p = prevailing annual interest rate, decimal

I_g = general inflation rate, decimal

Equation 15.10 adjusts the prevailing interest rate for inflation. If there is no inflation, the real interest rate is equal to the prevailing rate. If the inflation rate is greater than or equal to the prevailing interest rate, the real interest rate is zero and the ownership costs are limited to the cost of taxes, insurance, and shelter. Purchasing a machine during times of high inflation tends to “lock in” costs and make machine ownership more attractive than leasing. Example Problem 15.4 illustrates the calculation of ownership costs.

Example Problem 15.4

The self-propelled combine of Example Problem 15.1 has a purchase price of \$100,000, an expected economic life of 10 years, and an expected salvage value of 10% of new cost. At time of purchase, the prevailing interest rate is 6.0%, while the general rate of inflation is 3%. Calculate (a) the specific annual ownership costs and (b) the total annual ownership costs.

Solution

(a) No data were given concerning taxes, insurance, and shelter, so they will be assumed to be 2% of the purchase price, that is, $K_{tis} = 0.02$. From Equation 15.10, the real interest rate is:

$$I_r = (0.06 - 0.03) / (1 + 0.03) = 0.029 \text{ or } 2.9\%$$

Then, from Equation 15.9, the specific ownership costs are:

$$C_{os} = (1 - 0.1) \left[\frac{0.029(1 + 0.029)^{10}}{(1 + 0.029)^{10} - 1} \right] + \frac{2}{100} = 0.125$$

(c) Finally, the total annual ownership costs are:

$$C_{oa} = \$100,000(0.125) = \$12,500/\text{year}$$

15.3.2 Operating costs

Operating costs are costs associated with use of a machine. They include the costs of labor, fuel and oil, and repair and maintenance. A constant hourly labor cost can be determined for hired operators. If the owner operates the machine, the labor cost is determined from alternative uses of the owner's time. If the cost of labor is unknown at the time of the analysis, a typical community labor rate can be used. Dividing the hourly labor cost by C_a gives the labor cost per hectare of land worked by the machine.

15.3.2.1 Costs of fuel and oil

For any given operation, per-hectare fuel (or oil) cost can be calculated using the following equation:

$$C_s = \frac{p_L Q_i}{C_a} \quad (15.11)$$

where C_s = per-hectare fuel (oil) costs, \$/ha

p_L = price of fuel (oil), \$/L

Q_i = fuel (oil) consumed by engine, L/h

C_a = effective field capacity during the operation, ha/h

Of the three independent variables in Equation 15.11, Q_i is the variable for which it is most difficult to determine a realistic value. The first step is to estimate the engine power required to perform the operation. In Section 15.2, the power requirements of various operations was discussed. Power requirements computed at the drawbar must be converted into equivalent PTO power, as was done in Example Problem 15.2. After the total equivalent PTO power is calculated, the specific fuel consumption of the engine can be estimated. ASAE Data D497 provides specific fuel consumption equations for gasoline, diesel, or LPG engines, but since most farm tractors now have diesel engines, only the diesel equation is given here:

$$\text{SFC}_v = 3.91 + 2.64X - 0.203\sqrt{173 + 738X}$$

$$\text{If } X > 0.856, \text{SFC}_v = 0.411 \text{ L/kW h} \quad (15.12)$$

where SFC_v = specific fuel consumption, volume basis, L/kW h

X = ratio of equivalent PTO power requirement to maximum available PTO power

Typical values of X range from approximately 0.2 for spraying operations to 0.85 for primary tillage. Multiplying SFC_v by the equivalent PTO power needed for the operation gives Q_i , the estimated fuel consumption to perform the operation.

The per-hectare cost of oil consumption can be calculated using Equation 15.11 with the word oil substituted for the word fuel. ASAE D497 gives equations for estimating oil consumption of gasoline, diesel, or LPG engines. The equation for diesel engines is:

$$Q_i = \frac{21.69 + 0.59P_r}{1000} \quad (15.13)$$

where Q_i = oil consumption, L/h

P_r = rated engine power, kW

Equation 15.13 is based on replacement of oil in the crankcase at the manufacturer's recommended change intervals; it does not include oil that must be added between oil changes, nor does it include hydraulic/transmission oil or other lubricants. Total cost of all lubricants is approximately equal to 10% to 15% of fuel costs.

15.3.2.2 Costs of repairs and maintenance

Costs for repairs and maintenance are highly variable depending on the care provided by the manager of the machine. Some expenditures will always be necessary to replace worn or failed parts and/or to repair damage from accidents. Repair and maintenance costs tend to increase with the size and complexity, and thus with the purchase price of the machine. The following equation from ASAE EP496 can be used to estimate accumulated repair and maintenance costs:

$$\frac{C_m}{P_u} = \text{RF1} \left[\frac{t}{1000} \right]^{\text{RF2}} \quad (15.14)$$

where C_m = accumulated repair and maintenance costs, dollars

t = accumulated use, h

RF1, RF2 = repair factors from Table 15.1

To correct for inflation, the purchase price in Equation 15.14 is multiplied by $(1+I_g)^n$, where n is the age of the machine in years. Note that the accumulated repair and maintenance costs vary from year to year. Average hourly costs of repairs and maintenance can be estimated by estimating the total economic life of the machine in

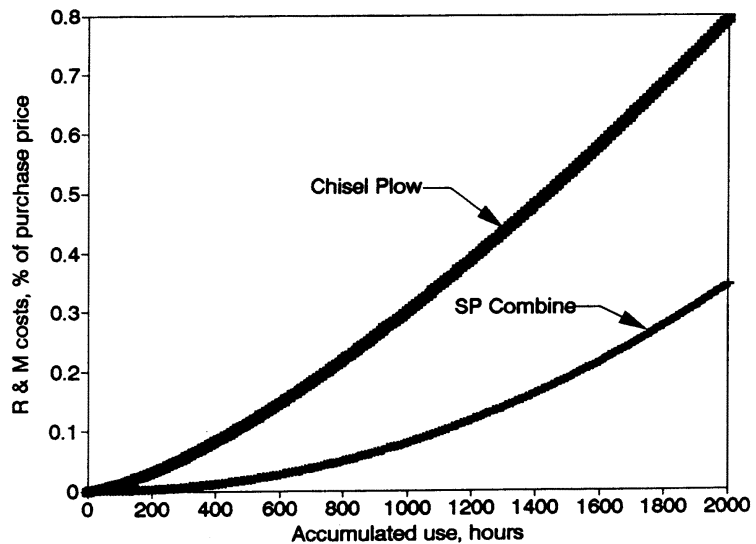


Figure 15.2 – Accumulated repair and maintenance costs of two machines as a percent of purchase price of the respective machines.

hours, using Equation 15.14 to calculate the total repair and maintenance costs over the life of the machine, and dividing the total by the economic life in hours. Then, by dividing the average cost by C_a , one can obtain the average repair and maintenance cost per hectare of area worked by the machine. Repair and maintenance costs are an important component of total costs. For example, use of Equation 15.14 with the data in Table 15.1 shows that, for a tractor, the total repair and maintenance costs over the life of a tractor can equal the purchase price of the tractor. Figure 15.2 illustrates the accumulation of repair and maintenance costs for two different machines. As a percent of purchase price, the chisel plow accumulates repair and maintenance costs much faster than the self-propelled combine. At the end of 2000 hours, for example, the accumulated repair and maintenance costs for the plow are 79.2% of purchase price. The corresponding figure for the combine is only 34.3%. However, the purchase price of the combine is about ten times that of the plow. Thus, in terms of dollars, the accumulated repair and maintenance costs for the combine are over 4 times those of the plow.

15.3.3 Timeliness costs

There is an optimum time of the year to perform some field operations and economic penalties are incurred if the operations are performed too early or too late. When harvesting a crop, for example, increasing fractions of the yield may be lost and/or the crop quality may be reduced if the harvest is started too early or delayed beyond the optimum time. In the extreme case, insufficient machine capacity may prevent completion of a harvest before adverse weather destroys the remainder of the crop. It is thus economically justifiable to increase machine costs through purchase of a machine of greater capacity when the larger machine will accomplish more timely

work. Thus the term *timeliness cost* is important in machinery cost analyses. The timeliness cost can be calculated by using the following equation:

$$C_t = \frac{K_t A Y V}{\lambda_o T C_a p_{wd}} \quad (15.15)$$

where C_t = timeliness cost, \$/ha

K_t = timeliness coefficient, fraction of annual crop value lost per day (see Table 15.4)

A = crop area, ha/yr

Y = crop yield, Mg/ha

V = crop value, \$/Mg

$\lambda_o = 2$ if operation commences or ends at the optimum time

$= 4$ if operation can be balanced evenly about the optimum time

T = expected time available for field work, h/day

C_a = effective field capacity of machine, ha/h

p_{wd} = probability of a good working day, decimal (see Table 15.5)

The factor, K_t , is the fraction of the crop yield that is lost for each day of delay of an operation. It is apparent that the timeliness coefficient varies with the type of operation. Given an optimum planting date, for example, planting earlier or later than that date will diminish the crop yield. Since the actual planting period can be balanced around the optimum date, $\lambda_o = 4$ for planting. Conversely, there is no timeliness coefficient associated with tillage unless tillage delays subsequently delay planting. For most harvesting operations, $\lambda_o = 2$ because it is often not feasible to begin harvesting until the crop is mature. Note that the denominator of Equation 15.15 relates to the rapidity with which an operation can be completed, i.e., working more hours per day and/or using a machine of greater capacity decreases the time required to complete an operation. Use of $\lambda_o = 4$ indicates an early start on the operation and thus earlier completion. Weather also affects the number of calendar days required to complete an operation, since the operation must be interrupted during bad weather. As indicated in Table 15.5, p_{wd} varies with geographic location and also varies throughout the year in most geographic locations. Example Problem 15.5 illustrates the calculation of operating costs.

Example Problem 15.5

The self-propelled combine of Example Problems 15.1 through 15.4 is harvesting corn in the midwest USA in early September. The crop value is \$78/Mg. The combine is used an average of 10 hours per day and 200 hours per year. From Example Problem 15.3, the engine uses 54.2 kW of power on average during combining. However, power demand for combining can be 30% higher and additional power is needed if the grain bin is unloaded while the combine is combining; thus, a 100 kW engine is on the combine. Diesel fuel costs \$0.50/liter, while motor oil costs \$1.20/liter. Labor costs are \$12.00 per hour. Calculate (a) the total operating costs per hectare, excluding timeliness costs, (b) the timeliness penalty costs, and (c) total costs per hectare.

Table 15.4. Timeliness coefficients (ASAE Standard D497).

Operation	K _T , 1/day		
Tillage (depends on whether planting is delayed by prior tillage)	0.000-0.010		
Seeding			
Corn (Indiana, Illinois, Iowa, Eastern Nebraska, Eastern Kansas)			
Available moisture in root zone at planting, cm	<u>April</u>	<u>May</u>	<u>June</u>
10	0.010	0.000	0.002
20	0.006	0.001	0.003
30	0.003	0.004	0.007
Wheat, Utah	0.008		
North Dakota	0.007		
Soybeans, Wisconsin, May & June	0.005		
Missouri, Illinois, June	0.006		
Double crop after wheat, Illinois	0.010		
Cotton, Lubbock, Texas			
April	0.004		
May	0.020		
Mississippi, April & May	0.007		
Barley, Utah	0.008		
North Dakota	0.007		
Oats, Illinois and Michigan	0.010		
Wisconsin after May 6	0.012		
Alabama, Fall	0.000		
Utah	0.008		
Rape, Manitoba	0.003		
Rice, California, May	0.010		
Row Cultivation, Illinois, soybeans	0.011		
Rotary hoeing, Iowa, soybeans	0.028		
Harvest			
Haymaking, Michigan, June	0.018		
Shelled corn, Iowa	0.003		
Ear corn, Illinois, after Oct. 26	0.007		
Soybeans, Illinois (depends on variety)	0.006-0.010		
Wheat, Ohio	0.005		
Cotton, Alabama	0.002		
Rice, California	0.009		
Sugar cane, Queensland, Australia			
pre-optimum	0.002		
post-optimum	0.003		

Table 15.5. Probabilities for a good working day (ASAE Data 497.4).

Average date	Region	Soil	Notes	Central Illinois	State of Iowa	South-eastern Michigan	State of South Carolina	Southern Ontario Canada	Mississippi Delta	Probability level, percent										
										Wettable period		50		90		50		90		
Jan. and Feb.																				
Mar. 7																				
Mar. 21																				
Apr. 4																				
Apr. 18																				
May 2																				
May 16																				
May 30																				
June 13																				
June 27																				
July 11																				
July 25																				
Aug. 8																				
Aug. 22																				
Sept. 5																				
Sept. 19																				
Oct. 3																				
Oct. 17																				
Nov. 1																				
Nov. 15																				
Nov. 29																				
Dec. 13																				

Adjust for Sundays and holidays by multiplying pwd's above by 0.86, 0.82, 0.78 and 0.75 for months 0, 1, 2 and 3 holidays.

Solution

(a) From Example Problem 15.1, the field capacity of the combine is 3.24 ha/h. Thus, the per-hectare labor costs are:

$$\$12.00 / 3.24 = \$3.70/\text{ha}$$

Next, the per-hectare fuel and oil costs will be calculated. From Equation 15.12, the ratio of actual to maximum power is $54.2/100 = 0.54$. Then the specific fuel consumption of the engine is:

$$\text{SFC}_v = 3.91 + 2.64(0.54) - 0.203(173 + 738 \times 0.54)^{0.5} = 0.483 \text{ L/kW h}$$

The hourly fuel consumption is:

$$Q_{if} = 0.483(54.2) = 26.2 \text{ L/h}$$

From Equation 15.11, making use of the effective field capacity from Example Problem 15.1, the per-hectare fuel costs are:

$$C_{sf} = 0.50(26.2) / 3.24 = \$4.03/\text{ha}$$

Next, from Equation 15.13, the estimated oil consumption rate is:

$$Q_{io} = (21.69 + 0.59 \times 100) / 1000 = 0.08 \text{ L/h}$$

Again, from Equation 15.11, the per-hectare oil costs are:

$$C_{so} = 1.20(0.08) / 3.24 = \$0.03/\text{ha}$$

To calculate the per-hectare costs of repair and maintenance, Equation 15.14 is first used to calculate the accumulated repair and maintenance costs after 10 years of use at 200 hours per year. Also, the purchase price is corrected for the 3% inflation rate, that is, the adjusted price is:

$$P_u = \$100,000(1 + 0.03)^{10} = \$134,392 \text{ adjusted price}$$

Then, from Equation 15.14 and using RF factors from Table 15.1:

$$C_{rm} = 134,392(0.14)(2000/1000)^{2.1} = \$80,661 \text{ total repair and maintenance costs}$$

Harvesting at a rate of 3.24 ha/h for 2000 hours, the combine harvests 6840 ha during its economic lifetime. Therefore, the per-hectare costs for repair and maintenance are:

$$80,661/6840 = \$11.79/\text{ha}$$

The total per-hectare operating cost, excluding the timeliness penalty cost, is:

$$3.70 + 4.03 + 0.03 + 11.79 = \$19.55/\text{ha}$$

(b) The timeliness penalty cost is calculated using Equation 15.15. From Table 15.4, $K_\tau = 0.003$. From Table 15.5, averaging values for Illinois and Iowa in late October, $p_{wd} = 0.61$ at the 90% probability level. Harvesting at the rate of 3.24 ha/h for 200 hours per year, the combine harvests 648 ha/year. Then, inserting values into Equation 15.15 as given in the three example problems, the timeliness cost penalty is:

$$C_t = \frac{0.003(648)(12)(78)}{2(10)(3.24)(0.61)} = \$46.03/\text{ha}$$

(c) From Example Problem 15.4, the \$12,500 annual ownership costs divided over 648 ha harvested annually are \$19.29 per hectare. Thus, the total per-hectare costs are:

\$19.29/ha	ownership costs
19.55/ha	operating costs excluding timeliness penalty
<u>46.03/ha</u>	timeliness penalty cost
\$84.87/ha	total costs

Harvesting costs consumed about 9% of the total revenues from growing the corn crop, that is, $12 \text{ Mg/ha}(\$78)/\text{Mg} = \$936/\text{ha}$. The combine used in Example Problems 15.1 through 15.3 may not have been of optimum capacity. In Section 15.4, a method for selecting the optimum capacity will be presented.

15.4 MACHINERY SELECTION AND REPLACEMENT

15.4.1 Machinery selection

Choosing the appropriate field capacity for a machine is an important problem for both the machine designer and the farm operator. From the farm operator's viewpoint, there is an optimum field capacity for maximum profit and the goal is to determine that optimum capacity. Since the farm operator will want to purchase a machine of optimum capacity, the machine designer also has a vital interest in designing machines of optimum size for various farm sizes. The problem of machinery selection is illustrated in Figure 15.3, in which machines of various sizes are considered for a farm of a given size. Three types of costs are illustrated in the figure. The machinery costs include all ownership and operating costs except labor, which is displayed separately. The timeliness costs are also shown. The per-hectare machinery costs increase with machine size because the land area is fixed and larger machines cost more than small machines. Larger machines decrease the labor costs by completing the work more quickly. Note that, if timeliness is not considered, the smallest machines would be most economical. However, timeliness costs rise sharply when machines are too small to complete the work in a timely manner. As indicated in Figure 15.3, the optimum machine size is one that minimizes the sum of the timeliness costs and the machinery costs including labor.

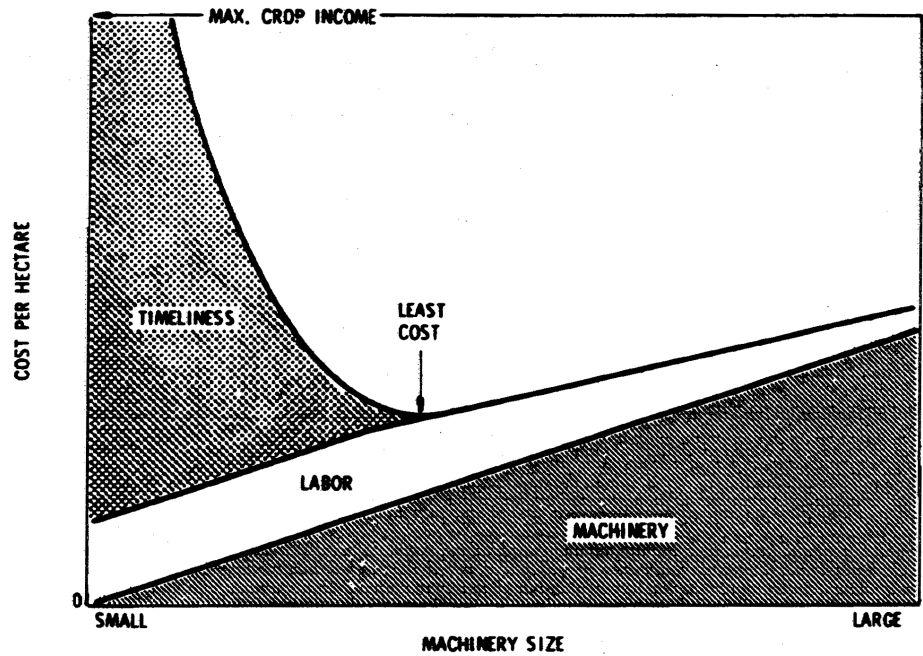


Figure 15.3 – Costs related to machinery size for a specific farm (Burrows and Siemens, 1974).

Mathematically, the field capacity giving least total cost for an individual machine can be determined by combining all of the cost equations into one equation and differentiating with respect to field capacity. The result is given in the following equation:

$$C_{\text{aopt}} = \sqrt{\frac{A}{C_{\text{os}} K_p} \left[L_c + T_{\text{fc}} + \frac{K_{\tau} A Y V}{\lambda_o T p_{\text{wd}}} \right]} \quad (15.16)$$

where C_{aopt} = optimum effective field capacity, ha/h

L_c = labor cost, \$/h

T_{fc} = specific ownership costs of tractor, \$/h

K_p = unit price function, described below

A value for T_{fc} can be determined by using the following equation:

$$T_{\text{fc}} = \frac{C_{\text{oat}}}{\tau_{\text{At}}} \quad (15.17)$$

where T_{fc} = Amount charged to machine for tractor use, \$/h

C_{oat} = annual ownership cost of tractor, \$/yr (from Equation 15.6)

τ_{At} = total annual use of tractor, h/yr

An alternative method of estimating C_{oat} makes use of the following equation developed by Buckmaster:

$$C_{\text{oat}} = 278 P_{\text{pto}}^{0.122} \tau_{\text{Lt}}^{-0.437} \tau_{\text{At}}^{-0.958} I_r^{0.244} P_{\text{act}} \quad (15.18)$$

where P_{pto} = rated PTO power of tractor, kW

P_{act} = actual power demand on tractor used in operation, kW

τ_{Lt} = economic life of tractor, years

The remaining quantities in Equations 15.16 and 15.18 were previously defined, except for K_p , the unit price function. It is defined as the increased price for one additional unit of field capacity. A value for K_p can be determined by comparing the prices of a group of machines that vary only in capacity. If the sales price is plotted versus field capacity for the group of machines, the slope of the line is equal to K_p . If the increased capacity is expressed on a width basis, as for a tillage machine, then the purchase price should be plotted versus width. The slope of the line is then the price per unit of increased width and K_p can be calculated using the following equation:

$$K_p = \frac{10P_w}{v \eta_f} \quad (15.19)$$

where K_p = unit price function, \$ · h/ha

P_w = price per unit of increased width, \$/m

v = travel speed, km/h

η_f = field efficiency, decimal

Equation 15.16 can estimate the optimum capacity of a single machine. Usually, however, a family of machines is required in farming operations and these machines should have field capacities that are compatible with each other and with the tractor. For example, a tractor, plow, disk, planter, combine, and possibly other implements may be required to grow soybeans. Each of the implements has a definite period during the year during which its work should be accomplished. The term *scheduling* is defined as determining the time periods during the year when each operation can be performed. After the scheduling is completed, the required capacity can be calculated by using the following equation:

$$C_a = \frac{A}{\tau_{\text{ad}} T p_{\text{wd}}} \quad (15.20)$$

where C_a = effective field capacity required to complete the work, ha/h

A = area to be worked, ha

τ_{ad} = available time to complete the work, days

T = length of each working day, h/day

p_{wd} = probability of a good working day, decimal (see Table 15.5)

The tractor must be large enough to provide power to the implement with the greatest power demand. If the implements vary widely in power demand, the tractor will be used inefficiently on the implements with the lowest power demand. Thus, to provide greatest overall efficiency and profit, it may be best to choose some implements with greater capacity than would be calculated using Equation 15.16 or 15.20. The calcula-

tions become even more complex when the size of the farm justifies ownership of more than one tractor and/or more than one combine. Further, the use of constant timeliness coefficients (K_t) is an over-simplification. Realistically, there is little or no reduction in crop yield if operations can be accomplished during the normally scheduled periods. The daily penalty for delayed work should be assessed only after the scheduled period. To achieve greater realism, digital computer programs have been developed for scheduling farm machinery operations and for selecting optimum systems of farm machinery (see, for example, Rotz et al., 1983, or Siemens et al., 1990). Except for the simplest of systems, it is necessary to use such programs to obtain realistic results. Example Problem 15.6 illustrates the calculation of optimum size of a single machine.

Example Problem 15.6

Using data from Example Problems 15.1 through 15.5, calculate the optimum combine capacity for harvesting the corn. Assume that, from an analysis of the purchase prices of two self-propelled combines, the unit price function is \$20,000 h/ha.

Solution

The required data for use in Equation 15.16 are already available. Note that $T_{fc} = 0$ in this example, since no tractor is used with the self-propelled combine. The optimum size is:

$$C_{\text{aopt}} = \sqrt{\frac{648}{0.125(20,000)} \left[12 + 0 + \frac{0.003(648)(12)(78)}{2(10)(0.61)} \right]} = 6.46 \text{ ha/h}$$

By using Equation 15.1, the reader may verify that a combine traveling at 5 km/h with a 24-row corn head working in 75-cm rows with a field efficiency of 72% would have the optimum capacity. It would be instructive to rework Example Problems 15.1 through 15.5 to observe the changes in the various costs as a result of using the larger combine.

15.4.2 Machinery replacement

All machines eventually reach the end of their economic life and the owner must decide when to replace each machine. There are a number of reasons why the owner might decide to replace a given machine. Machine damage suffered as a result of an accident might be so great that replacement would be less expensive than repairing the damage. The machine might become obsolete. As previously mentioned, a machine is obsolete when it is out of production and repair parts are no longer available, or when it can be replaced by another machine or method that will produce a greater profit.

Table 15.6. An example of average unit accumulated costs.

End of Year	Remain- ing Value	R&M Costs	Depr.	Int.	Acc. Depr.	Acc. Int.	Acc. R&M	Total Acc. Costs, \$	Acc. Use, ha	Unit Acc. Costs, \$/ha
1	2000	10	1000	200	1000	200	10	1210	100	12.10
2	1400	50	600	136	1600	336	60	1996	200	9.98
3	1000	70	400	96	2000	432	130	2562	300	8.54
4	700	100	300	68	2300	500	230	3030	400	7.58
5	500	200	200	48	2500	548	430	3478	500	6.96
6	350	300	150	34	2650	582	730	3962	600	6.60
7	225	350	125	23	2775	605	1080	4460	700	6.37
8	125	450	100	14	2875	619	1530	5024	800	6.28
9	100	550	25	9	2900	628	2080	5608	900	6.23
10	75	600	25	7	2925	635	2680	6240	1000	6.24

Combines, balers, and other processing machines generally become obsolete faster than tractors, since tractors need only supply power. A machine should be replaced when the anticipated frequency of breakdowns becomes so large that the machine is no longer reliable. Large economic penalties can result when field work is delayed and an unreliable machine can cause delays. Finally, a machine should be replaced when it is anticipated that the cost of repairs will begin to increase the average unit accumulated cost above the minimum. For example, Table 15.6 shows repair and maintenance, depreciation, and interest costs over the life of a \$3000 machine that is used on 100 ha annually. The unit accumulated costs reach a minimum at the end of year 9 of the machine life in this example. The machine should be replaced before the tenth year unless it is replaced earlier for other reasons.

PROBLEMS

- 15.1 A self-propelled combine is equipped with an 8-row corn head for 75-cm rows. (a) What is the maximum speed the combine should be operated in corn yielding 9.4 Mg/ha if the theoretical field capacity of the combine is 28 Mg/h? (b) What is the theoretical field capacity of the combine in ha/h?
- 15.2 A self-propelled combine is equipped with a 5-m grain platform. (a) At what speed must the combine be operated to fully use its separating capacity of 0.28 Mg/h in harvesting soybeans with a yield of 2.7 Mg/ha? (b) Considering the data in Table 15.1, what is the maximum recommended speed for harvesting the soybeans? (c) What is the theoretical capacity of this combine, in ha/h, in harvesting soybeans? (d) Is the theoretical field limited by gathering capacity or separating capacity of the combine?
- 15.3 A company is planning to design a family of self-propelled combines with a range of field capacities. All of the combines will be designed to operate at the typical speed listed in Table 15.1. Corn heads and 2, 4, 6, 8, 10, and 12

- rows will be marketed, all for 75-cm row spacing and with separating capacities to match the corn heads. (a) If the field efficiency of the 2-row machine is 70%, calculate the total time losses, $\tau_a + \tau_h$, that are incurred in harvesting one hectare. (b) Assuming that these time losses would remain unchanged for the combines larger than 2-row capacity, calculate and plot the field efficiency versus size of the corn heads. (c) As an alternate assumption, calculate and plot the allowable total time losses, $\tau_a + \tau_h$, that could be tolerated per hectare if all of the combines were to have the same field efficiency.
- 15.4 Same as Problem 15.3, except that a family of row-crop planters is to be designed. All of the planters will operate at a typical speed of 6.4 km/h and the field efficiency of the 2-row planter is 60%.
- 15.5 (a) Assuming that 100% of the machine width is utilized, calculate and plot the total allowable lost time as a fraction of theoretical operating time, i.e., $(\tau_a + \tau_h) / \tau_t$, versus field efficiency. (b) Repeat part a but with 95% of the machine utilized. Plot both curves on the same graph. (c) Using data from Table 15.1, mark the curves to show the allowable lost time for typical field efficiency of a potato harvester and a field cultivator assuming 95% of the width of the field cultivator is utilized.
- 15.6 Calculate and plot specific annual ownership costs versus economic life for life ranging from 1 to 20 years. Include two curves, one for a general inflation rate of 2% when the prevailing interest rate is 7% and one for a general inflation rate of 20% when the prevailing interest rate is 25%. Assume salvage value is 10% of purchase price, while taxes, insurance, and shelter are 2% of purchase price.
- 15.7 Same as Problem 15.6, except calculate and plot specific annual ownership costs versus real interest rate for interest rates ranging from 0% to 10%. Plot two curves, one for a 5-year economic life and one for a 10-year life.
- 15.8 A tractor with rated PTO power of 90 kW is used to perform a tillage operation which requires 75 kW equivalent PTO power. The effective field capacity is 2 ha/h. Fuel cost is \$0.75/L and oil cost is \$1.25/L. Calculate (a) the specific fuel consumption, (b) the fuel consumption in L/h, (c) the per-hectare fuel costs, (d) the oil consumption in L/h, and (e) the per-hectare oil costs.
- 15.9 Same as Problem 15.8, except that the rated power of the tractor is 80 kW.
- 15.10 Same as Problem 15.8, except that the rated power of the tractor is 120 kW.
- 15.11 (a) Assuming a zero rate of inflation, calculate and plot accumulated repair and maintenance costs as a percent of machine purchase price for a chisel plow. These dimensionless costs are to be plotted versus accumulated hours of use from zero to the estimated life of the plow, as given in Table 15.1. (b) Repeat part a, but with an inflation rate of 10%. Put the curves for zero and 10% inflation on the same graph.
- 15.12 Repeat Problem 15.11, except for a two-wheel drive tractor.
- 15.13 Repeat Problem 15.11, except for a self-propelled combine.

- 15.14 An 12-row conventional row-crop planter is to be used to plant 180 ha of soybeans with 75-cm row spacing in early June in Central Illinois. The soybeans have an anticipated yield of 2.7 Mg/ha and an anticipated selling price of \$250/Mg. (a) Using typical travel speed and field efficiency for the planting operation (see Table 15.1), calculate the field capacity and (b) the timeliness cost assuming the farmer works 10-hour days and wants to be assured of a 90% probability of having the required number of good working days.
- 15.15 Repeat Problem 15.14, except use a 6-row planter.
- 15.16 Repeat Problem 15.14, except use the planter to plant 200 ha of soybeans.
- 15.17 A conventional row-crop planter is to be used to plant 200 ha of soybeans with 75-cm row spacing in early May in Central Illinois. The soybeans have an estimated yield of 2.7 Mg/ha and an anticipated selling price of \$190/Mg. The farmer works 10-hour days. The planter is pulled by a \$70,000 tractor that is used 400 hours per year (only a fraction of that total time is used with the planter) with an economic life of 15 years. For both the planter and tractor, assume salvage value of 10%, interest rate of 5% and $K_{t,s} = 2\%$. The economic life of the planter is 10 years and labor costs are \$10.00 per hour. List prices are \$22,000, \$38,000 and \$60,000 for 8, 12 and 16-row planters, respectively. Calculate (a) the total annual ownership costs and (b) specific ownership costs of the tractor, (c) the specific annual ownership costs, (d) unit price function and (e) optimum effective field capacity of the planter. (f) If the planter works at the typical speed and field capacity given in Table 15.1, select the best available planter, i.e., how many rows would it have?
- 15.18 Same as Problem 15.17, except that the planter is used to plant corn (maize) in Iowa in early May. Also, there are 30 cm of available moisture in the root zone. The anticipated corn yield is 9.4 Mg/ha and the anticipated selling price of the corn is \$78/Mg.
- 15.19 Suppose that 10 days were available to do the planting described in Problem 15.17. What size planter would be selected to allow such scheduling?
- 15.20 Rework Example Problem 15.6, except let the hours worked per day vary from 6 to 16 hours. From the results, plot optimum capacity versus hours worked per day.

SIMULATION PROBLEMS

The simulator, Machinery Size Selector, on the CD-ROM was developed to explore the effect of relevant variables on the optimum size of some common farm machines. The simulator is based on theory in Chapter 15. Machine purchase price – size relationships were based on costs in 2005. The user can use the fifth web site above to find the CPI adjustment factor to use to adapt the spreadsheet for later years. Most of the other input variables in the simulator can be taken from the tables in Chapter 15. The user should use judgment in applying the results. If the optimum machine size seems excessive, for example, column K may show only a relatively small increase in total cost to use a much smaller machine.

- S15.1 (a) Use the simulator to find the optimum width of a moldboard plow to be used on 400 ha per year when the tillage depth is 20 cm. Assume the crop is corn yielding 12 Mg/ha and the corn price is \$78/Mg. The real interest rate is 3%, fuel is \$0.50/liter, oil is \$1.25/liter, the plow is used 10 hrs/day and the labor cost is \$10/hr. The remaining variables can be found in the tables in Chapter 15. Use a mid-range value for the timeliness coefficient, i.e., 0.005. Some iteration will be required to find an acceptable machine life and engine size. (b) After the optimum machine size is found, observe the changes in the various columns as the machine size is increased and consider whether the trends seem reasonable. (c) Now explore the effect of various input variables, e.g., crop yield and price, interest rate, fuel and oil prices, and labor hourly cost on the optimum machine size.
- S15.2 Rework Simulation Problem S15.1, except use a field cultivator at a depth of 18 cm.
- S15.3. Rework Simulation Problem S15.1, except use a tandem disk at a depth of 14 cm.
- S15.4 Rework Simulation Problem S15.1, except use a big round baler on 70 ha annually. The crop yield is 8 Mg/ha and the crop value is \$100/Mg.
- S15.5 Rework Simulation Problem S15.1, except use a self-propelled forage harvester on 150 ha annually. The crop yield is 8 Mg/ha and the crop value is \$90/Mg.
- S15.6 Rework Simulation Problem S15.1, except use a self-propelled combine on 400 ha annually. The crop yield is 12 Mg/ha and the crop value is \$78/Mg.

Relevant websites

(Warning: The following websites were relevant at time of publication of the book, but webmasters are free to change or eliminate websites at any time).

<http://www.extension.iastate.edu/Publications/PM952.pdf>

<http://www.machinerylink.com/articles/doane.pdf>

http://www.farmdoc.uiuc.edu/manage/machinebuilding_index.html

http://www2.agriculture.purdue.edu/ssmc/Frames/June04_SSMC.pdf

<http://www1.jsc.nasa.gov/bu2/inflateCPI.html>

ENGINEERING PRINCIPLES OF AGRICULTURAL MACHINES,

2nd Edition

Errata

(updated July 2006)

Page 18. 3rd line from the bottom, symbol should be > rather than <, as: $2\Psi_1(1 - 1/\phi)$ for $\phi > 1$

Page 24. Equation 2.9 should be:

$$\frac{p_{cme}}{p_1} = \frac{r - r^k + \Theta_r(r - r^{2-k} r_{co}^{k-1} + r r_{co}^{-1}(k-1)(r_{co} - 1))}{(k-1)(r-1)}$$

where p_{cme} = cycle mean effective pressure, kPa

p_1 = absolute pressure at beginning of compression, kPa

$\Theta_r = \Theta_3/\Theta_1$

$\lambda = k(\gamma^{-1} - 1)$

$r_{co} = (\lambda + 1)/(\lambda + (\Theta_3/\Theta_1)r^{k-1})$ = fuel cutoff ratio

$k = 1.4$ for air standard cycle

Page 36. Equation 2.24 should be: $\rho_a = \frac{29p_a}{8.314\Theta_a}$

$$\Theta_{rc} = 1 + \frac{p_{rc}^{0.286} - 1}{\eta_c}$$

Page 38. Equation 2.27 should be:

Page 79. Equation 4.23 should be: $PD = \frac{P}{\sin(180/N)}$

Page 85. Equation 4.26 should be: $\tan(\phi_{jo}) = \cos(\alpha) \tan(\phi_{ji})$

Page 117. Problem 5.2, use $\Delta p = 32$ MPa.

Page 118. Problem 5.7(a), start with Equation 5.9, not 5.19.

Page 118. Problem 5.8, the first sentence should include “.. as given by Equations 5.3 and 5.5” not “Problems 5.3 and 5.4.”

Page 119. Problem 5.8(c), assume $C_f = 1.9 \times 10^7$, not 0.025×10^8 .

Page 137. Problem 6.4, the latitude of the benchmark should be $40^\circ 3' 21.20''$ N Latitude.

Page 138. Problem 6.5, the latitude of the benchmark should be $40^\circ 3' 21.17''$ N Latitude.

Page 219. The equation above 8.46 should begin with a lowercase e, as: $eL_f + eL_r + b S_f - (b + d) S_r = 0$.

Page 383. Figure 11.36, photos for d and e are switched.